

Dissertation

(kumulativ)

zur Erlangung des akademischen Grades

Doctor rerum naturalium (Dr. rer. nat.)

Well-defined polyesters for applications in life science

vorgelegt dem Rat der Chemisch-
Geowissenschaftlichen Fakultät
der Friedrich-Schiller-Universität Jena

Damiano Bandelli
geboren *am 14. Juni 1989*
in Bagno a Ripoli, Florenz, Italien

Gutachter:

1. Prof. Dr. Ulrich S. Schubert, Friedrich Schiller Universität Jena
2. Prof. Dr. Felix H. Schacher, Friedrich Schiller Universität Jena

Tag der öffentlichen Verteidigung: 13.07.2022

Table of contents

Table of contents

Documentation of authorship.....	3
Dokumentation der Autorenschaft.....	9
1. Introduction.....	17
2. Challenges in polyester synthesis: From polycondensation to ROP.....	21
3. ROP of lactide and various lactones catalyzed by Strontium isopropoxide	27
4. Tailor-made block and gradient copolymers matching the HHB of P ϵ CL.....	33
5. Statistical copolyesters of ϵ - and δ -caprolactone	39
6. Designed monomers to modify PLA	46
7. Summary	54
8. Zusammenfassung.....	58
9. References.....	62
List of abbreviations.....	67
Curriculum Vitae.....	69
Publication List	71
Acknowledgements.....	75

Documentation of authorship

This section contains a list of the individual contributions to the publications reprinted in this thesis.

† Leading author

Damiano Bandelli, ^{1†} Julien Alex, ² Christine Weber, ³ Ulrich S. Schubert, ⁴ Polyester				
Pub1	stereocomplexes beyond PLA: Could synthetic opportunities revolutionize established material blending? <i>Macromol. Rapid Commun.</i> 2019 , <i>41</i> , 1900560.			
Author	1	2	3	4
Conceptual development	×		×	
Preparation of the manuscript	×	×		
Correction of the manuscript			×	×
Supervision of J. Alex	×		×	
Supervision of D. Bandelli			×	×
Proposed publication equivalent	0.5			

Damiano Bandelli, ^{1†} Christine Weber, ² Ulrich S. Schubert, ³ Strontium isopropoxide: A			
Pub2	highly active catalyst for the ROP of lactide and various lactones. <i>Macromol. Rapid Commun.</i> 2019 , <i>40</i> , 1900306.		
Author	1	2	3
Conceptual development		×	×
Test reactions	×		
Kinetic studies and interpretation	×		
MALDI analyses and interpretation	×		
Preparation of the manuscript	×		
Correction of the manuscript		×	×
Supervision of D. Bandelli		×	×
Proposed publication equivalent	1.0		

Documentation of authorship

Pub3 Damiano Bandelli,^{1†} Christian Helbing,^{2†} Christine Weber,³ Michael Seifert,⁴ Irina Muljajew,⁵ Klaus D. Jandt,⁶ Ulrich S. Schubert,⁷ Maintaining the hydrophilic–hydrophobic balance of polyesters with adjustable crystallinity for tailor–made nanoparticles, *Macromolecules* **2018**, *51*, 5567–5576.

Author	1	2	3	4	5	6	7
Conceptual development	×	×	×				
Kinetic studies and interpretation	×						
Polymer syntheses and structural characterization	×						
DSC and TGA studies	×						
PLM and AFM studies		×		×			
Nanoparticle preparations	×						
DLS measurements	×				×		
Preparation of the manuscript	×	×	×				
Correction of the manuscript			×	×	×	×	×
Supervision of D. Bandelli			×				×
Supervision of C. Helbing						×	
Supervision of I. Muljajew					×		×
Proposed publication equivalent	1.0						

Documentation of authorship

Pub4	Damiano Bandelli, ^{1†} Irina Muljajew, ² Karl Scheuer, ³ Johannes B. Max, ⁴ Christine Weber, ⁵ Felix H. Schacher, ⁶ Klaus D. Jandt, ⁷ Ulrich S. Schubert, ⁸ Copolymerization of caprolactone isomers to obtain nanoparticles with constant hydrophobicity and tunable crystallinity, <i>Macromolecules</i> 2020 , <i>13</i> , 5208–5217.							
Author	1	2	3	4	5	6	7	8
Conceptual development	×							
Kinetic studies and interpretation	×							
Polymer syntheses and structural characterization	×							
DSC and TGA studies	×							
WAXS analysis				×				
Nanoparticle preparations	×							
Fluorescence measurements		×						
DLS measurements	×							
AFM analysis			×					
Preparation of the manuscript	×							
Correction of the manuscript		×	×	×	×	×	×	×
Supervision of J. B. Max						×		
Supervision of D. Bandelli					×			×
Supervision of I. Muljajew					×			×
Supervision of K. Scheuer							×	
Proposed publication equivalent	1.0							

Documentation of authorship

Pub5 Damiano Bandelli,^{1†} Julien Alex,^{2†} Christian Helbing,³ Nico Ueberschaar,⁴ Helmar Görls,⁵ Peter Bellstedt,⁶ Christine Weber,⁷ Klaus D. Jandt,⁸ Ulrich S. Schubert,⁹ Poly(3-ethylglycolide): A well-defined polyester matching the hydrophilic hydrophobic balance of PLA, *Polym. Chem.* **2019**, *10*, 5440–5451

Author	1	2	3	4	5	6	7	8	9
Conceptual development	×						×		
Kinetic studies	×	×							
Polymer synthesis and characterization	×	×							
GC measurements				×					
X-Ray analyses					×				
Decoupling NMR measurements						×			
TGA and DSC analyses	×	×							
Nanoparticle preparation and DLS		×							
SEM measurements			×						
Preparation of the manuscript	×	×							
Correction of the manuscript							×	×	×
Supervision of J. Alex	×						×		
Supervision of D. Bandelli							×		×
Proposed publication equivalent	1.0								

Documentation of authorship

Author	1	2	3	4	5	6
Pub6 Michael Dirauf, ^{1†} Damiano Bandelli, ² Christine Weber, ³ Helmar Görls, ⁴ Michael Gottschaldt, ⁵ Ulrich S. Schubert, ⁶ TBD-Catalyzed Ring-Opening Polymerization of Alkyl-Substituted Morpholine-2,5-Dione Derivatives, <i>Macromol. Rapid Commun.</i> 2018 , <i>39</i> , 1800433.						
Conceptual development			×		×	
Monomer syntheses and analyses	×					
X-Ray analyses				×		
Kinetic studies	×					
MALDI analyses	×					
Preparation of the manuscript	×					
Correction of the manuscript			×		×	×
Supervision of M. Dirauf		×	×			×
Supervision of D. Bandelli			×			×
Proposed publication equivalent		0.5				

Documentation of authorship

Pub7 Karl Scheuer,^{1†} Damiano Bandelli,² Christian Helbing,³ Christine Weber,⁴ Julien Alex,⁵ Johannes B. Max,⁶ Alexis Hocken,⁷ Ondrej Stranik,⁸ Lisa Seiler,⁹ Frederike Gladigau,¹⁰ Ute Neugebauer,¹¹ Felix H. Schacher,¹² Ulrich S. Schubert,¹³ and Klaus D. Jandt,¹⁴ Self-assembly of copolyesters into stereocomplex crystallites tunes the properties of polyester nanoparticles, *Macromolecules* **2020**, *53*, 8340–8351.

Author	1	2	3	4	5	6	7	8	9	10	11	12	13	14
Conceptual development	×	×		×										
Bulk stereocomplex preparation		×			×									
DSC analyses					×									
DLS studies on stereocomplexation	×													
Quenching experiments	×													
DLS and AFM on stereocomplex NPs	×		×				×							
WAXS analysis						×								
Raman spectroscopy								×	×	×	×			
Preparation of the manuscript	×													
Correction of the manuscript		×	×	×	×	×	×	×	×	×	×	×	×	×
Supervision of D. Bandelli				×			×							
Proposed publication equivalent		0.5												

Dokumentation der Autorenschaft

Dieser Abschnitt enthält eine Auflistung der einzelnen Beiträge zu den in dieser Arbeit abgedruckten Publikationen.

†Leitender Autor

Damiano Bandelli, ^{1†} Julien Alex, ² Christine Weber, ³ Ulrich S. Schubert, ⁴ Polyester				
Pub1	stereocomplexes beyond PLA: Could synthetic opportunities revolutionize established material blending? <i>Macromol. Rapid Commun.</i> 2019 , <i>41</i> , 1900560.			
Autoren	1	2	3	4
Konzeptionelle Entwicklung	×		×	
Erstellen des Manuskripts	×	×		
Korrektur des Manuskripts			×	×
Aufsicht über J. Alex	×		×	
Aufsicht über D. Bandelli			×	×
Vorgeschlagenes Veröffentlichungsäquivalent	0.5			

Damiano Bandelli, ^{1†} Christine Weber, ² Ulrich S. Schubert, ³ Strontium isopropoxide: A			
Pub2	highly active catalyst for the ROP of lactide and various lactones. <i>Macromol. Rapid Commun.</i> 2019 , <i>40</i> , 1900306.		
Autoren	1	2	3
Konzeptionelle Entwicklung		×	×
Testreaktionen	×		
Kinetische Studien und Interpretation	×		
MALDI-Analysen und Interpretation	×		
Erstellen des Manuskripts	×		
Korrektur des Manuskripts		×	×
Aufsicht über D. Bandelli		×	×
Vorgeschlagenes Veröffentlichungsäquivalent	1.0		

Documentation of authorship

Pub3 Damiano Bandelli,^{1†} Christian Helbing,^{2†} Christine Weber,³ Michael Seifert,⁴ Irina Muljajew,⁵ Klaus D. Jandt,⁶ Ulrich S. Schubert,⁷ Maintaining the hydrophilic–hydrophobic balance of polyesters with adjustable crystallinity for tailor–made nanoparticles, *Macromolecules* **2018**, *51*, 5567–5576.

Autoren	1	2	3	4	5	6	7
Konzeptionelle Entwicklung	×	×	×				
Kinetische Studien und Interpretation	×						
Polymersynthesen und strukturelle Charakterisierung	×						
DSC– und TGA–Studien	×						
PLM– und AFM–Studien		×		×			
Nanopartikelpräparation	×						
DLS–Messungen	×				×		
Erstellen des Manuskripts	×	×	×				
Korrektur des Manuskripts			×	×	×	×	×
Aufsicht über D. Bandelli			×				×
Aufsicht über C. Helbing						×	
Aufsicht über I. Muljajew					×		×
Vorgeschlagenes Veröffentlichungsäquivalent	1.0						

Documentation of authorship

Damiano Bandelli, ^{1†} Irina Muljajew, ² Karl Scheuer, ³ Johannes B. Max, ⁴ Christine Weber, ⁵ Felix H. Schacher, ⁶ Klaus D. Jandt, ⁷ Ulrich S. Schubert, ⁸ Copolymerization of caprolactone isomers to obtain nanoparticles with constant hydrophobicity and tunable crystallinity, <i>Macromolecules</i> 2020 , <i>13</i> , 5208–5217.								
Pub4	1	2	3	4	5	6	7	8
Autoren								
Konzeptionelle Entwicklung	×				×			
Kinetische Studien und Interpretation	×							
Polymersynthesen und strukturelle Charakterisierung	×							
DSC– und TGA–Studien	×							
WAXS–Analyse				×				
Nanopartikelpräparation	×							
Fluoreszenzmessungen		×						
DLS–Messungen	×							
AFM–Analyse			×					
Erstellen des Manuskripts	×							
Korrektur des Manuskripts		×	×	×	×	×	×	×
Aufsicht über J. B. Max						×		
Aufsicht über D. Bandelli					×			×
Aufsicht über I. Muljajew					×			×
Aufsicht über K. Scheuer							×	
Vorgeschlagenes Veröffentlichungsäquivalent	1.0							

Documentation of authorship

Pub5 Damiano Bandelli,^{1†} Julien Alex,^{2†} Christian Helbing,³ Nico Ueberschaar,⁴ Helmar Görls,⁵ Peter Bellstedt,⁶ Christine Weber,⁷ Klaus D. Jandt,⁸ Ulrich S. Schubert,⁹ Poly(3-ethylglycolide): A well-defined polyester matching the hydrophilic hydrophobic balance of PLA, *Polym. Chem.* **2019**, *10*, 5440–5451

Autoren	1	2	3	4	5	6	7	8	9
Konzeptionelle Entwicklung	×						×		
Kinetische Studien	×	×							
Polymersynthesen und Charakterisierung	×	×							
GC-Messungen				×					
Röntgenkristallstrukturanalyse					×				
Spezielle NMR-Messungen						×			
DSC- und TGA-Studien	×	×							
Nanopartikelpräparation und DLS-Messungen		×							
SEM-Messungen			×						
Erstellen des Manuskripts	×	×							
Korrektur des Manuskripts							×	×	×
Aufsicht über J. Alex	×						×		
Aufsicht über D. Bandelli							×		×
Vorgeschlagenes Veröffentlichungsäquivalent	1.0								

Documentation of authorship

Pub6 Michael Dirauf, ^{1†} Damiano Bandelli, ² Christine Weber, ³ Helmar Görls, ⁴ Michael Gottschaldt, ⁵ Ulrich S. Schubert, ⁶ TBD-Catalyzed Ring-Opening Polymerization of Alkyl-Substituted Morpholine-2,5-Dione Derivatives, <i>Macromol. Rapid Commun.</i> 2018 , <i>39</i> , 1800433.						
Autoren	1	2	3	4	5	6
Konzeptionelle Entwicklung			×		×	
Monomersynthesen und –analysen	×					
Röntgenkristallstrukturanalyse				×		
Kinetische Studien	×					
MALDI-Analyse	×					
Erstellen des Manuskripts	×					
Korrektur des Manuskripts			×		×	×
Aufsicht über M. Dirauf		×	×			×
Aufsicht über D. Bandelli			×			×
Vorgeschlagenes Veröffentlichungsäquivalent		0.5				

Documentation of authorship

Pub7 Karl Scheuer,^{1†} Damiano Bandelli,² Christian Helbing,³ Christine Weber,⁴ Julien Alex,⁵ Johannes B. Max,⁶ Alexis Hocken,⁷ Ondrej Stranik,⁸ Lisa Seiler,⁹ Frederike Gladigau,¹⁰ Ute Neugebauer,¹¹ Felix H. Schacher,¹² Ulrich S. Schubert,¹³ and Klaus D. Jandt,¹⁴ Self-assembly of copolyesters into stereocomplex crystallites tunes the properties of polyester nanoparticles, *Macromolecules* **2020**, *53*, 8340–8351.

Author	1	2	3	4	5	6	7	8	9	10	11	12	13	14
Konzeptionelle Entwicklung	×	×		×										
Stereokomplex-Präparation im Bulk		×			×									
DSC-Analyse					×									
DLS-Studien zur Stereokomplexierung	×													
Zeitabhängige Stereokomplexierung	×													
DLS und AFM derder stereokomplexierten NP	×		×				×							
WAXS-Analyse						×								
Raman-Spektroskopie								×	×	×	×			
Erstellen des Manuskripts	×													
Korrektur des Manuskripts		×	×	×	×	×	×	×	×	×	×	×	×	×
Aufsicht über D. Bandelli				×			×							
Vorgeschlagenes Veröffentlichungsäquivalent		0.5												

Erklärung zu den Eigenanteilen des Promovenden/der Promovendin sowie der weiteren Doktoranden/Doktorandinnen als Koautoren an den Publikationen und Zweitpublikationsrechten bei einer kumulativen Dissertation

Für alle in dieser kumulativen Dissertation verwendeten Manuskripte liegen die notwendigen Genehmigungen der Verlage („Reprint permissions“) für die Zweitpublikation vor.

Die Co-Autoren der in dieser kumulativen Dissertation verwendeten Manuskripte sind sowohl über die Nutzung, als auch über die oben angegebenen Eigenanteile informiert und stimmen dem zu.

Die Anteile der Co-Autoren an den Publikationen sind in diesem Kapitel aufgeführt (Documentation of authorship).

Ich bin mit der Abfassung der Dissertation als publikationsbasiert, d.h. kumulativ, einverstanden und bestätige die vorstehenden Angaben. Eine entsprechend begründete Befürwortung mit Angabe des wissenschaftlichen Anteils des Doktoranden/der Doktorandin an den verwendeten Publikationen werde ich parallel an den Rat der Fakultät der Chemisch-Geowissenschaftlichen Fakultät richten.

Damiano Bandelli

Datum

Ort

Unterschrift

Prof. Dr. Ulrich S. Schubert

Datum

Ort

Unterschrift

Selbständigkeitserklärung

Ich erkläre, dass ich die vorliegende Arbeit selbständig und unter Verwendung der angegebenen Hilfsmittel, persönlichen Mitteilungen und Quellen angefertigt habe.

Ort, Datum

Unterschrift der Verfasserin/des Verfassers

1. Introduction

The development in polymer chemistry has enabled a vast landscape of applications from packaging to nanomedicine. In this regard, polyesters represent a promising class of polymeric materials not only exhibiting degradability,¹ but also featuring biocompatibility.²⁻⁴ Due to these facts, polyesters are commercially available and are mostly based on poly(lactic acid) (PLA), poly(lactic-co-glycolic acid) (PLGA) and poly ϵ -caprolactone (P ϵ CL). Their industrial production rely on the ring opening polymerization (ROP) of glycolides and lactones (**Figure 1.1**).⁵⁻⁶ Representing cyclic diesters of α -hydroxy acids, glycolides can be prepared from biomolecules such as glycolic and lactic acid.⁷⁻⁸ In addition, lactones represent a class of monomers obtained from natural resources and can be found in nature, *e.g.* in fruit and milk derivatives.^{6,9} The ROP of such monomers enables the preparation of well-defined polyesters that are commonly employed for the preparation of packaging materials,¹⁰ biomedical goods as well as nanoparticles.¹¹⁻¹² Such materials can be degraded, resulting in the starting material for the synthesis of new polyesters.³

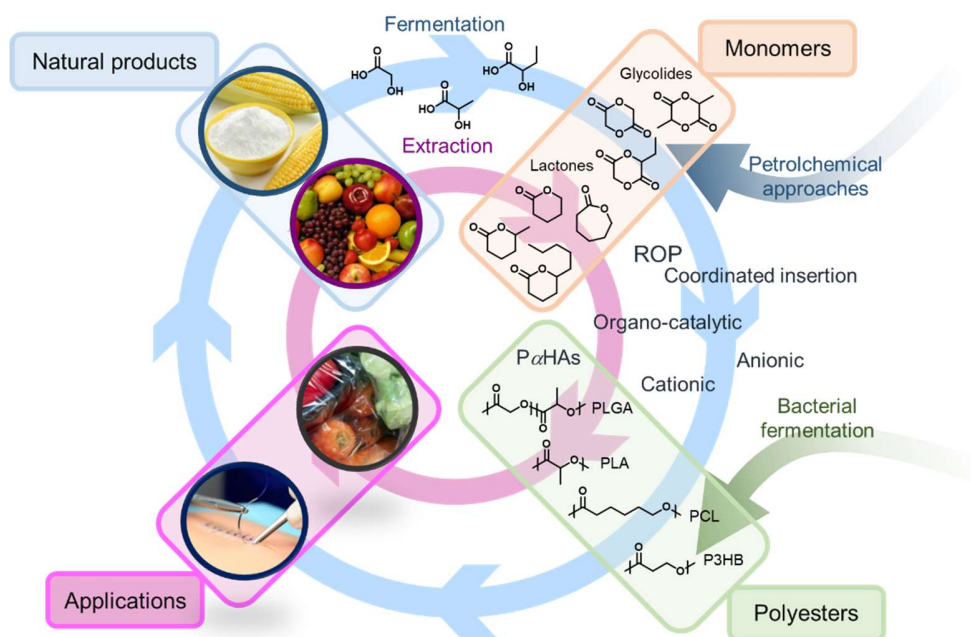


Figure 1.1. From synthesis to degradation of polyester materials.

1. Introduction

Nowadays, the development of polyester nanoparticles for drug delivery applications represent a central topic due to the modularity of size, morphology and properties.¹³⁻¹⁵

Representing the most common route toward polyester synthesis, the ROP allows functionalization, enabling the decoration of the target polyesters with stealth polymers, biologically active labels and fluorescence markers. They may be introduced as polymerization initiators, but also post polymerization modification can be used for functionalization, however representing an additional step to be considered in the polyester design.

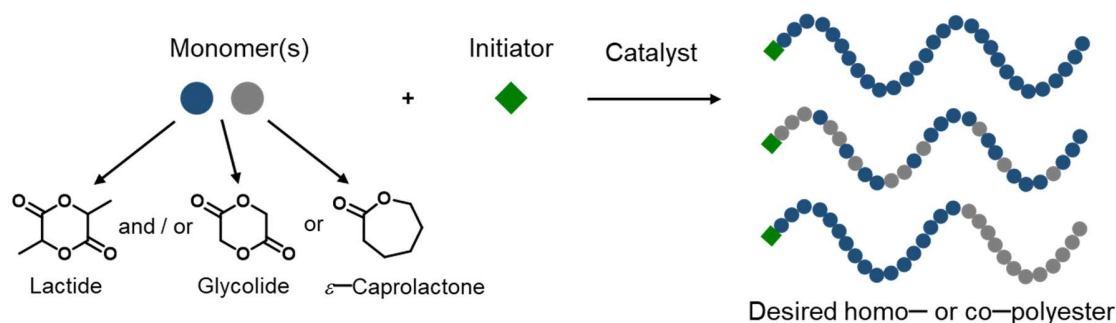


Figure 1.2. The synthetic approach toward well-defined polyesters.

In addition, also the formulation of stable nanoparticle dispersions represents a central aspect, enabling the encapsulation of drugs,^{11, 16} and it is usually performed employing stabilizers in order to avoid nanoparticle aggregation.¹⁷

The final application of such systems for drug delivery is based on the efficiency in the drug release which is usually dependent on the degradation of the polyester chain.

Despite the interest in polyesters as starting materials for the preparation of highly potent carrier materials to be used in medicine, the list of polyesters on the market is restricted to the classical PLA, PLGA and P ϵ CL, with a limited range of thermal and mechanical properties. In order to tune such properties, with the aim to enhance the performances of the final material, the preparation of new polyesters is a current necessity in polyester research.

1. Introduction

In this regard, the polymer design plays a key role for the preparation of high performing polymeric species. In fact, a vast landscape of variables, such as molar masses, thermal properties, crystallinities and hydrophilicities, represents a complex multidimensional parameter space that should be carefully evaluated and altered. Nowadays, new polymers for drug delivery applications have to meet complex requirements including targeted functionalization reactions. However, the change of one property often goes along with the variation of another one, such as *e.g.* a thermal property, the crystallinity or the polymer hydrophobicity. Already a careful polymer design could come in hand, allowing to keep one or more parameters, *e.g.* molar mass, hydrophobicity, unaltered while changing the target properties.

The scope of this thesis is to define how polyester design can be tuned in order to access libraries of materials that feature a constant hydrophilic hydrophobic balance (HHB) and similar molar masses, with a selective variation of thermal and mechanical properties of bulk materials as well as nanoparticles. Representing the method of choice for the preparation of the polyesters employed in this thesis, **Chapter 2** contains an overview of the preparation and the ROP of glycolides as well as lactones and introduces the concept of stereocomplexes. As such ROP require catalysts, **Chapter 3** introduces the common catalysts and highlights the development of the novel, non-toxic catalyst strontium isopropoxide.

Two polymeric libraries mimicking the HHB of P ϵ CL and PLA are reported in **Chapters 4 to 6**, representing a central research area within the CRC 1278 (“PolyTarget”), financed by the German Research Foundation (DFG) and entitled “Controlling the degradation behavior of polymeric nanoparticles by structurally tailored thermal properties” (Project A06). Synthetic approaches rely on i) the copolymerization of two monomers with different in HHB in a tailored ratio, ii) the copolymerization of caprolactone isomers, iii) the development of a new constitutional isomer for lactide and its (co)polymerization, and iv) the formation of stereocomplexes from stereo-defined

1. Introduction

PLA and PLA-based copolymers. The strategic concept is further verified by determination of the HHB, as well as thermal and mechanical properties of the according polyester nanoparticles.

.

2. Challenges in polyester synthesis: From polycondensation to ROP

Parts of this chapter have been published: **Pub1**) Damiano Bandelli, Julien Alex, Christine Weber, Ulrich S. Schubert, “Polyester stereocomplexes beyond PLA: Could synthetic opportunities revolutionize established material blending?”, *Macromol. Rapid Commun.* **2019**, *41*, 1900560.

Representing an extremely versatile polymeric class employed for a wide range of commercial applications, from packaging materials to biomedical materials, polyesters such as polylactic acid (PLA), poly(lactic-*co*-glycolic acid) (PLGA) and polycaprolactone (P ϵ CL) are commercially available.

Nowadays their industrial synthesis relies on the ring opening polymerization (ROP) of selected monomers such as lactide (LA), glycolide and ϵ -caprolactone (ϵ CL). However, the first development for the oligomerization and polymerization of an α -hydroxy acid such as glycolic and lactic acid was reported from Carothers at the beginning of the 20th century *via* polycondensation reactions.¹⁸ The basic concept behind polycondensation is based on the reactivity of functional groups such as carboxylic acid and alcohol moieties. Representing AB monomers bearing both carboxyl and hydroxyl functionalities, α -hydroxy acids, and in particular lactic acid, have been extensively employed for polycondensation often yielding oligomers (**Figure 2.1**).¹⁹⁻²⁰ In this regard various approaches can be employed in order to increase the molar mass of the resulting polyester. However, high temperatures and low pressures are often required in order to obtain high molar mass poly(α -hydroxy acids).¹⁹

Similarly to lactic acid, also other α -hydroxy acids such as 2-hydroxybutyric acid and 2-hydroxy-3-methylbutyric acid oligomerize *via* polycondensation processes. In contrast to α -hydroxy acids, β -hydroxy acids are scarcely employed in polycondensation reactions. In fact, their polycondensation has only been successfully reported for a derivative of malic acid, albeit with comparably low molar mass and high dispersity.²¹

2. Challenges in polyester synthesis: From polycondensation to ROP

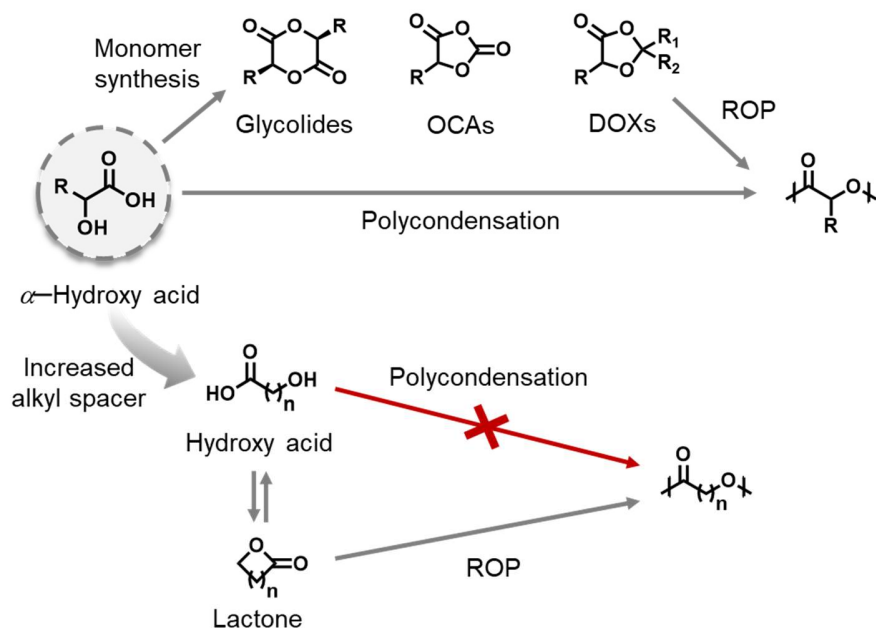


Figure 2.1. Polycondensation and ROP of selected monomers for the preparation of polyesters from hydroxy acids.

In contrast, the ROP requires the use of heterocycles as monomers, making the synthesis of hydroxy acid derivatives a central aspect.²² Based on α -hydroxy acids, glycolides represent the common choice as monomers.⁵ In addition, also *O*-carboxyanhydrides (OCAs) and dioxolanones (DOXs) can be employed for the same purpose.²³⁻²⁵

The ROP of such monomers enables an improved control of molar masses and dispersity in comparison to polycondensation, also enabling the tuning of the stereochemistry of the final polyesters. Besides, it enables further extension of the polyester library from derivatives of β -, γ -, δ -, ϵ - as well as ω -hydroxy acids that are commonly found as lactones.

Representing the monomer of choice for industrial polyester production and academic research, glycolides are usually obtained *via* prepolymer backbiting, direct cyclization and acylation/cyclization (**Figure 2.2**).⁸ Prepolymer backbiting as well as direct cyclization enable the preparation of symmetric glycolides bearing the same substituents in position 3 and 6 of the

2. Challenges in polyester synthesis: From polycondensation to ROP

dioxanedione ring (**Figure 2.2**). The prepolymer backbiting is industrially employed for the preparation of glycolide and lactide, and it has been reported for the preparation of a large series of glycolides bearing alkyl,²⁶⁻²⁹ alkynyl,³⁰ PEGylated³¹ and aromatic substituents (**Figure 2.2**).³²⁻³⁴

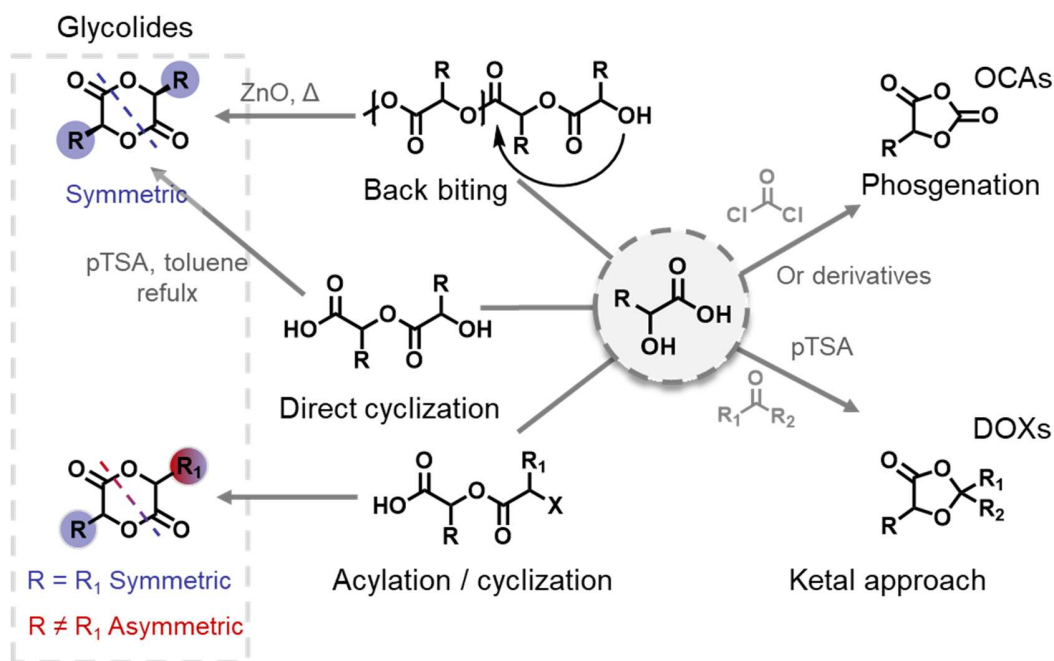


Figure 2.2. Synthetic approaches towards the preparation of monomers for the synthesis of poly(α -hydroxy acids) *via* ROP.

In contrast, the acylation/cyclization pathway is usually employed for the preparation of asymmetric glycolides. This approach is based on a two-step reaction of an acyl bromide derivative with a hydroxy acid. Subsequent to the acylation reaction, a cyclization is conducted in order to access the desired glycolide bearing alkyl,^{26-27, 35} alkynyl,³⁶ halogenated,³⁷ PEGylated,³⁸ azide³⁶ and aromatic^{35, 38-40} moieties. The same approach has been used for the preparation of morpholinediones (see **Chapter 5**).⁴¹

2. Challenges in polyester synthesis: From polycondensation to ROP

The ROP of glycolides often results in polymers with predictable molar masses and low dispersities. For this purpose, a plethora of catalysts and initiators has been developed (see **Chapter 3**).

Representing cyclic esters, also lactones can be employed for the preparation of polyesters *via* ROP approaches. Among them, only ϵ -caprolactone (ϵ CL) is employed in industry and it is produced *via* the Baeyer–Villiger oxidation of cyclohexanone.⁴² In addition, a series of δ -lactones can be synthesized or even can be directly found in nature, *e.g.* derived from fruits or milk.⁴³⁻⁴⁶ The polymerization of such heterocycles can be performed according to ROP pathways. However, in contrast to glycolides, the polymerization of lactones is prone to the influence of the ring size and the presence of substituents.⁴⁷⁻⁴⁸ In order to overcome the different polymerizability of lactones, the development of novel catalysts allowing to enable the polymerization is a central aspect of the polymer design and is further discussed in **Chapter 3**.

The ROP of glycolides as well as lactones allow the preparation of homo and copolyesters with predictable molar masses and moderate dispersities. Moreover, starting from a chiral monomer, the retention of stereochemistry enables access to stereo-defined polymers. Mostly isotactic PLA is obtained through polymerization of L- or D-lactide, respectively. In contrast, atactic chains result from polymerization of racemic lactide.⁴⁹ The variation in stereoregularity is often connected with a variation of thermal and mechanical polymer properties.⁵⁰ Additionally, the thermal and mechanical properties of stereoregular polyesters such as PLA can be further modified through stereocomplexation. The latter represents a specific blending process in which polymer chains of different configuration interact forming new crystallite domains due to stereoselective association (**Figure 2.3**).⁵⁰⁻⁵¹

2. Challenges in polyester synthesis: From polycondensation to ROP

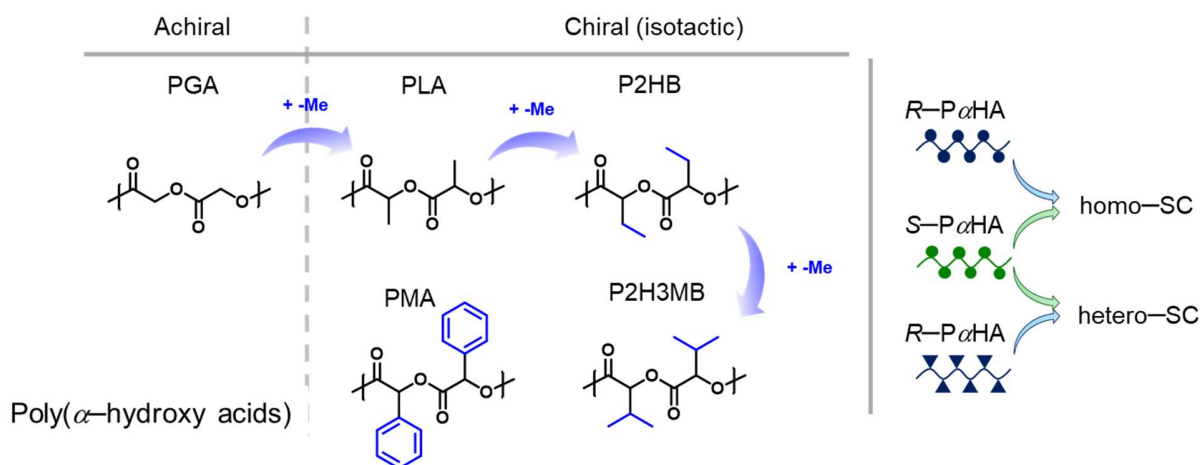


Figure 2.3. Schematic representation of the achiral and chiral poly(α -hydroxy acids) potentially suited for stereocomplexation and kind of stereocomplexes: Poly(glycolic acid) (PGA), poly(2-hydroxybutanoic acid) (P2HB), poly(2-hydroxy-3-methylbutanoic acid) (P2H3MB) and poly(mandelic acid) (PMA).

For polyesters, the blending of of L- and D- configured isotactic chains in equimolar concentration, also referred to as stereocomplex (SC), results in the increase of the melting temperature and the formation of new domains with increased crystallinity. Dynamic scanning calorimetry (DSC) and X-ray diffraction represent common methods to verify stereocomplexation.⁵⁰ In addition, polarized light microscopy, atomic force microscopy and nuclear magnetic resonance studies are useful to provide further insights, either with respect to mechanical properties or on a structural level.⁵⁰⁻⁵¹ Besides PLA, also other polyesters such as poly(2-hydroxybutanoic acid) (P2HB) and poly(2-hydroxy-3-methylbutanoic acid) (P2H3MB) are suited for stereocomplexation.⁵²⁻⁵³ In addition to blending of polyester chains of the same nature (Homo-SC, e.g. PLLA/ PDLA), the range of poly(α -hydroxy acids) capable of SC formation enables additional variation of properties through blending of different types of polyester chains with opposite configuration (Hetero-SC).

2. Challenges in polyester synthesis: From polycondensation to ROP

Despite the high interest in the variation of properties through stereocomplexation, SC are mostly prepared from homopolymers. In this regard, the use of block or statistical copolymers could increase the range of applicable materials. Already a small variation in the structure of the standard PLA could serve this purpose, as is introduced in **Chapter 6** of this thesis.

3. ROP of lactide and various lactones catalyzed by Strontium isopropoxide

Parts of this chapter have been published: **Pub2)** Damiano Bandelli, Christine Weber, Ulrich S. Schubert, “Strontium isopropoxide: A highly active catalyst for the ROP of lactide and various lactones”, *Macromol. Rapid Commun.* **2019**, *40*, 1900306.

Polyesters such as PLA, PLGA and P ϵ CL represent biodegradable and biocompatible materials often employed for biomedical applications. Their industrial synthesis is often achieved by means of ROP employing tin octanoate (Sn(Oct)₂) as catalyst. Besides, a vast series of metal complexes and organic catalysts has been developed enabling a fine tuning of molar masses, dispersity, end-group fidelity and stereochemistry.^{49, 54-55} Among metal catalysts, aluminum based complexes often represent the catalyst of choice in academia.⁵⁵ In this category, the studies on the aluminum isopropoxide catalyzed ROP of glycolides and lactones enabled the discovery of the coordination insertion mechanism.⁵⁶⁻⁵⁷ Since then other metal alkoxides, *e.g.* based on tin,⁵⁸ titanium,⁵⁹ lanthanum,⁶⁰ have been developed and used.

In addition, also organic compounds, often used as ligands in the metal complex design, can catalyze the ROP of cyclic esters.⁴⁹ Already pyridine and 4-dimethylaminopyridine (DMAP) can be used for this purpose. Besides, cyclic amidines, cyclic guanidines,⁶¹ thioureas, phosphazenes and *N*-heterocyclic carbenes represent highly active organo-catalysts for the ROP of lactide and lactones (**Figure 3.1**).⁶²

3. ROP of lactide and various lactones catalyzed by Strontium isopropoxide

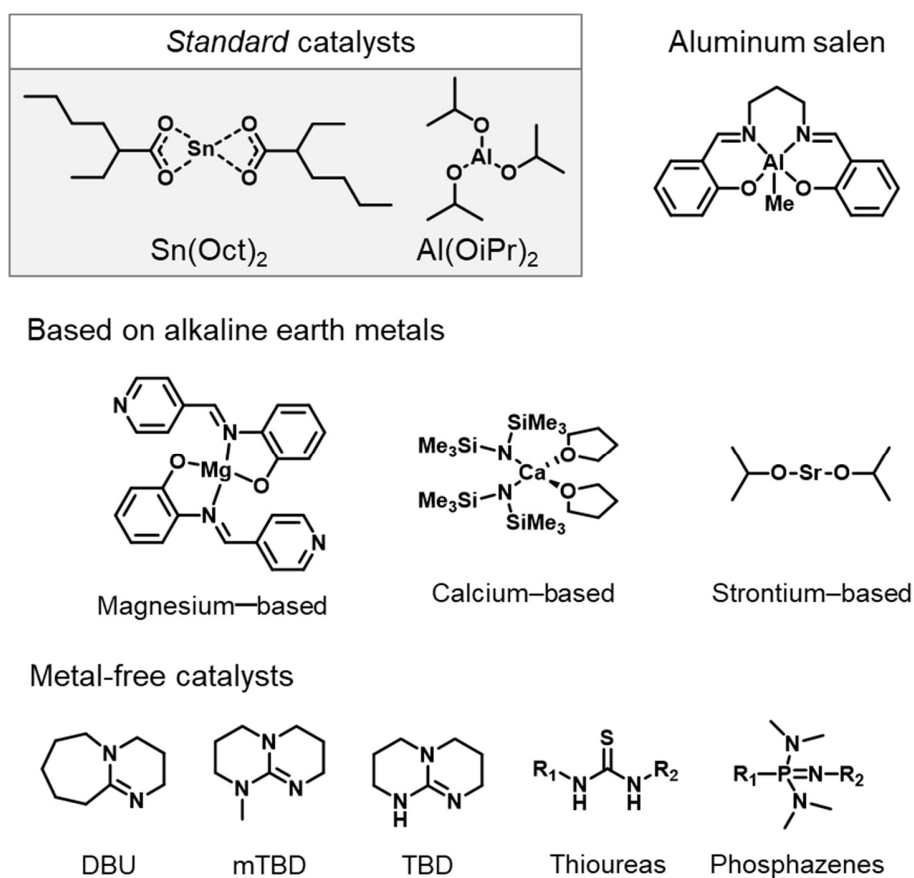


Figure 3.1. Schematic representation of metal based and metal-free catalyst employed for the ROP of glycolides and lactones.

The large variety of catalysts developed are often used for the ROP of lactide, ϵ -caprolactone (ϵCL) and δ -valerolactone (δVL) that represent the standard monomers. However a variation in the chemical structure of the monomer is accompanied by a variation of polymerizability, making the catalyst design a central aspect.⁴⁸ Already the standard $\text{Sn}(\text{Oct})_2$ is able to promote the polymerization of substituted glycolides in bulk or in solution.⁶³ However, temperatures above 100 °C are often required. Due to this fact, the polymerization of substituted lactones, e.g. δ -caprolactone and δ -decalactone, is often accomplished using organic catalysts.^{48, 64}

3. ROP of lactide and various lactones catalyzed by Strontium isopropoxide

Since polyesters find application in biomedical fields, also the toxicity of the catalyst represents a central point to be taken into account. In fact, only low traces of heavy metals are tolerated by the Food and Drug Administration (FDA) for food packaging and sutures. However, if biomedical applications are intended, the replacement of toxic compounds with suitable alternatives is required. Among the vast series of metal complexes and organic catalysts able to replace $\text{Sn}(\text{Oct})_2$, alkaline–earth complexes seen previously also feature biocompatibility.⁶⁵⁻⁶⁶ Among them, strontium salts represent well–known active agents for bone remineralization and can prevent osteoporosis.⁶⁷

Avoiding a delicate ligand design, the commercially available strontium isopropoxide ($\text{Sr}(\text{OiPr})_2$) served for the purpose of polymerizing L–lactide (LLA) (**Figure 3.2**). Already test reactions revealed its high activity at room temperature in toluene employing a lactide to catalyst ratio up to 200. Moreover, the addition of dodecanol (DodOH) as co–initiator resulted in high conversions but lower molar masses.

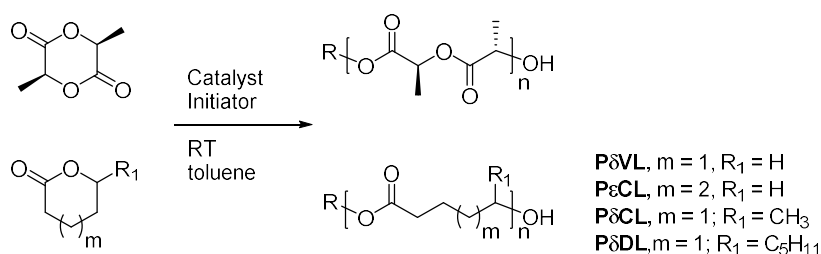


Figure 3.2. Schematic representation of the ROP of glycolides and lactones.

Kinetic studies were performed employing a [LLA] to $[\text{Sr}(\text{OiPr})_2]$ ratio of 100 with or without dodecanol as co–initiator. The linear evolution of molar masses over conversion confirmed a good reaction control, moreover moderate to low dispersity values were seen over the course of the polymerization (**Figure 3.3**). Besides, the comparison of the theoretically expected and experimental molar masses were in excellent agreement with the molar masses determined by SEC,

3. ROP of lactide and various lactones catalyzed by Strontium isopropoxide

thereby confirming that i) both isopropanolate moieties of the catalyst are active during polymerization, and ii) the molar mass of the PLA could be tailored by the polymerization time as well as by the amount of alcohol to serve as additional initiating species.

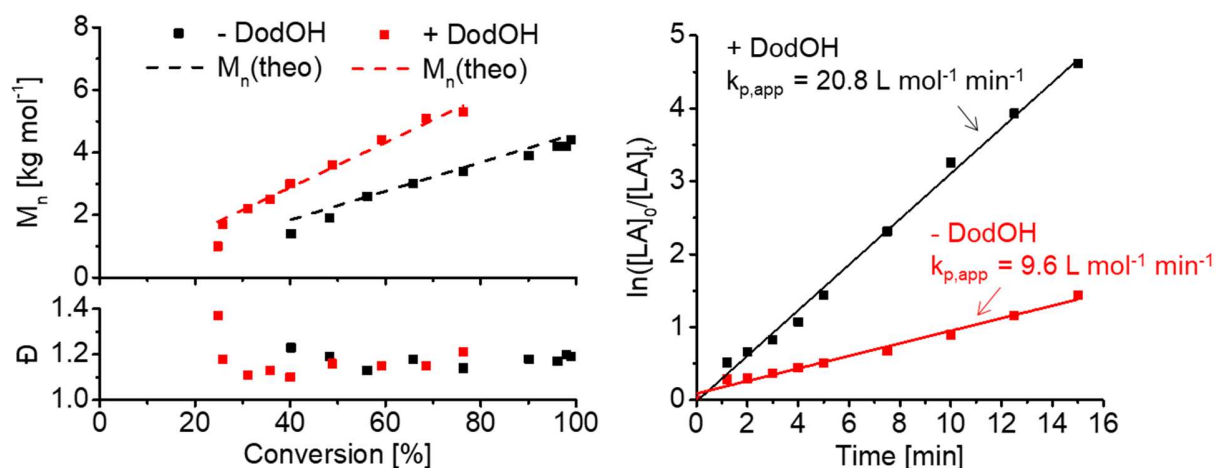


Figure 3.3. Kinetic plots for the $\text{Sr}(\text{OiPr})_2$ catalyzed ROP of LLA at room temperature in toluene employing a $[\text{LLA}]:[\text{Sr}(\text{OiPr})_2]$ of 100:1 with or without one equivalent of dodecanol in comparison with Sr. **Left.** Molar mass and dispersity evolution over conversion (dots) and $M_{n,\text{theo}}$ (dotted lines) according to $M_{n,\text{theo}} = M(\text{LLA}) \times [\text{LLA}]_0/[\text{I}]_0 \times \text{conversion}$ assuming the initiation from all isopropanolate and DodOH moieties ($[\text{I}]_0 = 2[\text{Sr}(\text{OiPr})_2]_0 + [\text{DodOH}]_0$). **Right.** First-order kinetic plots of the ROP of LA with a linear fit according to $\ln([\text{LLA}]_0/[\text{LLA}]_t) = k_{p,\text{app}} \times [\text{I}]_0 \times t$.

MALDI–ToF–MS revealed an increase of molar masses over reaction time (**Figure 3.4**), also showing discrimination effects at high monomer conversion, making this technique unsuitable for the calculation of molar masses. However, a zoom into the most intense region of each spectrum revealed that both isopropyl and dodecyl α -functionalized PLA chains were produced from the reaction with dodecanol. A typical spacing between two neighbouring peaks ($\Delta m/z = 72$) corresponded to single lactoate repeating units.⁶⁸ In contrast to most reports, cyclic species were not observed in any mass spectra, hinting towards the fact that the m/z difference might be caused

3. ROP of lactide and various lactones catalyzed by Strontium isopropoxide

by the catalytic mechanism rather than by chain transfer reactions. This was confirmed by the MALDI–ToF mass spectrum of a purified PLA sample with lower molar mass. Although the ROP was driven to high conversion, cyclic species were still not found in the spectrum.

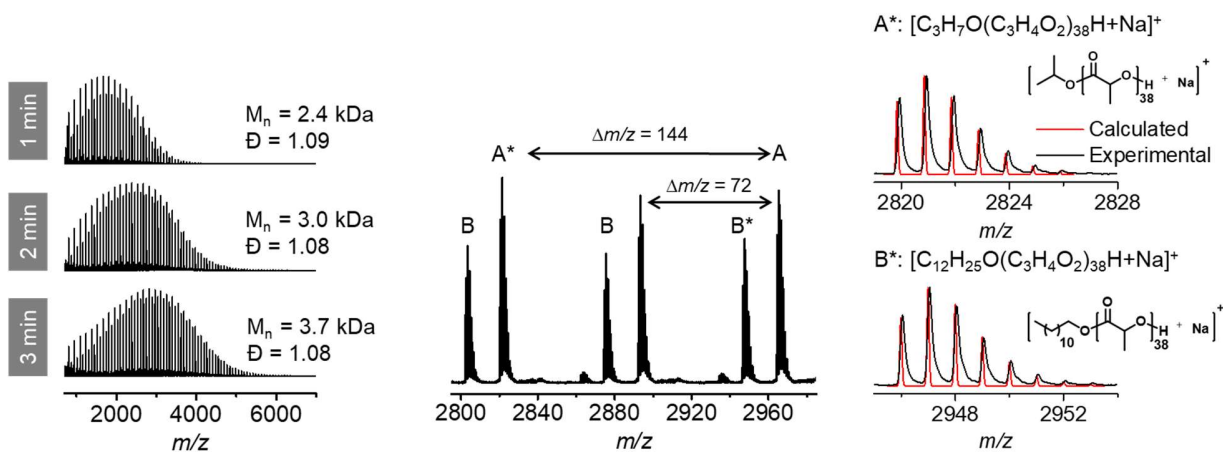


Figure 3.4. MALDI–ToF–MS analysis of the $Sr(OiPr)_2$ catalyzed ROP of LLA employing a $[LLA]:[Sr]:[DodOH] = 100:1:1$. **Left.** Overlay of mass spectra after 1, 2 and 3 minutes reaction time. **Centre.** Zoom–in in the most abundant region of the sample collected after a reaction time of 2 minutes and peak assignments. **Right.** Overlay of the experimental and calculated isotopic patterns of the peaks indicated by an asterix.

Due to the high reactivity of the catalyst for the polymerization of lactide, the same experimental settings were used for the ROP of a series of ϵ - and δ -lactones employing a monomer to catalyst ratio of 100. Representing the most common lactones, ϵ CL and δ VL were firstly selected. Their homopolymerization resulted in quantitative conversions after a reaction time of 1 minute. Due to the high reactivity, multimodal SEC elugrams with dispersity values above 3.8 were obtained, suggesting that transesterifications play a role during their polymerization. In contrast, a methyl substituted δ VL such as δ CL, could be easily polymerized in presence of dodecanol, resulting in moderate dispersity of 1.16 after a reaction time of 15 minutes. The same held true for the

3. ROP of lactide and various lactones catalyzed by Strontium isopropoxide

polymerization of the pentyl substituted δ VL, δ DL. The polymerization of such monomers was furthermore evaluated *via* kinetic studies.

SEC analyses revealed bimodal molar mass distributions for samples taken at the beginning of the ROP, which transformed to unimodal signals during the course of the ROP. The dispersity decreased to values below 1.2 for monomer conversions above 50%, ruling out commonly observed transesterification processes as reason for this unusual polymerization behavior. Moreover, as reported for the polymerization of other lactones, the first order kinetic plot for irreversible polymerizations revealed a non-linear behavior as results of equilibrium processes during polymerization.

In summary, the strontium isopropoxide-catalyzed ROP of several monomers resulted in a fast polymerization already at room temperature. The synthesis of the industrially relevant PLA from LLA revealed a good molar mass control, low dispersity and excellent end-group fidelity, making strontium isopropoxide a suitable alternative to toxic catalyst tin octanoate that is currently applied in industry. Strontium isopropoxide also enabled a fast and controlled polymerization of the substituted δ CL and δ DL, *i.e.* two monomers featuring great potential for future medical applications. Although largely disregarded in the current literature, they enable significant alteration of thermal and mechanical properties, as will be discussed in the following chapters.

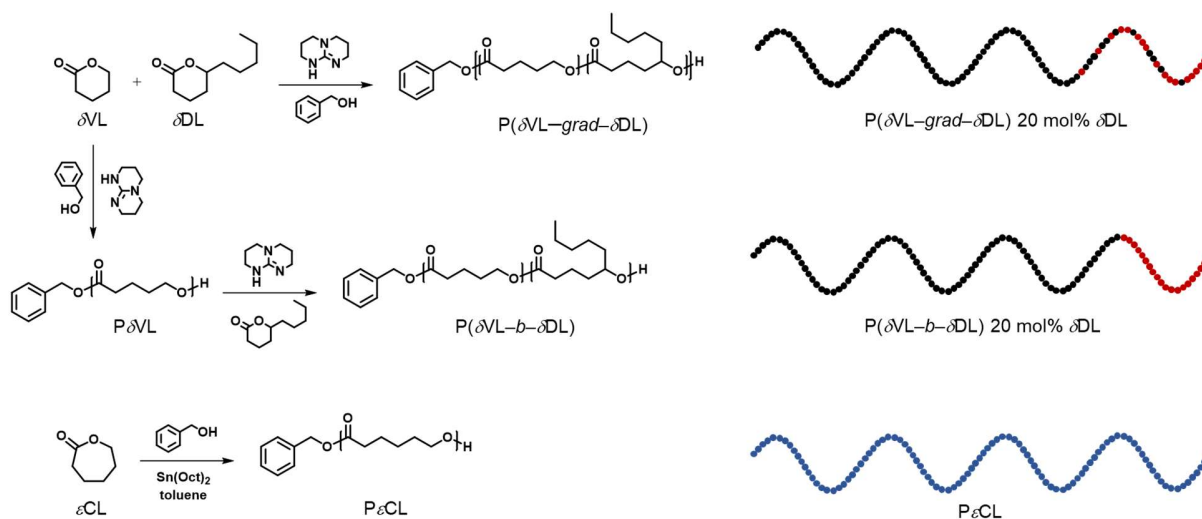
4. Tailor-made block and gradient copolymers matching the HHB of P ϵ CL

Parts of this chapter have been published: **Pub3**) Damiano Bandelli, Christian Helbing, Christine Weber, Michael Seifert, Irina Muljajew, Klaus D. Jandt, Ulrich S. Schubert, “Maintaining the hydrophilic–hydrophobic balance of polyesters with adjustable crystallinity for tailor-made nanoparticles”, *Macromolecules* **2018**, *51*, 5567–5576.

Poly(ϵ -caprolactone) (P ϵ CL) represents one of the most investigated polyesters in academia due to its biocompatibility and biodegradability and it is commercialized (*e.g.* Resomer®). Its relatively low melting temperature (T_m) around 60 °C suggests its employment in drug delivery applications.⁶⁹ However, a slow degradation *via* hydrolysis is often observed due to the high degree of crystallinity.⁷⁰ In this regard, the copolymerization with a selected comonomer can result in the decrease of the degree of crystallinity, affecting the drug release.⁷¹⁻⁷² However, if the application as nanoparticle drug carrier is intended, the choice of a suitable comonomer represents a central aspect in order to vary or maintain parameters such as molar mass, thermal properties, degree of crystallinity and hydrophilic–hydrophobic balance (HHB).

In order to unravel the structure–property relationship, the selective variation of a single feature should be achieved keeping constant the other features. For this purpose, the copolymerization of the two δ -lactones, δ -valerolactone (δ VL) and δ -decanolactone (δ DL) was approached in order to keep the overall P ϵ CL hydrophobicity while varying the degree of crystallinity of the polyester material (**Scheme 4.1**). For this goal, a final copolymer composition comprising 20 mol% of δ DL was targeted in order to access block and gradient copolymers keeping the overall HHB constant.

4. Tailor-made block and gradient copolymers matching the HHB of P ϵ CL



Scheme 4.1. Schematic representation of the chemical structure of the ROP of δ -valerolactone (δ VL), δ -decanolactone (δ DL) and ϵ -caprolactone (ϵ CL) yielding copolyesters featuring the same hydrophobicity.

Kinetic studies on the homopolymerization of both δ VL and δ DL represented the first step toward copolymerization and were performed at room temperature in bulk employing TBD as catalyst and benzyl alcohol (BnOH) as initiator with a $[M]_0:[I]_0$ of 100:1. The polymerization of both lactones featured a good control of molar masses and moderate dispersity, also revealing the higher reactivity of the unsubstituted δ VL in line with literature reports.⁷³⁻⁷⁵ As a consequence, two well-defined homopolymers P δ VL (**P2**) and P δ DL (**P3**) were synthesized featuring a similar degree of polymerization.

With respect to the synthesis of well-defined block copolymers comprising both δ VL and δ DL units, a short P δ VL sample was synthesized ($[\delta$ VL] $_0:[I]_0$ of 20:1, **P1**, **Table 4.1**) and analyzed by means of MALDI-ToF-MS. The isotopic patterns were assigned to P δ VL functionalized with a benzyl group in α -position and a hydroxyl group in ω -position, while no cyclic or water-initiated

4. Tailor-made block and gradient copolymers matching the HHB of P ϵ CL

species were detected. As a result, the excellent end-group fidelity of the ROP enabled the preparation of a P δ VL sample that was used as macroinitiator for the preparation of block copolymers comprising δ VL as well as δ DL units. The block copolymerization was performed in bulk at room temperature and the reaction times were set on the basis of the homopolymerization kinetics. SEC analysis on the initial P δ VL and the P δ VL-*b*-P δ DL (**P4**) revealed the shift to higher molar mass. Additionally, ^1H NMR analysis confirmed the successful copolymerization and enabled the calculation of the δ DL mole fraction of 20 mol% that was the target composition in order to mimic the HHB of P ϵ CL.

Table 4.1: Selected structural characterization data of the synthesized (co)polymers.

Sample	Polymer	Feed [mol%] δ VL/ δ DL	Conv. ¹ [%] δ VL/ δ DL	Theo. ² [mol%] δ VL/ δ DL	NMR ³ [mol%] δ VL/ δ DL	M_n [kg mol ⁻¹] NMR ³	M_n [kg mol ⁻¹] SEC ⁴	\mathcal{D} SEC ⁴
P1 ⁵	P δ VL	100 / 0	98 / -	100 / 0	100 / 0	2.7	3.8	1.47
P2	P δ VL	100 / 0	93 / -	100 / 0	100 / 0	9	9	1.33
P3	P δ DL	0 / 100	- / 84	0 / 100	0 / 100	14	14	1.55
P4	P δ VL- <i>b</i> -P δ DL	n.a.	70 / 17	80 / 20	82 / 18	11	11	1.35
P5	P(δ VL- <i>grad</i> - δ DL)	75 / 25	98 / 82	78 / 22	80 / 20	11	11	1.66
P6	P ϵ CL	n.a.	99 (ϵ CL)	n.a.	n.a.	9	9	1.30

¹ Conversion determined by integration of suitable signals in the ^1H NMR spectra of the reaction solution.

² Calculated from feed ratio and the individual monomer conversions.

³ Composition determined by integration of suitable signals in the ^1H NMR spectra of the purified polymers.

⁴ Eluent CHCl_3 , RI detection, PMMA calibration.

⁵ MALDI-ToF-MS (DCTB + NaI): $M_n = 2.8 \text{ kg mol}^{-1}$, $\mathcal{D} = 1.14$.

Additionally, the statistical copolymerization of the two δ -lactones was investigated in detail *via* a kinetic study in order to achieve the target δ DL fraction of 20 mol% and to determine the copolymer

4. Tailor-made block and gradient copolymers matching the HHB of P ϵ CL

microstructure. In line with homopolymerization data, δ VL was incorporated faster compared to δ DL during the statistical copolymerization, while the increase of the molar mass during polymerization hinted toward the formation of a copolymer with a strong gradient. Based on the kinetic study, a gradient copolymer with the desired composition and similar molar mass as **P4** was prepared (**P5**).

The set of copolymers **P4** and **P5** was complemented with a P ϵ CL sample (**P6**) with similar molar mass that was hence used as reference for further characterization. Considering the application of the polyesters **P4** to **P6**, the bulk properties were investigated by means of differential scanning calorimetry (DSC). Such analysis revealed that the block copolymer **P4** featured a similar melting point as the P ϵ CL **P6** (**Figure 4.1**). The comparison with the DSC analysis conducted on **P2** and **P3** revealed that the melting point of **P4** could be ascribed to the semicrystalline P δ VL block. However, the degree of crystallinity calculated from the enthalpy of melting was lower for **P4** compared to for **P6**.⁷⁶ Both melting point and degree of crystallinity of the gradient copolyester **P5** were different from **P6**. In conclusion, the (co)polyester design enabled the selective variation of the sole degree of crystallinity in comparison with the well-known P ϵ CL.

4. Tailor-made block and gradient copolymers matching the HHB of P ϵ CL

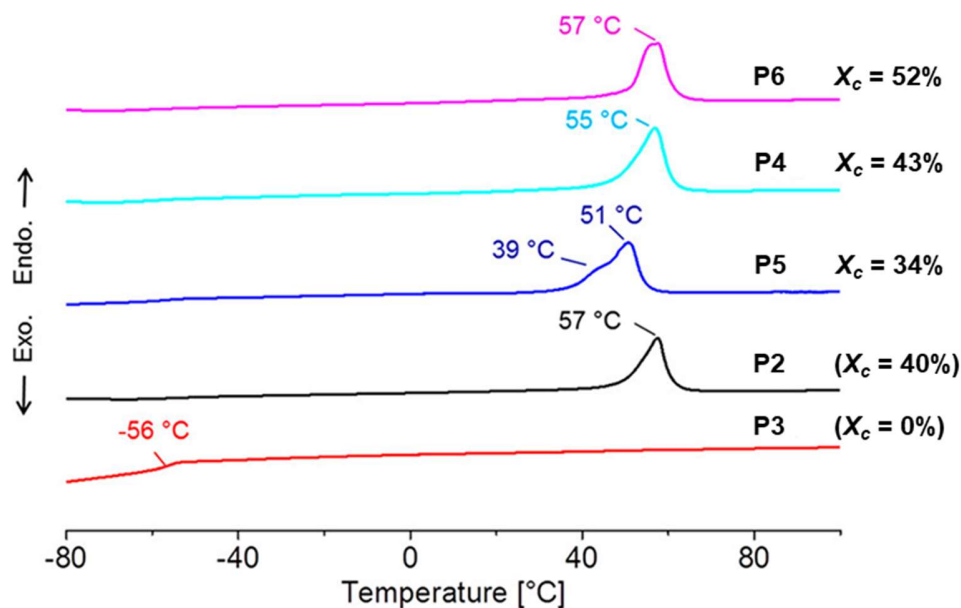


Figure 4.1. DSC thermograms of the polyesters **P4** to **P6** with constant HHB and the P δ VL and P δ DL homopolymers **P2** and **P3**. The melting temperature is indicated next to the melting peaks, while the degree of crystallinity X_c is listed on the right. The measurements were performed from -100 to 200 °C (second heating run, heating rate 20 K min^{-1}).

Representing the next step toward applications, polyester nanoparticles were produced from the polyesters **P4** to **P6** *via* nanoprecipitation. Stable nanoparticle suspensions were prepared featuring a similar hydrodynamic diameter of 170 nm from dynamic light scattering (DLS) measurements (**Figure 4.2**). Additionally, atomic force microscopy (AFM) measurements were employed to assess nanoparticle stiffness, which correlated with the bulk crystallinity.

4. Tailor-made block and gradient copolymers matching the HHB of P ϵ CL

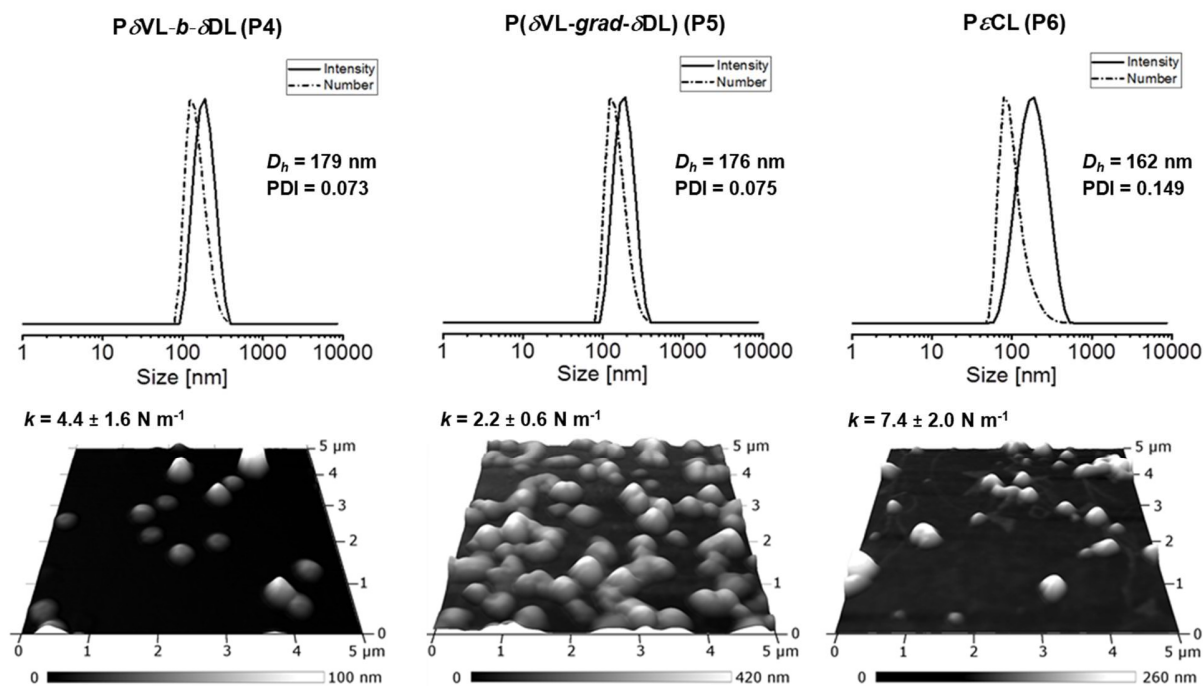


Figure 4.2. DLS size distribution plots of the nanoparticle suspensions (upper part) prepared by nanoprecipitation of **P4** to **P6** and 3D AFM-height images of dried nanoparticles (lower part).

The copolymerization of the two lactones, δ VL and δ DL, proved to be a useful tool to prepare polyesters featuring similar molar masses, but varying thermal properties. However, the use of both δ VL and δ DL only enabled to access a small library of copolymers matching the HHB of P ϵ CL. Aiming to correlate the bulk polyester properties to the degradation and release behavior of loaded polyester nanoparticles featuring the same HHB, a larger polymer library was required, as will be described in the next chapter.

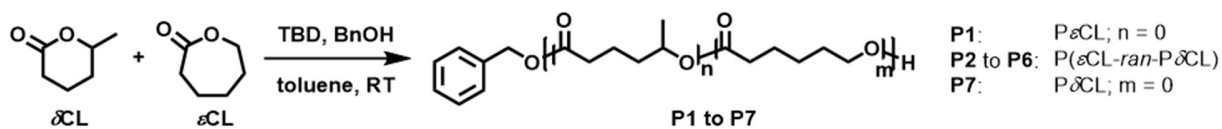
5. Statistical copolyesters of ϵ - and δ -caprolactone

Parts of this chapter have been published: **Pub4**) Damiano Bandelli, Irina Muljajew, Karl Scheuer, Johannes B. Max, Christine Weber, Felix H. Schacher, Klaus D. Jandt, Ulrich S. Schubert, “Copolymerization of caprolactone isomers to obtain nanoparticles with constant hydrophobicity and tunable crystallinity”, *Macromolecules* **2020**, *13*, 5208–5217.

Synthetic approaches toward the preparation of polyesters with a similar hydrophobicity represent a central aspect of this thesis. As reported in **Chapter 4**, the ROP of selected monomers enables the preparation of tailor-made copolyesters reaching a target monomer composition. However, the necessity to focus on a target composition resulted in a small polyester library. In order to overcome this disadvantage, the copolymerization of the two structural isomers ϵ -caprolactone (ϵ CL) and δ -caprolactone (δ CL) was approached.

In order to access a library of polycaprolactones with varying ϵ CL and δ CL composition, a preliminary evaluation of the polymerizability of both monomers was performed at room temperature in toluene employing TBD as catalyst and BnOH as initiator (**Scheme 5.1**). Despite representing isomeric species, an extensive kinetic evaluation revealed that the δ CL was not able to polymerize at low catalyst loading, as proven by SEC and ^1H NMR analysis. In contrast, ϵ CL polymerized efficiently already with low amount of TBD, in line with data reported in literature.⁶¹

5. Statistical copolyesters of ϵ - and δ -caprolactone



Scheme 5.1. Schematic representation of the chemical structure of the ROP of δ -caprolactone (δCL) and ϵ -caprolactone (ϵCL) yielding copolyesters featuring the same hydrophobicity.

Kinetic analysis on the ring opening copolymerization of both monomers were performed on five monomer feed ratios ($[\epsilon\text{CL}]_0$ to $[\delta\text{CL}]_0$) between 80:20 and 50:50, but keeping the initial overall monomer concentration to 4 mol L^{-1} and a monomer to catalyst to initiator ratio of 100:2:1. For all copolymerizations studied, a linear increase of the molar masses (from SEC analysis) over monomer conversion ($^1\text{H NMR}$) was detected, proving a good molar mass control during the polymerization process. The first order kinetic plots for all copolymerizations revealed a linear behavior for both lactones. However, the increase of the δCL fraction in the feed resulted in a decrease of the apparent polymerization constant for ϵCL ($k_{p,\text{app}}(\epsilon\text{CL})$), while $k_{p,\text{app}}(\delta\text{CL})$ increased. However, no variation of the copolymer composition was detected for the feed ratios investigated, suggesting the formation of random copolymers. In order to verify that, the kinetic data were used for the calculation of reactivity ratios according to Mayo–Lewis, Meyer–Lowry as well as Beckingham–Sanoja–Lynd (BSL) kinetic models.⁷⁷⁻⁸⁰ The application of Mayo–Lewis method pointed toward to a stronger tendency of both monomers toward homopropagation ($r_{\epsilon\text{CL}} = 3.1$ and $r_{\delta\text{CL}} = 7.1$). However, the overall conversions of around 18% were relatively high for this classical method. Based on the resolution of the kinetic equation for the statistical copolymerization of two monomers, assuming an irreversible polymerization, the Meyer–Lowry approach enabled the use of each kinetic analysis for the determination of the reactivity ratios. An almost constant reactivity ratio of 0.50 was found for δCL for all copolymerization reactions. In contrast, the reactivity ratio calculated for ϵCL slightly changed throughout the series of kinetic studies but consistently

5. Statistical copolyesters of ϵ - and δ -caprolactone

remained below 1. In this regard, the method reported by Beckingham *et al.* (BSL method) was applied to the kinetic datapoints. Similar to Meyer–Lowry, the BSL method hinted toward the presence of a random copolymerization of ϵ CL and δ CL. The resulting calculated reactivity ratios were used to depict a model representation of the copolyesters based on conditional probabilities followed by the calculation of the average block length of both ϵ CL and δ CL segments estimated from the reactivity ratios.⁸¹⁻⁸³

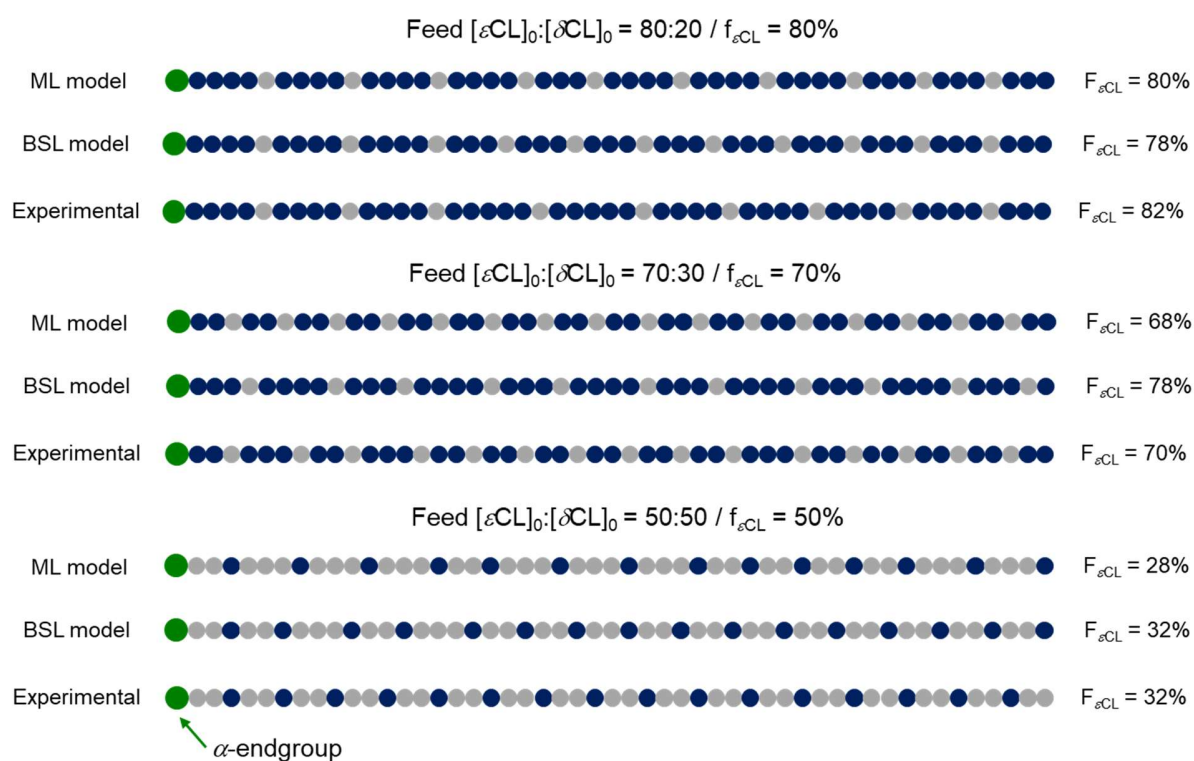


Figure 5.1. Representation of the microstructures obtained from experimental data and probability calculations based on the Meyer–Lowry (ML) and Beckingham (BSL) models for a DP value of 50 employing an initial $[\epsilon\text{CL}]_0:[\delta\text{CL}]_0$ ratio of 80:20, 70:30, and 50:50. The benzyl α -end group is depicted in green, the ϵ CL and δ CL units are depicted in blue and gray, respectively.

5. Statistical copolyesters of ϵ - and δ -caprolactone

The evaluation of the microstructures obtained from conditional probabilities was done employing the “experimental” microstructures that were based on the experimental data obtained during the kinetic analysis (**Figure 5.1**). Irrespective of the initial feed ratios, both BSL as well as ML models gave similar results as the experimental evaluation, hinting toward a random order.

A library of copolyesters was hence synthesized P(ϵ CL-*ran*- δ CL) **P8** to **P12** on the basis of both homopolymerization and copolymerization kinetic data. In addition, the homopolymers P ϵ CL (**P7**) and P δ CL (**P13**) were prepared (**Table 5.1**).

Table 5.1. Selected structural characterization data of the synthesized (co)polyesters.

Sample	Polymer	ϵ CL / δ CL				NMR		SEC ⁴	
		Feed [mol%]	Conversion ¹ [%]	Theor. ² [mol%]	NMR ³ [mol%]	$M_{n,theo}$ ² [kg mol ⁻¹]	$M_{n,NMR}$ ³ [kg mol ⁻¹]	$M_{n,SEC}$ [kg mol ⁻¹]	\bar{D}
P7 ⁵	P ϵ CL	100 / 0	47 / 0	100 / 0	100 / 0	11	13	19	1.17
P8 ⁶	P(ϵ CL- <i>ran</i> - δ CL)	80 / 20	89 / 62	85 / 15	87 / 13	9	13	21	1.57
P9 ⁶	P(ϵ CL- <i>ran</i> - δ CL)	75 / 25	81 / 63	79 / 21	81 / 19	9	10	19	1.41
P10 ⁶	P(ϵ CL- <i>ran</i> - δ CL)	70 / 30	75 / 62	74 / 26	75 / 25	8	10	19	1.30
P11 ⁶	P(ϵ CL- <i>ran</i> - δ CL)	60 / 40	64 / 64	59 / 41	61 / 39	7	9	16	1.26
P12 ⁶	P(ϵ CL- <i>ran</i> - δ CL)	50 / 50	51 / 67	43 / 57	45 / 55	7	7	15	1.21
P13 ⁷	P δ CL	0 / 100	0 / 44	0 / 100	0 / 100	10	9	6	1.09

¹ Determined by the integration of monomer and polymer signals from the ¹H NMR spectra of the reaction solution between 4 and 5 ppm.

² Calculated from the single monomer conversions and the feed ratio.

³ Determined by the integration of suitable signals from the ¹H NMR spectra of the purified polyesters.

⁴ Eluent CHCl₃, RI detection, PS calibration.

⁵ [ϵ CL]₀: [BnOH]₀: [TBD]₀ = 200:1:1; [ϵ CL]₀ = 2 mol L⁻¹

⁶ [CL]₀: [BnOH]₀: [TBD]₀ = 100:1:2; [CL]₀ = 4 mol L⁻¹

⁷ [δ CL]₀: [BnOH]₀: [TBD]₀ = 200:1:4; [δ CL]₀ = 4 mol L⁻¹

5. Statistical copolyesters of ϵ - and δ -caprolactone

The library of polycaprolactones with similar molar masses but varied ϵ CL content was investigated with respect to bulk properties in view of further applications (*e.g.* in the biomedical field). In this instance, DSC analysis revealed that only the copolyesters **P7** to **P10** showed a melting event, while cold crystallization was not detected during the first, as well as the second and the third heating run (first and second heating at 20 °C min⁻¹ and third heating at 10 °C min⁻¹). During the cooling run performed at 20 °C min⁻¹ a crystallization event was recorded for the copolyesters **P7** to **P9**. Additionally, the melting temperature (T_m) as well as the crystallization temperature (T_c) linearly decreased with ϵ CL fraction (**Figure 5.2**). WAXS analysis were performed in order to access the degree of crystallinity (X_c) of the copolyester series. Similar to the trend depicted for T_m and T_c , the X_c decreased linearly for the samples **P7** to **P12**. With a ϵ CL composition of 45 mol%, **P12** represented the only amorphous sample. In fact, **P13**, the homopolymer from δ CL, revealed three distinctive reflexes at 2θ of 18.4, 20.0, and 21.3 and a degree of crystallinity of 8%.

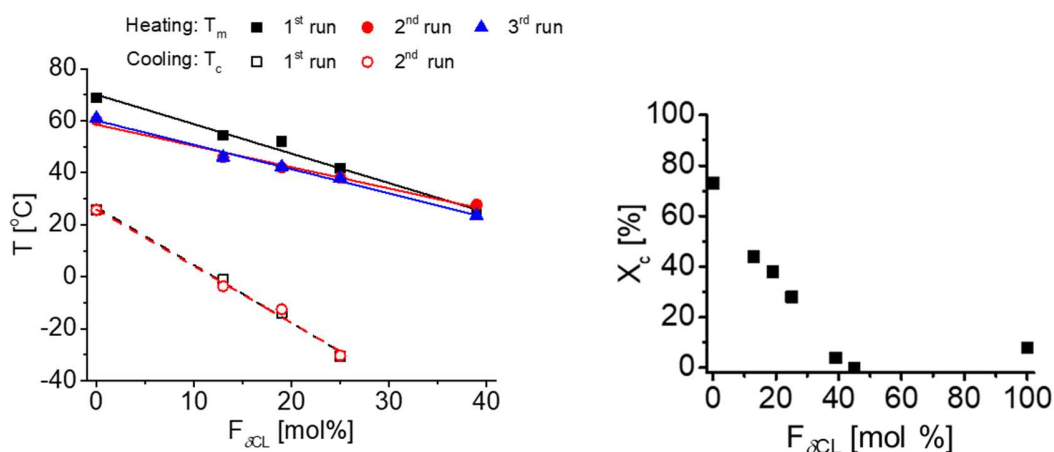


Figure 5.2. Left: Dependence of the melting temperature (T_m) and the crystallization temperature (T_c) on the fraction of δ CL in the copolymer ($F_{\delta CL}$). **Right:** Dependence of the degree of crystallinity (X_c) on the fraction of δ CL in the copolymer ($F_{\delta CL}$).

5. Statistical copolyesters of ϵ - and δ -caprolactone

The variation of both melting temperature and degree of crystallinity of the **P7** to **P13** series suggested their possible application for the preparation of stable nanoparticle suspensions for drug encapsulation. In this regard, a preliminary preparation of stable nanoparticle suspensions was achieved *via* nanoprecipitation employing the same protocol applied for the **P4** to **P6** series described in **Chapter 4**. DLS as well as AFM analysis performed on the final suspensions revealed the presence of nanoparticles with a hydrodynamic diameter between 115 and 138 nm and low to moderate dispersity. As final step for the material development, the evaluation of the nanoparticle HHB was a fundamental proof of concept for the validation of the synthetic efforts. For this purpose, a similar nanoprecipitation protocol was performed in order to prepare pyrene loaded nanoparticles from the two homopolymers **P7** and **P13** and the copolymer **P12**. DLS analysis performed on the three suspensions revealed the presence of nanoparticles with diameters between 120 and 160 nm and low to moderate dispersity ($0.084 < \text{PDI} < 0.103$). Fluorescence spectroscopy (FS, **Figure 5.3**) of the suspensions revealed a similar I_1 to I_3 ratio of 1.22 for all the suspensions. This last result indicated that the three nanoparticles featured similar hydrophobicity, since the fluorescence spectra of pyrene (in particular the ratio between the I_1 and I_3 bands) is related to the chemical and physical environment.

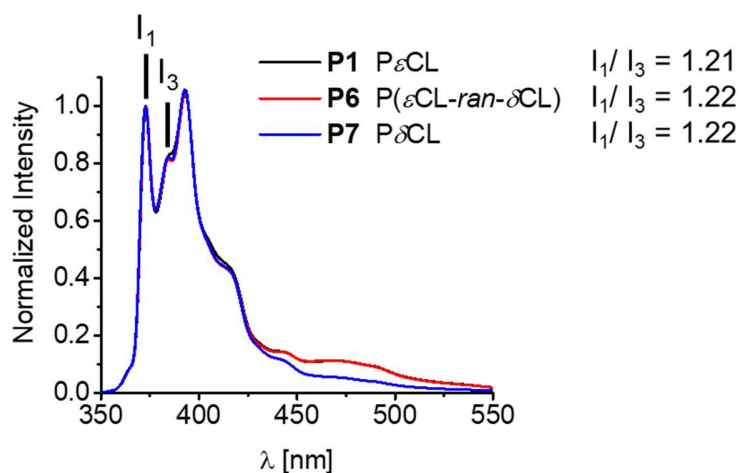


Figure 5.3. Normalized fluorescence spectra of pyrene loaded nanoparticles formed from **P7**, **P12**, and **P13** ($\lambda_{\text{ex}} = 339 \text{ nm}$, $\text{co}(\text{polymer}) = 5 \mu\text{g mL}^{-1}$, $\text{co}(\text{pyrene}) = 0.05 \mu\text{g mL}^{-1}$).

The copolymerization of the two caprolactone isomers, δCL and ϵCL , was performed and refined for the preparation of well-defined copolyesters with a random microstructure. The variation of composition in the series from **P7** to **P13** resulted in a varied bulk degree of crystallinity. In order to unambiguously prove the constant hydrophobicity of the nanoparticle suspensions, pyrene encapsulation was performed, resulting in nanoparticles with similar HHB.

Aiming to correlate the nanoparticle properties with the degradation features, the current research effort is based on the enzymatic degradation of model nanoparticles. Moreover, the encapsulation of pharmaceutical active ingredients as well as *in vitro* performance studies of anti-inflammatory drugs are currently under investigation.

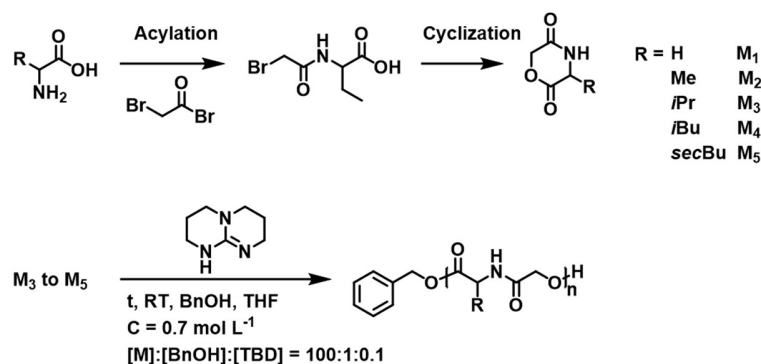
This chapter described the concept of copolymerization of caprolactone isomers to result in a library of homo- and random copolyesters with tunable thermal and mechanical properties and constant HHB. Aiming towards generalization and expansion of the concept, the development of a similar library of polyesters matching the HHB of PLA is described in the next chapter.

6. Designed monomers to modify PLA

Parts of this chapter have been published: **Pub5**) Damiano Bandelli, Julien Alex, Christian Helbing, Nico Ueberschaar, Helmar Görls, Peter Bellstedt, Christine Weber, Klaus D. Jandt, Ulrich S. Schubert, “Poly(3-ethylglycolide): A well-defined polyester matching the hydrophilic hydrophobic balance of PLA”, *Polym. Chem.* **2019**, *10*, 5440–5451. **Pub6**) Michael Dirauf, Damiano Bandelli, Christine Weber, Helmar Görls, Michael Gottschaldt, Ulrich S. Schubert, “TBD-Catalyzed ring-opening polymerization of alkyl-substituted morpholine-2,5-dione derivatives”, *Macromol. Rapid Commun.* **2018**, *39*, 1800433. **Pub7**) Karl Scheuer, Damiano Bandelli, Christian Helbing, Christine Weber, Julien Alex, Johannes B. Max, Alexis Hocken, Ondrej Stranik, Lisa Seiler, Frederike Gladigau, Ute Neugebauer, Felix H. Schacher, Ulrich S. Schubert, and Klaus D. Jandt, “Self-assembly of copolyesters into stereocomplex crystallites tunes the properties of polyester nanoparticles”, *Macromolecules* **2020**, *53*, 8340–8351.

In the previous chapters, the synthesis as well as the properties of well-defined polylactones featuring the same hydrophobicity as poly(ϵ -caprolactone) were introduced. In addition, polyesters from α -hydroxy acids represents another class of polymers used for medical goals.⁸⁴ As already described in **Chapter 2**, the ROP of selected monomers such as lactide and glycolide can be tuned in order to obtain the target material. Moreover, the change in monomer structure is often accompanied by the variation of macroscopic features such as thermal and mechanical properties, as well as the hydrophobicity of the resulting polymer. In order to obtain a series of materials varying properties of PLA but retaining its HHB, the acylation/cyclization pathway introduced in **Chapter 2** was applied for the preparation of 3-ethylglycolide (EtGly), an isomer of lactide. In addition, the acylation/cyclization pathway was adopted for the preparation of a series of morpholine-2,5-diones (**Scheme 6.1**) enabling access to polyesteramides.

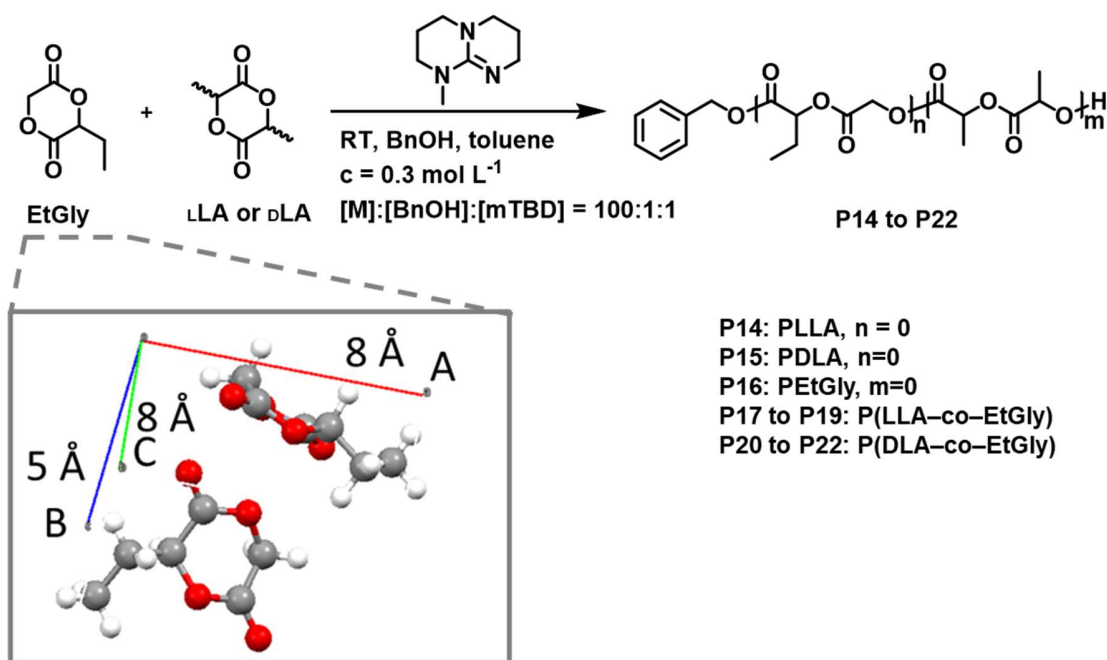
6. Designed monomers to modify PLA



Scheme 6.1. Schematic representation of the synthesis and ROP morpholine-2,5-diones from glycine (**M2**), alanine (**M3**), valine (**M4**), leucine (**M5**) and isoleucine (**M6**).

For the preparation of the monomers **M1** to **M5**, 2-bromoacetyl bromide was employed for the acylation of glycine, L-alanine, L-valine, L-leucine and L-isoleucine (**Scheme 6.1**). The resulting linear precursor was cyclized at high dilution in order to avoid oligomerization. The final products were purified and analyzed by means of NMR spectroscopy, ESI MS, crystal structure and elemental analysis. In line with literature data, the synthesis of **M1** to **M5** was accomplished with low to moderate yields between 22 and 34%.⁸⁵⁻⁸⁷ The polymerization of these monomers was successfully accomplished *via* the TBD-catalyzed ROP, resulting in a series of polydepsipeptides with varied hydrophobicity. Particular focus was given on detailed kinetic studies of the homopolymerization of the two isomers **M4** and **M5** featuring butyl substituents as well as the valine-based monomer **M3** in THF at RT. It was confirmed that the resulting polydepsipeptides featured controllable and uniform end groups if monomer conversions were kept below 50%, which will enable access to well-defined polydepsipeptide block copolymers.

6. Designed monomers to modify PLA



Scheme 6.2. Schematic representation of the chemical structure of 3-ethylglycolide (EtGly), its crystal structure and the ROP with L- or D-lactide yielding polyesters **P14** to **P22**.

The same acylation/cyclization pathway was employed for the preparation of EtGly from 2-bromoacetyl bromide and racemic 2-hydroxybutyric acid, as was confirmed by the same set of analysis methods as described above (**Scheme 6.2**). The ROP of EtGly was performed in direct comparison to that of L- as well as D-lactide (LLA and DLA, respectively) employing the organobase mTBD as catalyst, BnOH as initiator in toluene at room temperature with a $[M]_0:[BnOH]_0:[mTBD]_0$ ratio of 100:1.

Kinetic analysis of homopolymerization of EtGly, LLA and DLA revealed a good control of the molar masses in all the range of conversion investigated (**Figure 6.1**). Irrespective of the monomer used, a fast initiation was followed by a decrease of the apparent polymerization rate, indicated by the non-linear behavior of the first order kinetic plot. A similar process was reported for the polymerization of LLA catalyzed by the cyclic amidine DBU, suggesting that multiple polymerization pathways, *e.g.* nucleophilic and hydrogen bonding, can play a role during

6. Designed monomers to modify PLA

polymerization.⁸⁸ In all cases, MALDI-ToF-MS analysis revealed the presence of well-defined polyesters with a benzyl α - and a hydroxyl ω -end group.

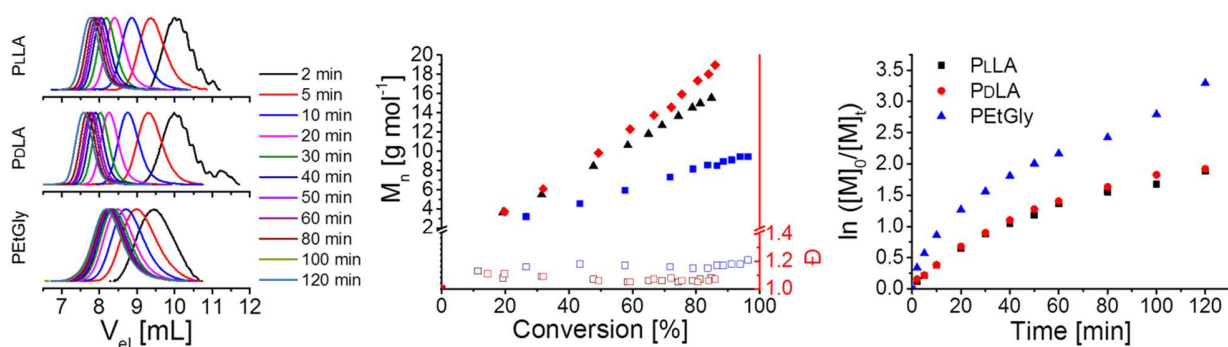


Figure 6.1. Kinetic plots for the mTBD catalyzed ROP of LLA, DLA and EtGly at room temperature in toluene employing a $[M]_0:[BnOH]_0:[mTBD]_0$ of 100:1:1. **Left.** SEC curves. **Middle.** Molar mass and dispersity evolution over conversion. **Right.** First-order kinetic plots.

Having established the synthesis and the polymerization of a set of tailor-made monomers, the isomers EtGly, LLA and DLA were selected for the preparation of polyesters featuring a constant hydrophobicity. The according homopolymers PLLA and PDLA represented isotactic materials as demonstrated by proton homonuclear decoupling experiments. In contrast, the polymer obtained from the racemic EtGly represented an atactic material. In order to access a library of copolyesters with similar molar masses but varied mechanical properties, the statistical copolymerization of L- or DLA with EtGly as comonomer was performed employing the same polymerization settings as for the homopolymerization, and utilizing an EtGly feed of 5, 10 and 20% at room temperature in toluene (**Table 6.1**).

6. Designed monomers to modify PLA

Table 6.1: Selected structural characterization data of the synthesized (co)polyesters.

Sample	Polymer	LA / EtGly			NMR		SEC ⁴	
		Feed [mol%]	Conversion [%] ¹	NMR ² [mol%]	M _{n, theo} ³ [kg mol ⁻¹]	M _{n, NMR} ² [kg mol ⁻¹]	M _{n, SEC} [kg mol ⁻¹]	D
P14	PLLA	100 / 0	85	100 / 0	12	11	16	1.06
P15	PDLA	100 / 0	85	100 / 0	12	12	19	1.06
P16	PEtGly	0 / 100	97	0 / 100	14	10	12	1.06
P17	P(EtGly- <i>stat</i> -LLA)	95 / 05	75	95 / 05	11	11	16	1.11
P18	P(EtGly- <i>stat</i> -LLA)	90 / 10	74	89 / 11	11	11	13	1.20
P19	P(EtGly- <i>stat</i> -LLA)	80 / 20	69	78 / 22	10	10	12	1.23
P20	P(EtGly- <i>stat</i> -DLA)	95 / 05	77	96 / 04	11	12	19	1.10
P21	P(EtGly- <i>stat</i> -DLA)	90 / 10	79	91 / 9	11	11	18	1.21
P22	P(EtGly- <i>stat</i> -DLA)	80 / 20	77	78 / 22	11	10	15	1.28

¹ Determined by the integration of monomer and polymer signals from the ¹H NMR spectra of the reaction solution between 4 and 5 ppm.

² Determined by the integration of suitable signals from the ¹H NMR spectra of the purified polyesters.

³ Calculated from the single monomer conversions and the feed ratio.

⁴ Eluent CHCl₃, RI detection, PS calibration.

Similarly to the library of PCLs (**Chapter 4 and 5**), the thermal properties of the homo- and copolyesters **P14** to **P22** were studied by means of DSC. Data revealed the decrease of the glass transition and the melting temperature with increasing amount of EtGly in the polyesters. Moreover, the degree of crystallinity calculated from the enthalpy of melting followed the same trend, revealing that the addition of small amounts of EtGly in the material ($\leq 20\%$) resulted in a strong variation of thermal properties (**Figure 6.2**)

6. Designed monomers to modify PLA

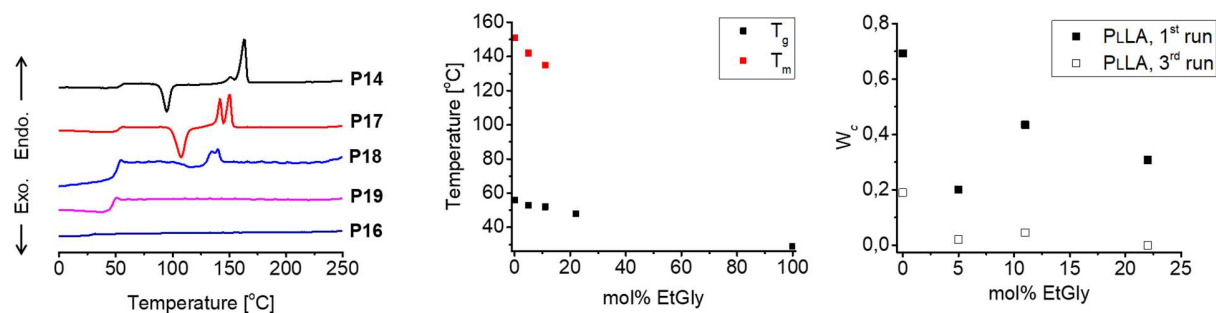


Figure 6.2. DSC analysis of the polyester library based on PLLA (**P14** and **P16** to **P19**). **Left:** DSC thermograms of the third heating run performed from -20 to 260 °C at a heating rate of 10 °C min^{-1} . **Middle:** Dependency of the melting and glass transition temperature on the molar fraction of EtGly during the third heating run. **Right:** Dependency of the degree of crystallinity on the molar fraction of EtGly during the first and the third heating run.

In order to further alter the material properties, the two isotactic PLAs (**P14** and **P15**) as well as the PLLA and PDLA-based copolyesters (**P17** to **P22**) were employed for the preparation of stereocomplexes *via* solution casting in tetrahydrofuran. The dried materials were characterized by means of DSC and WAXS analysis. The equimolar mixture of **P14** and **P15** resulted in the increase of melting temperature from 163 °C of the homocrystallites to 199 °C of the stereocomplex crystallites. A similar behavior was detected for the equimolar mixture of **P17** / **P20** containing 5% EtGly, **P18** / **P21** containing 10% EtGly, and **P19** / **P22** containing 20% EtGly. WAXS analysis further confirmed the stereocomplex formation showing the presence of the typical PLA stereocomplex reflex at a 2θ of 12 in the equimolar mixtures. An in-depth study of the stereocomplexation kinetics also enabled the preparation of stable nanoparticle suspensions that were furthermore analyzed *via* AFM as well as Raman spectroscopy, revealing the formation of stereocomplex nanoparticles with varied mechanical properties.

6. Designed monomers to modify PLA

As a proof of concept, pyrene containing nanoparticles were prepared from **P14** to **P16** following the same procedure as described in **Chapter 5**. The PLA-based nanoparticles featured a similar I_1 / I_3 ratio of 1.26 and, therefore, a similar hydrophobicity (**Figure 6.3**). The I_1 / I_3 ratio for the PLA nanoparticles was higher compared to the average value of the PCL-based nanoparticles of 1.22. Since the increase of the I_1 / I_3 ratio is related to an increase in the hydrophilicity of the system, the higher I_1 / I_3 ratio of the PLA nanoparticles suggested higher hydrophilicity, which is in line with the classical methods proposed by Davies and Griffith for the calculation of HHB.

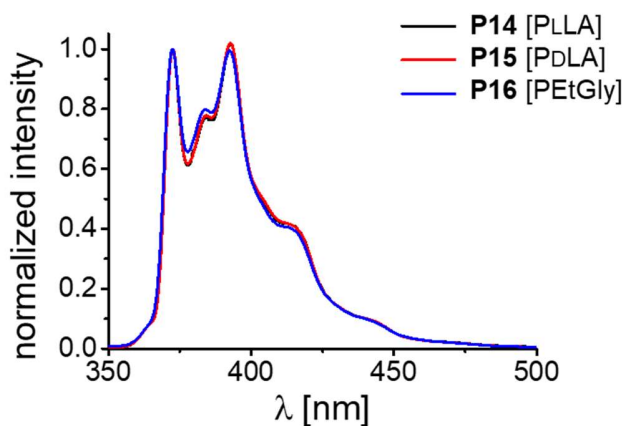


Figure 6.3. Normalized fluorescence spectra of pyrene loaded nanoparticles formed from **P14** to **P16** ($\lambda_{\text{ex}} = 339 \text{ nm}$, $c(\text{polymer}) = 5 \mu\text{g mL}^{-1}$, $c(\text{pyrene}) = 0.05 \mu\text{g mL}^{-1}$).

The acylation/cyclization pathways for the preparation of glycolide-like monomers was successfully applied for the synthesis of a series of morpholine-2,5-diones and a new lactide isomer, EtGly. Kinetic studies of homopolymerization of EtGly, L- and D-LA were the starting point for the preparation of a library of PLA-based copolyesters with tuned thermal properties. In this regard, the decrease of bulk melting point and degree of crystallinity was following a similar trend as the PCL library. Representing chiral polyesters, the P(EtGly-*stat*-LA) were successfully employed for the preparation of bulk stereocomplexes as well as nanoparticle stereocomplexes, with a further variation of thermal properties. Finally, fluorescence spectroscopy of pyrene-loaded

6. Designed monomers to modify PLA

nanoparticle suspensions revealed a constant HHB. The PLA-based library will be investigated with respect to encapsulation, release, and activity of various APIs within the framework of the SFB 1278 (PolyTarget) to unravel the question of how thermal and mechanical properties of nanoparticles influence their performance without having to consider the HHB as a third variable.

7. Summary

Polyesters represent a large family of materials that find extensive applications due to their biodegradability and biocompatibility. Their industrial production usually relies on the ring opening polymerization (ROP) of selected monomers, such as lactones and glycolides, enabling the preparation of poly(lactic acid) (PLA), poly(lactic-*co*-glycolic acid) (PLGA) as well as poly(ϵ -caprolactone) (P ϵ CL). The high biocompatibility of such materials enable their applications in medical fields for the preparation of prosthetic materials as well as for the preparation of drug delivery carriers.^{12, 89-91} Despite that, two main concerns are currently affecting their applications: The use of toxic catalysts such as tin salts during polymerization, and the limited range of polyester materials on the market.

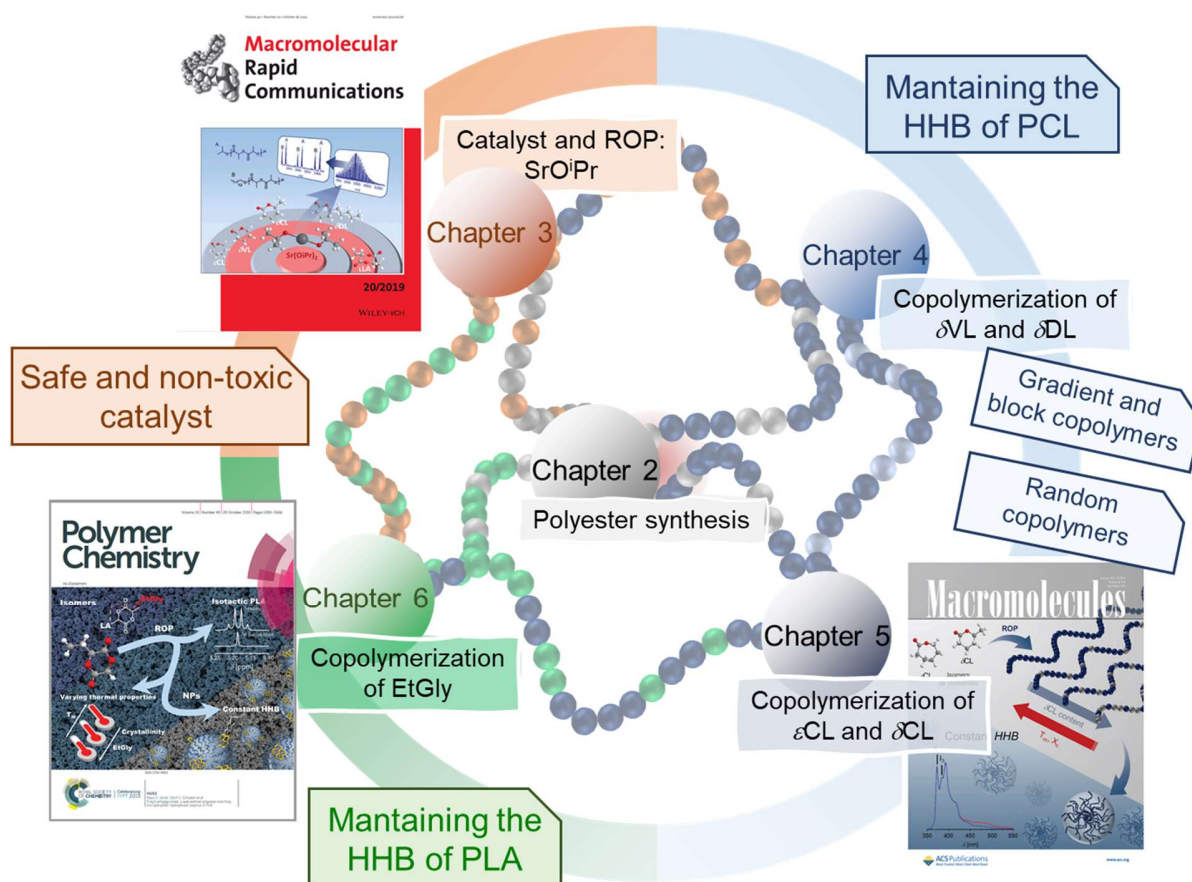


Figure 7.1. Overview of the topic discussed in this thesis.

7. Summary

Representing a less toxic alternative to heavy metal complexes, strontium isopropoxide was introduced in this work as a catalyst for the polymerization of L-lactide, proving a high activity already at room temperature. The strontium-based catalyst featured also high activity and an excellent molar mass control during the homopolymerization of substituted δ -lactones that otherwise often require high reaction times.

Taking lactide as basic structure, the replacement of one ester bond with an amide bond results in another class of monomers, the morpholine-2,5-diones, whose polymerization lead to polydepsipeptides featuring both esters and amide bonds. For a series of natural amino acids, the corresponding glycolic acid-based monomers were synthesized. Their polymerization was accomplished in a controlled manner *via* organocatalyzed ROP for the first time.

While these new materials further broaden the parameter space to be applied as carriers for drug delivery systems, the latter is far from being understood due to the multidimensional parameter space presented through alterations such as molar mass, carrier size, copolymer composition, *etc.*, even if only established materials are considered. A fundamental understanding necessitates unraveling the parameter space, which is not an easy task as variation of one parameter frequently goes along with alteration of another one. The research presented in this thesis contribute to understanding of how thermal as well as mechanical properties affect the performance of polyester-based nanocarriers. In particular, the third variable of the hydrophilic hydrophobic balance was eliminated through careful design of the polyester materials. For this purpose, three methods were identified: (i) The copolymerization of two lactone monomers in a pre-determined ratio, (ii) the copolymerization of isomers, and (iii) blending of suitable (co)polymers to result in further alteration of thermal and mechanical properties through stereocomplexation. All approaches were directed towards the synthesis of libraries of polyesters with the same HHB as P ϵ CL or PLA.

7. Summary

In a first study, the copolymerization of δ -valerolactone and δ -decalactone was performed *via* a TBD catalyzed ROP. As a result, the preparation of a short library of a block and a gradient copolymer matching the hydrophilic hydrophobic balance of P ϵ CL was accomplished and resulted in a variation of thermal properties (T_m). Stable nanoparticles suspensions were prepared, and their stiffness was correlated to the as bulk crystallinity. Whereas this study demonstrated the feasibility of the approach, it was limited to a series of three polymers due to the necessity of a discrete ratio of the two comonomers.

The library of polyesters with the same hydrophobicity as P ϵ CL was enlarged on the basis of the random copolymerization of the two isomers ϵ CL and δ CL, enabling to vary other properties than the HHB irrespective of the copolymer composition as random copolymers were obtained. DSC and WAXS investigations revealed that increasing the δ CL fraction in the polyesters resulted in a decrease of the melting point and the degree of crystallinity of the bulk materials. In addition to their eligibility to form nanoparticles of similar size in aqueous dispersion, encapsulation of pyrene confirmed a constant HHB, demonstrating the feasibility of the synthetic concept.

The transfer of the concept towards PLA relied on the new monomer 3-ethylglycolide (EtGly), which was homo- as well as copolymerized with L- and D-lactide. The resulting polymer libraries featured similar molar masses and low dispersities, as well as a decrease of melting temperatures and degree of crystallinity with the increase of the racemic EtGly in the copolymers. All PLA-mimicking nanoparticles also featured a constant HHB. The fact that it was different from that of the PCL-based materials stresses the feasibility of the initial concept as well as the necessity to perform such research. Stereocomplex properties made from these materials followed a similar trend, offering another possibility to vary thermal and mechanical properties of polymer nanoparticles while maintaining the HHB.

7. Summary

As a result, two libraries of polyester and their nanoparticles with same HHB, similar molar mass but varying thermal properties were established. The materials are currently being further investigated with respect to their performance as nanoparticulate drug delivery systems. Due to the use of materials developed within this thesis with constant HHB, these ongoing studies will provide definitive answers to the question if thermal and mechanical properties of NP, in fact, influence their performance.

As an outlook, the future of such materials will be focused on their nanoparticle preparation and properties. For this goal, the addition of stabilizers will be of utmost importance in order to shield the polyester core allowing an evaluation of enzymatic degradation. Moreover, the preparation of functional block copolymer with stealth properties will be tackled with respect to a future application also *in vivo*.

8. Zusammenfassung

Polyester stellen eine große Familie von Materialien dar, die aufgrund ihrer biologischen Abbaubarkeit und Biokompatibilität umfangreiche Anwendungen finden. Ihre industrielle Produktion beruht in der Regel auf der Ringöffnungspolymerisation (ROP) ausgewählter Monomere wie Lactonen oder Glykoliden, was Poly(milchsäure) (PLA), Poly(milchsäure-*co*-glykolsäure) (PLGA) und Poly(ϵ -caprolacton) (P ϵ CL) zugänglich macht. Die hohe Biokompatibilität solcher Materialien ermöglicht ihre Anwendung im medizinischen Bereich zur Herstellung von Prothesenmaterialien sowie von Wirkstoffträgern.^{12, 89-91} Die Verwendung von toxischen Katalysatoren wie Zinnsalzen während der Polymerisation und die begrenzte Auswahl an Polyestermaterialien auf dem Markt stellen aktuelle Herausforderungen dar.

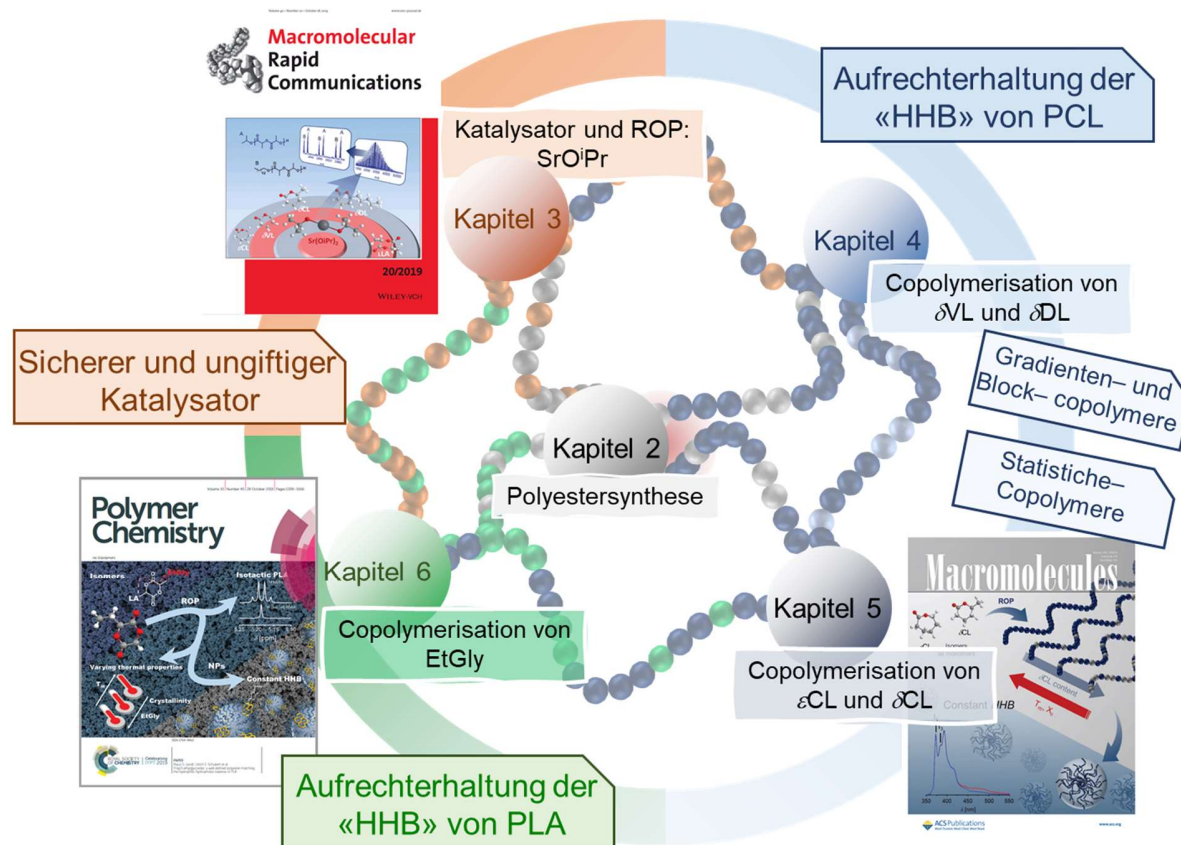


Figure 8.1. Überblick über das Thema dieser Arbeit.

8. Zusammenfassung

Als Alternative zu Schwermetallkomplexen wurde in dieser Arbeit Strontiumisopropoxid als Katalysator für die Polymerisation von L-Lactid vorgestellt. Vor Allem die hohe Aktivität bei Raumtemperatur und die ausgezeichnete Molmassenkontrolle bei der Homopolymerisation von substituierten δ -Lactonen, die sonst oft lange Reaktionszeiten erfordern, ist hierbei herauszustellen.

Ausgehend von Lactid als Grundstruktur führt der Ersatz einer Esterbindung durch eine Amidbindung zu einer anderen Klasse von Monomeren, den Morpholin-2,5-dionen, deren Polymerisation die Herstellung von Polydepsipeptiden erlaubt, die sowohl Ester- als auch Amidbindungen aufweisen. Für eine Reihe natürlicher Aminosäuren wurden die entsprechenden Monomere auf Basis der Glykolsäure synthetisiert. Ihre Polymerisation gelang erstmals kontrolliert über organokatalysierte ROP.

Diese neuen Materialien erweitern den mehrdimensionalen Parameterraum, der polymeren Trägern für Arzneimittel zu Grunde liegt. Dieser ist jedoch weit davon entfernt, verstanden zu werden, selbst wenn nur etablierte Materialien berücksichtigt werden, da Änderungen von Molmasse, Partikelgröße, Copolymerzusammensetzung usw. eigenständige Parameter darstellen. Da die Variation eines Parameters häufig mit der Änderung eines anderen einhergeht, ist ein grundlegendes Verständnis der einzelnen Variablen schwer zu erhalten.

Die in dieser Dissertation präsentierte Forschung trägt zum Verständnis des Einflusses thermischer und mechanischer Eigenschaften auf die Wirkweise von Polyester-basierten Nanoträgern bei. Insbesondere die dritte Variable, die hydrophile hydrophobe Balance (HHB), wurde durch sorgfältiges Design der Polyestermaterialien eliminiert. Zu diesem Zweck wurden drei Methoden identifiziert: (i) Die Copolymerisation von zwei Lactonmonomeren in einem vorbestimmten Verhältnis, (ii) die Copolymerisation von Isomeren und (iii) das Mischen geeigneter (Co)polymere, um eine weitere Veränderung von thermischen und mechanischen Eigenschaften durch

8. Zusammenfassung

Stereokomplexierung herbeizuführen. Alle Ansätze waren auf die Synthese von Bibliotheken von Polyestern mit der gleichen HHB wie P ϵ CL oder PLA gerichtet.

In einer ersten Studie wurde die Copolymerisation von δ -Valerolacton und δ -Decalacton über eine TBD-katalysierte ROP durchgeführt. Als Ergebnis wurde ein Block- und ein Gradienten-copolymer erhalten, deren HHB der von P ϵ CL entsprechen, während sich thermische Eigenschaften (T_m) unterschieden. Die Steifigkeit von stabilen Nanopartikeln ließ sich mit der Kristallinität der Bulkmaterialien korrelieren. Während diese Studie die Machbarkeit des Ansatzes demonstrierte, blieb er aufgrund der Notwendigkeit eines diskreten Verhältnisses der beiden Comonomere auf drei Polymere beschränkt.

Die Bibliothek von Polyestern mit der gleichen Lipophilie wie P ϵ CL wurde auf der Grundlage der statistischen Copolymerisation der beiden Isomere ϵ CL und δ CL vergrößert, und zwar unabhängig von der Copolymerzusammensetzung. DSC- und WAXS-Analysen zeigten, dass eine Erhöhung des δ CL-Anteils in den Polyestern zu einer Abnahme des Schmelzpunkts und des Kristallinitätsgrads führte. Die Verkapselung von Pyren in Nanopartikeln ähnlicher Größe in wässriger Dispersion zeigte eine konstante HHB der Materialien, was die Eignung des Synthesekonzepts bestätigte.

Die Übertragung des Konzepts auf PLA beruhte auf dem neuen Monomer 3-Ethylglycolid (EtGly), das sowohl homo- als auch mit L- und D-Lactid copolymerisiert wurde. Die resultierenden Polymerbibliotheken zeigten ähnliche Molmassen und niedrige Dispersitäten sowie eine Abnahme der Schmelztemperaturen und des Kristallinitätsgrads mit der Zunahme des racemischen EtGly in den Copolymeren. Alle PLA-analogen Nanopartikel wiesen auch eine konstante HHB auf. Die Tatsache, dass sich diese von denen der PCL-basierten Materialien unterschieden, unterstreicht die Notwendigkeit der Anwendung des entwickelten Konzepts, um

8. Zusammenfassung

Struktur–Eigenschafts–beziehungen polymerer Trägermaterialien sinnvoll aufzuklären. Die Eigenschaften der aus diesen Materialien hergestellten Stereokomplexe folgten einem ähnlichen Trend und bieten eine weitere Möglichkeit, die thermischen und mechanischen Eigenschaften von Polymernanopartikeln unter Beibehaltung der HHB zu variieren.

Als Ergebnis wurden zwei Bibliotheken von Polyestern und ihren Nanopartikeln mit gleichem HHB, ähnlicher Molmasse, aber unterschiedlichen thermischen Eigenschaften erhalten. Die Materialien werden derzeit hinsichtlich ihrer Leistungsfähigkeit als nanopartikuläre Drug-Delivery–Systeme weiter untersucht. Aufgrund der Verwendung von Materialien mit konstanter HHB, die in dieser Arbeit entwickelt wurden, werden diese laufenden Studien neue Antworten auf die Frage liefern, ob thermische und mechanische Eigenschaften von NP tatsächlich ihre Eigenschaften bezüglich Verkapselung und Freisetzung von pharmazeutischen Wirkstoffen beeinflussen.

Die Zukunft solcher Materialien wird sich auf ihre Herstellung und Eigenschaften von Nanopartikeln konzentrieren. Für dieses Ziel ist die Zugabe von Stabilisatoren von größter Bedeutung, um den Polyesterkerne abzusichern, wird jedoch den enzymatischen Abbau weiter beeinflussen. Darüber hinaus wird die Herstellung funktioneller Block–copolymerer mit Stealth-Eigenschaften im Hinblick auf eine zukünftige Anwendung auch *in vivo* angegangen.

9. References

1. X. Tang, E. Y. X. Chen, *Chem* **2019**, *5*, 284-312.
2. S. Y. Choi, M. N. Rhie, H. T. Kim, J. C. Joo, I. J. Cho, J. Son, S. Y. Jo, Y. J. Sohn, K.-A. Baritugo, J. Pyo, Y. Lee, S. Y. Lee, S. J. Park, *Metab. Eng.* **2020**, *58*, 47-81.
3. A. Larrañaga, E. Lizundia, *Eur. Polym. J.* **2019**, *121*, 109296.
4. V. Siracusa, *Polymers* **2019**, *11*, 1066.
5. S. Dutta, W. Hung, Chou, B. Huang, Hunn, C. Lin, Chieh, In *Synthetic Biodegradable Polymers*, Rieger, B.; Künkel, A.; Coates, G. W.; Reichardt, R.; Dinjus, E.; Zevaco, T. A., Eds. Springer Berlin Heidelberg: Berlin, Heidelberg, 2012; pp 219-283.
6. M. Das, B. Mandal, V. Katiyar, In *Advances in Sustainable Polymers: Synthesis, Fabrication and Characterization*, Katiyar, V.; Kumar, A.; Mulchandani, N., Eds. Springer Singapore: Singapore, 2020; pp 21-33.
7. C. Gao, C. Ma, P. Xu, *Biotechnol. Adv.* **2011**, *29*, 930-939.
8. Y. Yu, J. Zou, C. Cheng, *Polym. Chem.* **2014**, *5*, 5854-5872.
9. G. Dräger, A. Kirschning, R. Thiericke, M. Zerlin, *Nat. Prod. Rep.* **1996**, *13*, 365-375.
10. M. Rabnawaz, I. Wyman, R. Auras, S. Cheng, *Green Chem.* **2017**, *19*, 4737-4753.
11. J. Zhao, G. Weng, J. Li, J. Zhu, J. Zhao, *Mater. Sci. Eng. C* **2018**, *92*, 983-994.
12. F. Molavi, M. Barzegar Jalali, H. Hamishehkar, *J. Control. Release* **2020**, *320*, 265-282.
13. M. Elsabahy, K. L. Wooley, *Chem. Soc. Rev.* **2012**, *41*, 2545-2561.
14. Z. Xu, D. Wang, Y. Cheng, M. Yang, L. Wu, Ping, *Mater. Sci. Eng. C* **2018**, *92*, 1006-1015.
15. M. Mir, N. Ahmed, A. Rehman, *Colloids Surf. B* **2017**, *159*, 217-231.
16. F. R. Wurm, C. K. Weiss, *Front. Chem.* **2014**, *2*, 49.
17. O. Maksimenko, J. Malinovskaya, E. Shipulo, N. Osipova, V. Razzhivina, D. Arantseva, O. Yarovaya, U. Mostovaya, A. Khalansky, V. Fedoseeva, A. Alekseeva, L. Vanchugova, M. Gorshkova, E. Kovalenko, V. Balabanyan, P. Melnikov, V. Baklaushev, V. Chekhonin, J. Kreuter, S. Gelperina, *Int. J. Pharm.* **2019**, *572*, 118733.
18. W. H. Carothers, G. L. Dorough, F. J. v. Natta, *J. Am. Chem. Soc.* **1932**, *54*, 761-772.
19. T. Maharana, B. Mohanty, Y. S. Negi, *Prog. Polym. Sci.* **2009**, *34*, 99-124.
20. S. Kobayashi, *Polym. Adv. Technol.* **2015**, *26*, 677-686.
21. O. Coulembier, P. Degée, J. L. Hedrick, P. Dubois, *Prog. Polym. Sci.* **2006**, *31*, 723-747.

9. References

22. P. Dubois, O. Coulembier, J. M. Raquez, Handbook of ring-opening polymerization John Wiley & Sons: 2009.
23. S. A. Cairns, A. Schultheiss, M. P. Shaver, *Polym. Chem.* **2017**, *8*, 2990-2996.
24. B. Martin Vaca, D. Bourissou, *ACS Macro Lett.* **2015**, *4*, 792-798.
25. Y. Zhong, R. Tong, *Front. Chem.* **2018**, *6*, 641.
26. M. Yin, G. L. Baker, *Macromolecules* **1999**, *32*, 7711-7718.
27. T. Trimaille, M. Moeller, R. Gurny, *J. Polym. Sci., Part A: Polym. Chem.* **2004**, *42*, 4379-4391.
28. T. Trimaille, R. Gurny, M. Moeller, *J. Biomed. Mater. Res.* **2007**, *80A*, 55-65.
29. F. Jing, M. R. Smith, G. L. Baker, *Macromolecules* **2007**, *40*, 9304-9312.
30. X. Jiang, E. B. Vogel, M. R. Smith, G. L. Baker, *Macromolecules* **2008**, *41*, 1937-1944.
31. X. Jiang, M. R. Smith, G. L. Baker, *Macromolecules* **2008**, *41*, 318-324.
32. T. L. Simmons, G. L. Baker, *Biomacromolecules* **2001**, *2*, 658-663.
33. T. Liu, T. L. Simmons, D. A. Bohnsack, M. E. Mackay, M. R. Smith, G. L. Baker, *Macromolecules* **2007**, *40*, 6040-6047.
34. D. E. Noga, T. A. Petrie, A. Kumar, M. Weck, A. J. García, D. M. Collard, *Biomacromolecules* **2008**, *9*, 2056-2062.
35. U. Schöllkopf, W. Hartwig, U. Sprotte, W. Jung, *Angew. Chem. Int. Ed.* **1979**, *18*, 310-311.
36. M. Rubinshtein, C. R. James, J. L. Young, Y. J. Ma, Y. Kobayashi, N. C. Gianneschi, J. Yang, *Org. Lett.* **2010**, *12*, 3560-3563.
37. C.-U. Lee, R. Khalifehzadeh, B. Ratner, A. J. Boydston, *Macromolecules* **2018**, *51*, 1280-1289.
38. X. Jiang, E. B. Vogel, M. R. Smith III, G. L. Baker, *J. Polym. Sci., Part A: Polym. Chem.* **2007**, *45*, 5227-5236.
39. W. W. Gerhardt, D. E. Noga, K. I. Hardcastle, A. J. García, D. M. Collard, M. Weck, *Biomacromolecules* **2006**, *7*, 1735-1742.
40. A. Pedna, L. Rosi, M. Frediani, P. Frediani, *J. Appl. Polym. Sci.* **2015**, *132*, 42323.
41. A. Smelcerovic, P. Dzodic, V. Pavlovic, E. Cherneva, D. Yancheva, *Amino Acids* **2014**, *46*, 825-840.
42. J. Chen, X. Zhao, G. Zhang, B. Chen, W. Cai, *Chin. J. Chem. Eng* **2013**, *21*, 1404-1409.
43. V. Boucard, G. Broustal, J. M. Campagne, *Eur. J. Org. Chem.* **2007**, *2007*, 225-236.
44. J.-L. Hsu, J.-M. Fang, *J. Org. Chem.* **2001**, *66*, 8573-8584.

9. References

45. J. Y. Do, D. K. Salunkhe, L. E. Olson, *J. Food Sci.* **1969**, *34*, 618-621.
46. H. Tamura, M. Appel, E. Richling, P. Schreier, *J. Agric. Food Chem.* **2005**, *53*, 5397-5401.
47. W. Saiyasombat, R. Molloy, T. M. Nicholson, A. F. Johnson, I. M. Ward, S. Poshyachinda, *Polymer* **1998**, *39*, 5581-5585.
48. D. K. Schneiderman, M. A. Hillmyer, *Macromolecules* **2016**, *49*, 2419-2428.
49. M. J. Stanford, A. P. Dove, *Chem. Soc. Rev.* **2010**, *39*, 486-494.
50. H. Tsuji, *Macromol. Biosci.* **2005**, *5*, 569-597.
51. J. Slager, A. J. Domb, *Adv. Drug Deliv. Rev.* **2003**, *55*, 549-583.
52. H. Tsuji, A. Okumura, *Macromolecules* **2009**, *42*, 7263-7266.
53. S. R. Andersson, M. Hakkarainen, A.-C. Albertsson, *Polymer* **2013**, *54*, 4105-4111.
54. H. Li, R. M. Shakaroun, S. M. Guillaume, J.-F. Carpentier, *Chem. Eur. J.* **2020**, *26*, 128-138.
55. J. Gao, D. Zhu, W. Zhang, G. A. Solan, Y. Ma, W.-H. Sun, *Inorg. Chem. Front.* **2019**, *6*, 2619-2652.
56. M. Florczak, A. Kowalski, J. Libiszowski, K. Majerska, A. Duda, *Polimery* **2007**, *52*, 722.
57. A. Kowalski, A. Duda, S. Penczek, *Macromolecules* **1998**, *31*, 2114-2122.
58. A. Kowalski, J. Libiszowski, A. Duda, S. Penczek, *Macromolecules* **2000**, *33*, 1964-1971.
59. J.-B. Zeng, M. Srinivansan, Y.-D. Li, R. Narayan, Y.-Z. Wang, *J. Polym. Sci., Part A: Polym. Chem.* **2010**, *48*, 5885-5890.
60. M. Save, M. Schappacher, A. Soum, *Macromol. Chem. Phys.* **2002**, *203*, 889-899.
61. B. G. G. Lohmeijer, R. C. Pratt, F. Leibfarth, J. W. Logan, D. A. Long, A. P. Dove, F. Nederberg, J. Choi, C. Wade, R. M. Waymouth, J. L. Hedrick, *Macromolecules* **2006**, *39*, 8574-8583.
62. M. K. Kiesewetter, E. J. Shin, J. L. Hedrick, R. M. Waymouth, *Macromolecules* **2010**, *43*, 2093-2107.
63. M. Labet, W. Thielemans, *Chem. Soc. Rev.* **2009**, *38*, 3484-3504.
64. P. Lecomte, C. Jérôme, In *Synthetic Biodegradable Polymers*, Rieger, B.; Künkel, A.; Coates, G. W.; Reichardt, R.; Dinjus, E.; Zevaco, T. A., Eds. Springer Berlin Heidelberg: Berlin, Heidelberg, 2012; pp 173-217.
65. K. Rezwan, Q. Z. Chen, J. J. Blaker, A. R. Boccaccini, *Biomaterials* **2006**, *27*, 3413-3431.
66. P. Habibovic, J. E. Barralet, *Acta Biomater.* **2011**, *7*, 3013-3026.

9. References

67. J. Y. Reginster, E. Seeman, M. C. De Vernejoul, S. Adami, J. Compston, C. Phenekos, J. P. Devogelaer, M. D. Curiel, A. Sawicki, S. Goemaere, O. H. Sorensen, D. Felsenberg, P. J. Meunier, *J. Clin. Endocrinol. Metab.* **2005**, *90*, 2816-2822.
68. I. Yildirim, S. Crotty, C. H. Loh, G. Festag, C. Weber, P.-F. Caponi, M. Gottschaldt, M. Westerhausen, U. S. Schubert, *J. Polym. Sci., Part A: Polym. Chem.* **2016**, *54*, 437-448.
69. P. Grossen, D. Witzigmann, S. Sieber, J. Huwlyler, *J. Control. Release* **2017**, *260*, 46-60.
70. M. Bartnikowski, T. R. Dargaville, S. Ivanovski, D. W. Hutmacher, *Prog. Polym. Sci.* **2019**, *96*, 1-20.
71. V. Buchholz, S. Agarwal, A. Greiner, *Macromol. Biosci.* **2016**, *16*, 207-213.
72. V. Karavelidis, E. Karavas, D. Giliopoulos, S. Papadimitriou, D. Bikiaris, *Int. J. Nanomedicine* **2011**, *6*, 3021-3032.
73. R. C. Pratt, B. G. G. Lohmeijer, D. A. Long, R. M. Waymouth, J. L. Hedrick, *J. Am. Chem. Soc.* **2006**, *128*, 4556-4557.
74. K. K. Bansal, D. Kakde, L. Purdie, D. J. Irvine, S. M. Howdle, G. Mantovani, C. Alexander, *Polym. Chem.* **2015**, *6*, 7196-7210.
75. M. T. Martello, A. Burns, M. Hillmyer, *ACS Macro Lett.* **2012**, *1*, 131-135.
76. V. Arias, P. Olsén, K. Odelius, A. Höglund, A.-C. Albertsson, *Polym. Chem.* **2015**, *6*, 3271-3282.
77. F. R. Mayo, F. M. Lewis, *J. Am. Chem. Soc.* **1944**, *66*, 1594-1601.
78. V. E. Meyer, G. G. Lowry, *J. Polym. Sci., Part A: Polym. Chem.* **1965**, *3*, 2843-2851.
79. B. S. Beckingham, G. E. Sanoja, N. A. Lynd, *Macromolecules* **2015**, *48*, 6922-6930.
80. N. A. Lynd, R. C. Ferrier, B. S. Beckingham, *Macromolecules* **2019**, *52*, 2277-2285.
81. H. J. Harwood, W. M. Ritchey, *J. Polym. Sci., Part B: Polym. Lett.* **1964**, *2*, 601-607.
82. R. Galvan, M. Tirrell, *J. Polym. Sci., Part A: Polym. Chem.* **1986**, *24*, 803-807.
83. S. Harrisson, F. Ercole, B. W. Muir, *Polym. Chem.* **2010**, *1*, 326-332.
84. H. Tsujimoto, Y. Kawashima, In *Nanoparticle Technology Handbook (Third Edition)*, Naito, M.; Yokoyama, T.; Hosokawa, K.; Nogi, K., Eds. Elsevier: 2018; pp 451-460.
85. Y. Feng, D. Klee, H. Hoecker, *Macromol. Chem. Phys.* **1999**, *200*, 2276-2283.
86. Y. Feng, D. Klee, H. Hoecker, *Macromol. Biosci.* **2001**, *1*, 66-74.
87. Y. Feng, J. Knüfermann, D. Klee, H. Hoecker, *Macromol. Rapid Commun.* **1999**, *20*, 88-90.
88. N. J. Sherck, H. C. Kim, Y.-Y. Won, *Macromolecules* **2016**, *49*, 4699-4713.

9. References

89. N. U. Khaliq, D. Chobisa, C. A. Richard, M. R. Swinney, Y. Yeo, *Ther. Deliv.* **2021**, *12*, 37-54.
90. C. Wang, W. Huang, Y. Zhou, L. He, Z. He, Z. Chen, X. He, S. Tian, J. Liao, B. Lu, Y. Wei, M. Wang, *Bioact. Mater.* **2020**, *5*, 82-91.
91. M. Santoro, S. R. Shah, J. L. Walker, A. G. Mikos, *Adv. Drug Deliv. Rev.* **2016**, *107*, 206-212.

List of abbreviations

Al(OiPr) ₃	Aluminum isopropoxide
AFM	Atomic force microscopy
API	Active pharmaceutical ingredient
BnOH	Benzyl alcohol
BSL	Beckingham–Sanoja–Lynd
Đ	Dispersity
DBU	1,8-Diazabicyclo[5.4.0]undec-7-ene
ϵ CL	ϵ -Caprolactone
EtGly	3-Ethylglycolide
ESI	Electrospray ionization
δ CL	δ -Caprolactone
δ DL	δ -Decalactone
DodOH	Dodecanol
DOX	Dioxolanones
DLS	Dynamic light scattering
DMAP	4-Dimethylaminopyridine
DSC	Dynamic scanning calorimetry
δ VL	δ -Valerolactone
FDA	Food and Drug Administration
HHB	Hydrophilic hydrophobic balance
NMR	Nuclear magnetic resonance
$k_{p,app}$	Apparent polymerization rate constant
LA	Lactide
MALDI	Matrix assisted light desorption ionization
ML	Meyer–Lowry
M_n	Number average molar mass
mTBD	7-Methyl-1,5,7-triazabicyclo[4.4.0]dec-5-ene
MS	Mass spectrometry
OCA	<i>O</i> -Carboxyanhydride
PDI	Polydispersity index
P ϵ CL	Poly(ϵ -caprolactone)
P δ CL	Poly(δ -caprolactone)
P δ DL	Poly(δ -decalactone)
P δ VL	Poly(δ -valerolactone)

List of abbreviations

PEG	Poly(ethylene glycol)
PGA	Poly(glycolic acid)
P2HB	Poly(2-hydroxybutanoic acid)
P2H3MB	Poly(2-hydroxy-3-methylbutanoic acid)
PLA	Poly(lactic acid)
PLGA	Poly(lactic-co-glycolic acid)
P ϵ CL	Poly(ϵ -caprolactone)
PMA	Poly(mandelic acid)
ROP	Ring opening polymerization
RT	Room temperature
SEC	Size exclusion chromatography
SC	Stereocomplex
Sn(Oct) ₂	Tin(II)octanoate
Sr(OiPr) ₂	Strontium isopropoxide
TBD	1,5,7-Triazabicyclo[4.4.0]dec-5-ene
T_c	Crystallization temperature
T_g	Glass transition temperature
T_m	Melting temperature
THF	Tetrahydrofuran
ToF	Time-of-flight
WAXS	Wide angle X-ray scattering
X_c	Degree of crystallinity

Publication List

Peer-reviewed publications

1. W. Oberhauser, M. Bartoli, G. Petrucci, **D. Bandelli**, M. Frediani, L. Capozzoli, C. Cepek, S. Bhardwaj, L. Rosi, “Nitrile hydration to amide in water: Palladium–based nanoparticles vs molecular catalyst”, *J. Mol. Catal. A Chem.* **2015**, *410*, 26–33.
2. M. Frediani, W. Oberhauser, E. Passaglia, L. Rosi, **D. Bandelli**, M. Bartoli, G. Petrucci, in *Handbook of Composites from Renewable Materials, Functionalization*; John Wiley & Sons: Hoboken, NJ, USA **2017**, *4*, 47–68.
3. M. Sahn, **D. Bandelli**, M. Dirauf, C. Weber, U. S. Schubert, “Bifunctional initiators as tools to track chain transfer during the CROP of 2-oxazolines”, *Macromol. Rapid Commun.* **2017**, *38*, 1700396.
4. M. Sahn, L. M. Stafast, M. Dirauf, **D. Bandelli**, C. Weber, U. S. Schubert, “LCST behavior of poly(2–ethyl–2–oxazoline) containing diblock and triblock copolymers”, *Eur. Polym. J.* **2018**, *100*, 57–66.
5. **D. Bandelli**, C. Helbing, C. Weber, M. Seifert, I. Muljajew, K. D. Jandt, U. S. Schubert, “Maintaining the hydrophilic–hydrophobic balance of polyesters with adjustable crystallinity for tailor-made nanoparticles”, *Macromolecules* **2018**, *51*, 5567–5576.
6. M. Dirauf, **D. Bandelli**, C. Weber, H. Görls, M. Gottschaldt, U. S. Schubert, “TBD-Catalyzed ring-opening polymerization of alkyl-substituted morpholine-2,5-dione derivatives”, *Macromol. Rapid Commun.* **2018**, *39*, 1800433.
7. **D. Bandelli**, C. Weber, U. S. Schubert, “Strontium isopropoxide: A highly active catalyst for the ring–opening polymerization of lactide and various lactones”, *Macromol. Rapid Commun.* **2019**, *40*, 1900306.
8. **D. Bandelli**, J. Alex, C. Helbing, N. Ueberschaar, H. Görls, P. Bellstedt, C. Weber, K. D. Jandt, U. S. Schubert, “Poly(3–ethylglycolide): A well–defined polyester matching the hydrophilic hydrophobic balance of PLA”, *Polym. Chem.* **2019**, *10*, 5440–5451.

Publication List

9. **D. Bandelli**, J. Alex, C. Weber, U. S. Schubert, “Polyester stereocomplexes beyond PLA: Could synthetic opportunities revolutionize established material blending?”, *Macromol. Rapid Commun.* **2020**, *41*, 1900560.
10. P. Wei, F. H. Sobotta, C. Kellner, **D. Bandelli**, S. Hoepfner, S. Schubert, J. C. Brendel, U. S. Schubert, “Degradable polycaprolactone nanoparticles stabilized *via* supramolecular host–guest interactions with pH–responsive polymer–pillar[5]arene conjugates”, *Polym. Chem.* **2020**, *11*, 1985–1997.
11. **D. Bandelli**, I. Muljajew, K. Scheuer, J. B. Max, C. Weber, F. H. Schacher, K. D. Jandt, U. S. Schubert, “Copolymerization of caprolactone isomers to obtain nanoparticles with constant hydrophobicity and tunable crystallinity”, *Macromolecules* **2020**, *53*, 5208–5217.
12. K. Scheuer, **D. Bandelli**, C. Helbing, C. Weber, J. Alex, J. B. Max, A. Hocken, O. Stranik, L. Seiler, F. Gladigau, U. Neugebauer, F. H. Schacher, U. S. Schubert, K. D. Jandt, “Self–assembly of copolyesters into stereocomplex crystallites tunes the properties of polyester nanoparticles”, *Macromolecules* **2020**, *53*, 8340–8351.
13. A. Vollrath, C. Kretzer, B. Beringer-Siemers, B. Shkodra, J. A. Czaplowska, **D. Bandelli**, S. Stumpf, S. Hoepfner, C. Weber, O. Werz, U. S. Schubert, “Effect of crystallinity on the properties of polycaprolactone nanoparticles containing the dual FLAP/mPEGS–1 inhibitor BRP–187”, *Polymers* **2021**, *13*, 2557.

Patents

1. N. Windhab, M. Bindl, A. Karau., M. Seibel, T. Endres, U. S. Schubert, C. Weber, **D. Bandelli**, Novel catalyzed synthesis of biodegradable polyesters. WO2020225044A1, 2020.

Conferences

Oral contributions:

- 1 D. Bandelli, L. Rosia, M. Bartoli, W. Oberhauser, G. Petrucci, M. Frediani,
6th Czech–Italian–Spanish Conference on Molecular Sieves and Catalysis, Amantea, Italy,
14 – 17 June 2015

“Hydrosoluble palladium nanostructured catalyst for nitriles hydrolysis: Synthesis,
characterizations and applications”
- 2 D. Bandelli, M. Bartoli, W. Oberhauser, E. Passaglia, L. Rosi, M. Frediani, P. Frediani,
XIX National Congress of the Industrial Chemistry division from SCI, Salerno, Italy. 14 –
16 September 2015

“Palladium macrocomplexes based on polymers and copolymers from renewable
resources”
- 3 **D. Bandelli**, C. Weber, C. Helbing, K. Jandt, U. S. Schubert
MACROMEX2017, Los Cabos, Mexico, December 3 – 7, 2017

“Block and gradient copolyesters and their nanoparticles: A thermal and mechanical study”
- 4 **D. Bandelli**, C. Helbing, C. Weber, M. Seifert, I. Muljajew, K. D. Jandt, U. S. Schubert
European Conference on Gradient Copolymers (ECGC), Jena, Germany, 28 September
2018

“Block and gradient copolyesters and their nanoparticles: A thermal and mechanical study”
- 5 **D. Bandelli**, K. Scheuer, C. Weber, K. D. Jandt, U. S. Schubert, Summer school SFB
PolyTarget 1278 (Jena) and SFB 1066 (Mainz), Fulda, Germany, 24 – 28 June 2019

“Controlling the degradation behavior of polymeric nanoparticles by structurally tailored
thermal properties”

Publication List

Posters:

- 1 **D. Bandelli**, L. Rosi, M. Frediani, M. Bartoli, P. Frediani, XIX National Congress of the Industrial Chemistry division from SCI, Salerno, Italy. 14 – 16 September 2015

 “Microwave assisted pyrolysis of cellulose in a multimode batch reactor”

- 2 K. Scheuer, **D. Bandelli**, C. Weber, K. D. Jandt, U. S. Schubert, Summer school SFB PolyTarget 1278 (Jena) and SFB 1066 (Mainz), Fulda, Germany, 24 – 28 June 2019

 “Controlling the degradation behavior of polymeric nanoparticles by structurally tailored thermal properties”

- 3 **D. Bandelli**, K. Scheuer, C. Weber, K. D. Jandt, U. S. Schubert, Symposium on Innovative Polymers for the Nanomedicine of the 21st Century, Jena, Gemany, 15 – 17 July 2019

 “Controlling the degradation behavior of polymeric nanoparticles by structurally tailored thermal properties”

Acknowledgements

I really think that words are not enough to express entirely my gratitude to all the people that supported, guided and walked with me during this incredible experience, but I will try my best.

First, I would like to express my deepest gratitude to Professor Schubert for allowing me to work in a vibrant, enthusiastic and challenging environment. Everything, from the opportunity to work with advanced instrumentation and techniques to the group seminar sessions, strongly contributed to my professional and personal growth. Moreover, having the chance to join the SFB PolyTarget was an incredible opportunity that enabled me to work in a multidisciplinary environment. Thank you for being supportive and for challenging me with interesting topics.

Secondly, I would like to thank Professor Jandt and Professor Schacher for the fruitful cooperation during the SFB PolyTarget. Your insightful comments strongly improved the quality of my work and my training.

To Christine, during this long journey you patiently walked me through polymer science and always challenged me to be a better version of myself. I am sure that without our meetings, discussions and writing sessions this thesis would not have been possible.

I would like to acknowledge all the colleagues that contributed to my work during my PhD thesis. A special thanks go to Irina Muljajew, Michael Dirauf and Julien Alex, my latest laboratory colleagues in Jena. Irina, our discussions and your support for all the DLS and fluorescence spectroscopy measurements strongly enriched our work. Michy and Julien, being your daily laboratory supervisor during your thesis was the easiest task I ever had, your contribution was fundamental for this thesis. All you three are young talented chemists and I consider myself lucky for having worked with you.

Thanks to Dr. Martin Sahn, even if I did not use the data obtained during our collaboration in this thesis, your support was fundamental in my first years in Jena. I would like to thank the group of

Acknowledgements

Professor Jandt, in particular Dr. Christian Helbing and Karl Scheuer for their kind collaboration. Another thank goes to Johannes Max for his precious contribution with WAXS analyses, to Dr. Helmar Görls, Dr. Nico Ueberschaar, Dr. Peter Bellstedt and Prof. Neugebauer for their support, and to Dr. Johannes C. Brendel and Dr. Peng Wei for including me in their research. A special thanks to Dr. Grit Festag, Renzo Paulus, Nicole Fritz, Dr. Jürgen Vitz, Alexander Meier, Benjamin Friebe and to all the people that made all the instruments of ZAF and CEEC Jena I running smoothly (especially the glovebox).

Christine, Micky, Irina, Julien, “Paolino”, Ben, Flo and the “ZAF gang”: Even if labwork was not always giving the expected results, we always found the right catalyst for a good laugh. You made my stay in Jena happy, for this “le parole non sono sufficienti”. A presto!

Ed eccomi arrivato ad altri tipi di ringraziamenti. Quattro anni non sono un tempo che può passare velocemente. Lontani, tutti voi siete diventati la migliore versione di voi stessi.

Grazie Iside, Nicco, Fra, Giulia, Papo e Ale per avermi supportato e sopportato in questi anni.

Grazie alla mia famiglia, ad Aurora, Simone e Laura. Mi avete spinto, motivato, consolato e coccolato. Non solo negli ultimi cinque anni, ma sempre. Per voi, davvero, le parole non riescono a raccontare abbastanza.

Thanks to all of you,

Damiano

Publications **P1** to **P7**

P1: Reproduced with permission from D. Bandelli, J. Alex, C. Weber, U. S. Schubert, “Polyester stereocomplexes beyond PLA: Could synthetic opportunities revolutionize established material blending?”, *Macromolecular Rapid Communications* 2019, 41, 1900560; published by WILEY-VCH Verlag GmbH & Co. KGaA, Weinheim, 2019.

P2: Reproduced with permission from D. Bandelli, C. Weber, U. S. Schubert, “Strontium Isopropoxide: A Highly Active Catalyst for the Ring-Opening Polymerization of Lactide and Various Lactones”, *Macromolecular Rapid Communications* 2019, 40, 1900306; published by WILEY-VCH Verlag GmbH & Co. KGaA, Weinheim, 2019.

P3: Reprinted with permission from D. Bandelli, C. Helbing, C. Weber, M. Seifert, I. Muljajew, K. D. Jandt, U. S. Schubert, “Maintaining the hydrophilic–hydrophobic balance of polyesters with adjustable crystallinity for tailor–made nanoparticles”, *Macromolecules* 2018, 51, 5567–5576. Copyright 2018 American Chemical Society.

P4: Reprinted with permission from D. Bandelli, I. Muljajew, K. Scheuer, J. B. Max, C. Weber, F. H. Schacher, K. D. Jandt, U. S. Schubert, “Copolymerization of caprolactone isomers to obtain nanoparticles with constant hydrophobicity and tunable crystallinity”, *Macromolecules* 2020, 53, 5208–5217. Copyright 2018 American Chemical Society.

P5: Reproduced from D. Bandelli, J. Alex, C. Helbing, N. Ueberschaar, H. Görls, P. Bellstedt, C. Weber, K. D. Jandt and U. S. Schubert, *Polym. Chem.* 2019, 10, 5440–5451 DOI: 10.1039/C9PY00875F, with permission from the Royal Society of Chemistry.

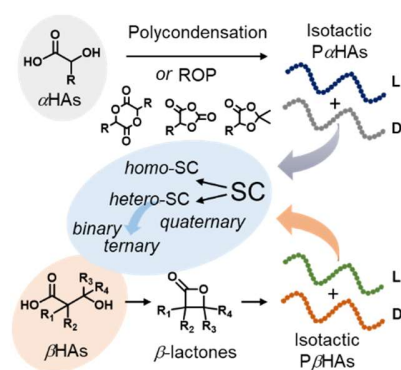
P6: Reproduced with permission from M. Dirauf, D. Bandelli, C. Weber, H. Görls, M. Gottschaldt, U. S. Schubert, TBD–Catalyzed Ring–Opening Polymerization of alkyl–substituted Morpholine–2,5–dione derivatives, *Macromol. Rapid Commun.* 2018, 39, 1800433, published by WILEY-VCH Verlag GmbH & Co. KGaA, Weinheim, 2018.

P7: Reprinted with permission from K. Scheuer, D. Bandelli, C. Helbing, C. Weber, J. Alex, J. B. Max, A. Hocken, O. Stranik, L. Seiler, F. Gladigau, U. Neugebauer, F. H. Schacher, U. S. Schubert, Klaus D. Jandt, Self–assembly of copolyesters into stereocomplex crystallites tunes the properties of polyester nanoparticles, *Macromolecules* 2020, 53, 8340–8351. Copyright 2020 American Chemical Society.

Publication P1

Polyester stereocomplexes beyond PLA: Could synthetic opportunities revolutionize established material blending?

D. Bandelli, J. Alex, C. Weber, U. S. Schubert, *Macromol. Rapid Commun.* **2019**, *41*, 1900560.





Polyester Stereocomplexes Beyond PLA: Could Synthetic Opportunities Revolutionize Established Material Blending?

Damiano Bandelli, Julien Alex, Christine Weber, and Ulrich S. Schubert*

This review summarizes the current literature regarding stereocomplexation of different polyesters based on α - as well as β -hydroxy acids beyond the well-known poly(lactic acid). Representing the initial step toward stereocomplexation, synthetic approaches needed to obtain and analyze isotactic polyesters are summarized. The basic technologies for the preparation and characterization of the respective stereocomplexes (SCs) are described, and published material properties are related to the structure of the respective polyesters. The variety of available SC materials is very limited despite the multiple options provided by state-of-the-art stereoselective monomer synthesis and polymerization methods. A combination of knowledge from the three scientific areas (i.e., organic chemistry, synthetic macromolecular chemistry, and materials science) thus has enormous potential to create novel materials with additional features enabled by the introduction of functional moieties to such materials besides the adjustment of thermal as well as mechanical properties.

1. Introduction

Ever since polymers were invented, they have been an interdisciplinary field between synthetic macromolecular chemistry, physical chemistry, physics, and materials science, in particular due to the manifold applications that were quickly found.

Polyesters as one example, are applied as packaging materials, for prosthesis, tissue engineering,^[1] and drug delivery.^[2–4] Representing a sustainable polymer class, they could solve current major problems such as environmental pollution due to microplastic contamination. This is mainly due to two facts: a) Many polyesters can be obtained from natural resources, and b) polyesters are biodegradable.^[5] Although initially obtained by polycondensation by Carothers in 1932,^[6] it was not until the 1950s that polyesters attracted considerable attention.^[7] Poly(lactic acid) (PLA), probably representing the most well-known polyester, is produced nowadays from

starch by fermentation yielding lactic acid, oligomerization and subsequent ring-opening polymerization (ROP) of lactide.^[8] Obtained via green chemistry, the ROP even enables to tailor molar masses and end groups. However, PLA represents a brittle material with a low processing window of 12 °C^[9] because the melting temperature is close to its degradation temperature.^[10] Its brittleness necessitates the use of plasticizers, that is, substances whose extensive use is debated because of leakage from the material and resulting effects on human health.

On the other hand, a simple statistical copolymerization with another monomer can easily alter a homopolymer's property, a fact that is well-known among the polymer community.^[11] The development of poly(lactic-co-glycolic acid) (PLGA), that

is, the copolymer of lactide and glycolide, represents an excellent example.^[12,13] The degradability as well as the thermal properties can be easily tuned, which has led to their commercialization under the trade name RESOMER.

In fact, there is a wealth of other monomers that can be applied for polyester synthesis, some even representing naturally occurring lactones. Already homopolymers offer a wide range of properties, and the parameter space offered by copolymerizations is far from being exploited, even by academia.^[14] However, industry has limited itself to more traditional polyesters including PLA, PLGA, or polycaprolactone (PCL). Although poly(3-hydroxy butyric acid) (P3HB)^[15] is simply produced by several microorganisms as a form of energy storage via fermentation with high molar mass, it has not found broad applications in commercial products so far. Why is that? Besides approval issues, in particular for bio-medical applications, economical reasons drive forward innovations in small steps. In view of that, blending represents an option to alter properties in a straightforward fashion minimizing the need to replace well-established materials.

Stereocomplexation represents a very specific type of blending that can occur when stereo-defined polymers with different tacticities or configurations are mixed. If stereoselective association prevails over the interactions between the parent polymers, new macromolecular arrangements are formed.^[16]

Nature has been structuring via chirality ever since. Proteins and DNA double helix represent well-known examples. In fact, the first report about stereocomplexation was published by Pauling and Corey regarding the formation of “racemate species” based on polypeptides in 1953,^[17] describing what is known today as stereocomplexes. Apart from other polyamides,^[18–20] polyethers,^[21,22] polythioethers,^[23] polyketones,^[24]

D. Bandelli, J. Alex, Dr. C. Weber, Prof. U. S. Schubert
 Laboratory of Organic and Macromolecular Chemistry (IOMC)
 Friedrich Schiller University Jena
 Humboldtstr. 10, 07743 Jena, Germany
 E-mail: ulrich.schubert@uni-jena.de

D. Bandelli, J. Alex, Dr. C. Weber, Prof. U. S. Schubert
 Jena Center for Soft Matter (JCSM)
 Friedrich Schiller University Jena
 Philosophenweg 7, 07743 Jena, Germany

© 2019 The Authors. Published by WILEY-VCH Verlag GmbH & Co. KGaA, Weinheim. This is an open access article under the terms of the Creative Commons Attribution License, which permits use, distribution and reproduction in any medium, provided the original work is properly cited.

DOI: 10.1002/marc.201900560



vinyl-based polymers,^[25] in particular, the polyester PLA is capable of undergoing stereocomplexation.^[26,27]

Resulting in altered material properties^[28] such as, slower hydrolysis kinetics,^[29] increased temperature stability, higher degree of crystallinity and, therefore, altered mechanical properties,^[26,30] these macroscopic properties are caused by structural features at the molecular level. Structural requirements for PLA stereocomplexation are based on crystallite formation,^[31] conformation of the individual macromolecules in a 10_3 α - or 3_1 helix,^[32] and ultimately tacticity. Playing with the latter, that is, with the configuration at the varying repeating units, actually offers another opportunity to alter polymer properties without even introducing structural isomers as building units.^[12] This can easily lead to different macroscopic properties such as melting temperature T_m , degree of crystallinity or degradation rate. Stereocomplexation of such materials can further be used to widen the application range, offering more opportunities, again simply by blending.

Modern polymer materials must not only be able to meet the requirement of one specific problem but include additional benefit to provide added value. Following nature's example, as in proteins, the introduction of functional moieties to established materials represents a reasonable approach. But how can this be realized for biodegradable polyesters,^[33] a material class that has not had thousands or millions of years of optimization time by the evolution? A small portion of functional monomers incorporated to a well-known matrix could serve the purpose. The combination with stereocomplexation would further expand the window of accessible properties compared to the isolated materials.

We provide an overview of synthetic approaches toward (functional) monomers suitable to produce polyesters, keeping in mind stereoselectivity as an ultimate requirement to produce novel materials suitable for stereocomplexation. Narrowing down the structural variety known for monomers, we briefly introduce opportunities to produce polyesters to finally further concentrate on the materials that have actually been utilized for this purpose. To encourage the scientific community to dive further into the interdisciplinary topic, we complement our review with a short introduction about the methods to produce stereocomplexes and to confirm their existence.

2. Strategies to Synthesize Stereo-Defined Polyesters

Polyesters that have been used for the preparation of stereocomplexes include poly(α -hydroxy acid)s ($P\alpha$ HA) and poly(β -hydroxy acid)s ($P\beta$ HA). $P\alpha$ HA are based on poly(glycolic acid) (PGA), a non-chiral polyester featuring low solubility in common organic solvents. Substitution at PGA's methylene groups results in stereocenters and, hence, in $P\alpha$ HA that could be suited for stereocomplexation (Figure 1). PLA represents the most well-known $P\alpha$ HA capable of stereocomplexation, but several other isotactic $P\alpha$ HA such as, for example, poly(2-hydroxybutyric acid) (P2HB),^[34] poly(2-hydroxy-3-methylbutyric acid) (P2H3MB),^[35] poly(phenyllactic acid) (PPhLA)^[36] or poly(mandelic acid) (PMA)^[37,38] have been synthetically accessed. $P\beta$ HA with stereoinformation represent substituted poly(3-hydroxypropanoic acid)s, several of which are known to undergo stereocomplexation (Figure 1).



Damiano Bandelli was born in Bagno a Ripoli (Florence, Italy) in 1989. He studied chemistry at the University of Florence. After his graduation in 2014 (M.Sc.), he continued his work in the laboratory of Prof. Rosi and Dr. Frediani (University of Florence). Since 2016, he has worked in the research group of Prof. Ulrich S. Schubert at the

Friedrich-Schiller University in Jena as a Ph.D. student. His research is focused on the development of tailor-made (co) polyesters for drug delivery applications.



Christine Weber studied chemistry at the Friedrich Schiller University in Jena (Germany) and carried out her Ph.D. studies in the research group of Prof. Ulrich S. Schubert at Friedrich Schiller University, where she is now a postdoc. Her research interests have since shifted from thermoresponsive polymers to the develop-

ment of functional novel biodegradable materials.



Ulrich S. Schubert performed his Ph.D. studies at the universities of Bayreuth and South Florida. After postdoctoral training at the University of Strasbourg, he obtained his Habilitation at TU Munich in 1999. From 1999 to 2000, he was a professor at the University of Munich, and from 2000 to 2007, he was a full professor at TU

Eindhoven. Since 2007, he has been a full professor at the Friedrich Schiller University Jena, Germany, and director of the Jena Center for Soft Matter. His current research interests include self-healing materials, organic batteries, high-throughput screening technology, and materials for smart delivery of drugs.

$P\alpha$ HA as well as $P\beta$ HA can be obtained via polycondensation or ROP. For both strategies, the corresponding α - or β -hydroxy acids represent the key starting materials introducing chirality. Hydroxy acids are a large family of compounds often found as biological products.^[39] Besides lactic acid, which can be obtained via bacterial fermentation in both enantiomeric

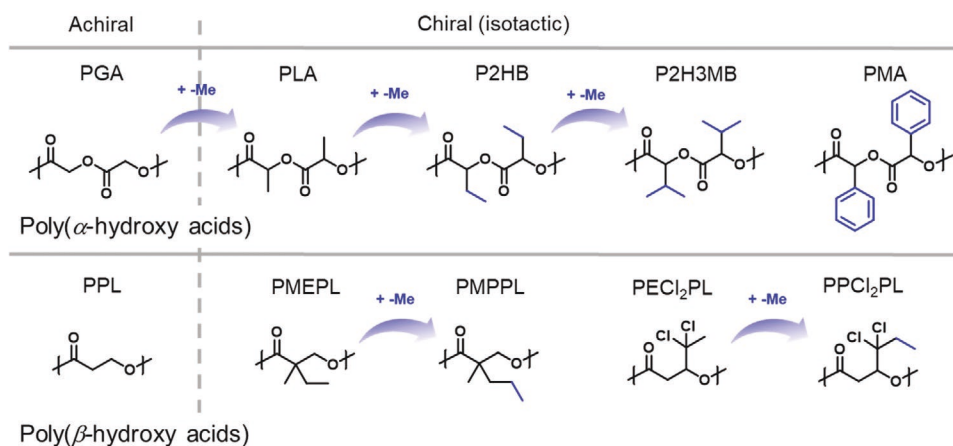


Figure 1. Schematic representation of the poly(α -hydroxy acids) and poly(β -hydroxy acids) potentially suited for stereocomplexation: poly(glycolic acid) (PGA), poly(2-hydroxybutanoic acid) (P2HB), poly(2-hydroxy-3-methylbutanoic acid) (P2H3MB), poly(propiolactone) (PPL), poly(α -methyl- α -ethyl- β -propiolactone) (PMEPL), poly(α -methyl- α -*n*-propyl- β -propiolactone) (PMPPL), poly(α -(1,1-bischloro)ethyl- β -propiolactone) (PECl₂PL), and poly(α -*n*-(1,1-bischloro)propyl- β -propiolactone) (PPCl₂PL).

forms, that is, L- or D-lactic acid,^[40] other α -hydroxy acids such as 2-hydroxybutanoic acid (2HB) or 2-hydroxy-3-methylbutanoic acid (2H3MB) can be synthesized in a similar fashion. In particular, these three monomers are frequently employed for the preparation of polyesters used in stereocomplexation. However, many other α -hydroxy acids are commercially available with high enantiopurity. Examples include 2-hydroxy-3-methylpentanoic acid, 2-hydroxy-3,3-dimethylbutyric acid, mandelic acid, 2-hydroxy-2-phenylpropionic acid, 3-phenyl lactic acid, and 2-hydroxy-2-methyl-3-phenylpropionic acid.

2.1. Polycondensation of α - and β -Hydroxy Acids

Already these simple hydroxy acids represent AB monomers to obtain the corresponding polyesters via polycondensation,^[41] a method that has been known since the first polycondensation of lactic acid was reported by Carothers in 1932.^[6] The approach has since been developed further to increase the molar mass of the PLA accessible by direct polycondensation (Figure 2).^[42,43] Post synthesis modifications through chain coupling or melt

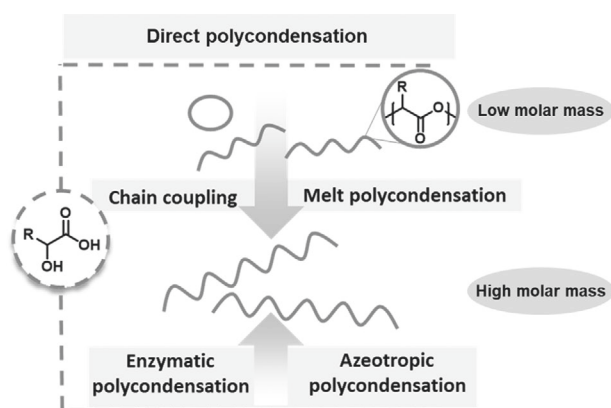


Figure 2. Schematic representation of polycondensation approaches of α -hydroxy acids.

treatment represent two routes that can be applied on a large scale. On the other hand, azeotropic and enzymatic polycondensation^[44] enable the preparation of high molar mass PLA from its α -hydroxy acid monomer.

Whereas polycondensation is used for polymerization of α -hydroxy acids such as lactic acid, 2HB, and 2H3MB, the polycondensation of β -hydroxy acids is less common. It has, to the best of our knowledge, only successfully been reported for a derivative of malic acid, albeit with comparably low molar mass and high dispersity.^[45]

A major benefit of polycondensation is the stereocontrol during polymerization as the configuration at the chiral center of the hydroxy acid is often retained.^[46,47] However, long reaction times, high temperatures and an efficient water removal are required, resulting in a moderate control of molar mass and dispersity.^[46,48]

2.2. ROP of α - and β -Hydroxy Acid Based Monomers

Enabling the tuning of molar masses and low polydispersity values, the ROP of glycolides and β -lactones has become a common procedure to prepare P α HA as well as P β HA, respectively. Stereocontrol is usually granted for ROP of enantiopure monomers,^[49,50] making their preparation a central issue. A large variety of catalysts can be employed to tune the polymerization of such monomers; however, the optimum reaction conditions have to be carefully evaluated based on the reaction mechanism as well as the properties of the monomers.^[14,51–53]

Being less exploited, the ROP of O-carboxyanhydrides (OCAs) represents an alternative route to yield P α HA, whereas the ROP of dioxolanones (DOXs) enables the synthesis of poly(ester ketals) as well as P α HA.

2.2.1. Monomer Synthesis and Polymerization to Yield P α HA via ROP

The stereo-controlled synthesis of cyclic esters from α -hydroxy acids represents a key step for the synthesis of the

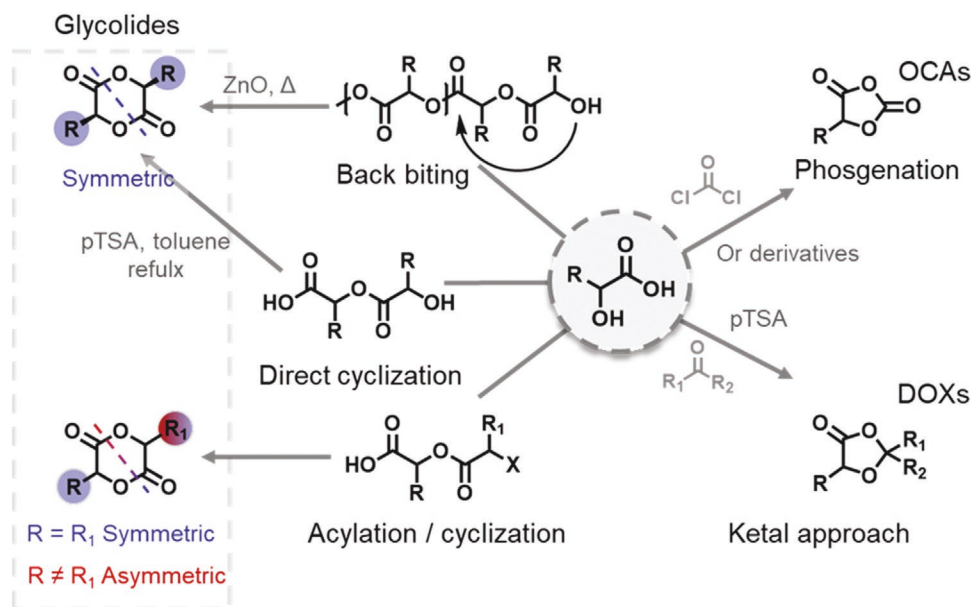


Figure 3. Schematic representation of synthetic strategies to obtain monomers for ROP to obtain P α HAs. pTSA, *p*-toluenesulfonic acid; OACs, O-carboxyanhydrides; DOX, dioxolanones.

corresponding polyesters to be used for stereocomplexation. Initial reports on the formation of cyclic diesters of α HA such as lactic or glycolic acid date back to the 19th century.^[54–56] Nowadays, glycolide (the cyclic diester of glycolic acid) and lactide (the cyclic diester of lactic acid) represent common monomers for the ROP to produce P α HA and are commercially available. All three stereoisomers of lactide, that is, *D*-lactide, *L*-lactide, *meso*-lactide as well as the racemate can be purchased. Prepolymer backbiting and the biotechnological synthesis (Figure 3) are the most common ways to produce lactide industrially.^[8,57] (3*S*,6*S*)-3,6-Diisopropyl-1,4-dioxane-2,5-dione (2 in Figure 4) represents the only other substituted glycolide on the market, to the best of our knowledge. Monomer synthesis hence represents a polymer chemist's first task if new polyester stereocomplexes are targeted.

Taking glycolide as basic structure, a substitution at both or only one methylene moiety leads to symmetric or asymmetric monomers, respectively (Figure 3). Direct cyclization and backbiting of oligomers exclusively yield symmetrically substituted glycolides, whereas asymmetric glycolides can only be produced via the acylation/cyclization pathway. In particular, the latter is suitable to introduce functional moieties, as recently reviewed by Yu et al.^[58] as well as by Becker and Wurm.^[59] The synthesis of OACs has been adopted from the more well-known NCAs,^[60–62] whereas the ketal approach yielding DOX represents a rather new field of research. As central issue with respect to stereocomplexation, we hence focus on enantiopurity of the cyclic esters reported here. It should be noted that, despite the vast series of monomers accessible via different reaction pathways, only few have been utilized for the synthesis of stereo defined polymers and the preparation of stereocomplexes.

Synthesis of Symmetrically Substituted Glycolides: The direct cyclization of α -hydroxy acids is a straightforward technique used for the preparation of symmetrically substituted glycolides

with alkyl,^[63–66] alkynyl,^[67] PEGylated,^[68] and aromatic^[69–71] substituents (Figure 4).

To minimize the formation of oligomers, the cyclization is performed in a diluted solution of the target α -hydroxy acid in toluene or xylenes at reflux conditions employing *p*-toluenesulfonic acid (*p*TSA) as a catalyst. The equilibrium reaction is driven toward the formation of the glycolide derivatives by removal of the condensation byproduct water using a Barrett trap. Typical reaction conditions involve several days of reaction time, as summarized in Table 1. Subsequent to simple purification by means of distillation or recrystallization, the products were obtained in low to moderate yields (15–71%).

Stereochemistry represents a central aspect to be taken into account. In glycolides obtained from chiral α -hydroxy acids, the carbon atoms adjacent to the ester moieties (positions 3 and 6) represent stereocenters (Figure 4). In principle, the two enantiomers with *R,R* and *S,S* configuration, respectively, as well as the *meso* form can result from cyclization.

In the majority of reports the cyclization is performed employing racemic α -hydroxy acids, resulting in a mixture of the two enantiomers and the *meso* form. Representing a diastereomer, the latter can be separated from the mixture of the two enantiomers in *R,R* and *S,S* configuration.^[66] However, when enantiopure α -hydroxy acids are converted, the stereochemistry is retained, as reported by Noga et al.^[71] for the dibenzyloxy functionalized glycolide 9, where epimerization was avoided.

Synthesis of Asymmetrically Substituted Glycolides: To enable access to asymmetrically substituted glycolides, a slightly more laborious route is required. The introduction of asymmetry takes advantage from the difference in reactivity of carboxylic acid derivatives. In a two or three-step synthetic approach, a hydroxy acid is first esterified using a halogen-substituted acyl bromide such as, for example, 2-bromoacetyl bromide, to

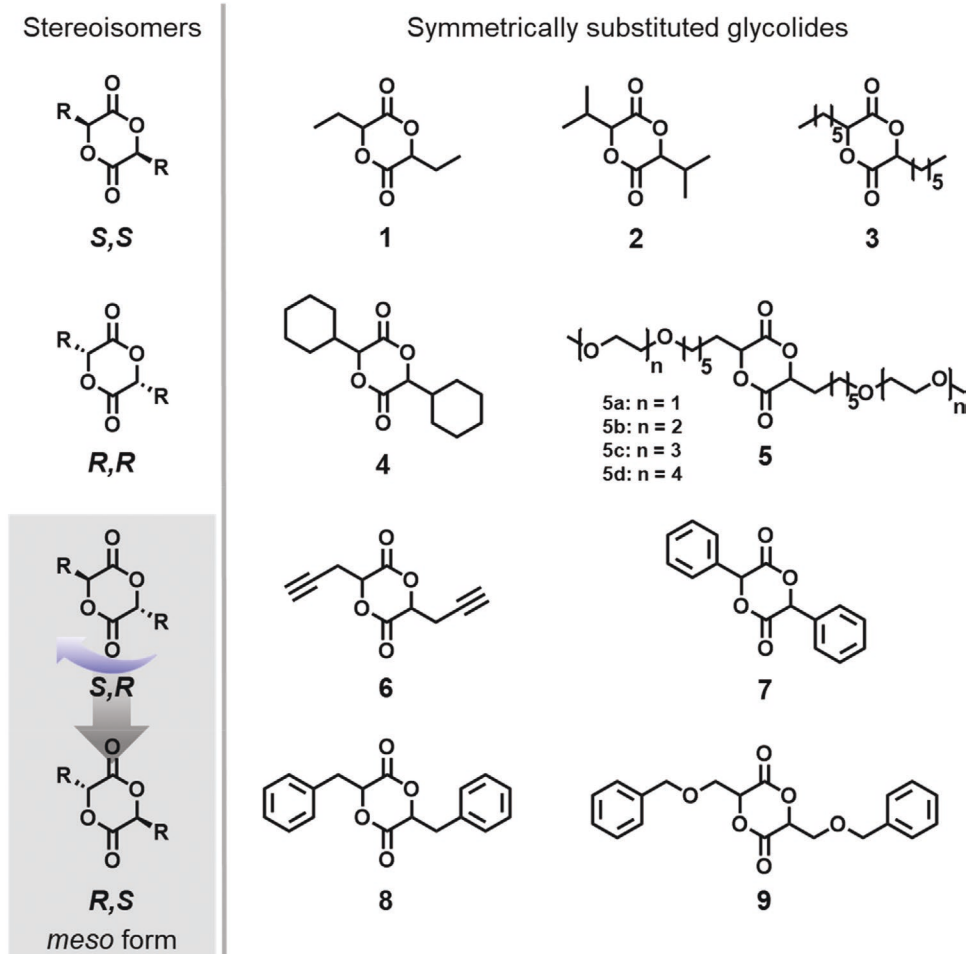


Figure 4. Schematic representation of symmetrically substituted glycolides obtained via the direct cyclization of α -hydroxy acids. Note that the stereoisomers with *R,S* configuration and *S,R* configuration represent identical *meso*-forms for all symmetric glycolides.

Table 1. Experimental overview of the symmetric glycolides obtained from direct cyclization. Structures are depicted in Figure 4.

Entry	Reaction conditions ^{a)}			Stereoisomer ratio RR or SS/ <i>meso</i>	Yield [%]	Ref.
	[α HA][mol L ⁻¹]	Catalyst loading [mol%]	Time[d]			
1	0.14	1	4	1/1	63	[63]
2	0.1	30	6	1/0 ^{b)}	16	[66]
3	0.1	30	4	1/1	65	[63]
	0.06	10	1	mixture	65	[65]
4	0.1	30	6	1/0 ^{b)}	21	[66]
5a	0.06	5	3	n.d.	41	[68]
5b	0.06	5	3	n.d.	28	[68]
5c	0.06	5	3	n.d.	21	[68]
5d	0.06	5	3	n.d.	15	[68]
6	0.09	5	3	mixture	34	[67]
7 ^{c)}	0.07	3	3	1/1	53	[69]
8	0.02	0.8	3	n.d.	42	[70]
9	0.03	2	20	1/0	21	[71]

^{a)}Catalyst: *p*-toluensulfonic acid. Reaction performed in reflux conditions. If not indicated otherwise, toluene was used as solvent; ^{b)}The ratio of the RR and SS forms was 1:1; ^{c)}Xylene was used as solvent.

produce a bromo-substituted carboxylic acid as linear precursor, which is converted to the desired product via an intramolecular nucleophilic substitution under basic conditions. The acylation reaction is either performed in bulk at 75–80 °C, or in solution at 0 or 25 °C in the presence of triethylamine as scavenger for the formed hydrobromic acid (Table 2). Subsequent to purification of the linear precursor, the cyclization step is performed in acetone or acetonitrile under reflux conditions at low concentrations, again employing a base as acid scavenger (e.g., triethylamine, sodium bicarbonate). The acylation as well as the cyclization step have been modified to account for the availability of the two main educts (22, 23, 25), including a replacement of the acyl bromide by a *N,N*-dicyclohexylcarbodiimide (DCC) activated carboxylic acid, as well as an additional Finkelstein reaction prior to the cyclization to increase the leaving group quality during the nucleophilic substitution.^[72]

Based on the acyl bromide used in the linear precursor synthesis, the substituted dilactones are based on glycolide, lactide, or can carry ethyl or other substituents (Figure 5). Singly substituted glycolides feature one asymmetric carbon atom. Hence racemates of the two enantiomers in *R* or *S* configuration are produced from racemic starting materials. For synthetic procedures, starting from other acyl bromides, two stereocenters are usually introduced, resulting in the four stereoisomers depicted in Figure 5.

The acylation/cyclization approach has been applied for the synthesis of a wide range of substituents, including alkyl,^[63,64,73] alkenyl, alkynyl,^[74] halogenated,^[75] PEGylated,^[76] azide-functional,^[74] and aromatic^[72,73,76,77] moieties (Figure 5). Alkenyl, alkynyl, and azide functionalities can serve as moieties for further modification, either at the monomer or in a post polymerization modification via click chemistry.^[59] Moreover, the synthetic route has been adopted for the preparation of substituted morpholine 2,5-diones from α -amino acids,^[78,79] as well as for the synthesis of cyclic diesters with larger ring size, such as salicidellactide (40 in Figure 5).^[77]

A comparison of the direct cyclization (vide supra) with the acylation/cyclization pathway was reported by Yin and Baker^[63] for the symmetrically substituted diethylglycolide (1 in Figure 4) from racemic reactants. The direct cyclization resulted in a higher yield of 63% comprising an equimolar ratio of diastereomers, whereas the two-step reaction yielded 41% of 1 and a decreased fraction of the *meso* form (4:1 mixture of the *R,R/S,S* and *R,S* diastereomers).

It should be noted that, despite the variety of reported asymmetrically substituted glycolides, in particular most compounds including a quaternary carbon atom have not been used as monomers for a ROP but rather served as intermediates for the synthesis of other classes of compounds, as performed by Schöllkopf et al. for 27–37.^[73]

ROP of Glycolides: The ROP of glycolides represents a well-established polymerization approach.^[49,80–82] Used for the industrial production of PLA and PLGA from lactide and glycolide, tin octanoate ($\text{Sn}(\text{Oct})_2$) is one of the most frequently employed catalysts.^[83–85] The polymerization mechanism proceeds via coordination insertion, based on the interaction of the tin center with one of the ester groups of the substituted glycolide and with a suitable initiator (e.g., alcohols). The latter interactions are developed at temperatures higher than 60 °C

and allow good stereocontrol during the polymerization as the configuration of the monomer is retained after the ROP.^[85,86] Besides $\text{Sn}(\text{Oct})_2$, a plethora of metal catalysts based on transition metals^[81,83,87,88] as well as alkaline earth metal complexes^[87,89] are able to promote the polymerization of lactide under mild conditions assuring the control of stereo-information, molar mass and dispersity during the polymerization. Delicate ligand design enables to tune the activity of the catalyst with respect to the stereochemistry of the monomer and, therefore, for example, to produce isotactic, syndiotactic or heterotactic polyesters.^[49,87,90,91]

More recently, metal free approaches led to the development of catalysts mostly based on organic bases,^[92–94] fluorinated alcohols,^[95] phosphazenes, organic acids and *N*-heterocyclic carbenes.^[96–98] These organic catalysts have been used for the ROP of lactide and lactones, assuring the tailoring of molar masses and dispersity of the final polyester. However, in comparison with the reaction mechanism of $\text{Sn}(\text{Oct})_2$, multiple activation pathways have been reported for organic base catalysts for the ROP of lactide and lactones.^[99–103] Several reports describe the tacticity of various PLA obtained from thiourea,^[104] phosphazene,^[105,106] *N*-heterocyclic carbene,^[107] or mTBD^[108] catalysis. Stereocomplexes from PLA obtained via thiourea catalysis have been successfully formed, showing the high potential of organocatalysts in the field, in particular as many are simply commercially available.^[109]

Synthesis and ROP of OCAs: The polymerization of OCAs represents an alternative route to access $P\alpha$ HAs. Providing a brief introduction into the topic, the reader is kindly referred to the excellent reviews by Vaca and Bourissou^[60] as well as by Zhong and Tong^[61] for a more detailed overview.

The synthesis of OCAs was firstly reported by Davies in 1951 from glycolic, lactic as well as mandelic acid with phosgene.^[110] More recently, phosgene has been replaced by diphosgene and triphosgene with similar reactivity,^[111,112] enabling access to a range of OCAs from various α -hydroxy acids (Figure 6). It should be noted that several enantiopure α -hydroxy acids can be obtained from the respective amino acids, as summarized by Basu et al.^[113] as well as Yin et al.^[114] Retaining the configuration of the α -hydroxy acid, the synthetic approach provides the respective OCA in typical yields between 40% and 85%.^[37,110–112,114–118]

Similar to the ROP of glycolides, the ROP of OCAs can be catalyzed by organobases such as DMAP^[111] or other pyridine derivatives,^[37] using alcohols as initiators. Whereas the ROP of a symmetrically substituted glycolide derivative yields the $P\alpha$ HA comprising two repeating units with the proper catalyst,^[108,119,120] the loss of carbon dioxide during the ROP provides the $P\alpha$ HA with a single hydroxy acid as repeating unit (Figure 6).^[111] The release of CO_2 represents also the major driving force for the ROP of OCAs, influencing not only the thermodynamics of the polymerization^[121] but also increasing the polymerization rate in comparison to a ROP of a glycolide under the same experimental conditions,^[111] as reported for the ROP of 42.

Many other catalyst types known from the ROP of glycolides such as *N*-heterocyclic carbenes or various metal-based catalysts are also suited to polymerize OCAs.^[61] In particular for the latter, ligand design enables stereocontrol during the ROP to

Table 2. Experimental overview of the asymmetrically substituted glycolides obtained from the acylation cyclization pathway. Structures are depicted in Figure 5.

Entry	Reaction conditions		Stereoisomer ratio RR:SS/SR:RS	Overall yield [%]	Ref.
	Acylation	Cyclization			
10	2-Bromopropionyl bromide, glycolic acid, 1,4-dioxane, 15 °C, 2 h	DMF, Na ₂ CO ₃ , 90 °C, 2.5 h	Racemate	43	[203]
11	2-Bromoacetyl bromide, 2-hydroxy- butyric acid, NEt ₃ , Et ₂ O, 0 °C, 6 h	Acetone, NaHCO ₃ , reflux, overnight	Racemate	27	[108]
12	1. 2-Bromoacetyl bromide, CH ₂ Cl ₂ , DMAP, 0 °C 2. Allyl-glycolic acid, NEt ₃ , RT, 16 h	DMF, Na ₂ CO ₃ , RT, 16 h	n.d.	40	[204]
13	2-Bromopropionyl bromide, hydroxy acid, ^{a)} bulk, 75–80 °C, 12 h	Acetone, NEt ₃ , reflux, 3 h	n.d.	35	[64]
14			n.d.	40	
15			n.d.	45	
16	2-Bromopropionyl bromide, 2-hydroxy-4-pentynoic acid, DMAP CH ₂ Cl ₂ , NEt ₃ , 0–25 °C, 18 h	DMF, Na ₂ CO ₃ , RT, 46 h	n.d.	41	[205]
17	2-Bromopropionyl chloride, hydroxy acid, ^{a)} NEt ₃ , CH ₃ CN, 0–25 °C, 0.5 h	CH ₃ CN, NEt ₃ , 70 °C, 3 h	n.d.	43	[74]
18			n.d.	46	
19	2-Bromopropionyl bromide, (S)-mandelic acid, NEt ₃ , CH ₃ CN, 0–25 °C, 1 h	Acetone, NaHCO ₃ , reflux, overnight	n.d.	n.d.	[77]
20	2-Bromopropionyl bromide, 2-cyclohexyl-2-hydroxyacetic acid, NEt ₃ , THF, 0–25 °C, overnight	Acetone, NaHCO ₃ , reflux, 2 days	n.d.	59	[66]
21	2-Bromopropionyl bromide, D,L-3-phenyllactic acid, bulk, 90 °C, 12 h	Acetone, NEt ₃ , reflux, 3 h	n.d.	35	[64]
22	2-Bromo-propionic acid, hydroxy acid, ^{a)} bulk, 75 °C, 6 h	1. Acetone, KI, reflux, 12 h 2. Acetone, DIEA, reflux, 9 h	n. d.	40	[72]
23	1. (S)-2-Bromo-propionic acid, HOBT, CH ₂ Cl ₂ , DCC 0–25 °C, 1 h 2. Hydroxy acid, ^{a)} CH ₂ Cl ₂ , 25 °C, 12 h	1. Acetone, KI, reflux, 12 h 2. Acetone, DIEA, reflux, 9 h	n. d.	66	[72]
24	2-Bromopropionyl chloride, hydroxy acid, ^{a)} NEt ₃ , CH ₃ CN, 0–25 °C, 0.5 h	CH ₃ CN, NEt ₃ , 70 °C, 3 h	Mixture	46	[74]
25	1. (S)-2-Bromo-propionic acid, HOBT, CH ₂ Cl ₂ , DCC 0–25 °C, 1 h 2. Hydroxy acid, ^{a)} CH ₂ Cl ₂ , 25 °C, 12 h	1. Acetone, KI, reflux, 12 h 2. Acetone, DIEA, reflux, 9 h	n.d.	70	[72]
26	2-Bromopropionyl bromide, trifluorolactic acid, NEt ₃ , CH ₃ CN, 0–25 °C, 3 h	CH ₃ CN, NaH, 0–25 °C, 3.5 h	1/8	27	[75]
27	2-Bromopropionyl bromide, α-hydroxyisobutyric acid, bulk, 75 °C, 12 h	Acetone, NEt ₃ , reflux, 3 h	n.d.	46	[64]
28	2-Bromopropionyl chloride, hydroxy acid, ^{a)} bulk, 80 °C, 2 h	Acetone, NEt ₃ , 60 °C, 1 h	n.d.	62	[73]
29			n.d.	72	
30			n.d.	75	
31			n.d.	66	
32			n.d.	73	
33			n.d.	85	
34			n.d.	67	
35			n.d.	70	
36			n.d.	85	
37			n.d.	80	
38	2-Bromooctadecanoyl chloride, hydroxy acid, ^{a)} NEt ₃ , Et ₂ O, 0 °C, 5 h	Acetone,	n.d.	12	[76]
39		NEt ₃ , reflux, 16 h	n.d.	10	
40	2-Bromopropionyl bromide, salicylic acid, NEt ₃ , CH ₃ CN, 0–25 °C, 1 h	Acetone, NaHCO ₃ , reflux, overnight	n.d.	n.d.	[77]

^{a)}Please see Figure 5 for the corresponding α-hydroxy acid. HOBT, 1-hydroxybenzo-triazole; DIEA, *N,N*-diisopropylethylamine; DMAP, 4-dimethylaminopyridine; DCC, *N,N'*-dicyclohexylcarbodiimide.

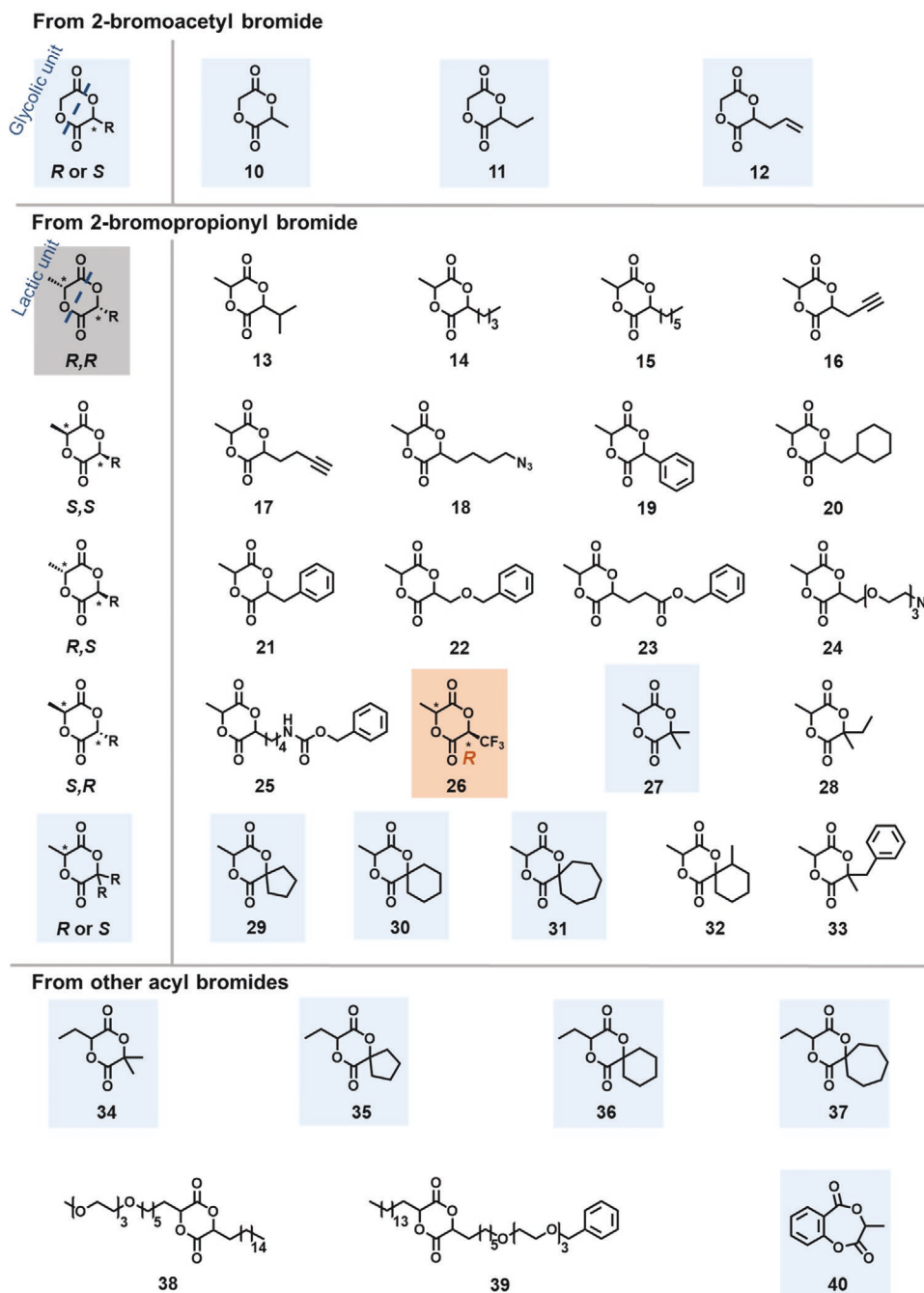


Figure 5. Schematic representation of asymmetrically substituted glycolides obtained via the acylation cyclization of α -hydroxy acids and the related salicidelactide (entry 40). Compounds marked in blue include two possible stereoisomers, whereas the presence of two or more stereocenters results in at least four different stereoisomers for all other compounds. For the compound marked in orange (entry 26) the stereochemistry of the asymmetric carbon is reversed due to the higher priority of the trifluoromethyl substituent.

obtain isotactic polyesters. It should be noted that the experimental conditions and the catalysts have to be carefully evaluated to minimize epimerization for organobase catalysts.^[37] Additional activation by hydrogen bonding through thiourea moieties has been recently reported to give stereoregular poly(43) with both *R* as well as *S* configuration.^[115] Initial differential scanning calorimetry (DSC) experiments even hinted

toward the formation of stereocomplexes, although more detailed analyses have not yet been reported.

Synthesis and ROP of 1,3-Dioxolan-4-ones: Recently the polymerization of 1,3-dioxolan-4-ones (DOXs) yielding P α HA has been reported by Cairns et al. (Figure 7).^[38] This route represents a valid alternative to OCAs and is based on non-toxic and inexpensive resources. Since the work of Cairns et al., only

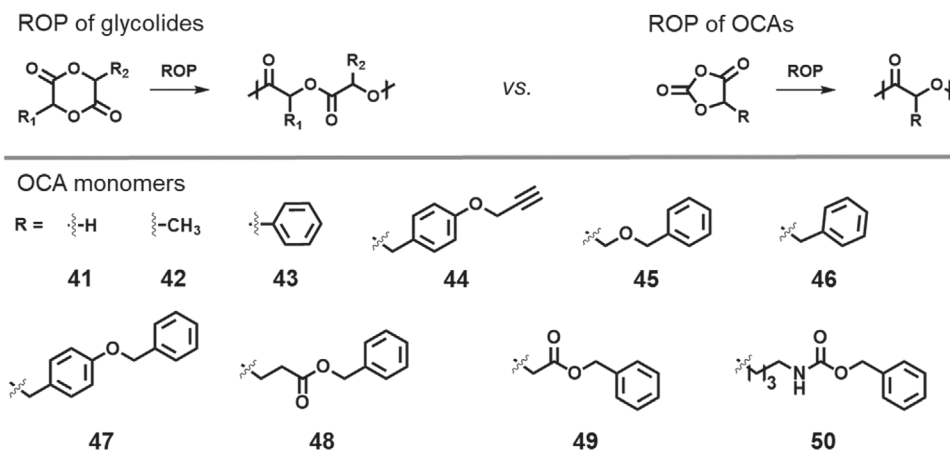


Figure 6. Schematic representation of the ring-opening polymerization (ROP) of *O*-carboxyanhydrides (OCAs) in direct comparison to the ROP of glycolides (top) and schematic representation of OCA monomers (bottom).

a few articles have been published regarding the polymerization of DOXs. However, the according monomers, that is, heterocycles that can be regarded as lactones as well as cyclic ketals, have long been known in the field of organic chemistry.

The synthesis of such compounds can be accomplished via an acid catalyzed reaction of α -hydroxy acids with aldehydes or ketones, respectively (Figure 3). The approach has provided aliphatic, aromatic and fluorinated DOX in yields between 20% and 95% (Figure 7).^[122–124] Interests in the regiochemistry of the conversion of citric or tartaric acid with formaldehyde or acetone from the 1970s^[123,125,126] have further triggered organic chemists to investigate the stereochemistry of the reaction. The configuration of the α -hydroxy acid is retained in 5-position of the DOX, and diastereomers are resulting from a *cis* or *trans* configuration of the substituent in 2-position, which is introduced via the carbonyl compound.^[122]

Modified synthetic routes include the use of, for example, 2,2-dimethoxypropane^[127] or alkynes^[128] as substitutes for acetone or aldehydes, respectively, as well as sophisticated methods to introduce more complex or two different substituents in 5-position of the 1,3-dioxolane ring.^[127,129,130]

The elimination of hydrochloric acid from the halide-substituted DOX **59**, **64**, or **74** yielded the alkylene functional heterocycles **60**, **65**, or **75**, respectively.^[131,132] Miyagawa et al. confirmed the excellent stability of the DOX **65** in the absence of radical initiators.^[132]

As first reported by Hillmyer for the respective 1,3-dioxanones yielding P β HA,^[133] a ROP initiated by an alcohol and catalyzed by Zn(Et)₂ can proceed also for DOX to produce P α HA (Figure 7, top).^[38] It should be noted that low amounts of the catalyst gave rise to poly(ester ketal)s, but at [catalyst ratios] / [initiator] ≥ 1 , exclusively polyesters were obtained.^[38,133] The latter is due to the loss of the carbonyl compound during the ROP via a Tishchenko reaction taking place at the catalytic metal center. The ROP including the elimination of the carbonyl compound proceeded in a more controlled fashion when aluminium-salen complexes were applied as catalysts.^[38,134] The catalysts were also successfully applied for **51–55**, **57–58**, **62**, and **71**. Careful adjustment of the salen ligand as well as the polymerization conditions enabled the preparation of isotactic

PMA.^[38] Organic bases were scarcely investigated for the copolymerization of lactide and **51**,^[38] whereas the standard catalyst Sn(Oct)₂ performed poorly for homopolymerizations of **51**, **52**, and **58** but yielded poly(ester ketal)s in a copolymerization with lactide.^[135] Also cationic homopolymerization of **52** and **67** failed but the ketal moieties could be introduced into a number of copolymers.^[136]

To summarize, the relatively new route to P α HAs has high potential, in particular as the range of monomers has not yet been fully exploited. For example, monomers such as the bis-dioxolanone **63**^[137] could serve as branching moieties to enable access to more sophisticated polymer architectures based on the ROP of DOX. However, a suitable polymerization approach yielding the sole polyester or polyesteracetal species represent challenges to be met if the application of such materials is intended.

2.3. Monomer Synthesis from β -Hydroxy Acids and Their ROP

The synthesis of poly(β -hydroxy acid)s via ROP can be achieved using β -lactones as monomers. Several β -lactones such as β -propiolactone, α - and β -methyl- β -propiolactone are commercially available. A variety of other substituted β -lactones can be obtained via many different reaction pathways that have been comprehensively reviewed.^[45,138] Besides the metal catalyzed insertion of carbon monoxide into epoxides,^[139–141] the recent discovery of β -lactone synthetase, an enzyme that is capable of catalyzing β -lactone synthesis from β -hydroxy acids,^[142,143] should be noted. However, the cyclization of β -bromo functionalized carboxylic acids under alkaline conditions in a nucleophilic substitution reaction represents the most direct route toward β -lactones (Figure 8).^[144] Variations include the usage of other leaving groups or activated carboxylic acid derivatives and hydroxyl groups.^[138]

The stereoselective [2 + 2] cycloaddition of a ketene and an aldehyde or a ketone, respectively, represents an alternative route that was reported by Wynberg and Staring in 1982.^[145] The initial catalyst quinidine^[145,146] has since been modified, resulting in a variety of substituted β -lactones that could

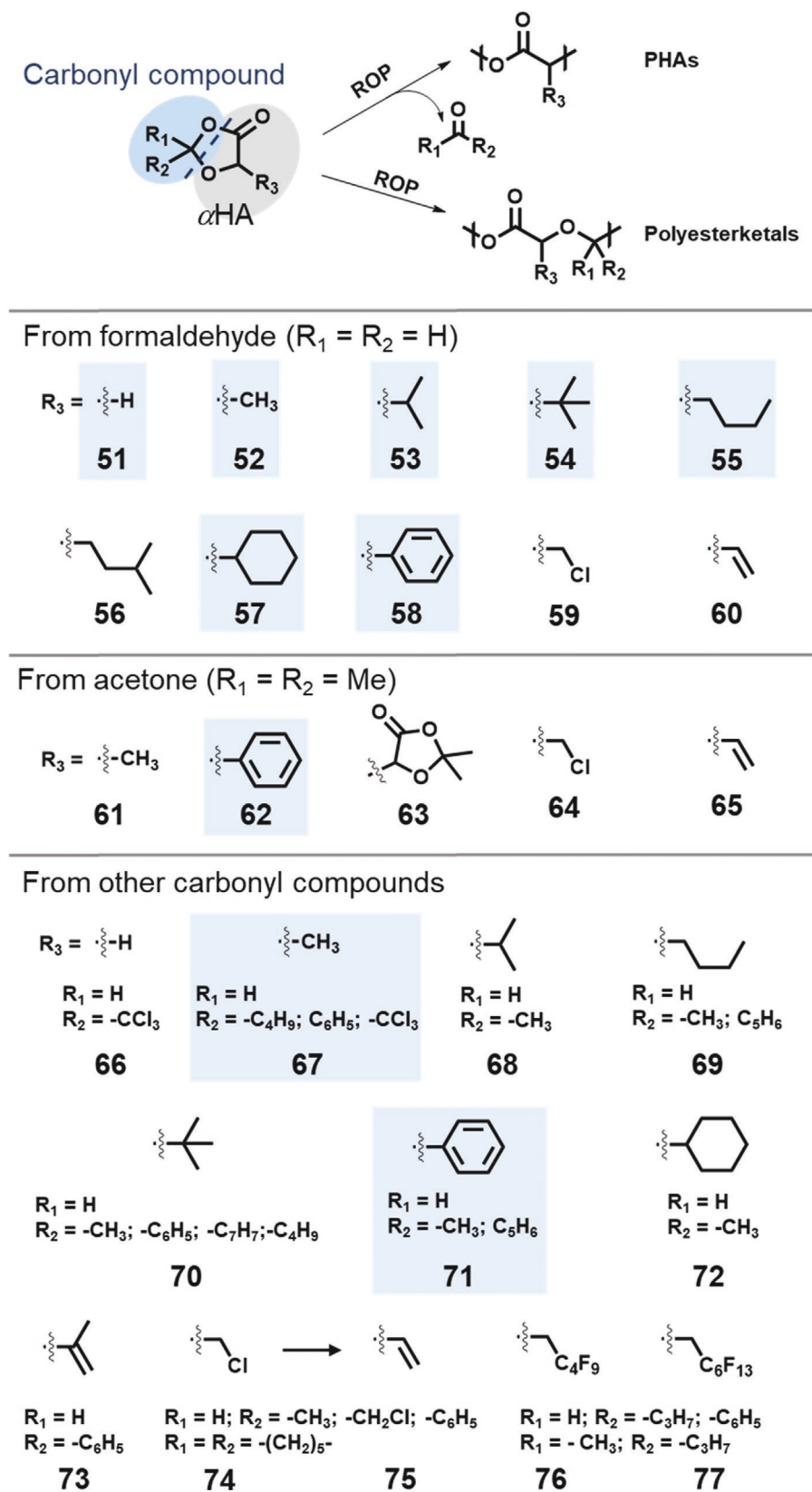


Figure 7. Schematic representation of the ROP of 1,3-dioxolan-4-ones (DOX) yielding P α HA or poly(ester ketal)s and DOX obtained from various α -hydroxy acids via the ketal approach.

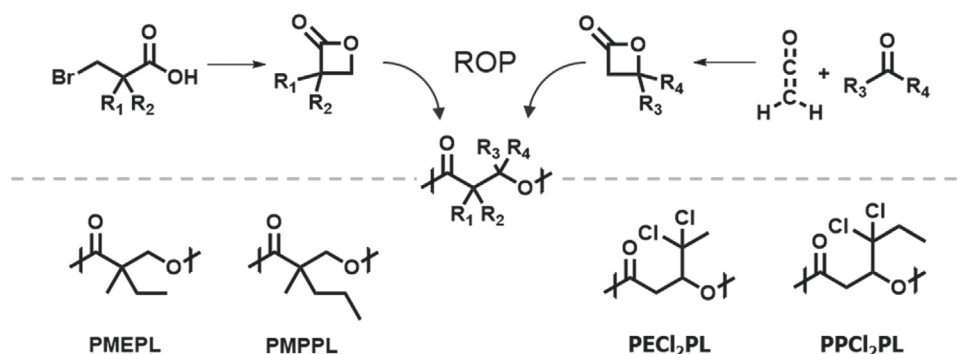


Figure 8. Schematic representation of common strategies to synthesize β -lactones and subsequent ring-opening polymerization to yield $P\beta$ HA.

be obtained with enantiomeric excesses between 65% and 97%.^[147,148] Catalysts such as BF_3 etherate yielded racemic products.^[149]

Similar as the ROP yielding $P\alpha$ HA, the ROP of β -lactones can be performed via anionic, coordination insertion, carbocationic, carbene-based and enzymatic processes.^[51,150,151] Among those mechanisms, the anionic ROP has been applied to obtain $P\beta$ HA used for stereocomplexation because of its excellent control of molar mass and stereochemistry.^[45] The polymerization of 1,3-dioxan-4-ones as alternative route toward $P\beta$ HA is described in Section 2.2.1.^[133]

3. Methods to Investigate Tacticity

The various synthetic routes yielding $P\alpha$ HA as well as $P\beta$ HA enable control of molar masses and dispersity. However, a certain stereoregularity of the obtained polyesters is of utmost importance for the formation of stereocomplexes from these materials. One could expect that the use of enantiopure monomers for the polymerization would result in polyesters with retained configuration. However, epimerization has been

reported,^[49] making the evaluation of tacticity a crucial point before stereocomplexation is attempted.

$P\alpha$ HA feature an asymmetrically substituted sp^3 hybridized carbon atom in α position of each ester moiety. The absolute configuration of two adjacent stereocenters in relation to each other, that is, a diad, can be defined on the basis of the Bovey formalism introduced for polyolefins (**Figure 9**).^[152] If the configuration is the same, that is, $-SS-$ or $-RR-$, an *iso*-diad (*i*) is present, whereas an altered configuration, that is, $-RS-$ or $-SR-$, produces a so-called *syndio*-diad (*s*). Triads and tetrads represent two or three successive diads and are defined in an analogous fashion involving three or four stereocenters, respectively. Transferred to the entire $P\alpha$ HA macromolecule, three major types of tacticities are resulting: In isotactic $P\alpha$ HA, each stereocenter features the same configuration, polyesters revealing alternating *S* and *R* configurations are defined as syndiotactic, whereas a random stereocenter configuration is observed in atactic polymers.

Nuclear magnetic resonance (NMR) spectroscopy represents the analytical technique of choice to determine the tacticity. The PLA methine protons appear as a quartet signal in a ^1H NMR spectrum. For isotactic PLA,^[153] only one quartet

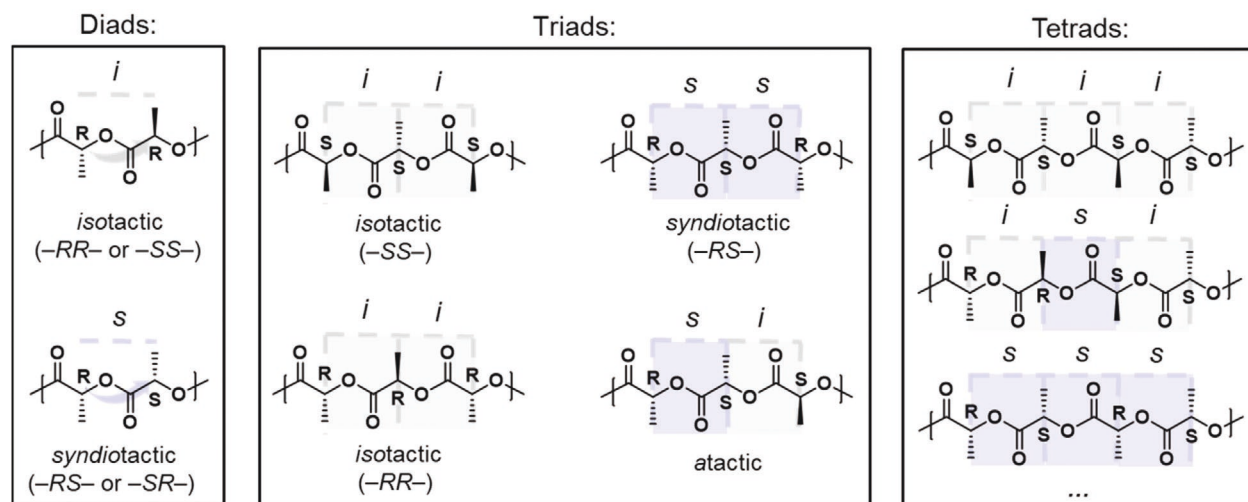


Figure 9. Schematic representation of diads, triads, and tetrads arising from the stereochemistry of PLA.

is observed. When the stereoregularity is disturbed, slightly shifted superimposed signals^[153] are obtained (**Figure 10**), which makes an individual integration or peak fitting very difficult. Through homonuclear decoupling by irradiation of an additional radiofrequency, the spin transitions become saturated and the splitting of all coupling partners with this certain nucleus collapses.^[154] The resulting singulets can be integrated in a much more straightforward fashion, enabling the determination of the stereosequence probability, if the, for example, tetrads, were previously assigned (see below). Although ¹³C NMR spectroscopy provides a better signal resolution, signals assigned to different tetrads may still overlap and cannot be unambiguously assigned.^[155,156] However, if assignments are known, also ¹³C NMR spectroscopy can be used to determine the stereosequence probability.^[157]

2D NMR spectroscopy is required for assignment of the signals in the ¹H and ¹³C NMR spectra and has, to the best of our knowledge, only been unambiguously performed for PLA to date (Figure 10, right).^[158,159] However, the presence of iso-

tactic P α HA can be verified based on ¹H NMR spectroscopy. It should be noted that homonuclear proton decoupling experiments can be helpful, in particular for PLA, but other P α HA such as, for example, PMA, already feature singulett methine signals.^[115]

Because the stereoregularity of polymers influences several properties such as the rotation of polarized light or the thermal properties, methods such as polarimetry or DSC can hint toward the presence of isotactic polyesters. However, as other parameters can exhibit additional influence, these methods should not be utilized as sole proof of tacticity.

4. Methods to Induce Stereocomplexation

Various methods to induce stereocomplexation have been developed during the last two decades,^[160] most of which represent classical procedures reported for PLA and can also be applied for the less common polyesters P α HAs and P β HAs. In

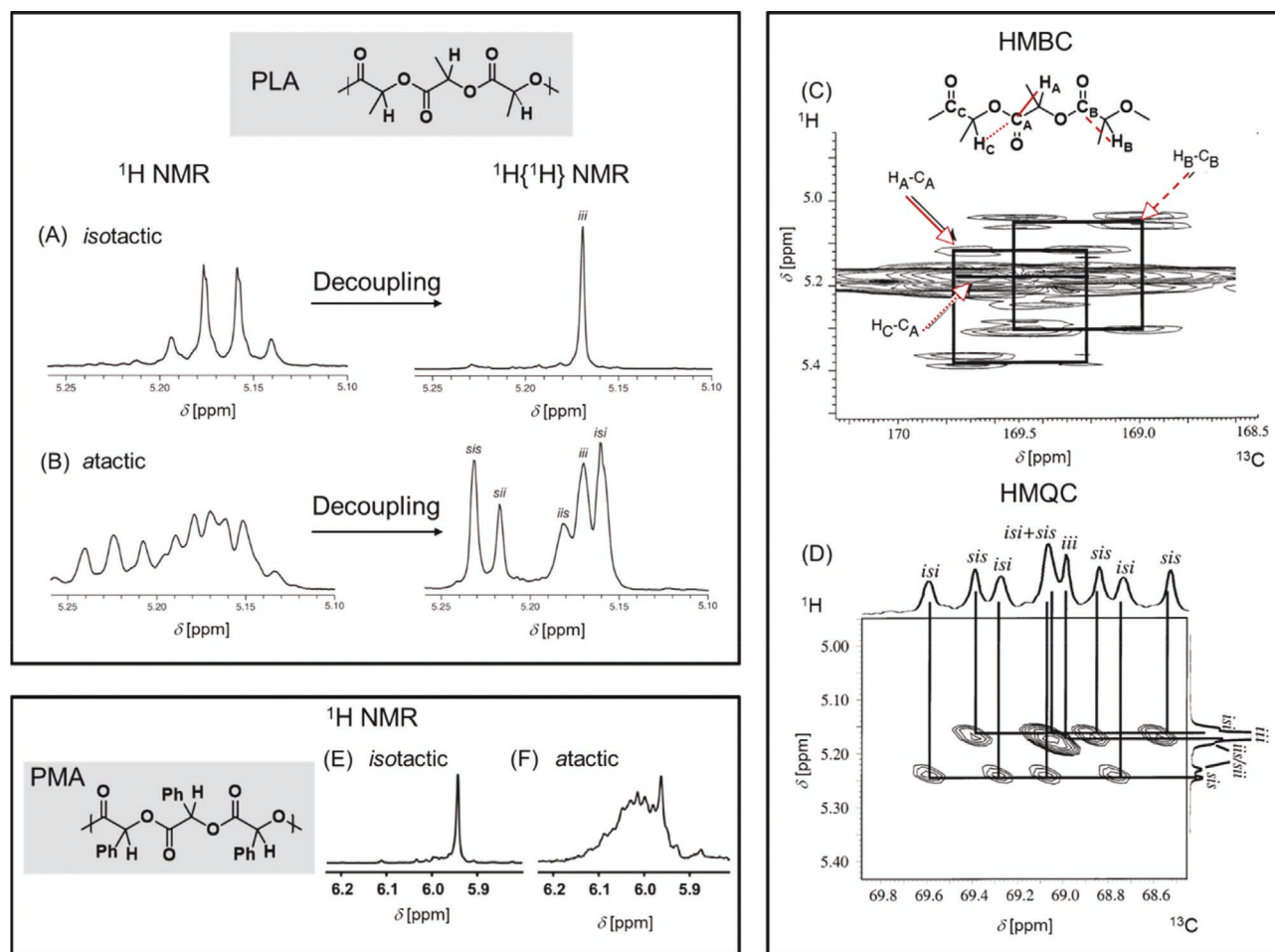


Figure 10. Left (top): Selective homonuclear decoupled ¹H NMR spectrum of A) isotactic and B) atactic PLA producing a singlet from initially quartet signals of the methine protons. Reproduced with permission.^[153] Copyright 2008, American Chemical Society. Right: Experimental NMR data for the evaluation of PLA synthesized using 5% ¹³C labeled L-lactide and 95% D-lactide.^[159] C) Zoomed-in HMBC spectrum in the region of the carbonyl coupling with the methine proton and schematic representation of the couplings. D) HMQC spectrum and full evaluation of tacticity at the tetrad level (see Figure 9). Reproduced with permission.^[159] Copyright 2002, American Chemical Society. Left (bottom): Zoom into the methine proton region of the ¹H NMR spectra of E) isotactic and F) atactic poly(mandelic acid). Reproduced with permission.^[115] Copyright 2019, American Chemical Society.

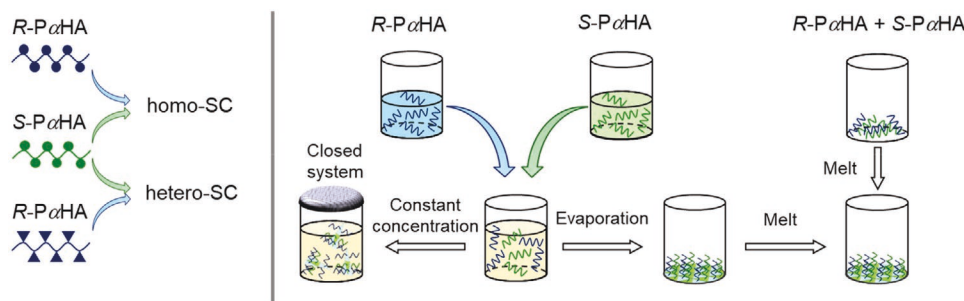


Figure 11. Schematic representation of solvent and melt procedures applied for stereocomplexation.

principle, stereocomplexation can occur whenever two isotactic polyesters of different configuration are present in a system allowing diffusion. Solution^[161] and melting^[162] approaches can be distinguished (**Figure 11**).^[163]

If both polyesters represent the same polymer type, for example, P_LLA is mixed with P_DLA, so-called homo-stereocomplexes (homo-SCs) are obtained. The same process can be applied for the blending of two different polymer types, for example, P_L2HB and P_DLA. The resulting material is called a hetero-SC. The extent of SC in the final material can be varied by the blending ratio of the two components, and the blending of three or more components results in ternary or quaternary stereocomplexes, respectively.^[16]

The solution methods imply the preparation and subsequent mixing of two different solutions containing D- and L-chains, respectively. The basic principle relies on the fact that every substance stays dissolved until a critical concentration is reached. The lower critical concentration of the stereocomplex compared to that of the D- and L-chains represents the driving force for the process. Due to the stronger interactions between stereocomplexes compared to the homopolymers, the good solvent for the homocrystallites becomes a poor or non-solvent for the stereocomplex. Chloroform,^[164] dichloromethane,^[165] THF at room temperature,^[166] or acetonitrile at ≈80 °C represent solvents suitable for this purpose.^[167] While PLA stereocomplexes from chloroform produced rather films,^[168] the precipitates from THF can be nanoparticles.^[166] At sufficient crystal thickness, stereocomplexes remain insoluble at elevated temperatures.^[26]

It should be noted that the concentration of the mixture can be kept constant, or the solvent is allowed to evaporate slowly, thereby increasing the concentration of the polymer mixture (solution casting). In general, solution casting is faster than the “constant concentration” method. The increase of the concentration in the solvent evaporation method is an additional driving force for SC formation.^[26]

Crystallization from the melt is probably the most frequently applied method. Either the solution casting sample is used for crystallization, or another bulk mixture is heated and quickly cooled to a certain crystallization temperature (T_c). Typically, T_c values are chosen between the T_m of the homocrystallites and the T_m of the stereocomplex crystallites.^[169,170] Other methods are quenching of the melt and subsequent crystallization by raising the temperature to a fixed T_c .^[171] However, the most straightforward way is simply crystallization during cooling from the melt.^[171]

5. Methods to Investigate Stereocomplexation

When isotactic polyesters with different configurations are mixed, the associative interactions between the chains of different configurations can prevail over the interactions of the parent polyesters entailing stereocomplexation. Due to the new stereoselective interactions, a different macromolecular packing is obtained, leading to a variation of the thermal as well as the mechanical properties of the final material. These properties can be used to verify the SC formation on an analytical basis.

In fact, DSC as a method to determine thermal properties of bulk materials is important not only for estimating suitable conditions for processing of materials from the melt, but it represents the usual and easily accessible way to investigate the success of an attempted stereocomplexation process. As depicted in **Figure 12** (left) for P2HB, the T_m of the two isotactic polymers in R or S configuration, respectively, is significantly lower compared to the T_m of the stereocomplex,^[172] a fact that is generally observed for polyester homo-SCs. In addition, the enthalpy of fusion ΔH_m of the homo-SCs is increased compared to that of the single components (See section 6).

Wide-angle X-ray scattering (WAXS) represents a complementary method to monitor stereocomplexation because the SC crystallites vary in lattice distances compared to crystallites of the pure isotactic polymer crystallites (Figure 12, right). As a consequence, WAXS represents a more sensitive method that is capable of following SC formation even if DSC results remained inconclusive.^[35] The combination of DSC and WAXS is hence a common and suitable approach to investigate novel SC materials.

In particular, to monitor the formation, the growth and morphology of SC crystallites over time, imaging methods such as polarized light microscopy (PLM) and atomic force microscopy (AFM) are very valuable.^[173,174] As depicted in **Figure 13** for the crystallization of P2HB,^[175] the radial growth rate of spherulites can be determined via PLM, whereas the laminar growth rate is accessible from AFM. The evaluation of radial growth rates revealed that SC crystallization occurred at higher temperatures but with significantly increased rate compared to homocrystallization. This shows that conditions for SC formation represent a major factor to be considered when tailoring the blend material properties. It should be noted that also data related to mechanical properties can be extracted from AFM, which can provide a

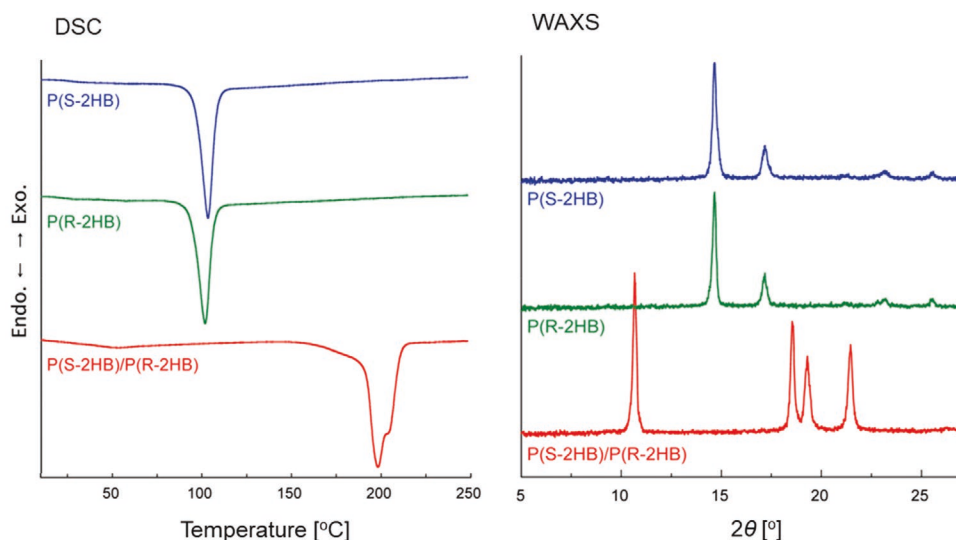


Figure 12. Thermal and WAXS analysis on the sole P2HB and the stereocomplex. A) DSC thermograms; B) WAXS analysis. Reproduced with permission.^[172] Copyright 2009, American Chemical Society.

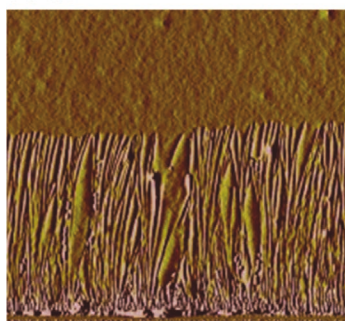
first indication with respect to application fields of these materials at an early stage of research.^[176]

Spectroscopic methods such as solid state NMR, Infrared or Raman spectroscopy are capable of tracking conformational changes, which occur during stereocomplexation.^[177–179] Although it was difficult to distinguish the SCs of Poly(α -methyl- α -ethyl- β -propiolactone) (PMEPL) from atactic species by solid state NMR spectroscopy in 1992,^[180] the instrumental possibilities have since significantly improved, enabling detailed insights into the structure of crystalline as well as amorphous regions for PLA SCs.^[181,182]

6. Homo-SCs

Homo-SCs represent the simplest type of SC as they are formed by blending the same polymer type in L and D configurations, respectively. As only two components are used for SC formation, homo-SCs represent binary SC. Access to the two isotactic polymers with opposite configuration is a clear prerequisite. There are hence only few polyester homo-SCs reported. These include the SCs from the P α HA (PLA,^[183] P2HB,^[34,172] P2H3MB^[35]), and the SCs from the P β HA (PMEPL,^[183,196–198] poly(α -(1,1-bis(chloro)ethyl- β -propiolactone)

AFM



PLM

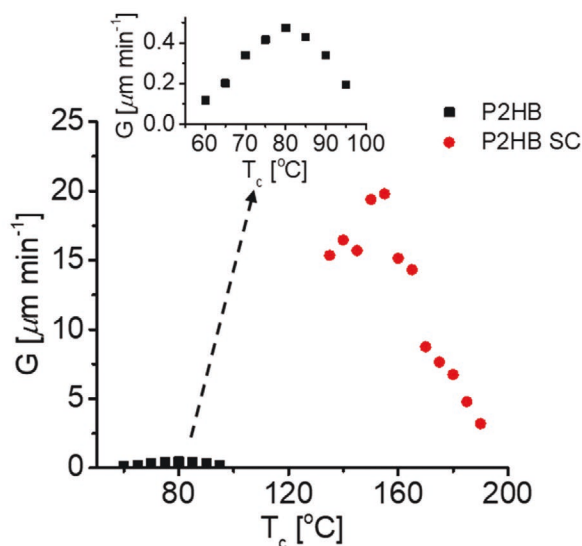


Figure 13. Investigation of SC crystallization of P2HB by means of AFM and PLM. PLM was used to determine the radial growth rates G that are plotted versus the crystallization temperature T_c . Adapted with permission.^[175] Copyright 2017, Elsevier.

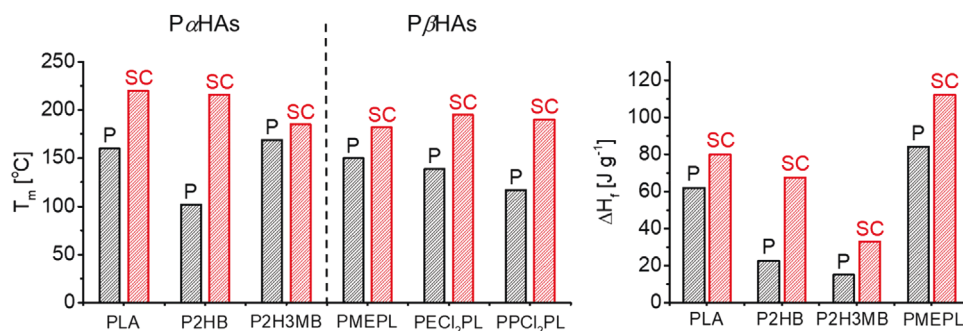


Figure 14. Melting temperatures T_m and enthalpies of fusion ΔH_f of crystallites of polyester homo-SC in direct comparison with the respective values of the isotactic polyesters. The ratio of the PLHA and P β HA was kept as 50:50 (wt%) during SC formation. Data were taken from literature publication (PLA,^[183] P2HB,^[188] P2H3MB,^[35] PMEPL,^[187] PECL₂PL,^[184] PPCL₂PL^[184]).

[PECL₂PL],^[184] poly(α -*n*-(1,1-bischloro)propyl- β -propiolactone) [PPCL₂PL]^[184]). The fourth homo-SC from the P α HA PMA has only very recently been suggested based on preliminary DSC investigations.^[115]

In general, DSC measurements indicated elevated T_m of SC crystallites compared to those of the pure isotactic P α HAs and P β HA (Figure 14). Although not reported for all SCs, the same trend can be observed considering the enthalpies of fusion ΔH_f .

Considering the substituents in α -position, the P α HA capable of SC formation feature substituents with increased steric demand (a methyl substituent for PLA, an ethyl substituent for P2HB, and an isopropyl substituent for P2H3MB). Although no clear trend is visible with respect to T_m , the ΔH_f of the crystallites systematically decreases with increasing bulkiness of the substituent for both, the crystallites of the isotactic polymers and the homo-SC crystallites. It should be noted that a complete resolution of the helical structures in the SC crystallites of P α HAs has, to the best of our knowledge, only been achieved for PLA so far.^[32] However, the higher spacing values obtained from WAXS analysis indicated that the higher steric hindrance of the substituents also increased the unit cell size for P2HB^[172] as well as P2H3MB.^[35]

Only the homo-SCs from the P β HA PMEPL and the P α HA P2HB were investigated in more detail. Research on PMEPL SCs has been conducted by Prud'homme and co-workers since 1984.^[185] Based on isotactic enantiopure P_LMEPL and P_DMEPL, the SC was formed. Additional blending with atactic polyester or excess of one enantiopure PMEPL isomer revealed that the crystallization of the SC controlled the morphology of the sample. The binary homo-SCs were further investigated by X-ray diffraction^[186] and solid state NMR^[180] studies to examine the SC structure in more detail. Crystallization from the melt resulted in crystallites of isotactic PMEPL in a zigzag conformation, whereas SC formation yielded a 2₁ helical structure and an increased unit cell. In an investigation regarding the effect of molar mass on the SC formation,^[187] P_DMEPL (molar mass [M_n] \approx 2 kg mol⁻¹) was blended via a solution approach with P_LMEPL of M_n between 3 and 33 kg mol⁻¹ in a 1:1 ratio. The SC formation was favored when blending polymers of opposite configuration with similar molar masses. Variation of the feed ratio during stereocomplexation revealed that the SC crystallites acted as a nucleation agents inducing the crystallization of the isotactic polymer used in excess.

The SC formation of the P α HA P2HB has been investigated in the Tsuji lab within the last decade.^[172] Initially, solution and melting approaches were compared for oligomeric species ($M_n \approx$ 3 kg mol⁻¹, $\bar{D} \geq$ 3.7), showing that melt crystallization resulted in more well-defined homo-SCs. Interested in a further comparison of properties of the SC material with the isotactic P2HB, the thermal and hydrolytic degradation was studied for higher molar mass P2HB ($M_n \approx$ 16 kg mol⁻¹).^[188] Whereas stereocomplexation did not affect thermal degradation, the hydrolytic degradation of the SC was significantly delayed due to a faster hydrolysis of amorphous domains, which were present to a lesser extent in the SC material. The effect of the molar mass of P2HB on the stereocomplexation process was investigated by combining six pairs of the isotactic P α HA of different configuration at similar M_n from 0.75 to 26 kg mol⁻¹.^[34] Whereas solution casting resulted in the formation of the sole stereocomplex, melt crystallization at 70 °C yielded a mixture of homo and SC crystallites. Elevated crystallization temperatures were needed to increase the fraction of SC crystallites.

7. Hetero-SCs

Hetero-SCs are formed when two different polymer types of *R* and *S* configuration are blended. The mixing of more than two components is also possible (Figure 15). The increasing level of complexity from homo-SCs, over binary hetero-SCs to ternary or even quaternary SCs makes the analysis by means of DSC and WAXS a challenging task. In this respect, a detailed comparison with analytical data of blends of the same configuration (where stereocomplexation can be excluded) can certainly be helpful. However, it should be clearly stated that even for binary blends, the structure of crystallites in a blend might be altered by other effects such as epitaxy. Hence, a stereocomplex is not necessarily formed, as reported by Prud'homme for the binary system PMEPL/PMPPL (poly(α -methyl- α -*n*-propyl- β -propiolactone)).^[189,190] In addition, partial SC formation has been observed while crystallites of the initial compounds remained visible, as reported for the binary hetero-SC formation of PLA and P2HB.^[191] On the other hand, the hetero stereocomplexation of P_L2HB and P_D2H3MB proceeded smoothly via solution casting as well as melt blending.^[192]

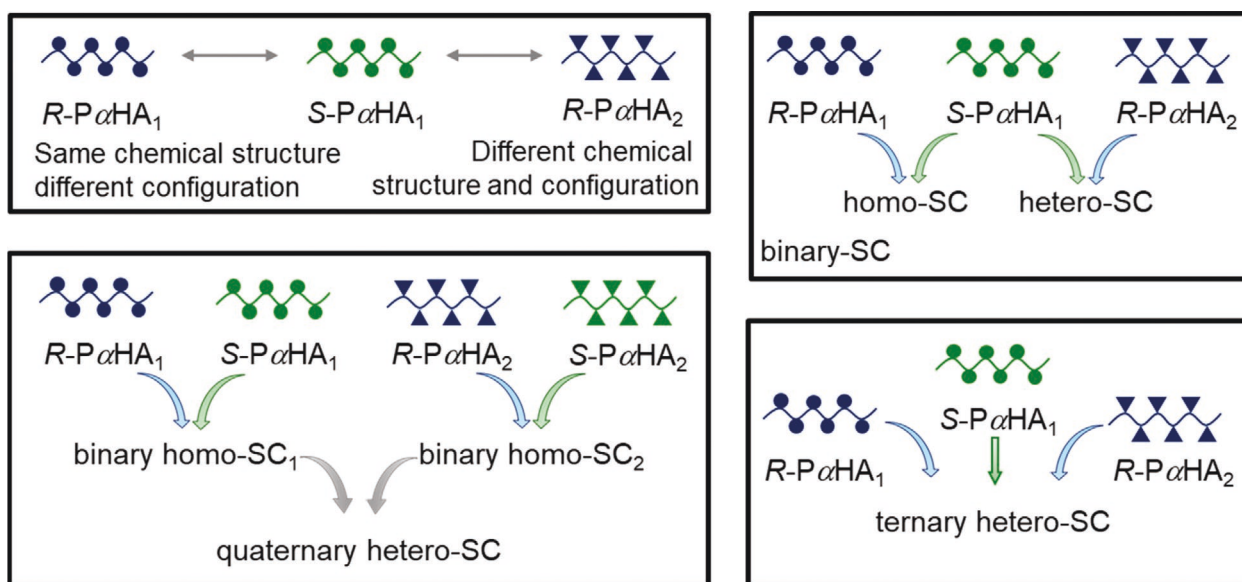


Figure 15. Schematic representation of the stereocomplexation of P α HAs yielding binary, ternary, and quaternary SCs.

7.1. Binary Hetero-SCs Composed of PLA and P2HB

The hetero-stereocomplexation of P2HB and PLA was investigated comprehensively in the Tsuji lab. Initially, P_L2HB synthesized by polycondensation and linear P_DLA obtained by ROP of D-lactide were blended in equal mass fractions.^[191] DSC and WAXS analysis indicated that SC formation via melt crystallization was unsuccessful but solution casting yielded partial crystallization in form of a hetero-SC. The melt crystallization conditions were further optimized by varying crystallization temperatures in feed ratios of 25, 50, and 75 mass% of the homopolymers in the binary blends (Figure 16, left).^[193] In fact, hetero-SCs could only be obtained by crystallization at around 160 °C, whereas amorphous blends were obtained at higher temperatures. Partially homocrystallites were formed upon crystallization at lower temperatures. PLM data suggested that the formation of stereocomplexes occurred at

the interface between the PLA and P2HB domains in these mixtures.

Additional variation of the polyester architecture by utilization of four-arm star-shaped polyesters synthesized by polycondensation using pentaerythritol further complicated the system, perturbing the formation of hetero-SC crystallites (Figure 16, right).^[194] Maintaining an equimolar ratio of P_LLA and P(_D2HB) in a P(_D2HB)-*b*-P_LLA block copolymer enhanced the SC formation of the two blocks of opposite configuration during melt crystallization, enabling the exclusive formation of SC crystallites in a wide crystallization temperature range from 70 to 160 °C.^[195]

7.2. Ternary and Quarternary Blends

SC formation and analysis are not straightforward already for binary hetero-SCs. The effects of the addition of a third

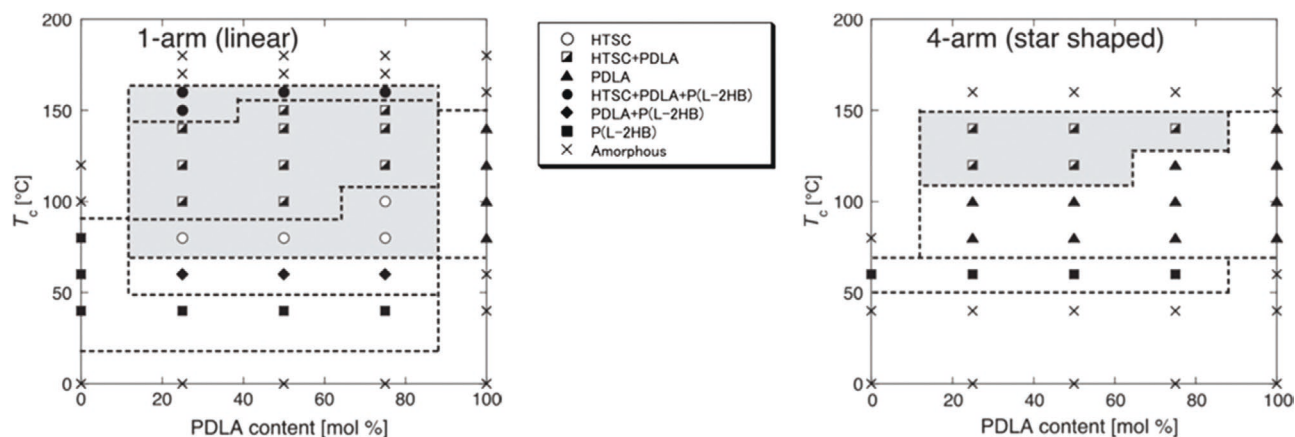


Figure 16. Formation of homo- and hetero-SC crystallites from P_DLA and P_L2HB by melt crystallization at varying temperatures T_c . Left: Linear P_DLA and P_L2HB. Right: 4 Arm star-shaped P_DLA and P_L2HB (HTSC, hetero stereocomplex). Adapted with permission.^[194] Copyright 2014, Wiley-VCH.

component were investigated by Tsuji and co-workers for ternary blends of PLA, P2HB and P2HB. PLM as additional characterization tool was of utmost importance, as sole analysis by means of DSC and WAXS was not sufficient to unravel the multiple crystallite types that were formed in such a complex blend. The addition of 10% of SCs resulted in an increased crystallization rate of the PLLA matrix.^[196] More specifically, P2HB homo-SC crystallites as well as Pd2HB/PLLA hetero-SC crystallites acted as nucleation agents during non-isothermal crystallization from the melt as well as during isothermal crystallization by heating. Variation of the PdLA, PL2HB, and Pd2HB ternary blend composition resulted in the formation of ternary SC crystallites with higher T_m as well as degree of crystallinity compared to those of the respective binary SCs at certain crystallization conditions, suggesting a random incorporation of PdLA and Pd2HB chains in the SC crystallites formed with PL2HB chains.^[197] Similar findings were reported using the even more complex quarternary blend of PL2HB/Pd2HB and PL2H3MB/Pd2H3MB, showing that quarternary SCs could be realized.^[198]

8. Conclusion and Future Perspectives

The P α HA PLA represents a well-investigated polymer with respect to SC formation.^[26] On the other hand, other polyesters have been scarcely investigated in this respect, although enantioselective monomer as well as polymer syntheses enable access to a multitude of new materials that could potentially be suitable for this purpose because isotactic polyesters have been or could theoretically be produced (Figure 17). Despite the current lack of comprehensive data, first structure property relationships can be deduced, showing that the steric hindrance induced by substituents plays a major role during tuning of

T_m and crystallinity of the SC materials. One should, however, consider that SC formation might not always be successful, as reported for PPhLA^[36] as well as for the blend of P3HB with PLA.^[199]

It should be noted that potential novel materials of that type require access to the, sometimes also novel, isotactic polyester of both configurations. With respect to avoiding this challenge, the statistical copolymerization of two monomers has to be stressed, as the variation of many properties is straightforward. One comonomer would serve the purpose of inducing stereocomplexation, whereas another comonomer would add additional functional features to the material if SC formation remains unperturbed, as in the case of PLGA.^[165] A multitude of interesting candidates (potentially) suitable for ROP copolymerization are described in Section 2 of this review.

It has been pointed out that, aside from PLA, the majority of P α HA used for SC formation have been obtained via polycondensation approaches. However, the use of mixed dimers for polymerization as reported for poly(lactic-*alt*-glycolic acid),^[200] or the combination with cross-metathesis polymerization as reported for poly(lactic-*alt*-caprolactic acid)^[201] represent recent approaches to further expand the range of accessible polyesters capable of SC formation. The regioselective copolymerization of cyclic anhydrides and epoxides is another unusual but very promising route to obtain alternating copolyesters,^[202] hinting toward the fact that isotactic alternating copolymers can undergo stereocomplexation in a similar fashion as isotactic homopolymers.

Substituted PCL analogs offer a vast parameter space for creating novel polyesters with defined tacticity. However, the corresponding lactone monomers for ROP are mainly available as racemates, a fact that could encourage organic chemists to make enantiopure starting materials more easily available

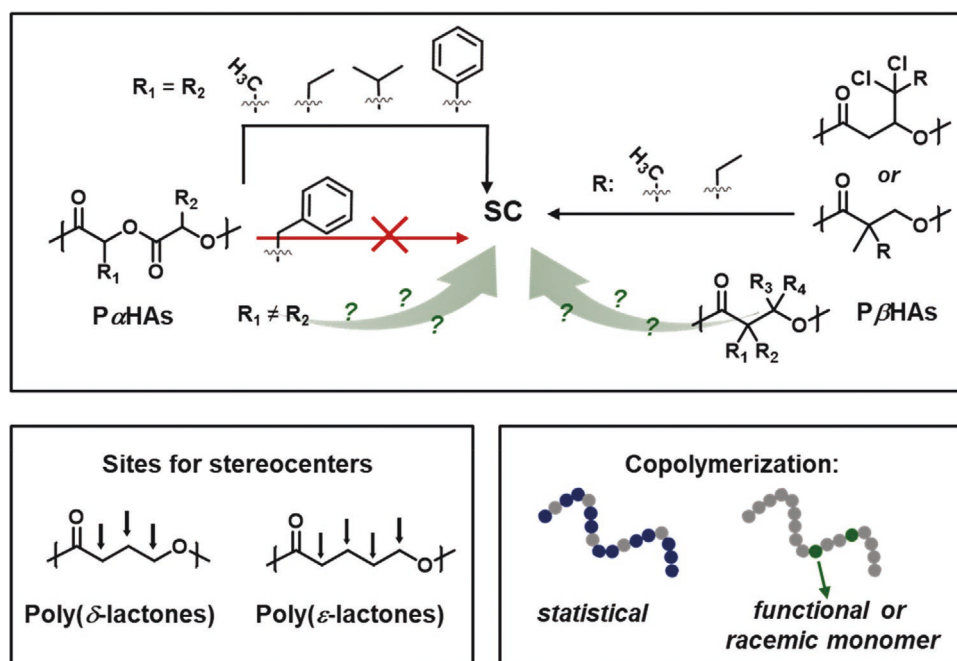


Figure 17. Schematic representation of P α HA and P β HA employed for stereocomplexation and opportunities to create novel SC materials by using alternative monomers and polyesters.

in order to investigate the resulting polyesters with respect to potential SC formation.

Synthetic polymer chemists are always eager to increase the level of complexity of available polymer architectures, including block, star-shaped, or graft copolymers. Whereas this could certainly be done for many isotactic P α HA and P β HA in a similar fashion as it has been achieved for PLA,^[26] the resulting materials would probably not be available in sufficient amounts to strive for large-scale industrial applications. On the other hand, a vast series of parameters based on the blending method can be adjusted in order to access new materials, which represents the material scientist's way to tailor the properties of materials. In addition, only small variations of an established macromolecule can have tremendous effects on the material properties, for example, by including additional features through copolymerization. Hence, the current request for sustainable new materials applicable in the biomedical field as well as for commodity polymers can only be met by maintaining the living cooperation between these two major fields of polymer research.

Supporting Information

Supporting Information is available from the Wiley Online Library or from the author.

Acknowledgements

This work was supported by the DFG-funded Collaborative Research Centre PolyTarget (SFB 1278, projects A06 and Z01).

Conflict of Interest

The authors declare no conflict of interest.

Keywords

poly(α -hydroxyacid)s, poly(β -hydroxyacid)s, polyesters, ring-opening polymerization, stereocomplexes

Received: October 22, 2019

Revised: November 15, 2019

Published online: December 3, 2019

- [1] F. Kabirian, B. Ditekowski, A. Zamanian, R. Heying, M. Mozafari, *Mater. Today Proc.* **2018**, *5*, 15586.
- [2] S. Aftab, A. Shah, A. Nadhman, S. Kurbanoglu, S. Aysil Ozkan, D. D. Dionysiou, S. S. Shukla, T. M. Aminabhavi, *Int. J. Pharm.* **2018**, *540*, 132.
- [3] E. Swider, O. Koshkina, J. Tel, L. J. Cruz, I. J. M. de Vries, M. Srinivas, *Acta Biomater.* **2018**, *73*, 38.
- [4] N. Olov, S. Bagheri-Khoulenjani, H. Mirzadeh, *J. Biomed. Mater. Res., Part A* **2018**, *106*, 2272.
- [5] L. N. Woodard, M. A. Grunlan, *ACS Macro Lett.* **2018**, 976.
- [6] W. H. Carothers, G. L. Dorough, F. J. van Natta, *J. Am. Chem. Soc.* **1932**, *54*, 761.

- [7] C. E. Lowe (El du Pont de Nemours and Co.), *US2668162A*, **1954**.
- [8] C. Gao, C. Ma, P. Xu, *Biotechnol. Adv.* **2011**, *29*, 930.
- [9] L. T. Lim, R. Auras, M. Rubino, *Prog. Polym. Sci.* **2008**, *33*, 820.
- [10] J. M. Becker, R. J. Pounder, A. P. Dove, *Macromol. Rapid Commun.* **2010**, *31*, 1923.
- [11] D. Garlotta, *J. Polym. Environ.* **2001**, *9*, 63.
- [12] R. A. Jain, *Biomaterials* **2000**, *21*, 2475.
- [13] J. M. Anderson, M. S. Shive, *Adv. Drug Delivery Rev.* **1997**, *28*, 5.
- [14] D. K. Schneiderman, M. A. Hillmyer, *Macromolecules* **2016**, *49*, 2419.
- [15] G. Barouti, C. G. Jaffredo, S. M. Guillaume, *Prog. Polym. Sci.* **2017**, *73*, 1.
- [16] J. Slager, A. J. Domb, *Adv. Drug Delivery Rev.* **2003**, *55*, 549.
- [17] L. Pauling, R. B. Corey, *Proc. Natl. Acad. Sci. USA* **1953**, *39*, 253.
- [18] T. Yoshida, S. Sakurai, T. Okuda, Y. Takagi, *J. Am. Chem. Soc.* **1962**, *84*, 3590.
- [19] I. Iribarren, C. Alemán, C. Regaño, A. Martínez de Ilarduya, J. J. Bou, S. Muñoz-Guerra, *Macromolecules* **1996**, *29*, 8413.
- [20] M. Tsuboi, A. Wada, N. Nagashima, *J. Mol. Biol.* **1961**, *3*, 705.
- [21] H. Sakakihara, Y. Takahashi, H. Tadokoro, N. Oguni, H. Tani, *Macromolecules* **1973**, *6*, 205.
- [22] K. L. Singfield, G. R. Brown, *Macromolecules* **1995**, *28*, 1290.
- [23] P. Dumas, N. Spassky, P. Sigwalt, *Macromol. Chem. Phys.* **1972**, *156*, 55.
- [24] Z. Jiang, M. T. Boyer, A. Sen, *J. Am. Chem. Soc.* **1995**, *117*, 7037.
- [25] T. G. Fox, B. S. Garrett, W. E. Goode, S. Gratch, J. F. Kincaid, A. Spell, J. D. Stroupe, *J. Am. Chem. Soc.* **1958**, *80*, 1768.
- [26] H. Tsuji, *Macromol. Biosci.* **2005**, *5*, 569.
- [27] Y. Ikada, K. Jamshidi, H. Tsuji, S. H. Hyon, *Macromolecules* **1987**, *20*, 904.
- [28] M. Saravanan, A. J. Domb, *Eur. J. Nanomed.* **2013**, *5*, 81.
- [29] H. Tsuji, *Biomaterials* **2003**, *24*, 537.
- [30] X. Shi, Z. Jing, G. Zhang, *J. Polym. Res.* **2018**, *25*, 71.
- [31] K. Tashiro, N. Kouno, H. Wang, H. Tsuji, *Macromolecules* **2017**, *50*, 8048.
- [32] T. Okihara, M. Tsuji, A. Kawaguchi, K.-I. Katayama, H. Tsuji, S.-H. Hyon, Y. Ikada, *J. Macromol. Sci., Part B: Phys.* **1991**, *30*, 119.
- [33] R. Tong, *Ind. Eng. Chem. Res.* **2017**, *56*, 4207.
- [34] H. Tsuji, S. Shimizu, *Polymer* **2012**, *53*, 5385.
- [35] S. R. Andersson, M. Hakkarainen, A.-C. Albertsson, *Polymer* **2013**, *54*, 4105.
- [36] H. Tsuji, H. Matsuoka, *Macromol. Rapid Commun.* **2008**, *29*, 1372.
- [37] A. Buchard, D. R. Carbery, M. G. Davidson, P. K. Ivanova, B. J. Jeffery, G. I. Kociok-Köhn, J. P. Lowe, *Angew. Chem., Int. Ed.* **2014**, *126*, 14078.
- [38] S. A. Cairns, A. Schultheiss, M. P. Shaver, *Polym. Chem.* **2017**, *8*, 2990.
- [39] T. Bhalla, V. Kumar, S. Bhatia, in *Advances in Industrial Biotechnology* (Eds: R. S. Singh, A. Pandey, C. Larroche), I. K. International Publishing House Pvt. Ltd., Delhi, India **2014**, p. 56.
- [40] F. A. Castillo Martinez, E. M. Balciunas, J. M. Salgado, J. M. Domínguez González, A. Converti, R. P. d. S. Oliveira, *Trends Food Sci. Technol.* **2013**, *30*, 70.
- [41] C. Vilela, A. F. Sousa, A. C. Fonseca, A. C. Serra, J. F. J. Coelho, C. S. R. Freire, A. J. D. Silvestre, *Polym. Chem.* **2014**, *5*, 3119.
- [42] T. Maharana, B. Mohanty, Y. S. Negi, *Prog. Polym. Sci.* **2009**, *34*, 99.
- [43] A. J. R. Lasprilla, G. A. R. Martinez, B. H. Lunelli, A. L. Jardini, R. M. Filho, *Biotechnol. Adv.* **2012**, *30*, 321.
- [44] S. Kobayashi, *Polym. Adv. Technol.* **2015**, *26*, 677.
- [45] O. Coulembier, P. Degée, J. L. Hedrick, P. Dubois, *Prog. Polym. Sci.* **2006**, *31*, 723.
- [46] K. Hiltunen, J. V. Seppälä, M. Härkönen, *Macromolecules* **1997**, *30*, 373.
- [47] D. S. Marques, M. H. Gil, C. M. S. G. Baptista, *J. Appl. Polym. Sci.* **2013**, *128*, 2145.
- [48] K. Hiltunen, M. Härkönen, J. V. Seppälä, T. Väänänen, *Macromolecules* **1996**, *29*, 8677.
- [49] M. J. Stanford, A. P. Dove, *Chem. Soc. Rev.* **2010**, *39*, 486.

- [50] C. M. Thomas, *Chem. Soc. Rev.* **2010**, 39, 165.
- [51] P. Dubois, O. Coulembier, J.-M. Raquez, *Handbook of Ring-Opening Polymerization*, John Wiley & Sons, New York **2009**.
- [52] S. Penczek, M. Cypryk, A. Duda, P. Kubisa, S. Słomkowski, *Prog. Polym. Sci.* **2007**, 32, 247.
- [53] P. Lecomte, C. Jérôme, in *Synthetic Biodegradable Polymers* (Eds: B. Rieger, A. Künkel, G.W. Coates, R. Reichardt, E. Dinjus, T.A. Zevaco), Springer, Berlin **2012**, p. 173.
- [54] C. A. Bischoff, P. Walden, *Ber. Dtsch. Chem. Ges.* **1893**, 26, 262.
- [55] H. Benninga, *A History of Lactic Acid Making: A Chapter in the History of Biotechnology*, Springer, Berlin **1990**.
- [56] J. Pelouze, *Liebigs Ann.* **1845**, 53, 112.
- [57] D. K. Yoo, D. Kim, D. S. Lee, *Macromol. Res.* **2006**, 14, 510.
- [58] Y. Yu, J. Zou, C. Cheng, *Polym. Chem.* **2014**, 5, 5854.
- [59] G. Becker, F. R. Wurm, *Chem. Soc. Rev.* **2018**, 47, 7739.
- [60] B. Martin Vaca, D. Bourissou, *ACS Macro Lett.* **2015**, 4, 792.
- [61] Y. Zhong, R. Tong, *Front. Chem.* **2018**, 6, 641.
- [62] C. Deng, J. Wu, R. Cheng, F. Meng, H.-A. Klok, Z. Zhong, *Prog. Polym. Sci.* **2014**, 39, 330.
- [63] M. Yin, G. L. Baker, *Macromolecules* **1999**, 32, 7711.
- [64] T. Trimaille, M. Möller, R. Gurny, *J. Polym. Sci., Part A: Polym. Chem.* **2004**, 42, 4379.
- [65] T. Trimaille, R. Gurny, M. Möller, *J. Biomed. Mater. Res., Part A* **2007**, 80A, 55.
- [66] F. Jing, M. R. Smith, G. L. Baker, *Macromolecules* **2007**, 40, 9304.
- [67] X. Jiang, E. B. Vogel, M. R. Smith, G. L. Baker, *Macromolecules* **2008**, 41, 1937.
- [68] X. Jiang, M. R. Smith, G. L. Baker, *Macromolecules* **2008**, 41, 318.
- [69] T. Liu, T. L. Simmons, D. A. Bohnsack, M. E. Mackay, M. R. Smith, G. L. Baker, *Macromolecules* **2007**, 40, 6040.
- [70] T. L. Simmons, G. L. Baker, *Biomacromolecules* **2001**, 2, 658.
- [71] D. E. Noga, T. A. Petrie, A. Kumar, M. Weck, A. J. García, D. M. Collard, *Biomacromolecules* **2008**, 9, 2056.
- [72] W. W. Gerhardt, D. E. Noga, K. I. Hardcastle, A. J. García, D. M. Collard, M. Weck, *Biomacromolecules* **2006**, 7, 1735.
- [73] U. Schöllkopf, W. Hartwig, U. Sprotte, W. Jung, *Angew. Chem., Int. Ed.* **1979**, 18, 310.
- [74] M. Rubinshtein, C. R. James, J. L. Young, Y. J. Ma, Y. Kobayashi, N. C. Gianneschi, J. Yang, *Org. Lett.* **2010**, 12, 3560.
- [75] C.-U. Lee, R. Khalifehzadeh, B. Ratner, A. J. Boydston, *Macromolecules* **2018**, 51, 1280.
- [76] X. Jiang, E. B. Vogel, M. R. Smith III, G. L. Baker, *J. Polym. Sci., Part A: Polym. Chem.* **2007**, 45, 5227.
- [77] A. Pedna, L. Rosi, M. Frediani, P. Frediani, *J. Appl. Polym. Sci.* **2015**, 132, 42323.
- [78] A. Smelcerovic, P. Dzodic, V. Pavlovic, E. Cherneva, D. Yancheva, *Amino Acids* **2014**, 46, 825.
- [79] M. Dirauf, D. Bandelli, C. Weber, H. Görls, M. Gottschaldt, U. S. Schubert, *Macromol. Rapid Commun.* **2018**, 39, 1800433.
- [80] S. Dutta, W.-C. Hung, B.-H. Huang, C.-C. Lin, in *Synthetic Biodegradable Polymers* (Eds: B. Rieger, A. Künkel, G. W. Coates, R. Reichardt, E. Dinjus, T.A. Zevaco), Springer, Berlin **2012**, p. 219.
- [81] J. Wei, P. L. Diaconescu, *Acc. Chem. Res.* **2019**, 52, 415.
- [82] N. U. Dharmaratne, J. U. Pothupitiya, M. K. Kiesewetter, *Org. Biomol. Chem.* **2019**, 17, 3305.
- [83] K. Masutani, Y. Kimura, in *Synthesis, Structure and Properties of Poly(lactic acid)* (Eds: M. L. Di Lorenzo, R. Androsch), Springer International Publishing, Cham, Switzerland **2018**, p. 1.
- [84] S. Jacobsen, H. G. Fritz, P. Degée, P. Dubois, R. Jérôme, *Polym. Eng. Sci.* **1999**, 39, 1311.
- [85] A. Kowalski, J. Libiszowski, T. Biela, M. Cypryk, A. Duda, S. Penczek, *Macromolecules* **2005**, 38, 8170.
- [86] X. Zhang, D. A. MacDonald, M. F. A. Goosen, K. B. McAuley, *J. Polym. Sci., Part A: Polym. Chem.* **1994**, 32, 2965.
- [87] A. B. Kremer, P. Mehrkhodavandi, *Coord. Chem. Rev.* **2019**, 380, 35.
- [88] Y. A. Chang, R. M. Waymouth, *J. Polym. Sci., Part A: Polym. Chem.* **2017**, 55, 2892.
- [89] J. Wu, T.-L. Yu, C.-T. Chen, C.-C. Lin, *Coord. Chem. Rev.* **2006**, 250, 602.
- [90] O. Dechy-Cabaret, B. Martin-Vaca, D. Bourissou, *Chem. Rev.* **2004**, 104, 6147.
- [91] N. Nomura, R. Ishii, M. Akakura, K. Aoi, *J. Am. Chem. Soc.* **2002**, 124, 5938.
- [92] B. G. G. Lohmeijer, R. C. Pratt, F. Leibfarth, J. W. Logan, D. A. Long, A. P. Dove, F. Nederberg, J. Choi, C. Wade, R. M. Waymouth, J. L. Hedrick, *Macromolecules* **2006**, 39, 8574.
- [93] R. Todd, G. Rubio, D. J. Hall, S. Tempelaar, A. P. Dove, *Chem. Sci.* **2013**, 4, 1092.
- [94] B. Lin, R. M. Waymouth, *J. Am. Chem. Soc.* **2017**, 139, 1645.
- [95] O. Coulembier, D. P. Sanders, A. Nelson, A. N. Hollenbeck, H. W. Horn, J. E. Rice, M. Fujiwara, P. Dubois, J. L. Hedrick, *Angew. Chem., Int. Ed.* **2009**, 48, 5170.
- [96] C. Thomas, B. Bibal, *Green Chem.* **2014**, 16, 1687.
- [97] S. Naumann, P. B. V. Scholten, J. A. Wilson, A. P. Dove, *J. Am. Chem. Soc.* **2015**, 137, 14439.
- [98] N. E. Kamber, W. Jeong, R. M. Waymouth, R. C. Pratt, B. G. G. Lohmeijer, J. L. Hedrick, *Chem. Rev.* **2007**, 107, 5813.
- [99] G. Nogueira, A. Favrelle, M. Bria, J. P. Prates Ramalho, P. J. Mendes, A. Valente, P. Zinck, *React. Chem. Eng.* **2016**, 1, 508.
- [100] N. J. Sherck, H. C. Kim, Y.-Y. Won, *Macromolecules* **2016**, 49, 4699.
- [101] L. Simón, J. M. Goodman, *J. Org. Chem.* **2007**, 72, 9656.
- [102] S. Koeller, J. Kadota, F. Peruch, A. Deffieux, N. Pinaud, I. Pianet, S. Massip, J.-M. Léger, J.-P. Desvergne, B. Bibal, *Chem. - Eur. J.* **2010**, 16, 4196.
- [103] A. P. Dove, R. C. Pratt, B. G. G. Lohmeijer, R. M. Waymouth, J. L. Hedrick, *J. Am. Chem. Soc.* **2005**, 127, 13798.
- [104] R. C. Pratt, B. G. G. Lohmeijer, D. A. Long, P. N. P. Lundberg, A. P. Dove, H. Li, C. G. Wade, R. M. Waymouth, J. L. Hedrick, *Macromolecules* **2006**, 39, 7863.
- [105] S. Liu, H. Li, N. Zhao, Z. Li, *ACS Macro Lett.* **2018**, 7, 624.
- [106] L. Zhang, F. Nederberg, J. M. Messman, R. C. Pratt, J. L. Hedrick, C. G. Wade, *J. Am. Chem. Soc.* **2007**, 129, 12610.
- [107] H. Li, B.-R. Ai, M. Hong, *Chinese J. Polym. Sci.* **2018**, 36, 231.
- [108] D. Bandelli, J. Alex, C. Helbing, N. Ueberschaar, H. Görls, P. Bellstedt, C. Weber, K. D. Jandt, U. S. Schubert, *Polym. Chem.* **2019**, 10, 5440.
- [109] N. Mase, Moniruzzaman, S. Yamamoto, Y. Nakaya, K. Sato, T. Narumi, *Polymers* **2018**, 10, 713.
- [110] W. Davies, *J. Chem. Soc.* **1951**, 1357.
- [111] O. Thillaye du Boullay, E. Marchal, B. Martin-Vaca, F. P. Cossío, D. Bourissou, *J. Am. Chem. Soc.* **2006**, 128, 16442.
- [112] Z. He, L. Jiang, Y. Chuan, H. Li, M. Yuan, *Molecules* **2013**, 18, 12768.
- [113] A. Basu, K. R. Kunduru, J. Katzhendler, A. J. Domb, *Adv. Drug Delivery Rev.* **2016**, 107, 82.
- [114] Q. Yin, L. Yin, H. Wang, J. Cheng, *Acc. Chem. Res.* **2015**, 48, 1777.
- [115] M. Li, Y. Tao, J. Tang, Y. Wang, X. Zhang, Y. Tao, X. Wang, *J. Am. Chem. Soc.* **2019**, 141, 281.
- [116] M. Yuan, Z. He, H. Li, L. Jiang, M. Yuan, *Polym. Bull.* **2014**, 71, 1331.
- [117] R. J. Pounder, D. J. Fox, I. A. Barker, M. J. Bennison, A. P. Dove, *Polym. Chem.* **2011**, 2, 2204.
- [118] Y. Li, Y. Niu, D. Hu, Y. Song, J. He, X. Liu, X. Xia, Y. Lu, W. Xu, *Macromol. Chem. Phys.* **2015**, 216, 77.
- [119] D. Bandelli, C. Weber, U. S. Schubert, *Macromol. Rapid Commun.* **2019**, 40, 1900306.
- [120] I. Yildirim, S. Crotty, C. H. Loh, G. Festag, C. Weber, P.-F. Caponi, M. Gottschaldt, M. Westerhausen, U. S. Schubert, *J. Polym. Sci., Part A: Polym. Chem.* **2016**, 54, 437.



- [121] C. Bonduelle, B. Martín-Vaca, F. P. Cossío, D. Bourissou, *Chem. - Eur. J.* **2008**, *14*, 5304.
- [122] N. Chapel, A. Greiner, J. Y. Ortholand, *Tetrahedron Lett.* **1991**, *32*, 1441.
- [123] L. A. Cort, R. A. Stewart, *J. Chem. Soc.* **1971**, 1386.
- [124] I. Chehidi, A. Ould Amanetoullah, M. M. Chaabouni, A. Baklouti, *J. Fluor. Chem.* **2010**, *131*, 66.
- [125] M. V. Gabrielsen, *Acta Chem. Scand. A* **1975**, *29*, 7.
- [126] R. Brettell, *J. Chem. Soc. C* **1972**, 611.
- [127] T. Hashimoto, K. Fukumoto, N. Abe, K. Sakata, K. Maruoka, *Chem. Commun.* **2010**, 46, 7593.
- [128] M. Neveux, B. Seiller, F. Hagedorn, C. Bruneau, P. H. Dimeuf, *J. Organomet. Chem.* **1993**, *451*, 133.
- [129] A. Battaglia, G. Barbaro, P. Giorgianni, A. Guerrini, A. Pepe, *Tetrahedron: Asymmetry* **2001**, *12*, 1015.
- [130] A. Guerrini, G. Varchi, A. Battaglia, *J. Org. Chem.* **2006**, *71*, 6785.
- [131] V. R. Likhterov, V. S. Étlis, L. A. Ternovskoi, *Chem. Heterocycl. Compd.* **1985**, *21*, 1077.
- [132] T. Miyagawa, F. Sanda, T. Endo, *J. Polym. Sci., Part A: Polym. Chem.* **2000**, *38*, 1861.
- [133] A. E. Neitzel, M. A. Petersen, E. Kokkoli, M. A. Hillmyer, *ACS Macro Lett.* **2014**, *3*, 1156.
- [134] Y. Xu, M. R. Perry, S. A. Cairns, M. P. Shaver, *Polym. Chem.* **2019**, *10*, 3048.
- [135] R. T. Martin, L. P. Camargo, S. A. Miller, *Green Chem.* **2014**, *16*, 1768.
- [136] K. Hyou, A. Kanazawa, S. Aoshima, *ACS Macro Lett.* **2019**, *8*, 128.
- [137] K. Zhu, J. H. Simpson, E. J. Delaney, W. A. Nugent, *J. Org. Chem.* **2007**, *72*, 3949.
- [138] H. W. Yang, D. Romo, *Tetrahedron* **1999**, *55*, 6403.
- [139] A. Stirling, M. Iannuzzi, M. Parrinello, F. Molnar, V. Bernhart, G. A. Luinstra, *Organometallics* **2005**, *24*, 2533.
- [140] J. W. Kramer, E. B. Lobkovsky, G. W. Coates, *Org. Lett.* **2006**, *8*, 3709.
- [141] M. Mulzer, G. W. Coates, *J. Org. Chem.* **2014**, *79*, 11851.
- [142] F. M. Raushel, *Biochemistry* **2017**, *56*, 1175.
- [143] J. K. Christenson, J. E. Richman, M. R. Jensen, J. Y. Neufeld, C. M. Wilmot, L. P. Wackett, *Biochemistry* **2017**, *56*, 348.
- [144] D. Grenier, R. E. Prud'Homme, A. Leborgne, N. Spassky, *J. Polym. Sci. A* **1981**, *19*, 1781.
- [145] H. Wynberg, E. G. J. Staring, *J. Am. Chem. Soc.* **1982**, *104*, 166.
- [146] R. Tennyson, D. Romo, *J. Org. Chem.* **2000**, *65*, 7248.
- [147] J. Douglas, J. E. Taylor, G. Churchill, A. M. Z. Slawin, A. D. Smith, *J. Org. Chem.* **2013**, *78*, 3925.
- [148] V. Gnanadesikan, E. J. Corey, *Org. Lett.* **2006**, *8*, 4943.
- [149] R. Voyer, R. E. Prud'Homme, *J. Polym. Sci., Part A: Polym. Chem.* **1986**, *24*, 2773.
- [150] R. Ligny, M. M. Hänninen, S. M. Guillaume, J.-F. Carpentier, *Chem. Commun.* **2018**, *54*, 8024.
- [151] A. Khalil, S. Cammas-Marion, O. Coulembier, *J. Polym. Sci., Part A: Polym. Chem.* **2019**, *57*, 657.
- [152] H. N. Cheng, *J. Appl. Polym. Sci.* **1988**, *36*, 229.
- [153] J. L. Robert, K. B. Aubrecht, *J. Chem. Educ.* **2008**, *85*, 258.
- [154] K. A. M. Thakur, R. T. Kean, E. S. Hall, J. J. Kolstad, E. J. Munson, *Macromolecules* **1998**, *31*, 1487.
- [155] N. Spassky, V. Simic, M. S. Montaudo, L. G. Hubert-Pfalzgraf, *Macromol. Chem. Phys.* **2000**, *201*, 2432.
- [156] J. E. Kasperczyk, *Macromolecules* **1995**, *28*, 3937.
- [157] J. Belleney, M. Wisniewski, A. Le Borgne, *Eur. Polym. J.* **2004**, *40*, 523.
- [158] M. H. Chisholm, S. S. Iyer, D. G. McCollum, M. Pagel, U. Werner-Zwanziger, *Macromolecules* **1999**, *32*, 963.
- [159] M. T. Zell, B. E. Padden, A. J. Paterick, K. A. M. Thakur, R. T. Kean, M. A. Hillmyer, E. J. Munson, *Macromolecules* **2002**, *35*, 7700.
- [160] H. Bai, S. Deng, D. Bai, Q. Zhang, Q. Fu, *Macromol. Rapid Commun.* **2017**, *38*, 1700454.
- [161] H. Tsuji, Y. Ikada, *Polymer* **1999**, *40*, 6699.
- [162] H. Urayama, T. Kanamori, K. Fukushima, Y. Kimura, *Polymer* **2003**, *44*, 5635.
- [163] H. Tsuji, *Adv. Drug Delivery Rev.* **2016**, *107*, 97.
- [164] H. Uehara, Y. Karaki, S. Wada, T. Yamanobe, *ACS Appl. Mater. Interfaces* **2010**, *2*, 2707.
- [165] H. Tsuji, Y. Ikada, *J. Appl. Polym. Sci.* **1994**, *53*, 1061.
- [166] D. Portinha, J. Belleney, L. Bouteiller, S. Pensec, N. Spassky, C. Chassenieux, *Macromolecules* **2002**, *35*, 1484.
- [167] H. Tsuji, S. H. Hyon, Y. Ikada, *Macromolecules* **1992**, *25*, 2940.
- [168] Y. Koide, H. Ikake, Y. Muroga, S. Shimizu, *Polym. J.* **2012**, *45*, 645.
- [169] J. Zhang, K. Tashiro, H. Tsuji, A. J. Domb, *Macromolecules* **2007**, *40*, 1049.
- [170] P. Pan, L. Han, J. Bao, Q. Xie, G. Shan, Y. Bao, *J. Phys. Chem. B* **2015**, *119*, 6462.
- [171] H. Tsuji, Y. Ikada, *Polymer* **1995**, *36*, 2709.
- [172] H. Tsuji, A. Okumura, *Macromolecules* **2009**, *42*, 7263.
- [173] J. D. Hoffman, R. L. Miller, H. Marand, D. B. Roitman, *Macromolecules* **1992**, *25*, 2221.
- [174] H. Tsuji, Y. Tezuka, *Biomacromolecules* **2004**, *5*, 1181.
- [175] A. Ghanbari, R. E. Prud'homme, *Polymer* **2017**, *112*, 377.
- [176] D. Bandelli, C. Helbing, C. Weber, M. Seifert, I. Muljajew, K. D. Jandt, U. S. Schubert, *Macromolecules* **2018**, *51*, 5567.
- [177] P. Pan, J. Yang, G. Shan, Y. Bao, Z. Weng, A. Cao, K. Yazawa, Y. Inoue, *Macromolecules* **2012**, *45*, 189.
- [178] G. Kister, G. Cassanas, M. Vert, *Polymer* **1998**, *39*, 267.
- [179] V. Arias, K. Odelius, A. C. Albertsson, *Macromol. Rapid Commun.* **2014**, *35*, 1949.
- [180] A. M. Ritcey, R. E. Prud'Homme, *Macromolecules* **1992**, *25*, 972.
- [181] W. Zhou, K. Wang, S. Wang, S. Yuan, W. Chen, T. Konishi, T. Miyoshi, *ACS Macro Lett.* **2018**, *7*, 667.
- [182] W. Chen, S. Wang, W. Zhang, Y. Ke, Y.-I. Hong, T. Miyoshi, *ACS Macro Lett.* **2015**, *4*, 1264.
- [183] H. Tsuji, S. H. Hyon, Y. Ikada, *Macromolecules* **1991**, *24*, 5651.
- [184] R. Voyer, R. E. Prud'Homme, *Eur. Polym. J.* **1989**, *25*, 365.
- [185] D. Grenier, R. E. Prud'homme, *J. Polym. Sci., Part B: Polym. Phys.* **1984**, *22*, 577.
- [186] A. M. Ritcey, J. Brisson, R. E. Prud'Homme, *Macromolecules* **1992**, *25*, 2705.
- [187] C. Fraschini, A. Pennors, R. E. Prud'homme, *J. Polym. Sci., Part B: Polym. Phys.* **2007**, *45*, 2380.
- [188] H. Tsuji, A. Okumura, *Polym. J.* **2011**, *43*, 317.
- [189] A. Soldera, R. E. Prud'homme, *Macromolecules* **1997**, *30*, 3107.
- [190] A. M. Ritcey, R. E. Prud'homme, *Macromolecules* **1993**, *26*, 1376.
- [191] H. Tsuji, S. Yamamoto, A. Okumura, Y. Sugiura, *Biomacromolecules* **2010**, *11*, 252.
- [192] H. Tsuji, T. Hayakawa, *Polymer* **2014**, *55*, 721.
- [193] H. Tsuji, F. Deguchi, Y. Sakamoto, S. Shimizu, *Macromol. Chem. Phys.* **2012**, *213*, 2573.
- [194] H. Tsuji, M. Suzuki, *Macromol. Chem. Phys.* **2014**, *215*, 1879.
- [195] H. Tsuji, K. Shimizu, Y. Sakamoto, A. Okumura, *Polymer* **2011**, *52*, 1318.
- [196] H. Tsuji, S. Yamamoto, A. Okumura, *J. Appl. Polym. Sci.* **2011**, *122*, 321.
- [197] H. Tsuji, M. Hosokawa, Y. Sakamoto, *Polymer* **2013**, *54*, 2190.
- [198] H. Tsuji, T. Tawara, *Polymer* **2015**, *68*, 57.
- [199] Y. Hu, H. Sato, J. Zhang, I. Noda, Y. Ozaki, *Polymer* **2008**, *49*, 4204.
- [200] H. Tsuji, M. Yamasaki, Y. Arakawa, *ACS Appl. Polym. Mater.* **2019**, *1*, 1476.
- [201] F.-R. Zeng, J.-M. Ma, L.-H. Sun, Z. Zeng, H. Jiang, Z.-L. Li, *Macromol. Chem. Phys.* **2018**, *219*, 1800031.
- [202] J. M. Longo, A. M. DiCiccio, G. W. Coates, *J. Am. Chem. Soc.* **2014**, *136*, 15897.
- [203] C.-M. Dong, K.-Y. Qiu, Z.-W. Gu, X.-D. Feng, *J. Polym. Sci., Part A: Polym. Chem.* **2000**, *38*, 4179.
- [204] M. Leemhuis, N. Akeroyd, J. A. W. Kruijtzter, C. F. van Nostrum, W. E. Hennink, *Eur. Polym. J.* **2008**, *44*, 308.
- [205] Y. Yu, J. Zou, L. Yu, W. Ji, Y. Li, W.-C. Law, C. Cheng, *Macromolecules* **2011**, *44*, 4793.



Supporting Information

for *Macromol. Rapid Commun.*, DOI: 10.1002/marc.201900560

Polyester Stereocomplexes Beyond PLA: Could Synthetic Opportunities Revolutionize Established Material Blending?

Damiano Bandelli, Julien Alex, Christine Weber, and Ulrich S. Schubert*

Copyright WILEY-VCH Verlag GmbH & Co. KGaA, 69469 Weinheim, Germany, 2019.

Supporting Information

Polyester stereocomplexes beyond PLA: Could synthetic opportunities revolutionize established material blending?

*Damiano Bandelli, Julien Alex, Christine Weber, and Ulrich S. Schubert**

Table S1: List of poly(α -hydroxy acids) exhibiting stereocomplexation and thermal properties before as well as after the blending process.

Sample (stereocomplex type) ^{a)}	Blending process (composition) ^{b)}	T _{g1} (T _{g2}) [° C]	T _{cc1} (T _{cc2}) [° C]	T _{m1} (T _{m2} , T _{m3}) [° C]	Range X _c [%]	Ref.
Polymeric species						
PLLA ^{c)}		n.r.	n.r.	111 (132)	-	[35, 172, 195, 196]
	M					

PDLA ^{c)}	M	n.r.	60	107 (138)	-	
PL2HB ^{d)}	S	27	70	75 to 114	33 to 61	[34,
	M	n.r.	n.r.	92 to 103	0 to 68	172,
PD2HB ^{d)}	S	27	79	76 to 115	28 to 65	191,
	M	n.r.	n.r.	88 to 111	0 to 66	195]
4 Arms PL2HB ^{d)}	M	25	n.r.	85	0 to 31	[193]
4 Arms PDLA ^{c)}	M	54	n.r.	152 to 164	0 to 63	
PL2H3MB ^{e)}	S	n.r.	n.r.	169 (179)	-	[35,
PD2H3MB ^{e)}	S	n.r.	n.r.	166 (174)	-	197,
						205]
Blends						
PLLA / PDLA (bh)	M (1:1)	43	n.r.	195	n.r.	[172]
PL2HB / PD2HB (bh)		41	n.r.	170 to 215	65 to 85	[34,
	S (1:1)		n.r.	172 to 214	59 to 89	172,
	M (1:1)	39				196]
PL2H3MB / PD2H3MB (bh)	(S) 1:1	n.r.	n.r.	183 (185)	n.r.	[35]
PL2HB / PDLA (be)	S (1:1)	28 (39)	69	101 (166, 184)	n.r.	[191]
	M (1:1)	26 (54)	97	166 (183)	n.r.	
	M _q (3:1)	25 (54)	89	105 (167)	n.r.	[192]
	M _q (1:1)	24 (53)	87	101 (167)	n.r.	
	M _q (1:3)	23 (54)	86	100 (168)	n.r.	
PD2HB / PLLA (be)	M _q (1:9)	50	105	165	n.r.	[195,
						196]
4 Arms PL2HB / PDLA	M (3:1)	25 (56)	95 to	85 (141 to	0 to 25	[205]

(be)			101	147,		
				161 to 164)		
	M (1:1)	28 (54)	83	145 to 149	0 to 6	
				(161 to 163)		
	M (1:3)	25 to 27 (51 to 55)	82	146 to 150	0 to 3	
				(162 to 165)		
PD2HB/ PL2HB / PLLA	M _q (1:1:18)	49	101	165 (213)	n.r.	[195]
(t)						
	M _q (5:1:4)	24 to 26 (51 to 53)	75 to 94	184 to 211	11 to 40	[196]
			(146)			
	M _q (2:1:1)	22 to 26 (45 to 54)	83 to 87	177 to 214	22 to 69	
	M _q (5:4:1)	30	81 to 85	206 to 215	24 to 81	
PL2HB / Pd2H3MB (be)	S (1:1)	n.r.	n.r.	204	n.r.	[205]
	M (1:1)	27 to 33	57	189 to 209	n.r.	
PL2HB / Pd2HB / PL2H3MB / Pd2H3MB	S (1:1:3:3)	n.r.	n.r.	204	75	[197]
(q)						
	M (1:1:3:3)	n.r.	n.r.	201	74	
	S (2:2:3:3)	n.r.	n.r.	205	79	
	M (2:2:3:3)	n.r.	n.r.	203	82	
	S (1:1:1:1)	n.r.	n.r.	208	81	
	M (1:1:1:1)	n.r.	n.r.	205	77	
	S (3:3:2:2)	n.r.	n.r.	208	81	

	M (3:3:2:2)	n.r.	n.r.	206	75
	S (3:3:1:1)	n.r.	n.r.	210	79
	M (3:3:1:1)	n.r.	n.r.	207	76
PD2HB- <i>b</i> -PLLA (b)	M	n.r.	93	169	0 to 60 ^[194]

^{a)} Stereocomplex types: bh, binary homostereocomplex; be, binary heterostereocomplex; b, binary heterostereocomplex from block copolymer; t, ternary heterostereocomplex; q, quaternary heterostereocomplex.

^{b)} Blending processes: S, solution casting; M, melt crystallization; M_q, melt quenching.

^{c)} M_n from 2.7 to 11 kg mol⁻¹, 1.25 ≤ Đ ≤ 1.9 from SEC analyses.

^{d)} M_n from 0.8 to 25 kg mol⁻¹, 1.32 ≤ Đ ≤ 3.9 from SEC analyses.

^{e)} M_n from 1.1 to 2.1 kg mol⁻¹, 1.8 ≤ Đ ≤ 2.5 from SEC analyses.

Table S2: List of poly (β-hydroxy acids) exhibiting stereocomplexation and thermal properties before as well as after the blending process.

Sample	T _g [°C]	Range T _m [° C]	Range X _c [%]	Ref.
Polymeric species				
PLMEPL	n.r.	143 to 156	33 to 39	[180, 185-
PdMEPL	n.r.	143 to 156	33 to 39	187]
PDMPPPL	n.r.	148	n.r.	[190]
PLMECl ₂ PL	94	138	n.r.	[184]
PdMECl ₂ PL	114	141	n.r.	
PLMPCl ₂ PL	93	125	n.r.	
PdMPCl ₂ PL	82	110	n.r.	
Blends ^{a)}				
PLMEPL / PdMEPL	n.r.	190 to 215	42 to 53	[180, 185,

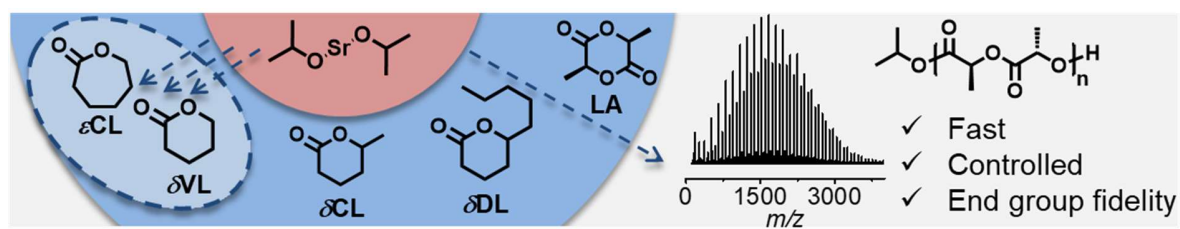
				[186]
PLMEPL / PDMPPL	n.r.	150	n.r.	[190]
PLMECl ₂ PL / PDMECl ₂ PL	n.r.	195	n.r.	[184]
PLMPCl ₂ PL / PDMPCl ₂ PL	n.r.	180 to 200	n.r.	

^{a)} From the mixture of equimolar solutions of isotactic chains.

Publication P2

Strontium Isopropoxide: A highly active catalyst for the Ring-Opening Polymerization of Lactide and various lactones

D. Bandelli, C. Weber, U. S. Schubert, *Macromol. Rapid Commun.* **2019**, *40*, 1900306.





Strontium Isopropoxide: A Highly Active Catalyst for the Ring-Opening Polymerization of Lactide and Various Lactones

Damiano Bandelli, Christine Weber, and Ulrich S. Schubert*

Commercially available strontium isopropoxide represents a suitable catalyst/initiator for the ring-opening polymerization (ROP) of lactide (LA), ϵ -caprolactone, δ -valerolactone, δ -caprolactone, and δ -decalactone. Well-defined polyesters are accessible via the solution polymerization of lactide in toluene with a [LA]:[Sr] ratio of 100:1 at room temperature with or without the addition of dodecanol as coinitiator. Kinetic studies and detailed analysis by means of matrix-assisted laser desorption ionization mass spectrometry reveal pseudo-first-order kinetics of the ROP as well as excellent endgroup fidelity of the polylactide (PLA) with isopropyl and dodecyl α -endgroups. Both isopropanolate moieties as well as the coinitiator each initiate PLA chains, enabling the synthesis of PLA with tailored molar mass. The polymerization of ϵ -caprolactone and δ -valerolactone confirms the high catalyst activity, which causes quantitative monomer conversion after 1 min polymerization time but broad molar mass distributions. In contrast, the catalyst is well suited for the ROP of the less reactive δ -caprolactone and δ -decalactone. Although kinetic studies reveal initially bimodal molar mass distributions, polyesters with dispersity values $\mathcal{D} < 1.2$ and unimodal molar mass distributions can be obtained at moderate to high monomer conversions.

In the last decades, polyesters have been subject to extensive investigation in the field of biomedicine due to their high tissue compatibility and biodegradability.^[1–3] Applications range from the formulation of well-defined micro- and nanomaterials for drug delivery to tissue engineering or implant materials.^[2,4] As materials approved by the U.S. Food and Drug Administration, polylactide (PLA), poly(lactide-co-glycolide) (PLGA), and poly(ϵ -caprolactone) (P ϵ CL) represent the most commonly used polyesters for this purpose and are commercially available

D. Bandelli, Dr. C. Weber, Prof. U. S. Schubert
Laboratory of Organic and Macromolecular Chemistry (IOMC)
Friedrich Schiller University Jena
Humboldtstr. 10
07743, Jena, Germany
E-mail: ulrich.schubert@uni-jena.de

D. Bandelli, Dr. C. Weber, Prof. U. S. Schubert
Jena Center for Soft Matter (JCSM)
Friedrich Schiller University Jena
Philosophenweg 7, 07743, Jena, Germany

The ORCID identification number(s) for the author(s) of this article can be found under <https://doi.org/10.1002/marc.201900306>.

© 2019 The Authors. Published by WILEY-VCH Verlag GmbH & Co. KGaA, Weinheim. This is an open access article under the terms of the Creative Commons Attribution License, which permits use, distribution and reproduction in any medium, provided the original work is properly cited.

DOI: 10.1002/marc.201900306

under the trade name Resomer. However, a range of alternative polyesters are accessible from various lactones that are commercially available and can be used to tailor, for example, the thermal or mechanical material properties.^[5] In particular, δ -lactones such as δ -valerolactone (δ VL), δ -caprolactone (δ CL), and δ -decalactone (δ DL) are naturally occurring and/or used as food additives.^[6] Differing in reactivity compared to the standard monomers lactide, glycolide, and ϵ -caprolactone (ϵ CL), many of these monomers cannot be efficiently polymerized using the standard catalyst tin octanoate ($\text{Sn}(\text{Oct})_2$), although alternative catalysts such as organic acids or bases have been successfully applied.^[5,7–10] Long reaction times or high catalyst loadings are usually required for their polymerization.^[5,7,8,11]

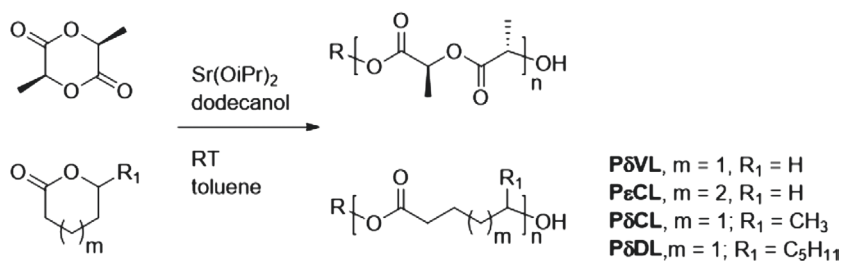
During selection of an appropriate ring-opening polymerization (ROP) catalyst, one has to consider that, besides influencing the ROP performance, the catalyst can be retained in the final material.^[12] Besides influencing the material properties,

in particular trace amounts of toxic catalysts based on, for example, tin or aluminum, represent a major concern if biomedical applications are intended. In contrast, catalyst residues could be advantageous, if the catalyst is based on elements that are beneficial at the site of action of the final polyester material.

Alkaline earth metal compounds based on calcium and strontium are well known as active agents for bone remineralization.^[13–16] In particular, strontium salts can prevent osteoporosis.^[17,18] Moreover, a range of magnesium, zinc, and calcium complexes are known to represent efficient ROP catalysts.^[19–21] Although extensive ligand design enables stereo-controlled ROP, the utmost majority of these complexes is not commercially available. The very few strontium-based ROP catalysts reported in the literature are all noncommercial compounds as well.^[22–26] On the other hand, the well-known ROP catalyst aluminum isopropoxide features a comparably simple structure, and other alkoxides have been utilized for the same purpose.^[27] Despite being commercially available, strontium isopropoxide ($\text{Sr}(\text{OiPr})_2$) has, to the best of our knowledge, not been studied in detail, although strontium amino isopropoxide (Sr-PO) has been applied for the ROP of lactide and ϵ CL by Tang et al. in 2003.^[28]

We hence explored the potential of $\text{Sr}(\text{OiPr})_2$ as initiator/catalyst for the polymerization of L-lactide (L-LA) and a series of lactones (Scheme 1).

In order to evaluate the catalytic performance of $\text{Sr}(\text{OiPr})_2$, preliminary tests on the ROP of L-LA were conducted at room



Scheme 1. Schematic representation of the ring-opening polymerization of L-lactide (top) and various lactones (bottom).

temperature (23 °C) in anhydrous toluene under inert atmosphere (Table 1). Keeping a constant monomer concentration of 0.5 mol L⁻¹, a first test screening was performed varying the monomer to catalyst ratio. All reactions were conducted with as well as without addition of an equimolar amount of dodecanol as coinitiator. For a [LLA]:[Sr] ratio of 20:1, quantitative monomer conversions were observed even at reaction times below 1 min, irrespective of the presence or absence of dodecanol. Size exclusion chromatography (SEC) indicated monomodal molar mass distributions of the obtained PLA. The same held true for an [LLA]:[Sr] ratio of 100:1 and a reaction time of 15 min, hinting toward a high activity of the catalyst for comparably low [LLA]:[Sr] ratios. Further increase of the [LLA]:[Sr] ratio to 200:1 resulted in moderate monomer conversions and bimodal molar mass distributions, even after comparably long polymerization times of 90 min. In these cases, the LLA conversion was increased when dodecanol was added, although SEC analysis revealed similar molar masses for both PLA samples. In contrast, the molar mass of PLA obtained with the lower [LLA]:[Sr] ratio was found to be lower when dodecanol was added.

We hence assumed that isopropanolate as well as dodecanol served as initiating species for PLA chains. To verify this assumption, detailed kinetic studies were performed at a [LLA]:[Sr] ratio of 100:1. Samples were taken periodically, quenched with a fourfold excess of benzoic acid and analyzed by means of ¹H nuclear magnetic resonance (NMR) spectroscopy, SEC, and matrix-assisted laser desorption/ionization time-of-flight mass spectrometry (MALDI-ToF-MS) in order to determine conversions, molar masses, dispersities as well as endgroup identities.

Figure 1 shows a zoom into the MALDI-ToF mass spectra measured from the kinetic sample taken after 2 min reaction time. For the ROP conducted without dodecanol, a single *m/z* distribution was observed, corresponding to PLA chains bearing an isopropanolate α-endgroup, as was clearly evident from the isotopic pattern overlay. The spacing between two neighboring peaks ($\Delta m/z = 72$) corresponded to single lactate repeating units, as reported for various ROP catalyzed by metal complexes.^[22,24] In contrast to most reports, cyclic species were not observed in any of our mass spectra, hinting toward the fact that the *m/z* difference might be caused by the catalytic mechanism rather than by chain transfer reactions.^[25] This was confirmed by the MALDI-ToF mass spectrum of a purified PLA sample with lower molar mass (entry 2 in Table 1). Although the ROP was driven to high conversion, cyclic species were still not found in the spectrum.

In contrast, two *m/z* series were evident from the mass spectra of the PLA obtained from the ROP with dodecanol addition. While the most abundant *m/z* series still corresponded to isopropanolate initiated chains, the additional *m/z* (labelled with 'B' in Figure 1B) was assigned to dodecanol initiated macromolecules, thereby confirming our assumption.

Table 1. Characterization data of the synthesized polyesters.

Entry	Monomer	[M]:[C]:[I] ^{a)}	[M] [mol L ⁻¹]	t [min]	Conversion [%] ^{b)}	<i>M</i> _{n, theo} [kg mol ⁻¹]	<i>M</i> _n ^{c)} [kg mol ⁻¹]	<i>D</i> ^{c)}
1	L-LA	20:1:1	0.5	0.17	>99	1.0	1.0	1.41
2	L-LA	20:1:0	0.5	1	96	1.5	3.2	1.21
3	L-LA	100:1:1	0.5	15	>99	4.9	13	1.16
4	L-LA	100:1:0	0.5	15	>99	7.3	16	1.16
5	L-LA	200:1:1	0.5	90	72	6.9	20	1.29
6	L-LA	200:1:0	0.5	90	52	7.5	19	1.27
7	ε-CL	100:1:1	0.5	1	>99	3.9	1.5	5.10
8	ε-CL	100:1:0	0.5	1	>99	5.8	3.0	6.56
9	δ-VL	100:1:1	0.5	1	>99	3.4	n.a.	n.a.
10	δ-VL	100:1:0	0.5	1	>99	5.1	4.0	3.80
11	δ-CL	110:1:1	4.0	15	82	3.2	5.0	1.16
12	δ-CL	110:1:0	4.0	15	6	0.4	1.2	1.49
13	δ-DL	110:1:1	4.0	15	52	3.0	5.0	1.16
14	δ-DL	110:1:0	4.0	15	32	2.8	5.0	1.19

^{a)}[M]:[C]:[I] corresponds to the initial molar ratio of [monomer]:[Sr(OiPr)₂]:[dodecanol] used for the polymerization; ^{b)}Determined by integration of suitable signals in the ¹H NMR spectra of the reaction solution; ^{c)}Eluent CHCl₃, RI detection, polystyrene (PS) calibration.

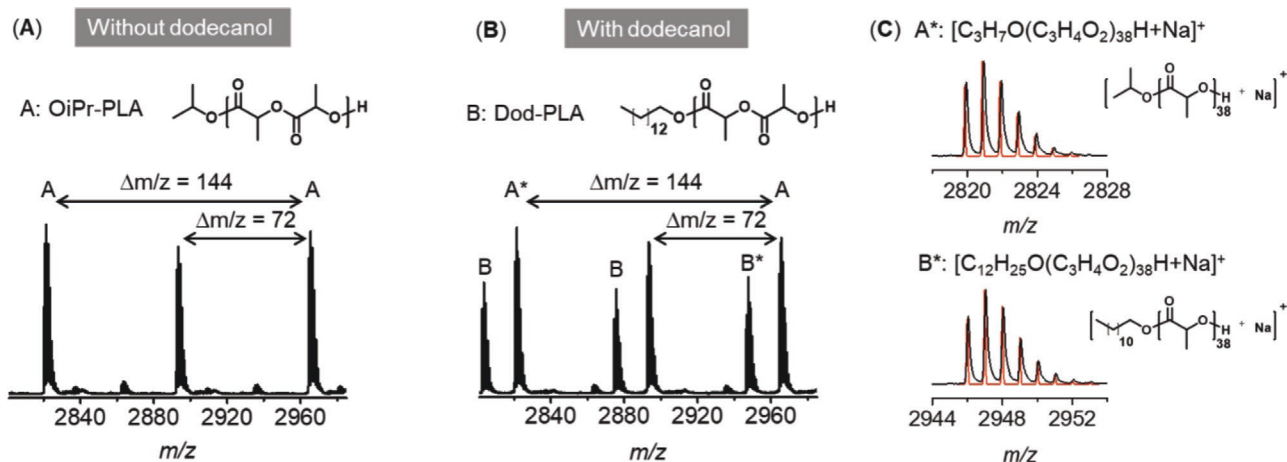


Figure 1. Zoom into the MALDI-ToF mass spectra (DCTB, NaI) of the PLA samples collected after 2 min of the Sr(OiPr)₂-mediated ROP of L-lactide and assignment of the peaks to the polymer structure. A) ROP without dodecanol ([L₂LA]:[Sr(OiPr)₂]:[DodOH] = 100:1:0). B) ROP with dodecanol ([L₂LA]:[Sr(OiPr)₂]:[DodOH] = 100:1:1). C) Overlay of experimental and theoretical isotopic patterns of the peaks indicated by an asterisk.

An increase of the molar mass throughout the kinetic studies was already evident from the MALDI-ToF mass spectra (Figure 2A). However, mass spectrometry does not represent a quantitative method, and mass discrimination effects were observed in the spectra at higher monomer conversions.

In order to access reliable molar mass values, SEC measurements in THF with PLA calibration were performed. Monomodal molar mass distributions and dispersity values (\bar{D}) mostly below 1.2 were detected for all kinetic samples (Figure 2B). The molar mass of the PLA increased in a linear fashion with monomer conversion. As expected from the preliminary test reactions, the molar masses of the PLA samples prepared with dodecanol were consistently lowered in comparison with those obtained without dodecanol. The theoretically expected molar masses were calculated according to $M_n(\text{theo}) = M(\text{LA}) \times [\text{M}]_0/[\text{I}]_0 \times \text{conversion}$ taking into account the fact that two isopropanolate moieties per Sr(OiPr)₂ molecule and each dodecanol molecule would initiate a PLA chain, corresponding to an effective $[\text{M}]/[\text{I}]$ ratio of 50 or 33 for the reaction without or with dodecanol, respectively. The resulting values were in excellent agreement with the molar masses determined by SEC, thereby confirming that a) both isopropanolate moieties of the catalyst are active during polymerization, and b) the molar mass of the PLA could be tailored by the polymerization time as well as by the amount of alcohol to serve as additional initiating species. The theoretical molar mass values provided in Table 1 were hence calculated accordingly.

The linearity of the semi-logarithmic plot suggested pseudo-first-order kinetics during both polymerizations (Figure 2A). Already the larger slope of the linear fit according to $\ln([\text{L}LA]_0/[\text{L}LA]_t) = k_{p,\text{app}} \times [\text{I}]_0 \times t$ indicated that the apparent polymerization rate was increased if dodecanol was added. It should be noted that the two polymerizations differed with respect to the initiator concentration, as described above ($[\text{I}]_0 = 15 \text{ mmol L}^{-1}$ or $[\text{I}]_0 = 10 \text{ mmol L}^{-1}$ for the ROP conducted with or without dodecanol, respectively). However, the calculated apparent polymerization constant ($k_{p,\text{app}}$) should

be independent of the initiator concentration. Surprisingly, $k_{p,\text{app}}$ was doubled for the ROP conducted with dodecanol ($20.8 \text{ L mol}^{-1} \text{ min}^{-1}$ vs $9.6 \text{ L mol}^{-1} \text{ min}^{-1}$), hinting toward the fact that the addition of alcohol affected the reactivity of the catalyst, that is, the coordination at the metal center during the ROP.

The high reactivity of the catalyst for the synthesis of PLA suggested its applicability for the ROP of different commercially available ϵ - and δ -lactones. Test reactions conducted on ϵ CL and δ VL revealed quantitative conversions already after 1 min reaction time employing a monomer to catalyst ratio of 100:1, regardless of the addition of dodecanol (Table 1, entries 7–10). However multimodal SEC elugrams were obtained from the reaction mixtures with high dispersity ($\bar{D} > 3.8$) showing that these ROP could not be well controlled in terms of molar mass due to the high activity of the catalyst.^[29] Interestingly test reactions conducted on the less reactive δ CL and δ DL benefitted from the high activity of the catalyst, as the respective P δ CL and P δ DL could be obtained with low dispersity values in short reaction times (Table 1, entries 11–14). It is to mention that the polymerization of substituted lactones was reported using lanthanum isopropoxide^[30] and organic catalysts such as 1,5,7-triazabicyclo[4.4.0]dec-5-ene and diphenyl phosphate.^[5,11,31] However, their activity seems to be lower in comparison to the present work.

As particularly the ROP using dodecanol were promising, kinetic studies were performed using an initial monomer concentration of $[\text{M}]_0 = 4 \text{ mol L}^{-1}$ due to the high monomer equilibrium concentration of δ CL and δ DL (Figure 2).^[5] Despite the nonlinearity of the first-order kinetic plot, which is also observed for a range of other catalysts for other substituted lactone monomers,^[5,30] the molar mass increased in a linear fashion with monomer conversion, although SEC was used as a relative method here.

Interestingly, SEC analyses revealed bimodal molar mass distributions for samples taken at the beginning of the ROP, which transformed to unimodal signals during the course of the ROP. The dispersity decreased to values below 1.2 for

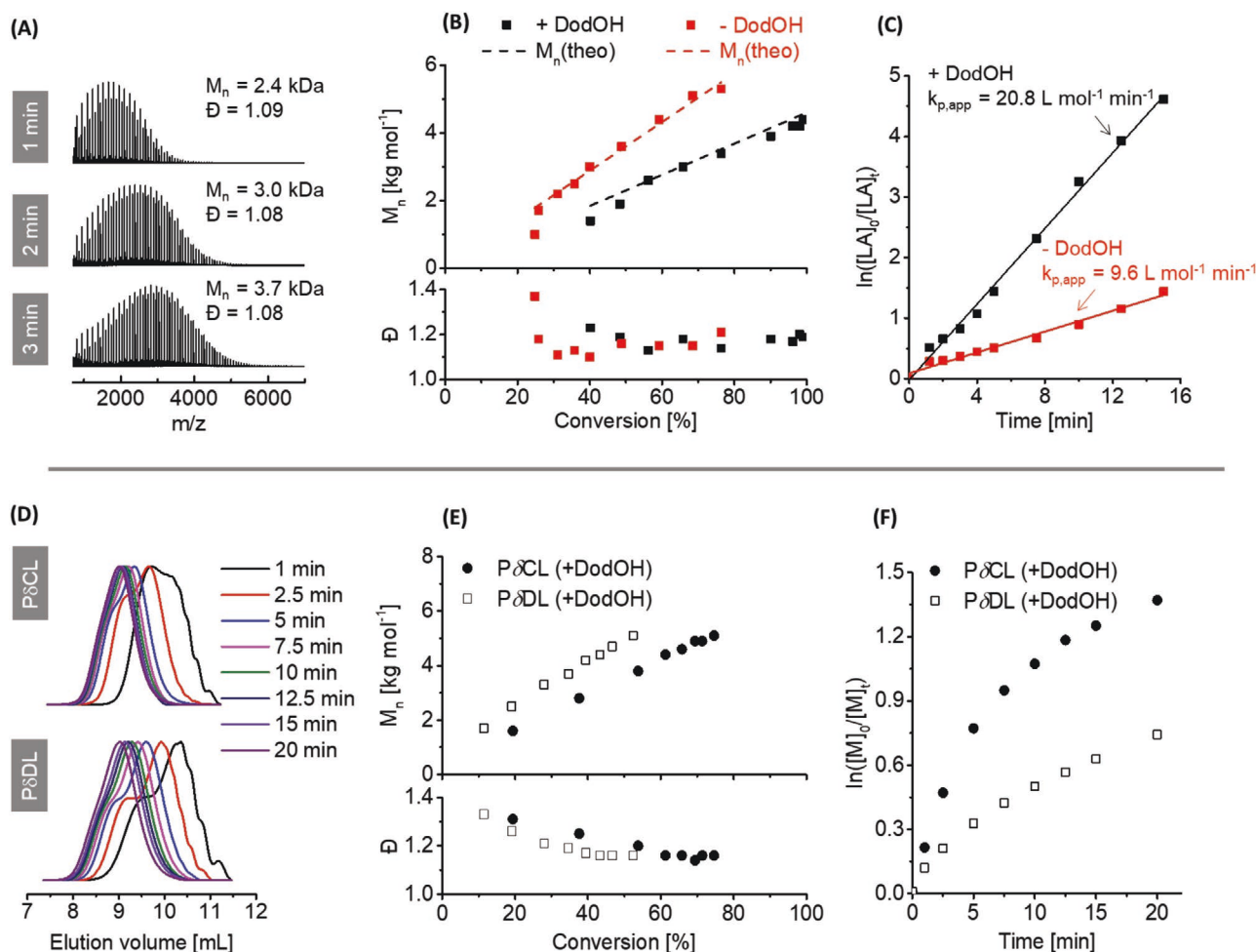


Figure 2. Kinetic studies for the strontium isopropoxide-mediated ROP of LA, δ CL, and δ DL conducted at room temperature in toluene ($[M]:[Sr(OiPr)_2] = 100:1$). A) Overlay of the MALDI-ToF mass spectra (DCTB, NaI) of the PLA samples collected after 1, 2, and 3 min for the reaction with dodecanol. B) Evolution of the molar mass with LA conversion (dots) (SEC: THF, RI detection, PLA calibration) and $M_{n,theo}$ (dotted lines) according to $M_{n,theo} = M(LA) \times [LA]_0/[I]_0 \times conversion$ assuming the initiation from all isopropanolate and DodOH moieties ($[I]_0 = 2[Sr(OiPr)_2]_0 + [DodOH]_0$). C) First-order kinetic plots of the ROP of LA with a linear fit according to $\ln([LA]_0/[LA]_t) = k_{p,app} \times [I]_0 \times t$. D) Overlay of the SEC elugrams for the ROP of δ CL and δ DL, respectively (CHCl $_3$, RI detection, PS calibration). E) Evolution of the molar mass with monomer conversion for the ROP of δ CL and δ DL, respectively ($[M]:[Sr(OiPr)_2]:[DodOH] = 100:1:1$). F) First-order kinetic plots for the polymerization of δ CL and δ DL, respectively ($[M]:[Sr(OiPr)_2]:[DodOH] = 100:1:1$).

monomer conversions above 50%, ruling out commonly observed transesterification processes as reason for this unusual polymerization behavior. One could speculate that catalyst rearrangements or oligomers^[32] with varying activity present in the reaction solution^[33] might cause this effect, which clearly requires extensive additional studies.

To summarize, strontium isopropoxide was successfully used for the ROP of lactide and a selection of lactones at room temperature using toluene as solvent. The ROP of lactide proceeded remarkably well controlled, indicating that both isopropanolate moieties initiated a PLA chain. The application of the same experimental settings for lactones revealed a very high activity for the ROP of unsubstituted ϵ CL and δ VL resulting in fast but uncontrolled polymerizations. In contrast, the less reactive δ CL and δ DL could be polymerized in a well-controlled manner, although the exact catalytic mechanism is subject to further investigation during our future research.

Supporting Information

Supporting Information is available from the Wiley Online Library or from the author.

Acknowledgements

This project was funded by the Thüringer Ministerium für Wirtschaft, Wissenschaft und Digitale Gesellschaft (Thuringian Ministry for Economic Affairs, Science and Digital Society, ProExzellenz II, NanoPolar). Moreover, the work was supported by the DFG-funded Collaborative Research Centre PolyTarget (SFB 1278, projects A06 and Z01). The authors further acknowledge Dr. Norbert Windhab (Evonik Nutrition & Care GmbH) for valuable discussions.

Conflict of Interest

The authors declare no conflict of interest.

Keywords

matrix-assisted laser desorption ionization time-of-flight mass spectrometry, polyesters, poly(lactic acid), ring-opening polymerization, strontium

Received: June 26, 2019

Revised: August 14, 2019

Published online: September 10, 2019

-
- [1] A. S. Gupta, *Nanomedicine* **2011**, *7*, 763.
[2] H. Liu, T. J. Webster, *Biomaterials* **2007**, *28*, 354.
[3] S. Tran, P.-J. DeGiovanni, B. Piel, P. Rai, *Clin. Transl. Med.* **2017**, *6*, 44.
[4] N. Kamaly, B. Yameen, J. Wu, O. C. Farokhzad, *Chem. Rev.* **2016**, *116*, 2602.
[5] D. K. Schneiderman, M. A. Hillmyer, *Macromolecules* **2016**, *49*, 2419.
[6] A. Prades, M. Dornier, N. Diop, J.-P. Pain, *Fruits* **2012**, *67*, 87.
[7] M. K. Kiesewetter, E. J. Shin, J. L. Hedrick, R. M. Waymouth, *Macromolecules* **2010**, *43*, 2093.
[8] B. G. G. Lohmeijer, R. C. Pratt, F. Leibfarth, J. W. Logan, D. A. Long, A. P. Dove, F. Nederberg, J. Choi, C. Wade, R. M. Waymouth, J. L. Hedrick, *Macromolecules* **2006**, *39*, 8574.
[9] S. Naumann, P. B. V. Scholten, J. A. Wilson, A. P. Dove, *J. Am. Chem. Soc.* **2015**, *137*, 14439.
[10] S. Naumann, F. G. Schmidt, W. Frey, M. R. Buchmeiser, *Polym. Chem.* **2013**, *4*, 4172.
[11] D. Bandelli, C. Helbing, C. Weber, M. Seifert, I. Muljajew, K. D. Jandt, U. S. Schubert, *Macromolecules* **2018**, *51*, 5567.
[12] T. H. Thi, M. Matsusaki, H. Hirano, H. Kawano, Y. Agari, M. Akashi, *J. Polym. Sci., Part A: Polym. Chem.* **2011**, *49*, 3152.
[13] K. Rezwan, Q. Z. Chen, J. J. Blaker, A. R. Boccaccini, *Biomaterials* **2006**, *27*, 3413.
[14] P. Habibovic, J. E. Barralet, *Acta Biomater.* **2011**, *7*, 3013.
[15] L. C. Palmer, C. J. Newcomb, S. R. Kaltz, E. D. Spoerke, S. I. Stupp, *Chem. Rev.* **2008**, *108*, 4754.
[16] W. Habraken, P. Habibovic, M. Epple, M. Bohner, *Mater. Today* **2016**, *19*, 69.
[17] S. J. Genuis, G. K. Schwalfenberg, *Clin. Nutr.* **2007**, *26*, 193.
[18] J. Y. Reginster, E. Seeman, M. C. De Vernejoul, S. Adami, J. Compston, C. Phenekos, J. P. Devogelaer, M. D. Curiel, A. Sawicki, S. Goemaere, O. H. Sorensen, D. Felsenberg, P. J. Meunier, *J. Clin. Endocrinol. Metab.* **2005**, *90*, 2816.
[19] J. Wu, T.-L. Yu, C.-T. Chen, C.-C. Lin, *Coord. Chem. Rev.* **2006**, *250*, 602.
[20] A. B. Kremer, P. Mehrkhodavandi, *Coord. Chem. Rev.* **2019**, *380*, 35.
[21] O. Dechy-Cabaret, B. Martin-Vaca, D. Bourissou, *Chem. Rev.* **2004**, *104*, 6147.
[22] L. Clark, G. B. Deacon, C. M. Forsyth, P. C. Junk, P. Mountford, J. P. Townley, J. Wang, *Dalton Trans.* **2013**, *42*, 9294.
[23] R. K. Kottalanka, A. Harinath, T. K. Panda, *RSC Adv.* **2015**, *5*, 37755.
[24] B. Liu, V. Dorcet, L. Maron, J.-F. Carpentier, Y. Sarazin, *Eur. J. Inorg. Chem.* **2012**, *2012*, 3023.
[25] I. Yildirim, S. Crotty, C. H. Loh, G. Festag, C. Weber, P.-F. Caponi, M. Gottschaldt, M. Westerhausen, U. S. Schubert, *J. Polym. Sci., Part A: Polym. Chem.* **2016**, *54*, 437.
[26] I. Yildirim, T. Yildirim, D. Kalden, G. Festag, N. Fritz, C. Weber, S. Schubert, M. Westerhausen, U. S. Schubert, *Polym. Chem.* **2017**, *8*, 4378.
[27] V. Simic, N. Spassky, L. G. Hubert-Pfalzgraf, *Macromolecules* **1997**, *30*, 7338.
[28] Z. Tang, X. Chen, Q. Liang, X. Bian, L. Yang, L. Piao, X. Jing, *J. Polym. Sci., Part A: Polym. Chem.* **2003**, *41*, 1934.
[29] H. R. Kricheldorf, R. Dunsing, A. Serra, *Macromolecules* **1987**, *20*, 2050.
[30] M. Save, M. Schappacher, A. Soum, *Macromol. Chem. Phys.* **2002**, *203*, 889.
[31] M. T. Martello, A. Burns, M. Hillmyer, *ACS Macro Lett.* **2012**, *1*, 131.
[32] V. Peruzzo, M. A. Chiurato, M. Favaro, P. Tomasin, *Mass Spectrom. Rev.* **2018**, *37*, 22.
[33] A. Kowalski, A. Duda, S. Penczek, *Macromolecules* **1998**, *31*, 2114.



Supporting Information

for *Macromol. Rapid Commun.*, DOI: 10.1002/marc.201900306

**Strontium Isopropoxide: A Highly Active Catalyst for
the Ring-Opening Polymerization of Lactide and Various
Lactones**

Damiano Bandelli, Christine Weber, and Ulrich S. Schubert*

Supporting Information

Strontium isopropoxide: A highly active catalyst for the ROP of lactide and various lactones.

*Damiano Bandelli, Christine Weber, Ulrich S. Schubert**

D. Bandelli, Dr. C. Weber, Prof. Dr. U. S. Schubert

Laboratory of Organic and Macromolecular Chemistry (IOMC), Friedrich Schiller University Jena,
Humboldtstr. 10, 07743 Jena, Germany

D. Bandelli, Dr. C. Weber, Prof. Dr. U. S. Schubert

Jena Center for Soft Matter (JCSM), Friedrich Schiller University Jena, Philosophenweg 7, 07743 Jena,
Germany

E-mail: ulrich.schubert@uni-jena.de

EXPERIMENTAL SECTION

Materials

L-Lactide (LLA, 98%) was purchased from Sigma Aldrich and recrystallized with ethylacetate prior to use. δ -Valerolactone (δ VL, 98%), δ -hexanolactone (δ CL, 99%) and δ -decalactone (δ DL, 97%) were purchased from TCI and used without purification. ϵ -Caprolactone (ϵ CL, 97%) was purchased from Sigma Aldrich, dried over calcium hydride and distilled. Dodecanol (DodOH, 98%) was purchased from Sigma Aldrich and recrystallized prior to use.

Strontium isopropoxide ($\text{Sr}(\text{OiPr})_2$) and anhydrous toluene were purchased from Sigma-Aldrich. All other chemicals were purchased from standard suppliers and used without further purification. All glassware was dried at 110 °C for 24 h prior to use for polymerization.

Instruments

All polymerizations were prepared in a MBraun UNILab Plus glove box workstation under nitrogen atmosphere (<0.1 ppm H_2O ; <0.1 ppm O_2). Proton nuclear magnetic resonance (^1H NMR) spectra were measured in CDCl_3 at room temperature using a Bruker AC 300 MHz spectrometer.

Size exclusion chromatography (SEC) measurements were performed on two different instruments. For all the samples a Shimadzu system was used. The system is equipped with a CBM-20A system controller, a LC-10AD VP pump, a RID-10A refractive index detector, a SPD-10AD VP UV detector and a SDV linear S column from PSS (Polymer Standards Service GmbH, Mainz, Germany) using chloroform : triethylamine : 2-propanol (94 : 4 : 2) as eluent at 40 °C at a flow rate of 1 mL min^{-1} . The system was calibrated against PS standards (400 to 100000 g mol^{-1}), which were purchased from PSS.

For all PLA samples, SEC measurements were repeated on a Shimadzu system equipped with a CBM-20A system controller, a LC-10AD VP pump, a RID-10A refractive index detector, a SPD-10AD VP UV

detector and a SDV linear M column from PSS at 30 °C using tetrahydrofuran as eluent at a flow rate of 1 mL min⁻¹. The system was calibrated against PLA standards (144 to 100000 g mol⁻¹), which were purchased from PSS.

For the measurements of the matrix-assisted laser desorption/ionization time-of-flight (MALDI-ToF) mass spectra, an Ultraflex III ToF/ToF instrument (Bruker Daltonics, Bremen, Germany) was used. The instrument is equipped with a Nd-YAG laser and a collision cell. All spectra were measured in the positive reflector mode using *trans*-2-[3-(4-*tert*-butylphenyl)-2-methyl-2-propenylidene] (DCTB) as matrix and sodium iodide (NaI) as doping salt. The instrument was calibrated prior to each measurement with an external PMMA standard (2,500 g mol⁻¹) from PSS.

Ring-opening polymerization

All polymerization mixtures were prepared in a glovebox at room temperature under nitrogen atmosphere (<0.1 ppm H₂O; <0.1 ppm O₂). For all the polymerizations a stock solution of catalyst in anhydrous toluene was used. If not noted otherwise the stock solution contained 21 mg (0.1 mmol) of Sr(OiPr)₂, 19 mg (0.1 mmol) of DodOH and 1 mL of anhydrous toluene for polymerizations conducted at a [M]:[DodOH]:[Sr(OiPr)₂] ratio of [100]:[1]:[1]. Similarly the stock solution contained 21 mg (0.1 mmol) of Sr(OiPr)₂ and 1 mL of anhydrous toluene for polymerizations conducted at a [M]:[DodOH]:[Sr(OiPr)₂] ratio of [100]:[0]:[1]. All reactions were quenched with a solution of benzoic acid in chloroform (four equivalents in comparison with the catalyst).

Homopolymerization of LLA (entry 1 in Table 1)

Corresponding to ratio of [LLA]:[Sr(OiPr)₂] of 20:1, PLA was obtained using 720 mg (5 mmol) of LLA and 460 μL of the stock solution containing the catalyst. After 60 seconds the polymerization mixture

was quenched, and a sample for the determination of the monomer conversion was taken. The crude PLA was precipitated into cold diethyl ether ($-22\text{ }^{\circ}\text{C}$), centrifuged at 5000 rpm for 5 minutes and the supernatant was removed. Afterwards the purified polyester was dried at $40\text{ }^{\circ}\text{C}$ in a vacuum oven overnight.

PLA: conv. = 96%. Yield = 88 %. ^1H NMR (300 MHz, CDCl_3 , δ): 1.51 (d, $-\text{CH}(\underline{\text{CH}_3})_2$), 1.60 (d, $-\text{OCH}\underline{\text{CH}_3}$), 5.05 (m, $-\underline{\text{CH}}(\text{CH}_3)_2$), 5.18 (q, $-\text{O}\underline{\text{CH}}\text{CH}_3$). SEC (CHCl_3 , PS calibration): $M_n = 3.2\text{ kg mol}^{-1}$; $\mathcal{D} = 1.21$. SEC (THF, PLA calibration): $M_n = 1.7\text{ kg mol}^{-1}$; $\mathcal{D} = 1.17$. MALDI ToF MS: $M_n = 2.4\text{ kg mol}^{-1}$; $\mathcal{D} = 1.15$

Homopolymerization of ϵCL (entry 7 and 8 in Table 1)

Corresponding to an initial ratio of $[\epsilon\text{CL}]:[\text{Sr}(\text{OiPr})_2]:[\text{DodOH}]$ of 100:1:1 or 100:1:0 respectively, $\text{P}\epsilon\text{CL}$ was obtained using 117 μL (117 mg, 1 mmol) of ϵCL , 1883 μL of anhydrous toluene and 92 μL of the stock solution containing the catalyst with or without dodecanol. After 1 minute of stirring, 150 μL of the polymerization mixture were withdrawn, quenched and analyzed by means of SEC and ^1H NMR spectroscopy.

Homopolymerization of δVL (entry 9 and 10 in Table 1)

Corresponding to an initial ratio of $[\delta\text{VL}]:[\text{Sr}(\text{OiPr})_2]:[\text{DodOH}]$ of 100:1:1 or 100:1:0 respectively, $\text{P}\delta\text{VL}$ was obtained using 97 μL (97 mg, 1 mmol) of δVL , 1811 μL of anhydrous toluene and 92 μL of the stock solution containing the catalyst with or without dodecanol. After 1 minute of stirring, 150 μL of the polymerization mixture were withdrawn, quenched and analyzed by means of SEC and ^1H NMR spectroscopy.

Homopolymerization of δ CL (entry 11 and 12 in Table 1)

Corresponding to an initial ratio of [δ CL]:[Sr(OiPr)₂]:[DodOH] of 110:1:1 or 110:1:0 respectively, P δ CL was obtained using 880 μ L (849 mg, 4 mmol) of δ CL, 920 μ L of anhydrous toluene and 180 μ L of the stock solution. The stock solutions were prepared dissolving 83 mg (0.4 mmol) of Sr(OiPr)₂ with or without 76 mg (0.4 mmol) of DodOH in 1 mL of anhydrous toluene. After 15 minutes of stirring, 150 μ L of the polymerization mixture were withdrawn, quenched and analyzed by means of SEC and ¹H NMR spectroscopy.

Homopolymerization of δ DL (entry 13 and 14 in Table 1)

Corresponding to an initial ratio of [δ DL]:[Sr(OiPr)₂]:[DodOH] of 110:1:1 or 110:1:0 respectively, P δ DL was obtained using 1428 μ L (1497 mg, 8 mmol) of δ DL, 372 μ L of anhydrous toluene and 180 μ L of the stock solution. The stock solutions were prepared dissolving 83 mg (0.4 mmol) of Sr(OiPr)₂ with or without 76 mg (0.4 mmol) of DodOH in 1 mL of anhydrous toluene. After 15 minutes of stirring, 150 μ L of the polymerization mixture were withdrawn, quenched and analyzed by means of SEC and ¹H NMR spectroscopy.

Polymerization kinetics

For the kinetic studies of the homopolymerization of LLA, δ CL and δ DL with a [M]:[Sr(OⁱPr)₂] ratio of [100]:[1], a vial was charged with 1 mmol of monomer and toluene. A sample of the resulting solution was withdrawn and used as time zero for ¹H NMR analyses. Afterwards 100 μ L of stock solution were added in order to start the reaction. The ROP proceeded at room temperature under stirring inside the glovebox. Aliquots were regularly withdrawn and quenched by addition of 50 μ L of

a solution of benzoic acid (4 equivalents in respect to $\text{Sr}(\text{OiPr})_2$) in chloroform. ^1H NMR and SEC analyses were performed from the quenched reaction mixtures in order to assess the monomer conversion, the molar mass, and the dispersity (\mathcal{D}). The samples obtained from the polymerization of LLA and δCL were furthermore analyzed by means of MALDI ToF mass spectrometry.

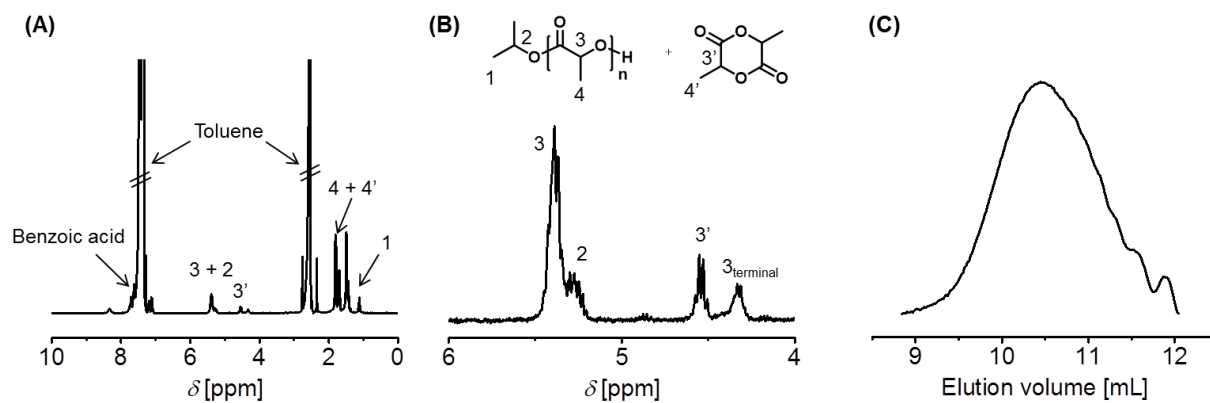


Figure S1: Characterization of entry **1** in **Table 1** employing a [LLA]:[Sr(OiPr)₂]:[DodOH] of 20:1:1. **A:** ¹H NMR spectrum (300 MHz, CDCl₃) of the reaction mixture and structural assignment. **B:** Zoom into the methine region and schematic representation of the structural assignment (peaks 3 and 3' were used to calculate conversion). **C:** SEC elugram (CHCl₃, RI detector).

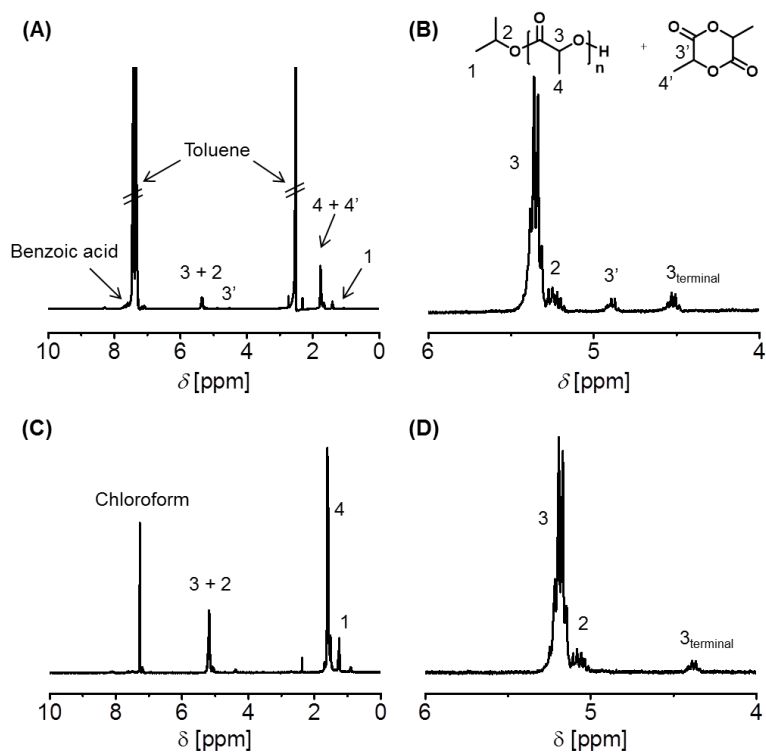


Figure S2: ^1H NMR spectrum (300 MHz, CDCl_3) of entry **2** in **Table 1** employing a $[\text{LLA}]:[\text{Sr}(\text{OiPr})_2]:[\text{DodOH}] = 20:1:0$. **A:** ^1H NMR spectrum of the reaction mixture and structural assignment. **B:** Zoom into the methine region and schematic representation of the structural assignment (peaks 3 and 3' were used to calculate conversion) of the reaction mixture. **C:** ^1H NMR spectrum of the purified PLA and structural assignment. **D:** Zoom in in the methine region and structural assignment of the pure sample.

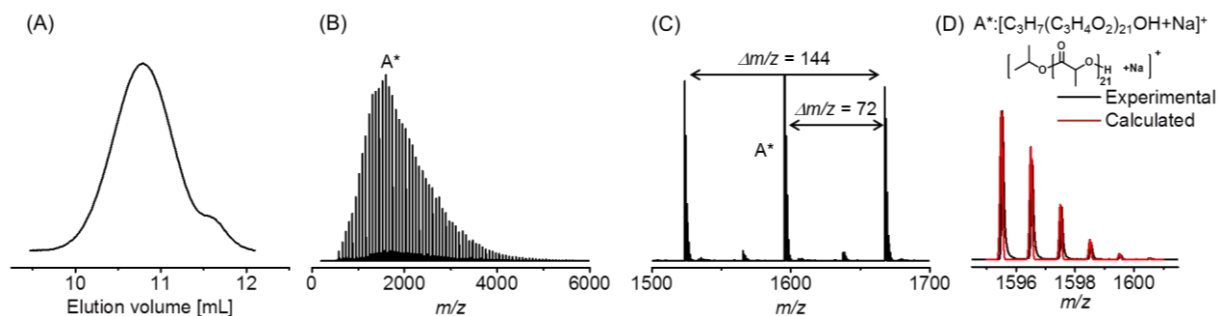


Figure S3: Characterization of **2** obtained *via* ROP of LA using strontium isopropoxide ($[\text{LLA}]/[\text{Sr}(\text{OiPr})_2] = 20:1$). **A:** SEC elugram (THF, RI, PLA cal.). **B:** MALDI-ToF mass spectrum (DCTB, NaI) (A^* is the most abundant peak). **C:** Zoom in to the most abundant m/z region of the mass spectrum. **D:** Overlay of the experimental and calculated isotopic pattern for the end group assignment.

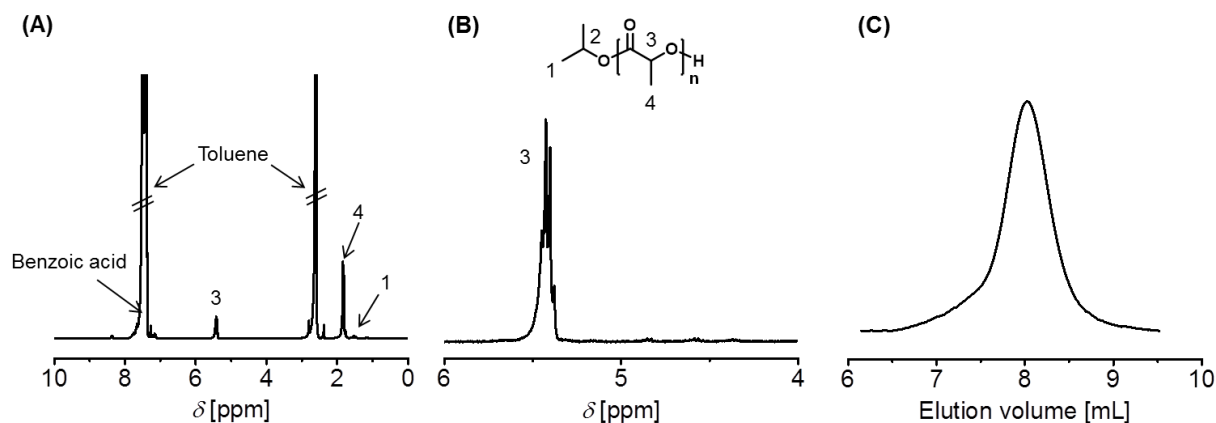


Figure S4: Characterization of entry **3** in **Table 1** employing a $[\text{LLA}]:[\text{Sr}(\text{OiPr})_2]:[\text{DodOH}]$ of 100:1:1. **A:** ^1H NMR spectrum (300 MHz, CDCl_3) of the reaction mixture and schematic representation of the structural assignment. **B:** Zoom in in the methine region and structural assignment. **C:** SEC elugram (CHCl_3 , RI detector).

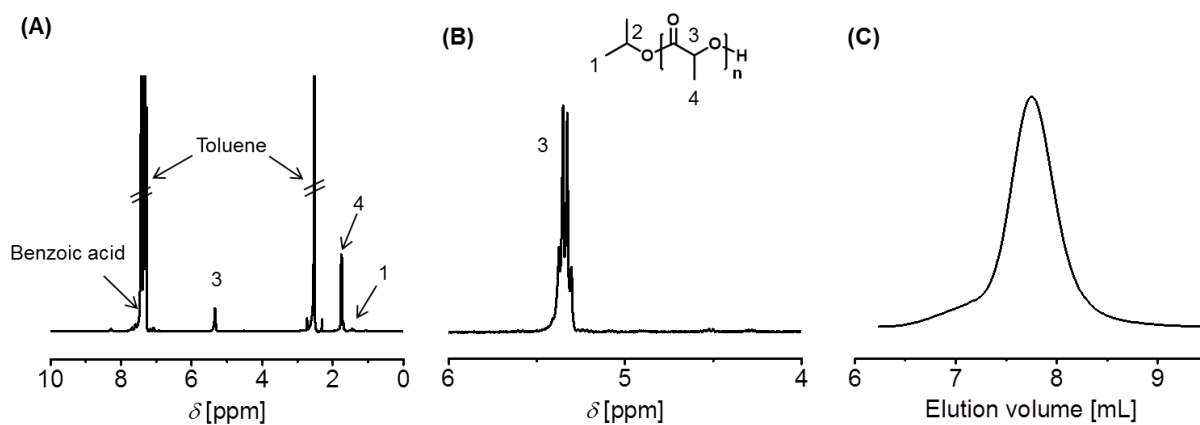


Figure S5: Characterization of entry **4** in **Table 1** employing a [LLA]:[Sr(OiPr)₂]:[DodOH] of 100:1:0. **A:** ¹H NMR spectrum (300 MHz, CDCl₃) of the reaction mixture and schematic representation of the structural assignment. **B:** Zoom in in the methine region and structural assignment. **C:** SEC elugram (CHCl₃, RI detector).

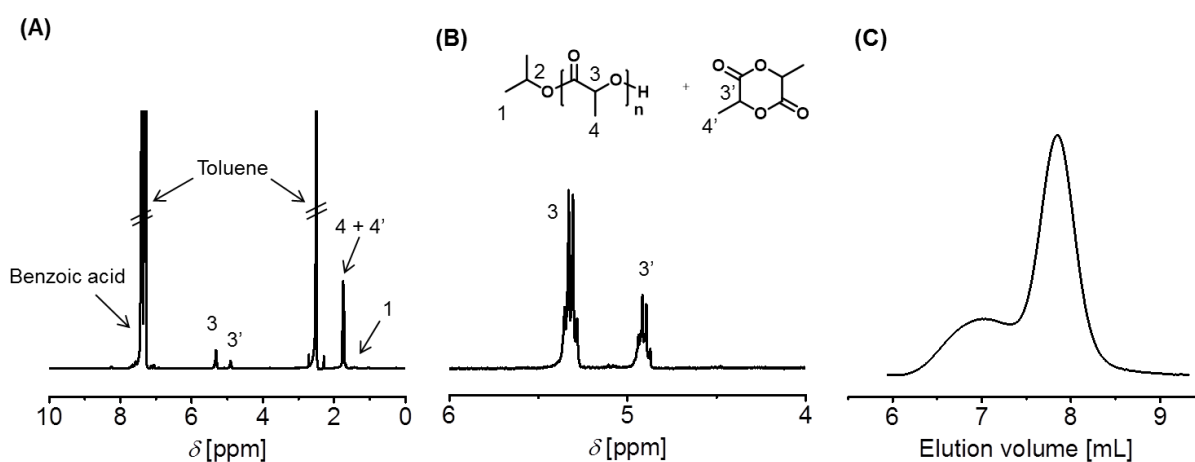


Figure S6: Characterization of entry **5** in **Table 1** employing a [LLA]:[Sr(OiPr)₂]:[DodOH] of 200:1:1. **A:** ¹H NMR spectrum (300 MHz, CDCl₃) of the reaction mixture and schematic representation of the structural assignment. **B:** Zoom in in the methine region and structural assignment (peaks **3** and **3'** were used to calculate conversion). **C:** SEC elugram (CHCl₃, RI detector).

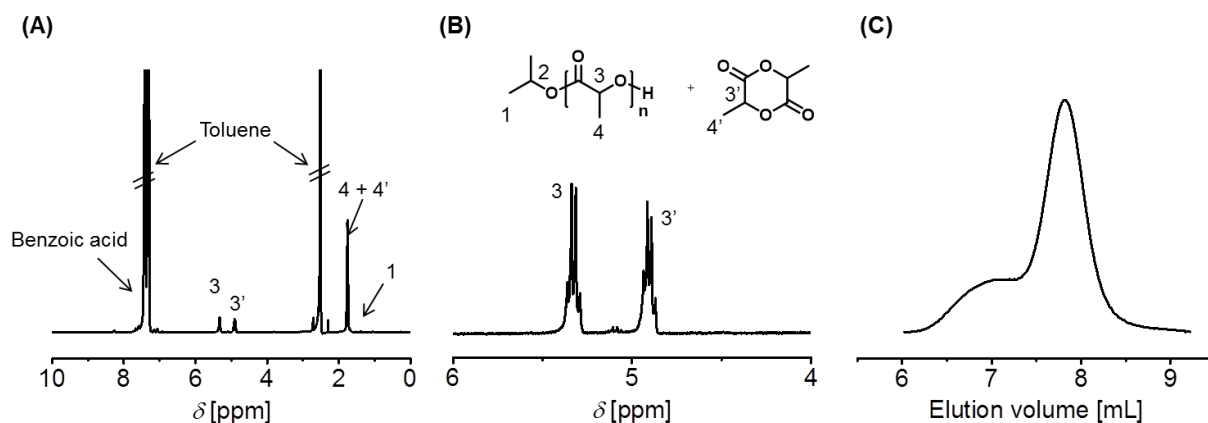


Figure S7: Characterization of entry **6** in **Table 1** employing a [LLA]:[Sr(OiPr)₂]:[DodOH] of 200:1:0. **A:** ¹H NMR spectrum (300 MHz, CDCl₃) of the reaction mixture and structural assignment. **B:** Zoom in in the methine region and schematic representation of the structural assignment (peaks 3 and 3' were used to calculate conversion). **C:** SEC elugram (CHCl₃, RI detector).

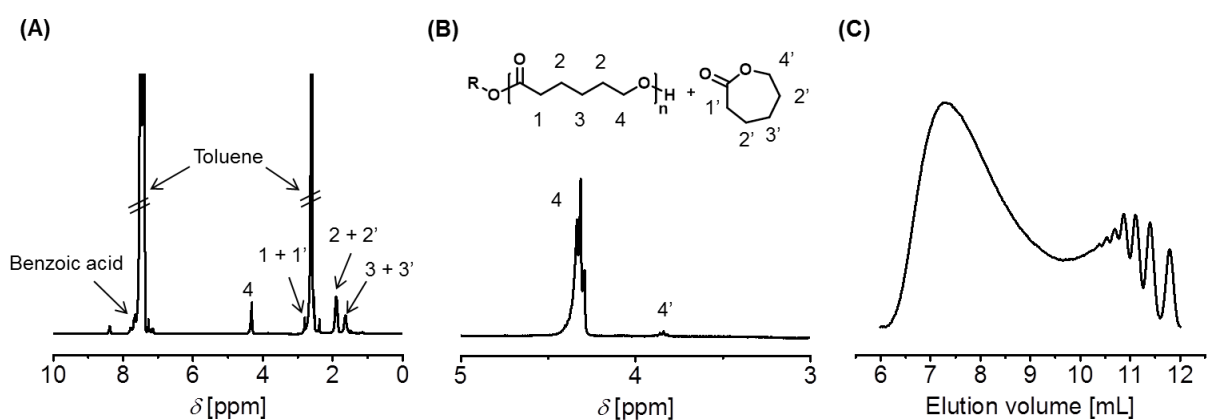


Figure S8: Characterization of entry **7** in **Table 1** employing a [ϵ CL]:[Sr(OiPr)₂]:[DodOH] of 100:1:1. **A:** ¹H NMR spectrum (300 MHz, CDCl₃) of the reaction mixture and schematic representation of the structural assignment. **B:** Zoom in in the methine region and structural assignment (peaks 4 and 4' were used to calculate conversion). **C:** SEC elugram (CHCl₃, RI detector).

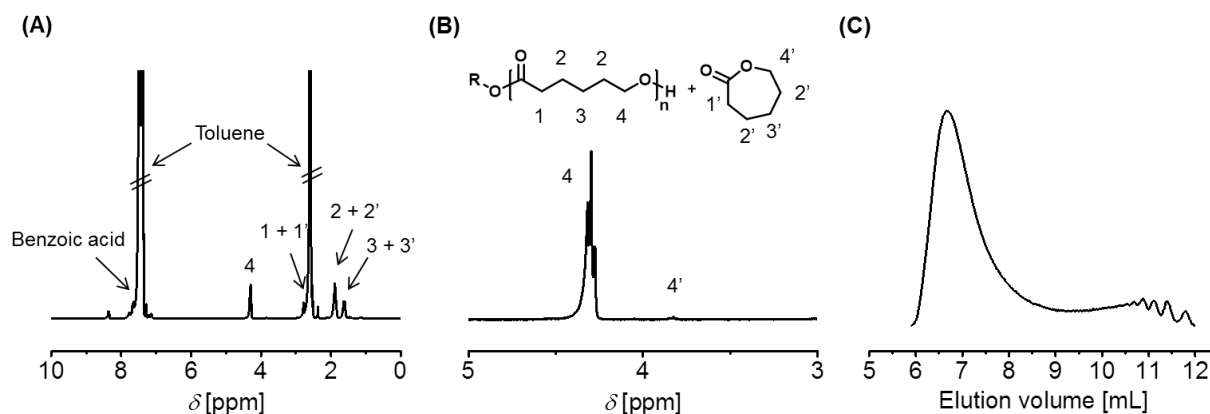


Figure S9: Characterization of entry **8** in **Table 1** employing a $[\epsilon\text{CL}]:[\text{Sr}(\text{OiPr})_2]:[\text{DodOH}]$ of 100:1:0.

A: ^1H NMR spectrum (300 MHz, CDCl_3) of the reaction mixture and schematic representation of the structural assignment. **B:** Zoom in in the methine region and structural assignment (peaks 4 and 4' were used to calculate conversion). **C:** SEC elugram (CHCl_3 , RI detector).

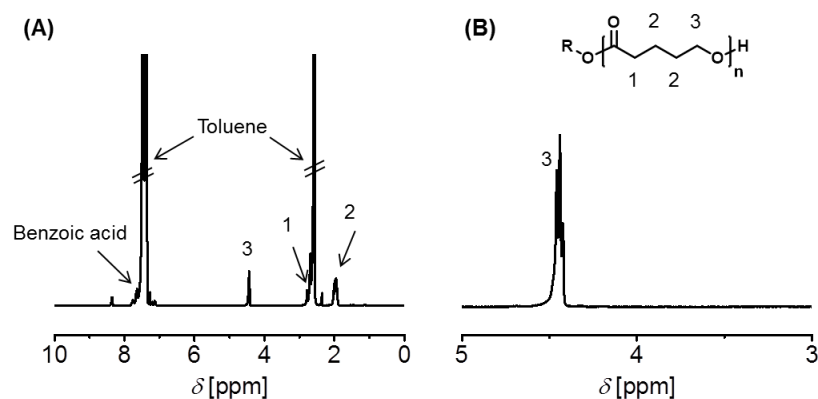


Figure S10: Characterization of entry **9** in **Table 1** employing a $[\delta\text{VL}]:[\text{Sr}(\text{OiPr})_2]:[\text{DodOH}]$ of 100:1:1. **A:** ^1H NMR spectrum (300 MHz, CDCl_3) of the reaction mixture and schematic representation of the structural assignment. **B:** Zoom in in the methine region and structural assignment.

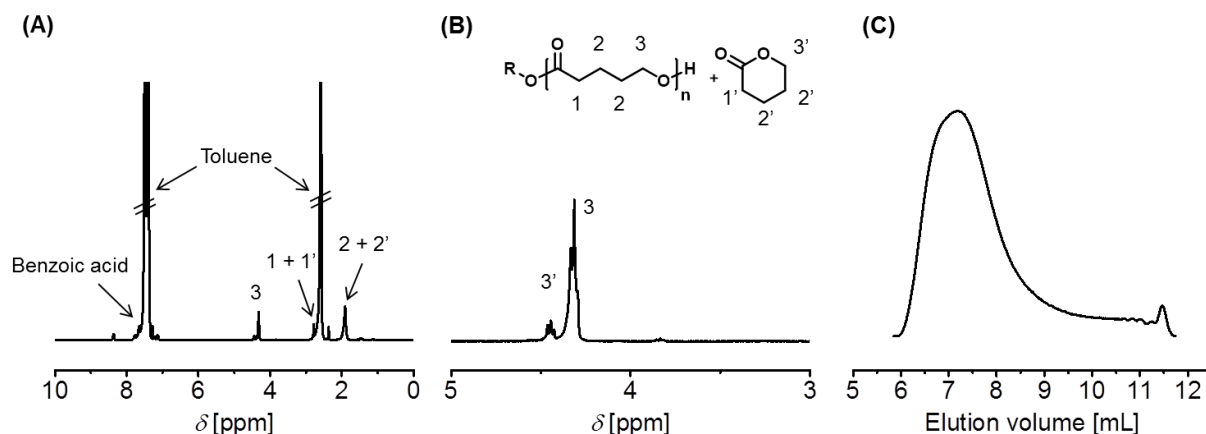


Figure S11: Characterization of entry **10** in **Table 1** employing a $[\delta\text{VL}]:[\text{Sr}(\text{OiPr})_2]:[\text{DodOH}]$ of 100:1:0. **A:** ^1H NMR spectrum (300 MHz, CDCl_3) of the reaction mixture and schematic representation of the structural assignment. **B:** Zoom in in the methine region and structural assignment (peaks 3 and 3' were used to calculate conversion). **C:** SEC elugram (CHCl_3 , RI detector).

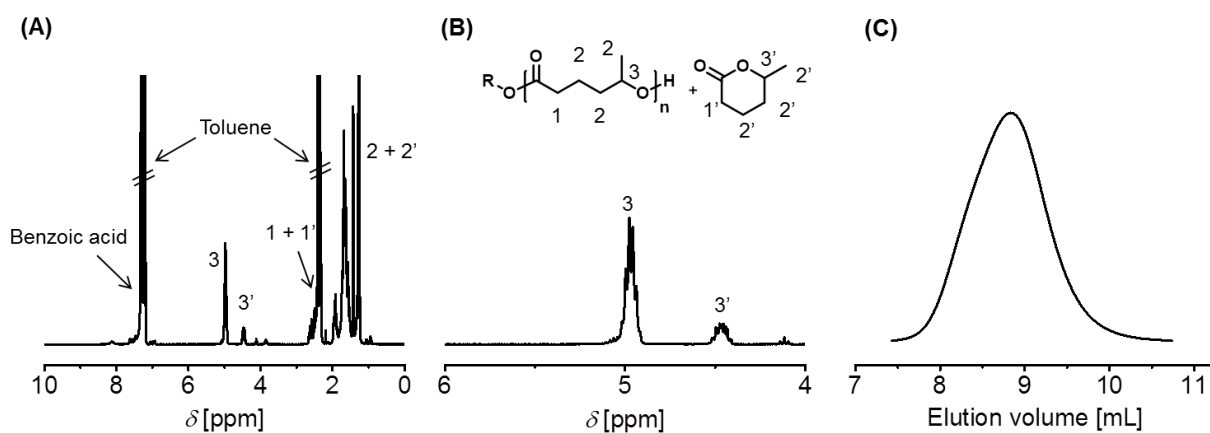


Figure S12: Characterization of entry **11** in **Table 1** employing a $[\delta\text{CL}]:[\text{Sr}(\text{OiPr})_2]:[\text{DodOH}]$ of 100:1:1. **A:** ^1H NMR spectrum (300 MHz, CDCl_3) of the reaction mixture and schematic representation of the structural assignment. **B:** Zoom in in the methine region and structural assignment (peaks 3 and 3' were used to calculate conversion). **C:** SEC elugram (CHCl_3 , RI detector).

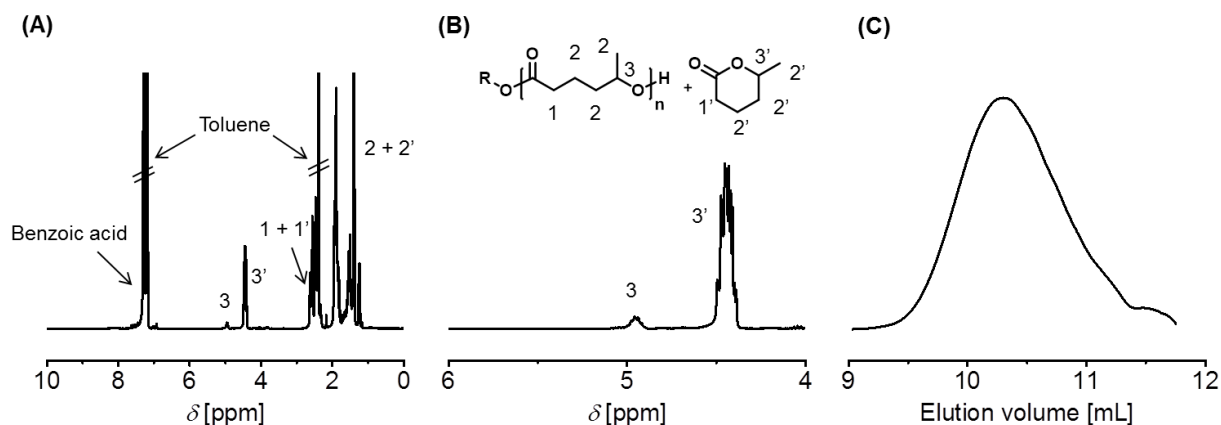


Figure S13: Characterization of entry **12** in **Table 1** employing a $[\delta\text{CL}]:[\text{Sr}(\text{OiPr})_2]:[\text{DodOH}]$ of 100:1:0. **A:** ^1H NMR spectrum (300 MHz, CDCl_3) of the reaction mixture and structural assignment. **B:** Zoom in in the methine region and schematic representation of the structural assignment (peaks 3 and 3' were used to calculate conversion). **C:** SEC elugram (CHCl_3 , RI detector).

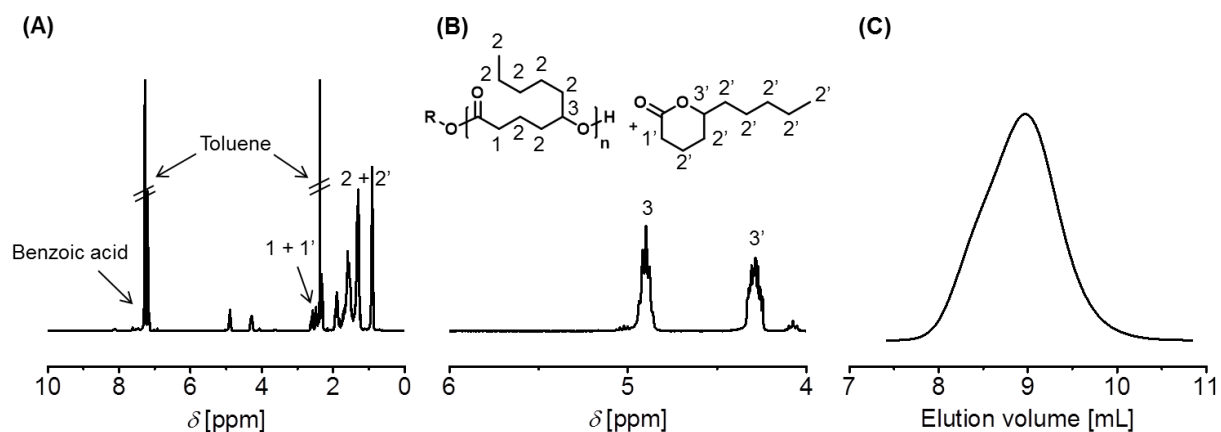


Figure S14: Characterization of entry **13** in **Table 1** employing a $[\delta\text{DL}]:[\text{Sr}(\text{OiPr})_2]:[\text{DodOH}]$ of 100:1:1. **A:** ^1H NMR spectrum (300 MHz, CDCl_3) of the reaction mixture and schematic representation of the structural assignment. **B:** Zoom in in the methine region and structural assignment (peaks 3 and 3' were used to calculate conversion). **C:** SEC elugram (CHCl_3 , RI detector).

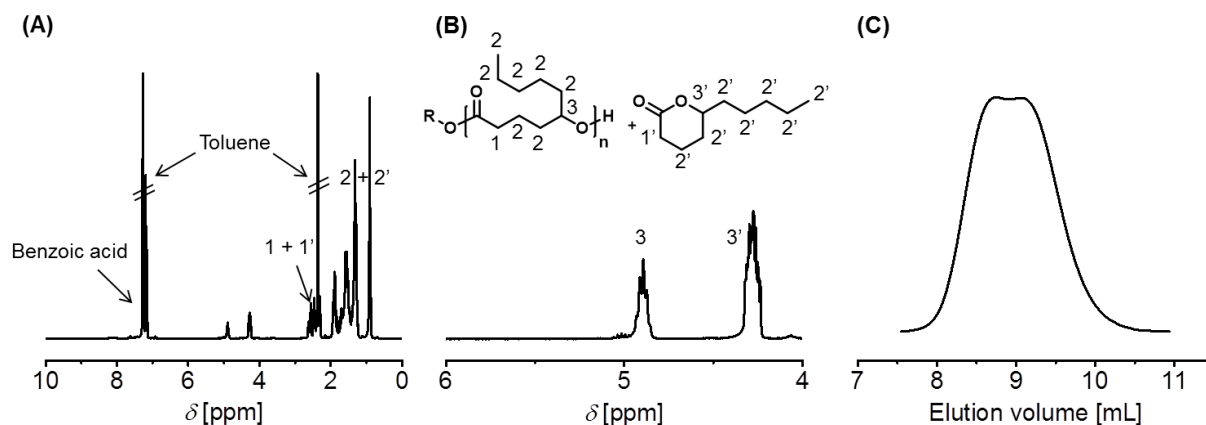


Figure S15: Characterization of entry **13** in **Table 1** employing a $[\delta\text{DL}]:[\text{Sr}(\text{OiPr})_2]:[\text{DodOH}]$ of 100:1:0. **A:** ^1H NMR spectrum (300 MHz, CDCl_3) of the reaction mixture and schematic representation of the structural assignment. **B:** Zoom in in the methine region and structural assignment (peaks 3 and 3' were used to calculate conversion). **C:** SEC elugram (CHCl_3 , RI detector).

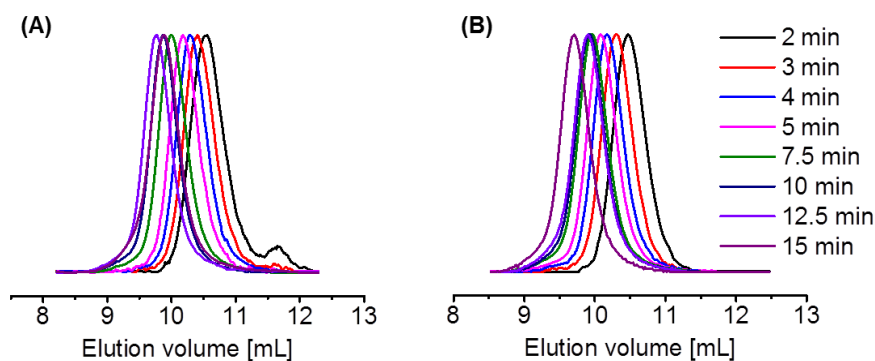
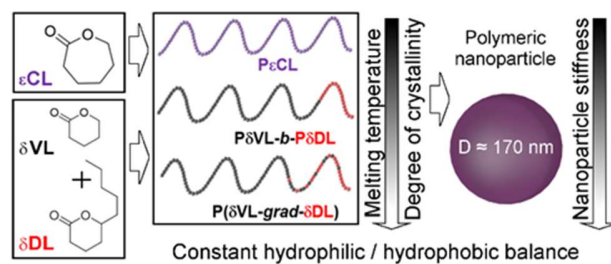


Figure S16: Overlay of the SEC elugrams (THF, RI detection, PLA calibration) for the kinetic studies of the ROP of LA in toluene (0.5 mol L^{-1}) at room temperature. **A:** Elugrams for the kinetic study without dodecanol ($[\text{LLA}]:[\text{Sr}(\text{OiPr})_2] = 100:1$). **B:** Elugrams for the kinetic study with dodecanol ($[\text{LLA}]:[\text{Sr}(\text{OiPr})_2]:[\text{DodOH}] = 100:1:1$).

Publication P3

Maintaining the hydrophilic–hydrophobic balance of polyesters with adjustable crystallinity for tailor–made nanoparticles

D. Bandelli, C. Helbing, C. Weber, M. Seifert, I. Muljajew, K. D. Jandt, U. S. Schubert,
Macromolecules **2018**, *51*, 5567–5576.



Maintaining the Hydrophilic–Hydrophobic Balance of Polyesters with Adjustable Crystallinity for Tailor-Made Nanoparticles

Damiano Bandelli,^{†,‡} Christian Helbing,^{‡,§} Christine Weber,^{†,‡} Michael Seifert,[§] Irina Muljajew,^{†,‡} Klaus D. Jandt,^{*,‡,§} and Ulrich S. Schubert^{*,†,‡}

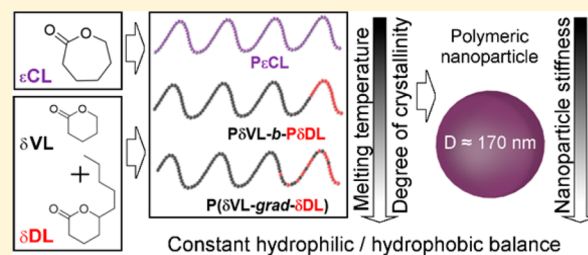
[†]Laboratory of Organic and Macromolecular Chemistry (IOMC), Friedrich Schiller University Jena, Humboldtstr. 10, 07743 Jena, Germany

[‡]Jena Center for Soft Matter (JCSM), Friedrich Schiller University Jena, Philosophenweg 7, 07743 Jena, Germany

[§]Chair of Materials Science (CMS), Department of Materials Science and Technology, Otto Schott Institute of Materials Research, Faculty of Physics and Astronomy, Friedrich Schiller University Jena, Löbdergraben 32, 07743 Jena, Germany

Supporting Information

ABSTRACT: To explore the relationship between thermal properties of a polymer and the biological performance of the resulting nanoparticle, all other parameters, including the hydrophobicity, should be kept constant. For this purpose, a gradient and a block copolyester were tailor-made via the triazabicyclodecene catalyzed ring-opening copolymerization of δ -valerolactone (δ VL) and δ -decalactone (δ DL) to match the hydrophobicity of poly(ϵ -caprolactone) (P ϵ CL). The degree of crystallinity of the semicrystalline materials was significantly reduced due to the incorporation of amorphous P δ DL segments, as confirmed by dynamic scanning calorimetry. Atomic force microscopy revealed short and randomly oriented crystals in the gradient copolymer but longer and parallel aligned crystals for the block copolymer and P ϵ CL. The stiffness of nanoparticles ($D_h \approx 170$ nm) prepared from the polyesters correlated to the bulk crystallinity. The set of nanoparticles with constant hydrophobicity and size will facilitate direct access to the influence of the nanoparticle crystallinity on biological processes such as enzymatic degradation, drug release, and cellular uptake.



INTRODUCTION

Polymeric nanoparticles represent highly promising materials for the targeted delivery of actives. They are often composed of a biodegradable polymer core serving as a reservoir for pharmaceutically active compounds, while stealth polymers¹ or targeting ligands² can be attached to its shell.³ The interdisciplinary field and the modularity of the concept offer a vast parameter landscape, rendering strict systematic investigations extremely complex. However, the latter are required to understand nanoparticle mediated drug delivery, which is one key factor for the development of a truly personalized medicine. Although the physicochemical characterization of nanoparticle carrier systems alone has been established,⁴ investigations of structure–property relationships with a predicting character regarding, e.g., release profiles of actives are still missing.

The vast majority of degradable nanocarriers is composed of polyesters such as poly(ϵ -caprolactone) (P ϵ CL) or polylactide (PLA).⁵ Encapsulated actives are released by enzymatic degradation.⁶ Besides other factors such as the hydrophobicity, the molar mass, or the chemical composition of the polymers, the crystallinity of polyesters influences the enzymatic degradation rate and, hence, the release from polyester-based nanoparticles.^{7–9} However, a clear statement can only be made

if only one parameter is varied, but all other parameters are kept constant. Although such investigations exist regarding the influence of the degree of crystallinity for PLA stereocomplexes in thin films,¹⁰ the issue is more complex for aqueous nanoparticle suspensions and has, to the best of our knowledge, not been clarified yet.

Whereas, e.g., the size of a polymer nanoparticle can be easily varied by using the identical polymer material,¹¹ a variation of the polyester crystallinity is often accompanied by a variation of the chemical composition. Unfortunately, a constant hydrophilic–hydrophobic balance (HHB) of the materials is difficult to maintain because polyesters with elongated alkyl spacers are more crystalline but also more hydrophobic than polyesters with shorter alkyl spacers.^{12,13}

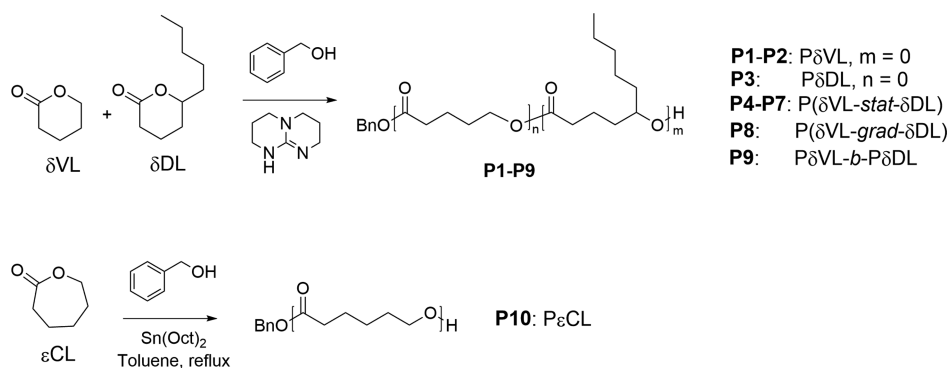
We therefore selected P ϵ CL as a well-known semicrystalline reference material and approached the issue by developing polyesters that would feature a different degree of crystallinity but the same hydrophobicity, i.e., the same fraction of ester moieties per polymer chain. The copolymerization concept relies on δ -lactones as monomers (Scheme 1). Lacking one

Received: April 30, 2018

Revised: June 19, 2018

Published: July 18, 2018

Scheme 1. Schematic Representation of the Ring-Opening Polymerization of ϵ -Caprolactone (ϵ CL), δ -Valerolactone (δ VL), and δ -Decalactone (δ DL) Yielding the Homo- and Copolyesters P1 to P10



methylene unit compared to P ϵ CL, poly(δ -valerolactone) (P δ VL) represents a semicrystalline polyester with a similar melting temperature as the reference material. Substituents at the six-membered monomer ring are known to significantly decrease the crystallinity of the corresponding polyesters, which in fact are often amorphous.¹³ We hence selected δ -decalactone (δ DL), comprising four additional methylene moieties compared to ϵ CL, as a second monomer to compensate for the “missing” methylene moiety of δ VL. A copolymer consisting of 80 mol % of δ VL and 20 mol % of δ DL would hence feature the same fraction of ester moieties as P ϵ CL.

δ -Lactones can be polymerized via ring-opening polymerization (ROP) using cationic initiators,¹⁴ the standard catalyst tin(II) octoate (Sn(Oct)₂),¹⁵ and organic base catalysts.^{16–20} The negative free enthalpy and entropy of the ROP of δ -lactones make the resulting polyesters polymers featuring a classical ceiling temperature.¹³ In view of this fact, we relied on the highly active catalyst triazabicyclodecene (TBD), which has already been successfully applied for the homopolymerization of δ VL²¹ and δ DL^{22,23} at room temperature.

The synthetic development of the tailor-made copolyesters we describe herein includes detailed kinetic studies to elucidate the microstructure and is complemented by an extensive characterization of the thermal and mechanical properties of the materials. Dynamic scanning calorimetry and polarized light microscopy were applied as integrating methods²⁴ to bulk samples. Atomic force microscopy^{25,26} was applied to correlate the bulk properties with the mechanical properties of nanoparticles prepared from the materials.

EXPERIMENTAL SECTION

Materials. δ -Valerolactone (δ VL, 98%) and δ -decalactone (δ DL, 97%) were purchased from TCI. ϵ -Caprolactone (ϵ CL, 97%) was purchased from Sigma-Aldrich and dried over calcium hydride. Benzyl alcohol (BnOH, 99.8%, water content <0.003%), 1,5,7-triazabicyclo[4.4.0]dec-5-ene (TBD), tin octanoate (Sn(Oct)₂), and anhydrous toluene were purchased from Sigma-Aldrich. All other chemicals were purchased from standard suppliers and used without further purification. All glassware was dried at 110 °C for 24 h prior to use for polymerization.

Instruments. All polymerizations were prepared in a MBraun UNILab Plus glovebox workstation under a nitrogen atmosphere (<0.1 ppm of H₂O; <0.1 ppm of O₂). Proton nuclear magnetic resonance (¹H NMR) spectra were recorded at room temperature in CDCl₃ on a Bruker Avance 300 MHz using the residual solvent resonance as internal standard. The chemical shifts are given in ppm relative to tetramethylsilane (TMS).

Size exclusion chromatography (SEC) measurements were performed on a Shimadzu system equipped with a CBM-20A system controller, a LC-10AD VP pump, a RID-10A refractive index detector, a SPD-10AD VP UV detector, and a SDV linear S column from PSS (Polymer Standards Service GmbH, Mainz, Germany) at 40 °C using chloroform:triethylamine:2-propanol (94:4:2) as eluent at a flow rate of 1 mL min⁻¹. The system was calibrated against PMMA standards (410–88 000 g mol⁻¹), which were purchased from PSS.

For the measurements of the matrix-assisted laser desorption/ionization time-of-flight (MALDI-ToF) mass spectra, an Ultraflex III ToF/ToF instrument (Bruker Daltonics, Bremen, Germany) was used. The instrument is equipped with a Nd:YAG laser and a collision cell. All spectra were measured in the positive reflector mode using *trans*-2-[3-(4-*tert*-butylphenyl)-2-methyl-2-propenylidene] (DCTB) as matrix and sodium iodide (NaI) as doping salt. The instrument was calibrated prior to each measurement with an external PMMA standard (2500 g mol⁻¹) from PSS.

Thermogravimetric analysis (TGA) was performed under a nitrogen atmosphere on a Netzsch TG 209 F1 Iris from room temperature to 600 °C at a heating rate of 10 K min⁻¹. Differential scanning calorimetry (DSC) measurements were performed on a Netzsch DSC 204 F1 Phoenix under a nitrogen atmosphere from –150 to 210 °C. Three cycles were recorded for each sample using a cooling rate of 20 K min⁻¹ between the heating runs. The first and the second heating run were conducted at a heating rate of 20 K min⁻¹. For the third heating run, a heating rate of 10 K min⁻¹ was applied. The glass transition temperature (T_g , inflection value reported) and the melting temperature (T_m) values are reported from the second heating run.

Dynamic light scattering (DLS) and ζ -potential measurements were performed on a Zetasizer Nano ZS (Malvern Instruments, Herrenberg, Germany) at 25 °C ($\lambda = 633$ nm) at an angle of 173°. Each measurement was performed five times. The mean particle size was approximated as the effective (Z-average) diameter and the width of the distribution as the dispersity index (PDI) of the particles obtained by the cumulants method assuming a spherical shape.

A Leica DM 2700 equipped with a linkam heating stage was used to prepare polymeric spherulites. For this purpose, a small amount of the polymer was placed on a clean glass slide and heat-treated with the same temperature profile as described for the DSC measurements. The formation of spherulites was clarified by light microscopy with crossed polarizers.

Shape and dimensions of the nanoparticles were investigated by scanning electron microscopy (SEM) with an AURIGA 60 Cross-Beam workstation (Carl Zeiss AG, Oberkochen, Germany). Additionally, atomic force microscopy (AFM) measurements were performed with a Dimension 3100 and Catalyst (both from Bruker, Veeco, Santa Barbara, CA) equipped with a nanoscope IV and VIII controller, respectively, to determine the nanoparticle shape and stiffness. Measurements were performed at room temperature by using standard tapping mode silicon cantilevers from Bruker (model RTESP, Veeco, Santa Barbara, CA) with a resonance frequency in the

Table 1. Selected Structural Characterization Data of the Synthesized (Co)polymers

sample	polymer	$\delta\text{VL}/\delta\text{DL}$			NMR ^c [mol %]	NMR		SEC	
		feed [mol %]	conv ^a [%]	theor ^b [mol %]		M_n^c [kg mol ⁻¹]	M_n^d [kg mol ⁻¹]	\bar{D}^d	
P1 ^e	P δVL	100/0	98/–	100/0	100/0	2.7	3.8	1.47	
P2	P δVL	100/0	93/–	100/0	100/0	9	9	1.33	
P3	P δDL	0/100	–/84	0/100	0/100	14	14	1.55	
P4	P(δVL -stat- δDL)	80/20	99/82	83/17	85/15	11	14	2.33	
P5	P(δVL -stat- δDL)	70/30	99/84	73/27	77/23	11	13	2.31	
P6	P(δVL -stat- δDL)	60/40	99/85	64/36	67/33	12	14	1.94	
P7	P(δVL -stat- δDL)	50/50	99/84	54/46	58/42	12	13	1.66	
P8	P(δVL -grad- δDL)	75/25	98/82	78/22	80/20	11	11	1.66	
P9	P δVL -b-P δDL	n.a.	70/17	80/20	82/18	11	11	1.35	
P10	PeCL	n.a.	99 (ϵCL)	n.a.	n.a.	9	9	1.30	

^aDetermined by integration of suitable signals in the ¹H NMR spectra of the reaction solution. ^bCalculated from feed ratio and monomer conversion. ^cDetermined by integration of suitable signals in the ¹H NMR spectra of the purified polymers. ^dEluent CHCl₃, RI detection, PMMA calibration. ^eMALDI-ToF MS: $M_n = 2.8 \text{ kg mol}^{-1}$, $\bar{D} = 1.14$.

range 315–364 kHz in air, a spring constant in the range 20–80 N m⁻¹, and a typical tip radius of less than 10 nm (typically 7 nm). The peak-force tapping mode was used to capture force–distance curves simultaneously to height profiles. To avoid a movement of the nanoparticles during the measurements, silicon substrates were modified with a thin layer of polyethylenimine (PEI).

Ring-Opening Polymerization. All polymerization mixtures were prepared in a glovebox at room temperature under a nitrogen atmosphere (<0.1 ppm of H₂O; <0.1 ppm of O₂). For the polymerizations catalyzed by TBD, a stock solution of initiator and catalyst was used. The stock solution contained 28 mg (0.2 mmol) of TBD, 20 μL (0.2 mmol) of BnOH, and 180 μL of anhydrous toluene for polymerizations conducted at a [BnOH]:[TBD] ratio of 1:1.

Polymerization Kinetics. For the kinetic studies of the homopolymerization of δVL and δDL , five vials were each charged with 1 mmol of monomer (corresponding to 110 μL of δVL and 179 μL of δDL). For the polymerization of δDL , 0.01 mmol of BnOH and 0.01 mmol of TBD were added to each vial from a stock solution in toluene to reach a ratio of $[\delta\text{DL}]:[\text{TBD}]:[\text{BnOH}] = 100:1:1$. According to a ratio of $[\delta\text{VL}]:[\text{TBD}]:[\text{BnOH}] = 100:0.1:1$, 0.01 mmol of BnOH and 0.001 mmol of TBD were used for the polymerization of δVL . The ROP proceeded at room temperature under stirring, and the reactions were quenched by addition of 1 mL of a solution of benzoic acid (1 equiv with respect to TBD) in chloroform after varying time intervals. ¹H NMR and SEC analyses were performed from the quenched reaction mixtures in order to assess the monomer conversion, the molar mass, and the dispersity (\bar{D}). The P δVL kinetics were conducted directly inside the glovebox. For the P δDL kinetics, the sample vials were prepared and sealed inside the glovebox and subsequently stirred outside of the glovebox at 23 °C.

For the kinetic studies of the statistical copolymerization, 0.75 mmol (70 μL) of δVL and 0.25 mmol (45 μL) of δDL were mixed inside each vial, and BnOH and TBD were added as described above to reach a ratio of $[\delta\text{VL}]:[\delta\text{DL}]:[\text{TBD}]:[\text{BnOH}] = 75:25:1:1$. The vials were transferred out of the glovebox, and kinetic samples were quenched and analyzed as described above.

Homopolymerization of δVL and δDL (P1 to P3). Corresponding to an initial ratio of $[\text{M}]:[\text{TBD}]:[\text{BnOH}]$ of 20:0.1:1, P1 was obtained as described above using 110 μL (1 mmol) of δVL and 10 μL of the stock solution containing TBD and BnOH. The polymerizations of P2 to P3 were conducted as described above (see kinetic studies). After the polymerization time indicated below, the polymerization mixtures were quenched, and a sample for the determination of the monomer conversion was taken. The crude polymers were precipitated into cold methanol (–22 °C), and the purified polyesters were dried at 40 °C in a vacuum oven overnight.

P δVL (P1). $t_{\text{pol}} = 13 \text{ min}$; conv = 98%. ¹H NMR (300 MHz, CDCl₃): $\delta/\text{ppm} = 1.68$ (broad, $-\text{CH}_2\text{CH}_2-$), 2.35 (t, $-\text{OC}(\text{O})\text{CH}_2-$), 4.08 (t, $-\text{CH}_2\text{O}-$), 5.15 (s, $\text{C}_6\text{H}_5(\text{CH}_2)\text{OC}(\text{O})-$), 7.36 (m,

C_6H_5-). SEC (CHCl₃, PMMA calibration): $M_n = 3.8 \text{ kg mol}^{-1}$; $\bar{D} = 1.47$. MALDI MS: $M_n = 2.8 \text{ kg mol}^{-1}$, $\bar{D} = 1.14$.

P δVL (P2). $t_{\text{pol}} = 50 \text{ min}$; conv = 93%; yield 90%. ¹H NMR (300 MHz, CDCl₃): $\delta/\text{ppm} = 1.68$ (broad, $-\text{CH}_2\text{CH}_2-$), 2.35 (t, $-\text{OC}(\text{O})\text{CH}_2-$), 4.08 (t, $-\text{CH}_2\text{O}-$), 5.15 (s, $\text{C}_6\text{H}_5(\text{CH}_2)\text{OC}(\text{O})-$), 7.36 (m, C_6H_5-). SEC (CHCl₃, PMMA calibration): $M_n = 9 \text{ kg mol}^{-1}$; $\bar{D} = 1.33$.

P δDL (P3). $t_{\text{pol}} = 24 \text{ h}$; conv = 84%; yield 50%. ¹H NMR (300 MHz, CDCl₃): $\delta/\text{ppm} = 0.86$ (t, CH_3-), 1.28 (t, $-\text{CH}_2-\text{CH}_2-\text{CH}_2-$), 1.57 (broad, $-\text{CH}_2-\text{CH}_2-\text{CH}(\text{OH})-\text{CH}_2-$), 2.30 (t, $-\text{OC}(\text{O})-\text{CH}_2-$), 5.12 (s, $\text{C}_6\text{H}_5(\text{CH}_2)\text{OC}(\text{O})-$), 7.36 (m, C_6H_5-). SEC (CHCl₃, PMMA calibration): $M_n = 14 \text{ kg mol}^{-1}$; $\bar{D} = 1.55$.

Statistical Copolymerization of δVL and δDL (P4 to P8). The statistical copolymers comprising δVL and δDL P4 to P7 were obtained as described above for the homopolymers P2 to P3. Keeping a constant ratio of $[\text{M}]_{\text{total}}:[\text{TBD}]:[\text{BnOH}] = 100:1:1$, the feed ratio of δDL and δVL was varied as indicated in Table 1. In an exemplary reaction for P4, 74 μL (0.8 mmol) of δVL was mixed with 36 μL (0.20 mmol) of δDL , 0.01 mmol of BnOH, and 0.01 mmol of TBD. The polymerization was conducted at room temperature for 18 h, and the analysis and purification were performed as described above.

Corresponding to a ratio of $[\delta\text{VL}]:[\delta\text{DL}]:[\text{TBD}]:[\text{BnOH}] = 75:25:1:1$, P8 was obtained using 69.6 μL (0.75 mmol) of δVL , 44.6 μL (0.25 mmol) of δDL , and 10 μL of the stock solution containing TBD and BnOH.

P(δVL -stat- δDL) (P8). $t_{\text{pol}} = 7.5 \text{ h}$; conv(δVL) = 98%; conv(δDL) = 82%; yield 82%. ¹H NMR (300 MHz, CDCl₃): $\delta/\text{ppm} = 0.89$ (t, CH_3 -DL), 1.28 (t, $\text{CH}_3-\text{CH}_2\text{CH}_2\text{CH}_2$ -DL), 1.63 (broad, $-\text{CH}_2-\text{CH}(\text{OH})-\text{CH}_2\text{CH}_2$ -DL), 2.35 (t, $-\text{OC}(\text{O})\text{CH}_2-$), 4.09 (t, $-\text{CH}_2\text{O}-\text{VL}$), 4.88 (t, $-\text{CH}_2\text{O}-\text{DL}$), 5.13 (s, $\text{C}_6\text{H}_5(\text{CH}_2)\text{OC}(\text{O})-$), 7.36 (m, C_6H_5-). SEC (CHCl₃, PMMA calibration): $M_n = 11 \text{ kg mol}^{-1}$; $\bar{D} = 1.66$.

Synthesis of P δVL -b-P δDL (P9). 20 μL of the stock solution and 185.8 μL (2 mmol) of δVL were used for the synthesis of the first block corresponding to a $[\text{M}]:[\text{TBD}]:[\text{BnOH}] = 100:0.1:1$. The polymerization was quenched after 32 min by the addition of 1 mL of a solution of benzoic acid (1 equiv in comparison with TBD) in chloroform. The first block was purified and analyzed as described above.

Conv = 70%; yield 53%; $M_{n,\text{theo}} = 7.1 \text{ kg mol}^{-1}$. ¹H NMR (300 MHz, CDCl₃): $\delta/\text{ppm} = 1.68$ (broad, $-\text{CH}_2\text{CH}_2-$), 2.35 (t, $-\text{OC}(\text{O})\text{CH}_2-$), 4.08 (t, $-\text{CH}_2\text{O}-$), 5.15 (s, $\text{C}_6\text{H}_5(\text{CH}_2)\text{OC}(\text{O})-$), 7.36 (m, C_6H_5-); $M_{n,\text{NMR}} = 7.7 \text{ kg mol}^{-1}$. SEC (CHCl₃, PMMA calibration): $M_n = 10 \text{ kg mol}^{-1}$; $\bar{D} = 1.18$.

For the chain extension, 75 mg (0.01 mmol) of the P δVL block was dissolved in 177 μL (1 mmol) of δDL by stirring for 2 h. Subsequently, 10 μL of a solution of TBD in toluene was added to result in an initial ratio of $[\text{M}]:[\text{TBD}]:[\text{P}\delta\text{VL}] = 100:1:1$. The reaction was performed at room temperature and quenched after 260

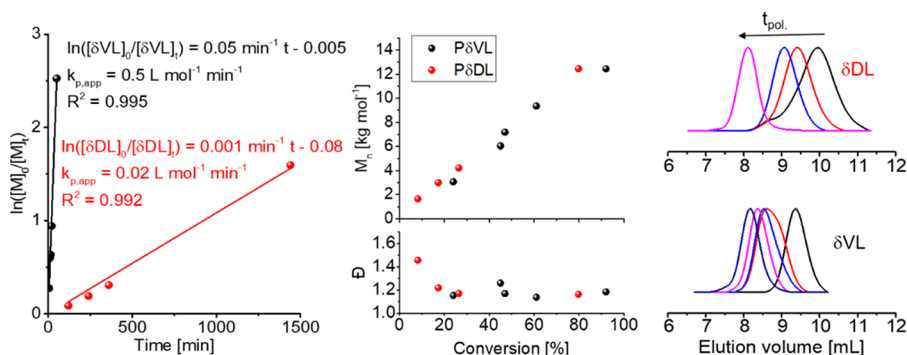


Figure 1. Kinetic studies of the homopolymerization of δVL and δDL conducted in bulk at room temperature using BnOH as initiator and TBD as catalyst ($[\delta DL]:[TBD]:[I] = 100:1:1$; $[\delta VL]:[TBD]:[I] = 100:0.1:1$). Left: first-order kinetic plot with a linear fit according to $\ln([M]_0/[M]) = k_{p,app}[I]_0 t$. Center: evolution of the molar mass with monomer conversion. Right: overlay of the SEC elugrams of the samples taken (CHCl_3 , RI detection).

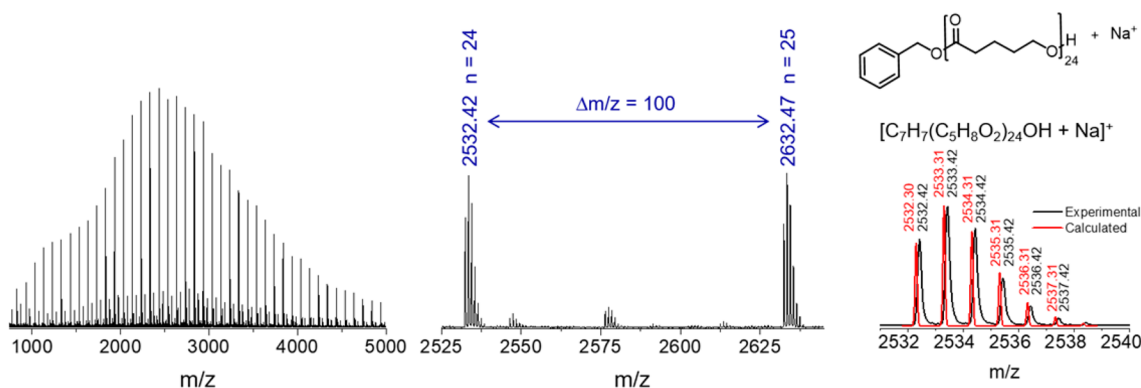


Figure 2. MALDI-ToF MS analysis of $P\delta VL$ (**P1**, DCTB, NaI). Left: full mass spectrum. Center: zoom into the most abundant m/z region. Right: overlay of the calculated and measured isotopic pattern for the structural assignment of the observed peaks.

min. The block copolymer **P9** was purified and analyzed as described above.

***P* δVL -*b*-*P* δDL (**P9**).** Conv = 17%; yield 24%. ¹H NMR (300 MHz, CDCl_3): δ /ppm = 0.89 (t, CH_3 -(DL)), 1.28 (t, CH_3 - $\text{CH}_2\text{CH}_2\text{CH}_2$ -(DL)), 1.63 (broad, $-\text{CH}_2-\text{CH}(\text{OH})-\text{CH}_2\text{CH}_2$ -(DL)), 2.35 (t, $-\text{OC}(\text{O})\text{CH}_2-$), 4.09 (t, $-\text{CH}_2\text{O}$ -(VL)), 4.88 (t, $-\text{CH}_2\text{O}$ -(DL)), 5.13 (s, $\text{C}_6\text{H}_5(\text{CH}_2)\text{OC}(\text{O})-$), 7.36 (s, C_6H_5-). SEC (CHCl_3 , PMMA calibration): $M_n = 11 \text{ kg mol}^{-1}$; $\bar{D} = 1.35$.

Poly(ϵ -caprolactone) (**P** ϵ CL, **P10**) was prepared charging 1108 μL (1 mol) of ϵ -CL, 10 μL (10 mmol) of BnOH, and 40 mg (10 mmol) of $\text{Sn}(\text{Oct})_2$ in a Schlenk round-bottom flask inside the glovebox. The flask was moved out of the glovebox, and 19 mL of anhydrous toluene was added under argon flux ($[M]_0 = 0.5 \text{ mol L}^{-1}$). The polymerization was performed at reflux conditions for 24 h. Aliquots of 200 μL were taken periodically and analyzed by means of SEC and ¹H NMR spectroscopy to monitor the evolution of the molar mass and the monomer conversion. Subsequent to cooling to room temperature, the final sample was taken, and the polymer solution was precipitated into cold methanol (-22°C). The purified **P** ϵ CL was dried at 40°C under reduced pressure overnight.

***P* ϵ CL (**P10**).** Conv = 99%; yield 93%. ¹H NMR (300 MHz, CDCl_3): δ /ppm = 1.41 (broad, $-\text{CH}_2\text{CH}_2\text{C}(\text{O})\text{O}-$), 1.47 (broad, $-\text{OCH}_2\text{CH}_2\text{CH}_2-$), 2.32 (t, $-\text{CH}_2\text{C}(\text{O})\text{O}-$), 4.10 (t, $-\text{CH}_2\text{O}-$), 5.13 (s, $\text{C}_6\text{H}_5(\text{CH}_2)\text{OC}(\text{O})-$), 7.37 (m, C_6H_5-). SEC (CHCl_3 , PMMA calibration): $M_n = 9 \text{ kg mol}^{-1}$; $\bar{D} = 1.30$.

Nanoparticle Preparation. Aqueous nanoparticle suspensions were prepared by dropping a polymer solution in THF into deionized water (see the Supporting Information for details). In a representative example, 5 mg of polymer was dissolved in 1 mL of THF and then 0.5 mL of this solution were dropped into 5 mL of deionized water under stirring (1000 rpm) at room temperature. The samples were left stirring for 3 h in order to evaporate the THF. DLS analyses were

performed 24 h after preparation. The samples were stored at 5°C , and DLS analyses were regularly performed for a period of 1 month in order to evaluate the stability of the nanoparticles.

RESULTS AND DISCUSSION

Homopolymerization of δVL and δDL . Prior to the synthesis of copolymers comprising δVL and δDL , kinetic studies of the homopolymerization of both monomers were conducted in bulk at room temperature utilizing TBD as a catalyst. Benzyl alcohol was used as initiator at an initial ratio of $[M]:[TBD]:[I]$ of 100:1:1 for the polymerization of δDL (Scheme 1). The significantly more reactive unsubstituted monomer δVL was polymerized using a lower amount of catalyst ($[M]:[TBD]:[I] = 100:0.1:1$). SEC analysis of the kinetic samples revealed mostly monomodal molar mass distributions for $P\delta DL$ as well as $P\delta VL$. In particular, the dispersity (\bar{D}) of the $P\delta VL$ samples remained low ($\bar{D} = 1.04$ – 1.12). For $P\delta DL$, the dispersity significantly decreased from $\bar{D} = 1.47$ to $\bar{D} = 1.09$ during the course of the polymerization. The molar masses of both polymers increased in a linear fashion with the monomer conversion, indicating that the molar mass of $P\delta DL$ and $P\delta VL$ can be well controlled under similar polymerization conditions. The linear kinetic plots depicted in Figure 1 (left) revealed that both ROP followed pseudo-first-order kinetics. Despite a 10-fold lower amount of catalyst used, the apparent polymerization rate constant $k_{p,app}$ is 25 times higher for δVL ($k_{p,app} = 0.5 \text{ L mol}^{-1} \text{ min}^{-1}$) compared to δDL ($k_{p,app} = 0.02 \text{ L mol}^{-1} \text{ min}^{-1}$), suggesting that a

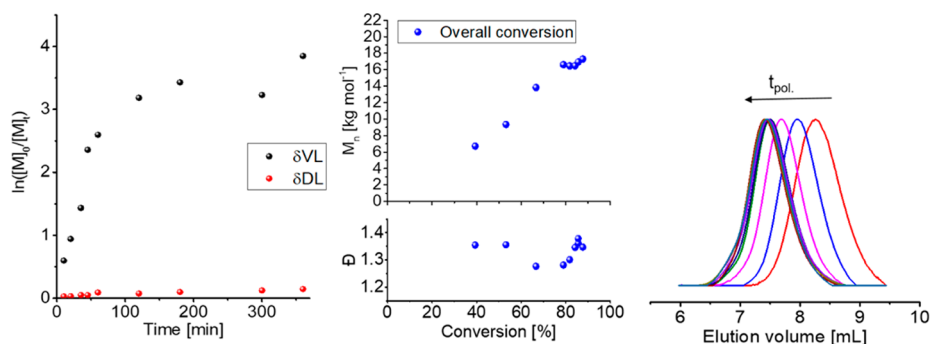


Figure 3. Kinetic studies of the statistical copolymerization of δ VL and δ DL conducted in bulk at room temperature using BnOH as initiator and TBD as catalyst ($[\delta$ VL]: $[\delta$ DL]:[TBD]:[I] = 75:25:1:1). Left: first-order kinetic plot for both monomers. Center: evolution of the molar mass with the overall monomer conversion. Right: overlay of the SEC elugrams of the samples taken (CHCl_3 , RI detection).

statistical copolymerization of the two monomers would result in copolymers with a strong gradient.

With respect to the synthesis of well-defined block copolymers comprising P δ VL and P δ DL, a high end group fidelity of the first block is of utmost importance for the reinitiation of the second block, i.e., the chain extension. For this purpose, MALDI-ToF MS analysis was performed for a P δ VL with a degree of polymerization (DP) of 20 (P1). The mass spectrum revealed a main distribution spaced by regular intervals of $\Delta m/z = 100$, corresponding to the mass of one repeating unit (Figure 2). The species could be assigned to sodiated P δ VL chains initiated by benzyl alcohol and terminated with a proton, as is demonstrated by the overlapping calculated and measured isotopic patterns. An additional less abundant m/z series could not be assigned to any water-initiated or cyclic polymer chains. In consequence, the obtained P δ VL would be suitable to act as a macroinitiator for a subsequent ROP of δ DL.

Statistical Copolymerization of δ VL and δ DL. In an initial screening, several statistical copolymerizations of δ VL and δ DL were performed to gain insight into a reasonable feed ratio of the monomers required to obtain a copolymer comprising 20 mol % δ DL. For this purpose, the fraction of δ DL in the feed was varied from 20 to 50 mol %. To account for the low reactivity of δ DL, the catalyst concentration was selected accordingly, resulting in an overall ratio of $[M]_{\text{total}}:[\text{TBD}]:[I]$ of 100:1:1 (Table 1). SEC analysis of the resulting copolymers P4 to P7 (see the Supporting Information) revealed rather broad molar mass distributions ($1.6 < \bar{D} < 2.4$) after a polymerization time of 16 h, most likely due to transesterification reactions. In particular, the SEC traces of P4 and P5, i.e., the copolymers comprising high molar fractions of the more reactive monomer δ VL, featured pronounced low molar mass tailing. Accordingly, the dispersity increases within the polymer series from P7 to P4. The individual monomer conversions were estimated from the ^1H NMR spectra of the unpurified samples. Because of overlapping signals in the spectra, the initial feed ratio of the two monomers was used as additional information (see the Supporting Information for details). Almost quantitative conversions of δ VL were reached, whereas around 80–85% of the less reactive δ DL was incorporated to the copolymers, as expected for the statistical copolymerization of two monomers with different reactivity. The final composition of P4 to P7 was determined via the integration of the methylene (δ VL repeating units) or methine (δ DL repeating units) proton signals neighboring the ester functionalities in the ^1H NMR spectra of the purified

copolymers (Figure S3). As shown in Table 1, the resulting compositions are in good agreement with the values calculated from the feed ratio and the monomer conversions for all copolymers.

To obtain a copolyester with the targeted composition of 80 mol % δ VL and 20 mol % δ DL, the feed ratio of the monomers was hence set to 75:25. Kinetic studies were performed to obtain detailed information about the expected compositional gradient along the polymer chain (Figure 3). In agreement with the kinetic plot for the homopolymerization of the two monomers, δ VL revealed a higher reactivity than δ DL, resulting in the formation of a gradient copolymer that is strongly enriched with δ VL repeating units at the beginning of the growing chain (see the Supporting Information). The linear increase of the molar mass with the overall monomer conversion and the unimodal molar mass distributions revealed that transesterifications were avoided despite the almost quantitative conversion of the more reactive δ VL. These polymerization conditions were hence applied to obtain a gradient copolyester with the same HHB of P ϵ CL (P8) that is composed of 80 mol % δ VL and 20 mol % δ DL.

Block Copolymerization. The targeted copolymer composition was achieved in a straightforward manner for the P δ VL-*b*-P δ DL block copolymer P9. To enable a fast initiation of the second block, the first block was synthesized via ROP of the more reactive δ VL. The resulting P δ VL with a DP of ≈ 76 served as macroinitiator for the less reactive δ DL. To avoid possible chain transfer reactions at high monomer conversions, the initial $[M]/[I]$ was set to 100 during the chain extension, which was driven to a conversion of 17%. In accordance with the monomer ratio thus expected, ^1H NMR spectroscopy revealed the targeted composition comprising 80 mol % δ VL and 20 mol % δ DL for the purified block copolymer. In addition, a clearly shifted molar mass distribution was observed by means of SEC measurements upon chain extension of the first block (see the Supporting Information).

In consequence, two tailor-made copolyesters with different microstructure were obtained that match the HHB of P ϵ CL (P10): the P δ VL-*b*-P δ DL block copolymer P9 and the P(δ VL-*grad*- δ DL) gradient copolymer P8. In addition, all three polymers featured a similar molar mass of around 9–11 kg mol $^{-1}$, making them perfect candidates for further investigation.

Bulk Properties. A differing degree of crystallinity or melting temperature of these tailor-made polyesters represented the next prerequisite to make them suitable materials

for our purpose. DSC measurements were hence performed using the bulk materials in the temperature range from -100 to 200 °C as the polyesters comprising P δ DL degraded above 200 °C (see the Supporting Information). As expected, the amorphous P δ DL **P3** revealed a low glass transition temperature T_g of -56 °C, whereas the P δ VL **P2** and the P ϵ CL **P10** represented semicrystalline materials with a melting temperature T_m of 57 °C (Figure 4). The fact that the T_m of the

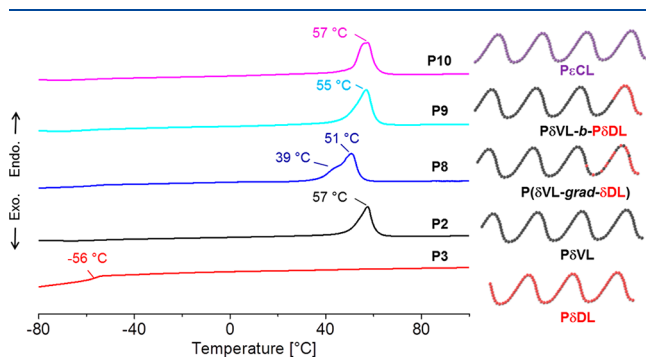


Figure 4. DSC thermograms of the polyesters **P8** to **P10** with constant HHB and the P δ VL and P δ DL homopolymers **P2** to **P3**. The measurement was performed from -100 to 200 °C (second heating run, heating rate 20 K min^{-1}).

P δ VL-*b*-P δ DL block copolymer **P9** remained almost unchanged ($T_m = 55$ °C) compared to that of the P δ VL homopolymer hints toward a phase segregation of the two building blocks in bulk. In contrast, the DSC thermogram of the P(δ VL-*grad*- δ DL) gradient copolymer **P8** revealed a nonsymmetrical broad endothermic peak at a significantly lower temperature. Although the crystallization of the P δ VL is impaired due to the incorporation of δ DL repeating units along the polymer chain, the strong gradient of **P9** allowed the formation of crystalline domains in the bulk material. Presumably, domains of varying composition melt at slightly different temperatures, explaining the broad transition.

The crystallinity of the materials is only resulting from the P δ VL segments, whereas the amorphous P δ DL fractions do not contribute. In consequence, the degree of crystallinity $X_{c,uw}$ was estimated from the DSC data using the melting enthalpies of fully crystalline P δ VL ΔH_f^0 .²⁷ As shown in Table 2, the three polyesters with constant HHB differ significantly with respect to their overall degree of crystallinity (from 24 to 52%). The P ϵ CL **P10** features the highest $X_{c,uw}$ and the $X_{c,uw}$ of the two copolymers is reduced. To compare the degree of crystallinity of the P δ VL domains of **P8** and **P9** to that of the P δ VL homopolymer, the δ VL mass fraction of the copolymers w_c was taken into account (eq 1).²⁸

$$X_{c,w} = \frac{\Delta H_f}{\Delta H_f^0 w_c} \quad (1)$$

Remarkably, the P δ VL domains in the P δ VL-*b*-P δ DL block copolymer **P9** revealed a similar $X_{c,w}$ as the P δ VL homopolymer, showing that the amorphous P δ DL domains do not interfere with the crystallization of the P δ VL block. In agreement with the broad melting transition, the $X_{c,w}$ is lowered for the P(δ VL-*grad*- δ DL) gradient copolymer **P8**. Here, the integration of δ DL mers in the crystalline P δ VL reduces the crystallizable domain size of the polymer chain and, thus, the bulk crystallinity.

The observations made by DSC measurements were supported by PLM measurements (Figure 5, left). For this purpose, polymer spherulites were prepared with the same temperature profiles as used for DSC measurements. The resulting light microscopy images confirmed the crystallinity of all three polymers because structures are visible due to a polarization of the light by birefringence induced by the polymeric crystals.²⁹

To obtain further information, we used AFM to investigate the surface in a more detailed fashion (Figure 5). Already the overview scans revealed that the alteration of the polymer chemistry significantly affected the bulk structure of the polyesters with constant HHB. The P ϵ CL homopolymer formed small spherulites, whereas a defined spherulite structure was not observable in the AFM images for the copolymers **P8** and **P9**. The variation in the polymer chain composition and, thus, the resulting varied crystallization behavior, visible in the DSC curves (Figure 4), are the reasons for the different surface structures. A closer look at the resulting crystalline surface morphology revealed that the differences in the chemical polymer structure from **P8** to **P10** not only induced different lamellar thicknesses (Table 2); furthermore, the lamellar crystal length and distribution changed. The gradient copolymer **P8** formed short and randomly oriented crystals. This observation explains the broad melting peak in the DSC, which correlates with a broad distribution of different crystal species.^{30,31} Likewise, the uniform long and parallel aligned crystals of the block copolymer **P9** and the P ϵ CL homopolymer **P10** are in agreement with the narrower DSC peak. The comparison of the lamella widths with the calculated polymer chain length (Table 2) revealed that the crystal domains are created by chain folds, which is typical for polymers.³²

Nanoparticles in Aqueous Suspension. Having successfully gained access to three polyesters with constant hydrophobicity but varied crystallinity, aqueous nanoparticle suspensions were prepared from **P8** to **P10** via nano-

Table 2. Bulk Properties of the Polyesters **P8**–**P10** with Constant HHB

polymer	<i>m</i> % δ VL	T_m^a [°C]	T_c^c [°C]	ΔH_f^a [J g^{-1}]	$X_{c,uw}^d$ [%]	$X_{c,w}^e$ [%]	l_{chain}^f [nm]	l_{lamella} [nm]
P2	P δ VL	57	22	72	40	40		
P3	P δ DL	– ^b	–	–	0	0		
P8	P(δ VL- <i>grad</i> - δ DL)	51	4	43	24	34	71	21.5 ± 2.6
P9	P δ VL- <i>b</i> -P δ DL	55	28	57	31	43	71	23.2 ± 7.2
P10	P ϵ CL	57	25	70	52	52	69	14.8 ± 2.0

^aDetermined by DSC in the second heating run. ^b $T_g = -56$ °C (inflection value, second heating run). ^cCrystallization temperature determined by DSC in the first cooling run. ^dEstimated from DSC using the ΔH_f of the fully crystalline materials from the literature ($\Delta H_f^0(\text{P}\delta\text{VL}) = 181.8$ J g^{-1} , $\Delta H_f^0(\text{P}\epsilon\text{CL}) = 136.1$ J g^{-1}).²⁷ ^eDegree of crystallinity of the P δ VL domains taking into account the mass fraction of δ VL in the copolymers. ^fCalculated for a completely extended chain considering the bond lengths and bond angles.

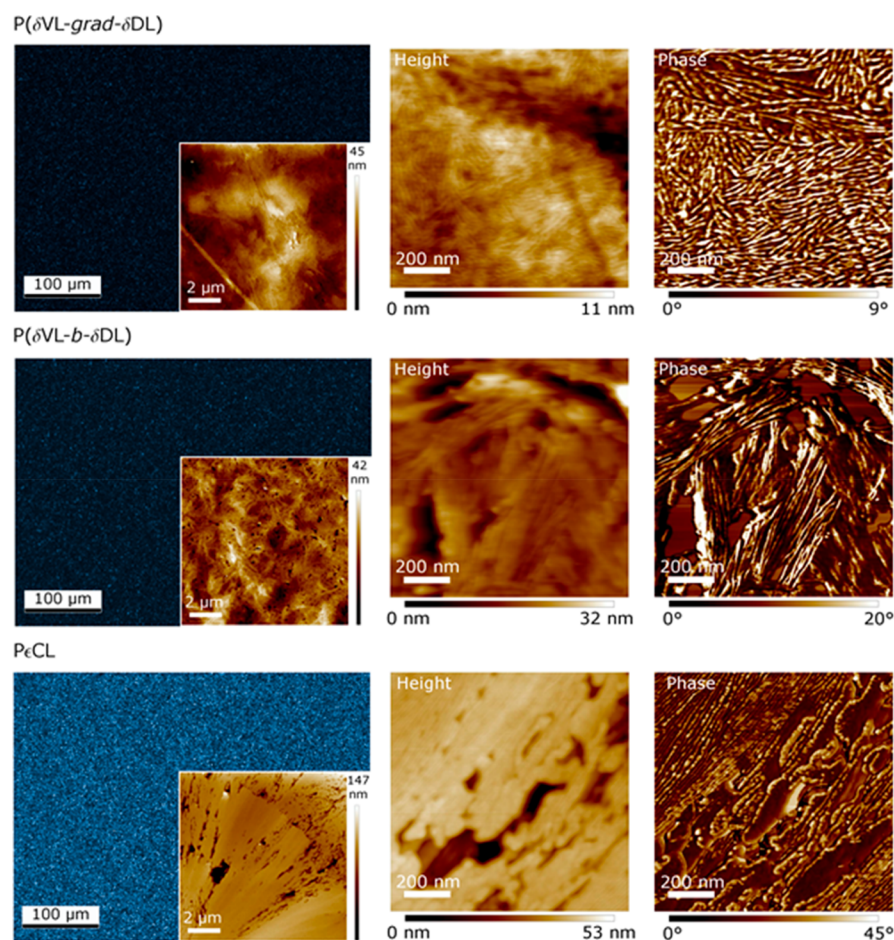


Figure 5. Left: polarized light microscopy images of **P8** to **P10** spherulites between polarizer and analyzer with a changed position of 90° . Overview AFM height images are shown as insets in the light microscopy pictures. Only for **P10**, a spherulite is recognizable. Center: magnified AFM height images (scale bars represent 200 nm). Right: magnified AFM phase images (scale bars represent 200 nm). The crystalline lamellae are visible for all three polymers (**P8**–**P10**).

precipitation according to a published protocol for polyesters with long alkyl spacers.³³ For this purpose, a solution of the polymer in THF was slowly dropped into water under vigorous stirring. Variation of the polymer concentration in the THF solution and the volume ratio of solvent (THF) to nonsolvent (water) facilitated access to particles with tailor-made hydrodynamic diameters (*Z*-average) between 50 and 230 nm (DLS analysis, see the [Supporting Information](#)). The utmost majority of the nanoparticle suspensions remained stable within a period of 4 weeks without the need of further stabilizers. In general, the nanoparticles formed from the copolyesters **P8** and **P9** revealed larger D_h if prepared under the same conditions as the corresponding P ϵ CL nanoparticles. However, an adjustment of the nanoprecipitation conditions of the individual polymers allowed to prepare nanoparticles of the same sizes from all three polyesters **P8** to **P10**. To simplify the investigation of the physical properties of the nanoparticles, a D_h of around 170 nm was selected for this purpose ([Table 3](#)). In accordance with the preliminary stability tests, all nanoparticles revealed negative zeta potentials (ζ) of approximately -30 mV, as common for polyester nanoparticles in aqueous suspension.^{34,35}

To assess whether the variation in crystallinity of the bulk materials was retained in the corresponding nanoparticles, they were investigated in detail by means of SEM and AFM ([Figure 6](#)). To avoid a movement of the nanoparticles during the

Table 3. DLS Data, ζ Potential, and Stiffness of Polymeric Nanoparticles Prepared in THF from Polymers with the Same HHB

	P(δ VL- <i>grad</i> - δ DL) (P8)	P δ VL- <i>b</i> -P δ DL (P9)	P ϵ CL (P10)
D_h^a [nm]	176	179	162
PDI	0.075	0.073	0.149
ζ [mV]	-28.6	-31.0	-27.8
stiffness ^b [$N\ m^{-1}$]	2.2 ± 0.6	4.4 ± 1.6	7.4 ± 2.0

^a D_h denotes the *Z*-average. ^bDetermined by AFM.

characterization, the substrates were functionalized with PEI. This polyelectrolyte layer induces a positive surface charge, immobilizing the nanoparticles electrostatically due to their negative ζ potential. SEM revealed a spherical shape of all polymeric nanoparticles. However, the diameters (around 200 nm) were found to be increased compared to the D_h from DLS. This effect was most significant for the polymer featuring the lowest degree of crystallinity (the gradient copolymer **P8**) and can be explained by collapsing of the nanoparticles onto the surface during the drying process. This is supported by the AFM images, which revealed a nanoparticle height that is lower than the nanoparticle diameter.

The degree of crystallinity of the nanoparticles is difficult to investigate in a direct manner. However, the stiffness and the

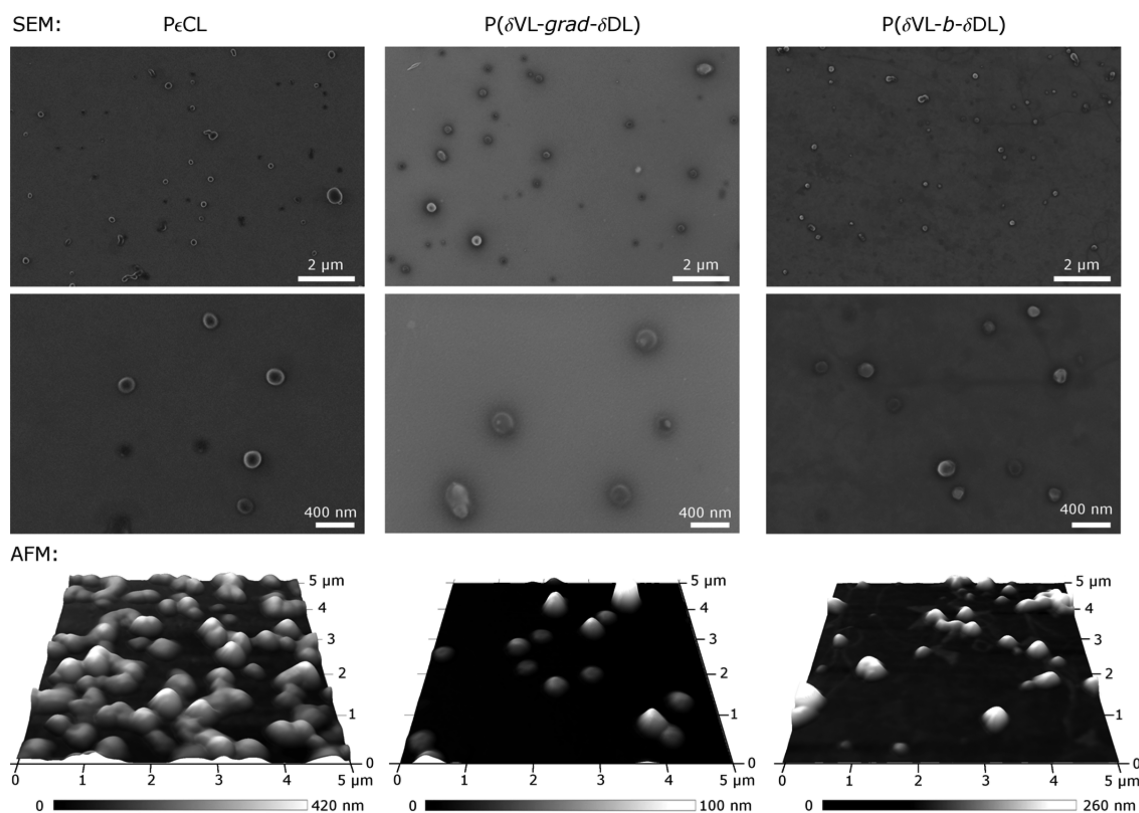


Figure 6. SEM images (upper part) and 3D AFM height images (lower part) of dried nanoparticles prepared from the three polymers (P8 to P10) by nanoprecipitation.

Young's modulus, which correlate with each other, are affected by the crystallinity of nanoparticles and can be deduced from AFM measurements.^{36,37} It should be noted that the cellular uptake of nanoparticles is directly affected by the stiffness of the materials and represents an additional key factor for successful nanoparticle-induced drug delivery.^{38,39} Force–distance curves were hence collected by means of AFM investigations. The resulting nanoparticle stiffness ranges from 2.2 to 7.4 N m⁻¹ and increases from the gradient copolymer P8, over the block copolymer P9, to the PεCL homopolymer P10 (Table 3). The degree of crystallinity of the bulk polymers follows the same trend (Table 2). On the basis of this comparison, we assume a correlation between the polymer bulk and nanoparticle crystallinity. In particular for the copolyesters P8 and P9, the mer sequences in the chemical structure represent the only chemical difference. Hence, the differences in the observed stiffness can only be induced by the increased degree of crystallinity from P8 to P9. It is expected that the degradation and, thus, the release rate of a drug from our polymeric nanoparticles will decrease with increasing degree of crystallinity. In contrast to the loosely packed amorphous domains, the close packing in the crystalline domains impairs the enzyme adsorption and, consequently, the enzymatic cleavage of the polyester chains in the bulk materials.⁷ The controlled HHB of our polymeric nanoparticles allows to develop direct structure–property relationships between crystallinity and degradation behavior and, hence, to adjust release profiles in the future.

CONCLUSION

The copolymerization of δVL and δDL enabled access to tailor-made polyester materials that feature the same hydro-

phobicity as PεCL but a varied degree of crystallinity. Stable nanoparticles in aqueous suspension of similar sizes were prepared from the three tailored materials. AFM measurements revealed that the bulk crystallinity correlates with the nanoparticle stiffness. The former can hence be directly applied as a first hint to deduce the nanoparticle crystallinity as additional influencing factors have been excluded by the copolymer design. Our future research will include the assessment of the nanoparticle crystallinity directly in suspension to investigate whether this observation can be generalized. The tailor-made nanoparticles presented here form the basis for studies regarding the enzymatic degradation, release profiles of encapsulated actives, and cellular uptake. The future utilization of a variety of actives and other designed polyesters will allow a clear statement about the effect of crystallinity on the release behavior.

ASSOCIATED CONTENT

Supporting Information

The Supporting Information is available free of charge on the ACS Publications website at DOI: 10.1021/acs.macromol.8b00925.

An additional kinetic study, NMR spectra, SEC elograms, TGA curves, nanoparticle preparation details and stability tests (PDF)

AUTHOR INFORMATION

Corresponding Authors

*(K.D.J.) E-mail k.jandt@uni-jena.de.

*(U.S.S.) E-mail ulrich.schubert@uni-jena.de.

ORCID 

Klaus D. Jandt: 0000-0002-7537-5603

Ulrich S. Schubert: 0000-0003-4978-4670

Author Contributions

D.B. and C.H. contributed equally.

Notes

The authors declare no competing financial interest.

ACKNOWLEDGMENTS

This project was funded by the Thüringer Ministerium für Wirtschaft, Wissenschaft, und Digitale Gesellschaft (Thuringian Ministry for Economic Affairs, Science and Digital Society, ProExzellenz II, NanoPolar). Moreover, the work was supported by the DFG-funded Collaborative Research Centre PolyTarget (SFB 1278, projects A06 and Z01). We gratefully acknowledge the partial financial support of the Thüringer Ministerium für Wirtschaft, Wissenschaft und Digitale Gesellschaft and the Deutsche Forschungsgemeinschaft (DFG), grant reference INST 275/389-1 FUGG; AOBJ: 640980.

REFERENCES

- (1) Knop, K.; Hoogenboom, R.; Fischer, D.; Schubert, U. S. Poly(ethylene glycol) in drug delivery: Pros and cons as well as potential alternatives. *Angew. Chem., Int. Ed.* **2010**, *49*, 6288–6308.
- (2) Press, A. T.; Traeger, A.; Pietsch, C.; Mosig, A.; Wagner, M.; Clemens, M. G.; Jbeily, N.; Koch, N.; Gottschaldt, M.; Beziere, N.; Ermolayev, V.; Ntziachristos, V.; Popp, J.; Kessels, M. M.; Qualmann, B.; Schubert, U. S.; Bauer, M. Cell type-specific delivery of short interfering RNAs by dye-functionalised theranostic nanoparticles. *Nat. Commun.* **2014**, *5*, 13.
- (3) Farokhzad, O. C.; Cheng, J. J.; Teply, B. A.; Sherifi, I.; Jon, S.; Kantoff, P. W.; Richie, J. P.; Langer, R. Targeted nanoparticle-aptamer bioconjugates for cancer chemotherapy in vivo. *Proc. Natl. Acad. Sci. U. S. A.* **2006**, *103*, 6315–6320.
- (4) Müller-Goymann, C. C. Physicochemical characterization of colloidal drug delivery systems such as reverse micelles, vesicles, liquid crystals and nanoparticles for topical administration. *Eur. J. Pharm. Biopharm.* **2004**, *58*, 343–356.
- (5) Czaplewska, J. A.; Majdanski, T. C.; Barthel, M. J.; Gottschaldt, M.; Schubert, U. S. Functionalized PEG-b-PAGE-b-PLGA triblock terpolymers as materials for nanoparticle preparation. *J. Polym. Sci., Part A: Polym. Chem.* **2015**, *53*, 2163–2174.
- (6) Azevedo, H. S.; Reis, R. L. Understanding the enzymatic degradation of biodegradable polymers and strategies to control their degradation rate. In *Biodegradable Systems in Tissue Engineering and Regenerative Medicine*; CRC Press: 2005; pp 177–201.
- (7) Buchholz, V.; Agarwal, S.; Greiner, A. Synthesis and enzymatic degradation of soft aliphatic polyesters. *Macromol. Biosci.* **2016**, *16*, 207–213.
- (8) Karavelidis, V.; Giliopoulos, D.; Karavas, E.; Bikiaris, D. Nanoencapsulation of a water soluble drug in biocompatible polyesters. Effect of polyesters melting point and glass transition temperature on drug release behavior. *Eur. J. Pharm. Sci.* **2010**, *41*, 636–643.
- (9) Karavelidis, V.; Karavas, E.; Giliopoulos, D.; Papadimitriou, S.; Bikiaris, D. Evaluating the effects of crystallinity in new biocompatible polyester nanocarriers on drug release behavior. *Int. J. Nanomed.* **2011**, *6*, 3021–3032.
- (10) Tsuji, H. Poly(lactide) stereocomplexes: Formation, structure, properties, degradation, and applications. *Macromol. Biosci.* **2005**, *5*, 569–597.
- (11) Perevyazko, I. Y.; Delaney, J. T.; Vollrath, A.; Pavlov, G. M.; Schubert, S.; Schubert, U. S. Examination and optimization of the self-assembly of biocompatible, polymeric nanoparticles by high-throughput nanoprecipitation. *Soft Matter* **2011**, *7*, 5030–5035.
- (12) Ceccorulli, G.; Scandola, M.; Kumar, A.; Kalra, B.; Gross, R. A. Cocrystallization of random copolymers of *ω*-pentadecalactone and *ε*-caprolactone synthesized by lipase catalysis. *Biomacromolecules* **2005**, *6*, 902–907.
- (13) Schneiderman, D. K.; Hillmyer, M. A. Aliphatic polyester block polymer design. *Macromolecules* **2016**, *49*, 2419–2428.
- (14) Lou, X.; Detrembleur, C.; Jérôme, R. Living cationic polymerization of δ -valerolactone and synthesis of high molecular weight homopolymer and asymmetric telechelic and block copolymer. *Macromolecules* **2002**, *35*, 1190–1195.
- (15) Kasyapi, N.; Bhowmick, A. K. Nanolamellar triblock of poly-d,l-lactide- δ -valerolactone-d,l-lactide with tuneable glass transition temperature and crystallinity for use as a drug-delivery vesicle. *RSC Adv.* **2014**, *4*, 27439–27451.
- (16) Dove, A. P. Organic catalysis for ring-opening polymerization. *ACS Macro Lett.* **2012**, *1*, 1409–1412.
- (17) Naumann, S.; Thomas, A. W.; Dove, A. P. Highly polarized alkenes as organocatalysts for the polymerization of lactones and trimethylene carbonate. *ACS Macro Lett.* **2016**, *5*, 134–138.
- (18) Lohmeijer, B. G. G.; Pratt, R. C.; Leibfarth, F.; Logan, J. W.; Long, D. A.; Dove, A. P.; Nederberg, F.; Choi, J.; Wade, C.; Waymouth, R. M.; Hedrick, J. L. Guanidine and amidine organocatalysts for ring-opening polymerization of cyclic esters. *Macromolecules* **2006**, *39*, 8574–8583.
- (19) Zhang, L.; Nederberg, F.; Pratt, R. C.; Waymouth, R. M.; Hedrick, J. L.; Wade, C. G. Phosphazene bases: A new category of organocatalysts for the living ring-opening polymerization of cyclic esters. *Macromolecules* **2007**, *40*, 4154–4158.
- (20) Kamber, N. E.; Jeong, W.; Waymouth, R. M.; Pratt, R. C.; Lohmeijer, B. G. G.; Hedrick, J. L. Organocatalytic ring-opening polymerization. *Chem. Rev.* **2007**, *107*, 5813–5840.
- (21) Pratt, R. C.; Lohmeijer, B. G. G.; Long, D. A.; Waymouth, R. M.; Hedrick, J. L. Triazabicyclodecene: A simple bifunctional organocatalyst for acyl transfer and ring-opening polymerization of cyclic esters. *J. Am. Chem. Soc.* **2006**, *128*, 4556–4557.
- (22) Bansal, K. K.; Kakde, D.; Purdie, L.; Irvine, D. J.; Howdle, S. M.; Mantovani, G.; Alexander, C. New biomaterials from renewable resources - amphiphilic block copolymers from δ -decalactone. *Polym. Chem.* **2015**, *6*, 7196–7210.
- (23) Martello, M. T.; Burns, A.; Hillmyer, M. Bulk ring-opening transesterification polymerization of the renewable δ -decalactone using an organocatalyst. *ACS Macro Lett.* **2012**, *1*, 131–135.
- (24) Meeus, J.; Scurr, D. J.; Chen, X.; Amssoms, K.; Davies, M. C.; Roberts, C. J.; Van den Mooter, G. Combination of (M)DSC and surface analysis to study the phase behaviour and drug distribution of ternary solid dispersions. *Pharm. Res.* **2015**, *32*, 1407–1416.
- (25) Armini, S.; Vakarelski, I. U.; Whelan, C. M.; Maex, K.; Higashitani, K. Nanoscale indentation of polymer and composite polymer-silica core-shell submicrometer particles by atomic force microscopy. *Langmuir* **2007**, *23*, 2007–2014.
- (26) Sitterberg, J.; Ozcetin, A.; Ehrhardt, C.; Bakowsky, U. Utilising atomic force microscopy for the characterisation of nanoscale drug delivery systems. *Eur. J. Pharm. Biopharm.* **2010**, *74*, 2–13.
- (27) Lorient, M.; Linossier, I.; Vallée-Réhel, K.; Fay, F. Syntheses, characterization, and hydrolytic degradation of P(ϵ -caprolactone-co- δ -valerolactone) copolymers: Influence of molecular weight. *J. Appl. Polym. Sci.* **2016**, *133*, 43007.
- (28) Arias, V.; Olsen, P.; Odelius, K.; Høglund, A.; Albertsson, A.-C. Selective degradation in aliphatic block copolyesters by controlling the heterogeneity of the amorphous phase. *Polym. Chem.* **2015**, *6*, 3271–3282.
- (29) Tagaya, A.; Koike, Y. Compensation and control of the birefringence of polymers for photonics. *Polym. J.* **2012**, *44*, 306–314.
- (30) Hölzer, S.; Büttner, T. N.; Schulze, R.; Arras, M. M. L.; Schacher, F. H.; Jandt, K. D.; Schubert, U. S. Mechanisms and kinetics of the crystal thickening of poly(butadiene)-block-poly(ethylene oxide) during annealing within the melting range. *Eur. Polym. J.* **2015**, *68*, 10–20.

(31) Schulze, R.; Arras, M. M. L.; Helbing, C.; Hoelzer, S.; Schubert, U. S.; Keller, T. F.; Jandt, K. D. How the calorimetric properties of a crystalline copolymer correlate to its surface nanostructures. *Macromolecules* **2014**, *47*, 1705–1714.

(32) He, W.-N.; Xu, J.-T. Crystallization assisted self-assembly of semicrystalline block copolymers. *Prog. Polym. Sci.* **2012**, *37*, 1350–1400.

(33) Herzog, K.; Müller, R. J.; Deckwer, W. D. Mechanism and kinetics of the enzymatic hydrolysis of polyester nanoparticles by lipases. *Polym. Degrad. Stab.* **2006**, *91*, 2486–2498.

(34) Hung, H.-I.; Klein, O. J.; Peterson, S. W.; Rokosh, S. R.; Osseiran, S.; Nowell, N. H.; Evans, C. L. PLGA nanoparticle encapsulation reduces toxicity while retaining the therapeutic efficacy of EtNBS-PDT in vitro. *Sci. Rep.* **2016**, *6*, 33234.

(35) Knecht, V.; Risselada, H. J.; Mark, A. E.; Marrink, S. J. Electrophoretic mobility does not always reflect the charge on an oil droplet. *J. Colloid Interface Sci.* **2008**, *318*, 477–486.

(36) Guo, D.; Xie, G.; Luo, J. Mechanical properties of nanoparticles: Basics and applications. *J. Phys. D: Appl. Phys.* **2014**, *47*, 013001.

(37) Paik, P.; Kar, K. K.; Deva, D.; Sharma, A. Measurement of mechanical properties of polymer nanospheres by atomic force microscopy: Effects of particle size. *Micro Nano Lett.* **2007**, *2*, 72–77.

(38) Banquy, X.; Suarez, F.; Argaw, A.; Rabanel, J.-M.; Grutter, P.; Bouchard, J.-F.; Hildgen, P.; Giasson, S. Effect of mechanical properties of hydrogel nanoparticles on macrophage cell uptake. *Soft Matter* **2009**, *5*, 3984–3991.

(39) Sun, J.; Zhang, L.; Wang, J.; Feng, Q.; Liu, D.; Yin, Q.; Xu, D.; Wei, Y.; Ding, B.; Shi, X.; Jiang, X. Tunable rigidity of (polymeric core)-(lipid shell) nanoparticles for regulated cellular uptake. *Adv. Mater.* **2015**, *27*, 1402–1407.

Supporting information for

Maintaining the hydrophilic hydrophobic balance of polyesters with adjustable crystallinity for tailor-made nanoparticles

*Damiano Bandelli,^{1,2#} Christian Helbing,^{2,3#} Christine Weber,^{1,2} Michael Seifert,³ Irina Muljajew,^{1,2} Klaus D. Jandt,^{2,3} * Ulrich S. Schubert^{1,2*}*

¹ Laboratory of Organic and Macromolecular Chemistry (IOMC), Friedrich Schiller University Jena, Humboldtstr. 10, 07743 Jena, Germany

² Jena Center for Soft Matter (JCSM), Friedrich Schiller University Jena, Philosophenweg 7, 07743 Jena, Germany

³ Chair of Materials Science (CMS), Department of Materials Science and Technology, Otto Schott Institute of Materials Research, Faculty of Physics and Astronomy, Friedrich Schiller University Jena, Löbdergraben 32, 07743 Jena, Germany

Both authors contributed equally.

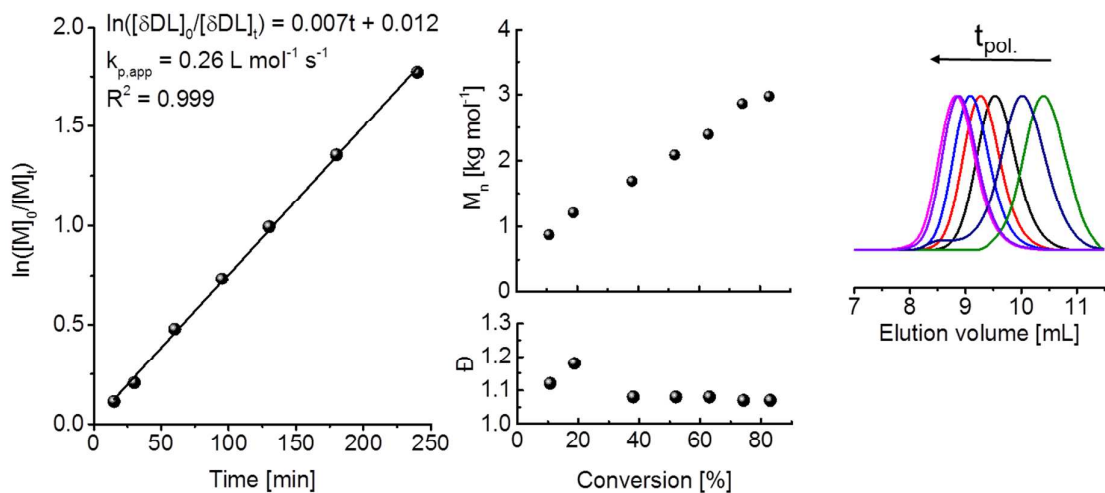


Figure S1: Kinetic studies of the homopolymerization of δDL conducted in bulk at room temperature using BnOH as initiator and TBD as catalyst ($[M]:[TBD]:[I] = 20:1:1$). **Left:** First-order kinetic plot with a linear fit according to $\ln([M]_0/[M]_t) = k_{p,app} [I]_0 t$. **Center:** Evolution of the molar mass with monomer conversion. **Right:** Overlay of the SEC elugrams of the samples taken (CHCl_3 , RI detection).

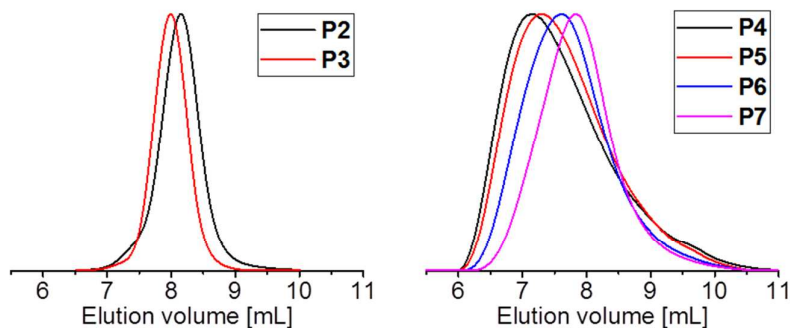


Figure S2: SEC elugrams (CHCl_3 , RI detection) of the P δVL (**P2**) and P δDL (**P3**) homopolymers and the statistical copolymers **P4** to **P7**.

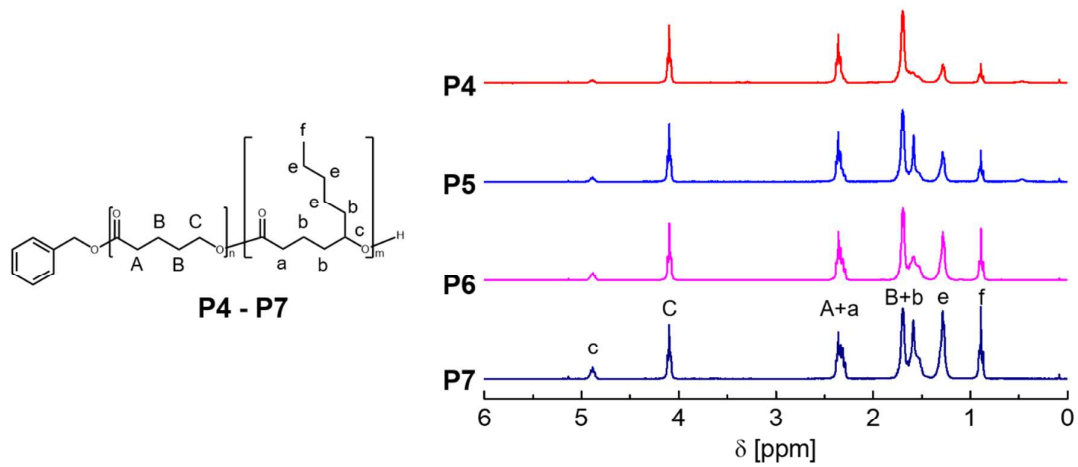


Figure S3: ^1H NMR spectra (300 MHz, CDCl_3) of the polymer series **P4** to **P7** after purification and structural assignment of the peaks. Signals **c** and **C** were used for the determination of the copolymer composition.

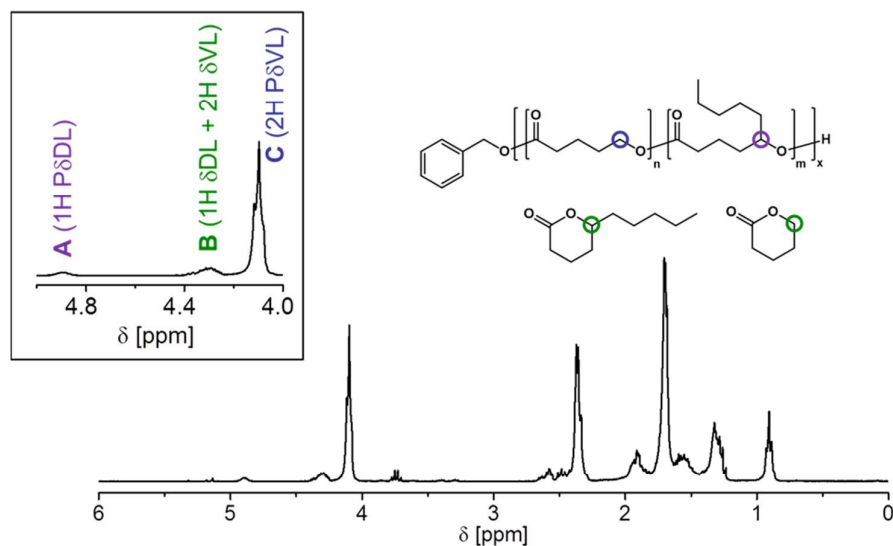


Figure S4: ^1H NMR spectrum (300 MHz, CDCl_3) of the kinetic sample taken after six hours during the copolymerization of δVL and δDL . The inset shows a zoom into the region of the spectrum used to determine the monomer conversions. The respective signals A-C are assigned to the structure of the polymer and the monomers.

Calculation of the monomer conversions

The overall conversion was calculated using the signal integrals assigned in **Figure S4** according to:

$$\text{conv}_{\text{Overall}} = \frac{\int A + \int C}{\int A + \int B + \int C} \quad (1)$$

To obtain the separate conversions of the two monomers, the following set of equations was used:

$$\int A = [\text{P}\delta\text{DL}] \quad (2)$$

$$\int C = 2[\text{P}\delta\text{VL}] \quad (3)$$

$$\int B = 2[\delta\text{VL}] + [\delta\text{DL}] \quad (4)$$

$$\frac{[\delta\text{VL}]_0}{[\delta\text{DL}]_0} = \frac{[\delta\text{VL}] + [\text{P}\delta\text{VL}]}{[\delta\text{DL}] + [\text{P}\delta\text{DL}]} \quad (5)$$

$[\delta\text{DL}]$ and $[\delta\text{VL}]$ denote the residual amounts of both monomers, whereas $[\text{P}\delta\text{DL}]$ and $[\text{P}\delta\text{VL}]$ denote the amounts of both monomers incorporated to the polymer. $[\delta\text{VL}]_0/[\delta\text{DL}]_0$ corresponds to the feed molar ratio of the two comonomers, which is known.

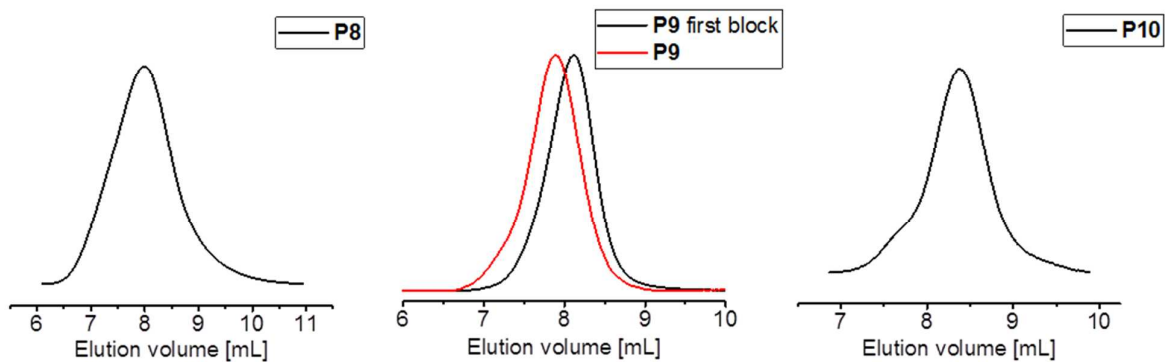


Figure S5: SEC elugrams (CHCl_3 , RI detection) of the three polyesters **P8** to **P10** featuring the same HHB.

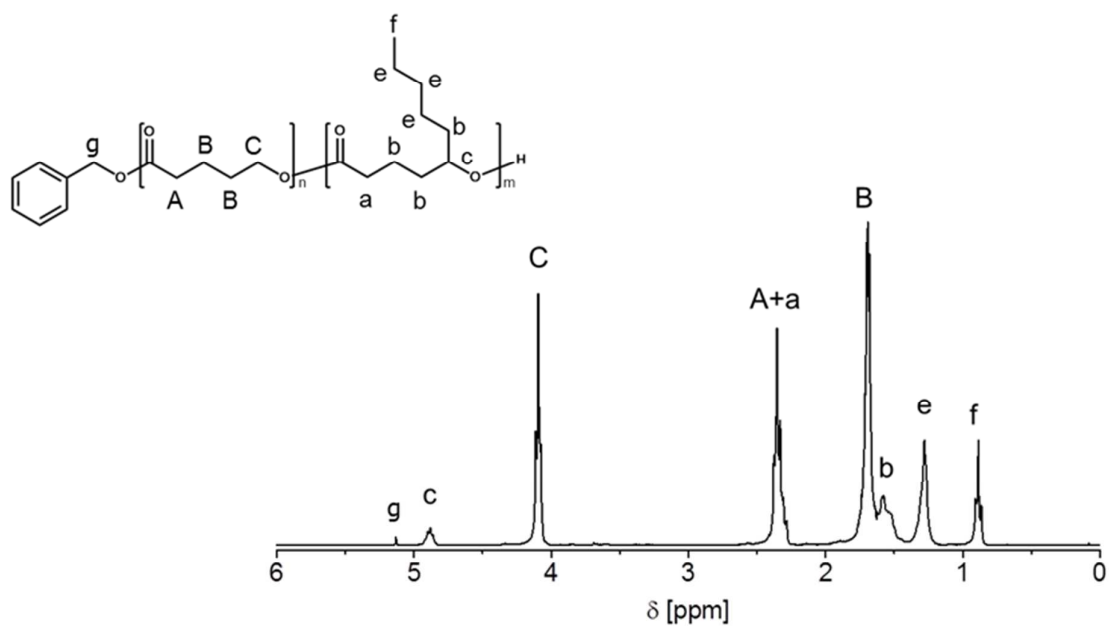


Figure S6: ^1H NMR spectrum (300 MHz, CDCl_3) of $\text{P}(\delta\text{VL-grad-}\delta\text{DL})$ (**P8**) and assignment of the signals to the structure of the polymer.

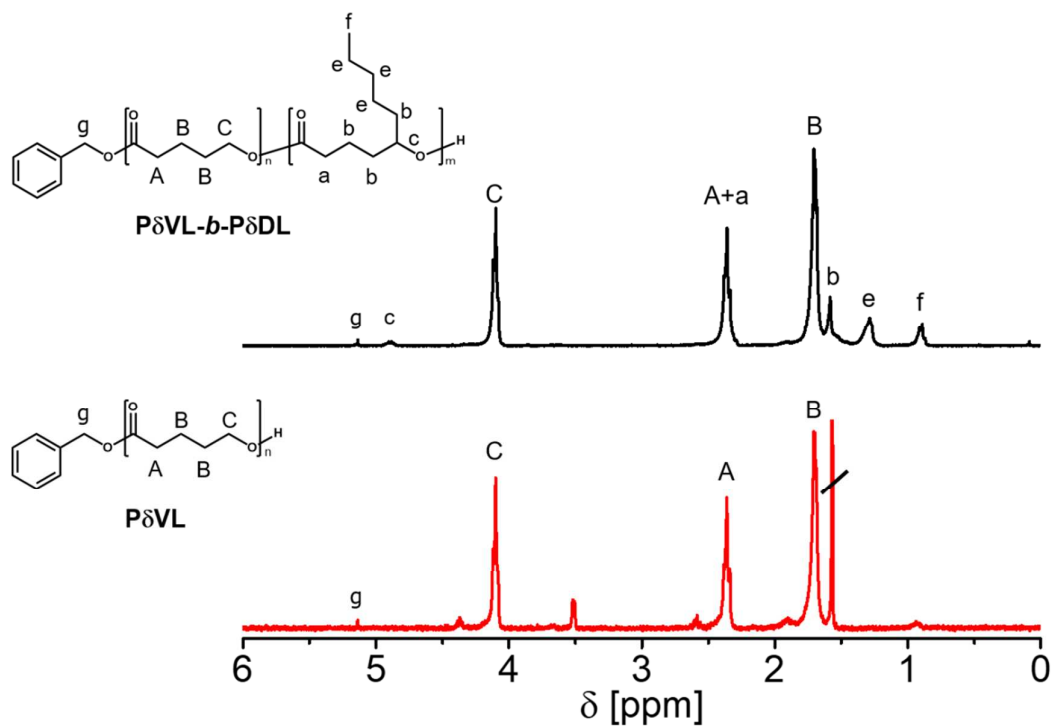


Figure S7: ^1H NMR spectra (300 MHz, CDCl_3) of $\text{P}\delta\text{VL}-b\text{-P}\delta\text{DL}$ (**P9**), the initial $\text{P}\delta\text{VL}$ macroinitiator and assignment of the signals to the structure of the polymer.

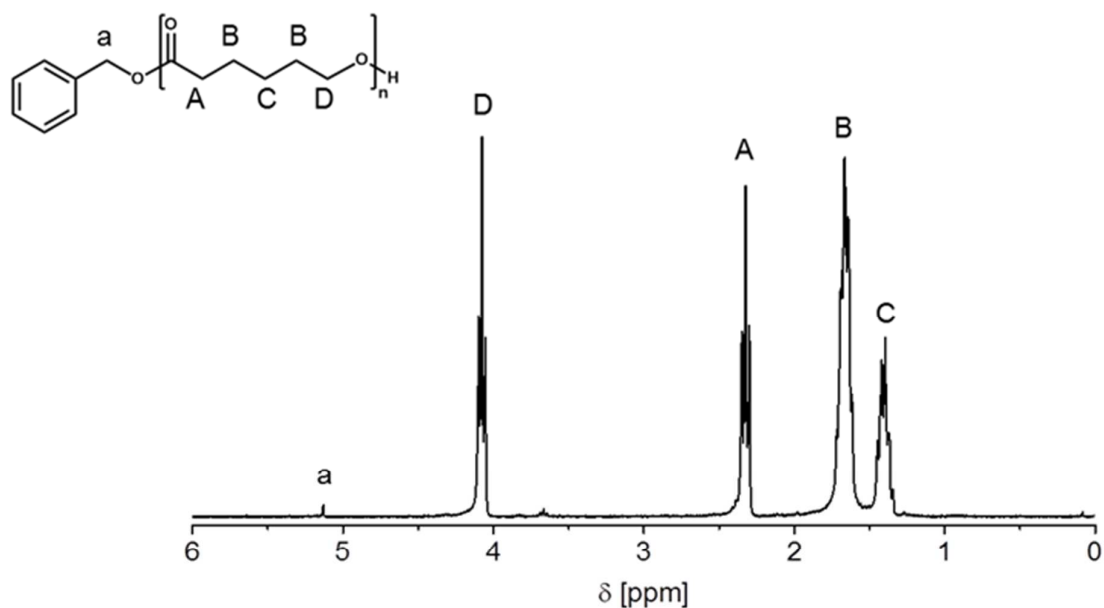


Figure S8: ^1H NMR spectrum (300 MHz, CDCl_3) of $\text{P}\epsilon\text{CL}$ (**P10**) and assignment of the signals to the structure of the polymer.

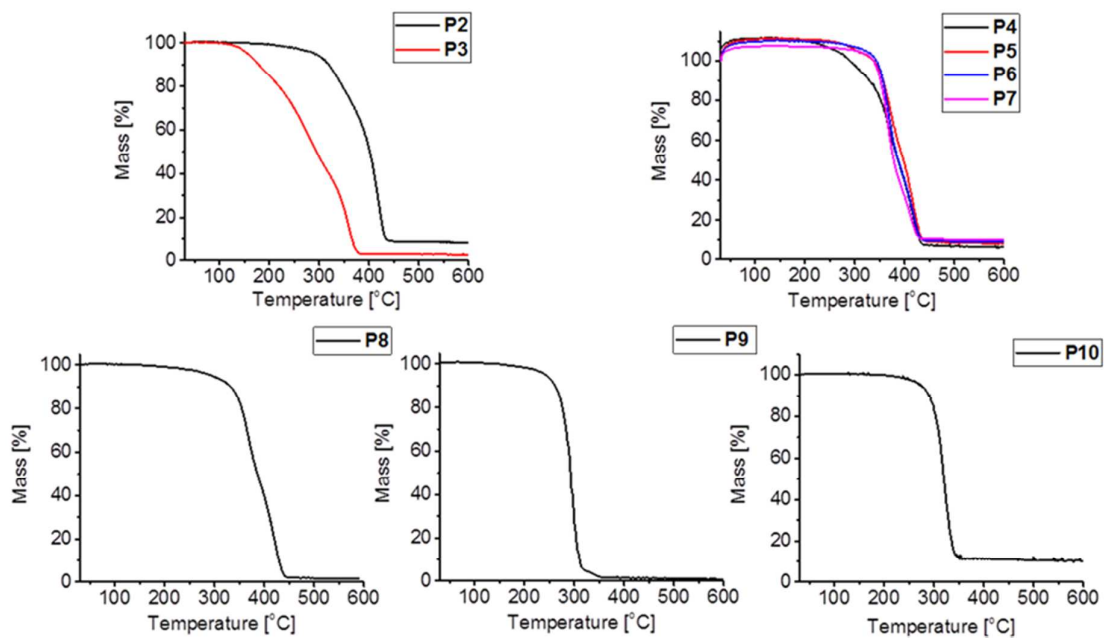


Figure S9: TGA thermograms of **P2** to **P10** (nitrogen atmosphere, heating rate 20 K min⁻¹).

Table S1: Detailed description of the nanoparticle screening performed from **P8-P10**.

Polymer	Sample	c(P) in THF [mg mL ⁻¹]	V(THF) [mL]	V(H ₂ O) [mL]	c(P) in H ₂ O [mg mL ⁻¹]
P ϵ CL	P10-NP 1	5	0.5	5	0.5
P ϵ CL	P10-NP 2	2.5	0.5	5	0.25
P ϵ CL	P10-NP 3	1	0.5	5	0.1
P ϵ CL	P10-NP 4	0.5	0.5	5	0.05
P ϵ CL	P10-NP 5	5	0.5	10	0.25
P ϵ CL	P10-NP 6	2.5	0.5	10	0.125
P ϵ CL	P10-NP 7	1	0.5	10	0.05
P ϵ CL	P10-NP 8	0.5	0.5	10	0.025
P(δ VL-grad- δ DL)	P8-NP 1*	5	0.5	5	0.5
P(δ VL-grad- δ DL)	P8-NP 2	2.5	0.5	5	0.25
P(δ VL-grad- δ DL)	P8-NP 3	1	0.5	5	0.1
P(δ VL-grad- δ DL)	P8-NP 4	0.5	0.5	5	0.05
P δ VL- <i>b</i> -P δ DL	P9-NP 2	2.5	0.5	5	0.25
P δ VL- <i>b</i> -P δ DL	P9-NP 3	1	0.5	5	0.1
P δ VL- <i>b</i> -P δ DL	P9-NP 4	0.5	0.5	5	0.05

* No stable nanoparticles were formed.

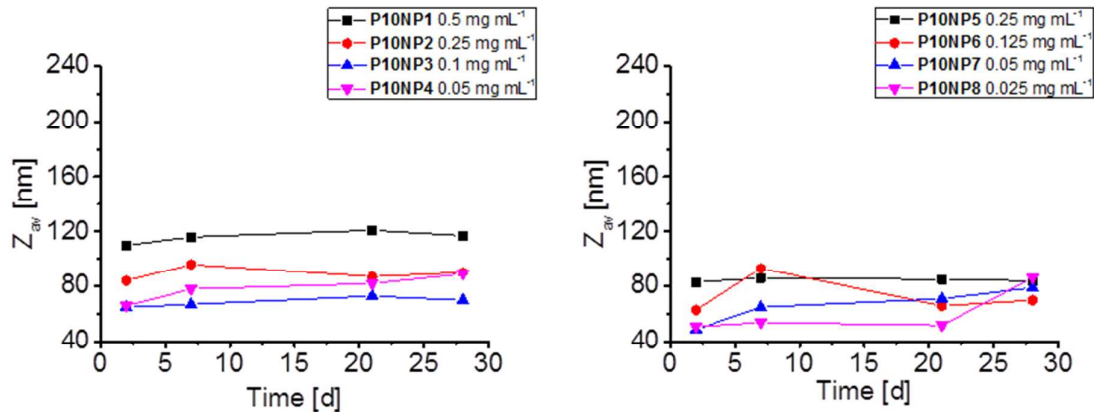


Figure S10: Stability of the nanoparticles prepared from P α CL **P10** in aqueous suspension upon storage at 5 °C. **Left:** Hydrodynamic diameters (DLS, Z-average) of the nanoparticle batches **P10NP1-4**. **Right:** Hydrodynamic diameters (DLS, Z-average) of the nanoparticle batches **P10NP5-8**.

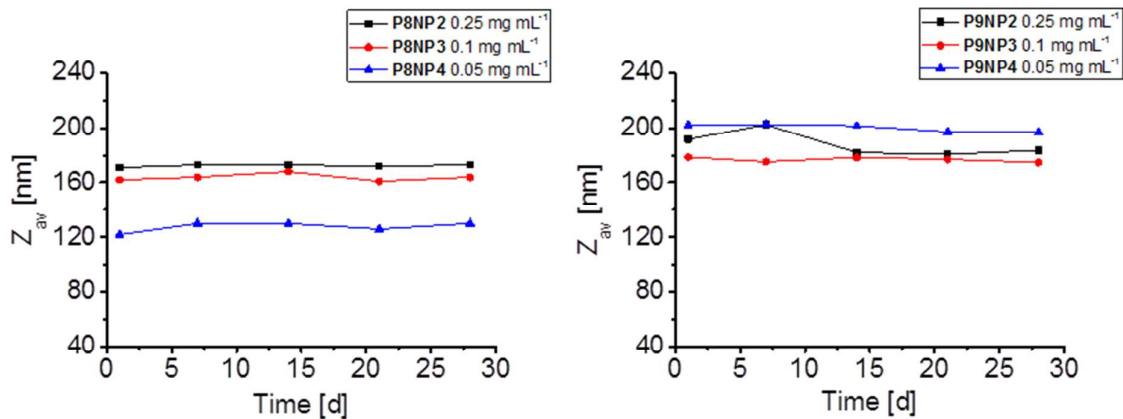


Figure S11: Stability of the nanoparticles prepared from P(δ VL-grad- δ DL) **P8** (left) and P δ VL-*b*-P δ DL **P9** (right) in aqueous suspension upon storage at 5 °C. Hydrodynamic diameters represent the Z-average as determined by DLS.

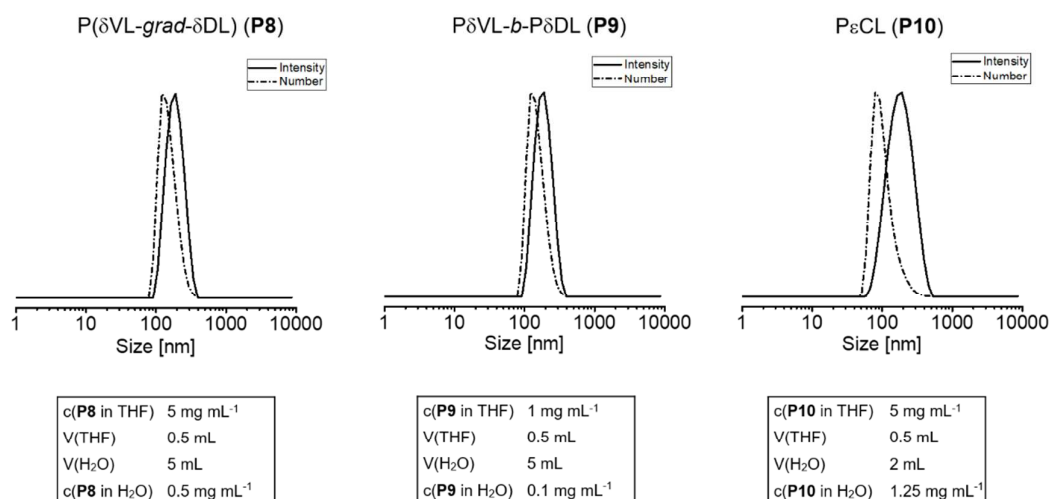
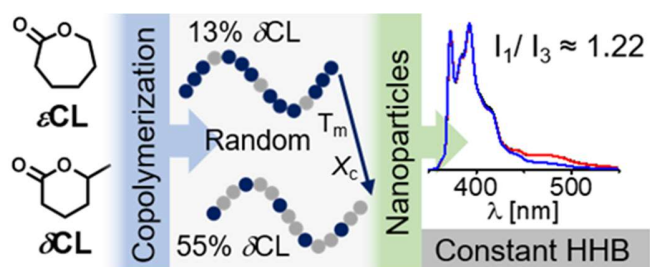


Figure S12: DLS size distributions of the nanoparticles prepared from **P8** to **P10** with hydrodynamic diameters of ≈ 170 nm. The full lines represent the intensity-weighted data, the dotted lines represent the number-weighted data.

Publication P4

Copolymerization of caprolactone isomers to obtain nanoparticles with constant hydrophobicity and tunable crystallinity

D. Bandelli, I. Muljajew, K. Scheuer, J. B. Max, C. Weber, F. H. Schacher, K. D. Jandt, U. S. Schubert, *Macromolecules* **2020**, *13*, 5208–5217.



Copolymerization of Caprolactone Isomers to Obtain Nanoparticles with Constant Hydrophobicity and Tunable Crystallinity

Damiano Bandelli, Irina Muljajew, Karl Scheuer, Johannes B. Max, Christine Weber, Felix H. Schacher, Klaus D. Jandt, and Ulrich S. Schubert*

Cite This: *Macromolecules* 2020, 53, 5208–5217

Read Online

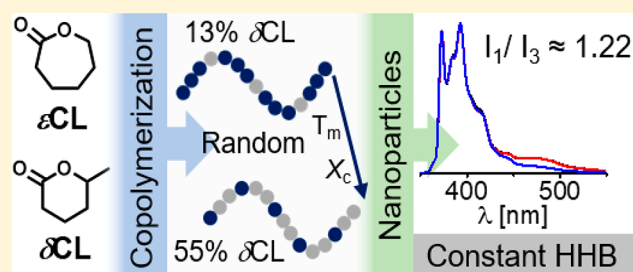
ACCESS |

Metrics & More

Article Recommendations

Supporting Information

ABSTRACT: To obtain a set of polycaprolactones (PCL) with varying crystallinity, the triazabicyclodecene-catalyzed copolymerization of the two constitutional isomers ϵ -caprolactone (ϵ CL) and δ -caprolactone (δ CL) was carried out at room temperature in toluene. Variation of the feed fraction of ϵ CL from 50% to 80% and the detailed kinetic studies accompanied by application of terminal as well as nonterminal kinetic models suggested the formation of random copolymers. Differential scanning calorimetry and wide-angle X-ray scattering investigations revealed the decrease of melting temperatures and degree of crystallinity with the ϵ CL fraction in the PCL. All copolymers were suited to obtain aqueous nanoparticle dispersions by means of nanoprecipitation. Encapsulation of the fluorescent probe pyrene confirmed a constant hydrophilic/hydrophobic balance of the nanoparticles.



INTRODUCTION

The preparation of polymeric nanoparticle carriers is a central subject for the development of compelling and personalized medicine.^{1,2} Already commercially available polymers can serve for the formulation of loaded nanoparticles as carriers for drug delivery applications,^{3–5} where the precise variation of the particle features, e.g., size, morphology, and eventual further compartmentalization,^{6,7} affect the targeting area.⁸ As a consequence, nanoparticles represent complex systems to be exploited systematically.^{4,9,10} The polymer design already plays a central role and is often accompanied by functionalization, enabling the preparation of well-defined polymers bearing biologically active labels,¹¹ fluorescent markers, or stealth polymers.^{12,13}

In this regard, polyesters represent an extremely versatile polymer class that can be obtained from natural and renewable resources.^{14–16} Due to the ester linkages, polyesters are also degradable via enzymatic catalysis.¹⁷ As a consequence, they are employed in the biomedical field not only within academic research, but also for industrial purposes.^{18–20} Currently, the majority of commercially available formulations are based on poly(lactic acid) (PLA), poly(lactic acid-co-glycolic acid) (PLGA), and polycaprolactone (PCL). These polyesters feature different thermal and mechanical properties, as well as different hydrophilic hydrophobic balance (HHB), resulting in different release activities during enzymatic degradation.^{21,22} However, the variation of a complete set of properties does not allow us to unambiguously decouple the effect of a single feature. The polymer design already enables constant selected properties, e.g., molar mass and HHB, making the synthesis of

the polyesters a central aspect in the multidimensional parameter space to be taken into account.²³

From a synthetic perspective, the fine-tuning of molar mass and dispersity is achieved via the ring opening polymerization (ROP) of the corresponding lactone, employing metal complexes as well as organobases as catalysts.^{24–27} However, the HHB of a resulting nanoparticle is more difficult to maintain while varying thermal properties.

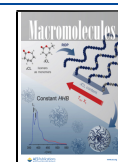
Taking advantage of the known bulk properties of several homopolymers,¹⁶ the copolymerization of established monomers already allows us to predict a variation of macroscopic properties. For instance, the addition of a comonomer during a statistical copolymerization results in the variation of thermal as well as mechanical properties of a given material.^{28–30} On the other hand, the incorporation of different amounts of comonomer in the copolymer will mostly alter the final HHB. The employment of constitutional isomers as monomers can prevent that if the general structure as a polyester is kept unchanged. This is because the proportion of ester vs methine, methylene, and methyl moieties is kept constant according to Davie's method.³¹

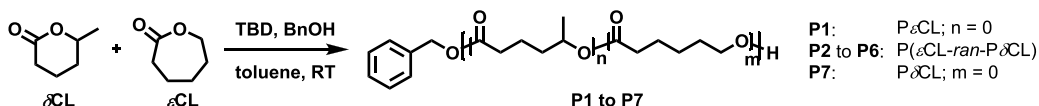
In this regard, the copolymerization of the two isomers ϵ -caprolactone (ϵ CL) and δ -caprolactone (δ CL) represents a

Received: March 1, 2020

Revised: May 13, 2020

Published: June 16, 2020



Scheme 1. ROP of δ -Caprolactone (δ CL) and ϵ -Caprolactone (ϵ CL) Yielding the Homo- and Co-polyesters P1 to P7

useful tool to access a library of materials featuring the same HHB. To the best of our knowledge, both monomers have only been copolymerized by Song et al., who focused on the enzymatic degradation of three statistical copolymers.³² However, detailed insights into the copolymerization kinetics and, hence, the copolymer microstructure remain unknown to date.

Representing a methyl-substituted lactone, δ CL featured a lower polymerizability compared to the unsubstituted ϵ CL when diphenylphosphate was used as a catalyst.¹⁶ As a consequence, one might expect the formation of gradient copolymers during a statistical copolymerization of ϵ CL and δ CL. As an efficient catalyst for the ROP of ϵ CL at room temperature,³³ we selected triazabicyclodecene (TBD), although it or other guanidinium base catalysts have, to the best of our knowledge, not yet been employed for the ROP of δ CL (Scheme 1).

We present an in-depth study of the copolymerization kinetics of ϵ CL and δ CL including the calculation of reactivity ratios. With the microstructure in hand, a set of copolymers with varied comonomer composition was studied with respect to bulk crystallinity by means of differential scanning calorimetry (DSC) and wide-angle X-ray scattering (WAXS). Representing a key toward future encapsulation of active pharmaceutical ingredients, stable nanoparticle dispersions were prepared and investigated regarding their HHB by fluorescence spectroscopy of encapsulated pyrene.

EXPERIMENTAL SECTION

Materials. ϵ -Caprolactone (ϵ CL, > 99%, TCI) and δ -caprolactone (δ CL, > 99%, TCI) were dried over calcium hydride and distilled at reduced pressure. The reaction solvent toluene (extra dry, Aldrich), the catalyst 1,5,7-triazabicyclo[4.4.0]dec-5-ene (TBD, 98%, Aldrich), and the initiator benzyl alcohol (BnOH, anhydrous, 99.8%, Aldrich) were stored under nitrogen atmosphere. Tetrahydrofuran (THF) for nanoparticle preparation was purified in a solvent purification system (SPS; Pure solv EN, InnovativeTechnology). All other chemicals were purchased from standard suppliers and were used without any further purification, unless stated otherwise.

Instruments. Polymerizations were conducted under nitrogen atmosphere in a MBraun UNILab Plus glovebox equipped with high efficiency box filters HEPA H13, a UNILab inert gas purification system and a vacuum pump.

Proton nuclear magnetic resonance (¹H NMR) spectra were measured in CDCl₃ at room temperature on a 300 MHz Bruker Avance I spectrometer. The residual ¹H peak of the deuterated solvent was used for chemical shift referencing.

Size-exclusion chromatography (SEC) measurements were performed utilizing a Shimadzu system equipped with a CBM-20A system controller, a LC-10AD pump, an RID-10A refractive index detector, and PSS (Polymer Standards Service GmbH, Mainz, Germany) SDV guard/linear S columns with chloroform/triethylamine (NEt₃)/*iso*-propanol (94:4:2) as eluent with a flow rate of 1 mL min⁻¹. The Techlab column oven was set to a constant temperature of 40 °C. Polystyrene (PS, 0.16 kg mol⁻¹ < M_n < 128 kg mol⁻¹) samples were used for calibration.

Matrix-assisted laser desorption ionization time-of-flight mass spectrometry (MALDI TOF MS) investigations were performed using an Ultraflex III ToF/ToF instrument from Bruker Daltonics equipped with a Nd:YAG laser. All spectra were measured in the

linear positive mode using *trans*-2-[3-(4-*tert*-butylphenyl)-2-methyl-2-propenyldiene]malononitrile (DCTB) as a matrix and sodium iodide as the doping salt. The instrument was calibrated with an external PMMA standard from PSS.

Thermogravimetric analysis (TGA) was performed under nitrogen atmosphere on a Netzsch TG 209 F1 Iris. Data were recorded from 30 to 600 °C at a heating rate of 20 °C min⁻¹. Differential scanning calorimetry (DSC) measurements were performed with a Netzsch 204 F1 Phoenix instrument under a nitrogen atmosphere from -100 to 210 °C applying a heating rate of 20 °C min⁻¹ in the first and second run and 10 °C min⁻¹ in the third run. The cooling rate between the heating runs was 20 °C min⁻¹.

Wide angle X-ray scattering (WAXS) measurements were performed on a Bruker AXS Nanostar, equipped with an Incoatec I μ SCu E025 microfocus X-ray source, operating at $\lambda = 1.54$ Å and a VANTEC 2000 detector. A pinhole setup with 750, 400, and 1000 μ m (in the order from source to sample) was used, and the sample-to-detector distance was 12 cm. The samples were fixed on a tape, and a corresponding baseline measurement was subtracted.

Dynamic light scattering (DLS) measurements were performed on a Zetasizer Nano ZS (Malvern Instruments, Herrenberg, Germany) at 25 °C ($\lambda = 633$ nm) at an angle of 173°. For each measurement, 3 \times 30 s runs were carried out in triplicate after an equilibration time of 30 s. The mean particle size was approximated as the effective (*Z*-average) diameter and the width of the distribution as the dispersity index (PDI) of the particles obtained by the cumulants method assuming a spherical shape.

Fluorescence spectra were recorded on a Jasco FP-8300 instrument using quartz cuvettes (Hellma analytics, 1 cm pathway). Measurements were performed at an excitation wavelength λ_{ex} of 339 nm from 350 to 550 nm with a scan speed of 20 nm min⁻¹ at an interval of 0.2 nm.

Atomic force microscopy (AFM) was performed with a Dimension 3100 and Multimode (both from Bruker, Veeco, Santa Barbara, CA) equipped with a nanoscope IV controller, as well as with a JPK-Nanowizard 3 (JPK BioAFM, Bruker Nano GmbH, Berlin, Germany) to determine the nanoparticle shape. Prior to each measurement, nanoparticle suspensions were deposited on Mica substrates, and the residual water was allowed to evaporate at room temperature. Measurements were performed at room temperature using standard tapping mode silicon cantilevers from Bruker (model RTESP, Veeco, Santa Barbara, CA) with a resonance frequency from 315 to 364 kHz in air, a spring constant in the range of 20 to 80 N m⁻¹, and a typical tip radius of less than 10 nm (typically 7 nm).

Ring Opening Polymerization. All polymerizations were performed at 23 °C in a glovebox under nitrogen atmosphere (<0.1 ppm of H₂O; < 0.1 ppm of O₂).

Homopolymerization Kinetics for ϵ CL and δ CL. The monomer was transferred into a vial and mixed with toluene. Afterward a solution containing BnOH, TBD, and toluene was added to adjust the initial monomer concentration [M]₀ and [M]₀: [BnOH]₀: [TBD]₀ ratio (Table S1 of the Supporting Information, SI). The ROP proceeded at room temperature. Aliquots were regularly withdrawn, quenched with a 4-fold excess of benzoic acid, and analyzed by means of ¹H NMR spectroscopy (Figure S1) and SEC to determine monomer conversions, molar masses, and dispersity values. In an exemplary reaction ([ϵ CL]: [BnOH]: [TBD] = 200:1:1; [ϵ CL]₀ = 2 mol L⁻¹), 444 μ L (4 mmol) of ϵ CL and 1.456 mL of toluene were transferred in a vial and stirred at room temperature to obtain a homogeneous solution. Subsequently, 100 μ L of a toluene solution containing 2.8 mg (0.02 mmol) of TBD and 2.2 mg (0.02 mmol) of BnOH were added to the mixture to start the reaction. Samples were

Table 1. Selected Structural Characterization Data of the Synthesized (Co)polyesters

sample	polymer	$\epsilon\text{CL}/\delta\text{CL}$			NMR			SEC ^d	
		feed [mol %]	conversion ^a [%]	theor. ^b [mol %]	NMR ^c [mol %]	$M_{n, \text{theo}}^b$ [kg mol ⁻¹]	$M_{n, \text{NMR}}^c$ [kg mol ⁻¹]	$M_{n, \text{SEC}}$ [kg mol ⁻¹]	\bar{D}
P1 ^e	P ϵCL	100/0	47/0	100/0	100/0	11	13	19	1.17
P2 ^f	P($\epsilon\text{CL-ran-}\delta\text{CL}$)	80/20	89/62	85/15	87/13	9	13	21	1.57
P3 ^f	P($\epsilon\text{CL-ran-}\delta\text{CL}$)	75/25	81/63	79/21	81/19	9	10	19	1.41
P4 ^f	P($\epsilon\text{CL-ran-}\delta\text{CL}$)	70/30	75/62	74/26	75/25	8	10	19	1.30
P5 ^f	P($\epsilon\text{CL-ran-}\delta\text{CL}$)	60/40	64/64	59/41	61/39	7	9	16	1.26
P6 ^f	P($\epsilon\text{CL-ran-}\delta\text{CL}$)	50/50	51/67	43/57	45/55	7	7	15	1.21
P7 ^g	P δCL	0/100	0/44	0/100	0/100	10	9	6	1.09

^aDetermined by the integration of monomer and polymer signals from the ¹H NMR spectra of the reaction solution between 4 and 5 ppm.

^bCalculated from the single monomer conversions and the feed ratio. ^cDetermined by the integration of suitable signals from the ¹H NMR spectra of the purified polyesters. ^dEluent CHCl₃, RI detection, PS calibration. ^e[ϵCL]₀:[BnOH]₀: [TBD]₀ = 200:1:1; [ϵCL]₀ = 2 mol L⁻¹. ^f[CL]₀: [BnOH]₀: [TBD]₀ = 100:1:2; [CL]₀ = 4 mol L⁻¹. ^g[δCL]₀: [BnOH]₀: [TBD]₀ = 200:1:4; [δCL]₀ = 4 mol L⁻¹.

taken after 1, 4, 5, 7.5, and 8 h, quenched with a 4-fold excess of benzoic acid, and analyzed as described above.

For bulk polymerizations, various vials were charged with the same amount of monomer, catalyst, and initiator. After varying the reaction time at room temperature, each vial was quenched by addition of a 4-fold excess of benzoic acid in toluene and analyzed as described above.

Statistical Copolymerization Kinetics for ϵCL and δCL . The two monomers were transferred into a vial to achieve five different monomer feed ratios [ϵCL]₀: [δCL]₀ of 80:20, 75:25, 70:30, 60:40, and 50:50. The overall monomer molar amount was fixed to 456 mg (4 mmol). Subsequently, 0.36 mL of toluene was added. The mixture was stirred at room temperature to obtain a homogeneous solution. Afterward 0.2 mL of a solution containing 4.3 mg (0.04 mmol) of BnOH and 11.1 mg (0.08 mmol) of TBD in toluene was added to adjust the overall initial monomer concentration [M]_{0,ovr} to 4 mol L⁻¹ and [M]_{0,ovr}: [BnOH]₀: [TBD]₀ ratio to 100:1:2 (Table S1). The ROP proceeded at room temperature. Aliquots were regularly withdrawn, quenched with a 4-fold excess of benzoic acid, and analyzed by means of ¹H NMR spectroscopy and SEC to determine monomer conversions, molar masses, and dispersity values.

In an exemplary reaction ([ϵCL]₀: [δCL]₀ = 70:30), 310 μL (2.8 mmol) of ϵCL , 132 μL (1.2 mmol) of δCL , 4.3 mg (0.04 mmol) of BnOH, 11.1 mg (0.08 mmol) of TBD, and 0.56 mL of toluene were used. The ROP proceeded at room temperature. Samples were withdrawn after 1, 2, 3, and 5 h, quenched with a 4-fold excess of benzoic acid, and analyzed via ¹H NMR spectroscopy and SEC.

Homopolymerization of ϵCL and δCL (P1 and P7). Corresponding to a ratio of [ϵCL]: [BnOH]: [TBD] of 200:1:1 and a [ϵCL]₀ of 2 mol L⁻¹, P ϵCL (P1) was obtained by adding 19.4 mL (175 mmol) of ϵCL and 67.2 mL of toluene to a round-bottom flask. Subsequent to complete dissolution at room temperature, 1 mL of a toluene solution containing 90.5 μL (0.87 mmol) of BnOH and 122 mg (0.87 mmol) of TBD was added to initiate the polymerization. Samples were withdrawn after 5, 7, and 8 h to monitor conversion, molar mass, and dispersity value. After 9 h of stirring at room temperature, the reaction mixture was quenched with a 4-fold excess of benzoic acid dissolved in toluene and a sample was taken to determine the monomer conversion. After a first precipitation of the polymers in cold methanol (-22 °C) followed by filtration, the polymer was redissolved in chloroform, reprecipitated in cold methanol (-22 °C), filtered, and dried in vacuum at 40 °C overnight to yield a white powder.

P ϵCL (P1): Conv. = 47%; yield: 7.6 g (38%). ¹H NMR (300 MHz, CDCl₃): δ /ppm = 1.39 (m, 209 H, -CH₂CH₂C(O)O-), 1.65 (m, 420 H, -OCH₂CH₂CH₂-), 2.31 (t, 208 H, -OC(O)-CH₂-), 4.06 (t, 207 H, -CH₂-O-), 5.11 (s, 2 H, C₆H₅-CH₂-), 7.35 (br, 5 H, C₆H₅-); SEC (CHCl₃, PS calibration): M_n = 19 kg mol⁻¹; \bar{D} = 1.17.

P δCL (P7) was synthesized employing a [δCL]: [BnOH]: [TBD] ratio of 200:1:4 at a [δCL]₀ of 4 mol L⁻¹. For this purpose, 19.29 mL (175.2 mmol) of δCL were dissolved in 19.5 mL of toluene at room

temperature. Subsequently, 5 mL of a toluene solution containing 90.66 μL (0.88 mmol) of BnOH and 488 mg (3.5 mmol) of TBD were added. After 2 h of stirring at room temperature, the reaction was terminated by addition of 1.5 equiv of benzoic acid in toluene. The mixture was stored at -22 °C for 3 days, forming a gel precipitate that was separated from the solution by decanting. The gel was dissolved in chloroform and precipitated from a 1/3 water/methanol mixture at room temperature. The precipitate was collected by centrifugation (5 °C, 7500 rpm, 5 min). The process was repeated twice, and the purified P7 was dried in vacuo at 40 °C overnight yielding a glassy gel.

P δCL (P7): Conv. = 44%; yield: 3.9 g (20%). ¹H NMR (300 MHz, CDCl₃): δ /ppm = 1.20 (d, 308 H, -CH₃), 1.59 (m, 473 H, -OCH(CH₃)CH₂CH₂-), 2.28 (t, 198 H, -OC(O)-CH₂-), 4.90 (m, 95 H, -CH(CH₃)-O-), 5.11 (s, 2 H, C₆H₅-CH₂-), 7.35 (br, 5 H, C₆H₅-); SEC (CHCl₃, PS calibration): M_n = 6.0 kg mol⁻¹; \bar{D} = 1.09.

General Procedure for the Statistical Copolymerization (P2 to P6). The reaction mixtures for the statistical copolymers of ϵCL and δCL were prepared in a similar fashion as that described above for the statistical copolymer kinetics. Corresponding to an [M]_{0,ovr}: [BnOH]: [TBD] ratio of 100:1:2 and an initial monomer concentration of 4 mol L⁻¹, 487 mg (3.5 mmol) of TBD, 181 μL (1.75 mmol) of BnOH and 4.877 mL of toluene were used. The feed ratio of ϵCL and δCL was varied as indicated below and in Table 1. Subsequent to polymerization at room temperature for 5 h, the reactions were terminated by addition of a 4-fold excess of benzoic acid. Aliquots of 200 μL were withdrawn from the solutions and used for SEC and ¹H NMR analyses. The remaining reaction mixtures were precipitated from cold methanol (-22 °C), kept at -22 °C for 1 h, and centrifuged (-10 °C, 8000 rpm, 5 min). Subsequent to removal of the supernatants, the copolymers were dissolved in 5 mL of THF, precipitated from 5 mL of water at room temperature, stored at 5 °C for 30 min, and centrifuged (5 min, 5 °C, 8000 rpm). Subsequent to removal of the supernatants, the precipitates were dried in vacuum at 40 °C overnight.

P($\epsilon\text{CL-ran-}\delta\text{CL}$) (P2): Corresponding to a [ϵCL]/[δCL] feed ratio of 80/20, 3.103 mL (28 mmol) of ϵCL and 0.77 mL (7 mmol) of δCL were used according to the general procedure.

Overall conv. = 81%; conv.(ϵCL) = 89%; conv.(δCL) = 62%; yield = 2.13 g (53%).

¹H NMR (300 MHz, CDCl₃): δ /ppm = 1.21 (d, 37 H, P δCL , -CH₃-), 1.39 (m, 153 H, P ϵCL , -CH₂CH₂C(O)O-), 1.62 (m, 426 H, P($\epsilon\text{CL-co-}\delta\text{CL}$), -OCH₂CH₂CH₂-), 2.30 (m, 172 H, P($\epsilon\text{CL-co-}\delta\text{CL}$), -OC(O)-CH₂-), 4.06 (t, 147 H, P ϵCL , -CH₂-O-), 4.90 (m, 11 H, P δCL , -CH₂-O-), 5.11 (s, 2 H, C₆H₅-CH₂-), 7.35 (br, 5 H, C₆H₅-); SEC (CHCl₃, PS calibration): M_n = 21 kg mol⁻¹; \bar{D} = 1.57.

P($\epsilon\text{CL-ran-}\delta\text{CL}$) (P3): Corresponding to a [ϵCL]/[δCL] feed ratio of 75/25, 2.909 mL (26.25 mmol) of ϵCL and 0.963 mL (8.75 mmol) of δCL were used according to the general procedure.

Overall conv. = 77%; conv.(ϵ CL) = 81%; conv.(δ CL) = 63%; yield = 1.58 g (40%).

^1H NMR (300 MHz, CDCl_3): δ /ppm = 1.21 (d, 55 H, P δ CL, CH_2 -), 1.39 (m, 149 H, P ϵ CL, $-\text{CH}_2\text{CH}_2\text{C}(\text{O})\text{O}-$), 1.62 (m, 455 H, P(ϵ CL-*co*- δ CL), $-\text{OCH}_2\text{CH}_2\text{CH}_2-$), 2.30 (m, 185 H, P(ϵ CL-*co*- δ CL), $-\text{OC}(\text{O})-\text{CH}_2-$), 4.06 (t, 147 H, P ϵ CL, $-\text{CH}_2-\text{O}-$), 4.90 (m, 17 H, P δ CL, $-\text{CH}_2-\text{O}-$), 5.11 (s, 2H, $\text{C}_6\text{H}_5-\text{CH}_2-$), 7.35 (br, 5H, C_6H_5-); SEC (CHCl_3 , PS calibration): M_n = 19 kg mol $^{-1}$; \bar{D} = 1.41.

P(ϵ CL-*ran*- δ CL) (P4): Corresponding to a $[\epsilon\text{CL}]/[\delta\text{CL}]$ feed ratio of 70/30, 2.715 mL (24.5 mmol) of ϵ CL and 1.156 mL (10.5 mmol) of δ CL were used according to the general procedure.

Overall conv. = 72%; conv.(ϵ CL) = 75%; conv.(δ CL) = 62%; yield = 2.02 g (50%).

^1H NMR (300 MHz, CDCl_3): δ /ppm = 1.21 (d, 72 H, P δ CL, CH_2 -), 1.39 (m, 145 H, P ϵ CL, $-\text{CH}_2\text{CH}_2\text{C}(\text{O})\text{O}-$), 1.62 (m, 429 H, P(ϵ CL-*co*- δ CL), $-\text{OCH}_2\text{CH}_2\text{CH}_2-$), 2.30 (m, 187 H, P(ϵ CL-*co*- δ CL), $-\text{OC}(\text{O})-\text{CH}_2-$), 4.06 (t, 139 H, P ϵ CL, $-\text{CH}_2-\text{O}-$), 4.90 (m, 22 H, P δ CL, $-\text{CH}_2-\text{O}-$), 5.11 (s, 2H, $\text{C}_6\text{H}_5-\text{CH}_2-$), 7.35 (br, 5H, C_6H_5-); SEC (CHCl_3 , PS calibration): M_n = 19 kg mol $^{-1}$; \bar{D} = 1.30.

P(ϵ CL-*ran*- δ CL) (P5): Corresponding to a $[\epsilon\text{CL}]/[\delta\text{CL}]$ feed ratio of 60/40, 2.327 mL (21 mmol) of ϵ CL and 1.541 mL (14 mmol) of δ CL were used according to the general procedure.

Overall conv. = 63%; conv.(ϵ CL) = 62%; conv.(δ CL) = 64%; yield = 1.74 g (44%).

^1H NMR (300 MHz, CDCl_3): δ /ppm = 1.21 (d, 94 H, P δ CL, CH_2 -), 1.39 (m, 100 H, P ϵ CL, $-\text{CH}_2\text{CH}_2\text{C}(\text{O})\text{O}-$), 1.62 (m, 470 H, P(ϵ CL-*co*- δ CL), $-\text{OCH}_2\text{CH}_2\text{CH}_2-$), 2.30 (m, 145 H, P(ϵ CL-*co*- δ CL), $-\text{OC}(\text{O})-\text{CH}_2-$), 4.06 (t, 86 H, P ϵ CL, $-\text{CH}_2-\text{O}-$), 4.90 (m, 28 H, P δ CL, $-\text{CH}_2-\text{O}-$), 5.11 (s, 2H, $\text{C}_6\text{H}_5-\text{CH}_2-$), 7.35 (br, 5H, C_6H_5-); SEC (CHCl_3 , PS calibration): M_n = 16 kg mol $^{-1}$; \bar{D} = 1.26.

P(ϵ CL-*ran*- δ CL) (P6): Corresponding to a $[\epsilon\text{CL}]/[\delta\text{CL}]$ feed ratio of 50/50, 1.939 mL (17.5 mmol) of ϵ CL and 1.926 mL (17.5 mmol) of δ CL were used according to the general procedure.

Overall conv. = 59%; conv.(ϵ CL) = 51%; conv.(δ CL) = 67%; yield = 1.10 g (28%).

^1H NMR (300 MHz, CDCl_3): δ /ppm = 1.21 (d, 127 H, P δ CL, CH_2 -), 1.39 (m, 75 H, P ϵ CL, $-\text{CH}_2\text{CH}_2\text{C}(\text{O})\text{O}-$), 1.62 (m, 361 H, P(ϵ CL-*co*- δ CL), $-\text{OCH}_2\text{CH}_2\text{CH}_2-$), 2.30 (m, 154 H, P(ϵ CL-*co*- δ CL), $-\text{OC}(\text{O})-\text{CH}_2-$), 4.06 (t, 68 H, P ϵ CL, $-\text{CH}_2-\text{O}-$), 4.90 (m, 41 H, P δ CL, $-\text{CH}_2-\text{O}-$), 5.11 (s, 2H, $\text{C}_6\text{H}_5-\text{CH}_2-$), 7.35 (br, 5H, C_6H_5-); SEC (CHCl_3 , PS calibration): M_n = 15 kg mol $^{-1}$; \bar{D} = 1.21.

Nanoparticle Preparation. P1 to P7 were dissolved in THF to provide a concentration of 1 mg mL $^{-1}$. 0.5 mL of the solution were dropped into 5 mL of Milli-Q water while stirring. The suspensions were stirred (1000 rpm) for 3 h at room temperature. The vials were left open overnight to allow evaporation of THF yielding aqueous dispersions of a final concentration of 0.1 mg mL $^{-1}$. Afterward DLS measurements were performed. The pyrene loaded nanoparticles were prepared by mixing 0.4 mL of polymeric THF solutions (c = 1.25 mg mL $^{-1}$) and 0.1 mL of a pyrene solution in THF (c = 50 μg mL $^{-1}$). 0.5 mL of the combined solution was dropped into 5 mL of Milli-Q water while stirring. The vials were left open overnight to allow evaporation of THF yielding aqueous dispersions of a final polymer concentration of 0.1 mg mL $^{-1}$ and a pyrene concentration of 1 μg mL $^{-1}$. After DLS measurements, the nanoparticle suspensions of P1, P6, and P7 were diluted 20 times and fluorescence spectra were measured (λ_{ex} = 339 nm, $c(\text{pyrene})$ = 2.4×10^{-7} mol L $^{-1}$).

Kinetic Modeling. Kinetic modeling was performed using Origin version Pro 2015. For the calculation of reactivity ratios, least-squares analysis based on standard functions was implemented for the kinetic models. The visual representations of the copolymer microstructures obtained employing the Meyer–Lowry (ML) and Beckingham (BSL) models were based on the calculation of conditional probabilities and the average block length of both ϵ CL and δ CL segments.^{34–36}

RESULTS AND DISCUSSION

The aim of our study was to obtain PCL with varied degrees of crystallinity. Since δ CL is rarely focused on, even in academic research,^{16,32,37} a broad screening of the homopolymerization conditions represented the initial step of this study. Therefore, the organobase TBD was used as a catalyst at room temperature and parameters such as [monomer] to [initiator] ratio and monomer concentration in toluene were varied (see the SI for details). Irrespective of the initial monomer concentration, the monomer concentration approached a threshold value of 0.55 mol L $^{-1}$ that represents the monomer equilibrium concentration $[\delta\text{CL}]_{\text{eq}}$ at room temperature (Figure 1). The value is in accordance with thermodynamic

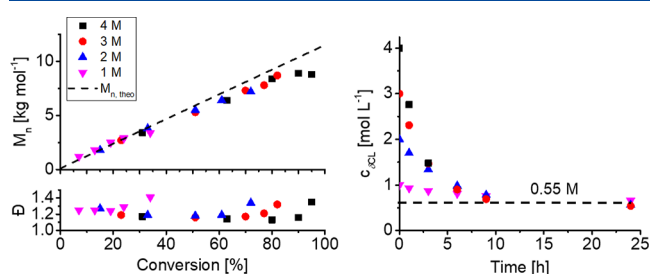


Figure 1. Kinetic plots for the TBD-catalyzed ROP of δ CL in toluene at room temperature employing an initial $[\delta\text{CL}]_0$: $[\text{BnOH}]_0$: $[\text{TBD}]_0$ ratio of 100:1:2 at initial monomer concentrations $[\delta\text{CL}]_0$ of 4, 3, 2, and 1 mol L $^{-1}$. Left: Dependence of the molar mass $M_{n,\text{SEC}}$ and dispersity on the monomer conversion. The dotted line represents the theoretical molar mass $M_{n,\text{theo}}$ calculated according to $M_{n,\text{theo}} = M_{\delta\text{CL}} \times ([\delta\text{CL}]_0/[\text{BnOH}]_0) \times \text{conversion} + M_{\text{BnOH}}$. Right: Evolution of the residual monomer concentration $[\delta\text{CL}]$ over time. The dotted line represents the monomer equilibrium concentration $[\delta\text{CL}]_{\text{eq}}$ of 0.55 mol L $^{-1}$.

data reported for the diphenyl phosphate catalyzed ROP of δ CL reported by Hillmyer and co-workers.¹⁶ Briefly, optimized polymerization conditions required at least 2 equiv of TBD with respect to the initiator BnOH. Similar to Lohmeijer et al.,³³ we observed that P ϵ CL with low dispersity required a reduced amount of TBD, i.e., $[\text{BnOH}]_0$: $[\text{TBD}]_0$ ratios of 1:1 or 1:0.5 (see SI for details). A $[\text{BnOH}]_0$: $[\text{TBD}]_0$ ratio of 1:2 as a compromise between the optimum ROP conditions of both monomers was selected for the statistical copolymerization. To account for $[\delta\text{CL}]_{\text{eq}}$, a rather high initial monomer concentration $[\text{CL}]_0$ of 4 mol L $^{-1}$ was investigated further.

Statistical Copolymerization of δ CL and ϵ CL. As Song et al. reported that a δ CL fraction in the feed $f_{\delta\text{CL},0}$ of 50% resulted in amorphous materials,³² we varied the feed ratio of ϵ CL and δ CL between 80:20 and 50:50. For this purpose, the kinetics of five different statistical copolymerizations were examined applying the conditions described above ($[\text{CL}]_0$: $[\text{BnOH}]_0$: $[\text{TBD}]_0$ = 100:1:2; $[\text{CL}]_0$ = 4 mol L $^{-1}$ in toluene at room temperature, Figures S15–S19).

Irrespective of the initial feed ratio, SEC revealed the occurrence of high molar mass tailing for conversions above 50%, in line with the results obtained for the homopolymerization of ϵ CL. However, dispersity values remained below 1.4 and the molar masses increased with conversion in a linear fashion. Because a monomer equilibrium concentration was not reached, the semilogarithmic plots suggested pseudo-first order polymerization kinetics up to such conversions. As evident from the apparent polymerization rate constants of the individual monomers $k_{p,\text{app}}$ (Table S3), the polymerizability of

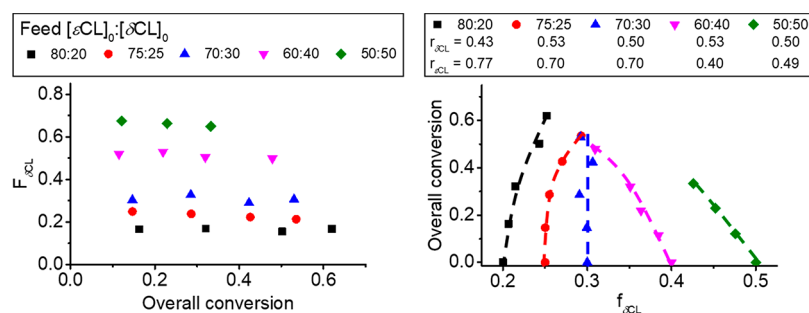


Figure 2. Monomer reactivity of ϵ CL and δ CL. Left: Evolution of the δ CL fraction in the copolymer ($F_{\delta\text{CL}}$) vs overall conversion. Right: Overall monomer conversion vs molar fraction of δ CL in the feed ($f_{\delta\text{CL}}$). The dotted lines represent fits according to the Meyer–Lowry equation.³⁹ Estimated reactivity ratios are indicated in the legend.

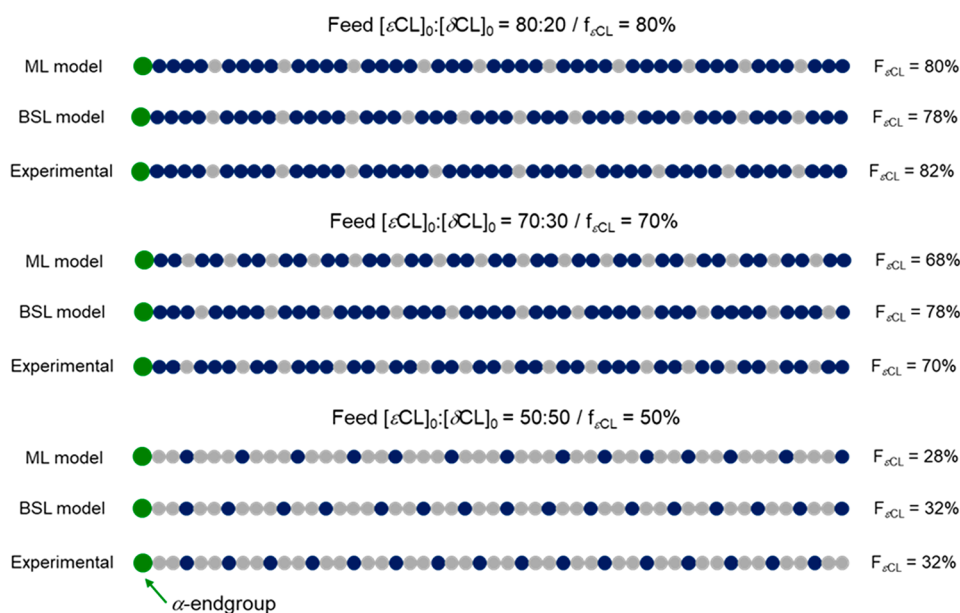


Figure 3. Schematic representation of the microstructures obtained from experimental data and probability calculations based on the Meyer–Lowry (ML) and Beckingham (BSL) models for a DP value of 50 employing an initial $[\epsilon\text{CL}]_0:[\delta\text{CL}]_0$ ratio of 80:20, 70:30, and 50:50. The benzyl α -end group is depicted in green, the ϵ CL and δ CL units are depicted in blue and gray, respectively.

the substituted lactone δ CL was increased in the copolymerization with ϵ CL compared to its homopolymerization.

In order to clarify the role of ϵ CL in the copolymerization with δ CL, the monomer reactivity ratios were of interest, reasoning the focus on low conversions during the kinetic studies. A range of analytical models can be used for this purpose and are often applied for irreversible polymerizations.^{38–40} Although equilibrium processes play a role in the ROP of lactones, the copolymerization of ϵ CL and δ CL resembled an irreversible reaction in the low conversion range investigated here. The Mayo–Lewis method³⁸ pointed toward a tendency of homopropagation for both monomers ($r_{\delta\text{CL}} = 7.1$ and $r_{\epsilon\text{CL}} = 3.1$). However, the overall conversions of around 18% were relatively high for this classical method (Figure S20). However, the wealth of data from the kinetic studies enabled a much clearer picture of the copolymer microstructure (Figure 2). For all copolymerizations, no significant variation of the δ CL fraction in the copolymer $F_{\delta\text{CL}}$ during the course of polymerization was observed. For the reactions up to a δ CL feed fraction $f_{\delta\text{CL},0}$ of 30%, the δ CL fraction was maintained in the copolymer. In contrast, increasing the $f_{\delta\text{CL},0}$ to 40% or 50% resulted in an elevated δ CL fraction in the copolymer ($F_{\delta\text{CL}} = 52\%$ or 66% , respectively). The observation is in agreement

with fitting results according to the Meyer–Lowry (ML) model,³⁹ which showed an almost constant reactivity ratio of δ CL for all copolymerizations ($r_{\delta\text{CL}} \approx$ of 0.50). In contrast, the estimated reactivity ratio of ϵ CL $r_{\epsilon\text{CL}}$ slightly changed throughout the series of kinetic studies but consistently remained below 1. In addition, the simple nonterminal method proposed by Beckingham et al.⁴⁰ in 2015 (BSL model) was tested although it assumes an ideal copolymerization taking place (Figure S21). Also in this case, slightly different reactivity ratios were found comparing the individual kinetic studies with varied comonomer feed fraction ($0.80 \leq r \leq 2.13$).

In summary, the ML as well as the BSL model hinted toward the presence of a random copolymerization of ϵ CL and δ CL. That is in line with observations made by Song et al., who investigated the copolymer microstructure by ¹³C NMR studies.³² The more accurate terminal ML model⁴¹ giving two independent reactivity ratios pointed toward a minor tendency to alternate as all reactivity ratios were below 1. However, none of the models took into account any equilibrium processes, and small differences in reactivity ratios might not be straightforward to picture as they could simply result from experimental error. The calculations were hence complemented with visual representations of selected copoly-

mer microstructures (Figure 3). The microstructures based on the ML and BSL models, respectively, were obtained on the basis of the conditional probabilities followed by the calculation of the average block length of both ϵ CL and δ CL segments estimated from the reactivity ratios.^{34–36} The average block length of the ϵ CL mers decreased from four ($f_{\epsilon\text{CL}} = 0.8$) to one ($f_{\epsilon\text{CL}} = 0.5$) within the copolymer series. The depictions of the microstructures labeled as “experimental” were directly and solely based on the $[\epsilon\text{CL}]_0:[\delta\text{CL}]_0:[\text{BnOH}]_0$ ratio of the two monomers and the individual monomer conversions after each time interval between sampling.

All three microstructures closely resembled each other, irrespective of the initial comonomer feed ratio. One can hence conclude that (a) the simplified BSL model gave similar results as the mathematically more challenging terminal ML model; and (b) despite the actual presence of equilibria during the ROP of ϵ CL and δ CL, our initial disregard of that fact was valid. Models developed for solely chain growth polymerization were hence reasonable to be applied here. It should, however, be stressed that maintaining monomer concentrations significantly above the monomer equilibrium concentrations $[M]_{\text{eq}}$ was an important prerequisite. These conclusions might not hold true for higher monomer conversions where $[M]_{\text{eq}}$ cannot be neglected anymore.

Synthesis of PCL Materials. The extensive kinetic investigations on the ROP of caprolactones described above enabled us to identify optimum polymerization conditions suited for the preparation of various PCL homo- and copolyesters on a gram scale. In order to exclude additional variation of properties due to molar mass effects, a DP value of 100 (corresponding to a molar mass M_n of 11 kg mol⁻¹) was targeted. To avoid broadening of the molar mass distributions at higher conversions, the two homopolymers P ϵ CL **P1** and P δ CL **P7** were synthesized employing a $[\text{CL}]_0:[\text{BnOH}]_0$ of 200:1 and terminated at conversions of around 50% (Table 1). In contrast, kinetic studies for the copolymers revealed low dispersity values also at higher conversions. Therefore, a $[\text{CL}]_0:[\text{BnOH}]_0$ of 100:1 was employed for the synthesis of **P2** to **P6**. In line with the kinetic studies, the conversion of ϵ CL increased from 50 to 90% with increasing molar fraction of ϵ CL in the feed, whereas the δ CL conversion was around 65% for all copolymers. In consequence, the molar fraction of ϵ CL in the purified copolymers was mostly increased in comparison with the feed.

Analyses of the purified copolyesters by means of ¹H NMR spectroscopy confirmed that. As depicted in Figure 4, signals assigned to both repeating units were seen, albeit mostly as overlapping signals. However, the methylene or methine proton signals neighboring the oxygen atoms of the ester moieties (peaks “d” and “D” in Figure 4) were well separated and hence used to determine the composition of **P2** to **P6**. The resulting values are in agreement with the values expected from the individual monomer conversions, confirming that the purification procedure did not alter the composition of the initial samples. In addition, the molar mass of the polyesters **P1** to **P7** was estimated from the ¹H NMR spectra utilizing peak integrals assigned to the benzylic methylene protons (“e” vs “d” and/or “D” in Figure 4). The resulting $M_{n,\text{NMR}}$ values tended to be slightly higher than $M_{n,\text{theo}}$, i.e., the molar mass expected from feed and conversion. This is most likely due to the accuracy of the end group determination method for molar masses around 10 kg mol⁻¹, because SEC analysis did not

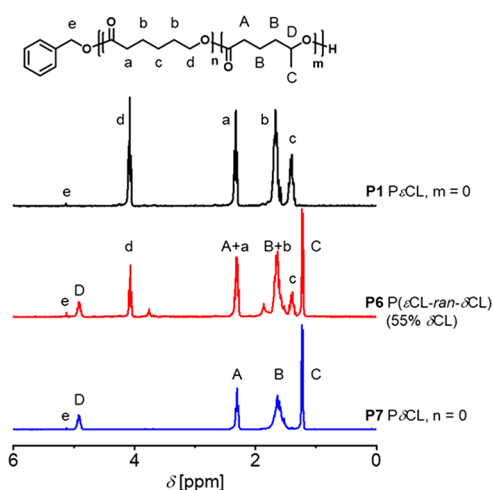


Figure 4. ¹H NMR spectra of P ϵ CL (**P1**), P δ CL (**P7**), the copolymer **P6** (300 MHz, CDCl₃), and assignment of the signals to the schematic representation of the structure of the copolyesters.

indicate any loss of low molar mass fractions throughout the purification process.

In line with the increased hydrodynamic volume of P ϵ CL compared to P δ CL in the chloroform based eluent used for SEC analysis, the molar masses $M_{n,\text{SEC}}$ were found to increase with the ϵ CL content throughout the polyester library. Also the dispersity value \bar{D} increased from 1.21 to 1.57 with the ϵ CL fraction for the copolymers **P2** to **P6**. This is most likely due to the formation of cyclic macromolecules through transesterification at higher conversions, as indicated by MALDI TOF mass spectrometry. Additional presence of TBD-initiated chains^{42,43} could neither be excluded nor be confirmed due to the resolution of the spectra (see SI). However, the two P ϵ CL and P δ CL homopolymers **P1** and **P7**, which were obtained under carefully optimized polymerization conditions, featured narrow molar mass distributions with dispersity values \bar{D} of 1.17 and 1.09, respectively.

Bulk Properties. As the crystallinity of polyesters can influence their degradation kinetics,³² analysis of the bulk materials by means of DSC and WAXS represented the next step to enable the determination of properties such as the melting temperature (T_m) and the degree of crystallinity (X_c). Subsequent to ensuring the thermal stability of the materials by means of TGA, DSC measurements were performed in the temperature range from -100 to 210 °C using three consecutive heating and cooling cycles (Table 2).

During the first heating run, the semicrystalline **P1** featured a melting temperature of 68 °C. Upon increasing the δ CL content in the copolymer, T_m decreased in a linear fashion to 24 °C for **P5** with a δ CL fraction $F_{\delta\text{CL}}$ of 39% (Figure 5). Although slightly lower T_m values were found for the semicrystalline **P1** to **P5** during the second and third heating run, the trend remained the same for polyesters with erased thermal prehistory. This observation is in line with the exothermic crystallization peaks recorded during the cooling runs for the samples **P1** to **P4**. Also here, an increased δ CL fraction resulted in a decreased T_c , suggesting that the comonomer δ CL affected the crystallization of the P ϵ CL domains. It should be noted that **P4** and **P5** additionally displayed cold crystallization during the second and third heating run. In addition, the enthalpy of melting decreased linearly with $F_{\epsilon\text{CL}}$, pointing toward a reduced degree of

Table 2. Bulk Properties of the Copolyesters Obtained by Means of DSC and WAXS Analysis

sample	polymer	$F_{\delta\text{CL}}$ [mol %]	first heating run ^a		WAXS ^b	first cooling run ^c		second heating run ^a	
			T_m [°C]	ΔH_f [J g ⁻¹]	X_c [%]	T_c [°C]	ΔH_c [J g ⁻¹]	T_m [°C]	$\Delta H_f - \Delta H_{cc}$ [J g ⁻¹]
P1	P ϵ CL	0	69	140	73	26	-93	60	87
P2	P(ϵ CL- <i>ran</i> - δ CL)	13	54	80	44	-4	-71	46	54
P3	P(ϵ CL- <i>ran</i> - δ CL)	19	52	50	38	-14	-43	42	49
P4	P(ϵ CL- <i>ran</i> - δ CL)	25	42	43	28	-29	-11	38	13
P5	P(ϵ CL- <i>ran</i> - δ CL)	39	24	2	4				
P6	P(ϵ CL- <i>ran</i> - δ CL)	55			0				
P7	P δ CL	100		n.d.	8				

^aPerformed from -100 to 210 °C with a heating rate of 20 °C min⁻¹. ^bPerformed at room temperature. ^cPerformed from 210 to -100 °C with a cooling rate of -20 °C min⁻¹.

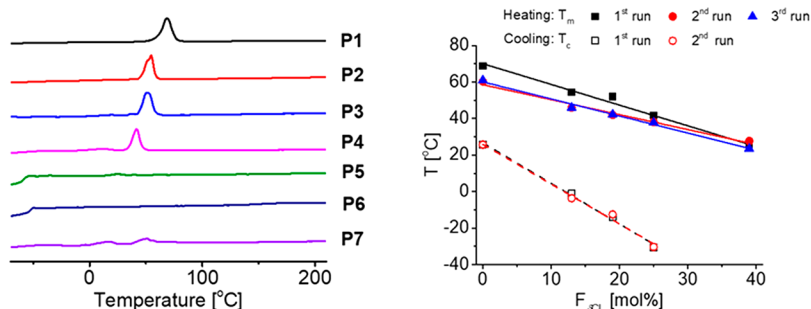


Figure 5. Left: DSC thermograms of the homo and copolyesters P1 to P7 (N₂, first heating run -100 to 210 °C, heating rate 20 °C min⁻¹). Right: Dependence of the melting temperature (T_m) and the crystallization temperature (T_c) on the fraction of δ CL in the copolymer ($F_{\delta\text{CL}}$).

crystallinity through incorporation of δ CL units in the P ϵ CL matrix (see SI).

Increasing the $F_{\delta\text{CL}}$ further resulted in the absence of a melting point, showing that a $F_{\delta\text{CL}}$ of 55% (P6) is sufficient to suppress the crystallinity induced by the P ϵ CL domains, which is in line with the average P ϵ CL block length of one determined by conditional probability calculations (Figure 3). However, the DSC thermogram of the P δ CL homopolymer P7 revealed multiple endothermic events in the first heating run, which were not visible in the second or third heating runs anymore.

WAXS analyses were performed to unambiguously determine the degree of crystallinity of the bulk materials P1 to P7. As reported in literature,^{44,45} the P ϵ CL P1 was semicrystalline with a degree of crystallinity of 73% and typical reflections at 2θ of 21.7 and 23.9 (Figure 6). The scattering pattern remained unaltered for the copolymers P2 to P5, suggesting that the introduction of δ CL comonomers did not affect the crystal structure of the P ϵ CL domains. However, increasing the

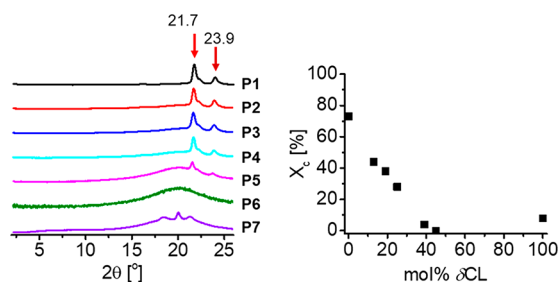


Figure 6. WAXS analysis for the homo and copolyesters P1 to P7. Left: WAXS diffractograms and assignment of the typical reflexes of P ϵ CL (P1). Right: Dependence of the degree of crystallinity (X_c) on the fraction of δ CL in the copolymer ($F_{\delta\text{CL}}$).

δ CL content resulted in lower scattering intensities, and, in consequence, lowered the degree of crystallinity. In fact, X_c of the polyesters P1 to P5 linearly decreased with the ϵ CL content (Figure 6). In line with DSC analyses, the copolyester P6 with a δ CL content of 55% represented an amorphous material.

WAXS analysis of the P δ CL homopolymer P7 showed the presence of low intensity scattering reflexes at 2θ of 18.4, 20.0, and 21.3 and a degree of crystallinity of 8%. The three new reflections did not superimpose with the scattering pattern of P1, suggesting that both polymers can, indeed, crystallize assuming different chain packing. However, the absence of the signals related to P7 in the WAXS diffractograms of P2 to P6 suggests an absence of such crystallites in the copolymers.

Nanoparticle Formulation. Having established a copolyester library with similar molar mass but varying degree of crystallinity, the preparation of stable aqueous nanoparticle dispersions represented the next step. Nanoprecipitation was hence performed according to an established protocol^{28,29} to yield dispersions of a final polymer concentration of 0.1 mg mL⁻¹ in water, avoiding the formation of agglomerates or polymer films. DLS measurements indicated hydrodynamic diameters between 115 and 138 nm and low to moderate dispersity (Table 3, SI). AFM was used as complementary technique to investigate the polymer nanoparticles from P1 to P7, revealing structures with an increased average size of 190 nm in diameter. However, the average height of 20 nm suggested that the nanoparticles collapsed on the surface of the substrate.

As final proof of concept for the preparation of polyester nanoparticles featuring the same HHB, pyrene was encapsulated employing the homopolymer P1 and P7 and the copolyester P6 (featuring a ϵ CL to δ CL ratio of 45 to 55). Frequently applied for the determination of the critical micellar concentration,^{46,47} pyrene can serve as a tool to determine the

Table 3. DLS Data of the Nanoparticles Obtained from the Polyesters P1 to P7

sample	P1	P2	P3	P4	P5	P6	P7
$F_{\epsilon\text{CL}}:F_{\delta\text{CL}}$ [mol %]	100:0	87:13	81:19	75:25	61:39	55:45	0:100
D_h^a [nm]	137	138	137	129	137	130	115
PDI	0.109	0.055	0.085	0.071	0.076	0.074	0.133

^a D_h denotes the Z-average.

hydrophobicity of its surrounding due to variation of the vibrational fine structure in its fluorescence spectrum. For this purpose, pyrene and the polymers were coprecipitated from THF into water keeping the pyrene to polymer mass ratio at 1% for all the samples. DLS analyses revealed hydrodynamic diameters between 120 and 160 nm and low to moderate dispersity ($0.084 < \text{PDI} < 0.103$; see SI). After a 20-fold dilution, the resulting pyrene-loaded nanoparticles were analyzed by means of fluorescence spectroscopy. The hydrophobicity of the nanoparticles was evaluated via the ratio of the I_1 and I_3 bands, resulting in a value of around 1.22 for all samples (Figure 7). This did not only confirm the constant

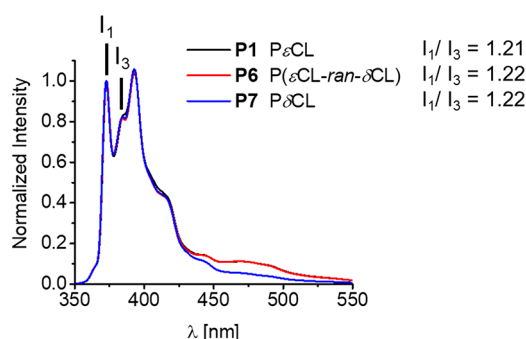


Figure 7. Normalized fluorescence spectra of pyrene loaded nanoparticles formed from P1, P6, and P7 ($\lambda_{\text{ex}} = 339$ nm, $\text{co}(\text{polymer}) = 5 \mu\text{g mL}^{-1}$, $\text{co}(\text{pyrene}) = 0.05 \mu\text{g mL}^{-1}$).

HHB for the PCL nanoparticles, but also hinted toward an increased hydrophobicity of the PCL particles in comparison to PLA ($I_1/I_3 \approx 1.3$),²⁹ thereby demonstrating the significance of a careful polymer design before structure property relationships with respect to nanoparticle performance can be drawn.

CONCLUSIONS

The copolymerization of the two constitutional isomers ϵCL and δCL represented a suitable approach to access a library of tailor-made polyesters with the same hydrophilic hydrophobic balance (HHB). An in-depth evaluation of the homo and copolymerization kinetics and application of the ML and BSL models suggested the presence of random copolymers. A comparison of the resulting microstructure estimated by conditional probability calculations with the microstructure directly obtained from kinetic data hinted toward the applicability of the kinetic models well below the monomer equilibrium concentration.

The copolymer microstructure and composition directly influenced the bulk crystallinity and melting temperature of the copolyesters, which both decreased in a linear fashion with the δCL fraction. The materials were suited to prepare stable aqueous nanoparticle dispersions of similar size and constant HHB, as indicated by encapsulation of the probe pyrene.

These carefully adjusted materials are currently investigated with respect to release of encapsulated active pharmaceutical ingredients to unambiguously clarify the effect of the crystallinity of polyester nanoparticles on enzymatic degradation.

ASSOCIATED CONTENT

Supporting Information

The Supporting Information is available free of charge at <https://pubs.acs.org/doi/10.1021/acs.macromol.0c00486>.

Additional description of the homopolymerization optimization and kinetic studies, calculation details, ¹H NMR spectra, SEC elugrams, MALDI TOF mass spectra including discussion, TGA and DSC thermograms, DLS and AFM data, and nanoparticle preparation details (PDF)

AUTHOR INFORMATION

Corresponding Author

Ulrich S. Schubert – Laboratory of Organic and Macromolecular Chemistry (IOMC) and Jena Center for Soft Matter (JCSM), Friedrich Schiller University Jena, 07743 Jena, Germany; orcid.org/0000-0003-4978-4670; Email: ulrich.schubert@uni-jena.de

Authors

Damiano Bandelli – Laboratory of Organic and Macromolecular Chemistry (IOMC) and Jena Center for Soft Matter (JCSM), Friedrich Schiller University Jena, 07743 Jena, Germany

Irina Muljajew – Laboratory of Organic and Macromolecular Chemistry (IOMC) and Jena Center for Soft Matter (JCSM), Friedrich Schiller University Jena, 07743 Jena, Germany

Karl Scheuer – Chair of Materials Science (CMS), Department of Materials Science and Technology, Otto Schott Institute of Materials Research, Faculty of Physics and Astronomy, Friedrich Schiller University Jena, 07743 Jena, Germany

Johannes B. Max – Laboratory of Organic and Macromolecular Chemistry (IOMC) and Jena Center for Soft Matter (JCSM), Friedrich Schiller University Jena, 07743 Jena, Germany

Christine Weber – Laboratory of Organic and Macromolecular Chemistry (IOMC) and Jena Center for Soft Matter (JCSM), Friedrich Schiller University Jena, 07743 Jena, Germany

Felix H. Schacher – Laboratory of Organic and Macromolecular Chemistry (IOMC) and Jena Center for Soft Matter (JCSM), Friedrich Schiller University Jena, 07743 Jena, Germany; orcid.org/0000-0003-4685-6608

Klaus D. Jandt – Jena Center for Soft Matter (JCSM) and Chair of Materials Science (CMS), Department of Materials Science and Technology, Otto Schott Institute of Materials Research, Faculty of Physics and Astronomy, Friedrich Schiller University Jena, 07743 Jena, Germany; orcid.org/0000-0002-7537-5603

Complete contact information is available at:

<https://pubs.acs.org/10.1021/acs.macromol.0c00486>

Notes

The authors declare no competing financial interest.

ACKNOWLEDGMENTS

The work was funded by the Deutsche Forschungsgemeinschaft (DFG, German Research Foundation)—project number 316213987—SFB 1278 (projects A01, A03, A06, Z01) and SCHA1640/18-1. We gratefully acknowledge the additional financial support of the Thüringer Ministerium für Wirtschaft, Wissenschaft, und Digitale Gesellschaft (Thuringian Ministry for Economic Affairs, Science and Digital Society, ProExzellenz II, NanoPolar) and the Deutsche Forschungsgemeinschaft (DFG), grant reference INST 275/389-1 FUGG; AOBJ: 640980. F.H.S. and U.S.S. acknowledge support from the Thuringian Ministry for Education, Science, and Culture (TMBWK, #B515-11028, SWAXS-JCSM).

REFERENCES

- (1) Fornaguera, C.; García-Celma, M. J. Personalized nanomedicine: A revolution at the nanoscale. *J. Pers. Med.* **2017**, *7*, 12.
- (2) Facklam, A. L.; Volpatti, L. R.; Anderson, D. G. Biomaterials for personalized cell therapy. *Adv. Mater.* **2020**, *32*, 1902005.
- (3) Casalini, T.; Rossi, F.; Castrovinci, A.; Perale, G. A perspective on polylactic acid-based polymers use for nanoparticles synthesis and applications. *Front. Bieng. Biotechnol.* **2019**, *7*, 259.
- (4) Mir, M.; Ahmed, N.; Rehman, A. u. Recent applications of PLGA based nanostructures in drug delivery. *Colloids Surf., B* **2017**, *159*, 217–231.
- (5) Englert, C.; Brendel, J. C.; Majdanski, T. C.; Yildirim, T.; Schubert, S.; Gottschaldt, M.; Windhab, N.; Schubert, U. S. Pharmapolymer in the 21st century: Synthetic polymers in drug delivery applications. *Prog. Polym. Sci.* **2018**, *87*, 107–164.
- (6) Xu, Z.; Wang, D.; Cheng, Y.; Yang, M.; Wu, L.-P. Polyester based nanovehicles for siRNA delivery. *Mater. Sci. Eng., C* **2018**, *92*, 1006–1015.
- (7) Liu, X.; Fan, X.; Jiang, L.; Loh, X. J.; Wu, Y.-L.; Li, Z. Biodegradable polyester unimolecular systems as emerging materials for therapeutic applications. *J. Mater. Chem. B* **2018**, *6*, 5488–5498.
- (8) Peres, C.; Matos, A. I.; Conniot, J.; Sainz, V.; Zupančič, E.; Silva, J. M.; Graça, L.; Sá Gaspar, R.; Prêat, V.; Florindo, H. F. Poly(lactic acid)-based particulate systems are promising tools for immune modulation. *Acta Biomater.* **2017**, *48*, 41–57.
- (9) Gao, S.; Tang, G.; Hua, D.; Xiong, R.; Han, J.; Jiang, S.; Zhang, Q.; Huang, C. Stimuli-responsive bio-based polymeric systems and their applications. *J. Mater. Chem. B* **2019**, *7*, 709–729.
- (10) Elsabahy, M.; Wooley, K. L. Design of polymeric nanoparticles for biomedical delivery applications. *Chem. Soc. Rev.* **2012**, *41*, 2545–2561.
- (11) Ekladios, I.; Colson, Y. L.; Grinstaff, M. W. Polymer–drug conjugate therapeutics: advances, insights and prospects. *Nat. Rev. Drug Discovery* **2019**, *18*, 273–294.
- (12) Cabral, H.; Miyata, K.; Osada, K.; Kataoka, K. Block copolymer micelles in nanomedicine applications. *Chem. Rev.* **2018**, *118*, 6844–6892.
- (13) Michalski, A.; Brzezinski, M.; Lapienis, G.; Biela, T. Star-shaped and branched polylactides: Synthesis, characterization, and properties. *Prog. Polym. Sci.* **2019**, *89*, 159–212.
- (14) Hillmyer, M. A.; Tolman, W. B. Aliphatic polyester block polymers: Renewable, degradable, and sustainable. *Acc. Chem. Res.* **2014**, *47*, 2390–2396.
- (15) Zhang, X.; Fevre, M.; Jones, G. O.; Waymouth, R. M. Catalysis as an enabling science for sustainable polymers. *Chem. Rev.* **2018**, *118*, 839–885.
- (16) Schneiderman, D. K.; Hillmyer, M. A. Aliphatic polyester block polymer design. *Macromolecules* **2016**, *49*, 2419–2428.
- (17) Bartnikowski, M.; Dargaville, T. R.; Ivanovski, S.; Huttmacher, D. W. Degradation mechanisms of polycaprolactone in the context of chemistry, geometry and environment. *Prog. Polym. Sci.* **2019**, *96*, 1–20.
- (18) Attia, M. F.; Brummel, B. R.; Lex, T. R.; Van Horn, B. A.; Whitehead, D. C.; Alexis, F. Recent advances in polyesters for biomedical imaging. *Adv. Healthcare Mater.* **2018**, *7*, 1800798.
- (19) Zhao, J.; Weng, G.; Li, J.; Zhu, J.; Zhao, J. Polyester-based nanoparticles for nucleic acid delivery. *Mater. Sci. Eng., C* **2018**, *92*, 983–994.
- (20) Castro-Aguirre, E.; Iñiguez-Franco, F.; Samsudin, H.; Fang, X.; Auras, R. Poly(lactic acid)—Mass production, processing, industrial applications, and end of life. *Adv. Drug Delivery Rev.* **2016**, *107*, 333–366.
- (21) Kamaraj, N.; Rajaguru, P. Y.; Issac, P. k.; Sundaresan, S. Fabrication, characterization, in vitro drug release and glucose uptake activity of 14-deoxy, 11, 12-didehydroandrographolide loaded polycaprolactone nanoparticles. *Asian J. Pharm. Sci.* **2017**, *12*, 353–362.
- (22) Budhian, A.; Siegel, S. J.; Winey, K. I. Controlling the in vitro release profiles for a system of haloperidol-loaded PLGA nanoparticles. *Int. J. Pharm.* **2008**, *346*, 151–159.
- (23) Bandelli, D.; Alex, J.; Weber, C.; Schubert, U. S. Polyester stereocomplexes beyond PLA: Could synthetic opportunities revolutionize established material blending? *Macromol. Rapid Commun.* **2020**, *41*, 1900560.
- (24) Lyubov, D. M.; Tolpygin, A. O.; Trifonov, A. A. Rare-earth metal complexes as catalysts for ring-opening polymerization of cyclic esters. *Coord. Chem. Rev.* **2019**, *392*, 83–145.
- (25) Bandelli, D.; Weber, C.; Schubert, U. S. Strontium isopropoxide: A highly active catalyst for the ring-opening polymerization of lactide and various lactones. *Macromol. Rapid Commun.* **2019**, *40*, 1900306.
- (26) Ottou, W. N.; Sardon, H.; Mecerreyes, D.; Vignolle, J.; Taton, D. Update and challenges in organo-mediated polymerization reactions. *Prog. Polym. Sci.* **2016**, *56*, 64–115.
- (27) Kamber, N. E.; Jeong, W.; Waymouth, R. M.; Pratt, R. C.; Lohmeijer, B. G. G.; Hedrick, J. L. Organocatalytic ring-opening polymerization. *Chem. Rev.* **2007**, *107*, 5813–5840.
- (28) Bandelli, D.; Helbing, C.; Weber, C.; Seifert, M.; Muljajew, I.; Jandt, K. D.; Schubert, U. S. Maintaining the hydrophilic–hydrophobic balance of polyesters with adjustable crystallinity for tailor-made nanoparticles. *Macromolecules* **2018**, *51*, 5567–5576.
- (29) Bandelli, D.; Alex, J.; Helbing, C.; Ueberschaar, N.; Görls, H.; Bellstedt, P.; Weber, C.; Jandt, K. D.; Schubert, U. S. Poly(3-ethylglycolide): a well-defined polyester matching the hydrophilic hydrophobic balance of PLA. *Polym. Chem.* **2019**, *10*, 5440–5451.
- (30) Liénard, R.; Zaldua, N.; Josse, T.; Winter, J. D.; Zübitor, M.; Mugica, A.; Iturrospe, A.; Arbe, A.; Coulembier, O.; Müller, A. J. Synthesis and characterization of double crystalline cyclic diblock copolymers of poly(ϵ -caprolactone) and poly(l(d)-lactide) (c(PCL-b-PL(D)LA)). *Macromol. Rapid Commun.* **2016**, *37*, 1676–1681.
- (31) Guo, X.; Rong, Z.; Ying, X. Calculation of hydrophile–lipophile balance for polyethoxylated surfactants by group contribution method. *J. Colloid Interface Sci.* **2006**, *298*, 441–450.
- (32) Song, Q.; Xia, Y.; Hu, S.; Zhao, J.; Zhang, G. Tuning the crystallinity and degradability of PCL by organocatalytic copolymerization with δ -hexalactone. *Polymer* **2016**, *102*, 248–255.
- (33) Lohmeijer, B. G. G.; Pratt, R. C.; Leibfarth, F.; Logan, J. W.; Long, D. A.; Dove, A. P.; Nederberg, F.; Choi, J.; Wade, C.; Waymouth, R. M.; Hedrick, J. L. Guanidine and amidine organocatalysts for ring-opening polymerization of cyclic esters. *Macromolecules* **2006**, *39*, 8574–8583.
- (34) Harwood, H. J.; Ritchey, W. M. The characterization of sequence distribution in copolymers. *J. Polym. Sci., Part B: Polym. Lett.* **1964**, *2*, 601–607.
- (35) Galvan, R.; Tirrell, M. On the average sequence length in copolymers. *J. Polym. Sci., Part A: Polym. Chem.* **1986**, *24*, 803–807.

(36) Harrison, S.; Ercole, F.; Muir, B. W. Living spontaneous gradient copolymers of acrylic acid and styrene: One-pot synthesis of pH-responsive amphiphiles. *Polym. Chem.* **2010**, *1*, 326–332.

(37) Save, M.; Schappacher, M.; Soum, A. Controlled ring-opening polymerization of lactones and lactides initiated by lanthanum isopropoxide, 1. General aspects and kinetics. *Macromol. Chem. Phys.* **2002**, *203*, 889–899.

(38) Mayo, F. R.; Lewis, F. M. Copolymerization. I. A basis for comparing the behavior of monomers in copolymerization; the copolymerization of styrene and methyl methacrylate. *J. Am. Chem. Soc.* **1944**, *66*, 1594–1601.

(39) Meyer, V. E.; Lowry, G. G. Integral and differential binary copolymerization equations. *J. Polym. Sci., Part A: Gen. Pap.* **1965**, *3*, 2843–2851.

(40) Beckingham, B. S.; Sanoja, G. E.; Lynd, N. A. Simple and accurate determination of reactivity ratios using a nonterminal model of chain copolymerization. *Macromolecules* **2015**, *48*, 6922–6930.

(41) Lynd, N. A.; Ferrier, R. C.; Beckingham, B. S. Recommendation for accurate experimental determination of reactivity ratios in chain copolymerization. *Macromolecules* **2019**, *52*, 2277–2285.

(42) Pascual, A.; Sardón, H.; Ruipérez, F.; Gracia, R.; Sudam, P.; Veloso, A.; Mecerreyes, D. Experimental and computational studies of ring-opening polymerization of ethylene brassylate macrolactone and copolymerization with ϵ -caprolactone and TBD-guanidine organic catalyst. *J. Polym. Sci., Part A: Polym. Chem.* **2015**, *53*, 552–561.

(43) Simón, L.; Goodman, J. M. The mechanism of TBD-catalyzed ring-opening polymerization of cyclic esters. *J. Org. Chem.* **2007**, *72*, 9656–9662.

(44) Muñoz-Bonilla, A.; Cerrada, M. L.; Fernández-García, M.; Kubacka, A.; Ferrer, M.; Fernández-García, M. Biodegradable polycaprolactone-titania nanocomposites: Preparation, characterization and antimicrobial properties. *Int. J. Mol. Sci.* **2013**, *14*, 9249–9266.

(45) Li, L.; Meng, F.; Zhong, Z.; Byelov, D.; de Jeu, W. H.; Feijen, J. Morphology of a highly asymmetric double crystallizable poly(ϵ -caprolactone-*b*-ethylene oxide) block copolymer. *J. Chem. Phys.* **2007**, *126*, 024904.

(46) Gu, L.; Shen, Z.; Zhang, S.; Lu, G.; Zhang, X.; Huang, X. Novel amphiphilic centipede-like copolymer bearing polyacrylate backbone and poly(ethylene glycol) and polystyrene side chains. *Macromolecules* **2007**, *40*, 4486–4493.

(47) Weber, C.; Wagner, M.; Baykal, D.; Hoepfener, S.; Paulus, R. M.; Festag, G.; Altuntas, E.; Schacher, F. H.; Schubert, U. S. Easy access to amphiphilic heterografted poly(2-oxazoline) comb copolymers. *Macromolecules* **2013**, *46*, 5107–5116.

Supporting information for

Copolymerization of caprolactone isomers to obtain nanoparticles with constant hydrophobicity and tunable crystallinity

*Damiano Bandelli,^{1,2} Irina Muljajew,^{1,2} Karl Scheuer,³ Johannes B. Max,^{1,2} Christine Weber,^{1,2}
Felix H. Schacher,^{1,2} Klaus D. Jandt,^{2,3} Ulrich S. Schubert^{1,2*}*

¹ Laboratory of Organic and Macromolecular Chemistry (IOMC), Friedrich Schiller University
Jena, Humboldtstr. 10, 07743 Jena, Germany

² Jena Center for Soft Matter (JCSM), Friedrich Schiller University Jena, Philosophenweg 7,
07743 Jena, Germany

³ Chair of Materials Science (CMS), Department of Materials Science and Technology, Otto Schott
Institute of Materials Research, Faculty of Physics and Astronomy, Friedrich Schiller University
Jena, Löbdergraben 32, 07743 Jena, Germany

* Correspondence to U. S. Schubert (ulrich.schubert@uni-jena.de)

Table S1: Details on the homopolymerization kinetics and test reactions for the ROP of ε -caprolactone and δ -caprolactone.

Entry	Monomer	[M] ₀ [mol L ⁻¹]	[M]:[BnOH]:[TBD]	n _M [mmol]	V _{ov} [mL]	Conversion [%] (time [h])	M _{n,SEC} [kg mol ⁻¹] (\bar{M})
1	δ CL	8.3	50:1:1	8.3	0.12	92 (4)	7 (1.13)
2	δ CL	8.3	100:1:1	8.3	0.12	2 (3)	n.d.
3	δ CL	8.3	100:1:2	8.3	0.12	67 (4)	7 (1.12)
4	δ CL	1	100:1:2	1	1	34 (24)	3 (1.41)
5	δ CL	2	100:1:2	2	1	72 (24)	7 (1.34)
6	δ CL	3	100:1:2	3	1	82 (24)	9 (1.32)
7	δ CL	4	100:1:2	4	1	83 (24)	9 (1.35)
8	δ CL	2	200:1:1	4	2	4 (24)	1 (1.17)
9	δ CL	2	200:1:2	4	2	7 (5.5)	1 (1.23)
10	δ CL	4	201:1:2	4	1	15 (48)	2 (1.21)
11	δ CL	4	200:1:4	4	1	51 (2)	7 (1.09)
12	δ CL	4	200:1:6	4	1	65 (2)	9 (1.10)
13	δ CL	4	200:1:8	4	1	73 (2)	9 (1.11)
14	ε CL	1	100:1:2	1	1	95 (24)	14 (1.95)
15	ε CL	2	100:1:2	2	1	92 (4.5)	13 (2.27)
16	ε CL	3	100:1:2	3	1	97 (4.5)	14 (2.62)
17	ε CL	4	100:1:2	4	1	68 (1)	14 (1.41)
18	ε CL	2	200:1:0.5	4	2	36 (24)	15 (1.15)
19	ε CL	4	200:1:0.5	4	1	48 (6)	18 (1.23)
20	ε CL	2	200:1:1	4	2	50 (8)	20 (1.17)

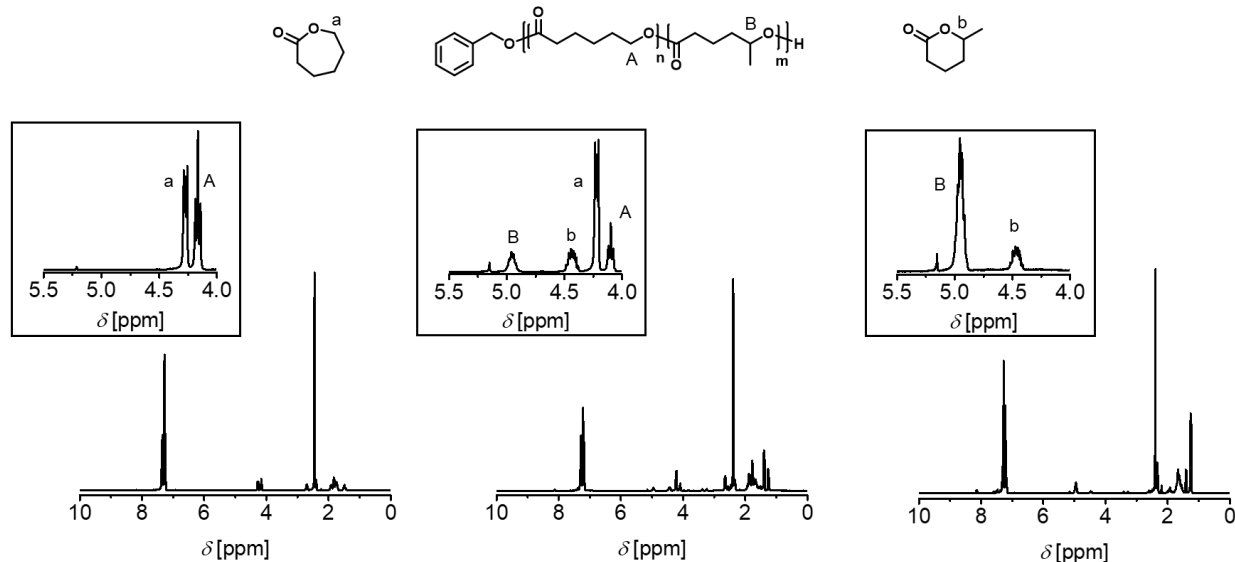


Figure S1: Exemplary ^1H NMR spectra (300 MHz, CDCl_3) of reaction mixtures of the ROP of ϵCL and δCL used to determine the monomer conversions. The zooms depict the chemical shift region used for the calculation assignments of the utilized signals to the schematic representation of monomers and polymers. **Left:** ^1H NMR spectrum of the homopolymerization reaction of ϵCL employing a $[\epsilon\text{CL}]_0:[\text{BnOH}]_0:[\text{TBD}]_0$ of 200:1:1, $[\epsilon\text{CL}]_0$ of 4 mol L^{-1} , collected after a reaction time of 8 h. **Center:** ^1H NMR spectrum of the statistical copolymerization reaction of ϵCL and δCL employing a $[\epsilon\text{CL}]_0 : [\delta\text{CL}]_0$ feed ratio of 50:50, a $[\text{CL}]_0:[\text{BnOH}]_0:[\text{TBD}]_0$ of 100:1:2 and $[\text{CL}]_0$ of 4 mol L^{-1} , collected after a reaction time of 3 h. **Right:** ^1H NMR spectrum of the homopolymerization reaction of δCL employing a $[\delta\text{CL}]_0:[\text{BnOH}]_0:[\text{TBD}]_0$ of 100:1:2, $[\delta\text{CL}]_0$ of 4 mol L^{-1} , collected after a reaction time of 9 h.

Homopolymerization kinetics of δ CL

First experiments were conducted in the bulk (**Figure S2-S3**) because the high initiator concentration during the ROP increases the overall polymerization rate. Although a low $[\delta\text{CL}]_0:[\text{BnOH}]_0:[\text{TBD}]_0$ ratio of 50:1:1 resulted in a linear increase of molar mass with respect to monomer conversion and a first order kinetic behavior, only low conversions were obtained at an increased feed ratio of 100:1:1. Also an increased catalyst amount (100:1:2) failed to increase the monomer conversion above 67%.

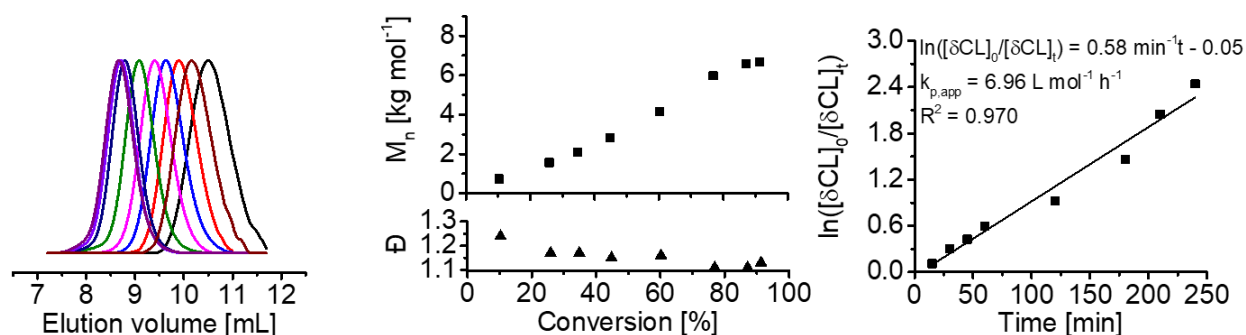


Figure S2: Kinetic studies of the ROP of δ CL in bulk employing a $[\delta\text{CL}]:[\text{BnOH}]:[\text{TBD}]$ of 50:1:1 (**Table S1**, entry **1**). **Left:** Overlay of SEC elugrams (CHCl_3 , RID). **Center:** Molar mass and dispersity evolution over conversion. **Right:** First order kinetic plot and linear extrapolation of experimental data (black line).

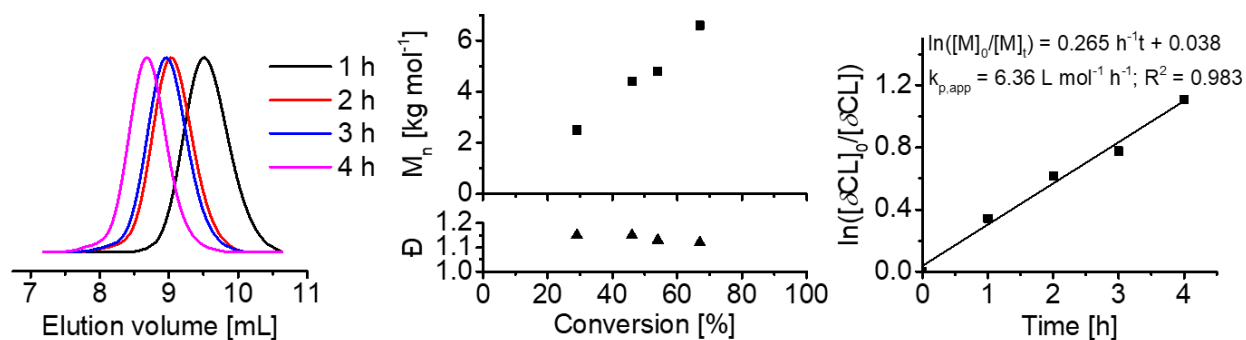


Figure S3: Kinetic studies of the ROP of δCL in bulk employing a $[\delta\text{CL}]:[\text{BnOH}]:[\text{TBD}]$ of 100:1:2 (**Table S1**, entry **3**). **Left:** Overlay of SEC elugrams (CHCl_3 , RID). **Center:** Molar mass and dispersity evolution over conversion. **Right:** First order kinetic plot and linear extrapolation of experimental data (black line).

We hence focused on the ROP of δCL in toluene. The feed ratio of 100:1:2 was kept constant, but the initial monomer concentration $[\delta\text{CL}]_0$ was varied ($[\delta\text{CL}]_0 = 1, 2, 3$ and 4 mol L^{-1} ; **Figure 1**, **Figure S4-S5**). SEC analyses revealed monomodal molar mass distributions for all samples, while the linear increase of the molar masses with respect to monomer conversion suggested a polymerization that was controlled with respect to molar mass. Low to moderate dispersity values (\bar{D}) below 1.4 were obtained. Besides, P δCL revealed a similar hydrodynamic volume as the calibration standard polystyrene (PS) in the chloroform-based eluent because the measured molar masses $M_{n,\text{SEC}}$ were in agreement with the values expected from the monomer to initiator ratio and conversion.

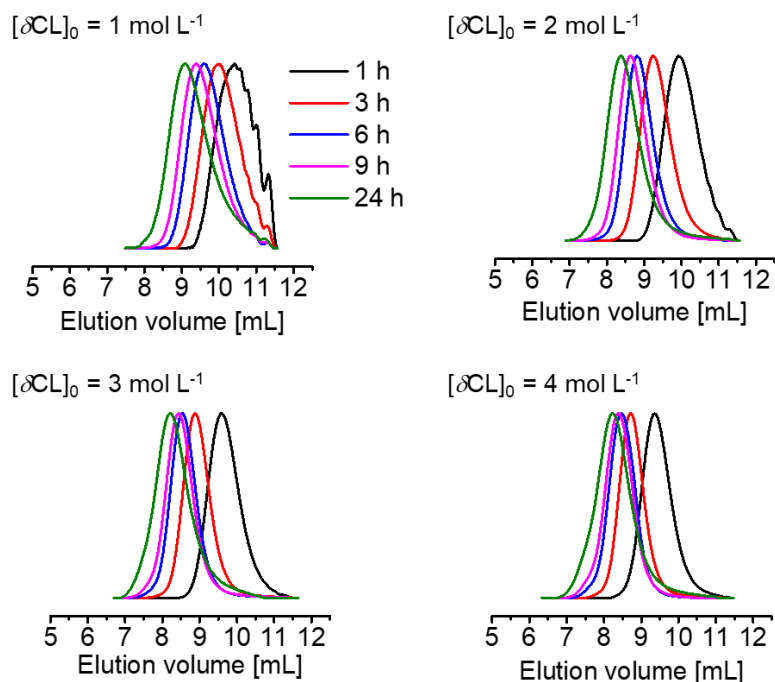


Figure S4: Overlay of SEC elugrams (CHCl_3 , RID) of the homopolymerization kinetics of δCL employing a $[\delta\text{CL}]:[\text{BnOH}]:[\text{TBD}]$ ratio of 100:1:2 and $[\delta\text{CL}]_0$ from 1 to 4 mol L^{-1} (**Table S1**, entries 4 to 7).

All solution ROP kinetics revealed a deviation from first-order behavior. The polymerization rate decreased throughout the course of the reaction. In principle, this may be due to termination, deactivation of the catalyst, or due to an equilibrium process. Irrespective of the initial monomer concentration, the monomer concentration approached a threshold value of 0.55 mol L^{-1} that represents the monomer equilibrium concentration $[\delta\text{CL}]_{\text{eq}}$ at room temperature. The value is in accordance with thermodynamic data reported for the diphenyl phosphate catalyzed ROP of δCL reported by Hillmyer and coworkers.¹ The respective kinetic equations describing the equilibrium process²⁻⁴ were hence applied to calculate the apparent polymerization rate constant ($k_{\text{p, app}}$ average value of $5.4 \text{ L mol}^{-1} \text{ h}^{-1}$).

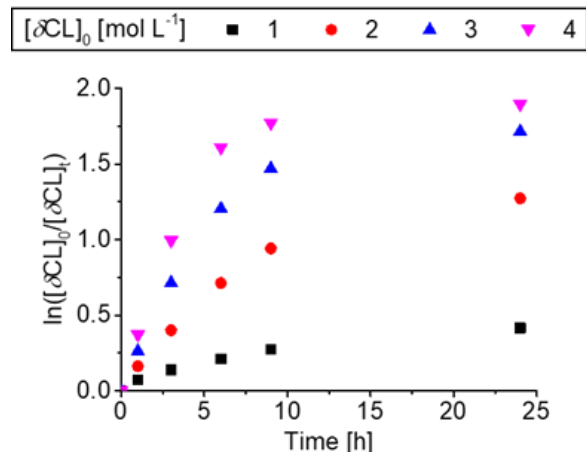


Figure S5: First order kinetic plots for the polymerization of δCL employing a $[\delta\text{CL}]:[\text{BnOH}]:[\text{TBD}]$ of 100:1:2 and $[\delta\text{CL}]_0$ from 1 to 4 mol L⁻¹ (**Table S1**, entries 4 to 7).

As the monomer equilibrium concentration prohibited a quantitative conversion of δCL , the monomer to initiator feed ratio was increased to 200:1 in order to obtain P δCL with higher degrees of polymerization (DP) and lower dispersity values. However, conversions remained low for polymerizations conducted using 1 or 2 equivalents of TBD. In contrast, an increased catalyst amount of 4, 6 or 8 equivalents enabled conversions above 50% as well as the synthesis of P δCL with narrow molar mass distribution ($\mathcal{D} \approx 1.10$, **Figure S6**). In conclusion, higher catalyst amounts were needed to obtain well-defined P δCL homopolymers.

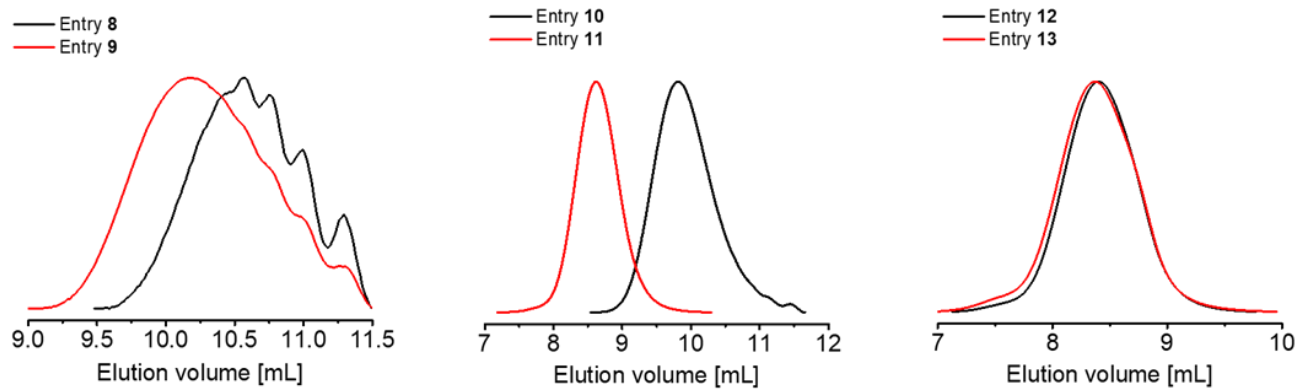


Figure S6: Overlay of SEC elugrams (CHCl₃, RID) of the homopolymerization of δ CL employing a [δ CL]:[BnOH] ratio of 200:1 (Table S1, entries 8 to 13).

Homopolymerization kinetics of ϵ CL

Unfortunately, the trend was reversed for the homopolymerization of ϵ CL. Similar to Lohmeijer *et al.*,⁵ we observed that P ϵ CL with low dispersity required a reduced amount of TBD, *i.e.* [BnOH]:[TBD] ratios of 1:1 or 1:0.5. A [BnOH]:[TBD] ratio of 1:2 as a compromise between the optimum ROP conditions of both monomers, *i.e.* ϵ CL and δ CL was selected for the statistical copolymerization and, hence, studied in detail with respect to an optimization of the monomer concentration $[\epsilon\text{CL}]_0$ in toluene. For this purpose, similar homopolymerization kinetics were conducted as described above for δ CL (**Figures S7-S13**). The unsubstituted ϵ CL polymerized faster ($k_{p, \text{app}}$ average value of $13.7 \text{ L mol}^{-1} \text{ h}^{-1}$) than the substituted lactone δ CL. In particular, for ROP at lower initial monomer concentration, rather high dispersity values ($\bar{D} \geq 1.9$) were observed. A $[\text{CL}]_0$ of 4 mol L^{-1} was also favorable with respect to the monomer equilibrium concentration of δ CL, as it allowed higher monomer conversions maintaining low dispersity. These conditions were hence selected for the statistical copolymerization of ϵ CL and δ CL.

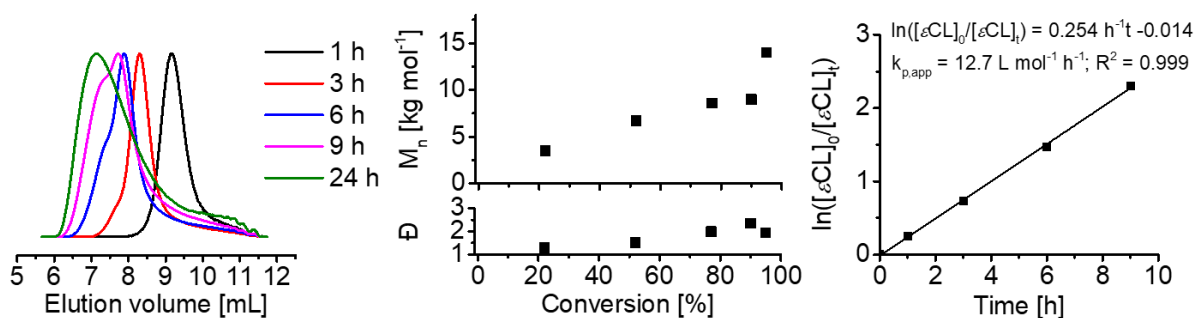


Figure S7: Kinetic studies of the ROP of ϵ CL employing a $[\epsilon\text{CL}]:[\text{BnOH}]:[\text{TBD}]$ of 100:1:2 and $[\epsilon\text{CL}]_0 = 1 \text{ mol L}^{-1}$ in toluene at room temperature (**Table S1**, entry 14). **Left:** Overlay of SEC elugrams (CHCl_3 , RID). **Center:** Dependence of the molar mass and dispersity on monomer conversion. **Right:** First order kinetic plot and linear extrapolation of experimental data (black line).

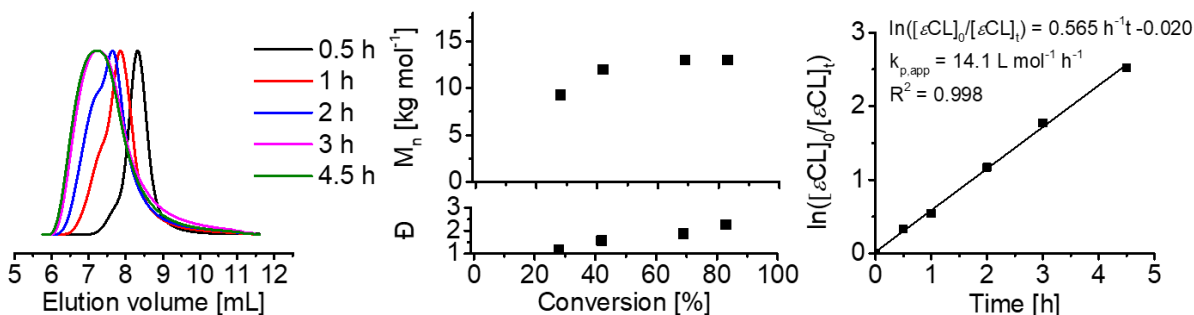


Figure S8: Kinetic studies of the ROP of ϵ CL employing a $[\epsilon\text{CL}]:[\text{BnOH}]:[\text{TBD}]$ of 100:1:2 and $[\epsilon\text{CL}]_0 = 2 \text{ mol L}^{-1}$ in toluene at room temperature (Table S1, entry 15). **Left:** Overlay of SEC elugrams (CHCl_3 , RID). **Center:** Dependence of the molar mass and dispersity on monomer conversion. **Right:** First order kinetic plot and linear extrapolation of experimental data (black line).

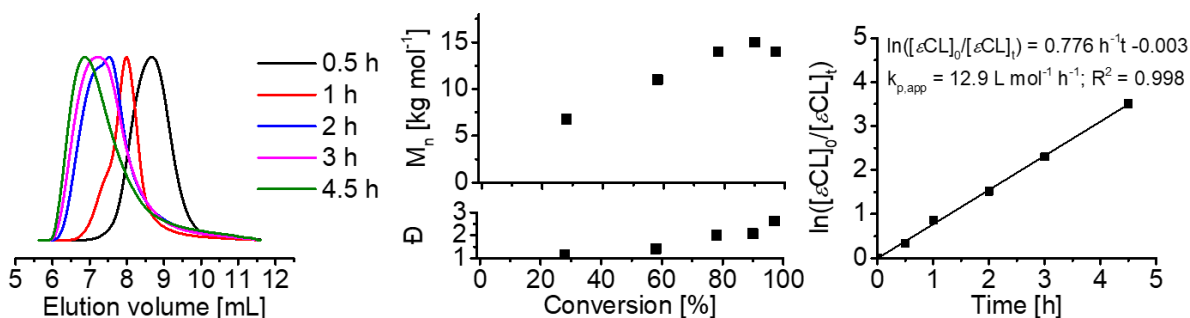


Figure S9: Kinetic studies of the ROP of ϵ CL employing a $[\epsilon\text{CL}]:[\text{BnOH}]:[\text{TBD}]$ of 100:1:2 and $[\epsilon\text{CL}]_0 = 3 \text{ mol L}^{-1}$ in toluene at room temperature (Table S1, entry 16). **Left:** Overlay of SEC elugrams (CHCl_3 , RID). **Center:** Dependence of the molar mass and dispersity on monomer conversion. **Right:** First order kinetic plot and linear extrapolation of experimental data (black line).

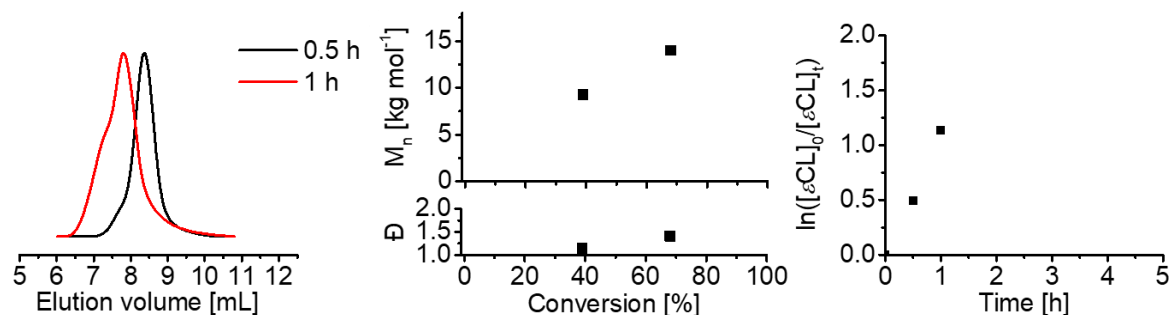


Figure S10: Test reactions of the ROP of ϵCL employing a $[\epsilon\text{CL}]:[\text{BnOH}]:[\text{TBD}]$ of 100:1:2 and $[\epsilon\text{CL}]_0 = 4 \text{ mol L}^{-1}$ in toluene at room temperature (Table S1, entry 17). **Left:** Overlay of SEC elugrams (CHCl_3 , RID). **Center:** Dependence of the molar mass and dispersity on monomer conversion. **Right:** First order kinetic plot.

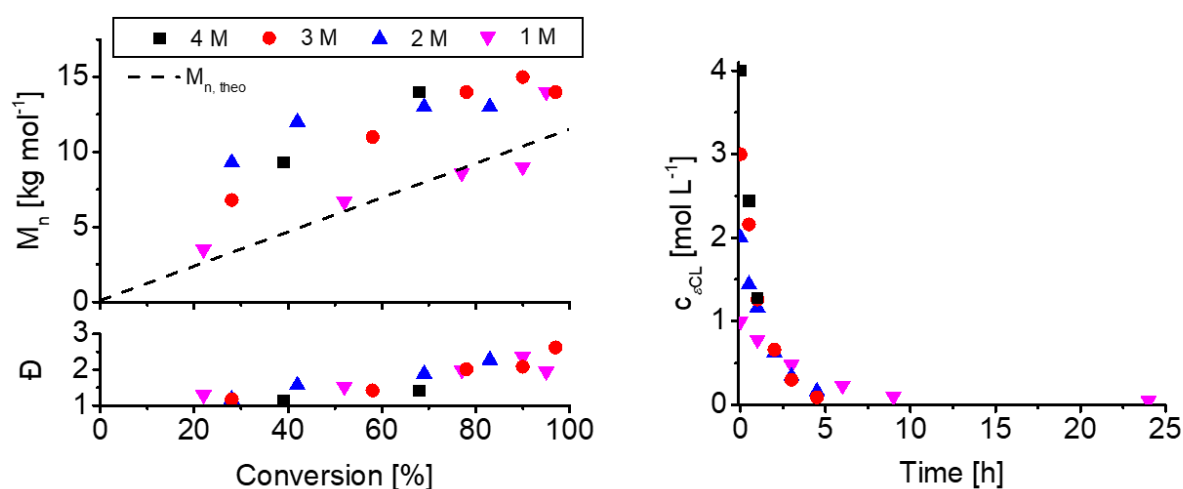


Figure S11: Kinetic plots for the TBD-catalyzed ROP of ϵCL in toluene at room temperature employing an initial $[\epsilon\text{CL}]_0:[\text{BnOH}]_0:[\text{TBD}]_0$ ratio of 100:1:2 at initial monomer concentrations $[\epsilon\text{CL}]_0$ of 4, 3, 2 and 1 mol L⁻¹. **Left:** Dependence of the molar mass $M_{n, \text{SEC}}$ and dispersity \bar{D} on the monomer conversion. The dotted line represents the theoretical molar mass $M_{n, \text{theo}}$ calculated according to $M_{n, \text{theo}} = M_{\epsilon\text{CL}} \times ([\epsilon\text{CL}]_0/[\text{BnOH}]_0) \times \text{conversion} + M_{\text{BnOH}}$. **Right:** Evolution of the residual monomer concentration $[\epsilon\text{CL}]$ over time.

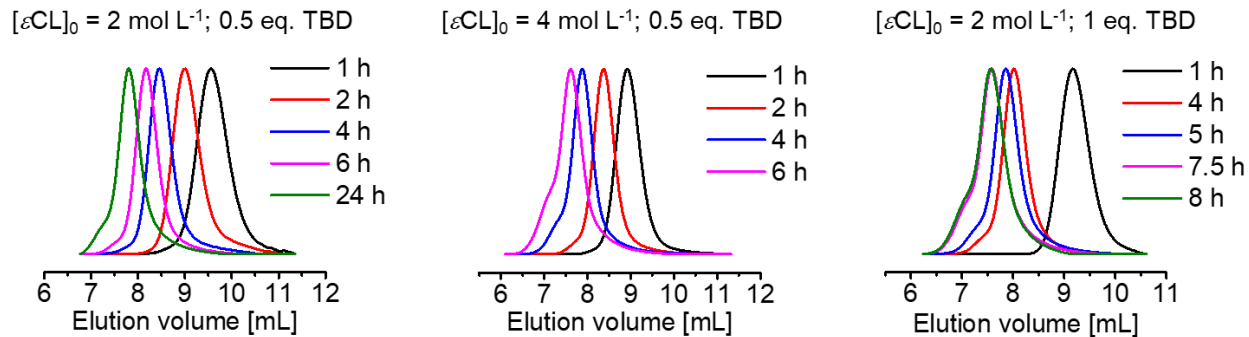


Figure S12: Overlay of SEC elugrams taken during the ϵ CL homopolymerization in toluene at room temperature employing a $[\epsilon\text{CL}]:[\text{BnOH}]$ ratio of 200:1. Initial monomer concentration $[\epsilon\text{CL}]_0$ and catalyst concentration were varied as indicated.

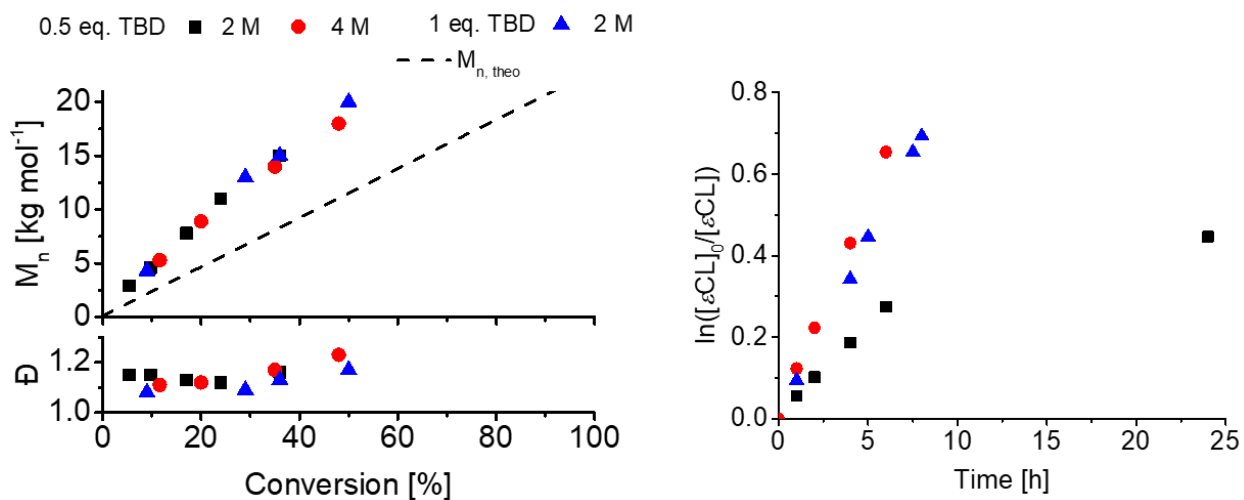


Figure S13: Kinetic plots for the polymerization of ϵ CL in toluene at room temperature employing a $[\epsilon\text{CL}]:[\text{BnOH}]$ of 200:1. Initial monomer concentration $[\epsilon\text{CL}]_0$ and catalyst concentration were varied as indicated in the legend. **Left:** Dependence of the molar mass $M_{n,\text{SEC}}$ and dispersity \bar{D} on the monomer conversion. **Right:** First order kinetic plots.

Additional discussion of the monomer equilibrium concentration

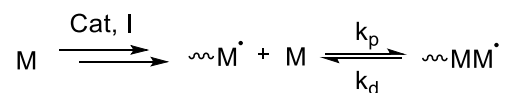
From a thermodynamic perspective, the homopolymerization of ϵ and δ -lactones show negative values for both enthalpy and entropy of polymerization. The latter results in a ceiling temperature for each monomer and a monomer equilibrium concentration ($[M]_{eq}$) that is dependent on the reaction temperature. The $[M]_{eq}$ can be hence calculated according to **equation 1**:

$$[M]_{eq} = \frac{\overline{DP}_n - 1}{\overline{DP}_n} \times e^{\left(\frac{\Delta H_p^0}{RT} - \frac{\Delta S_p^0}{R}\right)} \quad (\text{equation 1})$$

The homopolymerization kinetics of δ CL employing an initial monomer concentration of 1, 2, 3 and 4 mol L⁻¹ show that after an initial monomer conversion, a plateau in the monomer concentration is reached at 0.55 mol L⁻¹. The comparison with the value calculated from literature data show that 0.54 mol L⁻¹ represents the monomer equilibrium concentration for the polymerization of δ CL at 23 °C.³ The latter suggests that the plateau seen during polymerizations is related to equilibrium processes, and therefore the monomer consumption cannot proceed any further. Similarly to δ CL, also the consumption of ϵ CL proceeded with the development of a plateau in the monomer concentration vs. time plots. The low monomer equilibrium concentration of ϵ CL (1.2x10⁻² mol L⁻¹) enabled the high conversions reached during polymerization (**Figure S13**).⁴

Kinetic evaluation for the homopolymerization of δ CL and ϵ CL

Representing a reversible polymerization, the ROP of lactones is defined from a kinetic perspective, by a polymerization rate constant k_p as well as a depolymerization rate constant k_d .



The kinetic equation related to the reversible polymerization can be written as:

$$\frac{d[M]}{dt} = k_p[M][M^*] - k_d[MM^*] \quad (\text{equation 2})$$

where $[M]$, $[M^*]$ and $[MM^*]$ are the concentration of the monomer and the propagating species at time t , respectively. The resolution of **equation 2** leads to **equation 3**:²

$$[M] = [M]_{eq} + ([M]_0 - [M]_{eq}) \times e^{-k_{p,app}[I]_0 t} \quad (\text{equation 3})$$

where $[M]_0$ and $[I]_0$ are the initial concentration of monomer and initiator respectively, while $[M]_{eq}$ is the monomer equilibrium concentration.

However, the ROP of lactones catalyzed by mTBD/thioureas was dependent on the initial concentration of the catalyst. Equation 2 can be therefore rearranged as follows:⁵

$$[M] = [M]_{eq} + ([M]_0 - [M]_{eq}) \times e^{-k_{p,app}[C]_0 t} \quad (\text{equation 4})$$

The latter can be written as:

$$\text{Conversion [\%]} = 100 \times \left(1 - \frac{[M]_{eq}}{[M]_0}\right) \times (1 - e^{-k_{p,app}[C]_0 t}) \quad (\text{equation 5})$$

In principle, fitting of kinetic data to **equation 5** enables the calculation of parameters such as $[M]_{eq}$ and the apparent polymerization rate constant $k_{p,app}$. Aiming to calculate the kinetic constants of homopolymerization for δ CL as well as for ε CL, the conversion vs. time plot were fitted according to equation 4 (**Figure S14, Table S2**).

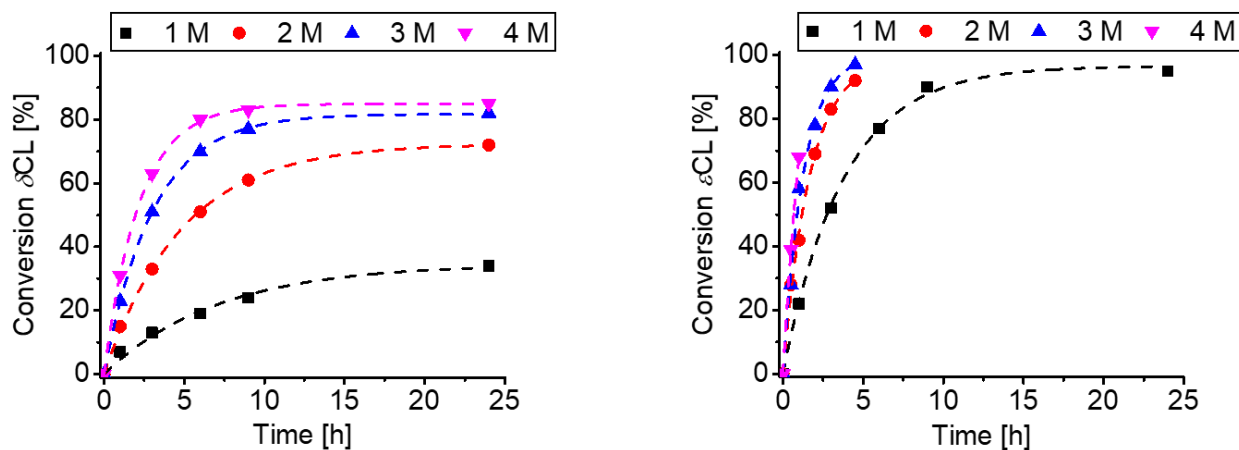


Figure S14: Fitting of kinetic data of the polymerization of δ CL and ε CL in toluene according to **equation 5** (room temperature, $[CL]:[BnOH]:[TBD] = 100:1:2$) (**Table S1**, entries **5 to 8** and **15 to 18**, respectively).

Table S2: Apparent polymerization rate constants and monomer equilibrium concentrations obtained from fitting of the kinetic data of the ROP of δ CL (entry 5 to 8) and ε CL (entry 15 to 17). The corresponding fits are depicted in **Figure S14**.

Entry ^{a)}	R ² ^{b)}	k _{p, app} ^{b)} [L mol ⁻¹ h ⁻¹]	[M] _{eq} ^{b)} [mol L ⁻¹]	[M] _{eq} ^{c)} [mol L ⁻¹]
5	0.985	7.05	0.65	0.54
6	0.999	5.15	0.55	0.54
7	0.999	5.43	0.55	0.54
8	0.999	5.67	0.60	0.54
15	0.998	13.3	0.034	0.015
16	0.997	14.8	0.017	0.015
17	0.994	12.9	0.015	0.015

^{a)} According to **Table S1**.

^{b)} Fitting the conversion over time plots according to **equation 5**.

^{c)} Calculated according to **equation 1** from literature data.

Copolymerization kinetics of ϵ CL and δ CL

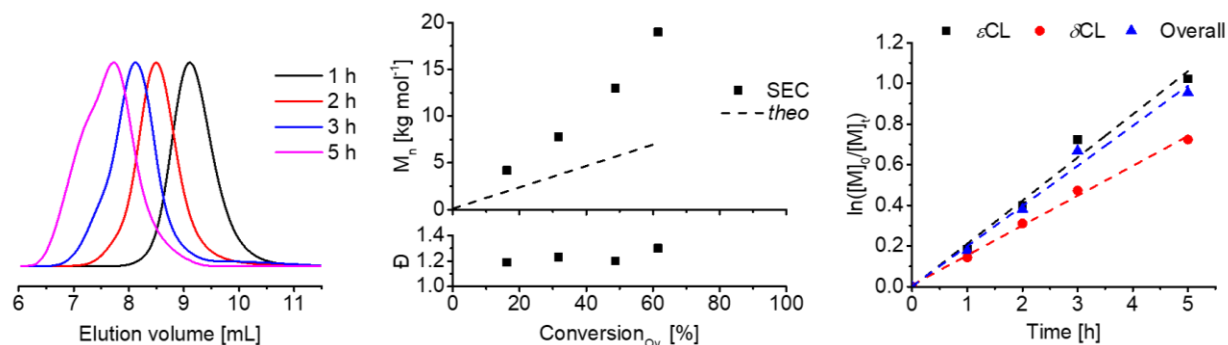


Figure S15: Kinetic studies of the copolymerization of ϵ CL and δ CL employing a $[\epsilon$ CL]: $[\delta$ CL]: $[\text{BnOH}]$: $[\text{TBD}]$ of 80:20:1:2 ($[\text{CL}]_0 = 4 \text{ mol L}^{-1}$ in toluene at room temperature). **Left:** Overlay of SEC elugrams (CHCl_3 , RID). **Center:** Dependence of the molar mass $M_{n,\text{SEC}}$ and dispersity \mathcal{D} on the overall monomer conversion. **Right:** First order kinetic plot and linear extrapolation of experimental data (dotted lines).

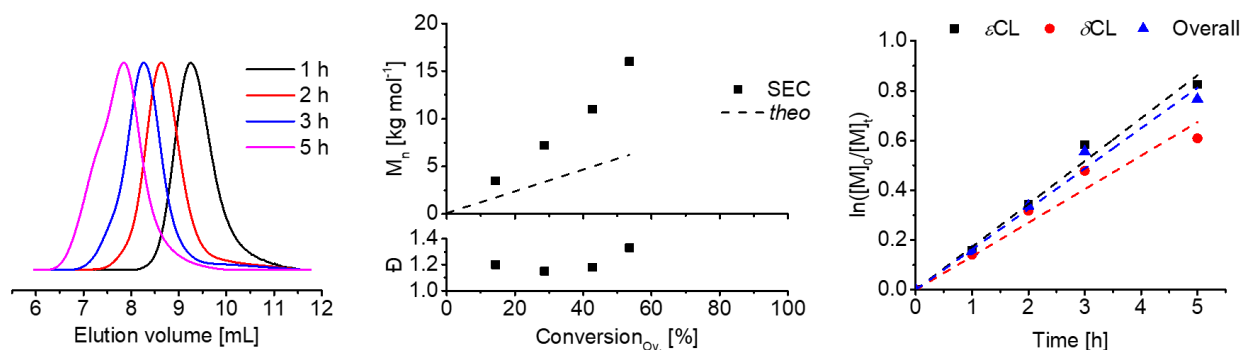


Figure S16: Kinetic studies of the copolymerization of ϵ CL and δ CL employing a $[\epsilon$ CL]: $[\delta$ CL]: $[\text{BnOH}]$: $[\text{TBD}]$ of 75:25:1:2 ($[\text{CL}]_0 = 4 \text{ mol L}^{-1}$ in toluene at room temperature) **Left:** Overlay of SEC elugrams (CHCl_3 , RID). **Center:** Dependence of the molar mass $M_{n,\text{SEC}}$ and dispersity \mathcal{D} on the overall monomer conversion **Right:** First order kinetic plot and linear extrapolation of experimental data (dotted lines).

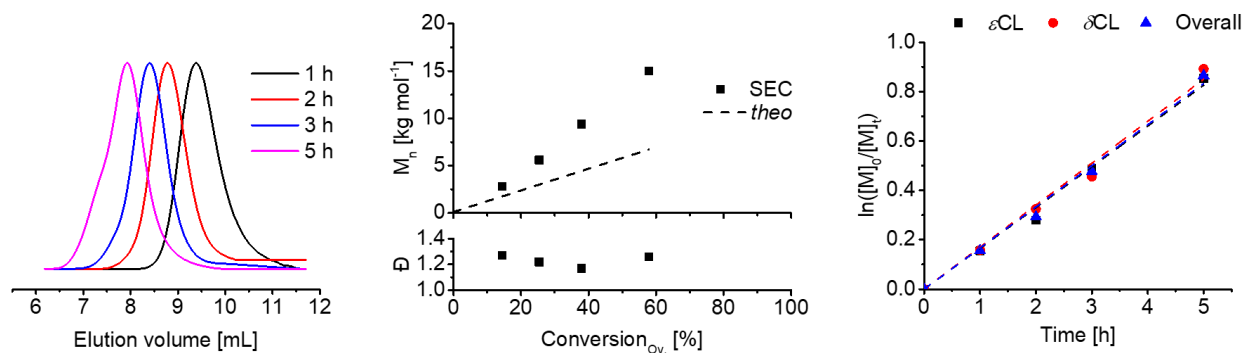


Figure S17: Kinetic studies of the copolymerization of ϵ CL and δ CL employing a $[\epsilon\text{CL}]:[\delta\text{CL}]:[\text{BnOH}]:[\text{TBD}]$ of 70:30:1:2 ($[\text{CL}]_0 = 4 \text{ mol L}^{-1}$ in toluene at room temperature). **Left:** Overlay of SEC elugrams (CHCl_3 , RID). **Center:** Dependence of the molar mass $M_{n,\text{SEC}}$ and dispersity \bar{D} on the overall monomer conversion **Right** First order kinetic plot and linear extrapolation of experimental data (dotted lines).

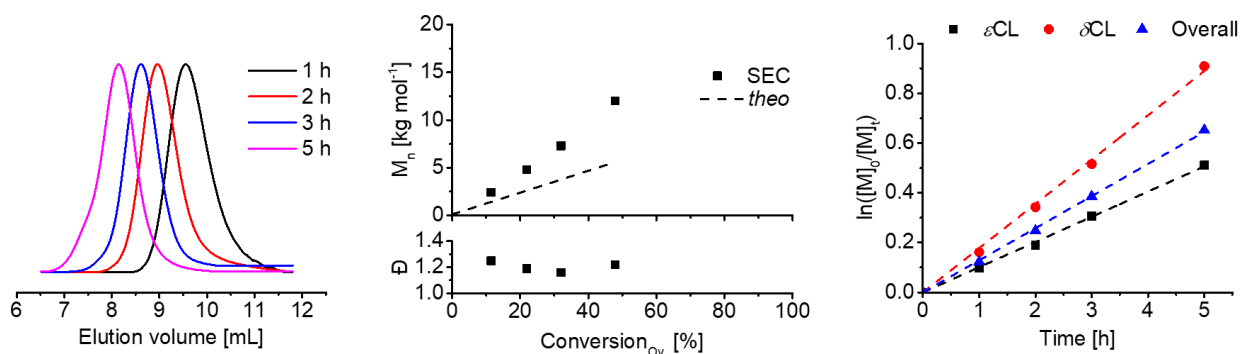


Figure S18: Kinetic studies of the copolymerization of ϵ CL and δ CL employing a $[\epsilon\text{CL}]:[\delta\text{CL}]:[\text{BnOH}]:[\text{TBD}]$ of 60:40:1:2 ($[\text{CL}]_0 = 4 \text{ mol L}^{-1}$ in toluene at room temperature). **Left:** Overlay of SEC elugrams (CHCl_3 , RID). **Center:** Dependence of the molar mass $M_{n,\text{SEC}}$ and dispersity \bar{D} on the overall monomer conversion **Right:** First order kinetic plot for the single and the overall monomer conversion and linear fitting (dotted lines).

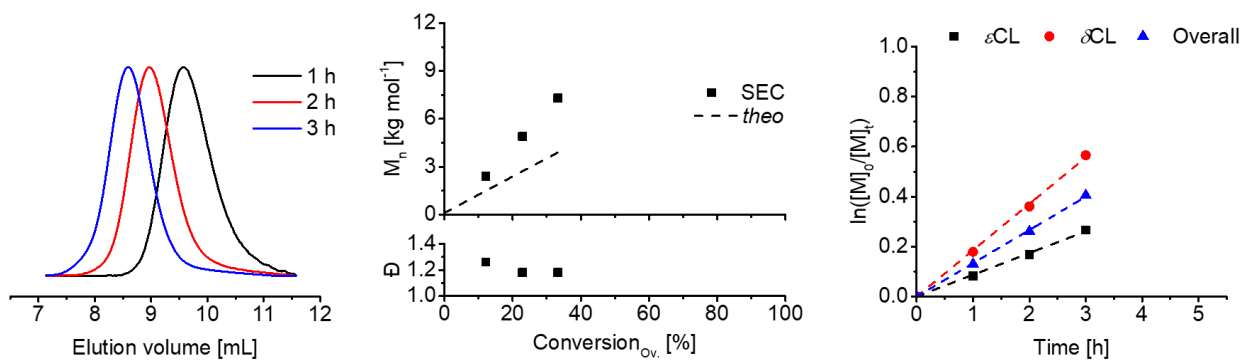


Figure S19: Kinetic studies of the copolymerization of ϵ CL and δ CL employing a $[\epsilon\text{CL}]:[\delta\text{CL}]:[\text{BnOH}]:[\text{TBD}]$ of 50:50:1:2 ($[\text{CL}]_0 = 4 \text{ mol L}^{-1}$ in toluene at room temperature). **Left:** Overlay of SEC elugrams (CHCl_3 , RID). **Center:** Dependence of the molar mass $M_{n,\text{SEC}}$ and dispersity \bar{D} on the overall monomer conversion **Right:** First order kinetic plot and linear extrapolation of experimental data (dotted lines).

Table S3: Calculations of the apparent polymerization rate ($k_{p, \text{app}}$) for the copolymerization studies (**Figure S15 to S19**) according to linear fitting of the semilogarithmic plot.

$[\epsilon\text{CL}]:[\delta\text{CL}]$	$k_{p, \text{app}, \epsilon\text{CL}} [\text{L mol}^{-1} \text{h}^{-1}]$	$k_{p, \text{app}, \delta\text{CL}} [\text{L mol}^{-1} \text{h}^{-1}]$	$k_{p, \text{app}, \text{ov.}} [\text{L mol}^{-1} \text{h}^{-1}]$
80:20	10.60	7.35	9.85
75:25	8.60	6.75	8.10
70:30	8.25	8.50	8.30
60:40	5.10	8.85	6.45
50:50	4.35	9.25	6.65

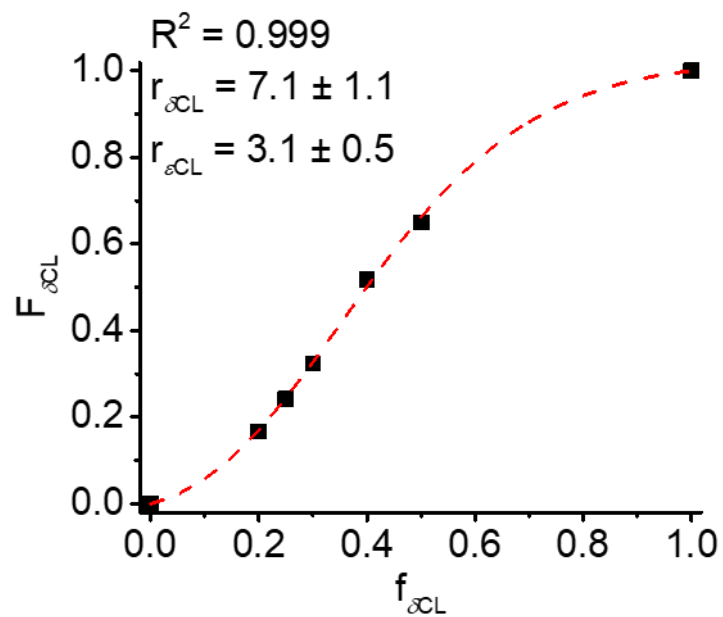


Figure S20: Dependence of the molar fraction of δCL in the copolymers ($F_{\delta\text{CL}}$) on the molar fraction of δCL in the feed ($f_{\delta\text{CL}}$) at an overall conversion of 18% and fitting according to Mayo-Lewis equation.

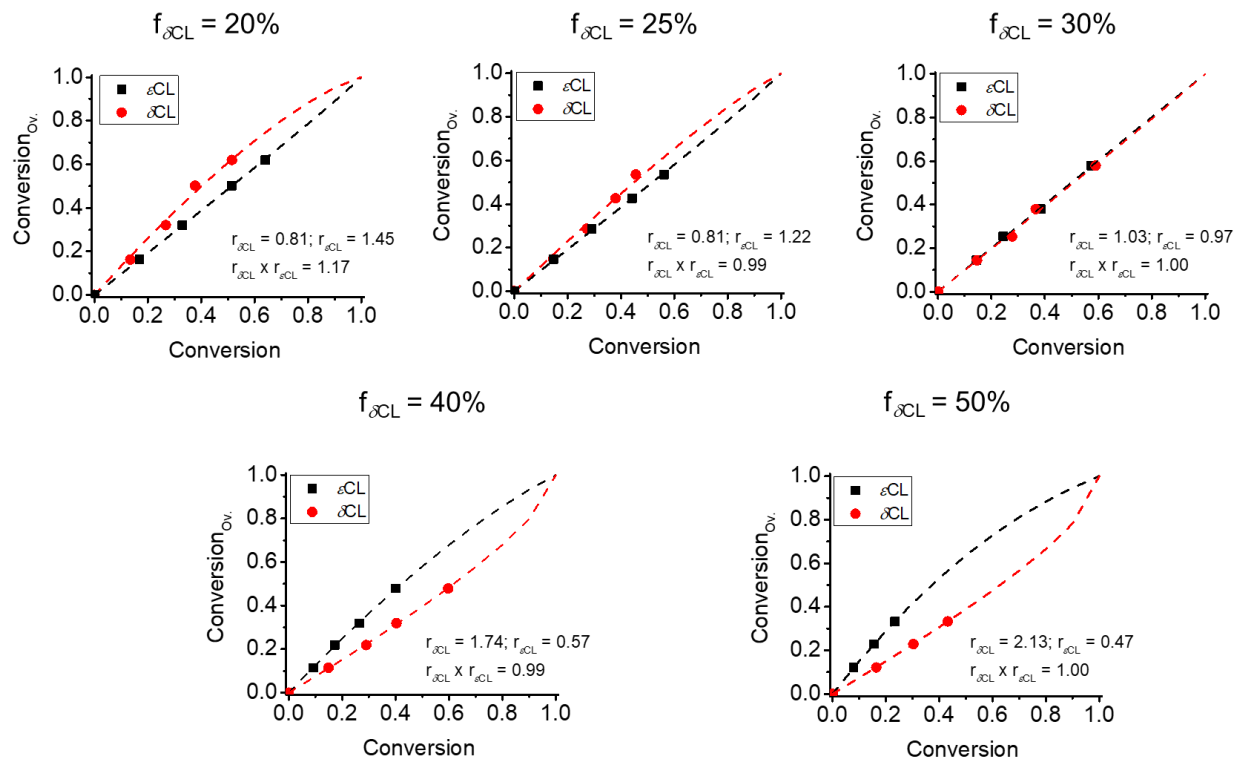


Figure S21: Evolution of the overall conversion over single monomer conversion for the copolymerization studies, fitting according to the Beckingham model, reactivity ratios obtained for each monomer feed investigated and estimation of the ideality of the copolymerization.

Characterization of PCL materials

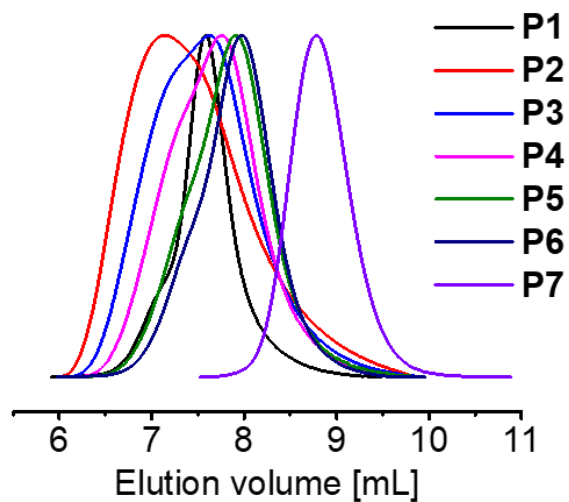


Figure S22: SEC elugrams of the purified homo and copolyesters **P1** to **P7** (CHCl_3 , RI detection).

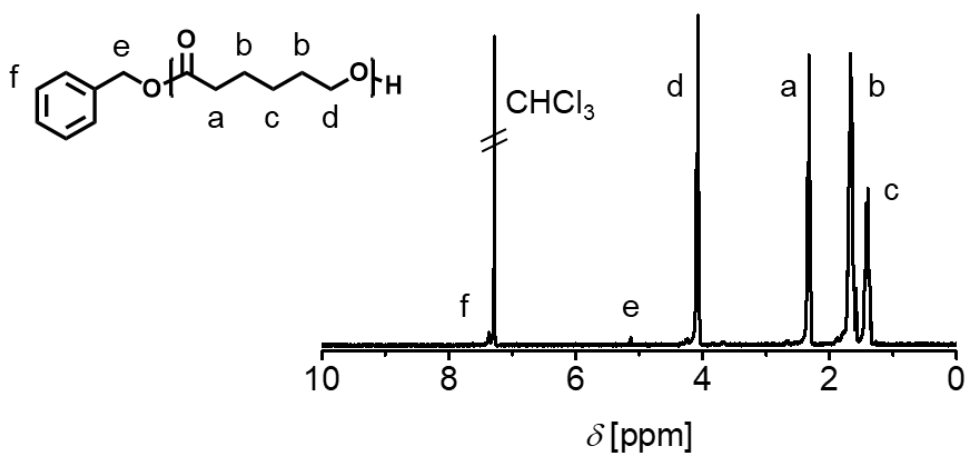


Figure S23: ^1H NMR spectrum (CDCl_3 , 300 MHz) of the purified $\text{P}\epsilon\text{CL}$ **P1** and assignment of the signals to the schematic representation of the structure.

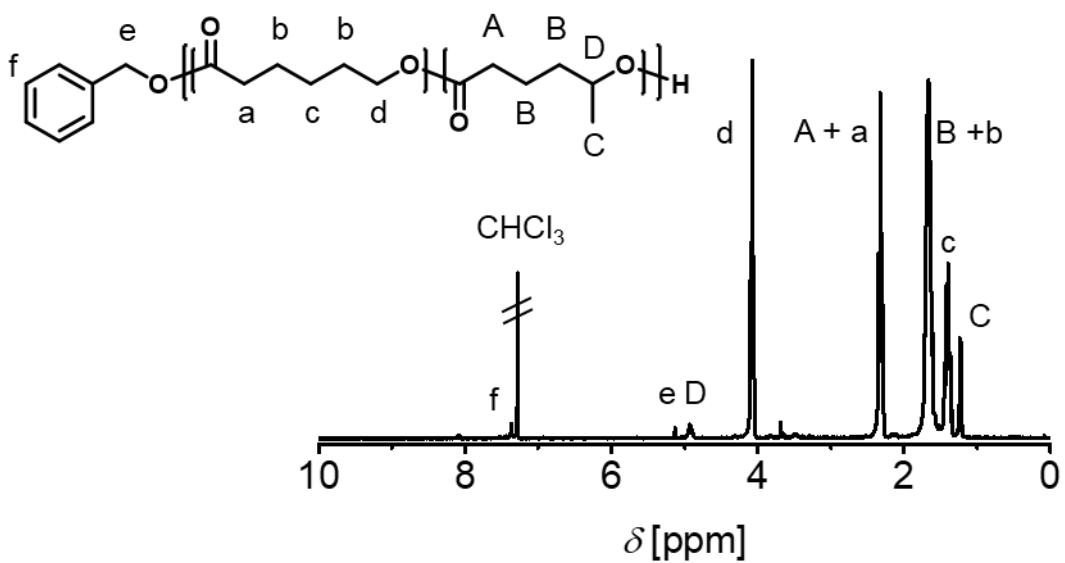


Figure S24: ¹H NMR spectrum (CDCl₃, 300 MHz) of the purified P(εCL-ran-δCL) **P2** and assignment of the signals to the schematic representation of the structure.

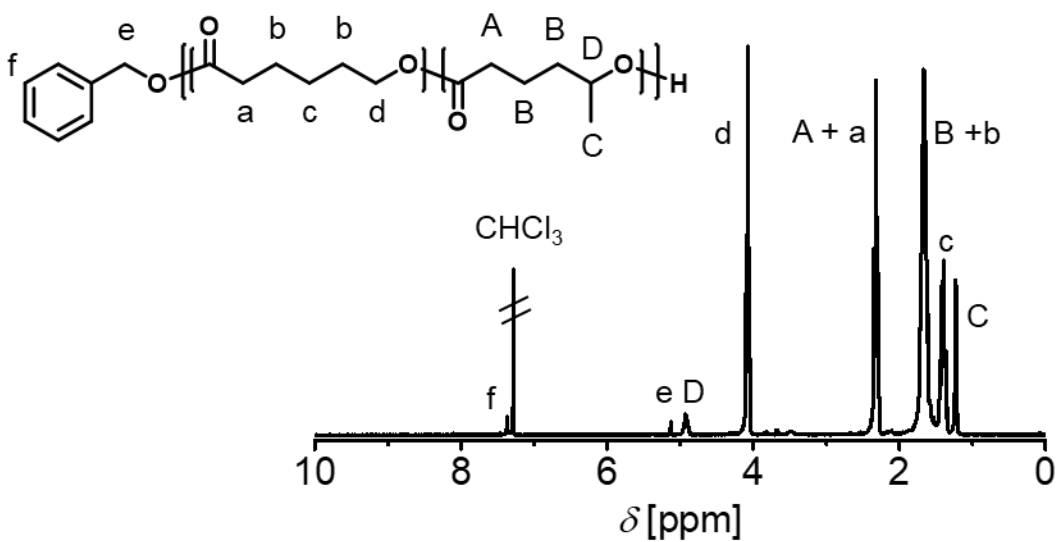


Figure S25: ¹H NMR spectrum (CDCl₃, 300 MHz) of the purified P(εCL-ran-δCL) **P3** and assignment of the signals to the schematic representation of the structure.

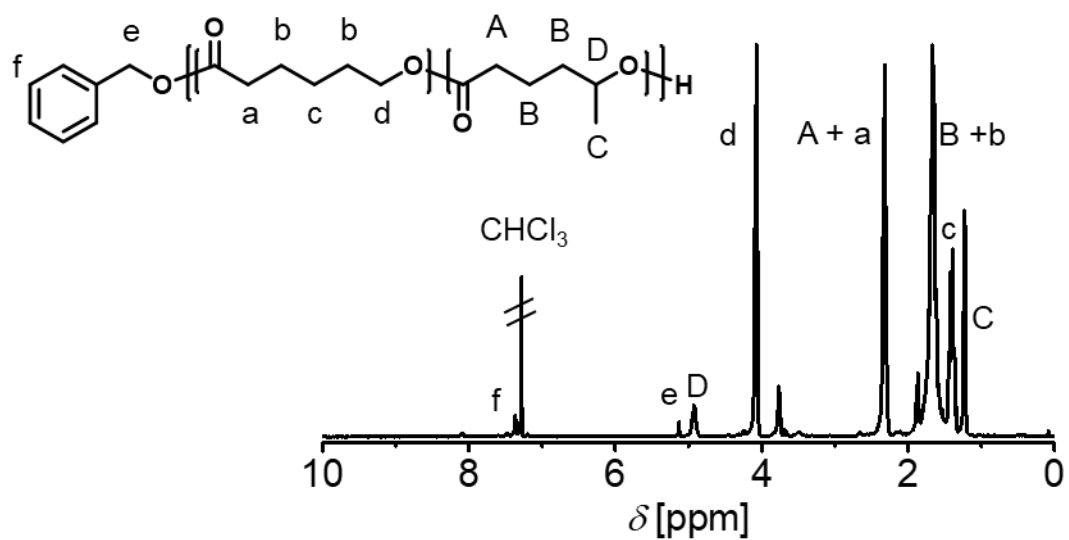


Figure S26: ^1H NMR spectrum (CDCl_3 , 300 MHz) of the purified $\text{P}(\epsilon\text{CL-}i\text{ran-}\delta\text{CL})$ **P4** and assignment of the signals to the schematic representation of the structure.

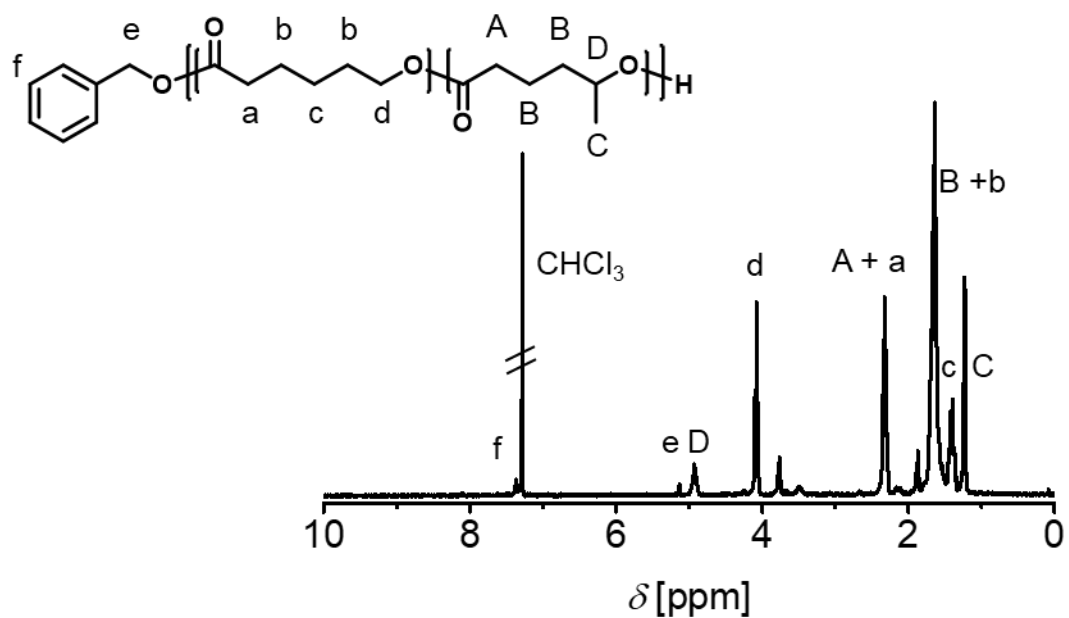


Figure S27: ^1H NMR spectrum (CDCl_3 , 300 MHz) of the purified $\text{P}(\epsilon\text{CL-}i\text{ran-}\delta\text{CL})$ **P5** and assignment of the signals to the schematic representation of the structure.

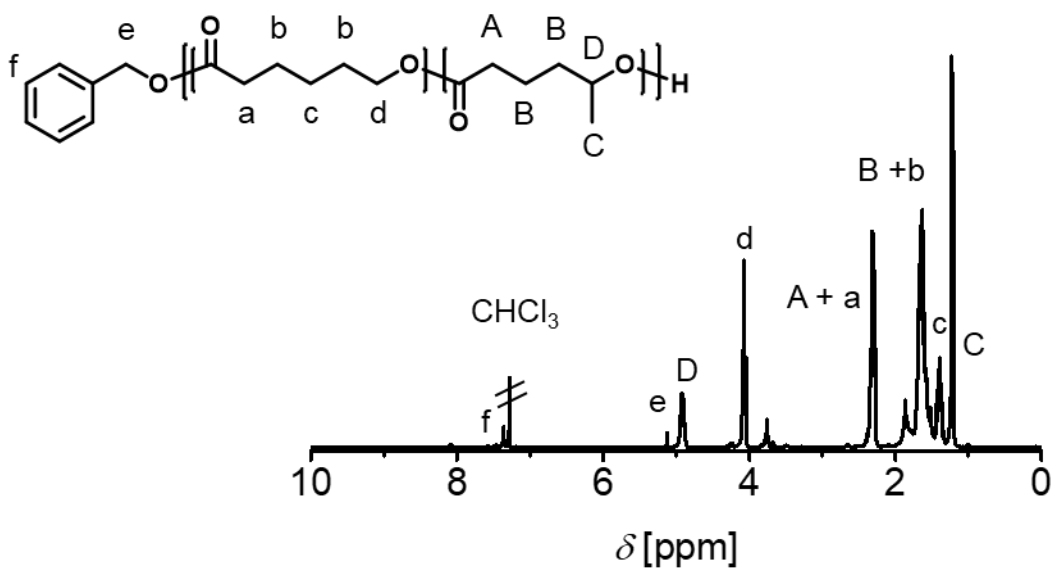


Figure S28: ^1H NMR spectrum (CDCl_3 , 300 MHz) of the purified $\text{P}(\epsilon\text{CL-ran-}\delta\text{CL})$ **P6** and assignment of the signals to the schematic representation of the structure.

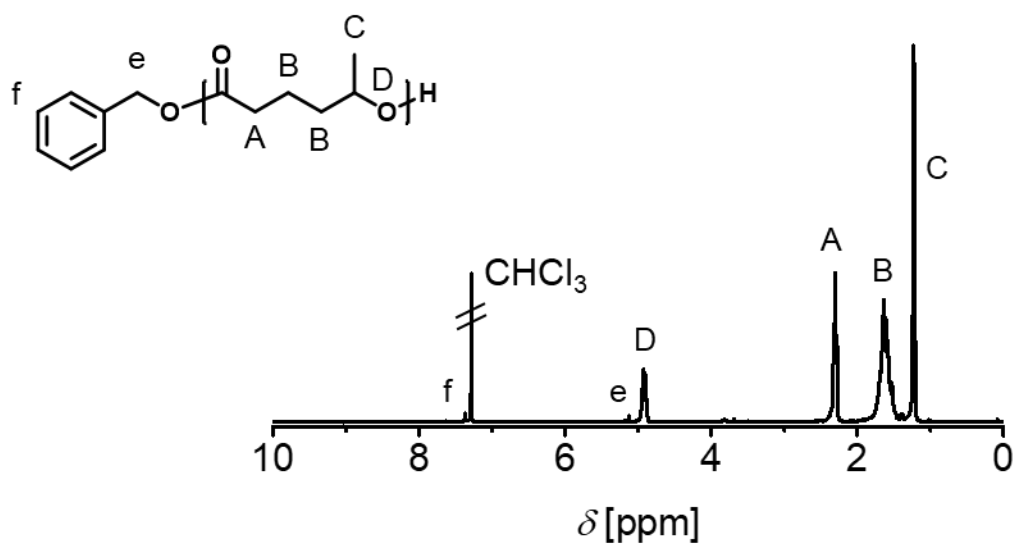


Figure S29: ^1H NMR spectrum (CDCl_3 , 300 MHz) of the purified $\text{P}\delta\text{CL}$ **P7** and assignment of the signals to the schematic representation of the structure.

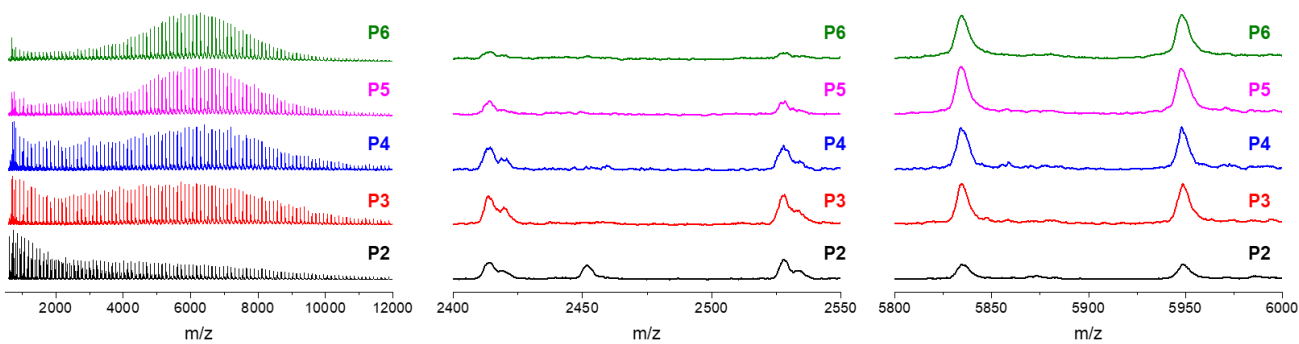


Figure S30: MALDI TOF mass spectra of P(ϵ CL-*ran*- δ CL) (DCTB, NaI, positive linear mode). Left: Full mass spectra. Center: Zoom into the region around $m/z = 2,500$. The zoomed region corresponds to one repeating unit. Peak assignments for **P2** revealing the most prominent side product signals are depicted below. Right: Zoom into the region around $m/z = 5,900$. The zoomed region corresponds to one repeating unit.

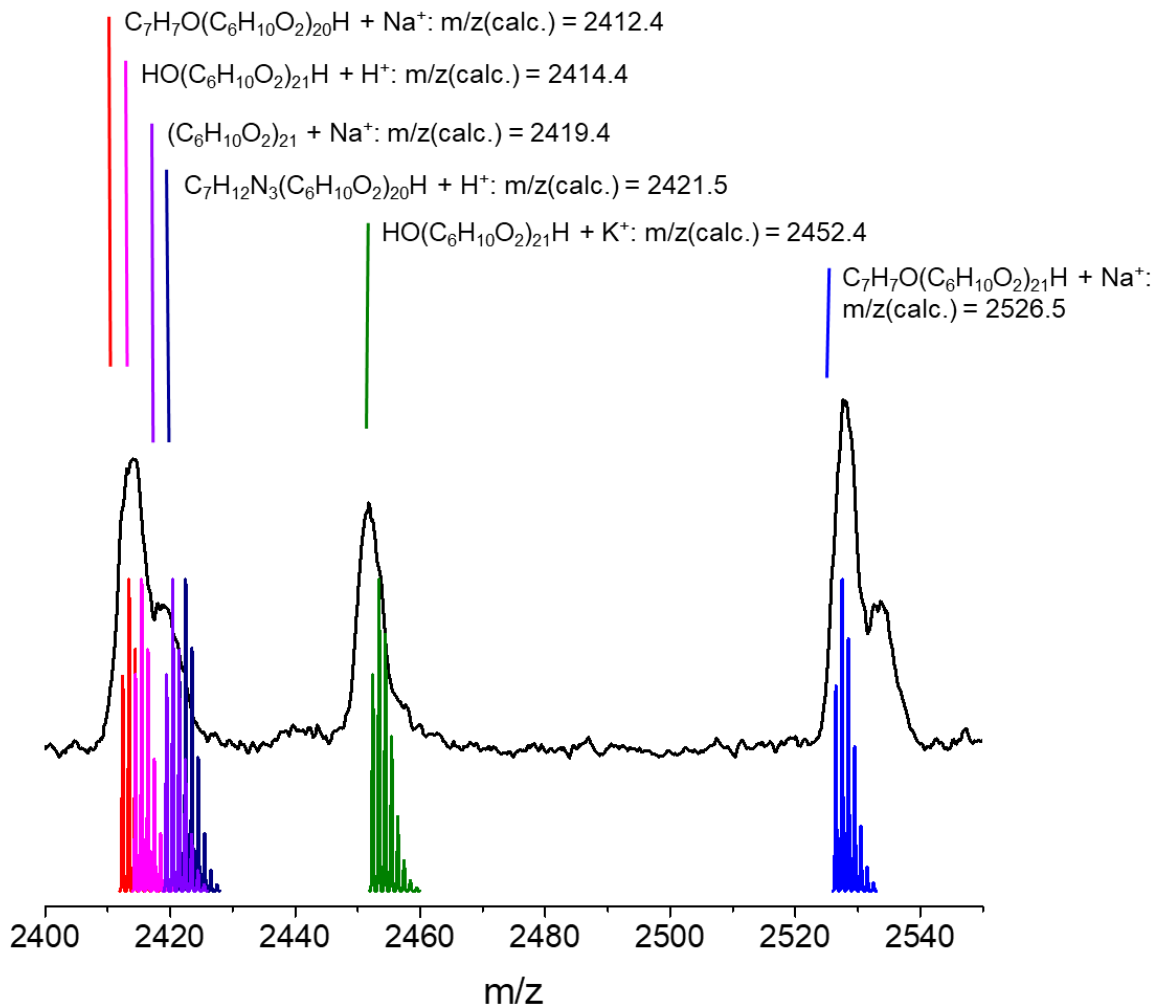


Figure S31: Zoom into the lower m/z region of the MALDI TOF mass spectrum of P(ϵ CL-*ran*- δ CL) **P2** (DCTB, NaI, positive linear mode) and assignment of the detected species *via* the corresponding calculated isotopic patterns. The m/z region corresponds to one repeating unit. The main series was assigned to sodiated PCL initiated by BnOH (red and blue, respectively) and overlaps with potentially present water initiated proton adducts (pink). The assignment of water initiated PCL as potassium adducts (green) confirmed their presence for **P2**, whereas the corresponding m/z signals were absent in the mass spectra of **P3-P6**. Sodiated cyclic PCL (purple) was assigned for all P(ϵ CL-*ran*- δ CL). It remained unclear if proton adducts of additional TBD initiated macromolecules (dark blue) are overlapping due to the resolution as the measurement conditions were optimized for the detection of higher molar mass species in the linear mode.

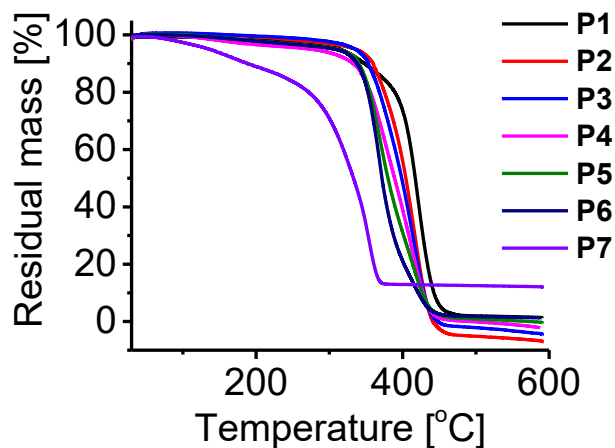


Figure S32: TGA thermograms of the polyester library **P1** to **P7** (N₂, 30 to 590 °C, heating rate 20 °C min⁻¹).

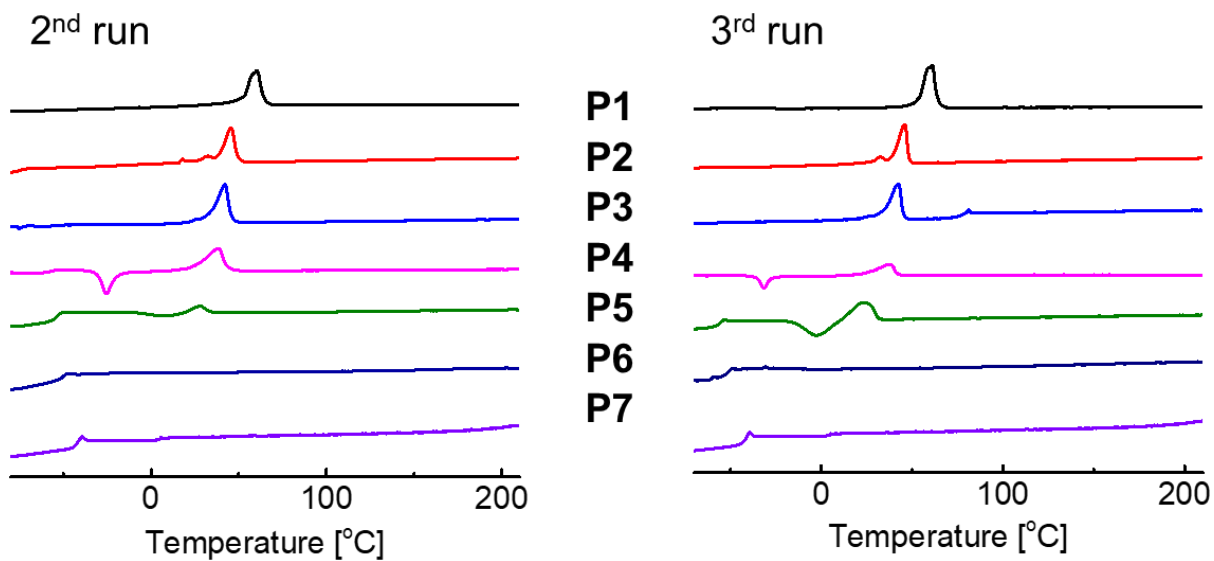


Figure S33: Additional DSC thermograms of the polyester library **P1** to **P7** (-100 to 210 °C). **Left:** Second heating run (heating rate of 20 °C min⁻¹). **Right:** Third heating run (heating rate of 10 °C min⁻¹).

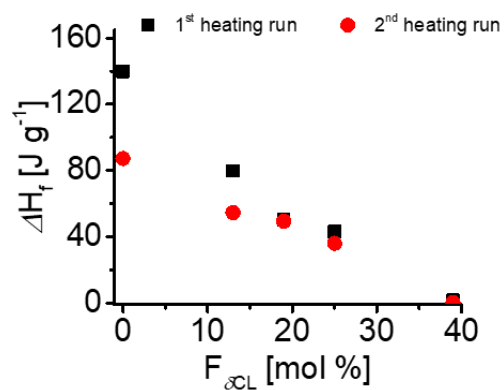


Figure S34: Dependence of the enthalpy of melting on the fraction of δ CL in the copolymer ($F_{\delta\text{CL}}$) during the first and the second heating runs (-100 to 210 °C; heating rate of 20 °C min⁻¹).

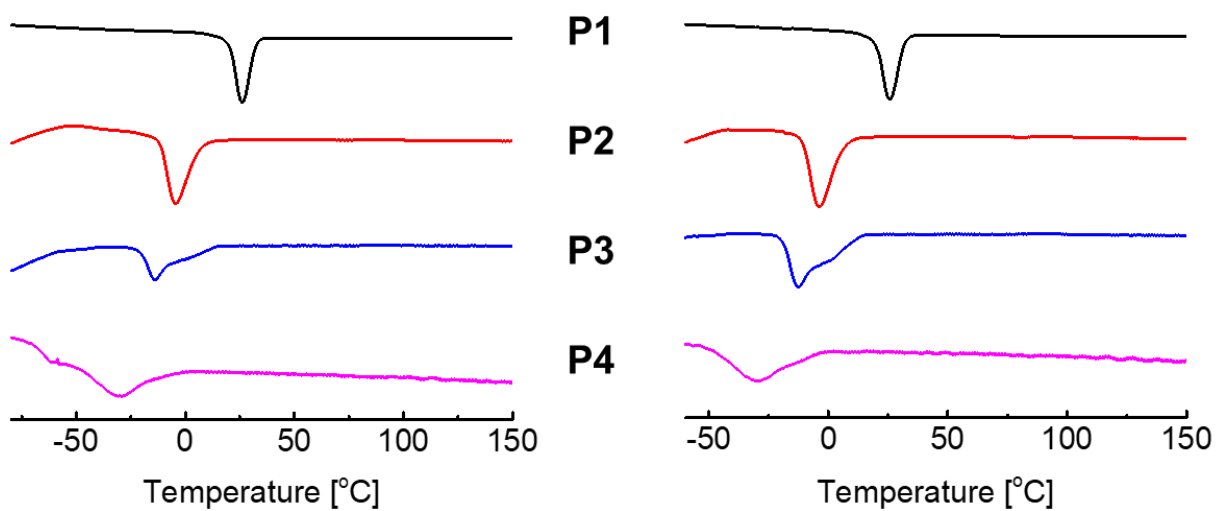


Figure S35: Additional DSC thermograms of the polyesters **P1** to **P4** (210 °C to -100 °C; cooling rate 20 °C min⁻¹). **Left:** First cooling run. **Right:** Second cooling run.

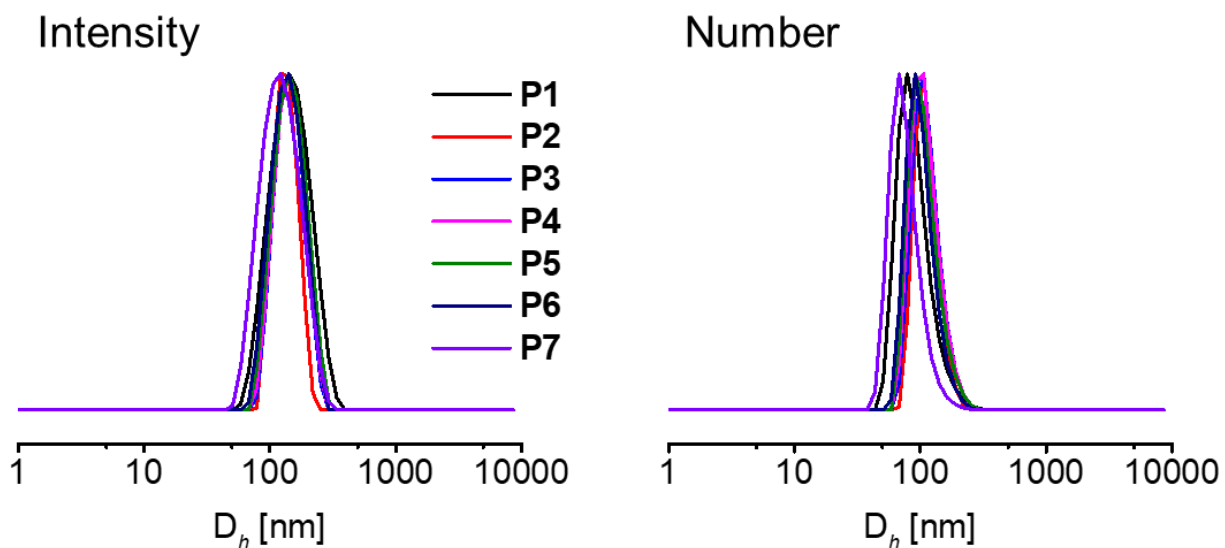


Figure S36: Size distributions of the nanoparticle dispersions of **P1** to **P7** obtained by DLS analysis ($c(\text{polymer}) = 0.1 \text{ mg mL}^{-1}$). **Left:** Intensity-weighted distributions. **Right:** Number-weighted distributions.

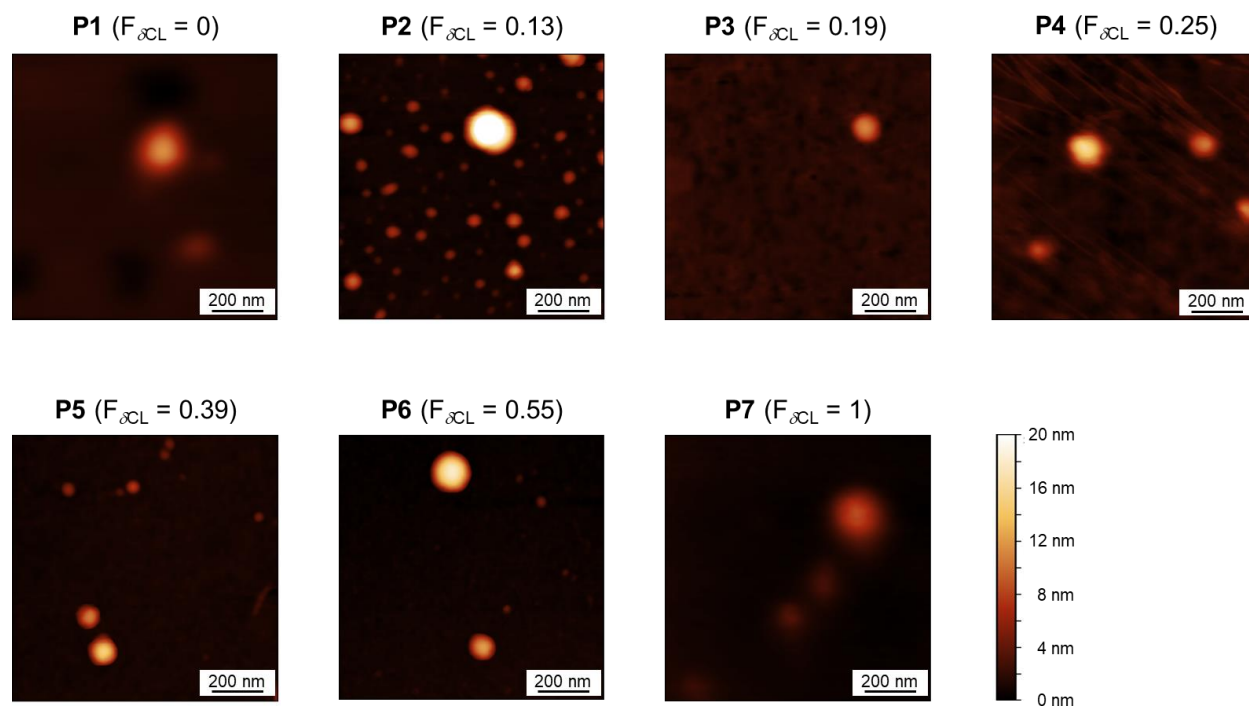


Figure S37: AFM height images of the nanoparticles obtained from **P1** to **P7**.

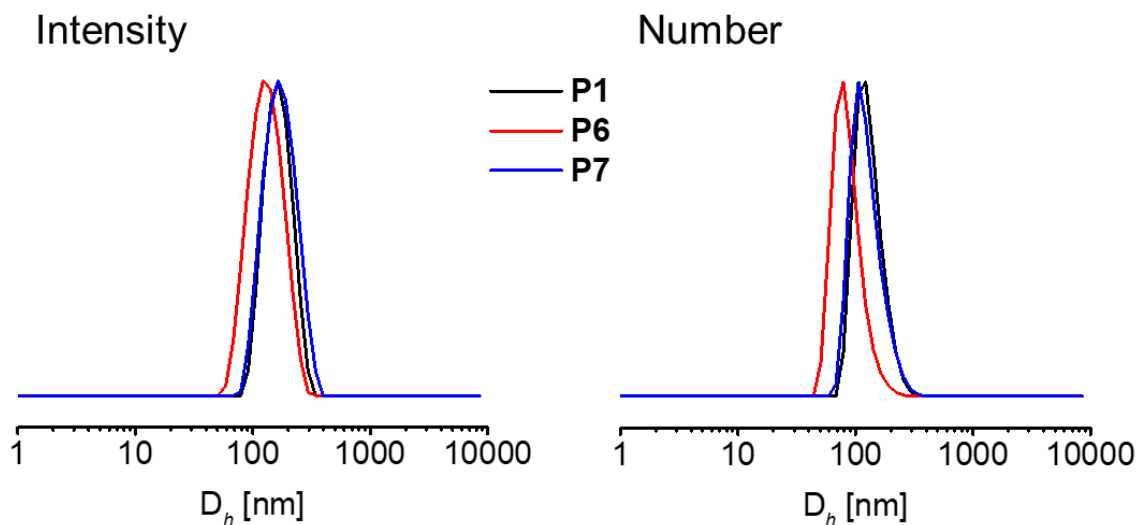


Figure S38: Size distributions of the pyrene encapsulated nanoparticle suspensions of **P1**, **P6** and **P7** obtained by DLS analysis ($c(\text{polymer}) = 0.1 \text{ mg mL}^{-1}$, $c(\text{pyrene}) = 1 \text{ } \mu\text{g mL}^{-1}$). **Left:** Intensity-weighted distributions. **Right:** Number-weighted distributions.

Table S4: DLS data of the pyrene loaded nanoparticles.

Sample	P1	P6	P7
$F_{\&L}$ [mol%]	0	55	100
D_h [nm]	158	120	160
PDI	0.097	0.103	0.103

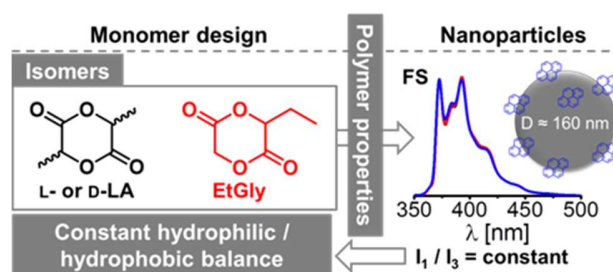
References

- [1] Schneiderman, D. K.; Hillmyer, M. A., Aliphatic polyester block polymer design. *Macromolecules* **2016**, *49*, 2419-2428.
- [2] Yin, M.; Baker, G. L., Preparation and characterization of substituted polylactides. *Macromolecules* **1999**, *32*, 7711-7718.
- [3] Hillmyer, M. A.; Tolman, W. B., Aliphatic polyester block polymers: Renewable, degradable, and sustainable. *Acc. Chem. Res.* **2014**, *47*, 2390-2396.
- [4] Dubois, P.; Coulembier, O.; Raquez, J.-M. in *Handbook of ring-opening polymerization*. John Wiley & Sons: 2009.
- [5] Lohmeijer, B. G. G.; Pratt, R. C.; Leibfarth, F.; Logan, J. W.; Long, D. A.; Dove, A. P.; Nederberg, F.; Choi, J.; Wade, C.; Waymouth, R. M.; Hedrick, J. L., Guanidine and amidine organocatalysts for ring-opening polymerization of cyclic esters. *Macromolecules* **2006**, *39*, 8574-8583.

Publication P5

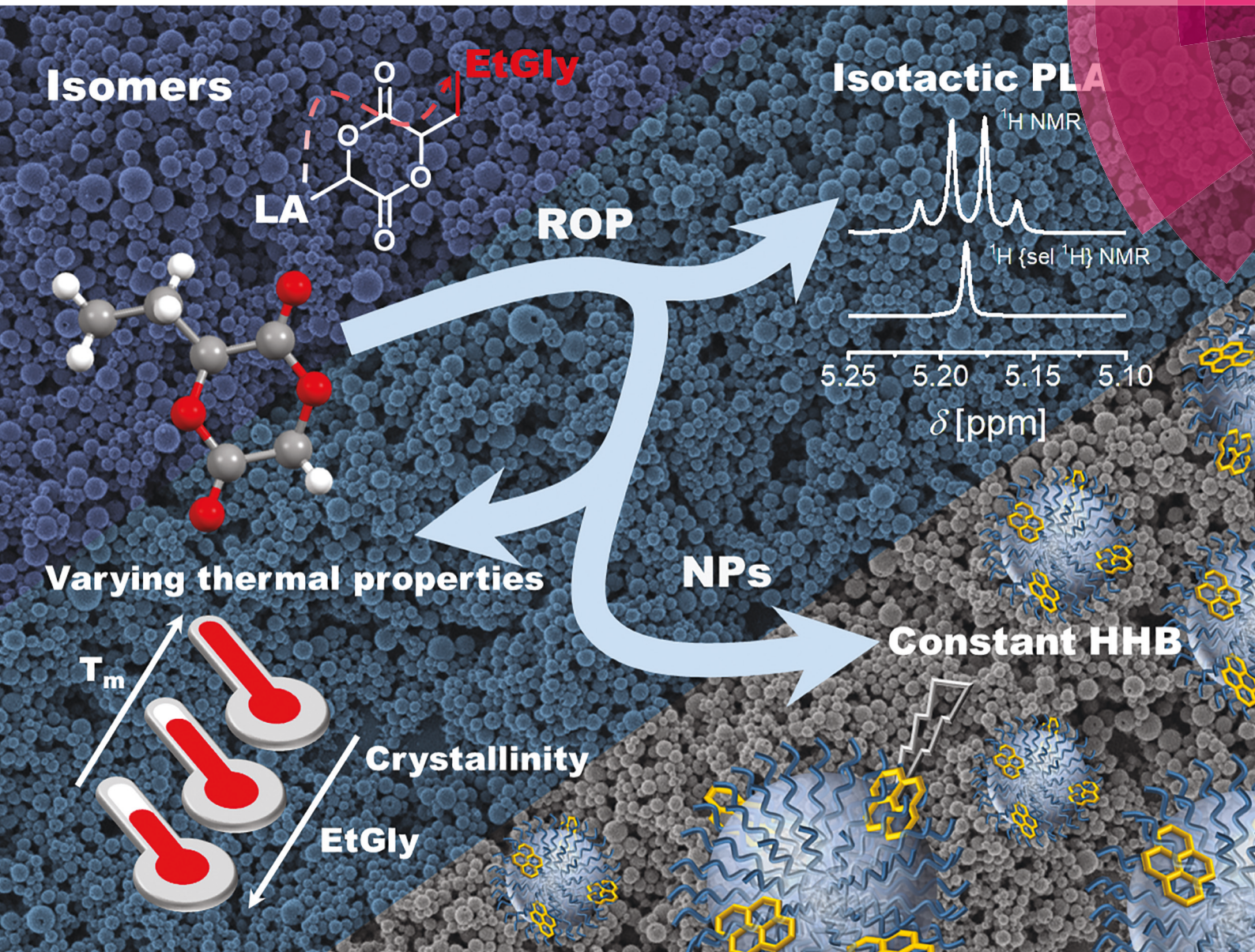
Poly(3-ethylglycolide): A well-defined polyester matching the hydrophilic hydrophobic balance of PLA

D. Bandelli, J. Alex, C. Helbing, N. Ueberschaar, H. Görls, P. Bellstedt, C. Weber, K. D. Jandt and U. S. Schubert, *Polym. Chem.* **2019**, *10*, 5440–5451.



Polymer Chemistry

rsc.li/polymers



ISSN 1759-9962



ROYAL SOCIETY OF CHEMISTRY

Celebrating IYPT 2019

PAPER

Klaus D. Jandt, Ulrich S. Schubert *et al.*

Poly(3-ethylglycidol): a well-defined polyester matching the hydrophilic hydrophobic balance of PLA



Cite this: *Polym. Chem.*, 2019, **10**, 5440

Poly(3-ethylglycolide): a well-defined polyester matching the hydrophilic hydrophobic balance of PLA†

Damiano Bandelli,^{‡a,b} Julien Alex,^{‡a,b} Christian Helbing,^c Nico Ueberschaar,^d Helmar Görls,^e Peter Bellstedt,^a Christine Weber,^{a,b} Klaus D. Jandt,^{*c} and Ulrich S. Schubert^{‡a,b}

The ring opening (co)polymerization of 3-ethyl-1,4-dioxane-2,5-dione (3-ethylglycolide, EtGly) and enantiopure lactide using benzyl alcohol as initiator and the organobase 7-methyl-1,5,7-triazabicyclo[4.4.0]dec-5-ene as catalyst yielded polyesters with predictable lactide and EtGly content between 5 and 20 mol%, molar masses around 11 000 g mol⁻¹ and dispersities below 1.3. Due to the amorphous nature of the atactic poly(3-ethylglycolide) (PEtGly), dynamic scanning calorimetry revealed increasing glass transition and melting temperatures with an increasing lactide content of the statistical copolymers. Nanoparticles with a diameter of 160 nm and spherical shape were obtained from each polyester by applying the nanoprecipitation method, as confirmed by dynamic light scattering and scanning electron microscopy investigation. The constant hydrophilic to hydrophobic balance (HHB) of PLA and PEtGly was confirmed by fluorescence spectroscopy using pyrene loaded nanoparticles, confirming that a set of materials was obtained suitable to enlighten the effect of crystallinity on nanoparticle degradation.

Received 15th June 2019,
Accepted 5th September 2019

DOI: 10.1039/c9py00875f

rsc.li/polymers

Introduction

Nanoparticulate drug carriers for delivering therapeutic compounds to target organs in the human body have been the subject of research for several decades.¹ In particular, aliphatic polyesters such as polylactide (PLA), poly(lactide-co-glycolide)

(PLGA) and polycaprolactone (PCL) are of interest for the encapsulation of hydrophobic drugs due to their biodegradability and high tissue compatibility.^{2,3} The encapsulation and the release behavior of drugs from polymeric nanoparticles is influenced by a large number of parameters such as temperature,⁴ molar mass of the polymers,⁵ additives⁶ and the shape of the nanomaterials.⁷ Moreover the particle size as well as the interaction of the encapsulated drug with the nanomaterial matrix, play a crucial role.^{5,8–13}

Since drug release depends on erosion of the particle surface, the diffusion of the drug out of the nanomaterial matrix as well as on the degradation of the nanomaterial,¹¹ it is expected that physico-chemical properties of nanocarrier materials affect the release behavior of drugs.^{14–17} In combination, these examples show that a multitude of factors contribute to the release kinetics. However, to elucidate the contributions of the individual properties to the performance of the system, systematic studies are required, keeping as many parameters constant as possible. To understand the influence of the thermal properties of the nanoparticle matrix material, other factors such as molar mass, shape, size and the hydrophilic to hydrophobic balance (HHB) should be kept constant. It is, however, not straightforward to decouple particularly the HHB from the thermal properties and the crystallinity for standard polyester materials because an alteration of the latter is frequently accompanied by a change of the former.^{15,18}

^aLaboratory of Organic and Macromolecular Chemistry (IOMC), Friedrich Schiller University Jena, Humboldtstr. 10, 07743 Jena, Germany.

E-mail: ulrich.schubert@uni-jena.de

^bJena Center for Soft Matter (JCSM), Friedrich Schiller University Jena, Philosophenweg 7, 07743 Jena, Germany

^cChair of Materials Science (CMS), Department of Materials Science and Technology, Otto Schott Institute of Materials Research, Faculty of Physics and Astronomy, Friedrich Schiller University Jena, Löbdergraben 32, 07743 Jena, Germany.

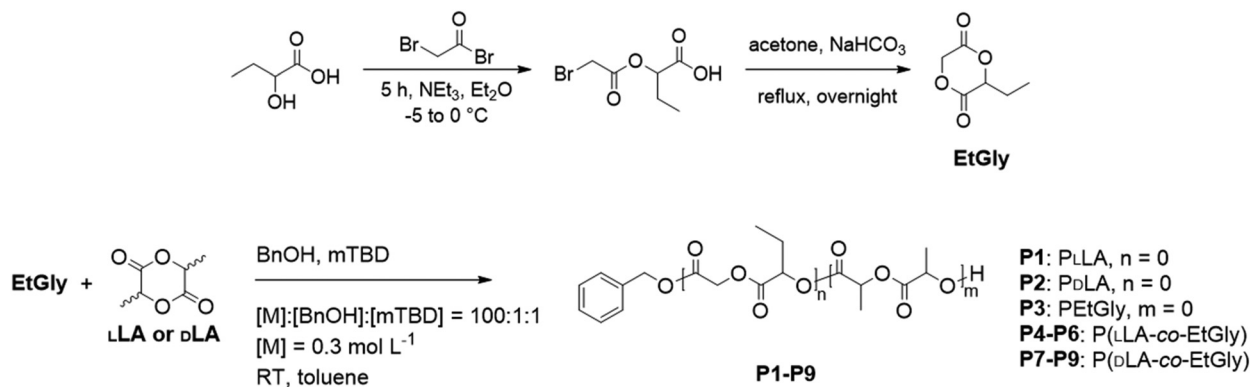
E-mail: k.jandt@uni-jena.de

^dMass Spectrometry Platform, Friedrich Schiller University Jena, Humboldtstr. 8, 07743 Jena, Germany

^eInstitute of Inorganic and Analytical Chemistry (IAAC), Friedrich Schiller University Jena, Humboldtstr. 8, 07743 Jena, Germany

† Electronic supplementary information (ESI) available: ¹H and ¹³C NMR spectra, FT-ATR-IR transmittance spectrum, GC chromatogram and CI mass spectrum of EtGly; SEC traces of reaction mixture and purified polymers **P1** to **P9**; detailed experimental descriptions, ¹H NMR spectroscopy and SEC of **P1** to **P9**; additional TGA and DSC thermograms, DLS size distributions and SEM micrographs of the nanoparticles and detailed summary of the nanoparticle characterization. See DOI: 10.1039/c9py00875f

‡ Both authors contributed equally.



Scheme 1 Schematic representation of the synthetic pathway yielding polyesters with the same hydrophilicity as PLA.

The two most common polyesters PLA and PLGA perfectly demonstrate the challenge: Encapsulated guests are released faster from an amorphous PLGA matrix than from a semicrystalline PLA matrix because PLGA is more prone to hydrolysis.^{19,20} However, PLGA is also less hydrophobic than PLA because glycolide lacks the two methyl substituents of lactide. Is the faster release kinetics from PLGA due to its amorphous nature or due to its increased hydrophilicity? In order to level out the HHB imbalance, we targeted the novel monomer 3-ethyl-1,4-dioxane-2,5-dione (3-ethylglycolide, EtGly) as being an isomer of lactide (Scheme 1). The ring-opening polymerization (ROP) of the cyclic dilactone EtGly, comprising a glycolic unit and a 2-hydroxybutyric unit, should enable access to a polyester featuring the same HHB as PLA. Small amounts of comonomers featuring opposite configuration are known to alter the thermal properties of semicrystalline isotactic PLA formed from enantiopure monomers.^{21,22} Consequently, the copolymerization of racemic EtGly and enantiopure lactide should enable access to a series of copolymers meeting the requirements as well.

As organic bases are well-working catalysts, *e.g.* for the ROP of lactide as well as its copolymerization with glycolide,^{23–25} the guanidine organobase 7-methyl-1,5,7-triazabicyclo[4.4.0]dec-5-ene (mTBD)²⁶ was selected as catalyst for the ROP to avoid the toxic standard catalyst tin(II) 2-ethylhexanoate (SnOct₂).²⁷ To exclusively vary the thermal properties and the degree of crystallinity (w_c), a library of nine polyesters with constant HHB and similar molar mass was targeted. The materials were analyzed by means of differential scanning calorimetry (DSC) and nanoparticles obtained from the corresponding polyesters were characterized by dynamic light scattering (DLS) and scanning electron microscopy (SEM) investigations.

Experimental section

Materials

L-Lactide (L-LA; 98%, Aldrich) was recrystallized from ethyl acetate prior to use. (*rac*)-2-Hydroxybutanoic acid (95%, abcr) and D-lactide (D-LA, 98%, abcr) were utilized without further

purification. The reaction solvent toluene (extra dry, Aldrich), the catalyst 7-methyl-1,5,7-triazabicyclo[4.4.0]dec-5-ene (mTBD, 98%, Aldrich) and the initiator benzyl alcohol (BnOH, anhydrous, 99.8%, Aldrich) were stored under nitrogen. The solvents utilized for column chromatography (ethyl acetate and *n*-hexane) were distilled before usage. R_f values were determined from pre-coated TLC sheets ALUGRAM® SIL G/UV₂₅₄ and silica gel 60 was used as packing material for the preparative columns (both delivered from Machery Nagel). Tetrahydrofuran (THF) for nanoparticle preparation was purified in a solvent purification system (SPS; Pure solv EN, InnovativeTechnology). All other chemicals were purchased from standard suppliers and were used without any further purification.

Instruments

Polymerizations were conducted under nitrogen atmosphere in a MBraun UNILab Plus glove box, which was equipped with high efficiency box filters HEPA H13, a UNILab inert gas purification system and a vacuum pump. Proton and carbon nuclear magnetic resonance (¹H and ¹³C NMR) spectra were measured in CDCl₃ or CD₂Cl₂ at room temperature on a 300 MHz Bruker Avance I or 400 MHz Bruker Avance III spectrometer. The residual ¹H peak of the deuterated solvent was used for chemical shift referencing. Homonuclear decoupling experiments were performed using a 500 MHz Bruker Avance III HD spectrometer equipped with a BBO Prodigy probe head. Elemental analysis was carried out using a Leco CHN-932. Melting points were determined with a melting point meter MPM-H2 from VWR international GmbH. Infrared (IR) spectra were measured with an IRAffinity-1 CE from Shimadzu equipped with a quest ATR diamond extended range X – single-reflection-ATR cuvette.

The crystallographic data were acquired as follows: The intensity data of EtGly was collected on a Nonius KappaCCD diffractometer, using graphite-monochromated Mo-K_α radiation. Data were corrected for Lorentz and polarization effects; absorption was taken into account on a semi-empirical basis using multiple-scans.^{28–30} The structure was solved by direct methods (SHELXS³¹) and refined by full-matrix least squares techniques against F_o^2 (SHELXL-97³¹). All hydrogen atoms

were located by difference Fourier synthesis and refined isotropically. All non-hydrogen atoms were refined anisotropically.³¹ MERCURY³² was used for structure representations.

Gas chromatography (GC) measurements were performed on a Shimadzu system (GC-2010 plus) equipped with an AOC-20s autosampler, a FID detector with a flow rate of 1.86 mL min⁻¹ and a PerkinElmer Elite-5MS column (30 m length, 0.25 mm ID, 0.25 μm film thickness, stationary phase: 5% diphenyl, 95% dimethyl polysiloxane using helium as carrier gas. After split injection (AOC 20i injector, 250 °C) the column oven was heated from 60 to 200 °C with a heating rate of 16 °C min⁻¹. GC-high resolution mass spectrometry (HRMS) measurements were performed on a GC/MS consisting of a Trace 1310 gas chromatograph coupled to a Q-Exactive GC mass spectrometer in EI and CI (methane as reactant gas) ionization mode (Thermo, Bremen, Germany, see ESI† for details).

Size-exclusion chromatography (SEC) measurements were performed utilizing a Shimadzu system equipped with a CBM-20A system controller, a LC-10AD pump, a RID-10A refractive index detector and a PSS (Polymer Standards Service GmbH, Mainz, Germany) SDV column with chloroform/triethylamine (NEt₃)/iso-propanol (94 : 4 : 2) as eluent with a flow rate of 1 mL min⁻¹. The column oven was set to a constant temperature of 40 °C. Polystyrene (PS) samples were used for calibration.

Matrix-assisted laser desorption/ionization time-of-flight mass spectrometry (MALDI-ToF MS) measurements were carried out using an Ultraflex III ToF/ToF instrument (Bruker Daltonics, Bremen, Germany). The spectrometer was equipped with a Nd-YAG laser. All spectra were recorded in the positive reflector mode. The instrument was calibrated with an external PMMA standard from PSS. *trans*-2-[3-(*tert*-Butylphenyl)-2-methyl-2-propenylidene]malononitril (DCTB, Sigma Aldrich) was used as matrix and sodium iodide (Sigma Aldrich) as additional salt. Separate solutions of analyte (10 mg mL⁻¹ in chloroform), DCTB (30 mg mL⁻¹ in chloroform) and sodium iodide (100 mg mL⁻¹ in acetone) were prepared. 5 μL of analyte solution, 15 μL of matrix solution and 5 μL of salt solution were mixed, and 1 μL of the resulting solution was deposited on the target plate according to the dried droplet spotting technique. Electro-spray ionization (ESI) time-of-flight mass spectrometry (MS) measurements of EtGly were performed utilizing a Bruker MicroQToF mass spectrometer.

Thermogravimetric analysis (TGA) was measured under nitrogen atmosphere on a STA Netzsch 449 F3 Jupiter. Data were recorded from 30 to 600 °C at a heating rate of 10 °C min⁻¹. Differential scanning calorimetry (DSC) measurements were performed with a Netzsch 204 F1 Phoenix instrument under a nitrogen atmosphere applying a heating rate of 20 °C min⁻¹ in the first and second run and 10 °C min⁻¹ in the third run. The temperature range was from -20 to 260 °C and the cooling rate between the heating runs was 20 °C min⁻¹.

Dynamic light scattering (DLS) and ζ-potential measurements were performed on a Zetasizer Nano ZS (Malvern Instruments, Herrenberg, Germany) at 25 °C (λ = 633 nm) at

an angle of 173°. For each measurement, 3 × 30 s runs were carried out in triplicates after an equilibration time of 30 s. The mean particle size was approximated as the effective (Z-average) diameter and the width of the distribution as the dispersity index (PDI) of the particles obtained by the cumulants method assuming a spherical shape. Fluorescence spectra were recorded on a Jasco FP-8300 instrument using spectroscopy-grade solvents and quartz cuvettes (1 cm pathway). The device was measuring from 350 to 550 nm with a scan speed of 20 nm min⁻¹ and a data interval of 0.2 nm. Shape and dimensions of the nanoparticles were investigated by scanning electron microscopy (SEM) with an AURIGA 60 CrossBeam® Workstation (Carl Zeiss AG, Oberkochen, Germany). Samples were previously coated with tungsten.

Synthesis of 3-ethyl-1,4-dioxane-2,5-dione (EtGly)

A solution of 2 g (*rac*)-2-hydroxybutanoic acid (19 mmol) and 2.68 mL triethylamine (NEt₃, 19 mmol) in 60 mL diethyl ether was cooled in an ice/sodium chloride bath to -5 °C and stirred for 20 minutes. Subsequently, a solution of 2.18 mL bromoacetyl bromide (25 mmol) in 5 mL diethyl ether was added dropwise within 30 minutes not allowing the reaction mixture to exceed 0 °C. The ice bath was removed and the reaction mixture was allowed to reach room temperature. The reaction mixture was stirred for another five hours at room temperature. Precipitates were removed by filtration and the remaining solution was concentrated under reduced pressure.

The crude yellow oil was dissolved in 1 L acetone and 20 g sodium bicarbonate (0.35 mol) were added in small portions. The reaction mixture was refluxed under vigorous stirring overnight. Subsequent to cooling to room temperature, the reaction mixture was filtered to remove the excess of salts. The solution was concentrated under reduced pressure and diluted with 1 to 2 mL of diethyl ether to precipitate salts and impurities. After filtration, the supernatant was washed with 2 mL distilled water and the aqueous phase was extracted three times with *ca.* 5 mL of diethyl ether. The combined organic phases were dried over sodium sulfate and evaporated under reduced pressure. The crude oil was purified by column chromatography (SiO₂, *n*-hexane/EtOAc, 5 : 1, *R_f* = 0.16) to obtain the product as colorless solid, which contained crystals suitable for crystallographic analysis.

3-Ethyl-1,4-dioxane-2,5-dione (EtGly). Yield = 27%. M.p.: 54.1 °C. ¹H NMR [ppm] (CDCl₃, 300 MHz): δ = 1.15 (t, 3H, *J* = 7.38, 7.41 Hz, CH₃), 2.11 (m, 2H, CH-CH₂-CH₃), 4.88 (dd, 1H, *J* = 4.94, 2.27, 4.95 Hz, CH-CH₂-CH₃), 4.94 (d, 2H, *J* = 1.80 Hz, CO-CH₂-O) ppm. ¹³C NMR (CDCl₃, 300 MHz): δ = 8.86 (C-1), 24.39 (C-2), 65.32 (C-4), 164.29 (C-5), 165.40 (C-6) ppm. IR [cm⁻¹]: $\tilde{\nu}$ = 2978 (CH₃), 2947 (CH₂), 2916 (CH), 1747 (O-C=O), 1076 (O-C-C(=O)); GC-MS: *m/z* (rel. intensity) = 145.04956 (100; calculation for C₆H₉O₄⁺ as [M + H]⁺: 145.04954, error: 0.17 ppm); 116.01054 (5; calculation for C₄H₄O₄⁺ as [M - CH₂ - CH₃]⁺: 116.01041, error: 1.09 ppm); 87.04412 (55; calculation for C₄H₇O₂, [O-(C=O)-CH-CH₂-CH₃ + H]⁺: 87.04406, error: 0.74 ppm); 59.049215 ([O-(C=O)-CH₂ + H]⁺); Elemental anal.

Calc. for $C_6H_8O_4$: C: 50.00; H: 5.60; found: C: 49.93; H: 5.56. Crystal Data for EtGly: $C_6H_8O_4$, $M_r = 144.12 \text{ g mol}^{-1}$, colourless prism, size $0.112 \times 0.110 \times 0.088 \text{ mm}^3$, monoclinic, space group $P2_1$, $a = 8.0925(9)$, $b = 5.0020(6)$, $c = 8.1097(9) \text{ \AA}$, $\beta = 92.838(1)^\circ$, $V = 327.87(6) \text{ \AA}^3$, $T = -140 \text{ }^\circ\text{C}$, $Z = 2$, $\rho_{\text{calcd}} = 1.460 \text{ g cm}^{-3}$, $\mu(\text{Mo-K}\alpha) = 1.24 \text{ cm}^{-1}$, multi-scan, transmin: 0.5867, transmax: 0.7456, $F(000) = 152$, 3303 reflections in $h(-7/10)$, $k(-6/6)$, $l(-10/8)$, measured in the range $2.51^\circ \leq \theta \leq 27.47^\circ$, completeness $\Theta_{\text{max}} = 100\%$, 1451 independent reflections, $R_{\text{int}} = 0.0352$, 1333 reflections with $F_o > 4\sigma(F_o)$, 123 parameters, 1 restraints, $R1_{\text{obs}} = 0.0436$, $wR2_{\text{obs}} = 0.0942$, $R1_{\text{all}} = 0.0504$, $wR2_{\text{all}} = 0.0995$, GOOF = 1.120, Flack-parameter 1.7(16), largest difference peak and hole: $0.346/-0.209 \text{ e \AA}^{-3}$.

Ring-opening polymerization

All polymerizations were performed at $23 \text{ }^\circ\text{C}$ in a glovebox under nitrogen atmosphere ($<0.1 \text{ ppm H}_2\text{O}$; $<0.1 \text{ ppm O}_2$). A stock solution of initiator and catalyst was used to achieve a ratio of $[\text{M}]/[\text{BnOH}]/[\text{mTBD}] = 100/1/1$ for all polymerizations.

Polymerization kinetics for L-LA, D-LA and EtGly

144 mg monomer (1 mmol) were dissolved in 3.3 mL toluene ($c = 0.3 \text{ mol L}^{-1}$). To start the polymerization, 20 μL stock solution containing 1.03 μL BnOH (0.01 mmol), 1.44 μL mTBD (0.01 mmol) and 17.53 μL toluene were added ($[\text{M}]/[\text{BnOH}]/[\text{mTBD}] = 100/1/1$). Samples were taken after 0, 2, 5, 10, 20, 30, 40, 50, 60, 80, 100 and 120 minutes. Each sample was quenched with a fourfold excess of benzoic acid (0.41 mg, 3.4 mmol) dissolved in chloroform.

The monomer conversion was determined by $^1\text{H NMR}$ spectroscopy for L- and D-LA. GC measurements were performed to obtain the conversion of EtGly.

General procedure for the homopolymerization (P1 to P3)

The monomer and toluene were added to a vial and stirred until complete dissolution ($c = 0.3 \text{ mol L}^{-1}$). Subsequently, a stock solution consisting of BnOH, mTBD and toluene was used to initiate the polymerization ($[\text{M}]/[\text{BnOH}]/[\text{mTBD}] = 100/$

1/1). After two hours of stirring at room temperature, the reaction mixture was quenched with a four fold excess of benzoic acid dissolved in toluene and a sample was taken to determine the monomer conversion. After precipitation of the polymers in ice-cold methanol, the homopolymers were dried *in vacuo* and yielded white powders. Further details are provided in the ESI.†

PLLA (P1). Conv. = 85%; yield = 66%. $^1\text{H NMR}$ (400 MHz, CDCl_3): $\delta/\text{ppm} = 1.60$ (d, 474H, $J = 7.12 \text{ Hz}$, H-1), 5.18 (q, 158H, $J = 7.07, 7.13, 7.09 \text{ Hz}$, H-2), $^1\text{H NMR}$ (300 MHz, CD_2Cl_2): $\delta = 1.56\text{--}1.58$ (br, 575H, H-1), 5.15–5.19 (br, 158H, H-2), 7.37 (br, 5H, H-3); SEC (CHCl_3 , PS calibration): $M_n = 16 \text{ kg mol}^{-1}$; $D = 1.06$.

PdLA (P2). Conv. = 85%; yield = 71%. $^1\text{H NMR}$ (400 MHz, CDCl_3): $\delta/\text{ppm} = 1.60$ (d, 504H, $J = 7.13 \text{ Hz}$, H-1), 5.18 (q, 168H, $J = 7.08, 7.12, 7.10 \text{ Hz}$, H-2), $^1\text{H NMR}$ (300 MHz, CD_2Cl_2): $\delta = 1.56\text{--}1.58$ (br, 576H, H-1), 5.15–5.21 (br, 168H, H-2), 7.37 (br, 5H, H-3); SEC (CHCl_3 , PS calibration): $M_n = 19 \text{ kg mol}^{-1}$; $D = 1.06$.

PEtGly (P3). Conv. = 97%; yield = 64%. $^1\text{H NMR}$ (400 MHz, CDCl_3): $\delta/\text{ppm} = 1.05$ (t, 210H, $J = 7.36, 7.66 \text{ Hz}$, H-1), 1.89–2.11 (br, 140H, H-2), 4.64–4.95 (br, 140H, H-4), 5.09–5.21 (br, 70H, H-3); SEC (CHCl_3 , PS calibration): $M_n = 12 \text{ kg mol}^{-1}$; $D = 1.19$.

General procedure for the statistical copolymerization (P4 to P9)

The statistical copolymers P4 to P9 were obtained as described for the homopolymers P1 to P3. A constant ratio of $[\text{M}]_{\text{total}} : [\text{TBD}] : [\text{BnOH}] = 100 : 1 : 1$ was kept, while the feed ratio of L- or D-LA and EtGly was varied as indicated in Table 1. All copolymerizations were performed at room temperature for two hours. In an exemplary reaction for P4, 352 mg (2.44 mmol) of L-LA and 19 mg (0.13 mmol) of EtGly were dissolved in 8.56 mL anhydrous toluene. The ROP was initiated by addition of a stock solution containing 2.66 μL BnOH (0.03 mmol), 3.35 μL mTBD (0.03 mmol) and 93.99 μL toluene. The polymerization proceeded at room temperature

Table 1 Selected structural characterization data of the synthesized (co)polymers

Sample	Polymer	mol% LA/EtGly feed	Conv. ^a [%]	mol% LA/EtGly NMR ^b	M_n [kg mol ⁻¹] NMR ^b	M_n [kg mol ⁻¹] SEC ^c	D SEC ^c
P1	PLLA	100/0	85	100/0	11	16	1.06
P2	PdLA	100/0	85	100/0	12	19	1.06
P3	PEtGly	0/100	97	0/100	10	12	1.19
P4	P(LLA- <i>stat</i> -EtGly)	95/05	75	95/05	11	16	1.11
P5	P(LLA- <i>stat</i> -EtGly)	90/10	74	89/11	11	13	1.20
P6	P(LLA- <i>stat</i> -EtGly)	80/20	69	78/22	10	12	1.23
P7	P(DLA- <i>stat</i> -EtGly)	95/05	77	96/04	12	19	1.10
P8	P(DLA- <i>stat</i> -EtGly)	90/10	79	91/09	11	18	1.21
P9	P(DLA- <i>stat</i> -EtGly)	80/20	77	78/22	10	15	1.28

^a Overall monomer conversion determined by integration of suitable signals in the $^1\text{H NMR}$ spectra of the reaction solution. The conversion for P3 was determined *via* GC analysis. ^b Determined by integration of suitable signals in the $^1\text{H NMR}$ spectra of the purified polymers. ^c Eluent CHCl_3 , RI detection, PS calibration. Values correspond to the purified polymers.

for two hours. The analyses and purification were performed as described above. Details for **P5** to **P9** are provided in the ESI.†

P(LLA-*stat*-EtGly) (P4). Feed L-LA/EtGly = 95/05; conv = 75%; yield = 74%. $^1\text{H NMR}$ (300 MHz, CDCl_3): δ/ppm = 1.00–1.07 (br, 12H, H-2), 1.50–1.79 (br, 483H, H-6), 1.92–2.04 (br, 11H, H-3), 4.59–4.89 (br, 7H, H-1), 5.14–5.21 (br, 152H, H-4, H-5), $^1\text{H NMR}$ (300 MHz, CD_2Cl_2): δ = 1.00–1.01 (br, 13H, H-2), 1.45–1.63 (br, 536H, H-6), 1.89–2.07 (br, 12H, H-3), 4.63–4.87 (br, 7H, H-1), 5.10–5.19 (br, 151H, H-4, H-5), 7.36 (br, 5H, H-7); SEC (CHCl_3 , PS calibration): M_n = 16 kg mol^{-1} ; D = 1.11.

Nanoparticle preparation

P1 to **P9** were dissolved in THF (see Table 3 for details). 0.5 mL of the polymer solution were dropped into 5 mL of milliQ water while stirring at a rate of 1000 rpm. THF was removed by stirring the nanoparticle suspension in an open glass vial overnight and DLS and zeta potential measurements were performed. The pyrene loaded nanoparticles were prepared using 1900 μL of polymeric THF solutions and 100 μL of a pyrene stock solution in THF ($c(\text{pyrene}) = 1 \text{ mg mL}^{-1}$ for **P1** and **P2** and $c(\text{pyrene}) = 0.3 \text{ mg mL}^{-1}$ for **P3** to afford a constant pyrene content of 1 mass% in the suspensions). Nanoparticle formulations from the THF mixtures were performed as described above. After DLS measurements, the nanoparticle suspensions of **P1** to **P3** were diluted 100 times and fluorescence spectra were measured ($\lambda_{\text{ex}} = 339 \text{ nm}$).

Results and discussion

Monomer synthesis

The synthesis of the heterocyclic monomer EtGly was accomplished in a two-step procedure adopted from well-known procedures published for similar monomers (Scheme 1).^{33–36} (*rac*)-2-Hydroxybutanoic acid was acylated with bromoacetyl bromide to yield the linear precursor in the presence of triethylamine (NEt_3) as scavenger for the formed HBr. The cyclization was afforded by refluxing the crude linear precursor with sodium bicarbonate overnight under highly diluted conditions to promote an intramolecular nucleophilic substitution. As typically observed for such syntheses,³⁶ the purified EtGly was obtained in low yields (27%). Detailed mass spectrometry analysis pointed towards a possible presence of macrocyclic impurities that could not be quantified and might have been produced during GC-MS analysis at temperatures above 250 $^\circ\text{C}$ (see ESI†). However, NMR spectroscopy supported the purity of the monomer, not indicating any diastereomers or meso forms. X-ray crystallography finally confirmed the identity of EtGly, which crystallized in a slightly twisted boat conformation (Fig. 1). The substitution of the ethyl moiety in bowsprit position allowed the endocyclic atoms to adopt bond angles according to their hybridization (Table S1†). EtGly was assigned to the space group $P2_1$ and the intermolecular interactions are primarily dominated by van der Waals forces.

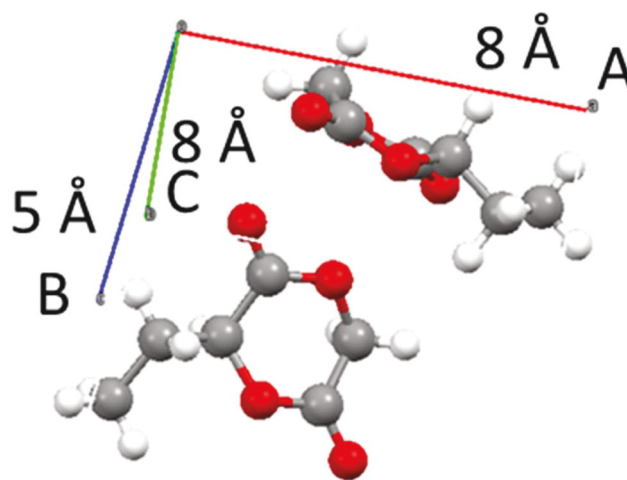


Fig. 1 Section of the packing of the crystal structures of the monomer EtGly obtained by X-ray scattering experiments.

Ring-opening polymerization

Employing mTBD as catalyst, kinetic studies were performed during the ROP of L-LA, D-LA and EtGly in toluene ($c = 0.3 \text{ mol L}^{-1}$) at room temperature. Benzyl alcohol was selected as initiator, keeping the initial ratio of $[\text{M}]/[\text{BnOH}]/[\text{mTBD}]$ constant at 100/1/1 for all the polymerizations, as the targeted polyesters should feature a similar molar mass. The conversions of L-LA and D-LA were determined *via* $^1\text{H NMR}$ analyses by integration of the methine protons peaks assigned to the monomers and the polymers. Due to overlapping signals in the $^1\text{H NMR}$ spectra, the conversion of EtGly was determined *via* GC investigation using the solvent as internal standard, although a complete baseline separation has not been realized.

The non-linear first-order kinetic plot depicted in Fig. 2 revealed that the apparent polymerization rate decreased throughout the course of the ROP in a similar fashion as reported for other monofunctional hydrogen bond acceptor catalysts such as 1,8-diazabicyclo[5.4.0]undec-7-ene (DBU).^{37–39} As expected, L-LA and D-LA featured the same kinetic behavior during the polymerization process but the polymerization rate of EtGly was significantly increased. Considering the fact that EtGly represents a monosubstituted glycolide, the latter is consistent with the increased reactivity of glycolide compared to, *e.g.*, lactide.²³ As reported for the $\text{Sn}(\text{Oct})_2$ catalyzed ROP of methylglycolide,⁴⁰ a nucleophilic attack at the monomer would preferably take place at the unsubstituted acyl moiety of the dioxanedione ring.

SEC traces from kinetic samples revealed unimodal molar mass distributions with dispersity values (D) below 1.08 for the PLAs and below 1.21 for PEtGly. The molar masses of all three polyesters increased in a linear fashion with monomer conversion during the course of the ROP. The molar masses of the homopolymers were hence well controlled using the same polymerization conditions.

The end group fidelity for the polymerization of EtGly was evaluated by means of MALDI-ToF-MS analysis on the sample

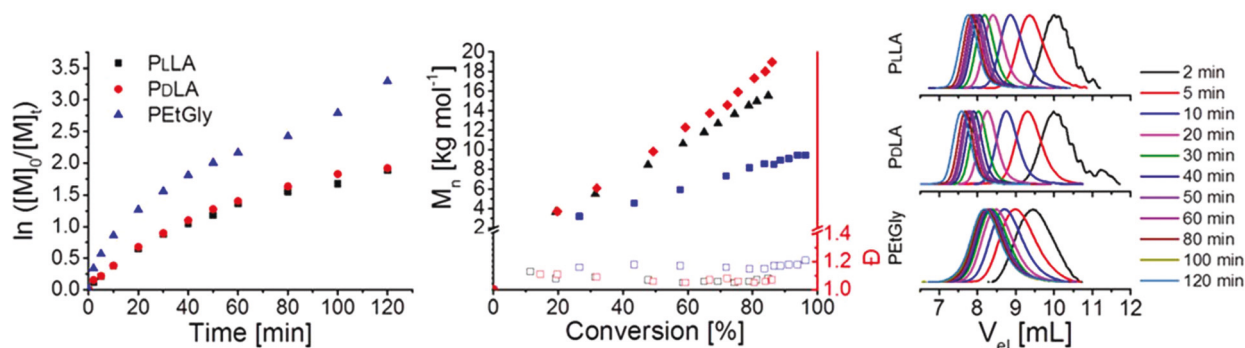


Fig. 2 Kinetic studies of the homopolymerization of L-LA, D-LA and EtGly conducted in toluene ($[M] = 0.3 \text{ mol L}^{-1}$) at room temperature using BnOH as initiator and mTBD as catalyst ($[M] : [mTBD] : [BnOH] = 100 : 1 : 1$). Left: First-order kinetic plot. Center: Evolution of the molar mass with monomer conversion. Right: Overlay of the SEC elugrams (CHCl_3 , RI detection, PS calibration).

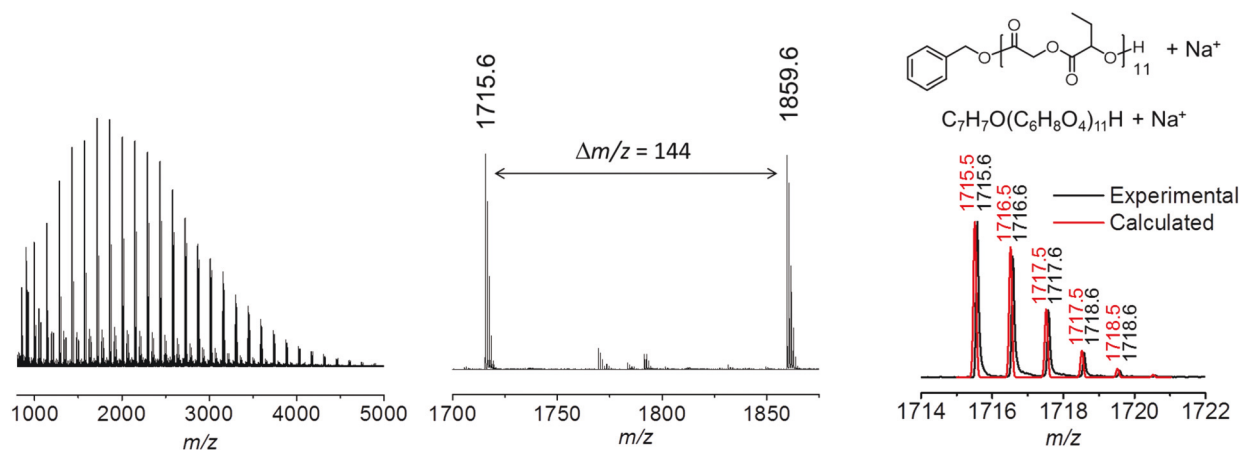


Fig. 3 MALDI-ToF MS analysis of the sample taken after two minutes during the polymerization of EtGly. Left: Full mass spectrum. Center: Zoom into the m/z region from 1700 to 1875. Right: Overlay of the calculated and measured isotopic patterns and assignment of the most abundant peak.

taken after two minutes, corresponding to a conversion of 26% ($M_{n,theo} = 3.8 \text{ kg mol}^{-1}$). The most abundant peak at $m/z = 1715.6$ was assigned to sodiated PEtGly chains initiated by benzyl alcohol and terminated by a proton as depicted in Fig. 3. The distance between two peaks of the main series of $\Delta m/z = 144$ corresponds to one EtGly repeating unit. Less abundant signals were assigned to chains with a carboxylic acid α - and a hydroxy ω -end group, possibly caused by water initiation or by deactivation of zwitterionic intermediates by water. Signals related to cyclic polymer chains caused by intramolecular transesterification could not be assigned.

The polymerization conditions were hence applied for the synthesis of the respective homopolymers PLLA (**P1**), PDLA (**P2**) and PEtGly (**P3**) as well as two series of statistical copolymers comprising 5, 10 and 20 mol% EtGly that are based on PLLA (**P4** to **P6**) and PDLA (**P7** to **P9**), respectively. For all polymerizations, the ratio of $[M] : [mTBD] : [BnOH]$ was kept constant at 100 : 1 : 1 to ensure a similar molar mass of the (co)polyesters (see Table 1). After two hours, the expected monomer conversions were reached for the homopolymers, whereas the overall

monomer conversions for the copolymer series ranged from 70 to 80%. Theoretical molar masses between 10 kg mol^{-1} and 12 kg mol^{-1} were hence expected. End group analyses by integration of end group and backbone signals in the ^1H NMR spectra confirmed these molar masses (Fig. S9–S17[†]). It should be stated that the theoretical molar mass of PEtGly (**P3**) might be biased by the GC analyses (see above), explaining the deviation of the expected ($M_n = 14 \text{ kg mol}^{-1}$) and achieved ($M_n = 10 \text{ kg mol}^{-1}$) molar mass values.

The successful incorporation of EtGly into PLLA as well as PDLA was also evident from the ^1H NMR spectra, as is exemplarily demonstrated by the overlay shown in Fig. 4. The methine and methylene proton region of the spectra proved to be suitable for the estimation of the copolymer compositions as the methylene proton signals assigned to the EtGly repeating units (peak 1 in Fig. 4) were separated from the overlapping methine proton signals (peaks 4 and 6 in Fig. 4). The resulting values calculated from these peak integrals are in good agreement with the feed ratio of the monomers (compare Table 1), demonstrating that the copolymer composition can be easily tailored.

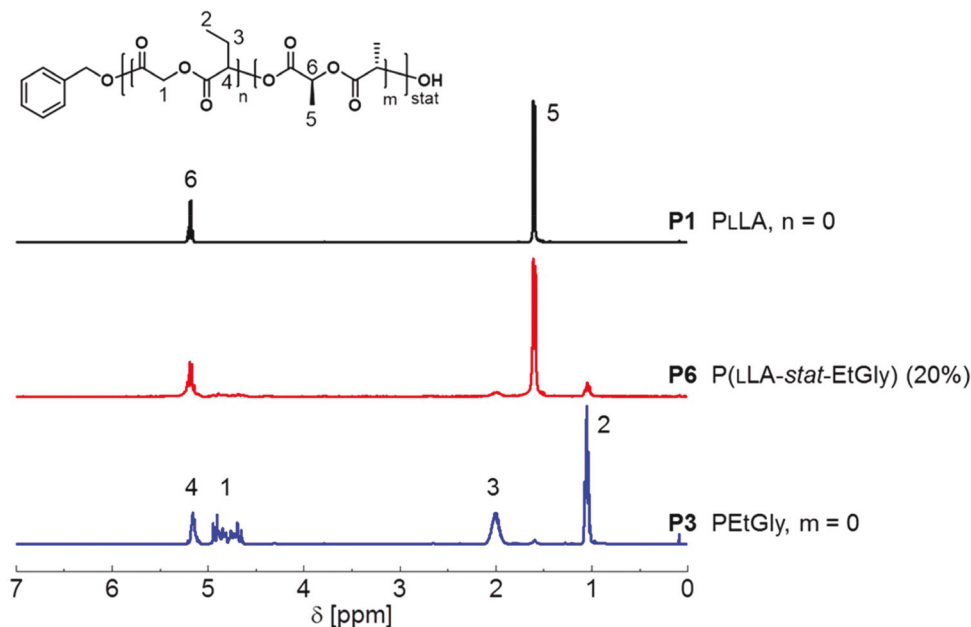


Fig. 4 ^1H NMR spectra of PLLA (**P1**, 400 MHz, CDCl_3), PEtGly (**P3**, 400 MHz, CDCl_3), the copolymer **P6** (300 MHz, CDCl_3) and schematic representation of the assignment of the signals to the structure of the polyesters.

Unimodal and narrow molar mass distributions ($D < 1.22$) were evident from SEC analysis of the reaction solutions (Fig. S7 and S8†). The molar mass distributions were retained subsequent to precipitation for the homopolymers **P1** to **P3** ($1.06 < D < 1.19$). Although precipitation into ice-cold methanol is a common purification procedure for the ROP of lactides,²⁶ an additional high molar mass distribution appeared in the SEC traces of the purified copolymers. In general, the peak was more prominent in polymers with higher EtGly content, in particular for the PLLA based copolymers. As the peak area corresponded to less than 8% and the overall dispersity never exceeded $D = 1.3$, a minor influence on the properties of the copolymers is assumed.

Stereochemistry of the homopolymers **P1** to **P3**

Proceeding slowly at room temperature, organic bases such as DBU can induce epimerization of lactide.⁴¹ Although no or negligible amounts of epimerization were observed after two days at room temperature, *i.e.* at conditions that are typically applied for a DBU catalyzed ROP,²⁶ other organic base catalysts result in partial loss of the stereoinformation of the monomer upon ROP.⁴² Less commonly used than DBU ($\text{p}K_{\text{a}} = 16.8$ in THF), the basicity of mTBD is increased ($\text{p}K_{\text{a}} = 17.9$ in THF).⁴³ To the best of our knowledge, it has not yet been investigated whether the configuration of lactide is retained during a mTBD catalyzed ROP.

Single frequency homonuclear decoupled ^1H NMR spectroscopy experiments⁴⁴ were hence conducted (Fig. 5). The selective decoupling of the methyl group protons of PLLA **P1** and PDLA **P2** resulted in a collapse of the quartet splitting of the methine proton signal. The resulting singlet corresponds

to iii tetrads,⁴⁴ verifying the presence of isotactic chains. The decoupling experiment on the PEtGly **P3**, which was obtained from the racemic EtGly monomer, showed a different result. After irradiation at the methylene proton frequency of the ethyl moiety, the overlapping triplets assigned to the protons at the stereocenters collapsed to at least four singlets. Both enantiomers should have therefore been statistically incorporated during the polymerization process, suggesting the presence of an atactic polyester.

Thermal properties in bulk

As the stereochemistry of all monomers was retained during the ROP process, the copolymerization of enantiopure L-LA or D-LA with defined fractions of the racemic EtGly should result in variations of the crystallinity of the resulting copolymers, while keeping the chain length as well as the HHB constant. Subsequent to TGA analysis to ensure the thermal stability of the materials (Fig. S18†), the bulk polyesters were thus investigated by means of DSC in the temperature range from -20 to 260 °C. After a first heating run at 20 °C min^{-1} , two additional heating runs were performed at 20 °C min^{-1} and 10 °C min^{-1} , respectively, to detect transitions of second and first order at optimum measurement conditions. As the glass transitions remained well detectable at the lower heating rate, the first and third heating runs are in the focus of the following discussion.

In general, no significant differences were found upon comparison of the results obtained from the two copolymer series based on PLLA and PDLA, respectively (Table 2). Fig. 6 exemplarily depicts the results of the PLLA copolymer series obtained in the third heating run, and further overlays are provided in

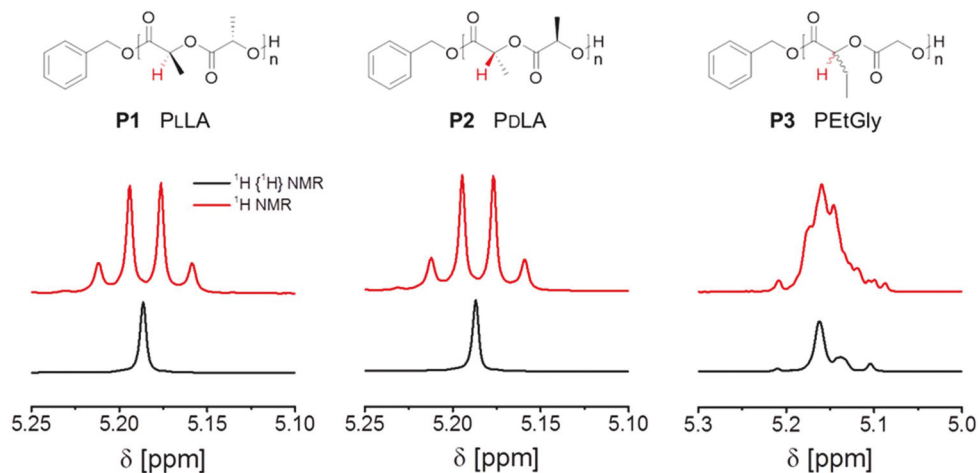


Fig. 5 Selective homonuclear decoupled ^1H NMR experiment (500 MHz, CDCl_3) and schematic representation of the structures of the polyesters **P1** to **P3**. Left: Collapsed signals of the methine protons of **P1**. Center: Collapsed signals of the methine protons of **P2**. Right: Collapsed signal of methine proton of **P3**.

Table 2 Thermal properties of the polyesters estimated from DSC analysis

Polymer	mol% EtGly	Third heating run ^b							First heating run ^d				
		T_g^a [°C]	T_c [°C]	T_m [°C]	ΔH_f [J g ⁻¹]	ΔH_c [J g ⁻¹]	w_c^c [%]	T_c [°C]	T_m [°C]	ΔH_f [J g ⁻¹]	ΔH_c [J g ⁻¹]	w_c^c [%]	
P1 PLLA	0	56	95	151/163	51	-33	19	—	158/165	64	—	69	
P2 PDLA	0	55	97	149/163	47	-37	11	—	157/166	68	—	73	
P3 PETGly	100	29	—	—	—	—	—	—	—	—	—	—	
P4 P(LLA- <i>stat</i> -EtGly)	5	53	108	142/150	35	-33	2	79	143/151	38	-20	20	
P5 P(LLA- <i>stat</i> -EtGly)	11	52	—	135/140	4	—	5	92	119/139	42	-2	43	
P6 P(LLA- <i>stat</i> -EtGly)	22	48	—	—	—	—	—	—	109/121	32	-4	31	
P7 P(DLA- <i>stat</i> -EtGly)	4	53	113	143/150	30	-30	0.4	97	155	50	-15	38	
P8 P(DLA- <i>stat</i> -EtGly)	9	51	119	137/142	6	-4	2	95	121/143	42	-12	31	
P9 P(DLA- <i>stat</i> -EtGly)	22	48	—	—	—	—	—	—	109/121	30	-4	28	

^a Inflection value. ^b Heating rate 10 °C min⁻¹. ^c Degree of crystallinity calculated according to eqn (1) using the ΔH_f of fully crystalline PLA from literature (ΔH_f° (PLA) = 93 J g⁻¹).⁴⁶ ^d Heating rate 20 °C min⁻¹.

the ESI (Fig. S19–S21†). Like PLLA and PDLA, the copolymers comprising EtGly represent semicrystalline materials. The typical double fusion events of PLA due to cold crystallization⁴⁵ were evident during DSC analysis of the copolymers as well. On the other hand, the PETGly homopolymer **P3** was amorphous, which is in line with its atactic structure.

Irrespective of the stereochemistry of the PLA, the glass transition temperatures T_g of the copolymers decreased in a linear fashion with increasing EtGly content, showing that the amorphous domains of the semicrystalline PLA-based materials are strongly affected by incorporation of the racemic comonomer (Fig. 7A). Similar observations hold true regarding the melting temperatures T_m of the two types of crystalline domains (Fig. 7B). As the T_m of polymers is directly correlated to their crystalline dimensions,^{47,48} this indicated that an increase of the amorphous EtGly content disturbed the PLA-crystal formation, resulting in smaller PLA crystals. Although the melting temperature $T_{m,1}$ of the crystallites formed during

cold crystallization differed in the first and third heating runs, the higher $T_{m,2}$ remained constant (Fig. S22†). It should, however, be stated that the initially semicrystalline copolymers comprising 20 mol% of EtGly were not able to recrystallize during the repeated heating and cooling cycles performed during the DSC measurements. In addition, the copolymers featuring 10 mol% EtGly did not recrystallize during the second heating run performed at a heating rate of 20 °C min⁻¹, demonstrating that the crystallization of the materials with higher EtGly fraction is slow.

The enthalpies of crystallization ΔH_c and the enthalpies of fusion ΔH_f were determined from the respective peak areas of the DSC thermograms to deduce structure–property relationships regarding the degree of crystallinity w_c of the two copolymer series. Higher EtGly content resulted in significantly decreased ΔH_f (Fig. 7C). The fact that ΔH_f is lower in the third heating run than for the polymers without any additional thermal pre-treatment again points towards low

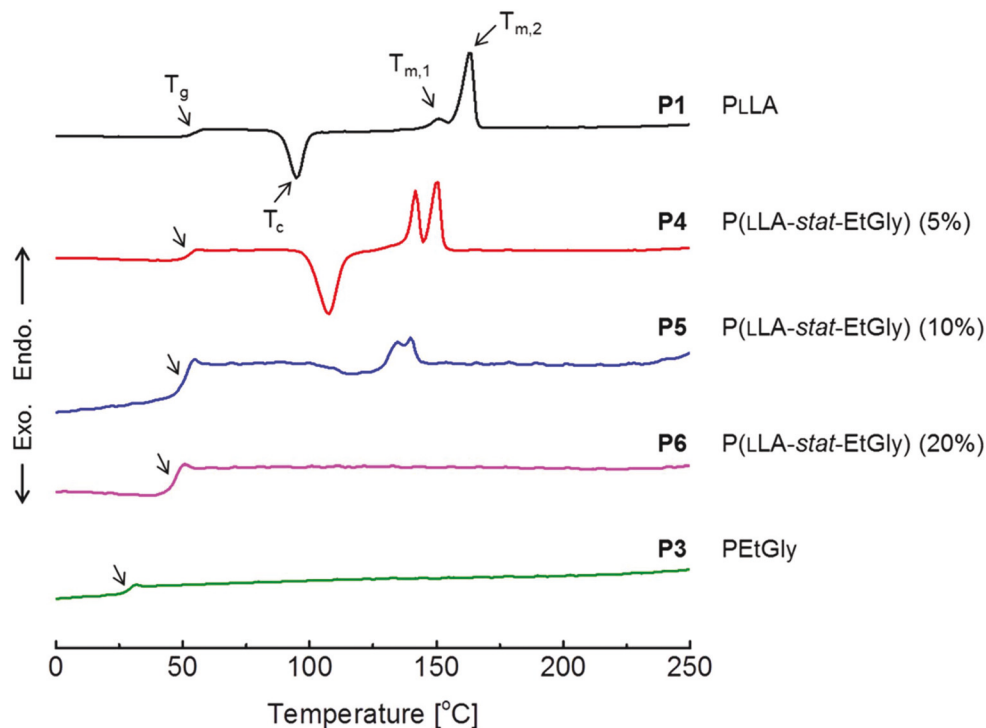


Fig. 6 DSC thermograms of the polyesters based on PLLA. The thermograms are shifted vertically for clarity. The measurements were performed from -20 to 260 °C (third heating run, heating rate 10 °C min^{-1} , cooling rate 20 °C min^{-1}).

crystallization rate of the polyesters. As the PEtGly homopolymer **P3** represented an amorphous sample, we assumed that the EtGly mers alone do not contribute to the crystallinity of the copolymers. The degree of crystallinity above the cold crystallization temperature has hence been roughly estimated by normalization with the enthalpy of fusion of PLA featuring infinite crystal thickness ΔH_f° . However, such a value would be of little significance for the polymer performance at room or body temperature. To assess the actual degree of crystallinity w_c via eqn (1), ΔH_c was hence taken into account.⁴⁹

$$w_c = \frac{(\Delta H_f + \Delta H_c)}{\Delta H_f^\circ(\text{PLA})} \quad (1)$$

The endo- and exothermal peaks in the DSC thermograms were sometimes rather broad, and the resulting w_c values should hence be considered with caution. However, Fig. 7D clearly shows that the crystallinity of PLA was significantly reduced already by incorporation of small fractions of EtGly, although being strongly affected by the thermal prehistory of the samples.

Nanoparticle formulation

To formulate particles small enough for biological applications and of uniform size, the nanoprecipitation method was applied.^{50,51} For this purpose, the polyesters were dissolved in THF and dropped rapidly into an excess of pure water under vigorous stirring. The organic solvent was allowed to evaporate

overnight, producing aqueous nanoparticle suspensions without the need for additional stabilizers. At constant polymer concentration of 0.5 mg mL^{-1} in the suspension, the polyesters based on PLA yielded nanoparticles featuring hydrodynamic diameters D_h between 150 and 170 nm, as indicated by DLS measurements (Fig. 8 and Fig. S23†). Although PEtGly **P3** produced larger nanoparticles under these conditions, the nanoparticle size has been tailored by decreasing the polymer concentration. It was thus possible to formulate nanoparticles from all polyesters with a uniform mean hydrodynamic diameter around 160 nm. The zeta potentials are always strongly negative ($\zeta \approx -30$ mV), indicating the stability of the particle suspensions (Table 3).

Analysis of the nanoparticles by means of SEM indicated a spherical shape of the nanoparticles formulated from each polyester (Fig. 9 and Fig. S24†). The majority of the particles featured diameters below 100 nm, which is most likely due to the drying process prior to the SEM measurements.

The tailor-made polyesters hence feature similar molar masses, different thermal properties and are suited to obtain nanoparticles of similar size. Although the copolymer design should ensure a constant HHB throughout the polymer library, the fluorescent probe pyrene^{52–55} was applied to provide in addition an experimental evidence for the fact. For this purpose, homopolymer nanoparticles formed from **P1** to **P3** were loaded with pyrene by nanoprecipitation using a THF solution of polymer and pyrene (Table S2†). The final pyrene

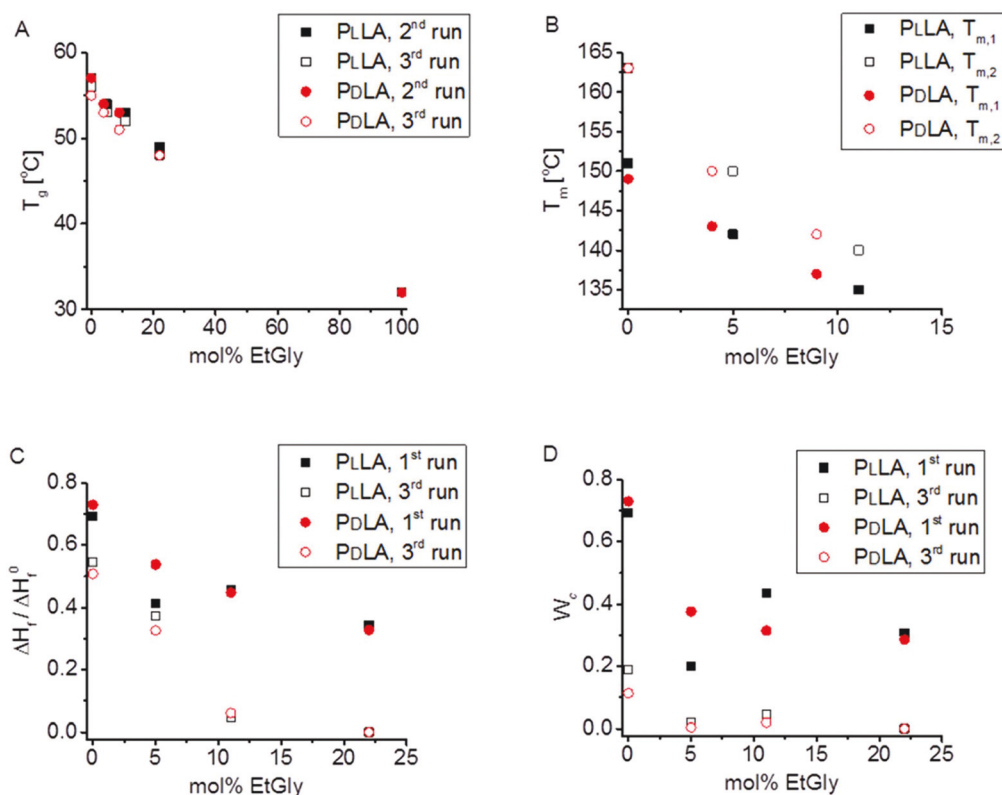


Fig. 7 Influence of the molar fraction of EtGly on the thermal properties of the copolyester series based on PLLA (P1, P3 to P6) and on PDLA (P2, P3, P7 to P9) as determined *via* DSC analysis (cooling rates: 20 °C min⁻¹, heating rate in the first run: 20 °C min⁻¹, heating rate in the second run: 20 °C min⁻¹, heating rate in the third run: 10 °C min⁻¹). A: Glass transition temperature T_g . B: Melting temperatures T_m of both crystallites determined in the third heating run. C: Enthalpy of fusion ΔH_f normalized by the ΔH_f of fully crystalline PLA (ΔH_f^0 (PLA) = 93 J g⁻¹).⁴⁶ D: Degree of crystallinity w_c calculated according to eqn (1).

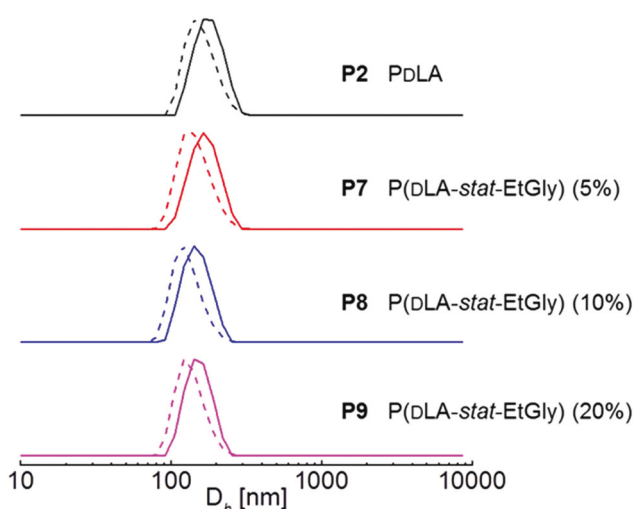


Fig. 8 DLS size distributions of the PDLA based nanoparticles prepared from P2 and P7 to P9 with hydrodynamic diameters $D_h \approx 160$ nm. The full lines represent the intensity-weighted data, the dotted lines represent the number-weighted data.

concentration ($c \approx 10^{-7}$ M) was set according to protocols that are well-established for the determination of critical micelle concentrations.^{56,57} Because the polymer concentration had to

Table 3 Nanoparticle size distributions and ζ -potentials determined by DLS measurements^a

Polymer	$c(P)$ in THF [mg mL ⁻¹]	$c(P)$ in H ₂ O [mg mL ⁻¹]	ζ [mV]	D_h [nm]	PDI
P1	5	0.5	-32	147	0.12
P2	5	0.5	-31	173	0.16
P3	1.5	0.15	-29	156	0.13
P4	5	0.5	-30	147	0.10
P5	5	0.5	-29	167	0.10
P6	5	0.5	-33	157	0.10
P7	5	0.5	-26	160	0.12
P8	5	0.5	-26	147	0.11
P9	5	0.5	-29	150	0.11

^a Prepared by dropping 0.5 mL THF solution into 5 mL water.

be varied in order to obtain nanoparticles of similar sizes, the ratio of pyrene to polymer was kept constant at 1 wt% to account for any quenching effects that might occur inside the nanoparticles. Fluorescence spectroscopy was utilized to judge the hydrophilicity of the pyrene environment *via* the vibrational fine structure of the emission spectrum. As depicted in Fig. 10, the I_1/I_3 ratio is very similar for all nanoparticle suspensions ($I_1/I_3 \approx 1.3$), confirming that the polymers indeed feature a constant HHB.

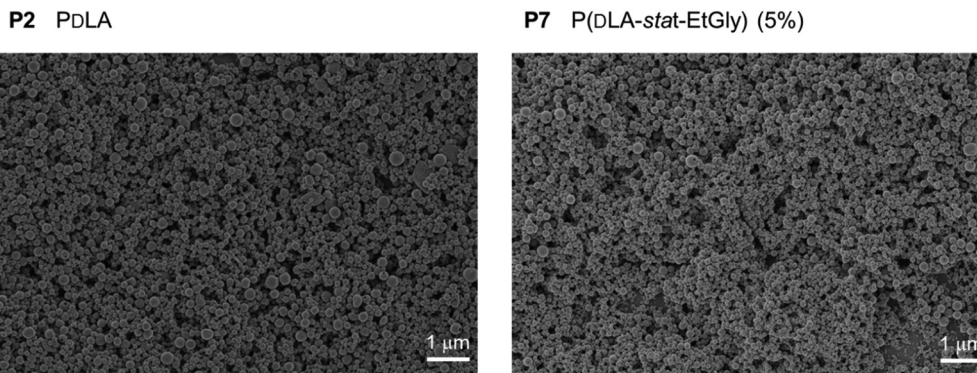


Fig. 9 SEM images of dried nanoparticles prepared from P2 and P7 by nanoprecipitation. Scale bars represent 1 μm .

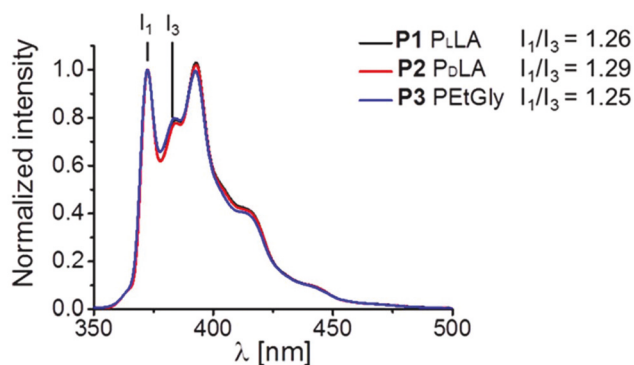


Fig. 10 Normalized fluorescence spectra of pyrene loaded nanoparticles formed from P1 to P3 ($\lambda_{\text{ex}} = 339 \text{ nm}$).

Conclusion

To understand the influence of the thermal properties and the crystallinity of a polyester matrix material on the release of encapsulated drugs, the (co)polymerization of the novel lactide isomer 3-ethyl-1,4-dioxane-2,5-dione (EtGly) represented the basis for the development of a series of polyesters matching the HHB of PLA. The stereochemistry of the enantiopure lactide monomers was retained during the mTBD catalyzed ROP performed at room temperature, resulting in a straightforward method to decrease the degree of crystallinity of well-defined P_LLA and P_DLA already upon incorporation of 5 to 20 mol% of the racemic EtGly in statistical copolymers. The copolymers featuring similar molar masses were suited to obtain stable nanoparticles with diameters around 160 nm and negative zeta potentials *via* nanoprecipitation. Fluorescence spectroscopy of the homopolymer nanoparticles using pyrene as probe confirmed the constant HHB of the polyester library.

Having established materials with constant HHB, molar mass and nanoparticle size, our future research will be focused on studying the release kinetics of encapsulated guest molecules from our tailor-made nanomaterials. The further expansion towards other polymers with constant HHB but

altered crystallinity would ultimately answer the question if and how the thermal properties of a polymer matrix play a crucial role during drug release.

Conflicts of interest

There are no conflicts to declare.

Acknowledgements

The authors thank Nicole Fritz for ESI and MALDI-ToF mass spectrometry analysis. The work was supported by the DFG-funded Collaborative Research Centre PolyTarget (SFB 1278, projects A06 and Z01). We gratefully acknowledge the additional financial support of the Thüringer Ministerium für Wirtschaft, Wissenschaft und Digitale Gesellschaft (Thuringian Ministry for Economic Affairs, Science and Digital Society, ProExzellenz II, NanoPolar) and the Deutsche Forschungsgemeinschaft (DFG), grant references INST 275/389-1 FUGG and INST 275/331-1 FUGG.

References

- 1 R. Singh and J. W. Lillard, *Exp. Mol. Pathol.*, 2009, **86**, 215–223.
- 2 K. E. Uhrich, S. M. Cannizzaro, R. S. Langer and K. M. Shakesheff, *Chem. Rev.*, 1999, **99**, 3181–3198.
- 3 B. D. Ulery, L. S. Nair and C. T. Laurencin, *J. Polym. Sci., Part B: Polym. Phys.*, 2011, **49**, 832–864.
- 4 T. Ishihara, N. Izumo, M. Higaki, E. Shimada, T. Hagi, L. Mine, Y. Ogawa and Y. Mizushima, *J. Controlled Release*, 2005, **105**, 68–76.
- 5 G. Mittal, D. K. Sahana, V. Bhardwaj and M. N. V. Ravi Kumar, *J. Controlled Release*, 2007, **119**, 77–85.
- 6 A. zur Mühlen, C. Schwarz and W. Mehnert, *Eur. J. Pharm. Biopharm.*, 1998, **45**, 149–155.
- 7 J. Zhao, H. Lu, S. Wong, M. Lu, P. Xiao and M. H. Stenzel, *Polym. Chem.*, 2017, **8**, 3317–3326.

- 8 J. A. Champion, Y. K. Katare and S. Mitragotri, *J. Controlled Release*, 2007, **121**, 3–9.
- 9 Z. P. Aguilar, in *Nanomaterials for Medical Applications*, Elsevier, 2013, ch. 5, pp. 181–234.
- 10 E. Allémann, J.-C. Leroux, R. Gurny and E. Doelker, *Pharm. Res.*, 1993, **10**, 1732–1737.
- 11 R. S. Langer and N. A. Peppas, *Biomaterials*, 1981, **2**, 201–214.
- 12 S. Yang, J. Zhu, Y. Lu, B. Liang and C. Yang, *Pharm. Res.*, 1999, **16**, 751–757.
- 13 L. Zeng, L. An and X. Wu, *J. Drug Delivery*, 2011, **2011**, 15.
- 14 C. C. Müller-Goymann, *Eur. J. Pharm. Biopharm.*, 2004, **58**, 343–356.
- 15 V. Karavelidis, D. Giliopoulos, E. Karavas and D. Bikiaris, *Eur. J. Pharm. Sci.*, 2010, **41**, 636–643.
- 16 M. Zilberman, *Acta Biomater.*, 2005, **1**, 615–624.
- 17 M. O. Omelczuk and J. W. McGinity, *Pharm. Res.*, 1992, **9**, 26–32.
- 18 V. Karavelidis, E. Karavas, D. Giliopoulos, S. Papadimitriou and D. Bikiaris, *Int. J. Nanomed.*, 2011, **6**, 3021–3032.
- 19 R. A. Jain, *Biomaterials*, 2000, **21**, 2475–2490.
- 20 J. M. Anderson and M. S. Shive, *Adv. Drug Delivery Rev.*, 1997, **28**, 5–24.
- 21 J. M. Becker, R. J. Pounder and A. P. Dove, *Macromol. Rapid Commun.*, 2010, **31**, 1923–1937.
- 22 L. Feng, B. Zhang, X. Bian, G. Li, Z. Chen and X. Chen, *Macromolecules*, 2017, **50**, 6064–6073.
- 23 H. Qian, A. R. Wohl, J. T. Crow, C. W. Macosko and T. R. Hoye, *Macromolecules*, 2011, **44**, 7132–7140.
- 24 F. Nederberg, B. G. G. Lohmeijer, F. Leibfarth, R. C. Pratt, J. Choi, A. P. Dove, R. M. Waymouth and J. L. Hedrick, *Biomacromolecules*, 2007, **8**, 153–160.
- 25 G. Nogueira, A. Favrelle, M. Bria, J. P. Prates Ramalho, P. J. Mendes, A. Valente and P. Zinck, *React. Chem. Eng.*, 2016, **1**, 508–520.
- 26 B. G. G. Lohmeijer, R. C. Pratt, F. Leibfarth, J. W. Logan, D. A. Long, A. P. Dove, F. Nederberg, J. Choi, C. Wade, R. M. Waymouth and J. L. Hedrick, *Macromolecules*, 2006, **39**, 8574–8583.
- 27 O. Dechy-Cabaret, B. Martin-Vaca and D. Bourissou, *Chem. Rev.*, 2004, **104**, 6147–6176.
- 28 *COLLECT*, *Data collection software*, Nonius BV, Netherlands, 1998.
- 29 Z. Otwinowski and W. Minor, in *Methods in Enzymology*, Academic Press, 1997, vol. 276, pp. 307–326.
- 30 G. Sheldrick, *Acta Crystallogr., Sect. A: Found. Crystallogr.*, 2008, **64**, 112–122.
- 31 G. Sheldrick, *Acta Crystallogr., Sect. C: Struct. Chem.*, 2015, **71**, 3–8.
- 32 C. F. Macrae, P. R. Edgington, P. McCabe, E. Pidcock, G. P. Shields, R. Taylor, M. Towler and J. van de Streek, *J. Appl. Crystallogr.*, 2006, **39**, 453–457.
- 33 F. Coumes, V. Darcos, D. Domurado, S. Li and J. Coudane, *Polym. Chem.*, 2013, **4**, 3705–3713.
- 34 M. Dirauf, D. Bandelli, C. Weber, H. Görls, M. Gottschaldt and U. S. Schubert, *Macromol. Rapid Commun.* 1800433, DOI: 10.1002/marc.201800433.
- 35 A. Pedna, L. Rosi, M. Frediani and P. Frediani, *J. Appl. Polym. Sci.*, 2015, **132**, 42323.
- 36 Y. Yu, J. Zou and C. Cheng, *Polym. Chem.*, 2014, **5**, 5854–5872.
- 37 C. Thomas and B. Bibal, *Green Chem.*, 2014, **16**, 1687–1699.
- 38 N. J. Sherck, H. C. Kim and Y.-Y. Won, *Macromolecules*, 2016, **49**, 4699–4713.
- 39 H. A. Brown, A. G. De Crisci, J. L. Hedrick and R. M. Waymouth, *ACS Macro Lett.*, 2012, **1**, 1113–1115.
- 40 C.-M. Dong, K.-Y. Qiu, Z.-W. Gu and X.-D. Feng, *J. Polym. Sci., Part A: Polym. Chem.*, 2000, **38**, 4179–4184.
- 41 I. A. Shuklov, H. Jiao, J. Schulze, W. Tietz, K. Kühlein and A. Börner, *Tetrahedron Lett.*, 2011, **52**, 1027–1030.
- 42 R. C. Pratt, B. G. G. Lohmeijer, D. A. Long, P. N. P. Lundberg, A. P. Dove, H. Li, C. G. Wade, R. M. Waymouth and J. L. Hedrick, *Macromolecules*, 2006, **39**, 7863–7871.
- 43 I. Kaljurand, T. Rodima, A. Pihl, V. Mäemets, I. Leito, I. A. Koppel and M. Mishima, *J. Org. Chem.*, 2003, **68**, 9988–9993.
- 44 J. L. Robert and K. B. Aubrecht, *J. Chem. Educ.*, 2008, **85**, 258.
- 45 M. Yasuniwa, S. Tsubakihara, Y. Sugimoto and C. Nakafuku, *J. Polym. Sci., Part B: Polym. Phys.*, 2004, **42**, 25–32.
- 46 V. Arias, P. Olsén, K. Odelius, A. Höglund and A.-C. Albertsson, *Polym. Chem.*, 2015, **6**, 3271–3282.
- 47 S. Hölzer, T. N. Büttner, R. Schulze, M. M. L. Arras, F. H. Schacher, K. D. Jandt and U. S. Schubert, *Eur. Polym. J.*, 2015, **68**, 10–20.
- 48 R. Schulze, M. M. L. Arras, C. Helbing, S. Hölzer, U. S. Schubert, T. F. Keller and K. D. Jandt, *Macromolecules*, 2014, **47**, 1705–1714.
- 49 L. Běhálek, M. Maršálková, P. Lenfeld, J. Habr, J. Bobek and M. Seidl, *Study of crystallization of polylactic acid composites and nanocomposites with natural fibres by DSC method*, 2013.
- 50 C. J. Martínez Rivas, M. Tarhini, W. Badri, K. Miladi, H. Greige-Gerges, Q. A. Nazari, S. A. Galindo Rodríguez, R. Á. Román, H. Fessi and A. Elaissari, *Int. J. Pharm.*, 2017, **532**, 66–81.
- 51 S. Schubert, J. J. T. Delaney and U. S. Schubert, *Soft Matter*, 2011, **7**, 1581–1588.
- 52 E. D. Goddard, N. J. Turro, P. L. Kuo and K. P. Ananthapadmanabhan, *Langmuir*, 1985, **1**, 352–355.
- 53 K. Kalyanasundaram and J. K. Thomas, *J. Am. Chem. Soc.*, 1977, **99**, 2039–2044.
- 54 G. Basu Ray, I. Chakraborty and S. P. Moulik, *J. Colloid Interface Sci.*, 2006, **294**, 248–254.
- 55 I. Yildirim, T. Bus, M. Sahn, T. Yildirim, D. Kalden, S. Hoepfener, A. Traeger, M. Westerhausen, C. Weber and U. S. Schubert, *Polym. Chem.*, 2016, **7**, 6064–6074.
- 56 L. Gu, Z. Shen, S. Zhang, G. Lu, X. Zhang and X. Huang, *Macromolecules*, 2007, **40**, 4486–4493.
- 57 C. Weber, M. Wagner, D. Baykal, S. Hoepfener, R. M. Paulus, G. Festag, E. Altuntas, F. H. Schacher and U. S. Schubert, *Macromolecules*, 2013, **46**, 5107–5116.

Supporting information for

Poly(3-ethylglycolide): A well-defined polyester matching the hydrophilic hydrophobic balance of PLA

*Damiano Bandelli,^{1,2#} Julien Alex,^{1,2#} Christian Helbing,³ Nico Ueberschaar,⁴ Helmar Görls,⁵
Peter Bellstedt,¹ Christine Weber,^{1,2} Klaus D. Jandt,^{3*} Ulrich S. Schubert^{1,2*}*

¹ Laboratory of Organic and Macromolecular Chemistry (IOMC), Friedrich Schiller University
Jena, Humboldtstr. 10, 07743 Jena, Germany

² Jena Center for Soft Matter (JCSM), Friedrich Schiller University Jena, Philosophenweg 7,
07743 Jena, Germany

³ Chair of Materials Science (CMS), Department of Materials Science and Technology, Otto
Schott Institute of Materials Research, Faculty of Physics and Astronomy, Friedrich Schiller
University Jena, Löbdergraben 32, 07743 Jena, Germany

⁴ Mass Spectrometry Platform, Friedrich Schiller University Jena, Humboldtstr. 8, 07743 Jena,
Germany

⁵ Institute of Inorganic and Analytical Chemistry (IAAC), Friedrich Schiller University Jena,
Humboldtstr. 8, 07743 Jena, Germany

Both authors contributed equally.

* Correspondence to K. D. Jandt (k.jandt@uni-jena.de) and U. S. Schubert (ulrich.schubert@uni-jena.de)

(rac)-3-Ethyl-1,4-dioxane-2,5-dione (EtGly):

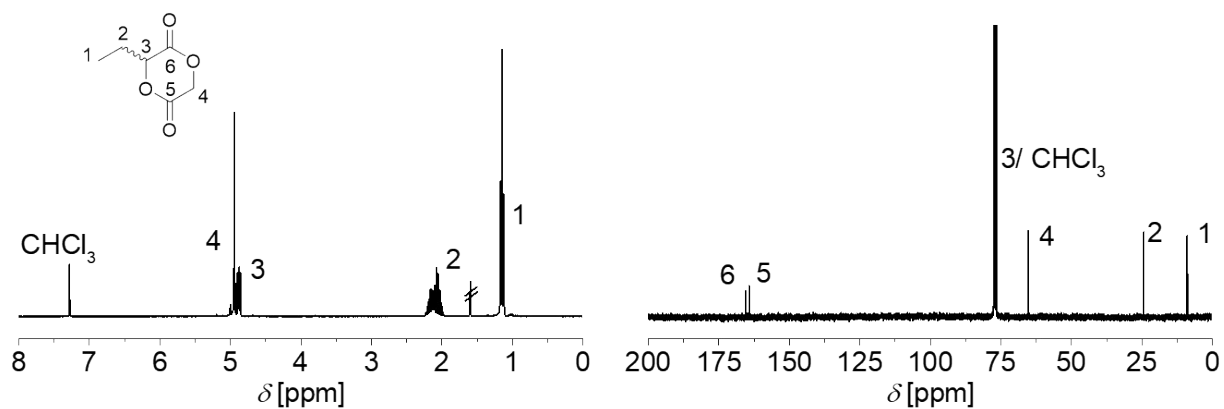


Figure S1: NMR characterization of the monomer EtGly (300 MHz, CDCl₃) and structural assignment of the signals. **Left:** ¹H-NMR spectrum. **Right:** ¹³C-NMR spectrum.

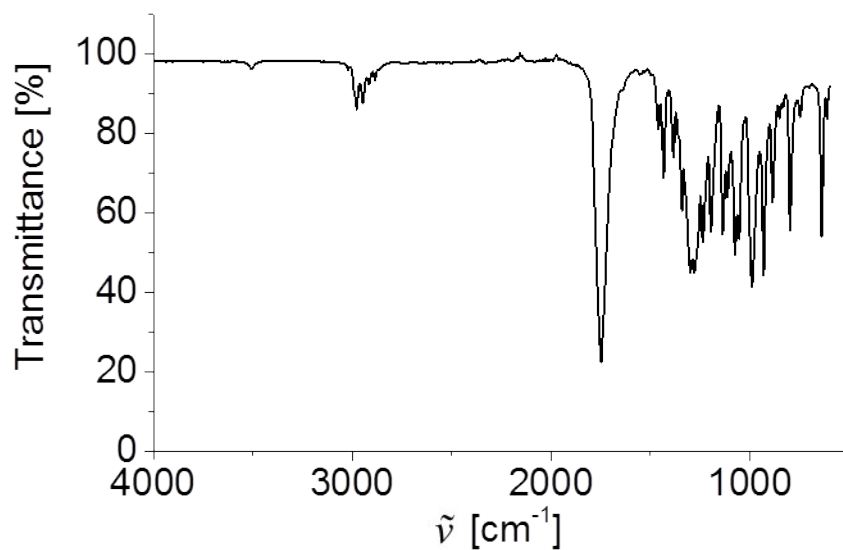


Figure S2: FT-ATR-IR transmittance spectrum of the monomer EtGly.

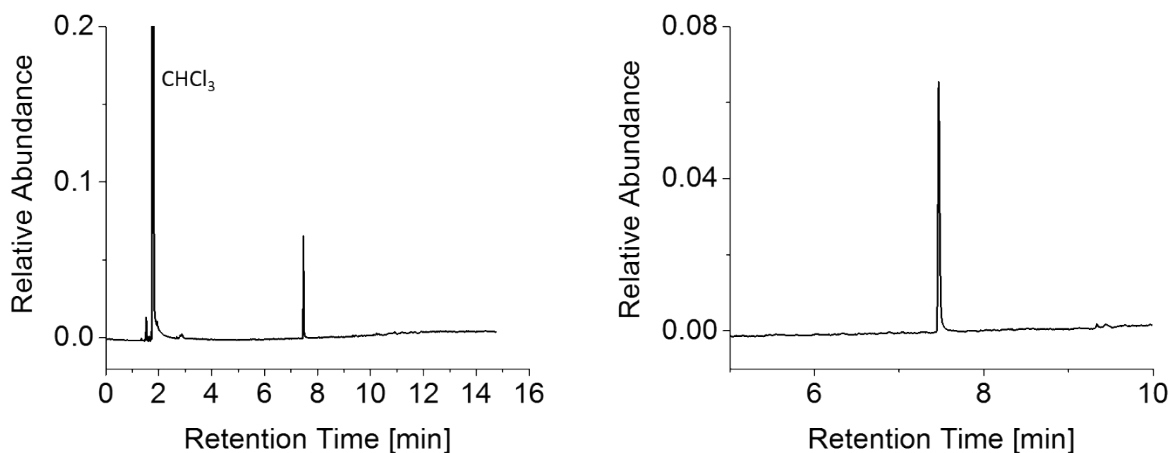


Figure S3: GC-FID chromatogram of the monomer EtGly (60 to 200 °C, heating rate 16 °C min⁻¹). **Left:** Full chromatogram. **Right:** Zoom into the region from 7 to 8 minutes.

Further discussion of the characterization of EtGly by means of mass spectrometry

Instrumentation

For GC-HRMS-measurements the following MS parameters were set: Resolution 120,000; AGC target 1×10^6 ; maximum ion time: 200 ms; scan range 50 to 600 m/z ; transfer line 1, 2 were at 280 °C and transfer line 3 at 250 °C. The ion source temperature was 300 °C and a combined EI/CI ion volume was installed. The filament delay was 3.90 min and the acquisition was performed between 4 and 23 min. For the CI mode methane 5.5 (Air Liquide, Düsseldorf, Germany) at a flow rate of $2 \text{ mL} \times \text{min}^{-1}$ was used. The Thermo GC trace 1310 coupled to a TriPlus RSH auto sampler was used with the following parameters: After initial 2 minutes at 40 °C the GC oven temperature was raised to 325 °C with $15 \text{ °C} \times \text{min}^{-1}$ and held for 2 min at 325 °C. The PTV injector was operated in split mode at 250 °C with a flow rate of $16 \text{ mL} \times \text{min}^{-1}$, split flow was 16 and the column flow $1 \text{ mL} \times \text{min}^{-1}$ in constant flow mode. The septum pure flow was set to $2 \text{ mL} \times \text{min}^{-1}$. After initial one minute at 250 °C the injector was

raised to 350 °C for one minute with a flow rate of 50 mL× min⁻¹ to clean the injector. The sample was injected using a 10 µL gas tight syringe after washing the syringe once with ethyl acetate and once with heptane. Before injection the syringe was rinsed thrice with 1 µL of the sample and three plunger strokes were applied to prevent air bubbles. Bottom sense was enabled and the sample was taken 0.2 mm above the bottom of the vial.

Results and discussion

Unfortunately, the expected mass of $m/z = 144$ was not detected by ESI MS (**Figure S4**). Instead, $m/z = 455.12$ and $m/z = 471.10$ were assigned to $[3M+Na]^+$ and $[3M+Na]^+$, respectively. These values could either result from physical adducts of three EtGly with a sodium or potassium ion, respectively, or from the isobaric macrocyclic trimer. Even if present only in trace amounts, the macrocyclic trimer could potentially be favorably ionized due to an easy complexation of the cation.¹ Aiming towards a distinction of the two possibilities, GC HRMS measurements were conducted utilizing both, EI as well as CI MS. **Figure S5** depicts the chromatograms of the total ion current (TIC). As confirmed by the EI and CI mass spectra, EtGly eluted at 9 min (group A, **Figure S6**). Additional peaks were detected at higher elution times, corresponding to column temperatures above 250 °C. Their intensity was significantly higher in GC-MS using EI compared to GC-MS performed with the milder CI method. The peaks were assigned to macrocycles composed of two or three EtGly, respectively. Similar species have been commonly detected by pyrolysis GC-MS of PLA,²⁻⁵ where various GC fractions were assigned to diastereomers. As a) such high temperatures come close to experimental conditions for GC-MS pyrolysis of PLA,² and b) PEtGly was prone to thermal degradation at even lower temperatures (see below for TGA thermograms), it could not be excluded that the monomer EtGly was prone to reaction during the GC MS analysis, thereby producing the detected macrocycles.

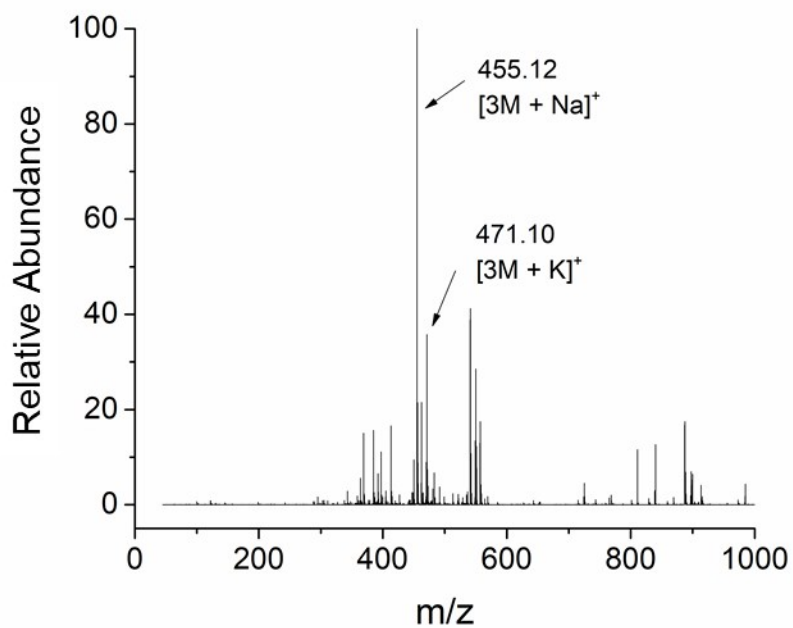


Figure S4: ESI mass spectrum (positive mode) of the monomer EtGly and structural assignments.

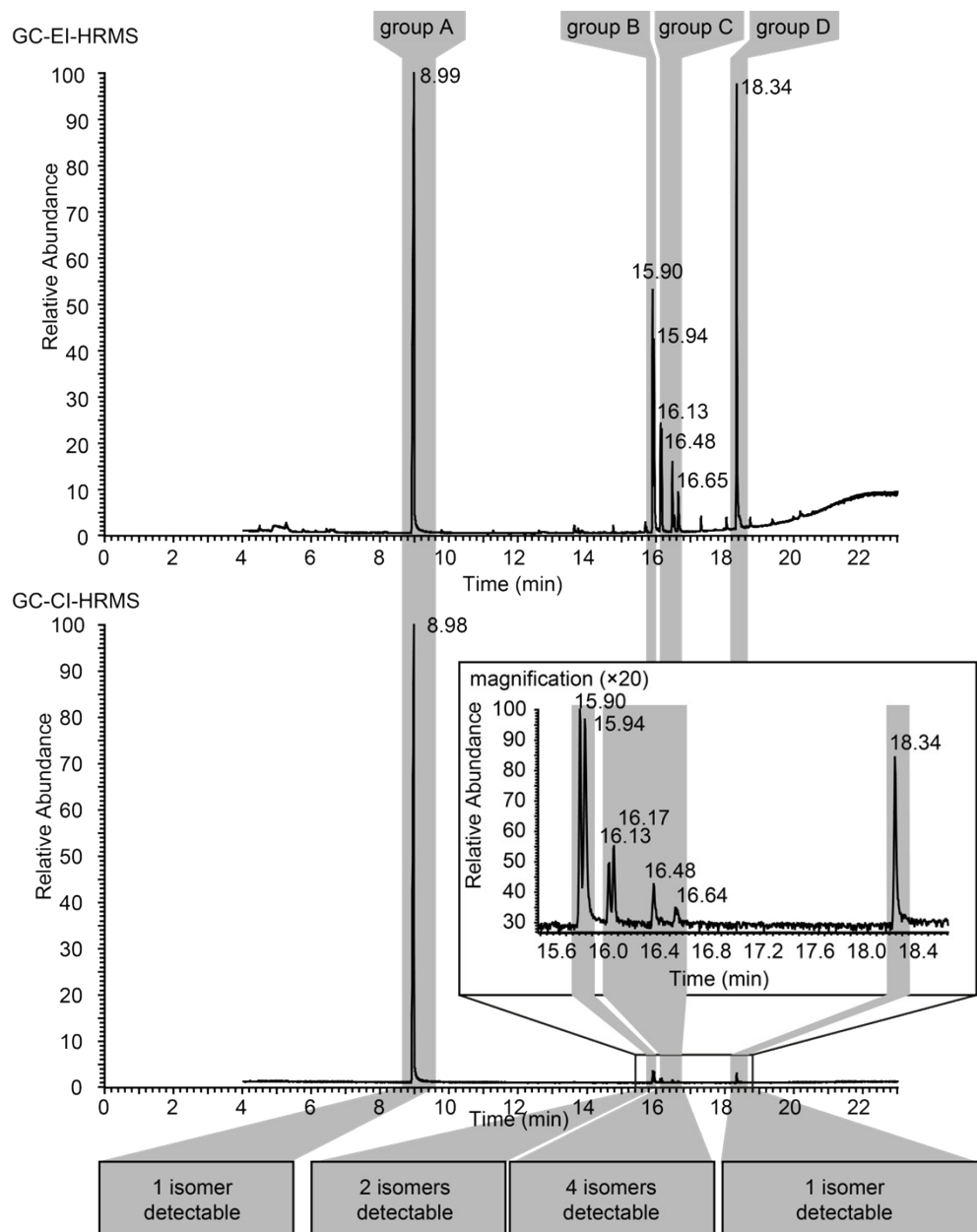
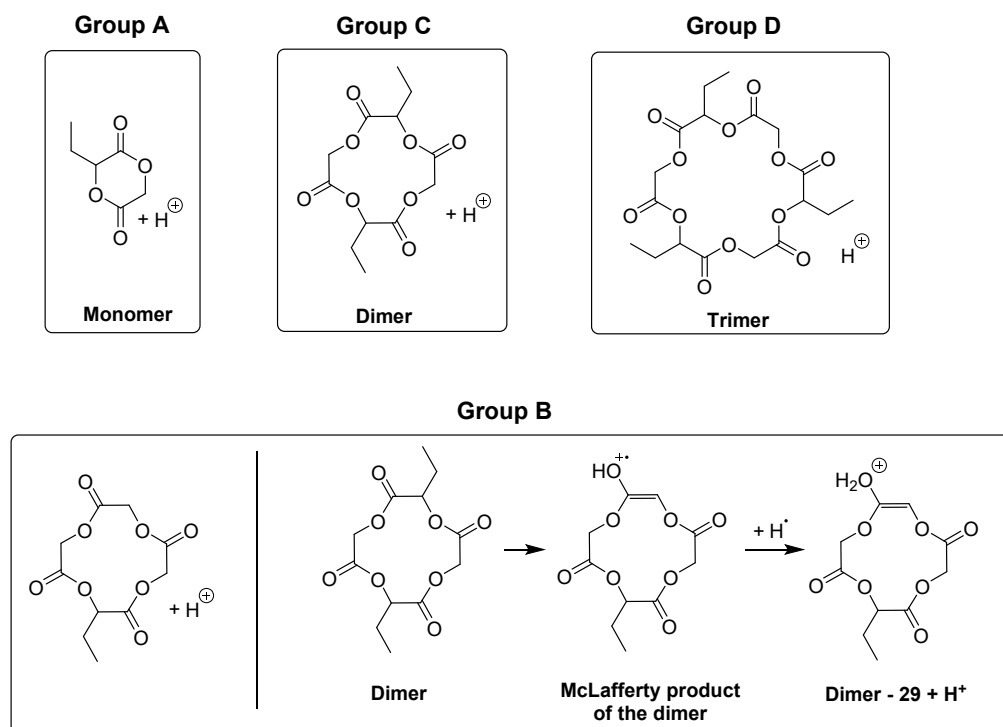


Figure S5: GC-chromatograms of the total ion current (TIC) of EtGly. **Top:** TIC from EI-ionization. **Bottom:** TIC from CI ionization including magnification. Based on their mass spectra, the peaks were assigned to four different compound groups (A to D, see **Table S1** and **Scheme S1**).

Table S1: Assignment of the peaks detected during GC-MS analysis of EtGly. TIC are depicted in Figure S5.

Peak number	t_{el} [min]	Group	Assignment	m/z CI [M+H] +	m/z EI
1	8.99	A	monomer	145	116; 58
2	15.90	B	dimer – 29 ^{a)}	261	244; 168; 128; 101
3	15.94	B	dimer – 29 ^{a)}	261	244; 168; 128; 101
4	16.13	C	dimer	289	272; 214; 186; 128; 70
5	16.17	C	dimer	289	272; 214; 186; 128; 70
6	16.48	C	dimer	289	272; 214; 186; 128; 70
7	16.64	C	dimer	289	272; 214; 186; 128; 70
8	18.34	D	trimer	433	272; 186; 128

^{a)} Compare **Scheme S1**.



Scheme S1: Schematic representation of the structure of the different species assigned by GC-MS analysis. The structure assigned to group B signals can either represent the protonized

molecular ion depicted on the bottom left, or be formed by McLafferty rearrangement of the dimer followed by addition of a hydrogen radical during CI.

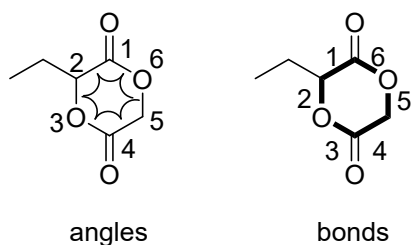


Figure S6: Schematic representation of the bond angles and lengths of the endocyclic atoms of EtGly used in **Table S1**.

Table S2: Bond angles and lengths of the endocyclic atoms of EtGly.

M1	1	2	3	4	5	6
Bond angle [°]	116.3	110.9	117.3	116.7	113.6	118.7
Bond length [Å]	1.51	1.46	1.34	1.50	1.44	1.34

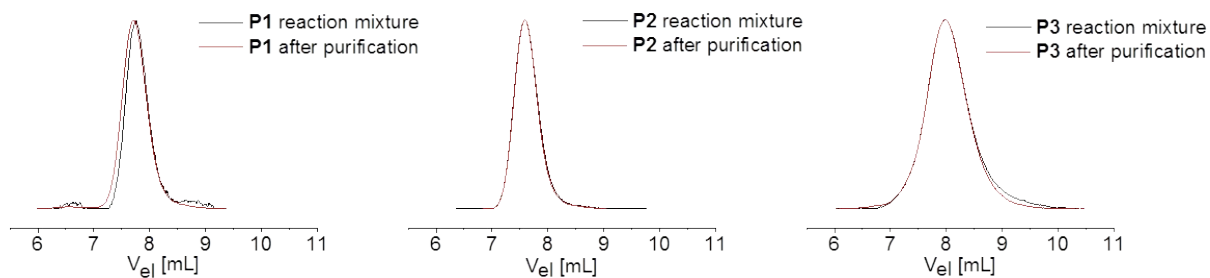


Figure S7: SEC elugrams (CHCl_3 , RI detection) of the homopolymers from reaction mixture (black) and after purification (red). **Right:** PLLA (**P1**). **Center:** P2 PDLA (**P2**). **Left:** PEtGly (**P3**).

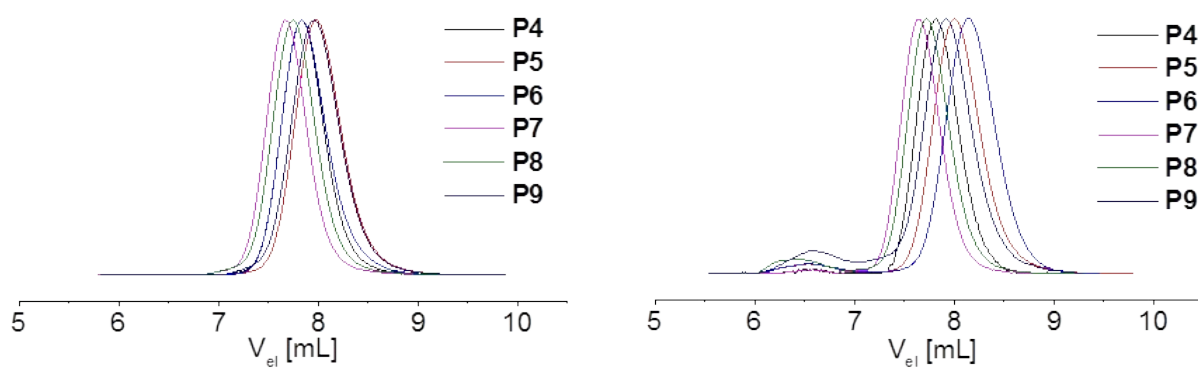


Figure S8: SEC elugrams (CHCl_3 , RI detection) of the statistical copolymers **P4-P9**. **Left:** Elugrams after quenching of the polymerization solution. **Right:** Elugrams after precipitation.

Poly(L-lactide) (P1):

800 mg L-Lactide (5.55 mmol) were dissolved in 18.50 mL toluene and the ROP was initiated using 111 μ L stock solution consisting of 5.74 μ L BnOH (0.06 mmol), 7.97 μ L mTBD (0.06 mmol) and 97.29 μ L toluene. The polymerization was quenched by addition of 27.4 mg benzoic acid (0,22 mmol).

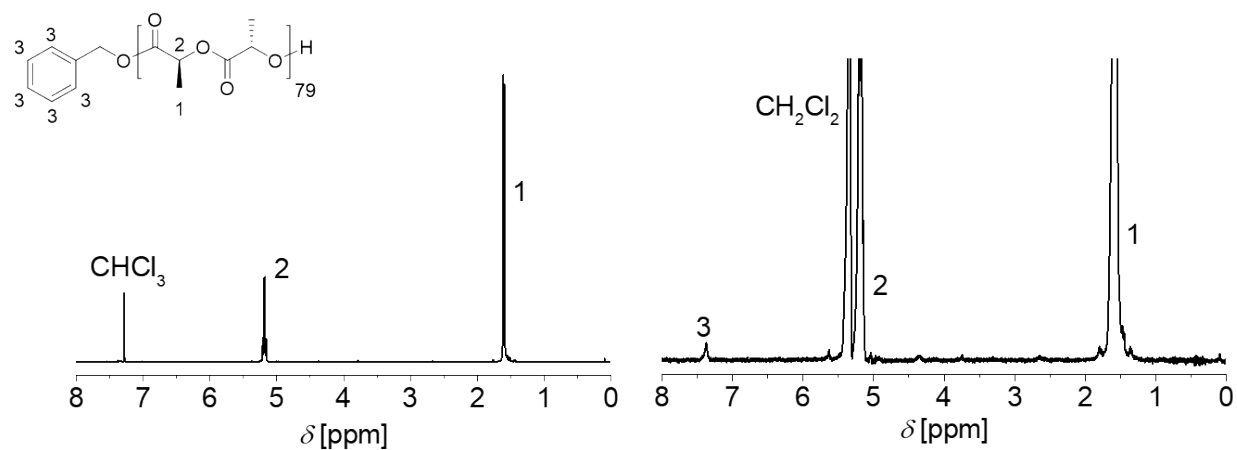


Figure S9: ^1H NMR characterization of PLLA (**P1**) and structural assignment of the signals. **Left:** ^1H NMR spectrum (400 MHz) in CDCl_3 . **Right:** ^1H NMR spectrum (300 MHz) in CD_2Cl_2 .

Poly(D-lactide) (P2):

800 mg D-Lactide (5.55 mmol) in 18.50 mL toluene and 111 μL stock solution containing 5.74 μL BnOH (0.06 mmol), 7.97 μL mTBD (0.06 mmol) and 97.29 μL toluene were used. The quenching was performed using 27.4 mg benzoic acid (0.22 mmol).

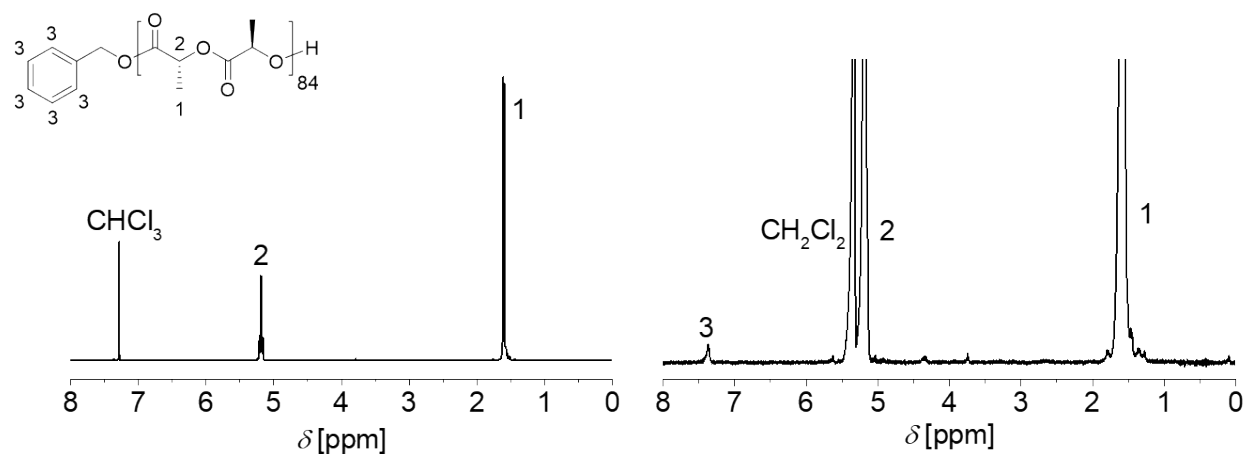


Figure S10: ^1H NMR characterization of PDLA (P2) and structural assignment of the signals. **Left:** ^1H NMR spectrum (400 MHz) in CDCl_3 . **Right:** ^1H NMR spectrum (300 MHz) in CD_2Cl_2 .

Poly(3-ethylglycolide) (P3):

535 mg EtGly (3.72 mmol) in 12.37 mL toluene and 74.24 μL stock solution consisting of 3.84 μL BnOH (0.04 mmol), 5.33 μL mTBD (0.04 mmol) and 65.07 μL toluene were utilized. The quenching was performed using 20.22 mg benzoic acid (0.17 mmol) dissolved in chloroform. Conversion was calculated from GC analysis.

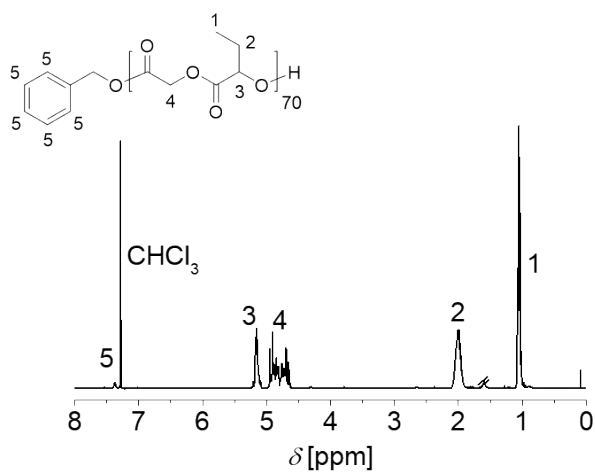


Figure S11: ^1H NMR spectrum (400 MHz, CDCl_3) of **P3** and structural assignment of the signals.

Poly(L-lactide-*stat*-3-ethylglycolide) (P4):

352 mg L-Lactide (2.44 mmol) and 19 mg EtGly (0.13 mmol) were used according to the general procedure in order to obtain a copolymer with 5% EtGly content.

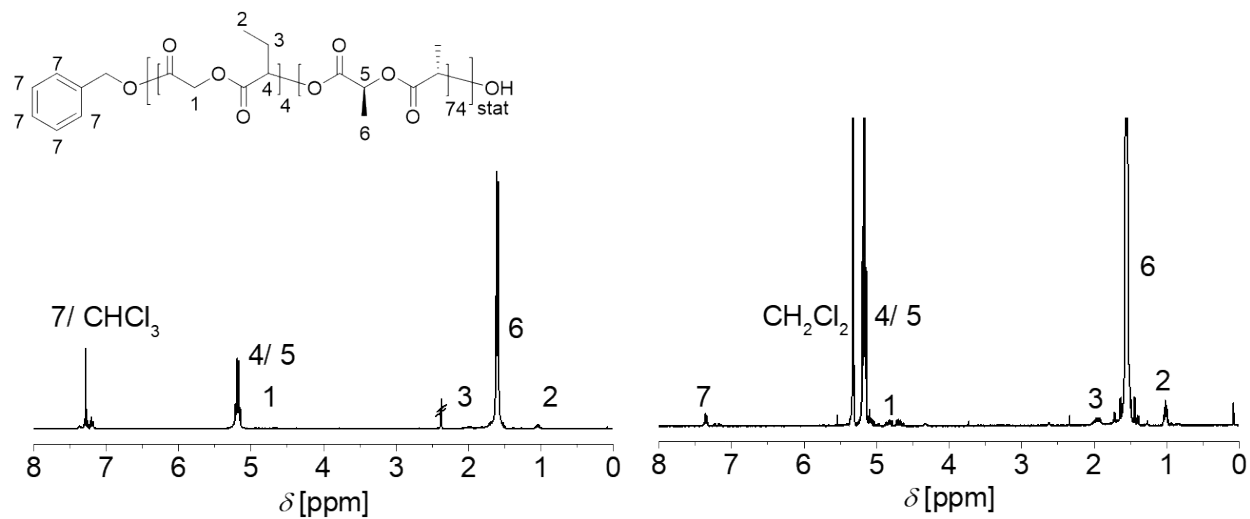


Figure S12: ¹H NMR characterization of **P4** and structural assignment of the signals. **Left:** ¹H NMR spectrum (300 MHz) in CDCl₃. **Right:** ¹H NMR spectrum (300 MHz) in CD₂Cl₂.

Poly(L-lactide-*stat*-3-ethylglycolide) (P5):

333 mg L-Lactide (2.31 mmol) and EtGly 37 mg (0.26 mmol) were used according to the general procedure in order to obtain a copolymer with 10% EtGly content.

P(LLA-*stat*-EtGly) (P5): feed LLA / EtGly = 90 / 10; conv = 74%; yield = 61%. $^1\text{H NMR}$ (300 MHz, CDCl_3): δ /ppm = 1.00 – 1.07 (br, 24H, H-2), 1.59 – 1.60 (br, 428H, H-6), 1.89 – 2.09 (br, 17H, H-3), 4.59 – 4.94 (br, 16H, H-1), 5.09 – 5.21 (br, 140H, H-4, H-5), $^1\text{H NMR}$ (300 MHz, CD_2Cl_2): δ = 1.04 – 1.06 (br, 25H, H-2), 1.45 – 1.63 (br, 484H, H-6), 1.93 – 2.06 (br, 18H, H-3), 4.67 – 4.90 (br, 17H, H-1), 5.10 – 5.23 (br, 142H, H-4, H-5), 7.39 (br, 5H, H-7); SEC (CHCl_3 , PS calibration): $M_n = 13 \text{ kg mol}^{-1}$; $D = 1.20$.

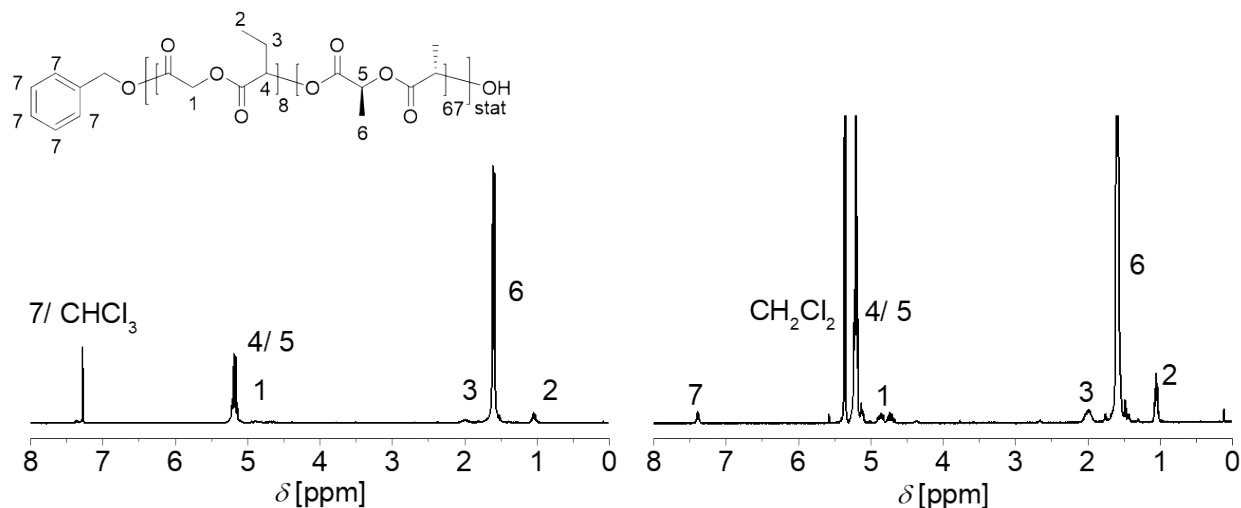


Figure S13: $^1\text{H NMR}$ characterization of P5 and structural assignment of the signals. **Left:** $^1\text{H NMR}$ spectrum (300 MHz) in CDCl_3 . **Right:** $^1\text{H NMR}$ spectrum (300 MHz) in CD_2Cl_2 .

Poly(L-lactide-*stat*-3-ethylglycolide) (P6):

296 mg L-Lactide (2.05 mmol) and 74.0 mg EtGly (0.51 mmol) were used according to the general procedure in order to obtain a copolymer with 20% EtGly content.

P(LLA-*stat*-EtGly) (P6): feed LLA / EtGly = 80 / 20; conv = 69%; yield = 61 %. $^1\text{H NMR}$ (300 MHz, CDCl_3): δ /ppm = 1.00 – 1.07 (br, 45H, H-2), 1.50 – 1.61 (br, 336H, H-6), 1.91 – 2.06 (br, 32H, H-3), 4.59 – 4.94 (br, 30H, H-1), 5.10 – 5.24 (br, 120H, H-4, H-5), $^1\text{H NMR}$ (300 MHz, CD_2Cl_2): δ = 1.04 – 1.07 (br, 46H, H-2), 1.47 – 1.60 (br, 373H, H-6), 1.93 – 2.08 (br, 32H, H-3), 4.67 – 4.91 (br, 30H, H-1), 5.12 – 5.23 (br, 119H, H-4, H-5), 7.40 (br, 5H, H-7); SEC (CHCl_3 , PS calibration): $M_n = 12 \text{ kg mol}^{-1}$; $D = 1.23$.

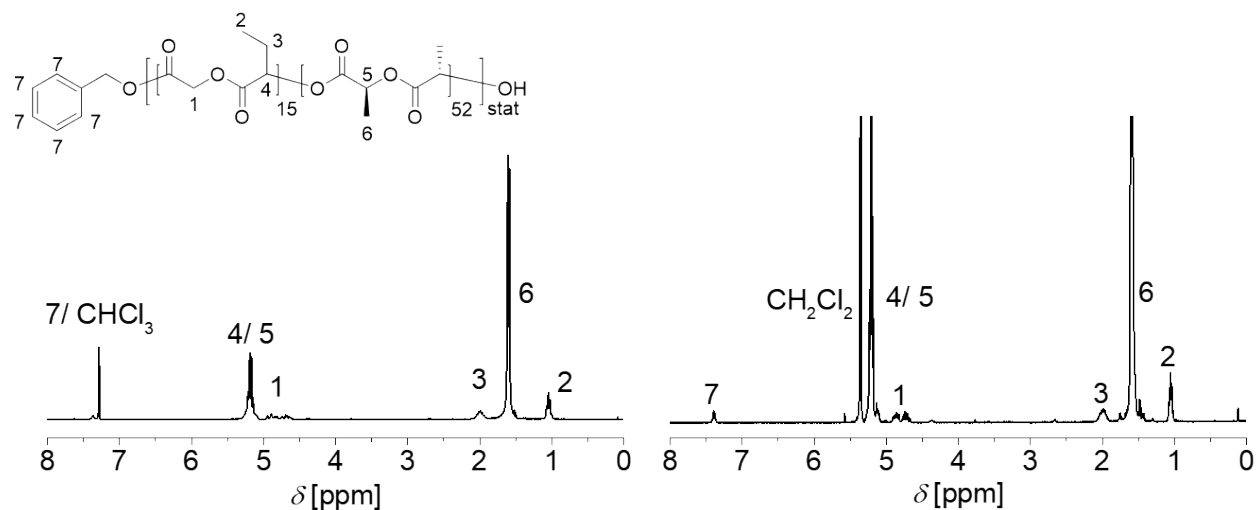


Figure S14: $^1\text{H NMR}$ characterization of P6 and structural assignment of the signals. **Left:** $^1\text{H NMR}$ spectrum (300 MHz) in CDCl_3 . **Right:** $^1\text{H NMR}$ spectrum (300 MHz) in CD_2Cl_2 .

Poly(L-lactide-*stat*-3-ethylglycolide) (P7):

352 mg D-Lactide (2.44 mmol) and 19 mg EtGly (0.13 mmol) were used according to the general procedure in order to obtain a copolymer with 5% EtGly content.

P(DLA-*stat*-EtGly) (P7): feed DLA / EtGly = 95 / 05; conv = 77%; yield = 72%. ^1H NMR (300 MHz, CDCl_3): δ /ppm = 1.02 – 1.07 (br, 9H, H-2), 1.50 – 1.71 (br, 461H, H-6), 1.89 – 2.06 (br, 7H, H-3), 4.59 – 4.94 (br, 6H, H-1), 5.10 – 5.21 (br, 145H, H-4, H-5), ^1H NMR (300 MHz, CD_2Cl_2): δ = 1.04 – 1.06 (br, 11H, H-2), 1.47 – 1.60 (br, 555H, H-6), 1.93 – 2.08 (br, 8H, H-3), 4.67 – 4.91 (br, 7H, H-1), 5.13 – 5.23 (br, 157H, H-4, H-5), 7.40 (br, 5H, H-7); SEC (CHCl_3 , PS calibration): M_n = 19 kg mol $^{-1}$; D = 1.10.

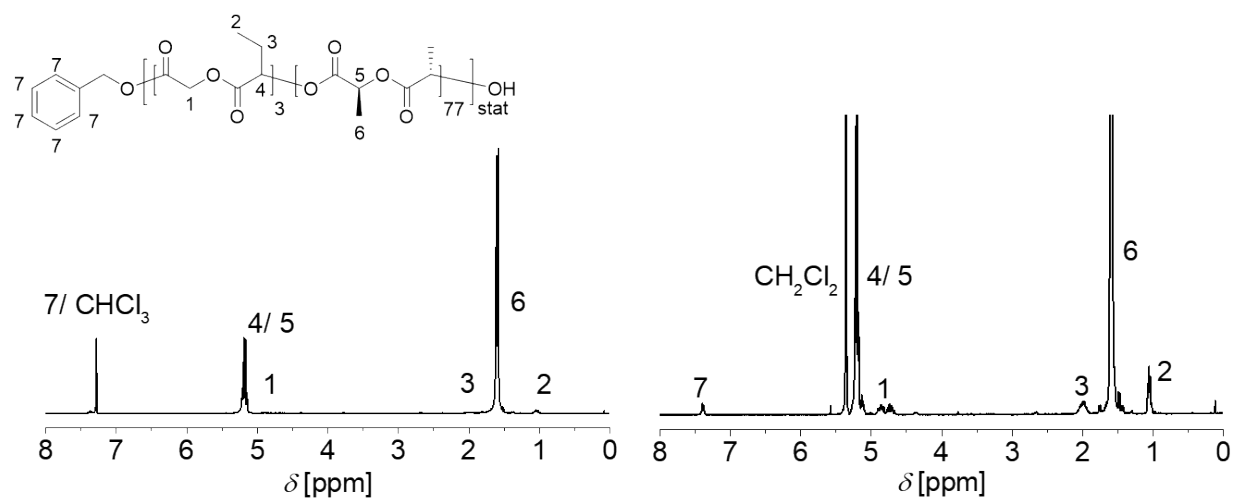


Figure S15: ^1H NMR characterization of P7 and structural assignment of the signals. **Left:** ^1H NMR spectrum (300 MHz) in CDCl_3 . **Right:** ^1H NMR spectrum (300 MHz) in CD_2Cl_2 .

Poly(L-lactide-*stat*-3-ethylglycolide) (P8):

333 mg D-Lactide (2.31 mmol) and 37 mg EtGly (0.26 mmol) were used according to the general procedure in order to obtain a copolymer with 10% EtGly content.

P(DLA-*stat*- EtGly) (P8): feed DLA / EtGly = 90 / 10; conv = 79%; yield = 71%. ^1H NMR (300 MHz, CDCl_3): δ [ppm] = 0.96 – 1.07 (br, 21H, H-2), 1.47 – 1.80 (br, 450, H-6), 1.92 -2.07 (br, 16H, H-3), 4.59 – 4.94 (br, 14H, H-1), 5.10 – 5.21 (br, 145H, H-4, H-5), ^1H NMR (300 MHz, CD_2Cl_2): δ = 1.04 – 1.06 (br, 23H, H-2), 1.49 – 1.60 (br, 513H, H-6), 1.92 – 2.08. (br, 16H, H-3), 4.67 – 4.91 (br, 14H, H-1), 5.10 – 5.23 (br, 149H, H-4, H-5), 7.39 (br, 5H, H-7); SEC (CHCl_3 , PS calibration): M_n = 18 kg mol $^{-1}$; D = 1.21.

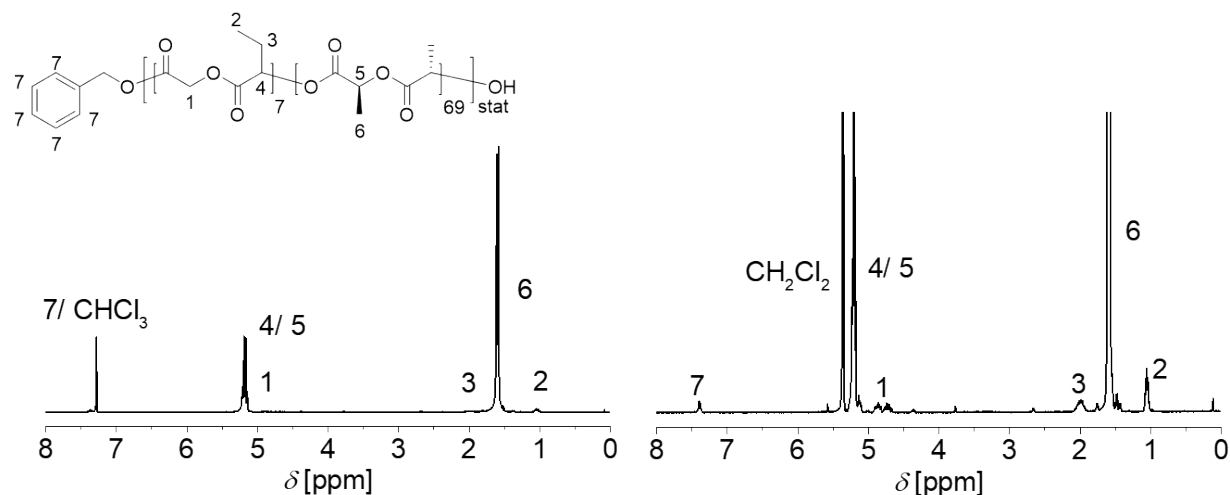


Figure S16: ^1H NMR characterization of **P8** and structural assignment of the signals. **Left:** ^1H NMR spectrum (300 MHz) in CDCl_3 . **Right:** ^1H NMR spectrum (300 MHz) in CD_2Cl_2 .

Poly(L-lactide-*stat*-3-ethylglycolide) (P9):

296 mg D-Lactide (2.05 mmol) and 74.0 mg EtGly (0.51 mmol) were used according to the general procedure in order to obtain a copolymer with 20% EtGly content.

P(DLA-*stat*-EtGly) (P9): feed DLA / EtGly = 80 / 20; conv = 77%; yield = 63%. ^1H NMR (300 MHz, CDCl_3): δ [ppm] = 1.00 – 1.07 (br, 48H, H-2), 1.50 – 1.80 (br, 354, H-6), 1.92 – 2.09 (br, 32H, H-3), 4.59 – 4.94 (br, 31H, H-1), 5.11 – 5.21 (br, 123H, H-4, H-5), ^1H NMR (300 MHz, CD_2Cl_2): δ = 1.04 – 1.07 (br, 51H, H-2), 1.47 – 1.60 (br, 426H, H-6), 1.93 – 2.08. (br, 36H, H-3), 4.67 – 4.91 (br, 32H, H-1), 5.11 – 5.23 (br, 129H, H-4, H-5), 7.40 (br, 5H, H-7); SEC (CHCl_3 , PS calibration): $M_n = 15 \text{ kg mol}^{-1}$; $D = 1.28$.

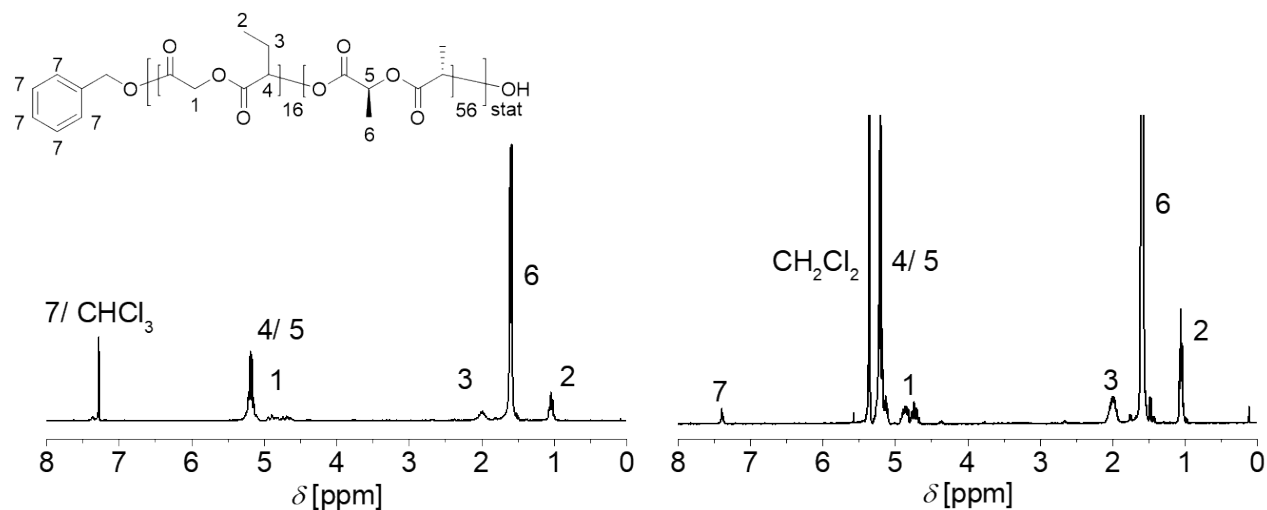


Figure S17: ^1H NMR characterization of P9 and structural assignment of the signals. **Left:** ^1H NMR spectrum (300 MHz) in CDCl_3 . **Right:** ^1H NMR spectrum (300 MHz) in CD_2Cl_2 .

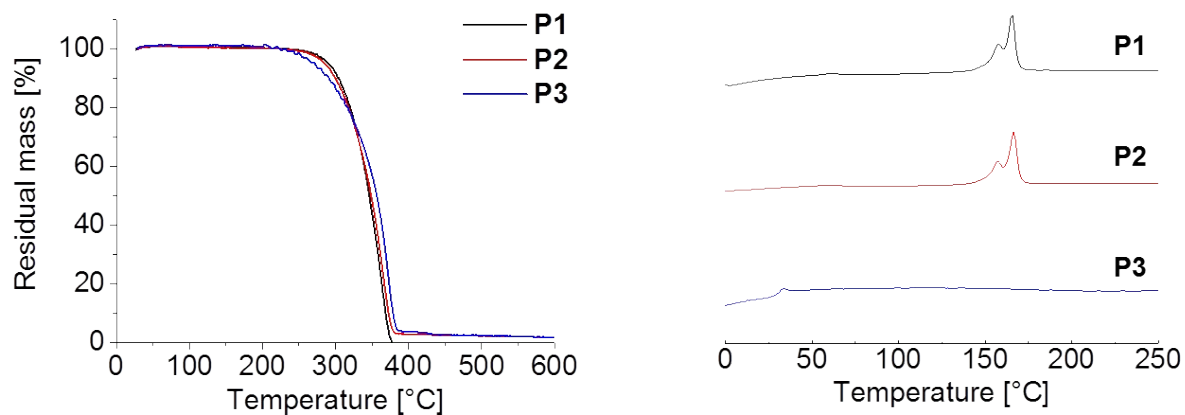


Figure S18: Thermal analysis of the homopolymers **P1** to **P3**. **Left:** TGA thermograms (nitrogen atmosphere, heating rate 20 K min⁻¹). **Right:** DSC thermograms from the first heating run (from –20 to 260 °C, heating rate 20 K min⁻¹).

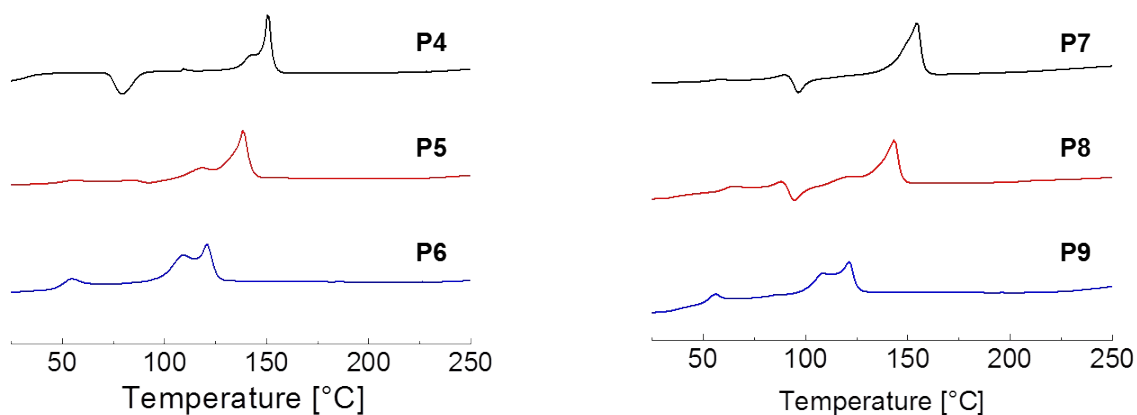


Figure S19: DSC thermograms of the copolyesters. The measurements were performed from –20 to 260 °C (first heating run, heating rate 20 K min⁻¹, cooling rate 20 K min⁻¹). **Left: P4 to P6** based on PLLA. **Right: P7 to P9** based on PDLA.

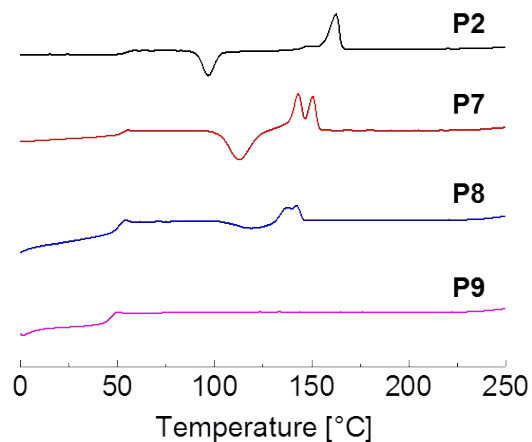


Figure S20: DSC thermograms of the PDLA based polyesters **P2** and **P7** to **P9**. The measurements were performed from -20 to 260 °C (third heating run, heating rate 10 K min^{-1} , cooling rate 20 K min^{-1}).

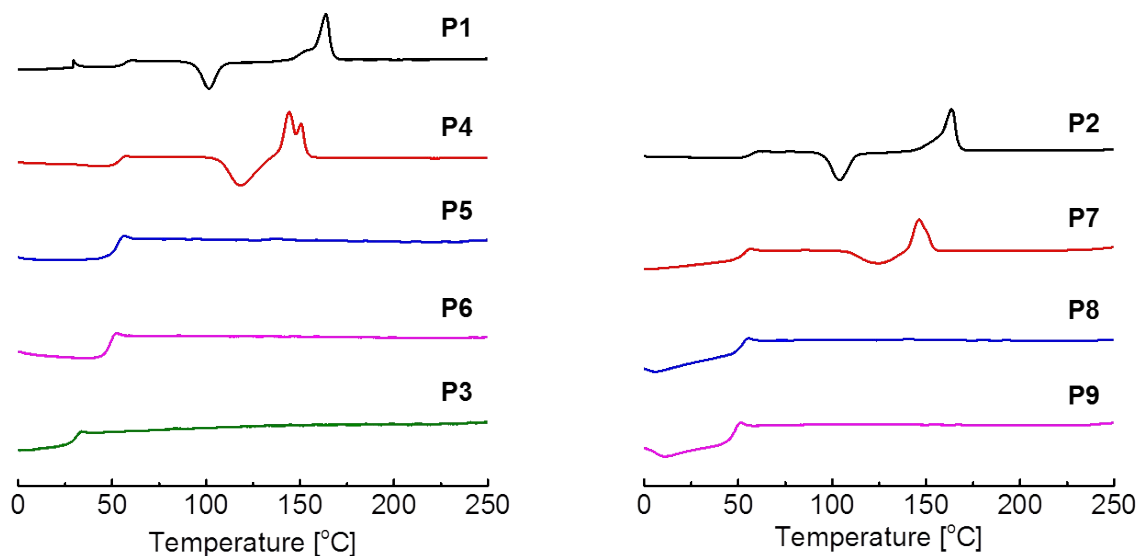


Figure S21: DSC thermograms of **P1** to **P9**. **Left:** PLLA based polyesters. **Right:** PDLA based polyesters. The measurements were performed from -20 to 260 °C (second heating run, heating rate 20 K min^{-1} , cooling rate 20 K min^{-1}).

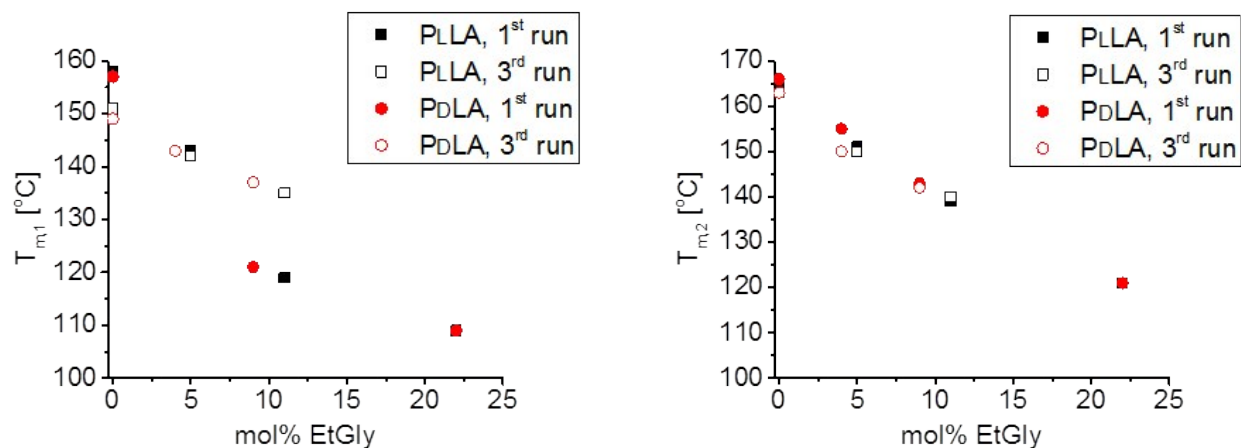


Figure S22: Influence of the molar fraction of EtGly on the melting temperatures of the copolyester series based on PLLA (**P1**, **P3** to **P6**) and on PDLA (**P2**, **P7** to **P9**) as determined *via* DSC analysis (cooling rates: 20 K min⁻¹, heating rate in the first run: 20 K min⁻¹, heating rate in the third run: 10 K min⁻¹). **Left:** First event of fusion ($T_{m,1}$). **Right:** Second event of fusion ($T_{m,2}$).

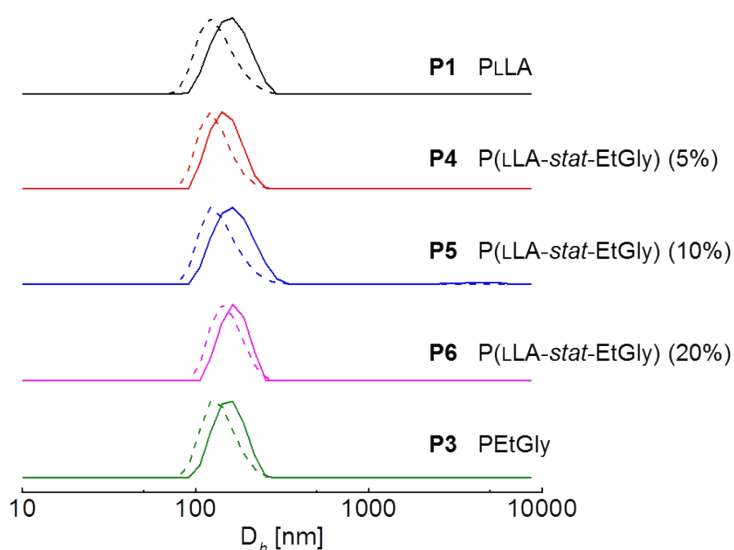
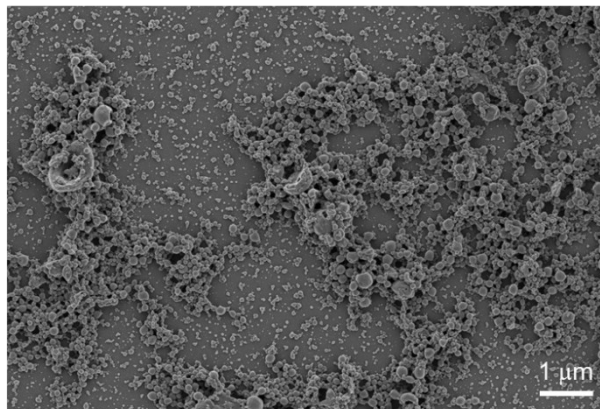
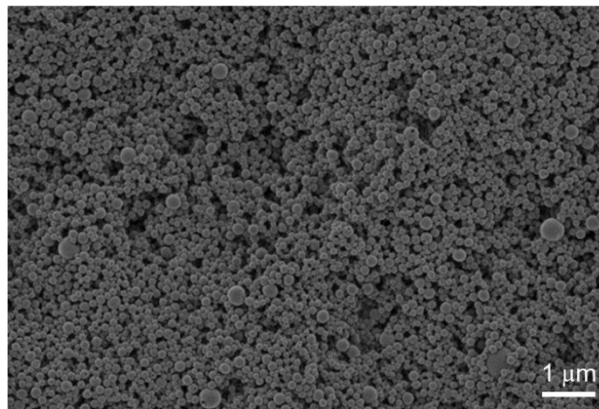


Figure S23: DLS size distributions of the nanoparticles prepared from **P1** and **P3** to **P6** with hydrodynamic diameters of $D_h \approx 150$ nm. The full lines represent the intensity weighted data, the dotted lines represent the number weighted data.

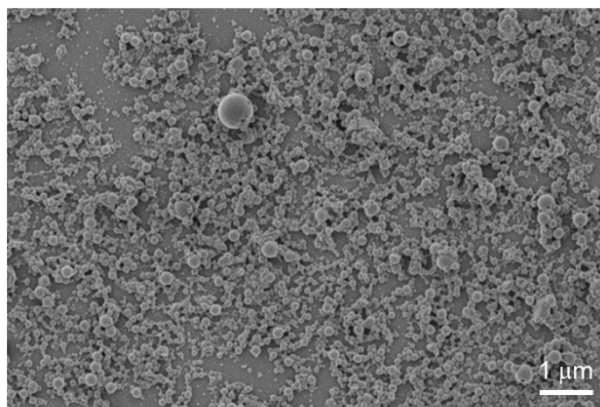
P1 (PLLA)



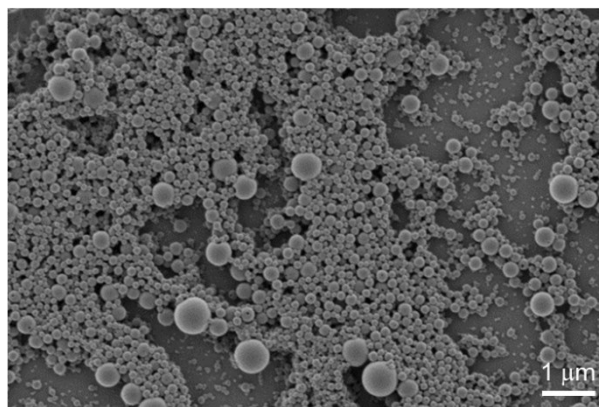
P4 (PLLA-*stat*-EtGly) (5%)



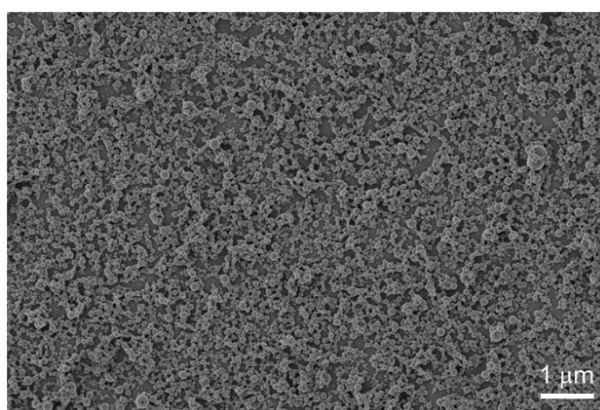
P5 (PLLA-*stat*-EtGly) (10%)



P6 (PLLA-*stat*-EtGly) (20%)



P8 (PDLA-*stat*-EtGly) (10%)



P9 (PDLA-*stat*-EtGly) (20%)

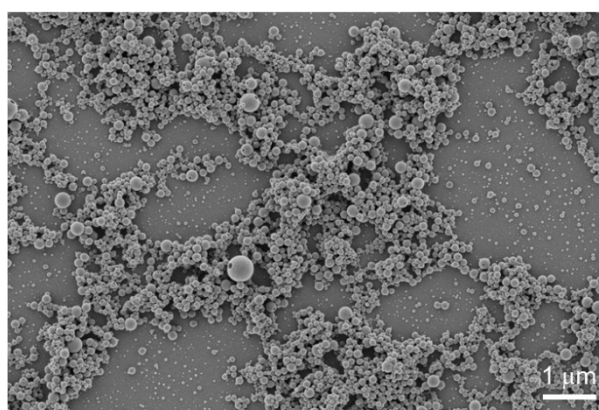


Figure S24: SEM images of dried nanoparticles prepared by nanoprecipitation. Scale bars represent 1 μm .

Table S3: Summary of nanoparticle size distributions, ζ -potential and fluorescence band ratio of the pyrene (Py) loaded nanoparticles.

Polymer	c(P1 to P3) in THF [mg mL ⁻¹]	c(Py) in THF [mg mL ⁻¹]	c(P1 to P3) in H ₂ O [mg mL ⁻¹]	c(Py) in H ₂ O [mg mL ⁻¹]	ζ [mV]	D _h [nm]	PDI	I ₁ / I ₃ ¹
P1	4.75	0.05	0.475	0.005	-33	149	0.13	1.26
P2	4.75	0.05	0.475	0.005	-39	149	0.11	1.29
P3	1.425	0.015	0.1425	0.0015	-33	171	0.20	1.25

¹ Fluorescence spectra recorded using 100 fold diluted nanoparticle suspensions.

References

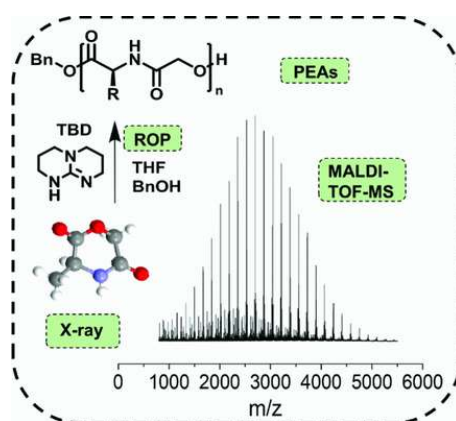
- [1] Prestegard, J. H.; Chan, S. I., Proton magnetic resonance studies of the cation-binding properties of nonactin. II. Comparison of the sodium ion, potassium ion, and cesium ion complexes. *J. Am. Chem. Soc.* **1970**, *92*, 4440-4446.
- [2] Aoyagi, Y.; Yamashita, K.; Doi, Y., Thermal degradation of poly[(R)-3-hydroxybutyrate], poly[ϵ -caprolactone], and poly[(S)-lactide]. *Polym. Degrad. Stabil.* **2002**, *76*, 53-59.
- [3] Arrieta, M. P.; Parres, F.; López, J.; Jiménez, A., Development of a novel pyrolysis-gas chromatography/mass spectrometry method for the analysis of poly(lactic acid) thermal degradation products. *J. Anal. Appl. Pyrolysis* **2013**, *101*, 150-155.
- [4] Khabbaz, F.; Karlsson, S.; Albertsson, A.-C., PY-GC/MS an effective technique to characterizing of degradation mechanism of poly (L-lactide) in the different environment. *J. App. Polym. Sci.* **2000**, *78*, 2369-2378.
- [5] Kopinke, F. D.; Remmler, M.; Mackenzie, K.; Möder, M.; Wachsen, O., Thermal decomposition of biodegradable polyesters—II. Poly(lactic acid). *Polym. Degrad. Stabil.* **1996**, *53*, 329-342.

Publication P6

TBD-Catalyzed Ring-Opening Polymerization of alkyl-substituted Morpholine-2,5-dione derivatives

M. Dirauf, D. Bandelli, C. Weber, H. Görls, M. Gottschaldt, U. S. Schubert,

Macromol. Rapid Commun. **2018**, *39*, 1800433.





TBD-Catalyzed Ring-Opening Polymerization of Alkyl-Substituted Morpholine-2,5-Dione Derivatives

Michael Dirauf, Damiano Bandelli, Christine Weber, Helmar Görls, Michael Gottschaldt, and Ulrich S. Schubert*

In a two-step synthesis, five different alkyl-substituted morpholine-2,5-dione monomers were synthesized from the natural amino acids glycine, alanine, valine, leucine, and isoleucine. The heterocyclic compounds crystallize in a boat-like conformation and are polymerized via 1,5,7-triazabicyclo[4.4.0]dec-5-ene (TBD)-catalyzed ring-opening polymerization (ROP) in tetrahydrofuran. Well-defined polymers could be obtained from the monomers based on valine, leucine, and isoleucine at a feed ratio of $M/I/TBD = 100/1/0.5$. Kinetic studies of the ROP reveal that the molar masses and dispersities ($\bar{M}_w/\bar{M}_n < 1.2$) could be well controlled, as confirmed by size exclusion chromatography and ^1H NMR spectroscopy. At conversions above 50%, the polymerization rate decreases and the dispersity slightly increases, presumably due to transesterification. Matrix-assisted laser desorption time-of-flight mass spectrometry indicates the presence of polymer chains with α -end groups derived from the initiator.

Among biocompatible and biodegradable polymers, polyesters represent the most commonly applied material in drug delivery research. In particular, poly(lactic acid) (PLA) is one of the most prominent and well-studied polyesters.^[1] Degradation occurs in alkaline environment or by enzymatic digestion.^[2,3] Poly(ester amide)s (PEAs) feature a rather similar degradation behavior as they contain hydrolysis-sensitive ester moieties alongside more stable amide bonds.^[4] The complete degradation of PEAs yields biocompatible hydroxy acids and amino acids, making them highly interesting for application in the field of drug delivery.^[5]

M. Dirauf, D. Bandelli, Dr. C. Weber, Prof. M. Gottschaldt, Prof. U. S. Schubert
Laboratory of Organic and Macromolecular Chemistry (IOMC)
Friedrich Schiller University Jena
Humboldtstr. 10, 07743 Jena, Germany
E-mail: ulrich.schubert@uni-jena.de

M. Dirauf, D. Bandelli, Dr. C. Weber, Prof. M. Gottschaldt, Prof. U. S. Schubert
Jena Center for Soft Matter
Friedrich Schiller University Jena
Philosophenweg 7, 07743 Jena, Germany
Dr. Helmar Görls
Laboratory of Inorganic and Analytical Chemistry (IAAC)
Friedrich Schiller University Jena
Humboldtstr. 8, 07743 Jena, Germany

The ORCID identification number(s) for the author(s) of this article can be found under <https://doi.org/10.1002/marc.201800433>.

DOI: 10.1002/marc.201800433

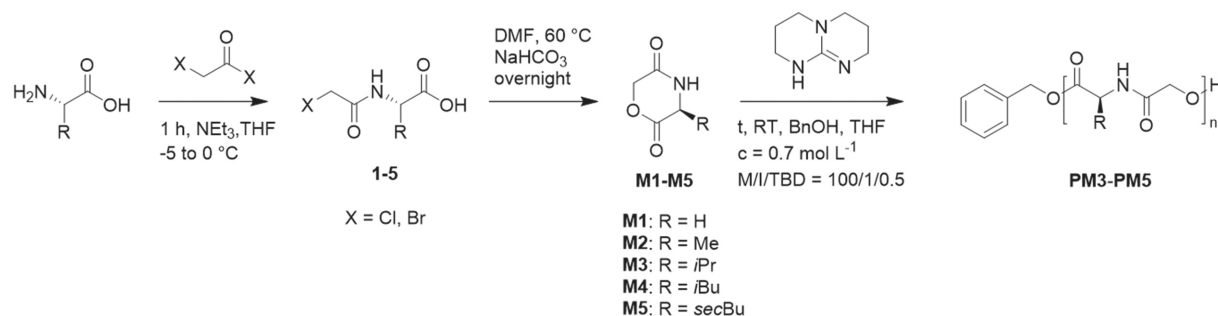
The ring-opening polymerization (ROP) of morpholine-2,5-dione derivatives represents one strategy to obtain PEAs.^[6–8] These heterocyclic monomers are commonly synthesized using natural amino acids as nonexpensive starting materials, which enables the adjustment of the resulting material properties by the choice of the amino acid.^[9] Similar to peptides, the substituent of the amino acid determines the hydrophilicity or lipophilicity of the resulting PEAs. As an example, polymers based on glycine or alanine would be less lipophilic than PEAs obtained from monomers made from the more hydrophobic valine, leucine, or isoleucine.

These monomers, that is, morpholine-2,5-dione^[10] (**M1**), (S)-3-methylmorpholine-2,5-dione^[11–13] (**M2**), and (S)-3-isobutylmorpholine-2,5-dione^[14] (**M4**), have

been reported to undergo homopolymerization by ROP in the presence of tin(II)-octoate ($\text{Sn}(\text{Oct})_2$), that is, the standard catalyst that is also used for the ROP of lactide. Feng et al. reported the polymerization of (S)-3-*iso*-propylmorpholine-2,5-dione (**M3**) in the presence of a lipase as a catalyst.^[15,16] Recently, a range of other metal alkoxides and acetates were applied as catalysts for the ROP of (S)-3-((S)-*sec*-butyl)morpholine-2,5-dione (**M5**).^[17]

All these polymerization procedures represent bulk reactions that are performed typically at temperatures above 100 °C. Besides the activity of the catalyst, the melting temperature of the monomer represents a limiting factor that prohibits an ROP under milder conditions. In consequence, current research is directed toward the copolymerization of morpholine-2,5-dione derivatives with lactide or glycolide.^[18–22] Although this approach helps to overcome the comparably low reactivity of the morpholine-2,5-diones,^[23] these $\text{Sn}(\text{Oct})_2$ -catalyzed bulk polymerizations still have to be performed at 120 °C due to the low activity of the catalyst.

On the other hand, highly potent organocatalysts for the ROP of cyclic esters or lactones in solution have been developed within the last decade.^[24] 1,5,7-Triazabicyclo[4.4.0]dec-5-ene (TBD),^[25–27] 1,8-diazabicyclo[5.4.0]undec-7-ene (DBU), or 7-methyl-1,5,7-triazabicyclo[4.4.0]dec-5-ene (MTBD) represent heterocyclic guanidine-based organobases suitable for this purpose. Among these, TBD is the most active catalyst^[28] and could, therefore, be able to compensate the relatively low reactivity of the morpholine-2,5-dione derivatives. Some organocatalysts



Scheme 1. Schematic representation of the synthetic approach toward well-defined polyesteramides.

have been investigated for the ROP of morpholine-2,5-diones with varied success.^[29,30]

However, to the best of our knowledge, a mild polymerization procedure of these cyclic monomers toward well-defined PEAs is missing to date. Due to the high melting temperatures of the monomers, an ROP suitable for this purpose must be performed in solution. This contribution describes the development of such ROP conditions for morpholine-2,5-dione derivatives based on glycine, alanine, valine, leucine, and isoleucine (**Scheme 1**).

Experimental Section

Our synthetic approach included the synthesis of five monomers, a broad variation of polymerization parameters to identify the optimum ROP conditions for these monomers to yield PEAs that are well defined in terms of molar mass, dispersity, and end groups. Subsequently, the TBD-catalyzed ROP in tetrahydrofuran (THF) at room temperature was investigated in depth by kinetic studies and matrix-assisted laser desorption ionization time-of-flight mass spectrometry (MALDI TOF MS).

In a modified literature approach,^[31,32] the monomer synthesis was accomplished via a two-step reaction starting from the natural L-amino acids. In a first step, a linear precursor molecule was obtained via an amidation reaction using either chloroacetyl chloride or bromoacetyl bromide. The subsequent intramolecular cyclization reaction was performed in a highly diluted DMF solution at 60 °C overnight to avoid the formation of oligomers. The optimized procedure was based on the use of chloroacetyl chloride and the cyclization of the nonrecrystallized

precursor, resulting in overall yields between 22% and 34% (see Supporting Information). The yields are comparable to those achieved via similar synthetic procedures reported in the literature.^[16,33,34]

In addition to the full characterization of the monomers by means of elemental analysis, mass spectrometry, NMR, and IR spectroscopy, the crystal structures of **M2** to **M5** were determined by X-ray crystallography (**Figure 1**). Urpi et al. reported a skew-boat conformation for **M1**, which was also found for **M2–M5**.^[35] Regardless of the amino acid, all substituents were located in the bowsprit position. A comparison of the bond angles shows the contribution of the planar geometry of the amide nitrogen atom ($119^\circ < \alpha 5 < 122^\circ$) to the ring strain. The sp^3 hybridized carbon atom carrying the substituent derived from the amino acid features a tetrahedral geometry ($108^\circ < \alpha 6 < 110^\circ$). In contrast, the bond angle around the methylene carbon atom is considerably enlarged ($111^\circ < \alpha 3 < 115^\circ$), hinting toward a higher ring strain at the glycolide section of the six-membered ring. Further discussion regarding the packing in the solid state and the contribution of hydrogen bonds is provided in the Supporting Information.

Intending a polymerization of the monomers **M1–M5** in solution, solubility tests represented the initial step. The more hydrophobic **M3–M5** were well soluble in THF, which represents a commonly used solvent for the ROP of, for example, lactide.^[36,37] In contrast, **M1** and **M2** could only be solubilized in more polar solvents, such as *N,N*-dimethylformamide, refluxing nitromethane or 0.5 M LiCl solution in THF. As homogeneous polymerization attempts using TBD as a catalyst and benzyl alcohol (BnOH) as an initiator failed in these solvents, an ROP in THF suspension was performed. Although size exclusion chromatography (SEC) analysis of the resulting polymers revealed multimodal molar mass distributions, the ROP proceeded at room temperature ($M/I/TBD = 100/1/0.1$), and molar masses of up to

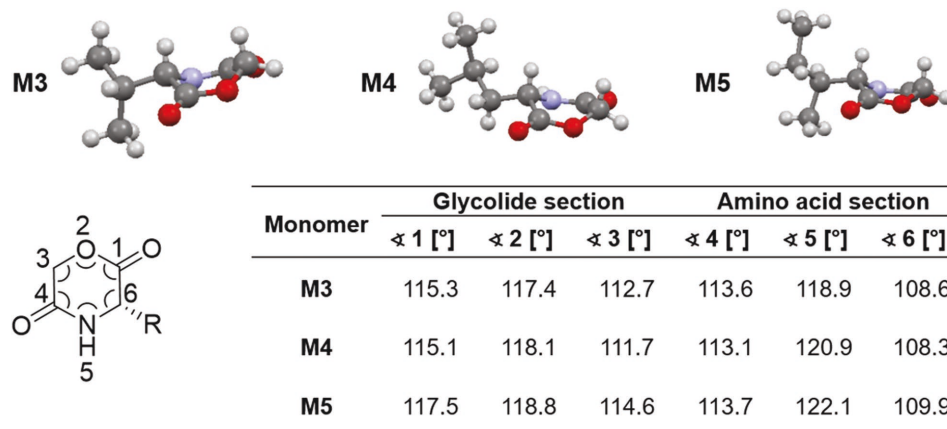


Figure 1. Boat-like conformation and selected bond angles of the monomers **M3–M5** obtained by X-ray crystallography. Standard deviation is omitted in view of clarity. The colored images are depicted in the Supporting Information.

6500 g mol⁻¹ were obtained ($\bar{D} \leq 1.41$, see Supporting Information), hinting toward the fact that TBD was capable of catalyzing the ROP of the morpholine-2,5-diones.

In consequence, the system THF/BnOH/TBD was further investigated using **M4** as a monomer that is soluble under these conditions. At a constant monomer concentration of 0.7 mol L⁻¹ and an M/I ratio of 100, the polymerization time and the catalyst concentration were varied. Irrespective of the polymerization time, only monomer conversions below 20% were achieved at an M/I/TBD ratio of 100/1/0.1, although unimodal molar mass distributions were evident after SEC analysis. An increased amount of TBD (M/I/TBD = 100/1/0.5) resulted in conversions above 80% but broad molar mass distributions ($1.7 \leq \bar{D} \leq 3.1$) at polymerization times above 1 h. In contrast, a PEA with a narrow and unimodal molar mass distribution ($\bar{D} = 1.12$) was obtained after a polymerization time of 30 min, showing that these ROP conditions were promising to obtain well-defined PEAs under mild conditions.

Polymerization kinetics was hence studied for **M3–M5** to evaluate if a controlled ROP could be realized for a set of monomers. All ROPs were performed in a glovebox under nitrogen atmosphere at room temperature (M/BnOH/TBD = 100/1/0.5, $[M]_0 = 0.7$ mol L⁻¹ in THF). Samples were periodically taken from the polymerization solutions, quenched with an at least tenfold excess of benzoic acid, and investigated by means of ¹H NMR spectroscopy and SEC in order to determine the monomer conversions and molar masses, respectively (Figure 2).

The semi-logarithmic kinetic plot revealed that the apparent polymerization rate decreased over time, which is indicative of “side reactions” taking place throughout the course of the polymerization. These could either represent termination reactions, or be caused by intermolecular chain transfer reactions. The fact that the molar mass of the PEAs did not increase in a linear fashion with monomer conversion hints toward the latter. In fact, this observation is in line with literature reports describing transesterifications using TBD as well as with the preliminary polymerization tests.^[38] However, these reactions came into effect only above monomer conversions of approximately 50%, as supported by the unimodal and narrow molar mass distributions of the PEAs ($\bar{D} \leq 1.17$), which consistently shifted toward lower elution volumes at increasing polymerization time for all three monomers. At higher conversions, the molar masses could not be easily controlled anymore and the dispersity increased ($M_n \leq 21\,000$ g mol⁻¹, $\bar{D} \leq 1.34$). However, PEAs with tailor-made molar masses up to 15 000 g mol⁻¹

should be accessible as long as the polymerization is quenched at monomer conversions of around 50%.

The monomers **M3** and **M5** revealed similar polymerization behavior, whereas the apparent polymerization rate of the L-leucine-based **M4** was significantly reduced. Due to the bond angles in the solid state and the generally higher reactivity of ester moieties, an activation of the ester moieties of the morpholine-2,5-diones by TBD can be assumed. However, X-ray crystallography indicated no significant difference of the ring strains upon comparison of **M3** to **M5**. However, the conformation in solution could differ, additionally allowing rotation of the *iso*-propyl, *iso*-butyl, and *sec*-butyl substituents of **M3** to **M5** in α -position of the ester carbonyl oxygen atom. One could thus speculate that the activation of the carbonyl moiety by the catalyst is hampered due to steric hindrance of the *iso*-butyl substituent of **M4** (compare structures depicted in Figure 2).

Current state of the art describes the ROP of lactones using organobases to proceed via two pathways:^[39,40] A) An activated alcohol pathway resulting in polymer chains carrying the according alcohol moiety as α -end group, and B) a nucleophilic attack of the catalyst at the monomer that would produce TBD initiated chains in our case. To investigate if the end groups of the PEAs **PM3–PM5** could be controlled by the established ROP conditions, MALDI TOF MS measurements were performed from samples taken after 10 min using 2,5-dihydroxybenzoic acid (DHB) as a matrix (Figure 3).

The distance between the detected peak series corresponded to the molar mass of one repeating unit, that is, $\Delta m/z = 157$ for the depsipeptide **PM3** based on L-valine, and $\Delta m/z = 171$ for **PM4** as well as **PM5** derived from L-leucine and L-isoleucine, respectively. In all three cases, the most abundant species could be assigned to the polymer chains initiated by benzyl alcohol with hydroxyl ω -end groups that are ionized with a sodium cation. The latter were formed due to the quenching of the ROP with benzoic acid. Less abundant m/z series were related to PEA chains with a carboxylic acid as well as a hydroxyl end group. These are either a result from initiation of the ROP by water, were formed by hydrolysis of covalently bound TBD at the α -chain end,^[41] or were generated by fragmentation during the ionization. Although the selective ionization of polymer chains with certain end groups cannot be excluded, MALDI TOF MS analysis revealed that the α -end groups of the PEAs could be predetermined by the alcohol used as initiator for the ROP of the morpholine-2,5-diones.

Five morpholine-2,5-dione monomers were obtained from the natural L-amino acids glycine, alanine, valine, leucine, and isoleucine in a two-step

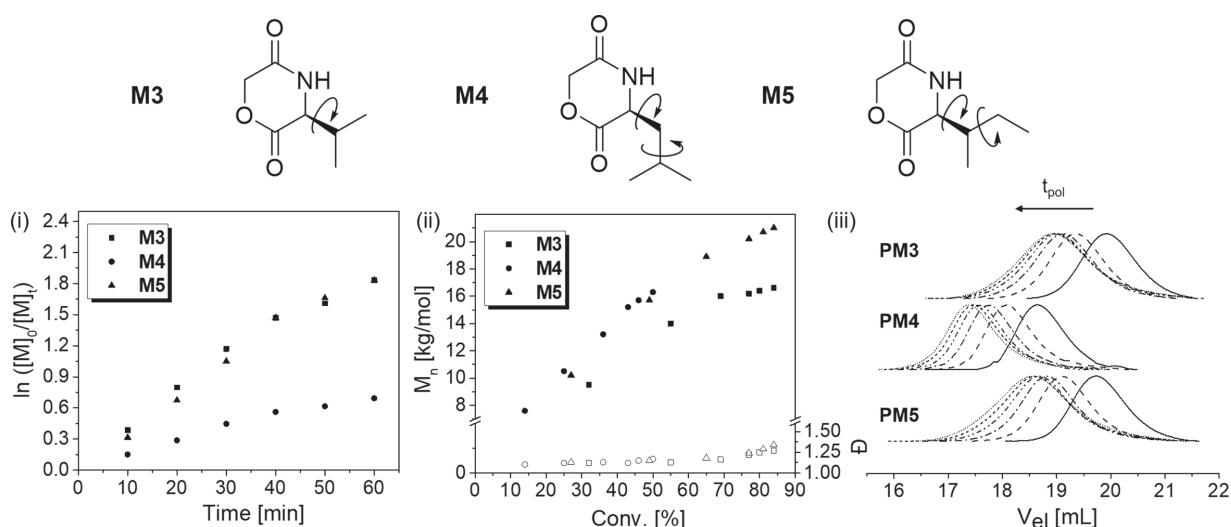


Figure 2. Kinetic studies of the ROP of **M3–M5** (M/I/TBD = 100/1/0.5, $[M]_0 = 0.7$ mol L⁻¹ in THF, RT). i) Semi-logarithmic kinetic plot. ii) Evolution of the molar mass and dispersities with the monomer conversion. iii) SEC traces (DMAC, 0.21% LiCl). SEC of the ROP of **M4** was measured on a slightly modified SEC setup.

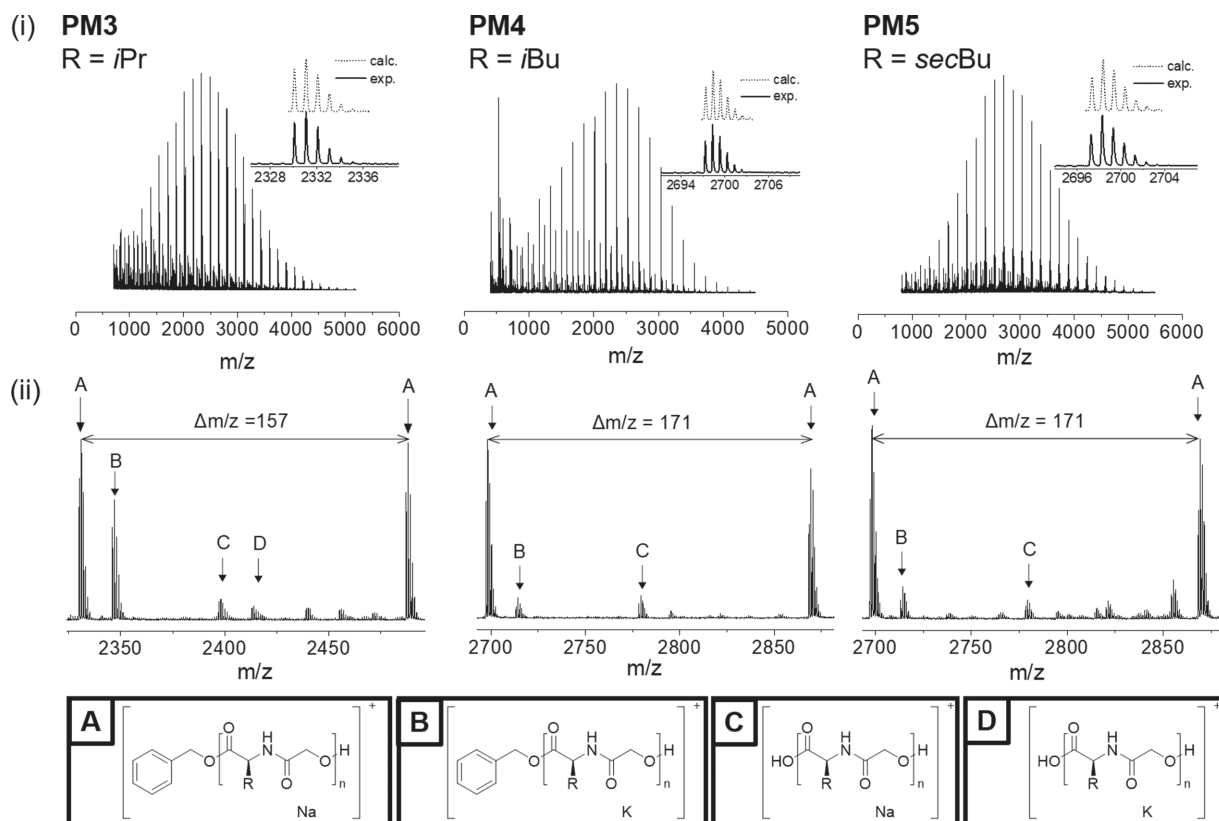


Figure 3. MALDI TOF mass spectra of samples taken from the polymerization mixture after 10 min (matrix: DHB). i) Full mass spectra. The insets show an overlay of the measured and calculated isotopic pattern of the most abundant species A. ii) Zoom into selected m/z regions displaying one repeating unit and assignment of the observed polymer species.

synthesis. TBD proved to be a suitable catalyst for the ROP of all five monomers in THF at room temperature yielding PEA homopolymers. In particular, the monomers **M3–M5** that were soluble in THF and are based on valine, leucine, and isoleucine could be polymerized in a controlled manner up to monomer conversions of 50%. As confirmed by kinetic studies and MALDI TOF MS investigations, the molar mass ($M_n \leq 15000 \text{ g mol}^{-1}$) as well as the α -end group of the resulting PEAs could be tailored, while the dispersity remained below 1.2.

Current research conducted in our laboratories is directed toward the application of these optimized ROP conditions for the synthesis of well-defined homo and block copolymers with varying molar masses. In particular, the utilization of macroinitiators featuring a stealth effect and the application of the PEAs as drug delivery vehicles is in the focus.

Supporting Information

Supporting Information is available from the Wiley Online Library or from the author.

Acknowledgements

The research was supported by the Deutsche Forschungsgemeinschaft (DFG) funded Collaborative Research Center PolyTarget (SFB 1278, projects A01 and Z01). The authors acknowledge Nicole Fritz for MALDI TOF MS measurements.

Conflict of Interest

The authors declare no conflict of interest.

Keywords

5-diones, amino acids, crystal structure, morpholine-2, poly(ester amide)s, ring-opening polymerization

Received: June 4, 2018
Revised: July 11, 2018
Published online: August 9, 2018

- [1] B. Tyler, D. Gullotti, A. Mangraviti, T. Utsuki, H. Brem, *Adv. Drug Delivery Rev.* **2016**, *107*, 163.
- [2] R. K. Kulkarni, E. Moore, A. Hegyeli, F. Leonard, *J. Biomed. Mater. Res., Part A* **1971**, *5*, 169.
- [3] S. H. Lee, I. Y. Kim, W. S. Song, *Macromol. Res.* **2014**, *22*, 657.
- [4] J. Schakenraad, P. Nieuwenhuis, I. Molenaar, J. Helder, P. J. Dijkstra, J. Feijen, *J. Biomed. Mater. Res., Part A* **1989**, *23*, 1271.
- [5] M. Winnacker, B. Rieger, *Polym. Chem.* **2016**, *7*, 7039.
- [6] P. J. Dijkstra, J. H. van Lochem, J. Feijen, *Makromol. Chem.* **1990**, *191*, 1813.
- [7] J. Helder, F. E. Kohn, S. Sato, J. W. van den Berg, J. Feijen, *Makromol. Chem. Rapid Commun.* **1985**, *6*, 9.

- [8] N. Yonezawa, F. Toda, M. Hasegawa, *Macromol. Rapid Commun.* **1985**, *6*, 607.
- [9] A. C. Fonseca, M. H. Gil, P. N. Simões, *Prog. Polym. Sci.* **2014**, *39*, 1291.
- [10] P. J. A. in't Veld, Z.-R. Shen, G. A. J. Takens, P. J. Dijkstra, J. Feijen, *J. Polym. Sci., Part A: Polym. Chem.* **1994**, *32*, 1063.
- [11] Y. Feng, C. Chen, L. Zhang, H. Tian, W. Yuan, *Trans. Tianjin Univ.* **2012**, *18*, 315.
- [12] Y. Feng, J. Lu, M. Behl, A. Lendlein, *Int. J. Artif. Organs* **2011**, *34*, 103.
- [13] X. Peng, M. Behl, P. Zhang, M. Mazurek-Budzyska, M. Y. Razzaq, A. Lendlein, *Polymer* **2016**, *105*, 318.
- [14] Y. Feng, D. Klee, H. Höcker, *Materialwiss. Werkstofftech.* **1999**, *30*, 862.
- [15] Y. Feng, D. Klee, H. Höcker, *Macromol. Biosci.* **2004**, *4*, 587.
- [16] Y. Feng, J. Knüfermann, D. Klee, H. Höcker, *Macromol. Rapid Commun.* **1999**, *20*, 88.
- [17] T. Naolou, A. Lendlein, A. T. Neffe, *Eur. Polym. J.* **2016**, *85*, 139.
- [18] K. Pagar, P. Vavia, *Sci. Pharm.* **2013**, *81*, 865.
- [19] C. Shi, F. Yao, J. Huang, G. Han, Q. Li, M. Khan, Y. Feng, W. Zhang, *J. Mater. Chem. B* **2014**, *2*, 1825.
- [20] C. Shi, Q. Li, W. Zhang, Y. Feng, X. Ren, *ACS Appl. Mater. Interfaces* **2015**, *7*, 20389.
- [21] Y. Feng, W. Lu, X. Ren, W. Liu, M. Guo, I. Ullah, W. Zhang, *Polymers* **2016**, *8*, 13.
- [22] J. Lv, J. Yang, X. Hao, X. Ren, Y. Feng, W. Zhang, *J. Mater. Chem. B* **2016**, *4*, 997.
- [23] M. Chisholm, J. Galucci, C. Krempner, C. Wiggenhorn, *Dalton Trans.* **2006**, 846.
- [24] W. N. Ottou, H. Sardon, D. Mecerreyes, J. Vignolle, D. Taton, *Prog. Polym. Sci.* **2016**, *56*, 64.
- [25] M. K. Kiesewetter, M. D. Scholten, N. Kirn, R. L. Weber, J. L. Hedrick, R. M. Waymouth, *J. Org. Chem.* **2009**, *74*, 9490.
- [26] M. K. Kiesewetter, E. J. Shin, J. L. Hedrick, R. M. Waymouth, *Macromolecules* **2010**, *43*, 2093.
- [27] R. C. Pratt, B. G. G. Lohmeijer, D. A. Long, R. M. Waymouth, J. L. Hedrick, *J. Am. Chem. Soc.* **2006**, *128*, 4556.
- [28] B. G. G. Lohmeijer, R. C. Pratt, F. Leibfarth, J. W. Logan, D. A. Long, A. P. Dove, F. Nederberg, J. Choi, C. Wade, R. M. Waymouth, J. L. Hedrick, *Macromolecules* **2006**, *39*, 8574.
- [29] R. C. Pratt, A. P. Dove, B. G. Lohmeijer, D. A. Culkin, R. M. Waymouth, J. L. Hedrick, *Polym. Prepr. (Am. Chem. Soc., Div. Polym. Chem.)* **2005**, *46*, 902.
- [30] R. C. Pratt, B. G. Lohmeijer, A. Mason, R. M. Waymouth, J. L. Hedrick, *Polym. Prepr. (Am. Chem. Soc., Div. Polym. Chem.)* **2006**, *47*, 101.
- [31] T. Ouchi, T. Nozaki, Y. Okamoto, M. Shiratani, Y. Ohya, *Macromol. Chem. Phys.* **1996**, *197*, 1823.
- [32] A. Pedna, L. Rosi, M. Frediani, P. Frediani, *J. Appl. Polym. Sci.* **2015**, *132*, 42323.
- [33] Y. Feng, D. Klee, H. Höcker, *Macromol. Biosci.* **2001**, *1*, 66.
- [34] Y. Feng, D. Klee, H. Höcker, *Macromol. Chem. Phys.* **1999**, *200*, 2276.
- [35] L. Urfi, X. Solans, M. Martínez-Palau, J. Puiggali, *Acta Crystallogr., Sect. C: Cryst. Struct. Commun.* **2006**, *62*, o262.
- [36] I. Yildirim, S. Crotty, C. H. Loh, G. Festag, C. Weber, P. F. Caponi, M. Gottschaldt, M. Westerhausen, U. S. Schubert, *J. Polym. Sci., Part A: Polym. Chem.* **2016**, *54*, 437.
- [37] I. Yildirim, C. Weber, U. S. Schubert, *Prog. Polym. Sci.* **2018**, *76*, 111.
- [38] M. T. Martello, A. Burns, M. Hillmyer, *ACS Macro Lett.* **2012**, *1*, 131.
- [39] L. Simón, J. M. Goodman, *J. Org. Chem.* **2007**, *72*, 9656.
- [40] N. J. Sherck, H. C. Kim, Y.-Y. Won, *Macromolecules* **2016**, *49*, 4699.
- [41] A. Pascual, H. Sardón, F. Ruipérez, R. Gracia, P. Sudam, A. Veloso, D. Mecerreyes, *J. Polym. Sci., Part A: Polym. Chem.* **2014**, *53*, 552.



Supporting Information

for *Macromol. Rapid Commun.*, DOI: 10.1002/marc.201800433

TBD-Catalyzed Ring-Opening Polymerization of Alkyl-Substituted Morpholine-2,5-Dione Derivatives

Michael Dirauf, Damiano Bandelli, Christine Weber, Helmar Görls, Michael Gottschaldt, and Ulrich S. Schubert*

Supporting Information

for *Macromol. Rapid Commun.*, DOI: 10.1002/marc.201800433

TBD catalyzed ring-opening polymerization of alkyl substituted morpholine-2,5-dione derivatives

Michael Dirauf, Damiano Bandelli, Christine Weber, Helmar Görls, Michael Gottschaldt, Ulrich S. Schubert*

M. Dirauf, D. Bandelli, Dr. C. Weber, Prof. Dr. M. Gottschaldt, Prof. Dr. U. S. Schubert
Laboratory of Organic and Macromolecular Chemistry (IOMC) Friedrich Schiller University
Jena, Humboldtstr. 10, 07743 Jena, Germany

M. Dirauf, D. Bandelli, Dr. C. Weber, Prof. Dr. M. Gottschaldt, Prof. Dr. U. S. Schubert
Jena Center for Soft Matter (JCSM), Friedrich Schiller University Jena, Philosophenweg 7,
07743 Jena, Germany

E-mail: ulrich.schubert@uni-jena.de

Dr. Helmar Görls

Laboratory of Inorganic and Analytical Chemistry (IAAC), Friedrich Schiller University Jena,
Humboldtstr. 8, 07743 Jena, Germany

Experimental Part

Materials

Solvents used for polymerizations and the precursor synthesis were dried in a solvent purification system (SPS; Pure solv EN, InnovativeTechnology). 1,5,7-Triazabicyclo[4.4.0]dec-5-ene (TBD, Sigma Aldrich), bromoacetyl bromide (Sigma Aldrich), chloroacetyl chloride (Sigma Aldrich) and the amino acids (TCI) were used without further purification.

Instrumentation

All NMR spectra were measured on a 300 MHz spectrometer from Bruker equipped with an Avance I console, a dual ^1H and ^{13}C sample head and a 60 × BACS automatic sample changer. The signals were determined by using the residual solvent signal as a reference. All

shifts are given in ppm in comparison to TMS as a reference. Infrared(IR) spectra were recorded using an IRAffinity-1 CE (Shimadzu) system equipped with a quest ATR diamond extended range X – single-reflection-ATR cuvette with a diamond crystal. Elemental analysis (EA) was performed with a Leco CHN-932. Melting points were determined using a VWR MPM-H2 melting point meter. Size exclusion chromatography (SEC) was measured on an Agilent 1200 series system, equipped with a PSS degasser, a G1310A pump and a Techlab oven (40 °C). A G1362A refractive index detector was utilized for data acquisition. The used eluent was a solution of 0.21 wt.% LiCl in DMAc, and the flow rate was 1 mL min⁻¹. A PSS Gram 30 and a PSS Gram 1000 column placed in series served as a column set. The molar masses were calculated using poly(methyl methacrylate) (PMMA) standards. Matrix-assisted laser desorption ionization mass spectrometry (MALDI-MS) measurements were carried out using an Ultraflex III ToF/ToF instrument (Bruker Daltonics) equipped with a Nd-YAG laser. All spectra were measured in the positive mode using 2,5 dihydroxybenzoic acid (DHB) as a matrix. Electro-spray ionization mass spectrometry (ESI-MS) was measured utilizing a Bruker MicroQToF mass spectrometer.

The intensity data for the compounds were collected on a Nonius KappaCCD diffractometer using graphite-monochromated Mo-K_α radiation. Data were corrected for Lorentz and polarization effects; absorption was taken into account on a semi-empirical basis using multiple-scans.^[1-3]The structures were solved by direct methods (SHELXS)^[4] and refined by full-matrix least squares techniques against Fo2 (SHELXL-97).^[4] All hydrogen atoms of the compounds **M2**, and **M3**, and the hydrogen atoms bonded to the nitrogen atoms of **M4** and **M5** were located by difference Fourier synthesis and refined isotropically. All other hydrogen atoms were included at calculated positions with fixed thermal parameters. The absolute chemical configuration of all compounds was determined by the absolute configuration of the starting materials. All non-hydrogen atoms were refined anisotropically.^[4] Crystallographic

data as well as structure solution and refinement details are summarized in **Table SI 2**.

MERCURY^[5] was used for structure representations.

General procedure for the precursor synthesis:

1 Equivalent of amino acid was suspended in dry tetrahydrofuran (THF). After addition of 1 equivalent NEt_3 , the mixture was stirred at room temperature for 20 minutes. Subsequently, the mixture was cooled to -5 to 0 °C in an ice bath. 1.5 equivalents bromoacetyl bromide respectively, in THF were added continuously over a period of 30 minutes. After removal of the ice bath, the mixture was allowed to reach room temperature while stirring for another 30 minutes. The mixture was filtered in order to remove the formed triethylammonium halide salt and the unreacted amino acid. Evaporation of the solvent usually left a slightly orange readily crystallizing oil, which was recrystallized from a suitable solvent.

2-Bromoacetyl-glycine (1): Compound **1** was synthesized according to the general procedure using 3.5 g (0.047 mol) glycine and 14.11 g (0.069 mol) bromoacetyl bromide. The oil was precipitated from cold diethylether. Yield: 55.4%. ^1H NMR(300 MHz, $\text{DMSO-}d_6$, compare **Figure SI 1**, δ): 3.80 (d, 2H, $J = 5.86$ Hz, $\text{NH-CH}_2\text{-CO}$), 3.93 (s, 2H, $\text{O-CH}_2\text{-CO}$), 8.60 (m, 1H, NH), 12.66 (s, 1H, COOH). Anal. calcd for $\text{C}_4\text{H}_6\text{BrNO}_3$: C 24.51, H 3.09, N 7.15, Br 40.77; found: C 25.13, H 3.19, N 6.59, Br 41.18.

2-Bromoacetyl-L-alanine (2): Compound **2** was synthesized according to the general procedure using 4 g (0.045 mol) L-alanine and 13.6 g (0.067 mol) bromoacetyl bromide. No crystallization of the oil was observed. It was used without further purification. Yield: n.d. (brownish oil). ^1H NMR (300 MHz, $\text{DMSO-}d_6$, compare **Figure SI 2**, δ): 1.27 (d, 3H, $J = 7.34$ Hz, CH_3) 3.90 (s, 2H, CH_2), 4.12 (m, 1H, CH), 8.62 (d, 1H, $J = 7.09$ Hz, NH).

2-Bromoacetyl-L-valine (3): Compound **3** was synthesized according to the general procedure using 4 g (0.034 mol) L-valine and 10.34 g (0.051 mol) bromoacetyl bromide. The

crude compound was recrystallized from ethyl acetate. Yield: 41.6%. ^1H NMR (300 MHz, $\text{DMSO-}d_6$, compare **Figure SI 3**, δ): 0.88 (d, 6H, $J = 6.81$ Hz, $(\text{CH}_3)_2$), 2.08 (m, 1H, CH- $(\text{CH}_3)_2$), 3.95 (m, 2H, CH_2), 4.15 (q, 1H, $J = 10.64, 8.24, 10.67$ Hz, NH-CH-CO) 8.46 (d, 1H, $J = 8.61$ Hz, NH), 12.78 (s, 1H, COOH) ppm; ^{13}C NMR (75 MHz, $\text{DMSO-}d_6$, compare **Figure SI 3**, δ): 18.3 (C-6), 19.5 (C-6), 30.6 (C-5), 29.5 (C-4), 57.9 (C-3), 166.8 (CO-NH), 173.0 (CO-OH) ppm; m.p. 130 °C (lit. 142 to 144 °C); ^{61}IR : $\nu = 3282$ (NH), 1705 (CO-OH), 1624 (CO-NH), 1558 (δ (NH)), 698 (ν (C-Br)); ESI-MS m/z (%): 260 (100) $[\text{M} + \text{Na}^+]$, 498 (23) $[2\text{M} + \text{Na}^+]$; Anal. calcd for $\text{C}_7\text{H}_{12}\text{BrNO}_3$: C 35.31, H 5.08, N 5.88, Br 33.56;found: C 35.37, H 5.20, N 5.96, Br 34.24.

2-Bromoacetyl-L-leucine (4): Compound **4** was synthesized according to the general procedure using 4 g (0.031 mol) L-leucine and 9.23 g (0.046 mol) bromoacetyl bromide. The compound was recrystallized from ethyl acetate. Yield: 44.0%. ^1H NMR (300 MHz, $\text{DMSO-}d_6$, compare **Figure SI 4**, δ): 0.85 (d, 3H, $J = 6.36$ Hz, CH_3), 0.90 (d, 3H, $J = 6.45$ Hz), 1.52 (m, 2H, $\text{CH}_2\text{-CH-}(\text{CH}_3)_2$), 1.62 (m, 1H, $\text{CH}_2\text{-CH-}(\text{CH}_3)_2$), 3.89 (dd, 2H, $J = 10.53, 17.03$ Hz, Br- $\text{CH}_2\text{-CO}$), 4.21 (q, 1H, $J = 7.95, 7.14, 7.90$ Hz, NH-CH-CO), 8.58 (d, 1H, $J = 8.02$ Hz, NH), 12.70 (s, 1H, COOH) ppm; ^{13}C NMR (75 MHz, $\text{DMSO-}d_6$, compare **Figure SI 4**, δ): 21.8 (C-1/C-2), 23.3 (C-1/C-2), 24.8 (C-3), 29.5 (C-4), 40.5 (C-5), 51.1 (C-6), 166.5 (C-7), 174.0 (C-8) ppm; m.p. 151 °C (lit. 149 to 151 °C); ^{67}IR : $\nu = 3298$ (NH), 1705 (CO-OH), 1632 (CO-NH), 1558 (δ (NH)), 667 (ν (C-Br));ESI-MS m/z (%): 274 (100) $[\text{M} + \text{Na}^+]$, 527 (34) $[2\text{M} + \text{Na}^+]$; Anal. calcd for $\text{C}_8\text{H}_{14}\text{BrNO}_3$: C 38.11, H 5.60, N 5.56, Br 31.69;found: C 38.47, H 5.62, N 5.44, Br 30.56.

2-Bromoacetyl-L-isoleucine (5):Compound **5** was synthesized according to the general procedure using 4 g (0.031 mol) L-isoleucine and 9.23 g (0.046 mol) bromoacetyl bromide. The compound was recrystallized from ethyl acetate. Yield: 36.0%. ^1H NMR (300 MHz, $\text{DMSO-}d_6$, compare **Figure SI 5**, δ): 0.86 (m, 6H, CH_3), 1.10-1.50 (dm, 2H, CH- $\text{CH}_2\text{-CH}_3$), 1.80 (m, 1H, $\text{CH}_3\text{-CH-CH}_2$) 3.95 (dd, 2H, $J = 10.80, 19.72$ Hz, Br- $\text{CH}_2\text{-CO}$), 4.19 (m, 1H,

NH-CH-CO), 8.48 (d, 1H, $J = 8.31$ Hz, NH), 12.79 (s, 1H, COOH) ppm; ^{13}C NMR (75 MHz, DMSO- d_6 , compare **Figure SI 5**, δ): 11.8 (C-1), 16.0 (C-2), 25.0 (C-3), 29.5 (C-4), 37.0 (C-5), 57.2 (C-6) ppm; m.p. 122 °C (lit. 119 to 119.5 °C); ^{18}IR : $\nu = 3294$ (NH), 1705 (CO-OH), 1631 (CO-NH), 1558 (δ (NH)), 690 (ν (C-Br)); ESI-MS m/z (%): 274 (100) $[\text{M} + \text{Na}^+]$, 527 (39) $[2\text{M} + \text{Na}^+]$; Anal. calcd for $\text{C}_8\text{H}_{14}\text{BrNO}_3$: C 38.11, H 5.60, N 5.56, Br 31.69; found: C 38.12, H 5.60, N 5.51, Br 30.00.

General procedure for the cyclization from purified precursors:

1 Equivalent of bromoacetylated amino acid was dissolved in DMF to achieve a concentration between 0.03 to 0.01 mol L^{-1} . 8 to 18 Equivalents of sodium bicarbonate were added and the reaction was stirred at 60 °C overnight. After cooling to RT, the mixture was filtered to separate the resulting sodium halide as well as the unreacted base. Evaporation of the solvent left a brownish readily crystallizing oil, which was recrystallized from a suitable solvent.

Morpholine-2,5-dione (M1): 4 g of **1** (0.021 mol; 1 eq.), 32 g sodium bicarbonate (0.38 mol; 18 eq.) and 1.6 L DMF were used. The crude compound was recrystallized from *isopropyl* alcohol. Yield: 18.9%. ^1H NMR (300 MHz, DMSO- d_6 , compare **Figure SI 6**, δ): 4.06 (d, 2H, $J = 2.3$ Hz, NH- CH_2 -CO), 4.71 (s, 2H, O- CH_2 -CO), 8.41 (s, 1H, NH) ppm; ^{13}C NMR (75 MHz, DMSO- d_6 , compare **Figure SI 6**, δ): 43.0 (C-1), 68.1 (C-2), 166.1 (CO-NH), 167.1 (CO-O) ppm; m.p. 189 °C (Lit. 192 to 193 °C); ^{19}IR : $\nu = 3197$ (NH), 1745 (CO-O), 1684 (CO-NH); ESI-MS m/z (%): 116 (100) $[\text{M} + \text{H}^+]$, 253 (71) $[2\text{M} + \text{Na}^+]$, 368 (53) $[3\text{M} + \text{Na}^+]$; Anal. calcd for $\text{C}_4\text{H}_5\text{NO}_3$: C 41.75, H 4.38, N 12.17; found: C 41.23, H 4.40, N 11.65.

(S)-3-Methylmorpholine-2,5-dione (M2): **2** (oil), 32 g sodium bicarbonate (0.38 mol) and 1.6 L DMF were used. The crude compound was recrystallized from chloroform. Yield: 16.7% (overall). ^1H NMR (300 MHz, DMSO- d_6 , compare **Figure SI 7**, δ): 1.33 (d, 3H, $J =$

6.99 Hz, CH₃), 4.30 (q, 1H, $J = 6.95, 6.97, 6.85$ Hz, NH-CH-CO), 4.75 (dd, 2H, $J = 15, 45, 74.22$ Hz, O-CH₂-CO), 8.55 (s, 1H, NH) ppm; ¹³C NMR (75 MHz, DMSO-*d*₆, compare **Figure SI 7**, δ): 17.4 (C-4), 48.4 (C-3), 68.4 (C-2), 166.7 (CO-NH), 169.9 (CO-O) ppm; m.p. 155 °C (lit. 154 to 156 °C); ⁹IR: $\nu = 3186$ (NH), 1748 (CO-O), 1697 (CO-NH), 1666 (δ (NH)); ESI-MS m/z (%): 130 (31) [M + H⁺], 152 (100) [M + Na⁺]; Anal. calcd for C₅H₇NO₃: C 46.51, H 5.46, N 10.85; found: C 46.28, H 5.41, N 10.70.

(S)-3-Iso-propylmorpholine-2,5-dione (M3): 3 g of **3** (0.013 mol), 8.5 g sodium bicarbonate (0.10 mol, 8 eq.) and 973 mL DMF were used. The crude compound was recrystallized from ethyl acetate. Yield: 29.5%. ¹H NMR (300 MHz, DMSO-*d*₆, compare **Figure SI 8**, δ): 0.94 (d, 3H, $J = 12.60$ Hz, CH₃), 0.96 (d, 3H, $J = 12.96$ Hz, CH₃), 2.18 (m, 1H, CH-(CH₃)₂), 3.97 (dd, 1H, $J = 2.60, 4.90$ Hz, NH-CH-CO), 4.74 (dd, 2H, $J = 15.99, 33.57$ Hz, O-CH₂-CO), 8.62 (s, 1H, NH) ppm; ¹³C NMR (75 MHz, DMSO-*d*₆, compare **Figure SI 8**, δ): 17.9 (C-5), 18.6 (C-5), 31.8 (C-7), 58.5 (C-3), 67.7 (C-2), 166.0 (CO-NH), 167.7 (CO-O) ppm; m.p. 97 °C (lit. 96 to 97 °C); ⁹IR: $\nu = 3229$ (NH), 1747 (CO-O), 1701 (CO-NH), 1670 (δ (NH)); ESI-MS m/z (%): 180 (79) [M + Na⁺], 337 (100) [2M + Na⁺], 353 (52) [2M + K⁺]; Anal. calcd for C₇H₁₁NO₃: C 53.49, H 7.05, N 8.91; found: C 53.92, H 7.05, N 8.77.

(S)-3-Iso-butylmorpholine-2,5-dione (M4): 2.6 g of **4** (0.010 mol; 1 eq.), 7 g sodium bicarbonate (0.082 mol; 8 eq.) and 794 mL DMF were used. The crude compound was recrystallized from ethyl acetate. Yield: 27.7%. ¹H NMR (300 MHz, DMSO-*d*₆, compare **Figure SI 9**, δ): 0.90 (t, 6H, $J = 5.65, 5.85$ Hz, (CH₃)₂), 1.62 (m, 2H, CH-CH₂-CH), 1.80 (m, 1H, CH₂-CH-(CH₃)₂), 4.15 (m, 1H, NH-CH-CO), 4.76 (m, 2H, O-CH₂-CO), 8.60 (s, 1H, NH) ppm; ¹³C NMR (75 MHz, DMSO-*d*₆, compare **Figure SI 9**, δ): 22.1 (C-1/C-2), 22.95 (C-1/C-2), 24.20 (C-3), 40.95 (C-4), 51.31 (C-5), 68.10 (C-6), 166.43 (C-7), 169.24 (C-8) ppm; m.p. 129 °C (lit. 129 to 130 °C); ¹⁰IR: $\nu = 3194$ (NH), 1744 (CO-O), 1678 (CO-NH); ESI-MS m/z (%): 194 (100) [M + Na⁺], 365 (27) [2M + Na⁺]; Anal. calcd for C₈H₁₃NO₃: C 56.13, H 7.65, N 8.18; found: C 55.92, H 7.59, N 7.97.

(S)-3-((S)-*Sec*-butyl)morpholine-2,5-dione (M5): 2 g of **5** (0.008 mol; 1 eq.), 6 g sodium bicarbonate (0,071 mol; 9 eq.) and 612 mL DMF were used. The crude compound was recrystallized from ethyl acetate. Yield: 9.5%. ¹H NMR (300 MHz, DMSO-*d*₆, compare **Figure SI 10**, δ): 0.87 (t, 3H, $J = 7.20, 7.35$ Hz, CH₂-CH₃), 0.94 (d, 3H, $J = 6.93$ Hz, CH-CH₃), 1.35 (dm, 2H, CH₂-CH₃), 1.90 (m, 1H, CH₃-CH-CH₂), 4.04 (m, 1H, NH-CH-CO), 4.74 (dd, 2H, $J = 15.97, 32.04$ Hz, O-CH₂-CO), 8.60 (s, 1H, NH) ppm; ¹³C NMR (75 MHz, DMSO-*d*₆, compare **Figure SI 10**, δ): 12.0 (C-1), 15.3 (C-2), 24.9 (C-3), 38.4 (C-4), 57.6 (C-5), 67.7 (C-6), 166.0 (CO-NH), 167.6 (CO-O) ppm; m.p. 108 °C (lit. 107 to 108 °C);^[10]IR: $\nu = 3186$ (NH), 1744 (CO-O), 1678 (CO-NH); ESI-MS m/z (%): 365 (100) [2M + Na⁺], 536 (19) [3M + Na⁺], 707 (6) [4M + Na⁺]; Anal. calcd for C₈H₁₃NO₃: C 56.13, H 7.65, N 8.18; found: C 54.82, H 7.47, N 8.01.

Optimized procedure for the monomer synthesis:

4 g of amino acid was suspended in 115 mL dry tetrahydrofuran. The suspension was cooled to -5 to 0 °C after addition of 1 equivalent triethylamine. Under temperature control, 1.5 equivalents chloroacetyl chloride in THF (20 mL) were added dropwise over a period of 30 min. The ice bath was removed after complete addition, the reaction mixture was stirred for another 30 min and allowed to reach room temperature. After filtration, the organic phase was washed with a mixture of distilled water and brine (1/1.5; v/v). The organic phase was dried over sodium sulfate. The volatiles were removed under reduced pressure after filtration. The residual brownish oil was used without further purification.

The oil was dissolved in 1.5 L DMF. 8 Equivalents of sodium bicarbonate were added. The mixture was stirred at 60 °C overnight. After cooling to room temperature, the remaining sodium bicarbonate and triethylammonium chloride were filtered off and the volatiles were removed under reduced pressure. 500 mL chloroform were added to the oil to precipitate

residual salts, which were removed by filtration. The filtrate was concentrated under reduced pressure and gave a brownish oil, which usually readily crystallized. The crude crystals were purified by recrystallization from ethyl acetate.

(S)-3-*Iso*-propylmorpholine-2,5-dione (M3): Yield: 23.7% (overall) characterization data see above.

(S)-3-*Iso*-butylmorpholine-2,5-dione (M4): Yield: 33.6% (overall) characterization data see above.

(S)-3-((S)-*Sec*-butyl)morpholine-2,5-dione (M5): Yield: 22.0% (overall) characterization data see above.

General procedure for the test polymerizations:

10 μL of a stock solution containing benzyl alcohol and TBD in THF were transferred to a solution of the desired morpholine-2,5-dione (0.5 mmol) in 710 μL THF (M/I/TBD = 100/1/0.5 of M/I/TBD = 100/1/0.1; $[\text{M}]_0 = 0.7 \text{ mol L}^{-1}$) in a glovebox. The mixture was stirred at room temperature for a varied period of time and quenched by the addition of a solution of benzoic acid (at least tenfold excess compared to TBD) in THF. The outcome was analyzed *via* $^1\text{H-NMR}$ and SEC measurements.

General procedure for the polymerization kinetics:

Inside a glovebox, a solution of TBD and benzyl alcohol was added to a solution of the monomer to reach a ratio of M/I/TBD of 100/1/0.5, while the initial monomer concentration $[\text{M}]_0$ was kept as 0.7 mol L^{-1} . The mixture was stirred inside the glovebox while taking a sample (250 μL) every ten minutes, which was quenched with at least a tenfold excess of

benzoic acid in THF, and further analyzed by means of ^1H NMR spectroscopy and SEC. Selected samples were also analyzed by MALDI-MS.

Characterization of the precursors 1-5:

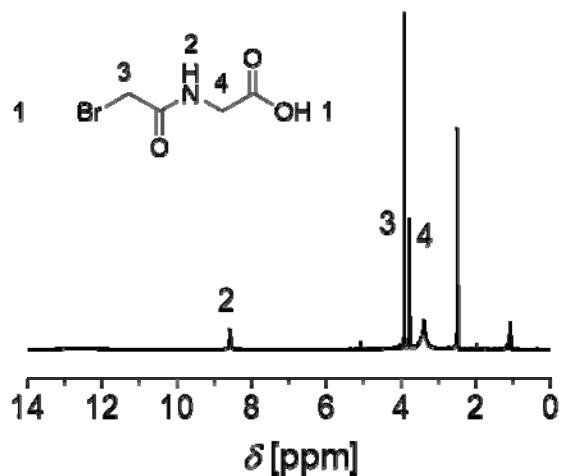


Figure SI 1. ^1H -NMR (300 MHz, DMSO-d_6) spectrum of the precursor compound 1.

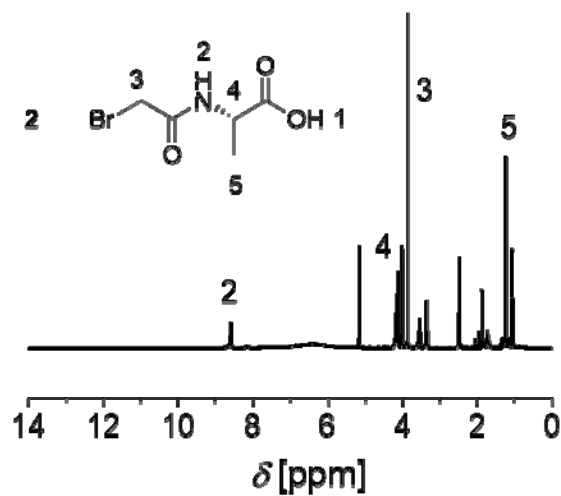


Figure SI 2. ^1H -NMR (300 MHz, DMSO-d_6) spectrum of the precursor compound 2.

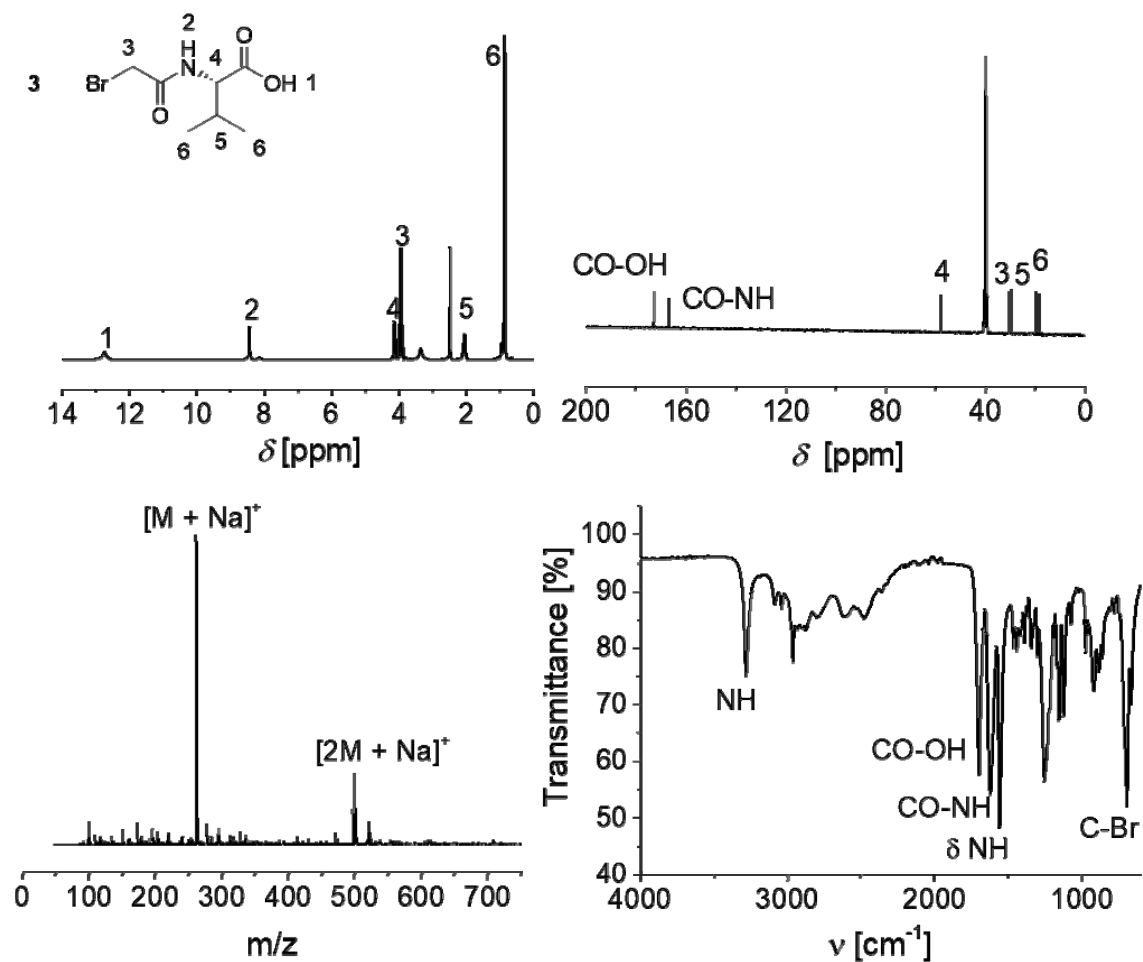


Figure SI 3. Characterization of the precursor compound **3**. Top left: $^1\text{H-NMR}$ spectrum (300 MHz, DMSO-d_6). Top right: $^{13}\text{C-NMR}$ spectrum (75 MHz, DMSO-d_6). Bottom left: ESI mass spectrum. Bottom right: FT-ATR-IR spectrum.

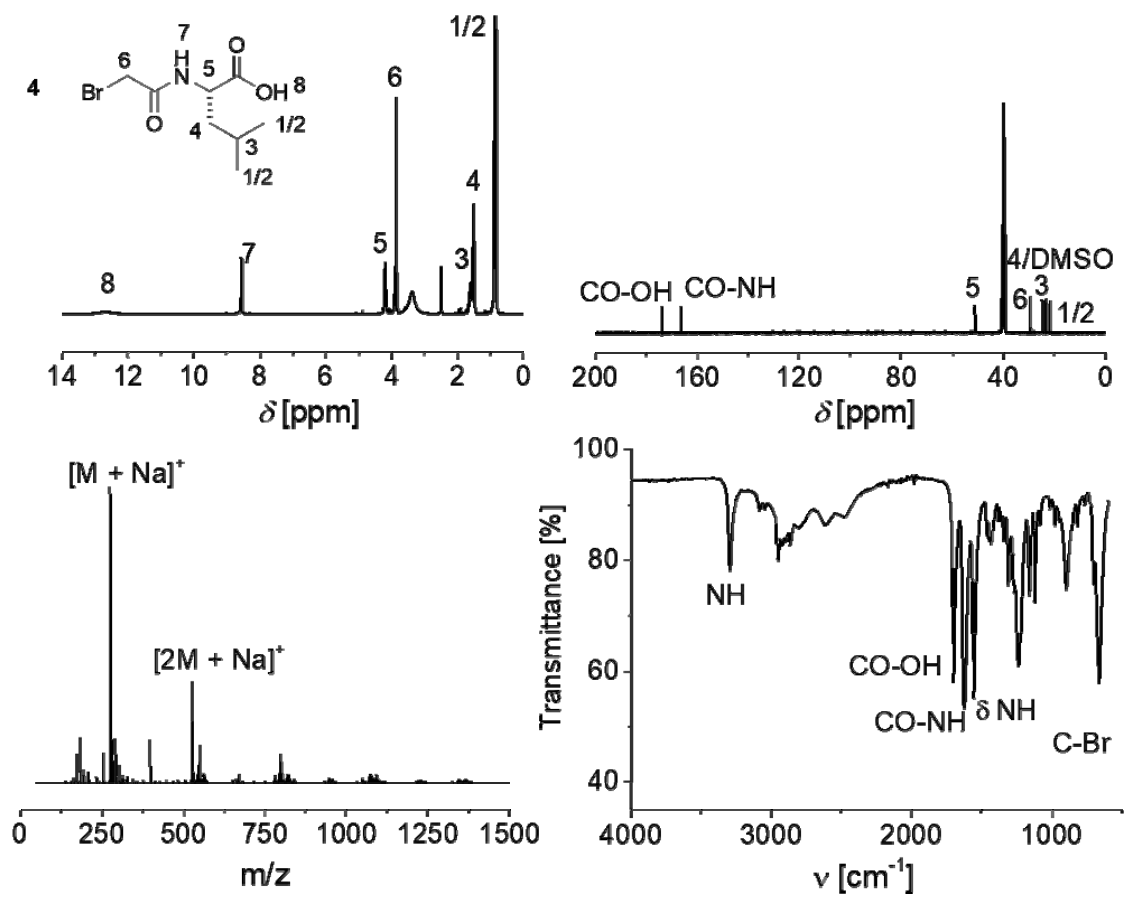


Figure SI 4. Characterization of the precursor compound 4. Top left: $^1\text{H-NMR}$ spectrum (300 MHz, DMSO-d_6). Top right: $^{13}\text{C-NMR}$ spectrum (75 MHz, DMSO-d_6). Bottom left: ESI mass spectrum. Bottom right: FT-ATR-IR spectrum.

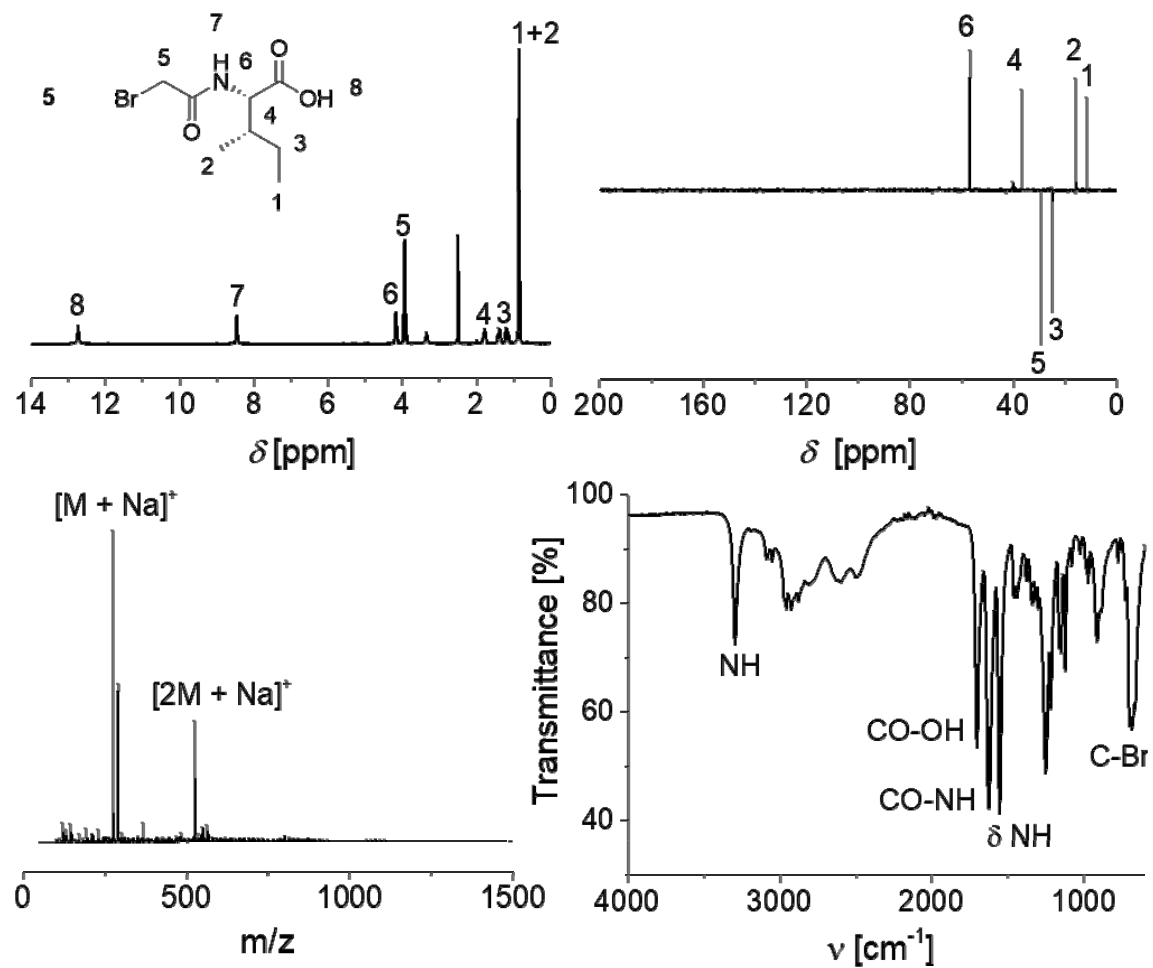


Figure SI 5. Characterization of the precursor compound **5**. Top left: ¹H-NMR spectrum (300 MHz, DMSO-d₆). Top right: DEPT 135 spectrum (75 MHz, DMSO-d₆). Bottom left: ESI mass spectrum. Bottom right: FT-ATR-IR spectrum.

Characterization of the monomers M1-M5:

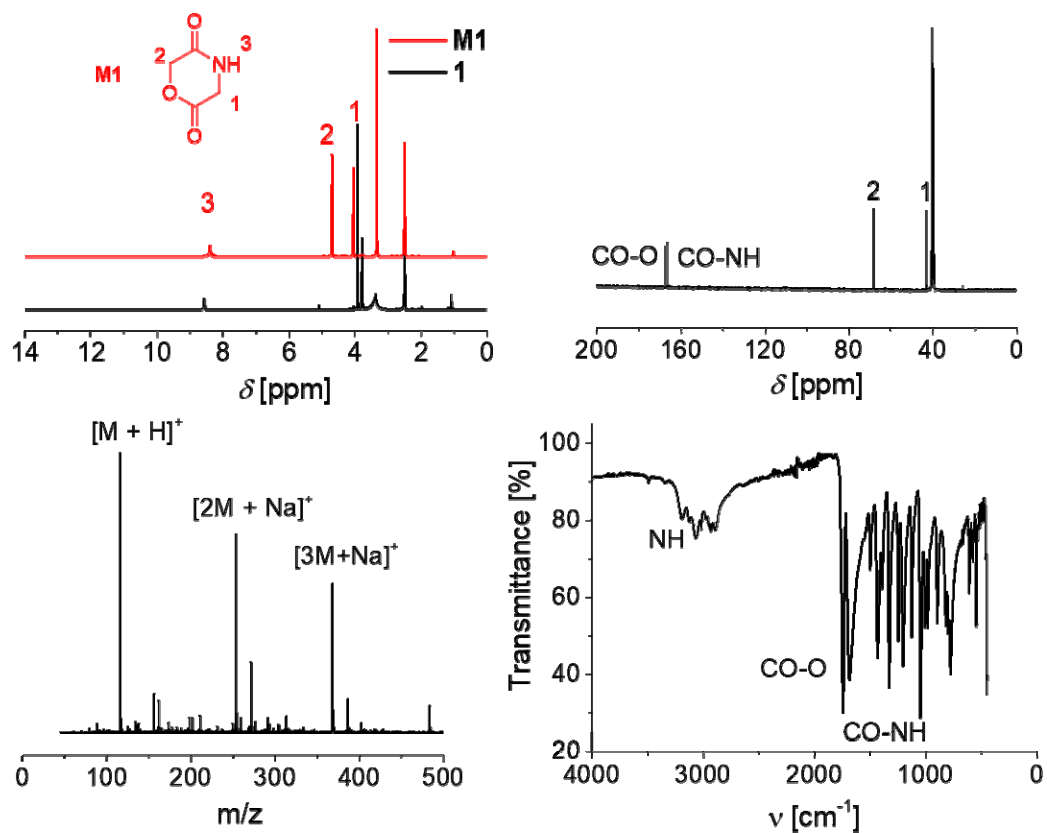


Figure SI 6. Characterization of the monomer **M1**. Top left: $^1\text{H-NMR}$ spectrum (300 MHz, DMSO-d_6). Top right: $^{13}\text{C-NMR}$ spectrum (75 MHz, DMSO-d_6). Bottom left: ESI mass spectrum. Bottom right: FT-ATR-IR spectrum.

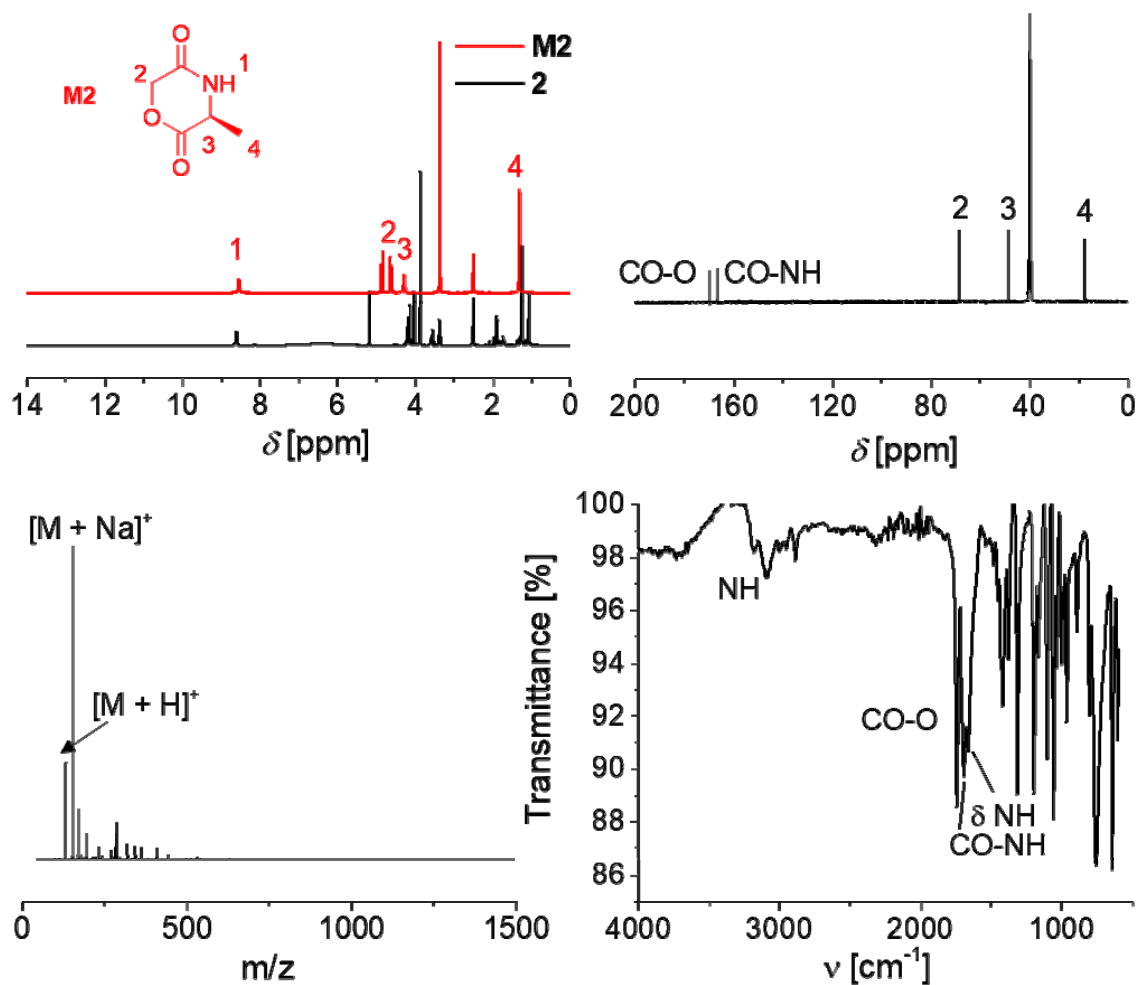


Figure SI 7. Characterization of the monomer **M2**. Top left: $^1\text{H-NMR}$ spectrum (300 MHz, DMSO-d_6). Top right: $^{13}\text{C-NMR}$ spectrum (75 MHz, DMSO-d_6). Bottom left: ESI mass spectrum. Bottom right: FT-ATR-IR spectrum.

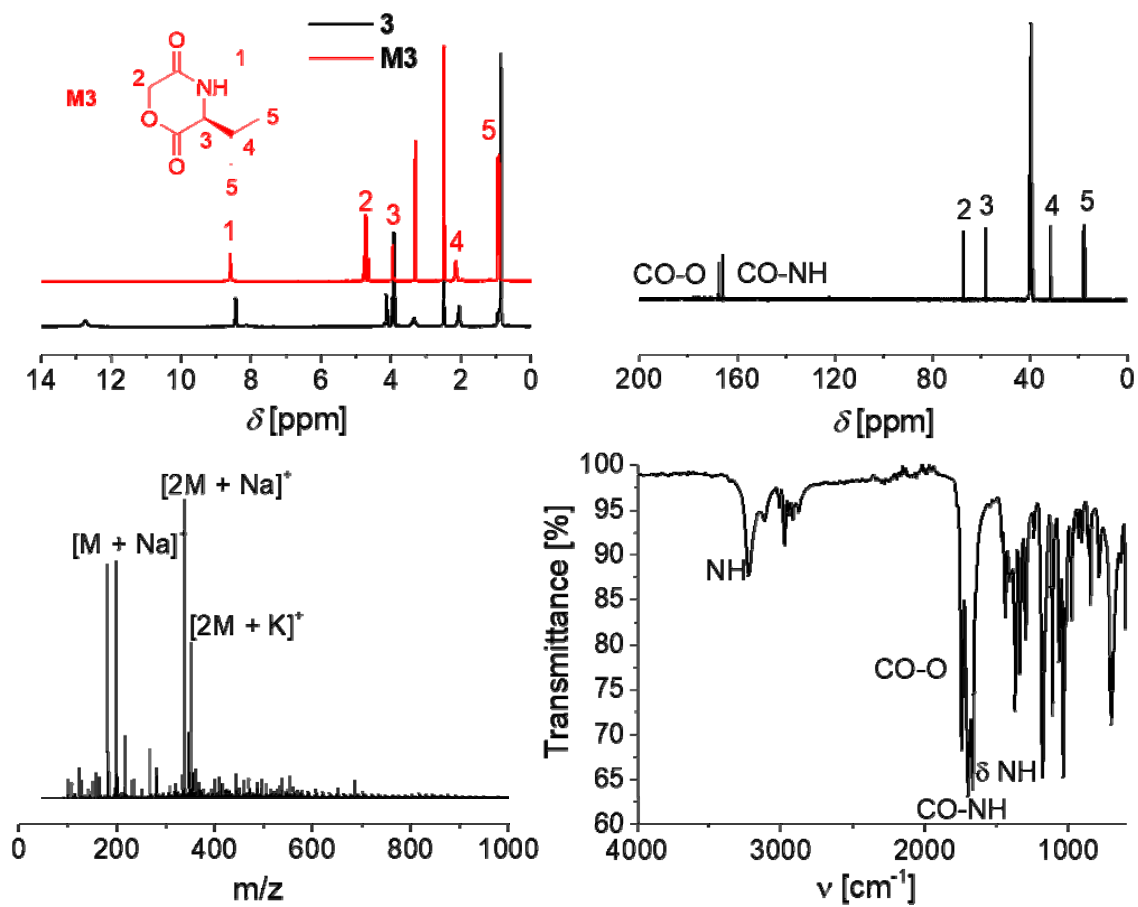


Figure SI 8. Characterization of the precursor compound **M3**. Top left: $^1\text{H-NMR}$ spectrum (300 MHz, DMSO-d_6). Top right: $^{13}\text{C-NMR}$ spectrum (75 MHz, DMSO-d_6). Bottom left: ESI mass spectrum. Bottom right: FT-ATR-IR spectrum.

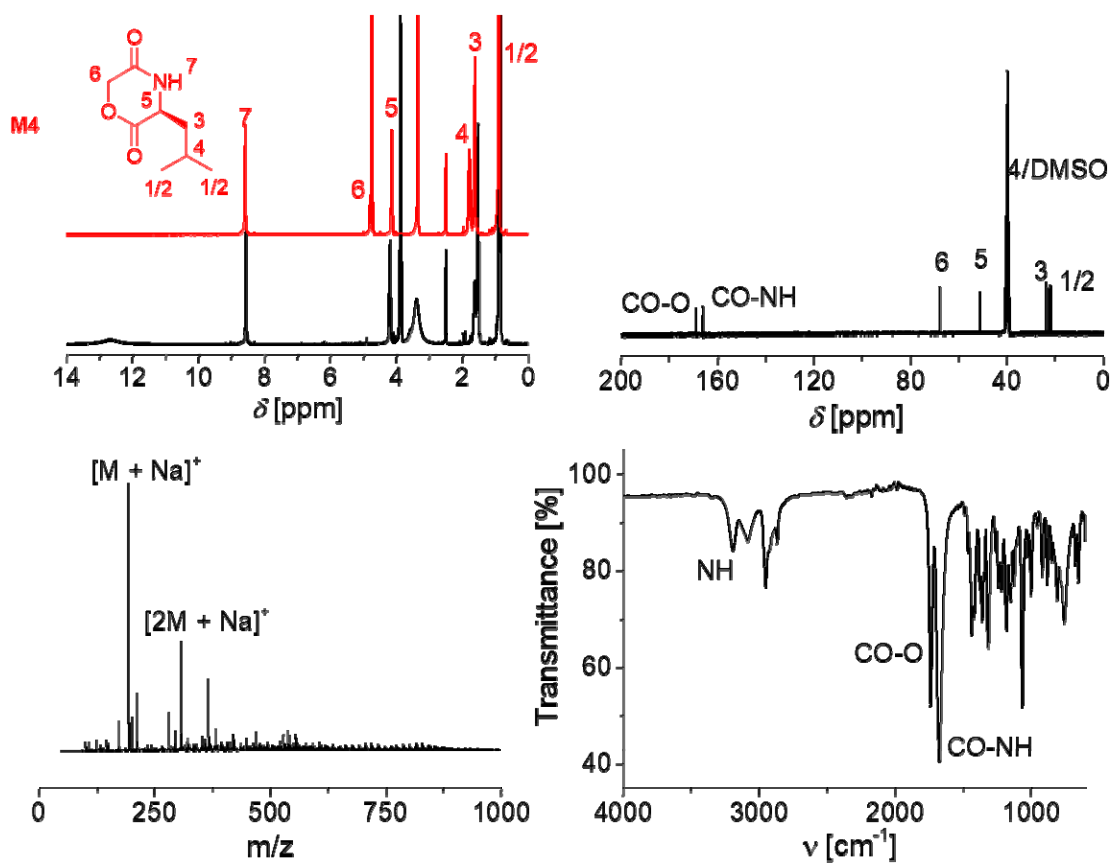


Figure SI 9. Characterization of the precursor compound **M4**. Top left: $^1\text{H-NMR}$ spectrum (300 MHz, DMSO-d_6). Top right: $^{13}\text{C-NMR}$ spectrum (75 MHz, DMSO-d_6). Bottom left: ESI mass spectrum. Bottom right: FT-ATR-IR spectrum.

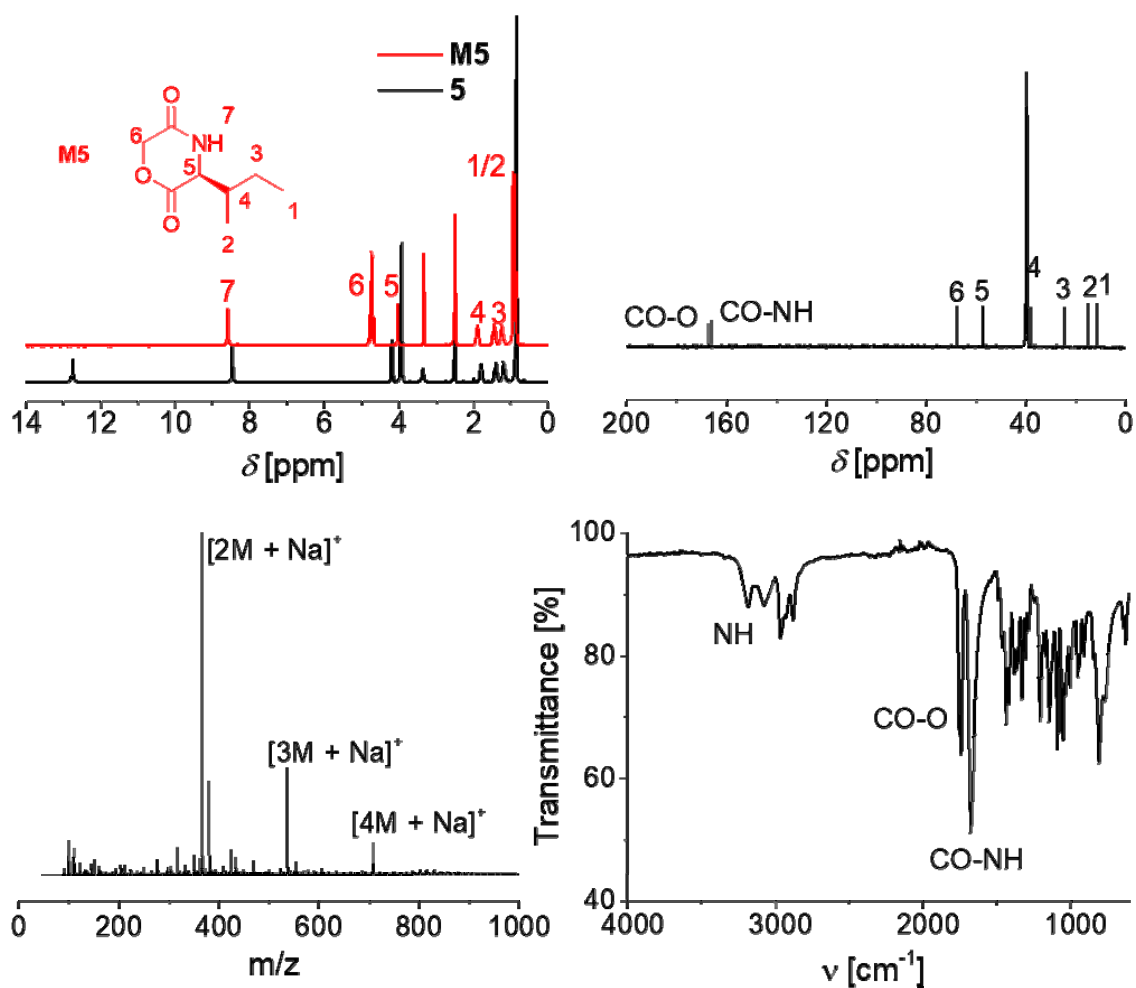


Figure SI 10. Characterization of the precursor compound **M5**. Top left: $^1\text{H-NMR}$ spectrum (300 MHz, DMSO-d_6). Top right: $^{13}\text{C-NMR}$ spectrum (75 MHz, DMSO-d_6). Bottom left: ESI mass spectrum. Bottom right: FT-ATR-IR spectrum.

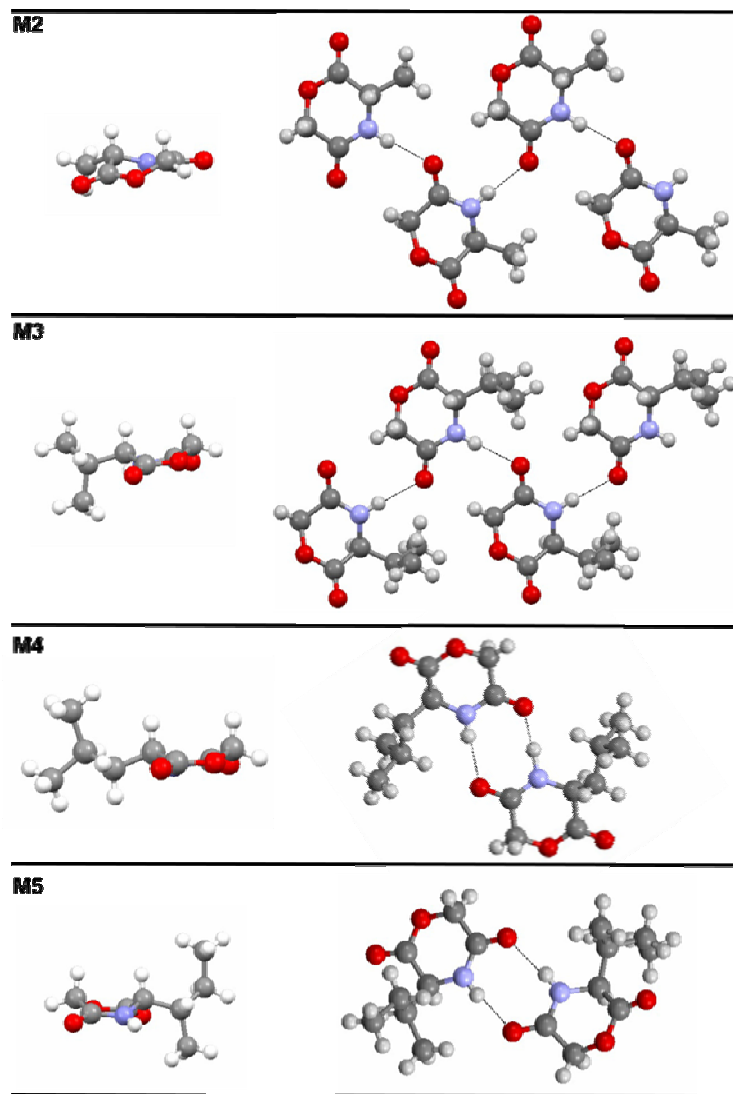


Figure SI 11.Section of the packing of the crystal structures of the monomers **M2** to **M5** obtained by x-ray scattering experiments.

Additional discussion of the packing of the crystal structures of the monomers in the solid

state:

All monomers were found to adopt a boat-like conformation in the solid state (see supporting information for selected bond lengths). Urpi *et al.* reported a similar skew-boat conformation for **M1**, which crystallized in centrosymmetric dimers due to intermolecular hydrogen bonding between the amide moieties. The uninvolved methylene groups reportedly formed weak hydrogen bonds to the uninvolved carbonyl moieties, generating a highly ordered three dimensional packing within the crystal. Due to the presence of alkyl substituents in the 3-position of the ring of **M2** to **M5**, hydrogen bonding between the individual molecules is limited to the amide groups. The monomers **M2** and **M3**, bearing a methyl and an *iso*-propyl group in 3-position, crystallized in chain-like superstructures. In contrast, **M4** and **M5** bearing *iso*-butyl and *sec*-butyl substituents, form dimers that are held together by two hydrogen bonds between the carbonyl oxygen and the hydrogen atom of the secondary amide. Presumably, the enlarged steric hindrance of the butyl moieties hampers chain formation.

Table SI 1. Selected bond distances of the morpholine-2,5-dione derivatives.

Monomer	d (H-bond) [Å]	d (C=O_{involved})^{a)} [Å]	d (C=O_{unaffected})^{b)} [Å]
M2	1.981	1.239	1.204
M3	2.118	1.234	1.207
M4	2.051 / 1.749	1.263 / 1.200	1.203 / 1.211
M5	1.972 / 2.028	1.246 / 1.239	1.203 / 1.209

a) C=O bond length of the carbonyl moiety involved in the hydrogen bonding b) C=O bond length of the carbonyl uninvolved in the hydrogen bonding.

Table SI 2. Crystal data and refinement details for the X-ray structure determinations of the compounds **M2toM5**.

Compound	M2	M3	M4	M5
formula	C ₅ H ₇ NO ₃	C ₇ H ₁₁ NO ₃	C ₈ H ₁₃ NO ₃	C ₈ H ₁₃ NO ₃
fw (g·mol ⁻¹)	129.12	157.17	171.19	171.19
T/°C	-140(2)	-140(2)	-140(2)	-140(2)
crystal system	orthorhombic	orthorhombic	monoclinic	monoclinic
space group	P 2 ₁ 2 ₁ 2 ₁	P 2 ₁ 2 ₁ 2 ₁	P 2 ₁	P 2 ₁
a/ Å	5.0496(2)	5.48180(10)	5.1650(3)	5.2704(2)
b/ Å	7.4115(3)	7.7614(2)	18.5336(6)	19.2998(7)
c/ Å	16.0833(5)	17.9027(4)	9.6232(4)	8.8292(3)
α/°	90	90	90	90
β/°	90	90	105.458(2)	106.703(2)
γ/°	90	90	90	90
V/Å ³	601.92(4)	761.70(3)	887.87(7)	860.19(5)
Z	4	4	4	4
ρ (g·cm ⁻³)	1.425	1.371	1.281	1.322
μ (cm ⁻¹)	1.19	1.07	0.98	1.01
measured data	8324	4732	7323	8964
data with I > 2σ(I)	1352	1681	2549	3436
unique data (R _{int})	1379/0.0262	1735/0.0231	3615/0.0506	3716/0.0279
wR ₂ (all data, on F ²) ^{a)}	0.0663	0.0648	0.1784	0.0802
R ₁ (I > 2σ(I)) ^{a)}	0.0254	0.0266	0.0716	0.0394
S ^{b)}	1.098	1.063	1.037	1.091
Res. dens./e·Å ⁻³	0.217/-0.157	0.206/-0.143	0.788/-0.316	0.192/-0.176
Flack-parameter	-0.2(10)	0.7(9)	1(3)	-0.2(9)
absorpt method	multi-scan	multi-scan	multi-scan	multi-scan
absorpt corr T _{min} /max	0.7070/0.7456	0.7047/0.7456	0.4465/0.7456	0.6851/0.7456
CCDC No.	1841471	1841472	1841473	1841474

^{a)} Definition of the R indices: $R_1 = (\sum ||F_o| - |F_c||) / \sum |F_o|$;

$wR_2 = \{\sum [w(F_o^2 - F_c^2)^2] / \sum [w(F_o^2)^2]\}^{1/2}$ with $w^{-1} = \sigma^2(F_o^2) + (aP)^2 + bP$; $P = [2F_c^2 + \text{Max}(F_o^2)]/3$;

^{b)} $S = \{\sum [w(F_o^2 - F_c^2)^2] / (N_o - N_p)\}^{1/2}$.

Test polymerizations:

Table SI 3. Initial polymerization tests of the TBD catalyzed ROP of the morpholine-2,5-dione derivatives **M1** to **M5** ($[M] = 0.7 \text{ mol L}^{-1}$).

M	Solvent	T [°C]	t [h]	M/I/TBD	Conv. ^{a)} [%]	M_n ^{b)} [g mol⁻¹]	Đ ^{b)}
M1	DMF	RT	1	100/1/0.1	-	-	-
M1	CH ₃ NO ₂	100	1	100/1/0.1	-	-	-
M1	THF ^{d)}	RT	1	100/1/0.1	24.7	4,500	1.41
M2	THF/LiCl ^{e)}	50	18	100/1/0.1	-	-	-
M2	THF ^{d)}	RT	1	100/1/0.1	23.8	6,500	1.27
M4	THF	RT	23.5	100/1/0.1	18.5	11,300	1.10
M4	THF	RT	18.5	100/1/0.5	89.6 ^{c)}	9,870	3.10
M4	THF	RT	5	100/1/0.5	92.5 ^{c)}	4,100	1.70
M4	THF	RT	1	100/1/0.5	82.1 ^{c)}	10,200	2.39
M4	THF	RT	0.5	100/1/0.5	37.5	13,300	1.12

a) Data obtained by integration of suitable signals in ¹H-NMR, b) data obtained by SEC (DMAc; 0.21 wt.% LiCl; RI detection, PMMA calibration), c) transesterification occurred, d) suspension polymerization and e) c = 0.5M.

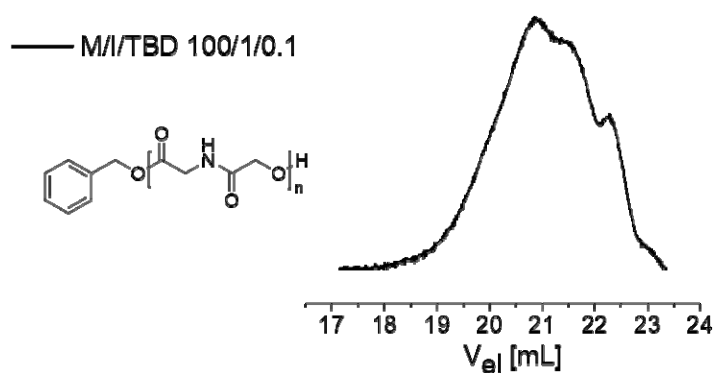


Figure SI 12. SEC elugram (DMAc, 0.21% LiCl, RI detection) of the suspension polymerization of **M1** in THF using 0.1 eq. TBD.

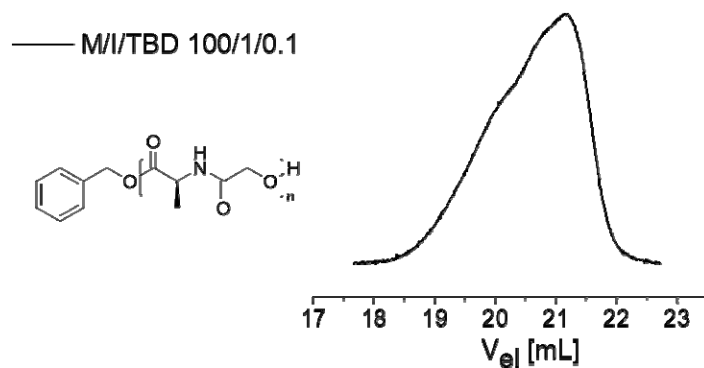


Figure SI 13. SEC elugram (DMAc, 0.21% LiCl, RI detection) of the suspension polymerization of **M2** in THF using 0.1 eq. TBD.

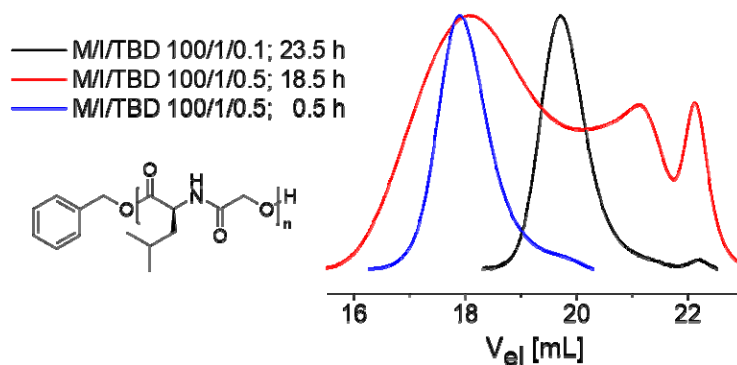


Figure SI 14. SEC elugrams (DMAc, 0.21% LiCl) of polymerization tests of **M4** in THF varying the amount of catalyst and polymerization time.

- [1] L. Krause, R. Herbst-Irmer, G. M. Sheldrick, D. Stalke, *J. Appl. Crystallogr.* **2015**, *48*, 3.
- [2] COLLECT, Data collection software, Nonius BV, Netherlands, **1998**.
- [3] Z. Otwinowski, W. Minor, *Methods in Enzymology*, Academic Press, **1997**, p. 307.
- [4] G. Sheldrick, *Acta Crystallogr., Sect. A: Found. Adv.* **2008**, *64*, 112.
- [5] C. F. Macrae, P. R. Edgington, P. McCabe, E. Pidcock, G. P. Shields, R. Taylor, M. Towler, J. van de Streek, *J. Appl. Crystallogr.* **2006**, *39*, 453.
- [6] E. Abderhalden, E. Haase, *Fermentforschung* **1931**, *12*, 313.

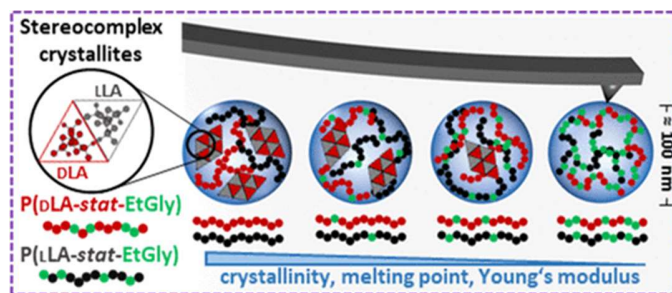
- [7] O. M. Friedman, A. M. Rutenberg, *J. Am. Chem. Soc.* **1950**, 72, 3285.
- [8] D. V. Santi, S. O. Cunnion, *Biochemistry* **1974**, 13, 481.
- [9] P. J. A. in 't Veld, P. J. Dijkstra, J. H. van Lochem, J. Feijen, *Makromol. Chem.* **1990**, 191, 1813.
- [10] Y. Feng, D. Klee, H. Keul, H. Höcker, *Macromol. Chem. Phys.* **2000**, 201, 2670.

Publication P7

Self-assembly of copolyesters into stereocomplex crystallites tunes the properties of polyester nanoparticles

K. Scheuer, D. Bandelli, C. Helbing, C. Weber, J. Alex, J. B. Max, A. Hocken, O. Stranik, L. Seiler, F. Gladigau, U. Neugebauer, F. H. Schacher, U. S. Schubert, Klaus D. Jandt,

Macromolecules **2020**, *53*, 8340–8351.



Self-Assembly of Copolyesters into Stereocomplex Crystallites Tunes the Properties of Polyester Nanoparticles

Karl Scheuer, Damiano Bandelli, Christian Helbing, Christine Weber, Julien Alex, Johannes B. Max, Alexis Hocken, Ondrej Stranik, Lisa Seiler, Frederike Gladigau, Ute Neugebauer, Felix H. Schacher, Ulrich S. Schubert,* and Klaus D. Jandt*

Cite This: *Macromolecules* 2020, 53, 8340–8351

Read Online

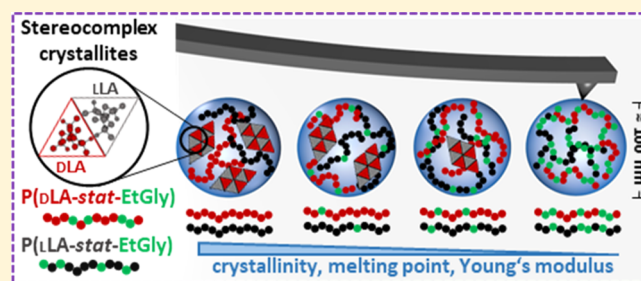
ACCESS |

Metrics & More

Article Recommendations

Supporting Information

ABSTRACT: Self-assembly of polyesters like PLLA and PDLA into stereocomplexes (SCs) is an interesting approach to tailor physical properties of polymeric nanoparticles without affecting their hydrophilicity. Here, we use the stereocomplexation of P(LA-*stat*-EtGly) and P(DLA-*stat*-EtGly) (EtGly: 3-ethylglycolide) to tune the melting temperature (T_m) and degree of crystallinity (w_c) of the bulk polymer. Using time-dependent blending experiments and characterization techniques, such as dynamic light scattering, wide-angle X-ray spectroscopy, differential scanning calorimetry, and atomic force microscopy, we tested the hypothesis that the amount of SCs within the nanoparticles impacts their mechanical properties. Our results show that T_m and w_c can be adjusted *via* the EtGly content. Interestingly, mechanical properties of the nanoparticles depend on the EtGly content as well as the self-assembly time of SCs before nanoparticle formation. This offers a high potential for their application in drug delivery, where their tunable properties will allow to adjust degradation and drug release behavior.



INTRODUCTION

Soft matter polymeric nanoparticles are promising candidates as matrix material for targeted drug delivery systems.^{1–3} Because of adjustable functional group transformations and the availability of a versatile polymeric architecture they are subject of the latest research.^{2,4–6} Drug uptake and release pattern as well as degradation into nontoxic products are the key transport properties of polymeric nanoparticle-based drug delivery systems. In particular, polyesters, such as polylactic acid (PLA), poly(lactic-*co*-glycolic acid), and poly- ϵ -caprolactone, are commonly used for nanoparticle formulation. They offer biocompatibility, biodegradability, straightforward formulation into nanoparticles, and can be modified with functional end groups.^{6–11} To control the key transport properties, it is essential to understand how they are impacted by a variety of factors. The hydrophilic/hydrophobic balance (HHB),^{12,13} the degree of crystallinity (w_c),^{14,15} the melting temperature (T_m) or the glass transition temperature (T_g)¹⁶ are such factors. An important aspect when investigating these parameters is the so-called third variable, a factor that is unintentionally altered and can impact the experimental outcome. An example for this is the HHB which is usually altered if T_m , T_g or w_c are varied by using copolymers of different compositions.^{15,16} This makes it crucial to keep the HHB constant while altering the polymer crystallinity to

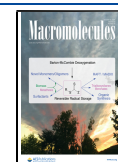
determine the structural effects on drug encapsulation and release.

To achieve this, several approaches exist, like varying copolymer types (block *vs* statistical copolymers)⁸ or combining different isomers in a copolymer.⁹ A third approach is the formation of so-called stereocomplexes (SCs), a polymer crystal structure that consists of polymer chains of opposing stereochemistry.^{17,18} PLA SCs are formed by stereoselective interactions of polymers with opposing chirality by which the L- and D-chains are pairwise packed in a triclinic unit cell.^{17–19} SC formation leads to stronger interactions between the L- and D-chains, compared to the homochiral crystals. This leads to an increased thermal stability and resistance against organic solvents, as well as to higher Young's modulus of the SCs.^{19,20} Typically SCs are formed from melt or from solution.^{20,21} During the SC formation from melt, PDLA and PLLA chains initially form homochiral crystal domains (so called α -domains) in a cold crystallization process when the crystallization temperature of the α -domains is reached.²²

Received: May 27, 2020

Revised: September 4, 2020

Published: October 2, 2020



Upon further heating, the α -domains melt and the chains then rearrange to the SC-structure, which does not transform back into α -domains upon cooling.²² On the other hand, SC formation from solution exploits the increased solvent stability of the SC crystals in comparison to the homocrystalline system.²³ Here, the L- and D chains self-assemble over long periods of time into SC crystals in organic solvents, such as chloroform, acetonitrile, or tetrahydrofuran (THF).^{23,24} The resulting self-assembled micro- and nanostructures of the SCs depend on the stereocomplexation process, the chain length, the presence of secondary polymeric species, and many other factors.^{20,25–37} Because of this and their unique properties, SCs offer potential to alter the T_m of a polymer without affecting its HHB.

In this study, we used P(DLA-*stat*-EtGly) and P(LLA-*stat*-EtGly), synthesized by Bandelli and Alex *et al.*,⁹ to investigate the impact of the 3-ethylglycolide (EtGly) content on the SC formation in solution. The constant HHB of the aqueous nanoparticle suspensions comprising PdLA, PLLA, as well as PEtGly (a polymer consisting of only EtGly) has previously been confirmed by fluorescence spectroscopy of encapsulated pyrene.⁹ Thus, the HHB of the entire system will not be affected by copolymerization or blending because the HHB of all components is the same, as no further additives are required. We further produced polymeric nanoparticles from those SCs with a constant HHB by nanoprecipitation and studied their structure property relationships. The mechanical properties of those nanoparticles depended on the EtGly content as well as the stereocomplexation time. Both parameters allow the adjustment of the nanoparticles' crystallinity. These polymeric nanoparticles will enable targeted experimental studies on how w_c and T_m of polyester-based nanoparticles impact their drug uptake, drug release, and their degradation behavior. Understanding these structure–property relationships is the key to future developments in nanomedicine and to tailor polymeric nanoparticles for targeted drug delivery.

MATERIALS AND METHODS

Copolymers and Chemicals. P(DLA-*stat*-EtGly) and P(LLA-*stat*-EtGly) with 0, 5, 10, and 20 mol % EtGly feeds were synthesized as described elsewhere.⁹ In brief, they were obtained by organo-catalyzed and benzyl alcohol initiated ring-opening copolymerization of EtGly with L- or D-lactide, respectively. They feature molar masses M_n of 10 kg mol⁻¹ and dispersity values D between 1.1 and 1.3. The statistical copolymers were used for the formulation of SCs. Stabilizer-free THF was used to dissolve the copolymers. Nanoprecipitation was performed in ultrapure water (MQW).

Stereocomplexation and Nanoprecipitation. P(DLA-*stat*-EtGly) and P(LLA-*stat*-EtGly) with EtGly contents of 0, 5, 10, and 20 mol % were dissolved in THF to obtain copolymer concentrations of 500 ng μL^{-1} , respectively. In order to prepare SCs, equimolar mixtures of P(DLA-*stat*-EtGly) and P(LLA-*stat*-EtGly) were produced for each EtGly content. These mixtures are referred to as the SC solution. The SCs formed in the SC solutions for up to 7 d. Continuous dynamic light scattering (DLS) measurements were performed to investigate the formation of SCs *in situ*. Additionally, 10 μL aliquots of the SC solutions were regularly withdrawn and drop cast on freshly cleaved mica substrates. These samples were dried at 25 °C at an ambient atmosphere. Atomic force microscopy (AFM) was used to determine the morphology of the SCs that had formed in THF. To obtain the bulk material for spherulite formation and lamellae structure investigation, the SC solution was drop cast on a microscopy glass slide.

Nanoprecipitation of the SCs was performed by producing SC solutions with a copolymer concentration of 1 $\mu\text{g } \mu\text{L}^{-1}$. After 1 min, 12 h, and after 7 d of SC formation, 0.5 mL of these SC solutions were gently poured into 2.5 mL of MQW under vigorous stirring. The vial was then left open for 3 h to let the THF evaporate, resulting in an aqueous nanoparticle dispersion. The hydrodynamic diameter (D_H) and the zeta potential (ζ_{Pot}) of the nanoparticles in dispersion was determined *via* DLS and electrophoretic light scattering (ELS). Additionally, 10 μL of the nanoparticle dispersion were drop cast on freshly cleaved mica substrates. The samples were dried at 25 °C in a normal atmosphere and further characterized by AFM.

DLS and ELS. DLS and ELS were used to observe stereocomplexation in THF as well as to determine the D_H and ζ_{Pot} of the nanoparticles after nanoprecipitation. The measurements were performed on a Zetasizer Nano ZS (Malvern Instruments, Herrenberg, Germany). The instrument operated in the 173° backscatter mode at 25 °C and a wavelength of $\lambda = 633$ nm.

Atomic Force Microscopy. AFM in tapping mode was used to image the formed SC structures, the lamellae structure of the bulk material and the nanoparticles. Further quantitative imaging (QI) was performed to obtain the Young's moduli of the nanoparticles. All AFM measurements were performed in air using a Dimension 3100, a MultiMode (both from Digital Instruments, Veeco, Santa Barbara, CA) equipped with a NanoScope IV Controller and a JPK NanoWizard (JPK BioAFM, Bruker Nano GmbH, Berlin, Germany). Standard tapping mode silicon cantilevers from Bruker (model RTESPA-300, Bruker, Santa Barbara, CA) with a resonance frequency around 300 kHz in air, a spring constant in the range of 20–80 N m⁻¹, and a tip radius of less than 10 nm (typically 7 nm) were used. To determine the Young's moduli of the NPs, we performed QI with an indentation depth of 7–10 nm. The Young's moduli were averaged for 77–103 datapoints of different nanoparticles. To determine statistically significant differences between the samples, a one-way ANOVA Dunn–Sidak test with $\alpha = 0.05$ was performed.

Polarized Light Microscopy. Polarized light microscopy (PLM) was performed in a N₂ atmosphere using a Leica DM2700 equipped with a Linkam heating stage (Linkam Scientific Instruments, Tadworth, UK). PLM was used to observe spherulite formation in the bulk material which was deposited on clean glass slides. The bulk material samples were heated to 225 °C, kept at this temperature for 3 min, and rapidly quenched to 150 °C, and kept at this temperature for 6 h. The heating rate for both, heating and cooling was 50 K min⁻¹. This procedure was based on the SC spherulite formation from the works of Bouapao *et al.* and Tsuji *et al.*^{29,30} who demonstrated the formation of SC spherulites from pure PLLA/PdLA-blends and from PLA-based copolymer blends.^{30,38}

Differential Scanning Calorimetry. Differential scanning calorimetry (DSC) was carried out using a Netzsch 204 F1 Phoenix (Netzsch, Selb, Germany) instrument to determine the bulk material properties T_g , T_m , and w_c . Three consecutive heating runs measured from –20 to 260 °C were performed under a N₂ atmosphere. The heating rate was adjusted in the first and second heating runs to 20 K min⁻¹ and in the third run to 10 K min⁻¹. The cooling rate between every heating run was 20 K min⁻¹. w_c at room temperature was calculated from eq 1^{39,40}

$$w_{c,\text{unweighted}}^{\text{DSC}} = \frac{(\Delta H_m + \Delta H_{cc})}{\Delta H_m^0(\text{PLA})} \cdot 100 \quad (1)$$

in which ΔH_m and ΔH_{cc} are the enthalpies for melting and cold crystallization, respectively. Equation 1 describes the overall crystallinity of our samples, whereas equation E₁ (Supporting Information) also takes into account the crystallizable fraction of the copolymers.⁴¹ Both w_c values were calculated by integrating the respective peak areas of the DSC thermograms. ΔH_m^0 represents the theoretical value for 100% crystallization and has a value of 142 J g⁻¹ according to Tsuji *et al.*²¹

Wide-Angle X-ray Scattering. Wide-angle X-ray scattering (WAXS) measurements were performed to investigate stereocomplexation in the bulk material. The instrument used was a Bruker

AXS Nanostar (Bruker, Billerica, Massachusetts, USA) equipped with an Incoatec 1 μ S Cu E025 microfocus X-ray source, operating at $\lambda = 1.54 \text{ \AA}$ and a VANTEC-2000 detector. A pinhole setup with 750, 400, and 1000 μm (in the order from source to sample) was used and the sample-to-detector distance was 12 cm. In addition to the SCs of varying EtGly contents, pure P Δ LA, P Δ LLA, and P Δ EtGly were investigated. w_c was calculated by using the eq 2

$$w_c^{\text{WAXS}} = \frac{S_c}{S_c + S_a} \cdot 100 \quad (2)$$

in which S_c is the integrated area of the crystalline peaks and S_a is the integrated area of the amorphous region of the WAXS pattern. We used the peak analysis tool of "OriginPro 2015" to analyze the data. The baselines of the WAXS patterns were fitted by hand. The peaks were also chosen manually. Subsequently, the area beneath the peaks alone and the area beneath the complete curve was calculated. The obtained values were used according to eq 2.

Raman Spectroscopy. Samples were placed on CaF₂ slides (Crystal GmbH) or on BOROFLOAT glass wafers for Raman characterization, either as solid samples or drop coated (5 μL and dried at room temperature). An upright Raman microscope was used to record the single spectra (WITec, Ulm, Germany) with 1800 L/mm grating. The Raman excitation laser (488 nm solid state laser, Excelsior 488, 15 mW before objective) was focused with a Nikon 10X NA 0.3, a Zeiss 10X NA 0.2, or a Nikon 100X NA 0.8 objective onto the sample. Spectra were recorded with integration times between 1 and 10 s per spectrum in 10 accumulations. The SC containing nanoparticles in suspension were locally enriched using an in-house produced DEP chip. The quadrupole DEP chip with a gold electrode structure on a fused silica wafer was fabricated and used as described previously;⁴² however, with a reduced distance of 5 μm between the electrodes. The sample (5–15 μL) was injected into 200 μL of 0.5 \times phosphate-buffered saline and single spectra were obtained by focusing a 405 nm laser (10 mW before objective) through a Nikon 60X NA 1 water immersion objective with a grating of 1800 L mm^{-1} and an integration time of 10 s. Statistical analysis was done using Python and results are visualized using Excel and Origin. Spectral preprocessing in Python involved spike removal, background removal, normalization, and resampling. For the calculation of the crystallinity in Excel, the amplitude of the fitted C=O band at 1760 cm^{-1} and the C–H deformation at 1310 cm^{-1} were used.

RESULTS AND DISCUSSION

Bulk Properties. The aim of this study is to demonstrate that the stereocomplexation of P(LLA-*stat*-EtGly) and P(Δ LA-*stat*-EtGly) tunes the properties of polymeric nanoparticles. However, prior to the formulation of nanoparticles, the impact of the EtGly content on SC formation, w_c and T_m of the bulk polymer had to be determined. For this, the bulk materials were investigated *via* WAXS and DSC, as well as PLM, Raman spectroscopy, and AFM. To determine the influence of the EtGly content on T_m of the SCs, DSC measurements were performed. In Figure 1, the DSC thermograms of the third heating run for the SCs and the P Δ LA-based copolymers are shown (refer to the Supporting Information S1–S6 for first and third heating run thermograms of SCs, P Δ LA-, and P Δ LLA-based copolymers including cooling). The T_m of all SCs was significantly higher in comparison to the corresponding copolymers' T_m , which represented the first indication of successful stereocomplexation.⁹ The T_m of the SCs decreased from 199 $^{\circ}\text{C}$ (0 mol % EtGly) to 174 $^{\circ}\text{C}$ (20 mol % EtGly), with increasing EtGly content. This T_m shift matches with the decreasing T_m at elevated EtGly contents for the pure copolymers, which are represented by the dotted lines, as shown in Figure 1.⁹

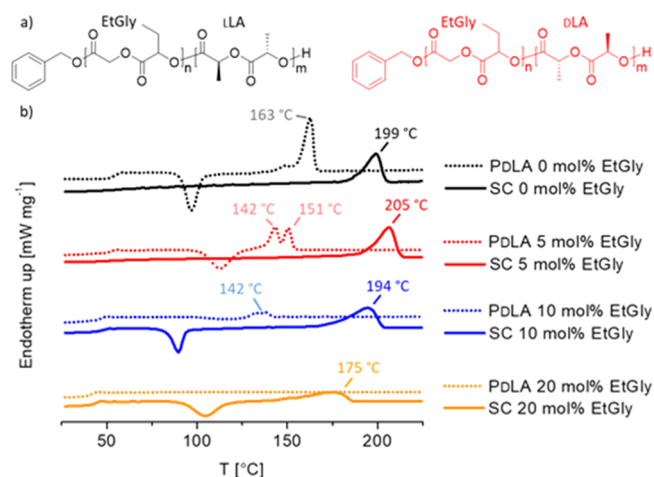


Figure 1. (a) Schematic representation of the structure for P(LLA-*stat*-EtGly) and P(Δ LA-*stat*-EtGly). (b) DSC thermograms (third heating run) of SCs with 0, 5, 10, and 20 mol % EtGly (solid lines). DSC thermograms (third heating run) of P Δ LA-based copolymers with 0, 5, 10, and 20 mol % EtGly (dotted lines).⁹ Additional data can be found in the Supporting Information S1–S6. Thermograms are shifted along the y-axis for clarity.

The T_m of the SCs containing 5 mol % EtGly sample is at 205 $^{\circ}\text{C}$ and, thus, even slightly higher than that of the SCs produced from pure P Δ LA and P Δ LLA after the third heating run. This indicates that the average SC crystallite size of the 0 mol % EtGly SCs is slightly smaller in comparison to the SCs containing 5 mol % EtGly. However, we have not observed this behavior during the first heating run, where a T_m of the 0 mol % SCs is at 238 $^{\circ}\text{C}$ and at 207 $^{\circ}\text{C}$ for the 5 mol % SCs. We conclude that small amounts of EtGly might not be able to suppress SC formation at all but to hinder their nucleation in the melt. As a result, if small amounts of EtGly are present fewer nuclei form from the melt but grow larger in size as they are less hindered by competitive growth of other crystallites. Despite this exception, the overall T_m shift toward lower temperatures with increasing EtGly contents can be explained by the presence of racemic EtGly as repeating unit, which does not crystallize itself and prevents further stereocomplexation. We assume that the EtGly segments in the polymer backbone sterically block the formation of SCs. Additionally, we observed cold crystallization for the SCs with 10 mol % EtGly and 20 mol % EtGly and for P Δ LA-based copolymers containing 0 and 5 mol % EtGly. The latter can be explained by the formation of an α' -phase upon heating, which also results in the observed double peak at T_m .⁴³ The former, however, cannot be explained that easily as the formation of a α' -phase would lead to distinctive melting peaks in the corresponding SC thermographs which were not observed. Thus, the presence of EtGly segments may suppress crystallite formation upon cooling. Therefore, both the nucleation rate and crystal growth are slowed down. The system has not reached the equilibrium state when the temperature falls below T_g at which the chain mobility is not sufficient to assemble into crystalline structures. Thus, upon heating above T_g , the chain mobility increases and the crystallization process continues.

Figure 2 shows the WAXS results of the SCs and P Δ LA-based copolymers as the reference (refer to the Supporting Information S7 for WAXS patterns of pure P Δ EtGly and P Δ LLA-based copolymers). Their WAXS patterns reveal a main intensity peak at an angle of 17 $^{\circ}$ and additional intensity peaks

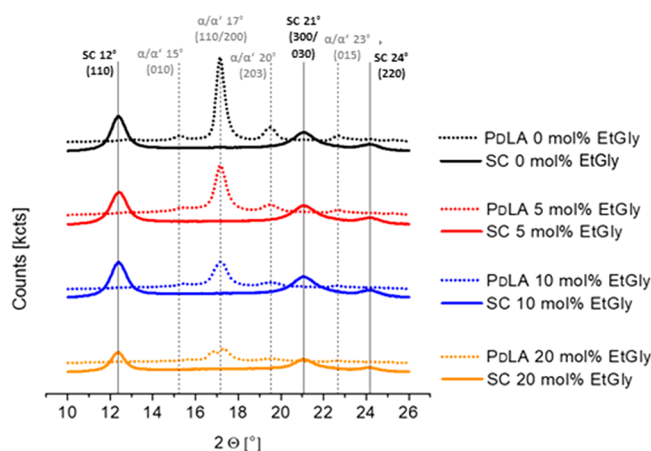


Figure 2. Bulk material WAXS patterns of the PdLA-based copolymers (dotted lines) as well as of SCs with 0, 5, 10, and 20 mol % EtGly (continuous lines). Additional data can be found in the Supporting Information S7. WAXS patterns are shifted along the y-axis for clarity.

at angles of 15, 20, and 23° which agrees with patterns of crystalline PLLA and PdLA reported in the literature.^{19,44,45} According to Shyr *et al.*, the 15° peak belongs to the (010) plane, the 17° peak to the (110/200) plane, the 20° peak to the (203) plane, and the 23° peak to the (015) plane of the orthorhombic α or α' -phase of the homochiral PLA crystals.⁴⁶ In contrast, the pattern for pure PEGly confirms that this material is amorphous (refer to the Supporting Information S7), in agreement with DSC investigations that are reported elsewhere.⁹ Interestingly, the WAXS patterns for PdLA and PLLA containing 20 mol % EtGly display a double peak at 17° with the first maximum located at 16.9° and the second at 17.4°. This might be caused by the high EtGly content of these samples leading to increased distortions in the crystal structure. The WAXS patterns of the equimolar mixtures of P(DLA-*stat*-EtGly) and P(LLA-*stat*-EtGly) with 0 mol % EtGly, 5 mol % EtGly, 10 mol % EtGly, and 20 mol % EtGly display three distinctive intensity peaks at angles of 12, 21, and 24°. According to Shyr *et al.*, the 12° peak belongs to the (110) plane, the 21° peak to the (300/030) plane, and the 24° peak to the (220) plane of the triclinic SC crystals in the bichiral blends of PdLA and PLLA and their copolymers.⁴⁶ These intensity peaks were not detected for homochiral PLLA or PdLA or their copolymers, respectively. This is a clear indication that stereocomplexation occurred in the bulk material of all samples and that no homochiral α or α' -phase has formed in the blended bichiral system, which is in line with the DSC results described above.^{19,47} Furthermore, the signal intensity varied between each sample, whereas no intensity peak shift was observed. This shows that the unit cell of the SCs remained unaffected by the EtGly mers. These are seemingly located within the amorphous regions of the polymer. This is supported by other reports on the crystallization behavior of SCs formed by copolymers that were discussed with respect to the effect of phase separation during stereocomplexation.^{30,48,49}

To determine the influence of the EtGly content on the overall crystallinity of our polymers at room temperature, we calculated the unweighted w_c of the SCs based on the WAXS measurements and the DSC results (Table 1). The w_c , weighted by the fraction of crystallizable mers is given in the

Table 1. Thermal Properties, Unweighted Degree of Crystallinity at Room Temperature from DSC and WAXS, and Lamellae Distance According to AFM of the SC Bulk Material (Additional Data can be Found in the Supporting Information T_{S1})

EtGly feed [mol %]	T_g [°C] ^a	T_m [°C] ^a	T_{cs} [°C] ^a	w_c^{DSC} [%] ^b	w_c^{DSC} [%] ^a	w_c^{WAXS} [%]	lamellae distance [nm]
0	n.a.	199	n.a.	52	39	45	18 ± 4
5	n.a.	206	n.a.	36	31	47	19 ± 4
10	47	194	90	32	16	41	23 ± 5
20	43	175	105	27	1	33	n.a.

^aData obtained and calculated from the third heating run (heating rate: 10 K min⁻¹). ^bData obtained and calculated from the first heating run (heating rate: 20 K min⁻¹).

Supporting Information T_{S1}, describing the crystallinity of the PLA crystalline domains formed in the copolymer samples in comparison to pure PLA. For both methods, we found that the w_c decreased with increasing EtGly content from 45 to 33% according to WAXS or from 52 to 27% for DSC (first heating run, see Supporting Information S2), respectively. The w_c^{WAXS} value of the 5 mol % sample of 47% was slightly higher than the one of the 0 mol % EtGly-containing SCs ($w_c^{\text{WAXS}} = 45\%$). However, the deviation is within the accuracy range for crystallinity calculations from WAXS measurements. According to DSC, the unweighted and weighted (see Supporting Information T_{S1}) w_c values show that, after the third heating run, the crystallinity of the 0 mol % EtGly sample is 39% and between 31 and 33% for the 5 mol % EtGly sample. Despite the accuracies of both methods (around 10–15%), the overall trend toward lower w_c with increasing EtGly content was displayed by both, DSC and WAXS analysis, and particularly evident when considering values from the third DSC heating run. The observation is caused by the slow crystallization kinetics, evident from the absence of a T_c during the DSC cooling runs but a cold crystallization during heating, in particular for samples with 10 and 20 mol % EtGly.

To gain deeper insights on the micro- and nanoscale structures of the resulting SCs, spherulites were formed and characterized by PLM and AFM. To obtain spherulites, we changed the temperature regime based on Bouapao *et al.* and Tsuji *et al.*^{29,30} The samples were heated to 225 °C, kept there for 3 min, rapidly quenched to 150 °C, and kept for 6 h. This led to the formation of mostly individual spherulites for all samples except the 20 mol % EtGly sample.

We carried out the AFM investigations of the lamellae at the edge of equally sized spherulites to determine the lamellae structure. Both, representative PLM images of the spherulites and AFM phase images of the corresponding lamellae structure can be seen in Figure 3. The distance between the lamellae within the spherulites increased with increasing EtGly content (Table 1). Thus, the number of amorphous regions between the lamellae increases as the EtGly content does. We assume that the EtGly rich areas of the polymer chain cannot undergo crystallization. The formation of crystalline regions relies on the presence of PLLA and PdLA within the copolymer backbone. However, it seems that increased EtGly contents can suppress the formation of spherulites at the chosen temperature as we obtained no spherulites for the 20 mol % EtGly samples with our treatment. This in combination with the lamellae structures found with AFM support the conclusion drawn from the DSC and WAXS results. Overall,

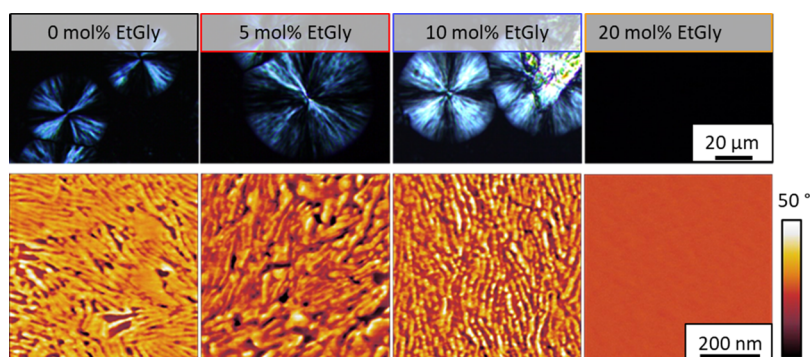


Figure 3. Bulk material morphology of SC spherulites containing 0, 5, 10, and 20 mol % EtGly. Top: SC spherulites in PLM. Bottom: AFM phase images of the SC lamellae structures.

this confirms that the degree of crystallinity of the homogeneous crystals⁹ and the SCs can be adjusted *via* the EtGly content.

In addition to WAXS and DSC, Raman spectroscopy is able to differentiate between neat PLA stereoisomers and SCs. Figure 4 shows mean Raman spectra of the polymers PLLA and

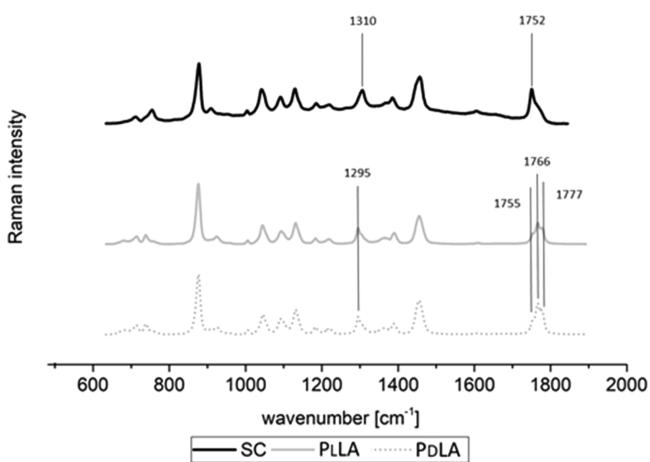


Figure 4. Mean Raman spectra of PLLA, PDLA, and the SC formed from both polymers. Additional data can be found in the Supporting Information T₅2, S8 and S9 (Raman spectra are shifted on the y-axis for clarity).

PDLA as well as of the SCs. The vibrational bands reveal the characteristic features of PLA and agree with spectra previously published in the literature.^{42,50,51} A band assignment is found in Table T₅2 in the Supporting Information. SCs present in the material can be identified by a sharp C=O stretching band centered at 1752 cm⁻¹ and the shape and the position of the C–H deformation band around 1300 cm⁻¹. Slight variations in the relative intensity of the broader shoulder around 1298 cm⁻¹ (for the C–H deformation band) and at 1770 cm⁻¹ (for the C=O stretching band) indicate different amorphous content. For the assignment of conformation and crystallinity, the C=O stretching vibration between 1730 and 1790 cm⁻¹ is of great interest.⁵¹ In semi-crystalline polymers (here, PLLA and PDLA in Figure 4), this region is split into three major overlapping bands centered at 1755, 1766, and 1777 cm⁻¹. In the highly ordered SCs, this looks very different (Figure 4). A strong, sharp band is found at 1752 cm⁻¹, which originates from the totally symmetric stretching vibration, and a broader shoulder occurs around 1770 cm⁻¹, which results from the

vibration of the more amorphous component. For all bulk SCs, the Raman spectra displayed those typical peaks (Figure S8 in the Supporting Information). This supports the findings from WAXS and DSC. Raman spectra of SC with various EtGly contents and w_c calculations can be found in the Supporting Information S8 and S9.

Stereocomplexation Dynamics. Stereocomplexation in solution is a self-assembly process that can take several days, depending on the polymer, solvent, and polymer concentration used.^{21,24} We were interested in how SCs are incorporated into polymeric nanoparticles upon nanoprecipitation. We investigated the dynamics of this process in THF before nanoprecipitation by long-time DLS measurements of the SC solution, accompanied by AFM investigations to monitor the formed structures. Figure 5a shows the measured D_H of the different solutions of PDLA and PLLA in THF prior to nanoprecipitation over a time of 7 d. For the SC solutions with 0, 5, 10, and 20 mol % EtGly, the data revealed a similar behavior. The measured D_H of SCs from pure PLLA and PDLA scattered strongly within the first 12 h of stereocomplexation and dropped to a relatively stable value afterward. This indicated the start of the SC formation in THF. From this point, we observed a continuous growth of the SCs after nucleation in DLS. The measured D_H of the 5 and 10 mol % EtGly samples behaved similarly, yet their DLS signals continued scattering within a broader size range than the DLS signal of the 0 mol % EtGly sample (see the Supporting Information S10). This is because the EtGly impacted the formation and growth of SCs in solution. Following this trend, we found that the signal of the 20 mol % EtGly sample revealed the least stable signal over time.

Additionally, we used AFM samples to monitor the size and morphology of the structures formed in THF (Figure 5b). The 0 mol % EtGly sample after 1 min of stereocomplexation formed only dendritic structures. After 12 h, we detected disc-like agglomerates embedded within an amorphous film. The latter almost completely disappeared after 4 d of incubation and the sample was covered with disc-like structures (see Supporting Information S11). Similar structures are also reported in the literature to be a typical structure for SCs formed in solution.^{23,24,52,53} We found first triangular-shaped SCs after 50 min of incubation, when no stable DLS signal was obtained (refer to the Supporting Information S13). This shows that the nucleation process started earlier than the DLS results suggest and that the first SC crystallites cannot be observed in the used DLS setup.^{23,24} After 7 d, the disc-like structures formed large agglomerates but no noticeable

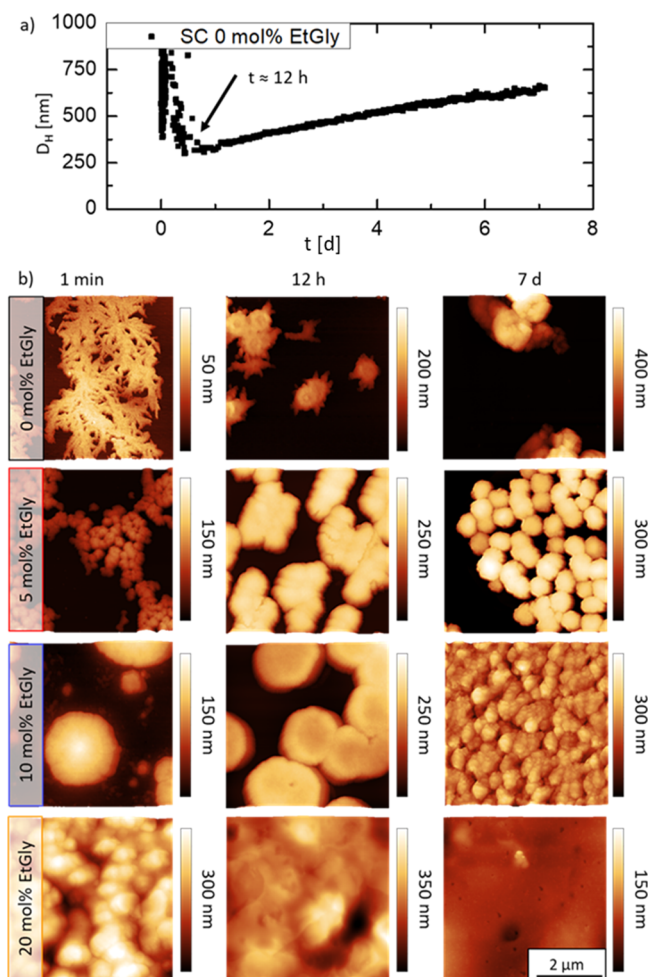


Figure 5. Time-dependent stereocomplexation in THF: (a) D_H of SCs with 0 mol % EtGly forming in THF over 7 d, the black arrow marks the time when a stable signal was obtained (DLS data). (b) AFM height images of the dried SC structures containing 0, 5, 10, and 20 mol % EtGly after 1 min, 12 h, and 7 d of stereocomplexation in THF. Additional data can be found in the Supporting Information S10–S12.

changes in shape were visible. In contrast to the 0 mol % EtGly samples, the 5 and 10 mol % samples formed polymeric dewetting structures instead of dendritic structures after 1 min as well as 12 h stereocomplexation. Like the 0 mol % EtGly samples, we found disc-like structures for the 5 mol % EtGly sample after 7 d, indicating the formation of SCs. However, the 10 mol % EtGly samples showed only round nodules which formed large agglomerates within a polymeric film after 7 d of incubation. Over the entire period, the 20 mol % EtGly sample only formed a film. This shows that increasing EtGly contents effectively suppressed the formation of SCs in solution within the observed time span of 7 d. Yet higher polymer concentrations or longer incubation times might lead to the formation of observable SC structures for the 10 mol % EtGly and 20 mol % EtGly samples as well.

These results strongly support the conclusions from the DSC, WAXS, PLM, and Raman data: increasing EtGly contents in the copolymers delay or block the formation of SCs. Further, this time-dependent behavior might be exploited as a second mechanism to control the amount of SCs incorporated into the polymeric nanoparticles, next to varying

the EtGly content of the copolymers. However, the smallest observed particles formed in THF featured hydrodynamic diameters of around 400–600 nm and above, according to DLS. In addition, the investigated structures in AFM ranged within these dimensions, which are too large to be considered as nanoparticles.

Nanoparticle Formation and Characterization. Based on the results of the stereocomplexation dynamics experiments (Figure 5), we produced polymeric nanoparticle dispersions after mixing the polymer solutions for 1 min, 12 h, and 7 d. We drop cast 0.5 mL of the polymer solution into 2.5 mL of MQW at room temperature under vigorous stirring. Afterward, the vial was left open for at least 3 h to allow evaporation of the THF. During this process, the THF diffused into the water, whereas the water insoluble polymer precipitated as nanoparticles.²⁰ Thus, the chain mobility was drastically decreased and the process of stereocomplexation stopped. Therefore, we will refer to the nanoprecipitation process in the following text as quenching. We determined ζ_{Pot} and D_H via ELS and DLS (see Supporting Information S13 for ζ_{Pot}) and also used AFM to investigate the particle morphology and Young's modulus. Figure 6 displays AFM height images from the QI measurements of the nanoparticles after 7 d of stereocomplexation prior to quenching. Images of particles quenched after 1 min and 12 h can be seen in the Supporting Information (Figure S14). The particles featured a round morphology and tended to agglomerate upon drying on the mica substrate. Their D_H ranged between 62 nm for the 20 mol % EtGly nanoparticles and increased with decreasing EtGly content up to 107 nm for the 0 mol % EtGly nanoparticles according to DLS (Figure 5b). The Young's modulus after 7 d of incubation also decreased with increasing amounts of EtGly from 1.7 ± 0.73 GPa for the 0 mol % EtGly nanoparticles toward 1.14 ± 0.48 GPa for the 20 mol % EtGly nanoparticles (representative force distance curves can be seen in the Supporting Information S15). This correlates well with the decreasing values of w_c and T_m , obtained from bulk material measurements of the SCs and of the copolymers prior to stereocomplexation (see Supporting Information T_S1).⁹ As discussed by Wang *et al.*, this points toward an increased crystallinity of the particles having lower EtGly contents and longer incubation times prior to nanoprecipitation.⁵⁴ In contrast, the mechanical properties of the NPs quenched after 1 min and 12 h revealed no relationship between their EtGly content and their Young's moduli or the EtGly content and the particle size, respectively (see Supporting Information S14). This is because after this amount of time, the self-assembly process of the SCs was interrupted at a stage where the amount of SCs incorporated into the nanoparticles (respectively the nanoparticles' crystallinity) strongly fluctuates. However, we observed that small particle sizes were accompanied by relatively high Young's moduli of 3 GPa and higher for the samples quenched after 1 min and 12 h of stereocomplexation. This is because of a higher impact of the substrate's properties on the measurement for lower particle sizes.

We assume that after 7 d of stereocomplexation, the amount of SCs within the polymeric nanoparticles depends on the EtGly content and contributes significantly to the particles Young's modulus. Also, the decreasing nanoparticle size might have impacted on the nanoparticles Young's modulus. We expected that smaller particle sizes lead toward higher Young's moduli because the substrate might have an increasing impact on the measurement. With the used AFM setup, the substrates

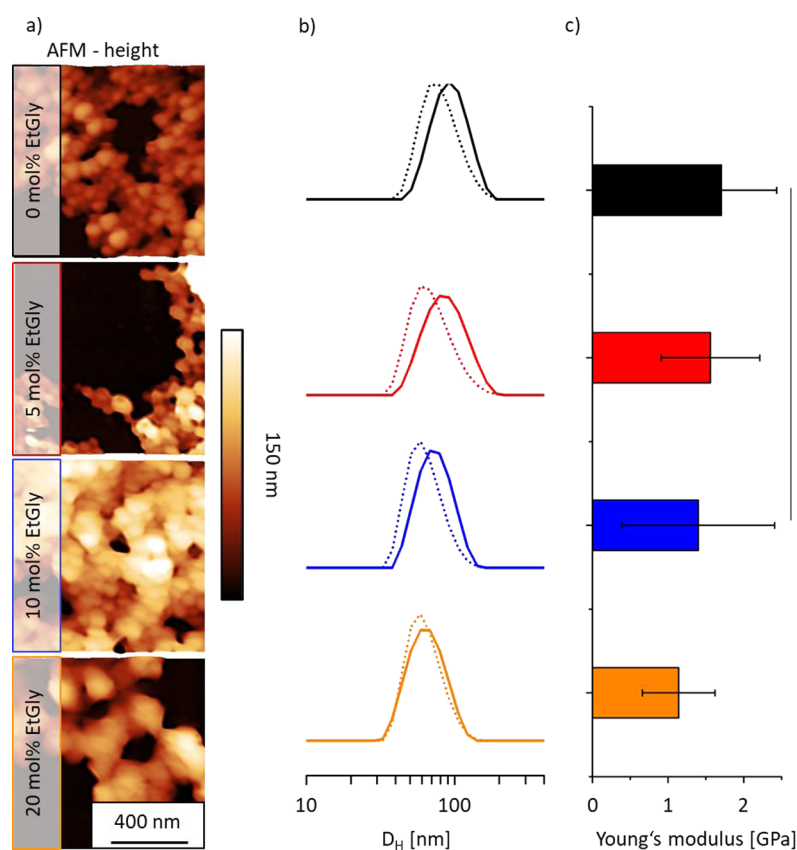


Figure 6. Polymeric nanoparticles quenched from SC solution: (a) AFM height images from QI measurements of the SC-containing nanoparticles with 0, 5, 10, and 20 mol % EtGly after 7 d of stereocomplexation prior to water quenching. (b) DLS size distributions of the nanoparticles dispersions with hydrodynamic diameters ranging from $D_H \approx 60\text{--}110$ nm; the full lines represent the size distributions by intensity, the dotted lines by volume. (c) Young's moduli of the particles determined *via* AFM, the error bars represent the standard deviation of all measurements. The vertical lines in (c) mark statistically significant differences according to a one-way ANOVA Dunn–Sidak test with $\alpha = 0.05$. Additional data can be found in the [Supporting Information S14](#).

Young's modulus was determined to be 32.6 ± 6.1 GPa, which is roughly 10 times higher than the Young's modulus of the nanoparticles. However, this is not the case here. If sufficient time for SC formation is given, the various amounts of SCs in the nanoparticles still cause detectable differences between samples with different EtGly content. In the case of the 1 min and 12 h samples, the stereocomplexation time was not sufficient. According to DLS (see [Supporting Information S10](#)), neither 1 min nor 12 h led to the formation of observable SCs in solution. Thus, upon quenching, the small amount of SCs within the nanoparticles did not impact their mechanical properties. Otherwise, we would expect a similar behavior of the particles quenched after 12 h as of those quenched after 7 d of incubation. Instead, we see an increased impact of the substrate on the measurements, as lower particle sizes led to higher Young's moduli. Combining these findings with the DLS data of the kinetic experiments, it can be assumed that after 7 d of stereocomplexation prior to quenching, sufficient amounts of SCs have been formed to impact the mechanical properties of the corresponding nanoparticles.

To support our assumptions based on AFM and DLS, we tried to obtain the nanoparticle crystallinity *via* Raman spectroscopy in both dried state and aqueous dispersion. [Figure 7](#) shows the conformation- and crystallinity-relevant spectral regions of the C–H deformation and the C=O stretching ([Figure 7a,b](#)) vibration of the nanoparticles in the dried state and in aqueous dispersion. Defined bands at 1752

and 1300 cm^{-1} were obtained for the nanoparticles containing 0 mol % EtGly after an incubation time of 7 d prior to nanoprecipitation, indicating the formation of significant amounts of SCs in this sample. The other samples displayed less defined bands with lower relative amplitudes which results from decreasing crystallinity of the nanoparticles. In [Figure 7c](#), the relative amplitudes at 1760 cm^{-1} are displayed for dry nanoparticles containing 0 mol % EtGly after 1 min, 12 h, and 7 d of stereocomplexation prior to nanoprecipitation, as well as for nanoparticles obtained after 7 d of incubation containing 5, 10, and 20 mol % EtGly (additional information can be found in the [Supporting Information Figure S16](#)). The data show that the crystallinity decreases as the EtGly content increases and as the stereocomplexation time decreases. Interestingly, the Raman spectra of the nanoparticles in dispersion looked very similar to the nanoparticles in the dried state. This proves that Raman spectroscopy is a suitable tool to determine the crystallinity of polymeric nanoparticles in dispersion. To the best of our knowledge, this has not been done before for a polymeric material. Therefore, our results point out that Raman spectroscopy is a valuable tool to monitor polymeric nanoparticles for drug delivery *in situ* in future research.

Mechanism of the Time-Dependent SC Content Increase of Polymeric Nanoparticles. To explain the morphological and mechanical data of the polymeric nanoparticles prepared by nanoprecipitation, the stereocomplexation kinetics as described above need to be considered.

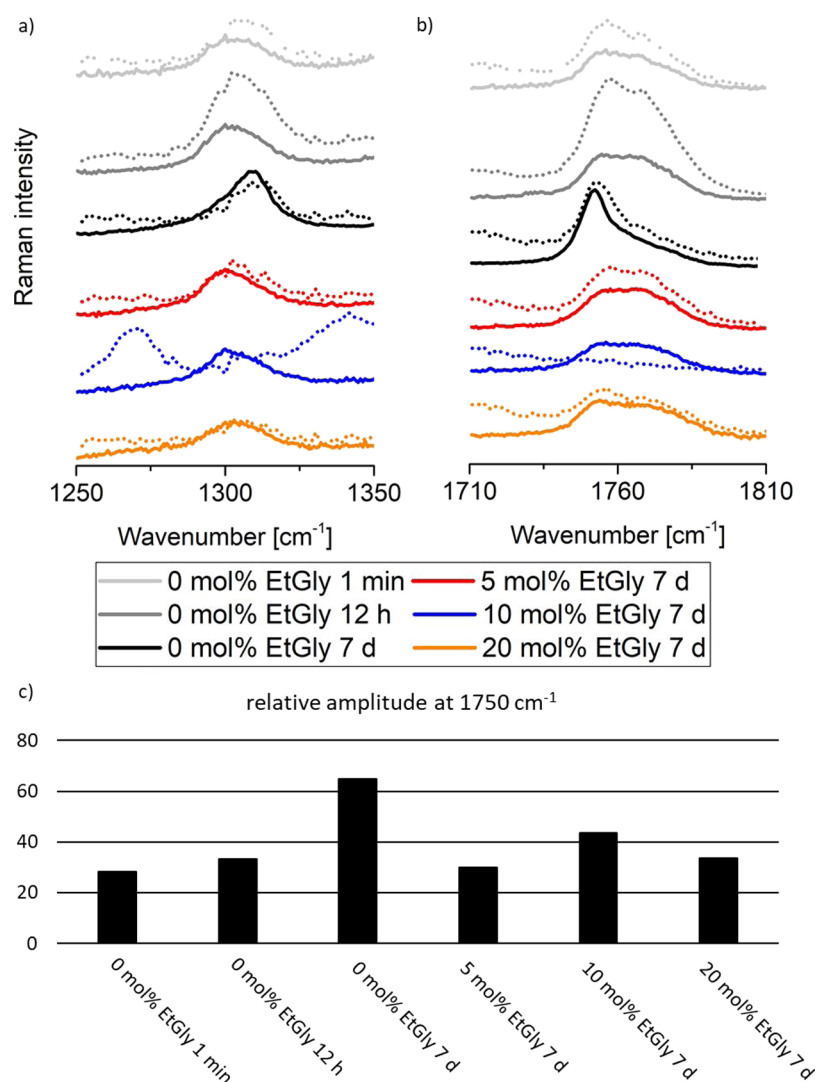


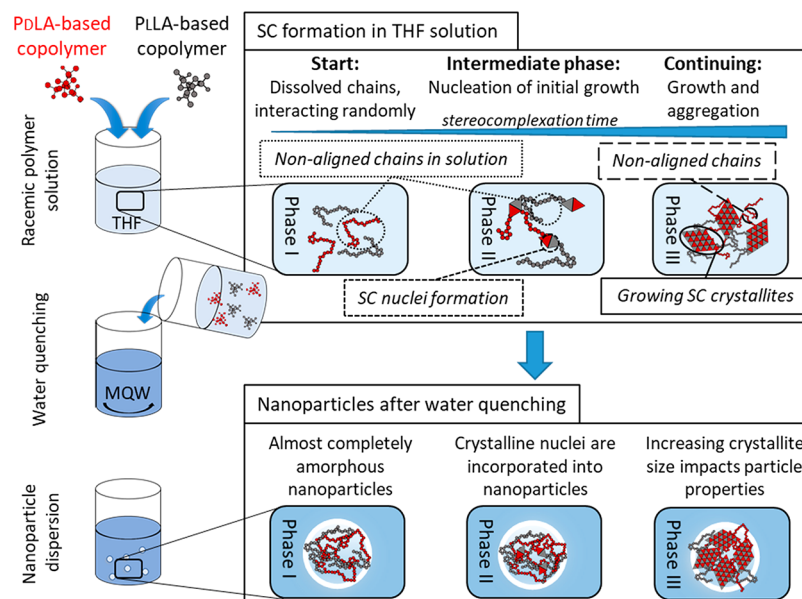
Figure 7. Raman spectroscopy data of nanoparticles with 0 mol % EtGly nanoprecipitated after 1 min, 12 h, and 7 d of stereocomplexation in THF and of nanoparticles containing 5, 10, and 20 mol % EtGly, nanoprecipitated after 7 d of stereocomplexation in THF (full lines: dry nanoparticles, dotted lines: nanoparticles in aqueous dispersion). (a) C–H region at 1310 cm⁻¹, (b) C=O region at 1750 cm⁻¹, (c) relative amplitude of the dried nanoparticles at 1750 cm⁻¹, lower amplitudes result from lower degrees of crystallinity. Additional information can be found in the Supporting Information Figure S16. Raman spectra are shifted along the y-axis for clarity.

Stereocomplexation is a self-assembly process.^{21,24,32} If stereocomplexation takes place in solution, the concentration-dependent mean free path between the polymer chains strongly impacts the rate of possible interactions between the L- and D-segments of the polymers. SCs have a significantly lower critical concentration threshold for precipitation from organic solvents in comparison to their homochiral counterparts. Therefore, these L- and D-interactions lead to the self-assembly of stable SC nuclei, which then start to grow.^{55,56} There are several studies on various materials that self-assemble into nanostructures, for example, on proteins but also on phase separations of copolymers and polymer blends.^{57–60}

Based on the knowledge of self-assembly processes in solution, we propose a mechanism for the time-dependent stereocomplexation in solution. After mixing the polymers in THF solution, there is a certain “lag-phase”.⁵⁷ During this lag phase, the polymer chains interact randomly, forming unstable SC nuclei that quickly dissolve again. No observable crystallization happens during this phase. However, because THF is a weak solvent for the SCs, the solution enters a state

of supersaturation upon mixing. This results in the precipitation of SC nuclei after the lag phase.^{21,56} In our DLS investigation of the SC formation in THF (Figure 5a), we observed a stabilization of the D_H at roughly 250 nm after 12 h. AFM monitoring revealed that at this time disc-like structures have formed, which subsequently grow in diameter over time if left in THF (Figure 5b). However, we monitored the structures formed in DLS via AFM in a 10 min period during the first hour of stereocomplexation. Here, we saw triangular structures appear after approximately 50 min of incubation, the corresponding AFM images can be seen in Figure S12 in the Supporting Information. These triangular structures might represent SC single crystals as was reported earlier by Slager *et al.*^{23,24} Because of this, the lag phase ended after approximately 50 min. This leads to the conclusion that nucleation started earlier than 12 h but was not detectable with DLS in the applied setup. These results also correspond well with previously reported experiments, supporting our model.^{52,61} After the formation of stable SC nuclei, crystals started growing. During this phase, the SCs increased in size as long as

Scheme 1. Model of the Self-Assembly of SCs in THF and the Effect of Quenching the SC Solution at Different Time Points; (I) “Lag-Phase”: Short Time after Mixing, No Stable/Observable SC Nuclei Form; Quenching Leads to Almost Completely Amorphous Nanoparticles; (II) “Nucleation and Initial Growth”: Stable SD Nuclei Form that Cannot be Observed in DLS; upon Quenching These Crystalline Nuclei Are Incorporated in Mostly Amorphous Nanoparticles; (III) “Growth and Aggregation”: the SCs in THF Grow over Time and Form Structures That Can Be Monitored *via* DLS; Depending on the Incubation Time, the Amount, and Size of SD Crystallites Incorporated into the Nanoparticles upon Water Quenching Impacts the Nanoparticles Size and Their Mechanical Properties



polymer chains could be incorporated into the crystal structure. Additionally, the SC crystals start to aggregate, which leads to the disc-like structures that we observed with AFM (see Figure 5b). This aggregation process leads to the observed stabilization of the DLS signal after 12 h (see Figure 5a). One factor that might influence the duration and outcome of the growth phase is therefore not only the presence of crystallizable polymer chains but also their accessibility toward each other. The presence of a noncrystallizable mer-species such as EtGly can reduce both the nucleation rate of SCs and their growth rate. It might also sterically block the formation of disc-like structures, which were not observed for elevated EtGly contents (see Figure 5b). This can happen up to a point where the formation of SCs is completely blocked. The absence of disc-like aggregates for the 20 mol % EtGly sample after 7 d of SC formation in THF (Figure 5b) and the suppression of spherulite formation in the bulk material (Figure 3) support this hypothesis.

If the SC solution is drop cast into water during stereocomplexation, the chain mobility is rapidly reduced within a very short period, preventing further SC growth. Thus, the internal structure of the formed nanoparticles reflects the current state of self-assembly at the moment of quenching. This proposed process on how the crystallites might be incorporated into the nanoparticles after quenching the SC solution is shown in Scheme 1. We assume that the polymeric nanoparticles were mostly amorphous when the SC solution was quenched after 1 min (Scheme 1, phase I). Size and Young's modulus of the nanoparticles therefore depended mainly on the quenching parameters. These quenching parameters, for example, the speed with which the polymer solution was injected into the water, the polymer concentration of the solution, and the stirring speed determine the diffusion rate of THF into the water. Thus, they control how rapidly the

chain mobility of the polymers is decreased. Variations of these parameters result in deviations in the mean free path length between the polymer chains after precipitation, impacting the mechanical properties of the material of the resulting nanoparticle. The same explanation is valid for the nanoparticle size and Young's modulus of SCs quenched after 12 h. At this point, data of the stereocomplexation dynamics suggests the presence of SCs in solution. However, we see that the SC aggregates more than double in size over the duration of a week, meaning that the actual amount of SCs after 12 h is still not sufficient to impact the nanoparticle properties. This aligns well with the Raman results. Only after 7 d, the sample showed high SC content.

However, because these nuclei are small in number and size, their impact on the nanoparticle size and Young's modulus is seemingly neglectable (Scheme 1, phase II). The main factor influencing these values is again the quenching parameters. Thus, neither the size of the quenched nanoparticles nor their Young's modulus correlated with their EtGly content after 1 min and 12 h of stereocomplexation prior to quenching (Figure 6b). Phase III (Scheme 1, phase III) is the growth and aggregation phase of SCs in the THF solution in which the size of the formed SCs increased gradually over time. This is supported by the DLS investigations of the SC formation in THF solution (Figure 5a). However, we found with AFM investigations after 7 d of incubation that the size of the formed aggregates depended on the composition of the polymers: less EtGly content resulted in larger, more defined structures (Figure 5b). Most likely, the average amount and size of SCs that are incorporated into the nanoparticles upon quenching depend on the copolymer composition during phase III. This means that the Young's modulus of the quenched nanoparticles and their size mainly depend on the EtGly content if sufficient time for SC formation is given

(Figure 5a). This is also supported by our Raman investigations. Although the applied setup may not be suitable to determine the absolute w_c value of the nanoparticles, comparison of the relative amplitudes beneath the C=O band and the C–H band at 1750 and 1310 cm^{-1} , respectively, showed that the amount of amorphous phases within the particles decreased when the stereocomplexation time prior to nanoprecipitation was increased and when the EtGly content decreased (see Figure 7).

All investigations in this study consistently indicate that high EtGly contents result in a lower stereocomplexation rate, decreased crystallinity, and lower melting temperatures. Because the melting temperature of a polymer correlates with the average crystallite thickness, an increase in EtGly content seemingly leads to thinner crystallites. Thus, the degree of crystallinity of the nanoparticles, quenched after 7 d of stereocomplexation in THF, can be adjusted by the EtGly content of the used copolymers. This proves that time-dependent stereocomplexation and stereocomplexation of copolymers can be used to control both, the degree of crystallinity and the mechanical properties of polymeric nanoparticles without affecting their HHB. These polymeric nanoparticles allow direct investigations of the impact of the nanoparticle crystallinity and T_m on the drug uptake and release as well as enzymatic degradation without the influence of other parameters such as a varied HHB.

CONCLUSIONS

In this study, we showed that stereocomplexation offers two alternative ways to control and adjust the crystallinity of polymeric nanoparticles, without changing the HHB of the overall system. While our approach focused on PLA-based polymers only, we assume that our findings can be transferred to other bichiral systems as well. The first way is the SC formation itself, which leads toward different crystal structures within the polymeric nanoparticles and toward higher T_m . The other way relies on the self-assembly mechanism and dynamics of SCs in solution. We demonstrated and discussed how the stereocomplexation dynamics impact the nanoparticle size and the nanoparticle properties. Understanding the stereocomplexation kinetics enables the adjustment of the nanoparticle properties *via* time-dependent quenching. Because SCs are formed in THF their formation is not affected by the quenching parameters. For the first time, the degree of crystallinity of SC containing nanoparticles in aqueous dispersion was adjusted *via* the EtGly content, stereocomplexation, and the stereocomplexation kinetics, while keeping the HHB of the system constant. This will enable systematic investigations on the dependence of the enzymatic degradation, the drug uptake, and the drug release on structural features of the polymeric nanoparticles. With these studies, we aim to develop a mechanistic model for the prediction of these dependencies with respect to a wide range of polymeric nanoparticles to be used in drug delivery.

ASSOCIATED CONTENT

Supporting Information

The Supporting Information is available free of charge at <https://pubs.acs.org/doi/10.1021/acs.macromol.0c01247>.

DSC thermograms of pure P(LLA-*stat*-EtGly), pure P(DLA-*stat*-EtGly), and SCs containing 0–20 mol % EtGly, WAXS patterns for P(LLA-*stat*-EtGly) containing

0–20 mol % EtGly and pure PEtGly, DLS data and AFM images of time-dependent SC formation in THF, ELS, and DLS data of SC containing nanoparticles, AFM images and Young's moduli of SC containing nanoparticles, T_m and w_c values for the noncomplexed copolymers, and Raman data of the bulk material, dried nanoparticles, and nanoparticles in dispersion (PDF)

AUTHOR INFORMATION

Corresponding Authors

Ulrich S. Schubert – Laboratory of Organic and Macromolecular Chemistry (IOMC) and Jena Center for Soft Matter (JCSM), Friedrich Schiller University Jena, Jena 07743, Germany; orcid.org/0000-0003-4978-4670; Email: ulrich.schubert@uni-jena.de

Klaus D. Jandt – Chair of Materials Science (CMS), Department of Materials Science and Technology, Otto Schott Institute of Materials Research, Faculty of Physics and Astronomy and Jena Center for Soft Matter (JCSM), Friedrich Schiller University Jena, Jena 07743, Germany; orcid.org/0000-0002-7537-5603; Email: k.jandt@uni-jena.de

Authors

Karl Scheuer – Chair of Materials Science (CMS), Department of Materials Science and Technology, Otto Schott Institute of Materials Research, Faculty of Physics and Astronomy, Friedrich Schiller University Jena, Jena 07743, Germany

Damiano Bandelli – Laboratory of Organic and Macromolecular Chemistry (IOMC) and Jena Center for Soft Matter (JCSM), Friedrich Schiller University Jena, Jena 07743, Germany; orcid.org/0000-0002-9968-2560

Christian Helbing – Chair of Materials Science (CMS), Department of Materials Science and Technology, Otto Schott Institute of Materials Research, Faculty of Physics and Astronomy, Friedrich Schiller University Jena, Jena 07743, Germany

Christine Weber – Laboratory of Organic and Macromolecular Chemistry (IOMC) and Jena Center for Soft Matter (JCSM), Friedrich Schiller University Jena, Jena 07743, Germany; orcid.org/0000-0003-0712-5255

Julien Alex – Laboratory of Organic and Macromolecular Chemistry (IOMC) and Jena Center for Soft Matter (JCSM), Friedrich Schiller University Jena, Jena 07743, Germany

Johannes B. Max – Laboratory of Organic and Macromolecular Chemistry (IOMC) and Jena Center for Soft Matter (JCSM), Friedrich Schiller University Jena, Jena 07743, Germany

Alexis Hocken – Chair of Materials Science (CMS), Department of Materials Science and Technology, Otto Schott Institute of Materials Research, Faculty of Physics and Astronomy, Friedrich Schiller University Jena, Jena 07743, Germany

Ondrej Stranik – Leibniz Institute of Photonic Technology, Jena 07743, Germany; orcid.org/0000-0001-8995-8132

Lisa Seiler – Leibniz Institute of Photonic Technology, Jena 07743, Germany; Institute of Physical Chemistry and Abbe School of Photonics, Friedrich Schiller University Jena, Jena 07743, Germany

Frederike Gladigau – Leibniz Institute of Photonic Technology, Jena 07743, Germany; Institute of Physical Chemistry and Abbe School of Photonics, Friedrich Schiller University Jena, Jena 07743, Germany

Ute Neugebauer – Laboratory of Organic and Macromolecular Chemistry (IOMC) and Institute of Physical Chemistry and

Abbe School of Photonics, Friedrich Schiller University Jena, Jena 07743, Germany; Leibniz Institute of Photonic Technology, Jena 07743, Germany; Center for Sepsis Control and Care, Jena University Hospital, Jena 07747, Germany

Felix H. Schacher – Laboratory of Organic and Macromolecular Chemistry (IOMC) and Jena Center for Soft Matter (JCSM), Friedrich Schiller University Jena, Jena 07743, Germany; orcid.org/0000-0003-4685-6608

Complete contact information is available at:
<https://pubs.acs.org/10.1021/acs.macromol.0c01247>

Notes

The authors declare no competing financial interest.

ACKNOWLEDGMENTS

The work was funded by the Deutsche Forschungsgemeinschaft (DFG, German Research Foundation)—project number 316213987—SFB 1278 (projects A06, A03, and Z01) and SCHA1640/18-1. We gratefully acknowledge the additional financial support of the Thüringer Ministerium für Wirtschaft, Wissenschaft und Digitale Gesellschaft (ProExzellenz II, “Nanopolar”) and the Deutsche Forschungsgemeinschaft (DFG), grant references INST 275/389-1 FUGG; AOBJ: 640980.

ABBREVIATIONS

LLA	L-lactide
DLA	D-lactide
EtGLy	3-ethylglycolide
T_m	melting temperature
w_c	degree of crystallinity
T_g	glass transition temperature
HHB	hydrophilic/hydrophobic balance
SC	stereocomplex
THF	tetrahydrofuran
MQW	ultrapure water
DLS	dynamic light scattering
AFM	atomic force microscopy
QI	quantitative imaging
DH	hydrodynamic diameter
ζ_{Pot}	zeta potential
ELS	electrophoretic light scattering
PLM	polarized light microscopy
DSC	differential scanning calorimetry
WAXS	wide angle X-ray scattering

REFERENCES

- (1) Dong, P.; Rakesh, K. P.; Manukumar, H. M.; Mohammed, Y. H. E.; Karthik, C. S.; Sumathi, S.; Mallu, P.; Qin, H.-L. Innovative nanocarriers in anticancer drug delivery—a comprehensive review. *Bioorg. Chem.* **2019**, *85*, 325–336.
- (2) Park, K. Controlled drug delivery systems: Past forward and future back. *J. Controlled Release* **2014**, *190*, 3–8.
- (3) El-Say, K. M.; El-Sawy, H. S. Polymeric nanoparticles: Promising platform for drug delivery. *Int. J. Pharm.* **2017**, *528*, 675–691.
- (4) Krause, H. J.; El Samaligy, M.; Rohdewald, P. Nanoparticles of biodegradable, synthetic material for pharmaceutical delivery. *DE 3341001 A1*, 1985.
- (5) Kreuter, J. [10] poly(alkyl acrylate) nanoparticles. *Methods in Enzymology*; Academic Press, 1985; Vol. 112, pp 129–138.
- (6) Prajapati, S. K.; Jain, A.; Jain, A.; Jain, S. Biodegradable polymers and constructs: A novel approach in drug delivery. *Eur. Polym. J.* **2019**, *120*, 109191.

(7) Pearce, A. K.; O'Reilly, R. K. Insights into active targeting of nanoparticles in drug delivery: Advances in clinical studies and design considerations for cancer nanomedicine. *Bioconjugate Chem.* **2019**, *30*, 2300–2311.

(8) Bandelli, D.; Helbing, C.; Weber, C.; Seifert, M.; Muljajew, I.; Jandt, K. D.; Schubert, U. S. Maintaining the hydrophilic–hydrophobic balance of polyesters with adjustable crystallinity for tailor-made nanoparticles. *Macromolecules* **2018**, *51*, 5567–5576.

(9) Bandelli, D.; Alex, J.; Helbing, C.; Ueberschaar, N.; Görls, H.; Bellstedt, P.; Weber, C.; Jandt, K. D.; Schubert, U. S. Poly(3-ethylglycolide): A well-defined polyester matching the hydrophilic hydrophobic balance of pla. *Polym. Chem.* **2019**, *10*, 5440–5451.

(10) Song, Q.; Wang, X.; Hu, Q.; Huang, M.; Yao, L.; Qi, H.; Qiu, Y.; Jiang, X.; Chen, J.; Chen, H.; Gao, X. Cellular internalization pathway and transcellular transport of pegylated polyester nanoparticles in caco-2 cells. *Int. J. Pharm.* **2013**, *445*, 58–68.

(11) Zweers, M. L. T.; Grijpma, D. W.; Engbers, G. H. M.; Feijen, J. The preparation of monodisperse biodegradable polyester nanoparticles with a controlled size. *J. Biomed. Mater. Res., Part B* **2003**, *66*, 559–566.

(12) Shin, I. G.; Kim, S. Y.; Lee, Y. M.; Cho, C. S.; Sung, S. Y. K. Methoxy poly(ethylene glycol)/ ϵ -caprolactone amphiphilic block copolymeric micelle containing indomethacin.: I. Preparation and characterization. *J. Controlled Release* **1998**, *51*, 1–11.

(13) Budhian, A.; Siegel, S. J.; Winey, K. I. Controlling the in vitro release profiles for a system of haloperidol-loaded plga nanoparticles. *Int. J. Pharm.* **2008**, *346*, 151–159.

(14) Jeong, J.-C.; Lee, J.; Cho, K. Effects of crystalline microstructure on drug release behavior of poly(ϵ -caprolactone) microspheres. *J. Controlled Release* **2003**, *92*, 249–258.

(15) Karavelidis, V.; Karavas, E.; Giliopoulos, D.; Papadimitriou, S.; Bikiaris, D. Evaluating the effects of crystallinity in new biocompatible polyester nanocarriers on drug release behavior. *Int. J. Nanomed.* **2011**, *6*, 3021–3032.

(16) Karavelidis, V.; Giliopoulos, D.; Karavas, E.; Bikiaris, D. Nanoencapsulation of a water soluble drug in biocompatible polyesters. Effect of polyesters melting point and glass transition temperature on drug release behavior. *Eur. J. Pharm. Sci.* **2010**, *41*, 636–643.

(17) Ikada, Y.; Jamshidi, K.; Tsuji, H.; Hyon, S. H. Stereocomplex formation between enantiomeric poly(lactides). *Macromolecules* **1987**, *20*, 904–906.

(18) Okihara, T.; Tsuji, M.; Kawaguchi, A.; Katayama, K.-I.; Tsuji, H.; Hyon, S.-H.; Ikada, Y. Crystal structure of stereocomplex of poly(l-lactide) and poly(d-lactide). *J. Macromol. Sci., Phys.* **1991**, *30*, 119–140.

(19) Brizzolara, D.; Cantow, H.-J.; Diederichs, K.; Keller, E.; Domb, A. J. Mechanism of the stereocomplex formation between enantiomeric poly(lactide)s. *Macromolecules* **1996**, *29*, 191–197.

(20) Saravanan, M.; Domb, A. J. A contemporary review on – polymer stereocomplexes and its biomedical application. *Eur. J. Nanomed.* **2013**, *5*, 81–96.

(21) Tsuji, H. Poly(lactide) stereocomplexes: Formation, structure, properties, degradation, and applications. *Macromol. Biosci.* **2005**, *5*, 569–597.

(22) Tashiro, K.; Kouno, N.; Wang, H.; Tsuji, H. Crystal structure of poly(lactic acid) stereocomplex: Random packing model of pdla and plla chains as studied by x-ray diffraction analysis. *Macromolecules* **2017**, *50*, 8048–8065.

(23) Slager, J.; Domb, A. J. Biopolymer stereocomplexes. *Adv. Drug Deliv. Rev.* **2003**, *55*, 549–583.

(24) Slager, J.; Brizzolara, D.; Cantow, H. J.; Domb, A. J. Crystallization and stereocomplexation governed self-assembling of poly(lactide)-b-poly(ethylene glycol) to mesoscale structures. *Polym. Adv. Technol.* **2005**, *16*, 667–674.

(25) Han, L.; Pan, P.; Shan, G.; Bao, Y. Stereocomplex crystallization of high-molecular-weight poly(l-lactic acid)/poly(d-lactic acid) racemic blends promoted by a selective nucleator. *Polymer* **2015**, *63*, 144–153.

- (26) Ishii, D.; Kimishima, M.; Otake, K.; Iwata, T. Enhanced crystallization of poly(lactide) stereocomplex by xylan propionate. *Polym. Int.* **2016**, *65*, 339–345.
- (27) Widhianto, Y. W.; Yamamoto, M.; Masutani, K.; Kimura, Y.; Yamane, H. Effect of the block length and the molecular weight on the isothermal crystallization behavior of multi-stereoblock poly(lactic acid)s. *Polym. Degrad. Stab.* **2017**, *142*, 178–187.
- (28) Tsuji, H.; Ikada, Y. Stereocomplex formation between enantiomeric poly(lactic acid)s. X. Binary blends from poly(d-lactide-co-glycolide) and poly(l-lactide-co-glycolide). *J. Appl. Polym. Sci.* **1994**, *53*, 1061–1071.
- (29) Bouapao, L.; Tsuji, H. Stereocomplex crystallization and spherulite growth of low molecular weight poly(l-lactide) and poly(d-lactide) from the melt. *Macromol. Chem. Phys.* **2009**, *210*, 993–1002.
- (30) Tsuji, H.; Tashiro, K.; Bouapao, L.; Hanesaka, M. Separate crystallization and cocrystallization of poly(l-lactide) in the presence of l-lactide-based copolymers with low crystallizability, poly(l-lactide-co-glycolide) and poly(l-lactide-co-d-lactide). *Macromol. Chem. Phys.* **2012**, *213*, 2099–2112.
- (31) Shao, J.; Tang, Z.; Sun, J.; Li, G.; Chen, X. Linear and four-armed poly(l-lactide)-block-poly(d-lactide) copolymers and their stereocomplexation with poly(lactide)s. *J. Polym. Sci., Part B: Polym. Phys.* **2014**, *52*, 1560–1567.
- (32) Sun, L.; Pitto-Barry, A.; Kirby, N.; Schiller, T. L.; Sanchez, A. M.; Dyson, M. A.; Sloan, J.; Wilson, N. R.; O'Reilly, R. K.; Dove, A. P. Structural reorganization of cylindrical nanoparticles triggered by polylactide stereocomplexation. *Nat. Commun.* **2014**, *5*, 5746.
- (33) Zhu, Y.; Akagi, T.; Akashi, M. Self-assembling stereocomplex nanoparticles by enantiomeric poly(γ -glutamic acid)-poly(lactide) graft copolymers as a protein delivery carrier. *Macromol. Biosci.* **2014**, *14*, 576–587.
- (34) Tam, Y. T.; Huang, C.; Poellmann, M.; Kwon, G. S. Stereocomplex prodrugs of oligo(lactic acid) n-gemcitabine in poly(ethylene glycol)-block-poly(d,l-lactic acid) micelles for improved physical stability and enhanced antitumor efficacy. *ACS Nano* **2018**, *12*, 7406–7414.
- (35) Chen, W.; Wang, S.; Zhang, W.; Ke, Y.; Hong, Y.-l.; Miyoshi, T. Molecular structural basis for stereocomplex formation of polylactide enantiomers in dilute solution. *ACS Macro Lett.* **2015**, *4*, 1264–1267.
- (36) Li, W.; Fan, X.; Wang, X.; Shang, X.; Wang, Q.; Lin, J.; Hu, Z.; Li, Z. Stereocomplexed micelle formation through enantiomeric pla-based γ -shaped copolymer for targeted drug delivery. *Mater. Sci. Eng., C* **2018**, *91*, 688–695.
- (37) Sun, Y.; He, C. Synthesis, stereocomplex crystallization, morphology and mechanical property of poly(lactide)-carbon nanotube nanocomposites. *RSC Adv.* **2013**, *3*, 2219–2226.
- (38) Tsuji, H.; Wada, T.; Sakamoto, Y.; Sugiura, Y. Stereocomplex crystallization and spherulite growth behavior of poly(l-lactide)-b-poly(d-lactide) stereodiblock copolymers. *Polymer* **2010**, *51*, 4937–4947.
- (39) Kong, Y.; Hay, J. N. The measurement of the crystallinity of polymers by dsc. *Polymer* **2002**, *43*, 3873–3878.
- (40) Xu, P.; Huang, X.; Pan, X.; Li, N.; Zhu, J.; Zhu, X. Hyperbranched polycaprolactone through raft polymerization of 2-methylene-1,3-dioxepane. *Polymers* **2019**, *11*, 318.
- (41) Nojima, S.; Fujimoto, M.; Kakihira, H.; Sasaki, S. Effects of copolymer composition on the crystallization and morphology of poly(ϵ -caprolactone)-block-polystyrene. *Polym. J.* **1998**, *30*, 968–975.
- (42) Schröder, U.-C.; Kirchhoff, J.; Hübner, U.; Mayer, G.; Glaser, U.; Henkel, T.; Pfister, W.; Fritzsche, W.; Popp, J.; Neugebauer, U. On-chip spectroscopic assessment of microbial susceptibility to antibiotics within 3.5 hours. *J. Biophot.* **2017**, *10*, 1547–1557.
- (43) Hsieh, Y.-T.; Nozaki, S.; Kido, M.; Kamitani, K.; Kojio, K.; Takahara, A. Crystal polymorphism of polylactide and its composites by x-ray diffraction study. *Polym. J.* **2020**, *52*, 755–763.
- (44) Mano, J. F.; Wang, Y.; Viana, J. C.; Denchev, Z.; Oliveira, M. J. Cold crystallization of plla studied by simultaneous saxs and waxes. *Macromol. Mater. Eng.* **2004**, *289*, 910–915.
- (45) Kawai, T.; Rahman, N.; Matsuba, G.; Nishida, K.; Kanaya, T.; Nakano, M.; Okamoto, H.; Kawada, J.; Usuki, A.; Honma, N.; Nakajima, K.; Matsuda, M. Crystallization and melting behavior of poly(l-lactic acid). *Macromolecules* **2007**, *40*, 9463–9469.
- (46) Shyr, T.-W.; Ko, H.-C.; Chen, H.-L. Homocrystallization and stereocomplex crystallization behaviors of as-spun and hot-drawn poly(l-lactide)/poly(d-lactide) blended fibers during heating. *Polymers* **2019**, *11*, 1502.
- (47) Na, B.; Zhu, J.; Lv, R.; Ju, Y.; Tian, R.; Chen, B. Stereocomplex formation in enantiomeric polylactides by melting recrystallization of homocrystals: Crystallization kinetics and crystal morphology. *Macromolecules* **2014**, *47*, 347–352.
- (48) Tsuji, H.; Deguchi, F.; Sakamoto, Y.; Shimizu, S. Hetero-stereocomplex crystallization and homocrystallization from the melt in blends of substituted and unsubstituted poly(lactide)s. *Macromol. Chem. Phys.* **2012**, *213*, 2573–2581.
- (49) Ma, C.; Pan, P.; Shan, G.; Bao, Y.; Fujita, M.; Maeda, M. Core-shell structure, biodegradation, and drug release behavior of poly(lactic acid)/poly(ethylene glycol) block copolymer micelles tuned by macromolecular stereostructure. *Langmuir* **2015**, *31*, 1527–1536.
- (50) Furukawa, T.; Sato, H.; Murakami, R.; Zhang, J.; Noda, I.; Ochiai, S.; Ozaki, Y. Raman microspectroscopy study of structure, dispersibility, and crystallinity of poly(hydroxybutyrate)/poly(l-lactic acid) blends. *Polymer* **2006**, *47*, 3132–3140.
- (51) Kister, G.; Cassanas, G.; Vert, M. Effects of morphology, conformation and configuration on the ir and raman spectra of various poly(lactic acid)s. *Polymer* **1998**, *39*, 267–273.
- (52) Tsuji, H.; Hyon, S. H.; Ikada, Y. Stereocomplex formation between enantiomeric poly(lactic acids). 5. Calorimetric and morphological studies on the stereocomplex formed in acetonitrile solution. *Macromolecules* **1992**, *25*, 2940–2946.
- (53) Slager, J.; Cohen, Y.; Khalfin, R.; Talmon, Y.; Domb, A. J. Peptides form stereoselective complexes with chiral polymers. *Macromolecules* **2003**, *36*, 2999–3000.
- (54) Wang, W.; Qi, H.; Zhou, T.; Mei, S.; Han, L.; Higuchi, T.; Jinnai, H.; Li, C. Y. Highly robust crystalsome via directed polymer crystallization at curved liquid/liquid interface. *Nat. Commun.* **2016**, *7*, 10599.
- (55) Erdemir, D.; Lee, A. Y.; Myerson, A. S. Nucleation of crystals from solution: Classical and two-step models. *Acc. Chem. Res.* **2009**, *42*, 621–629.
- (56) Vekilov, P. G. Nucleation. *Cryst. Growth Des.* **2010**, *10*, 5007–5019.
- (57) Gillam, J. E.; MacPhee, C. E. Modelling amyloid fibril formation kinetics: Mechanisms of nucleation and growth. *World J. Condens. Matter Phys.* **2013**, *25*, 373101.
- (58) Kawakami, K.; Bi, Y.; Yoshihashi, Y.; Sugano, K.; Terada, K. Time-dependent phase separation of amorphous solid dispersions: Implications for accelerated stability studies. *J. Drug Deliv. Sci. Technol.* **2018**, *46*, 197–206.
- (59) Zhang, X.; Yi, X.; Xu, Y. Phase separation time/temperature dependence of thermoplastics-modified thermosetting systems. *Front. Chem. Eng. China* **2008**, *2*, 276–285.
- (60) He, Y.; Eloi, J.-C.; Harmiman, R. L.; Richardson, R. M.; Whittell, G. R.; Mathers, R. T.; Dove, A. P.; O'Reilly, R. K.; Manners, I. Uniform biodegradable fiber-like micelles and block comicelles via “living” crystallization-driven self-assembly of poly(l-lactide) block copolymers: The importance of reducing unimer self-nucleation via hydrogen bond disruption. *J. Am. Chem. Soc.* **2019**, *141*, 19088–19098.
- (61) Tsuji, H.; Horii, F.; Hyon, S. H.; Ikada, Y. Stereocomplex formation between enantiomeric poly(lactic acid)s. 2. Stereocomplex formation in concentrated solutions. *Macromolecules* **1991**, *24*, 2719–2724.

1 Supplementary Information for

2 Self-assembly of copolymers into stereocomplex
3 crystallites tunes the properties of polyester
4 nanoparticles

5 *Karl Scheuer,¹ Damiano Bandelli,^{2,3} Christian Helbing,¹ Christine Weber,^{2,3} Julien Alex,^{2,3}*
6 *Johannes B. Max,^{2,3} Alexis Hocken,^{1, †} Ondrej Stranik,⁴ Lisa Seiler,^{4,5} Frederike Gladigau,^{4,5} Ute*
7 *Neugebauer,^{2,4,5,6} Felix H. Schacher,^{2,3} Ulrich S. Schubert,^{2,3} Klaus D. Jandt^{1,3}*

8 ¹Chair of Materials Science (CMS), Department of Materials Science and Technology, Otto Schott
9 Institute of Materials Research, Faculty of Physics and Astronomy, Friedrich Schiller University
10 Jena, Löbdergraben 32, 07743 Jena, Germany

11 ²Laboratory of Organic and Macromolecular Chemistry (IOMC), Friedrich Schiller University
12 Jena, Humboldtstr. 10, 07743 Jena, Germany

13 ³Jena Center for Soft Matter (JCSM), Friedrich Schiller University Jena, Philosophenweg 7, 07743
14 Jena, Germany

1 ⁴Leibniz Institute of Photonic Technology, Albert-Einstein-Straße 9, 07743 Jena, Germany

2 ⁵Institute of Physical Chemistry and Abbe School of Photonics, Friedrich Schiller University Jena,
3 Helmholtzweg 4, 07743 Jena, Germany

4 ⁶ Center for Sepsis Control and Care, Jena University Hospital, Am Klinikum 1, 07747 Jena,
5 Germany

6 † Current address: Department of Chemical Engineering, School for Engineering of Matter,
7 Transport and Energy, Arizona State University, Tempe, AZ 85287, USA

8 * Correspondence to K. D. Jandt (k.jandt@uni-jena.de); U. S. Schubert (ulrich.schubert@uni-
9 jena.de)

10

11 **Supporting Equation Es1:** Weighted degree of crystallinity ^{1,2}

12
$$w_{c,weighted} = \frac{(\Delta H_m + \Delta H_{cc})}{\Delta H_m^0(PLA) \times f} \cdot 100 \quad (Es1)$$

13 **Supporting table Ts1:** Enthalpies of cold crystallization (ΔH_{cc}) and melting (ΔH_m) as determined
14 by DSC measurements of the stereocomplexes used for calculation of the degrees of crystallinity.

f(Lactide) ^a	1 st heating run				3 rd heating run			
	ΔH_{cc} ^b [J g ⁻¹]	ΔH_m ^c [J g ⁻¹]	$w_{c,unweighted}$ ^d [%]	$w_{c,weighted}$ ^e [%]	ΔH_{cc} ^b [J g ⁻¹]	ΔH_m ^c [J g ⁻¹]	$w_{c,unweighted}$ ^d [%]	$w_{c,weighted}$ ^e [%]
1	-3	77	52	52	n.a.	55	39	39
0.95	n.a.	52	36	38	n.a.	44	31	33

0.9	n.a.	45	32	35	-22	44	16	18
0.8	n.a.	39	27	34	-30	30	1	2

1

2 ^a Lactide fraction.

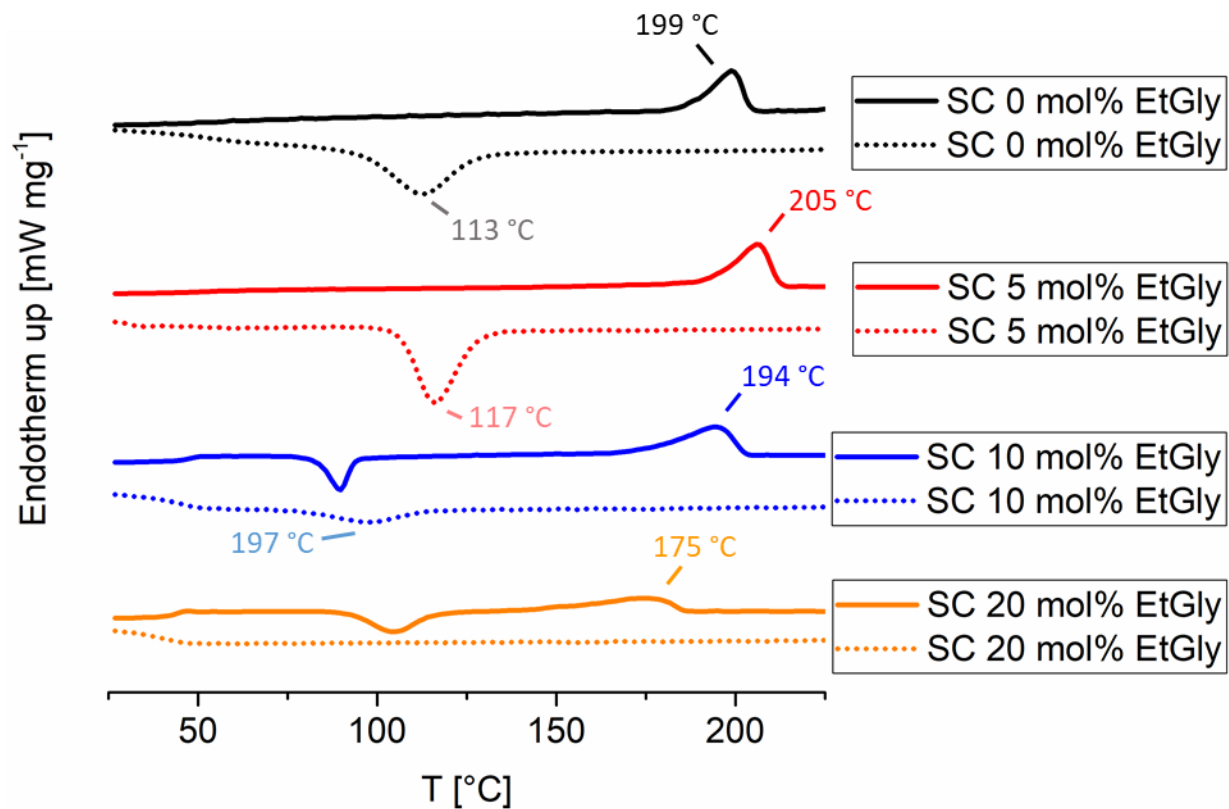
3 ^b Enthalpy of cold crystallization.

4 ^c Enthalpy of melting.

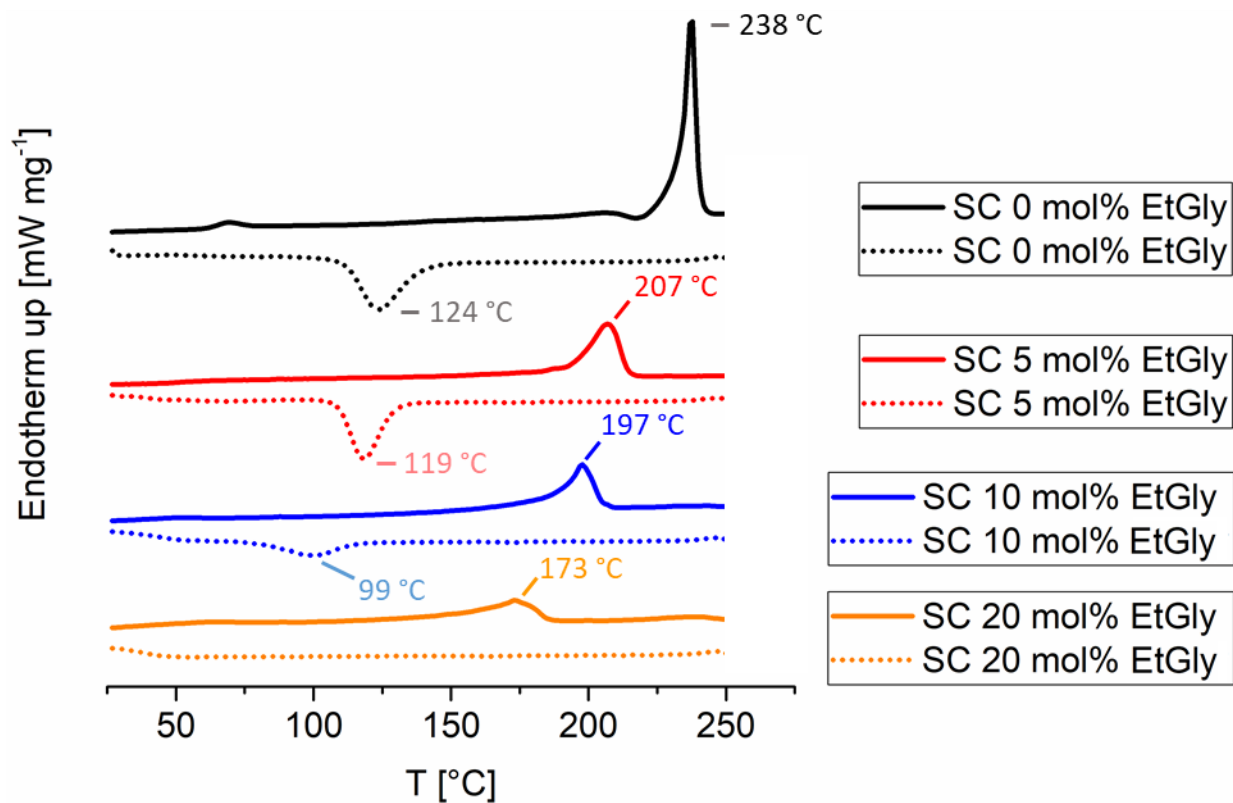
5 ^d Unweighted degree of crystallinity according to $w_{c,unweighted} = \frac{(\Delta H_m + \Delta H_{cc})}{\Delta H_m^0(PLA)} \cdot 100$

6 ^e Weighted degree of crystallinity according to $w_{c,weighted} = \frac{(\Delta H_m + \Delta H_{cc})}{\Delta H_m^0(PLA) \times f} \cdot 100$

7

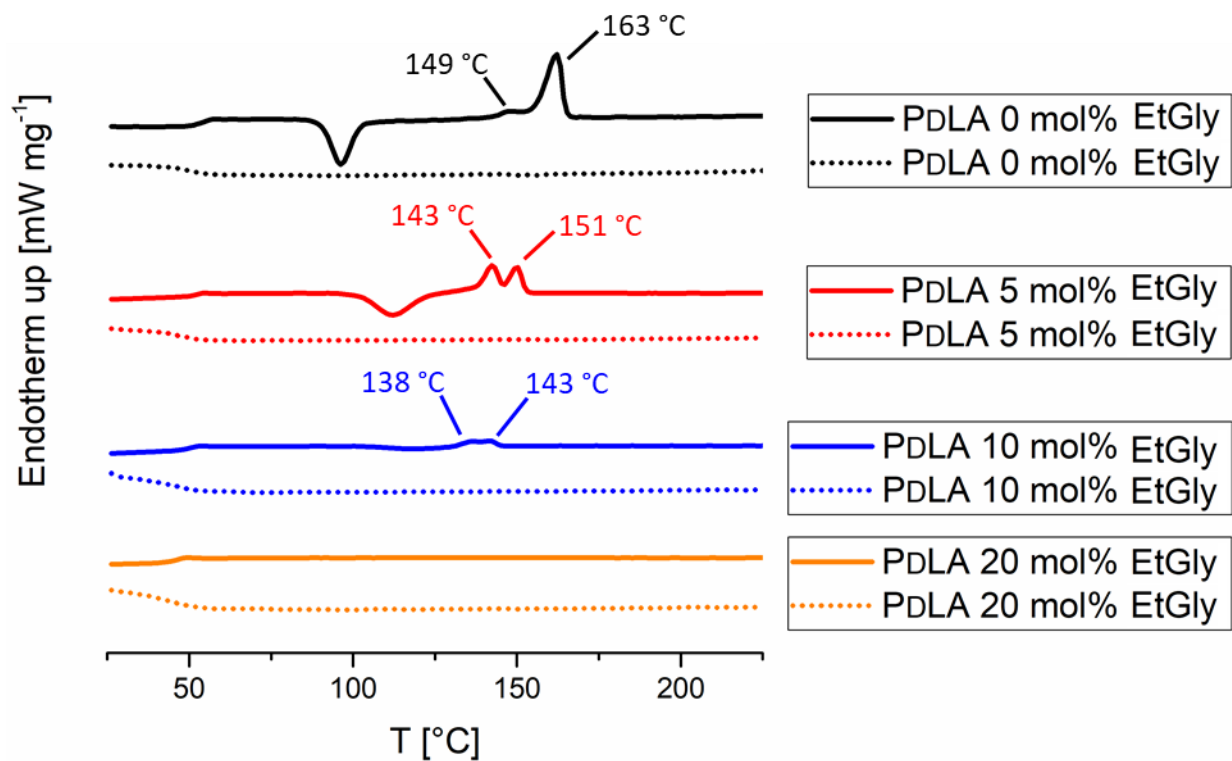


1
 2 **Figure S1.** DSC thermograms (third heating run) of SCs with 0, 5, 10 and 20 mol% EtGly (solid
 3 lines). DSC thermograms (third cooling run) of SCs with 0, 5, 10 and 20 mol% EtGly (dotted
 4 lines). Spectra shifted along the y-axis for clarity.

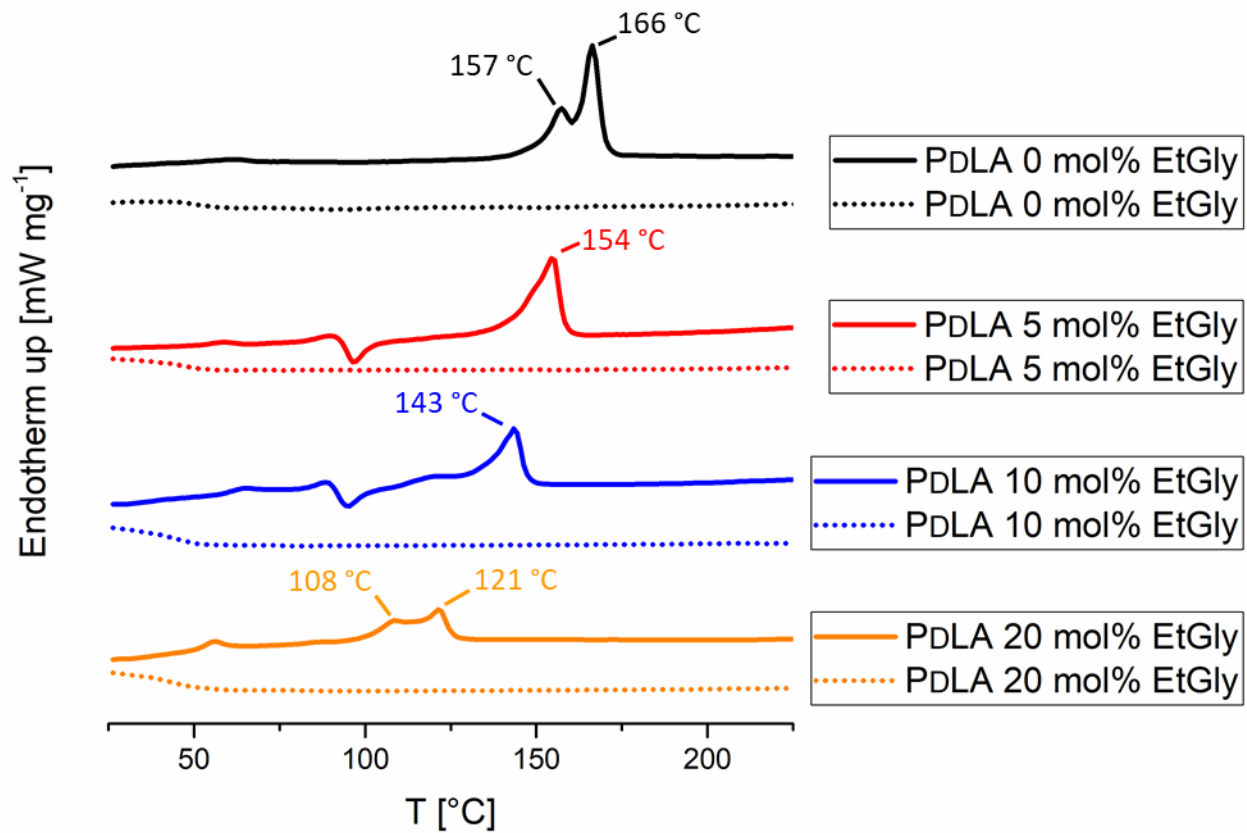


1
 2 **Figure S2.** DSC thermograms (first heating run) of SCs with 0, 5, 10 and 20 mol% EtGly (solid
 3 lines). DSC thermograms (first cooling run) of SCs with 0, 5, 10 and 20 mol% EtGly (dotted lines).
 4 Spectra shifted along the y-axis for clarity.

5
 6

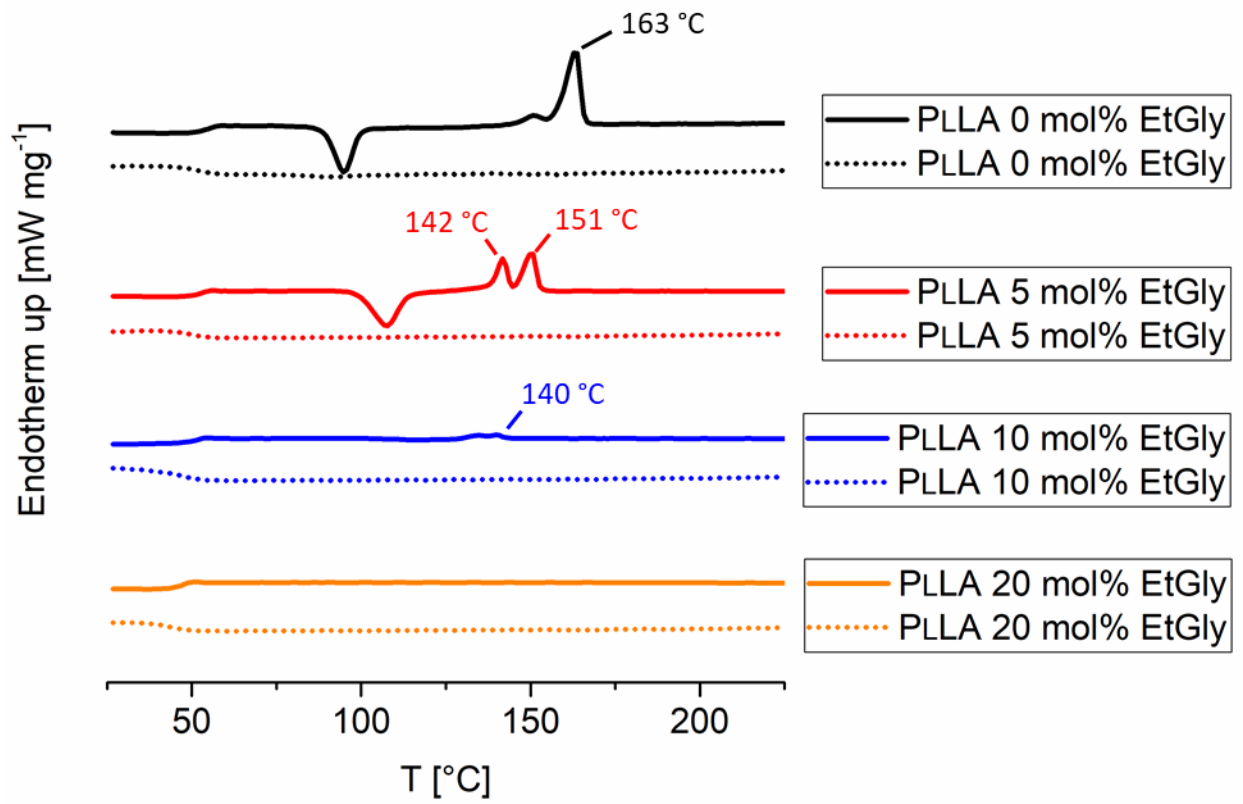


1
 2 **Figure S3.** DSC thermograms (third heating run) of PDLA with 0, 5, 10 and 20 mol% EtGly (solid
 3 lines). DSC thermograms (third cooling run) of PDLA with 0, 5, 10 and 20 mol% EtGly (dotted
 4 lines).³ Spectra shifted along the y-axis for clarity.

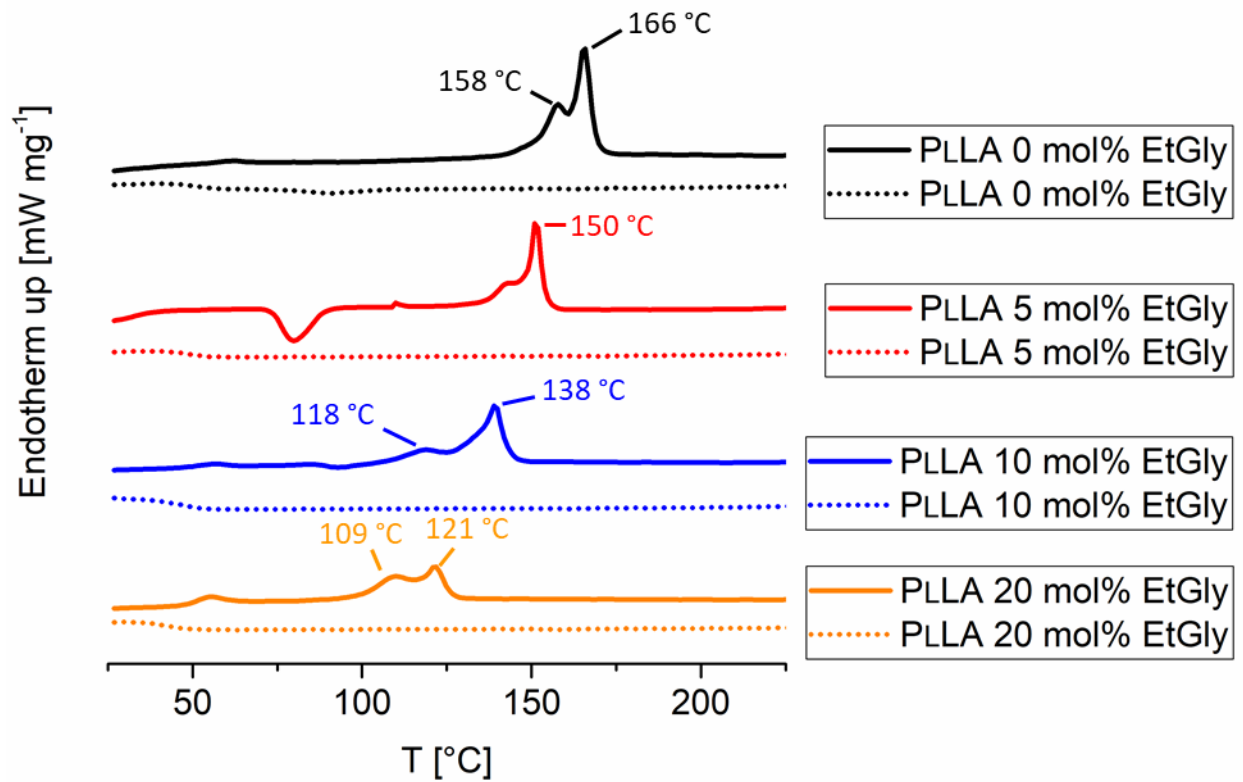


1
 2 **Figure S4.** DSC thermograms (first heating run) of PDLA 0, 5, 10 and 20 mol% EtGly (solid lines).
 3 DSC thermograms (first cooling run) of PDLA with 0, 5, 10 and 20 mol% EtGly (dotted lines).³
 4 Spectra shifted along the y-axis for clarity.

5

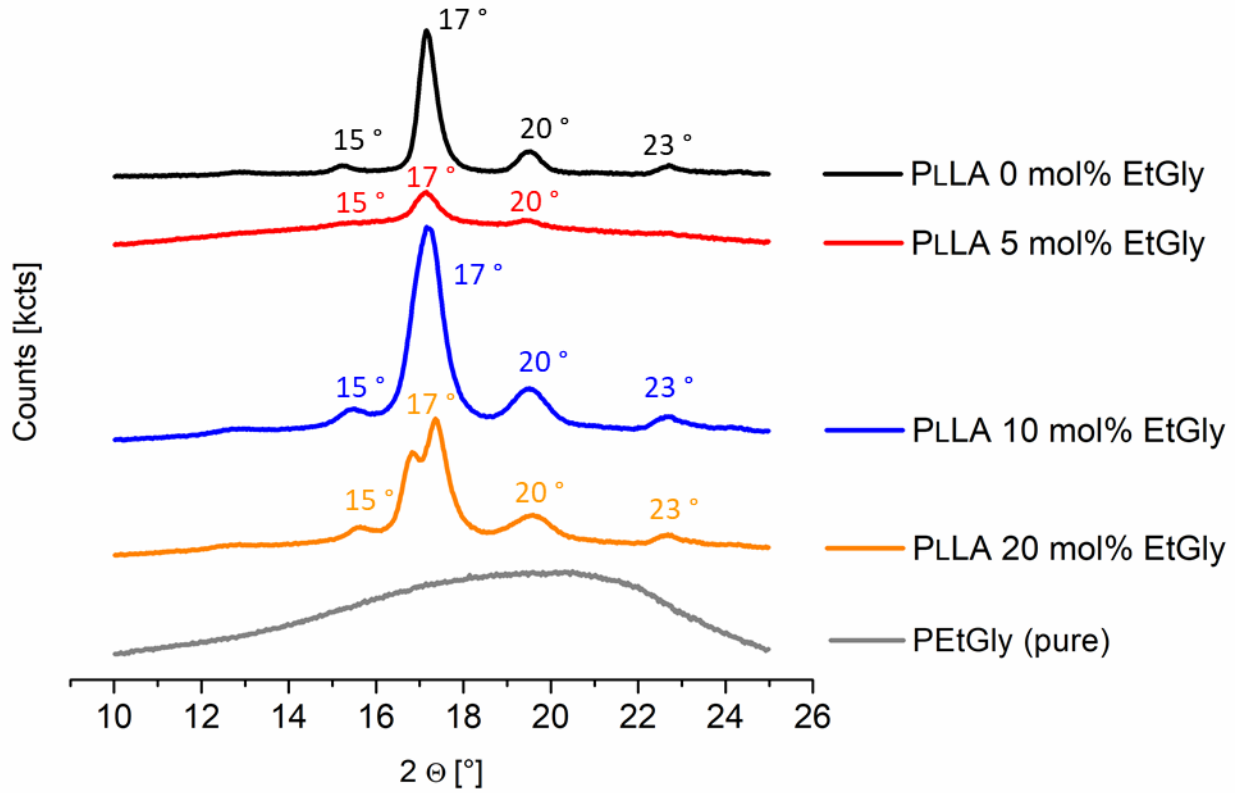


1
 2 **Figure S5.** DSC thermograms (third heating run) of PLLA with 0, 5, 10 and 20 mol% EtGly (solid
 3 lines). DSC thermograms (third cooling run) of PLLA with 0, 5, 10 and 20 mol% EtGly (dotted
 4 lines). ³ Spectra shifted along the y-axis for clarity.



1

2 **Figure S6.** DSC thermograms (first heating run) of PLLA with 0, 5, 10 and 20 mol% EtGly (solid
 3 lines). DSC thermograms (first cooling run) of PLLA with 0, 5, 10 and 20 mol% EtGly (dotted
 4 lines).³ Spectra shifted along the y-axis for clarity.



1
 2 **Figure S7.** Bulk material WAXS patterns of P(LLA-*stat*-EtGly) containing 0, 5, 10 and
 3 20 mol% EtGly and from pure PEGly. The 20 mol% EtGly pattern shows a double peak around
 4 17° with the first maximum at 16.9° and the second at 17.4°. Spectra shifted along the y-axis for
 5 clarity.

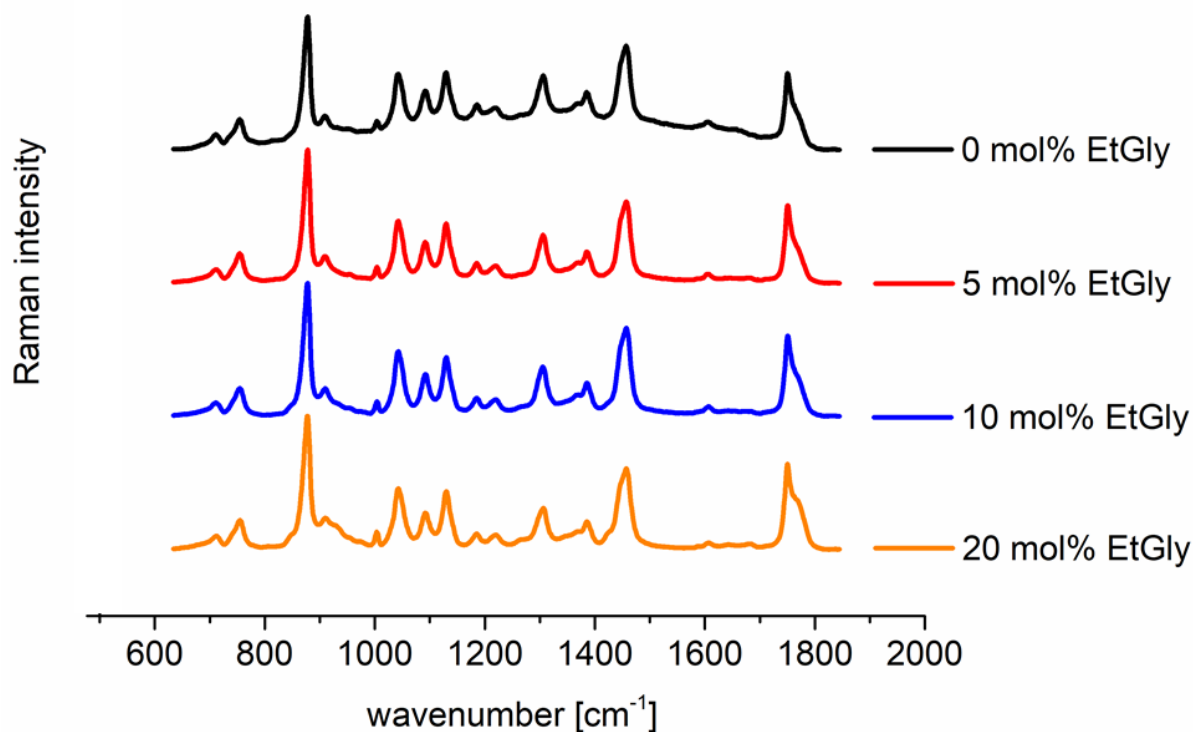
6
 7
 8
 9
 10
 11
 12
 13

1 **Supporting table Ts2.** Assignment of the Raman bands in bulk PDLA, PLLA and bulk SC. ⁴⁻⁸

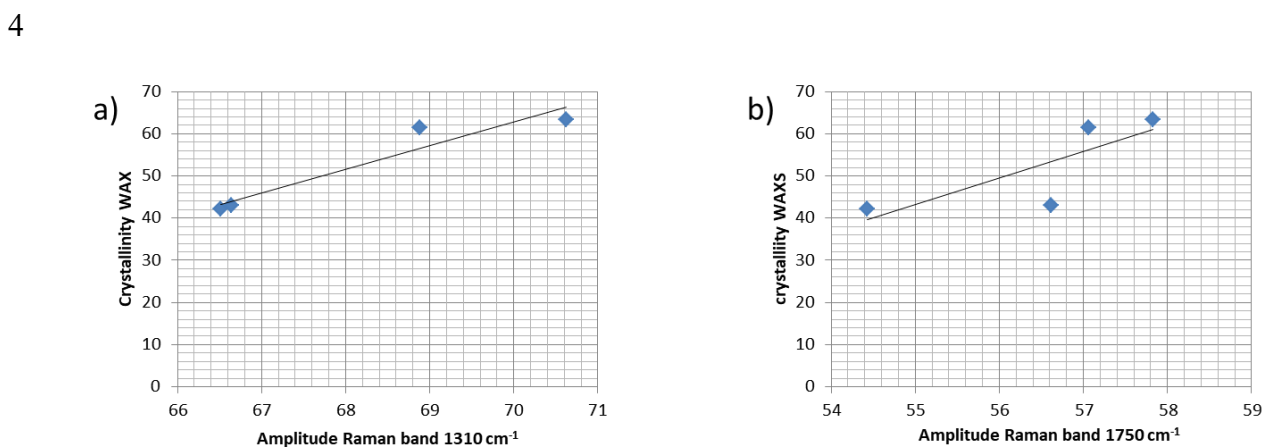
Raman band (cm ⁻¹)	Band assignment
1777 - 1749	C=O stretching
1458	CH ₃ asymmetric deformation
1387	CH ₃ symmetric deformation
1310	CH deformation
1295	CH deformation
1220	-
1188	COC asymmetric stretching
1131	CH ₃ asymmetric rocking
1092	COC symmetric stretching
1046	C-CH ₃ stretching
1006	-
925-911	Skeletal vibration (CC stretching and CH ₃ rocking)
880	C-COO stretching
757 - 713	C=O deformation

2

3 In order to correlate the degree of crystallinity and the Raman band intensities, Raman spectra of
4 stereocomplexes with different amounts of EtGly (between 0 and 20 mol%) were recorded and are
5 displayed in Figure S8. With all EtGly concentrations, stereocomplexes are formed as can be seen
6 from the sharp C=O stretching band centered at 1752 cm⁻¹ and the shape and position of the C-H
7 deformation band around 1300 cm⁻¹. Slight variations in the relative intensity of the broader
8 shoulder around 1298 cm⁻¹ (for the C-H deformation band) and at 1770 cm⁻¹ (for the C=O
9 stretching band) indicate different amorphous content. Both broad shoulders are increasing with
10 increasing EtGly content indicating a higher amorphous content and thus, reduced crystallinity
11 with increasing EtGly content. The relative amplitudes of the sharp bands at 1310 cm⁻¹ and
12 1752 cm⁻¹ in relation to their broader features (around 1289 cm⁻¹ and at 1770 cm⁻¹) are plotted
13 against the crystallinity values obtained from WAXS analysis in Figure S9. A linear regression
14 between the measured values was performed and the formula and the correlation coefficient are
15 given in the figure legend.



1
 2 **Figure S8.** Bulk material Raman spectra of bulk SCs containing 0, 5, 10 and 20 mol% EtGly.
 3 Spectra shifted along the y-axis for clarity.

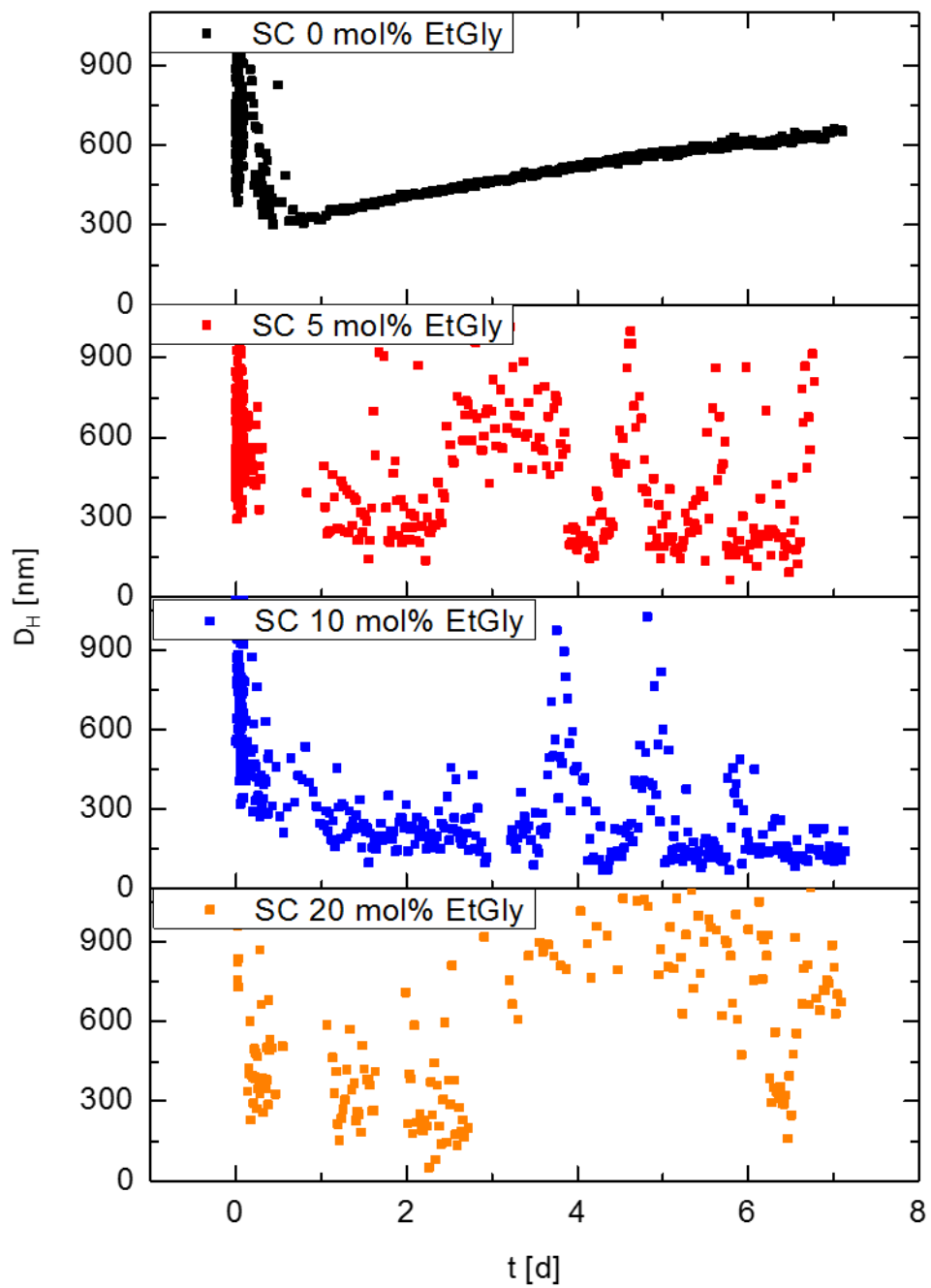


5
 6 **Figure S9.** Correlation of Raman spectral features and crystallinity as obtained from WAXS for
 7 the two Raman bands around 1310 cm⁻¹ (a) and at 1752 cm⁻¹ for SCs. Blue dots indicate averaged
 8 values obtained from SC polymers. The black line is a linear fit for a)

- 1 crystallinity = $5.5784 \cdot \text{amplitude of Raman band @}1310\text{cm}^{-1} - 327.71$, $R^2 = 0.9109$ and for b)
- 2 crystallinity = $6,2567 \cdot \text{amplitude of Raman band @}1750\text{cm}^{-1} - 300.84$, $R^2 = 0.6322$.

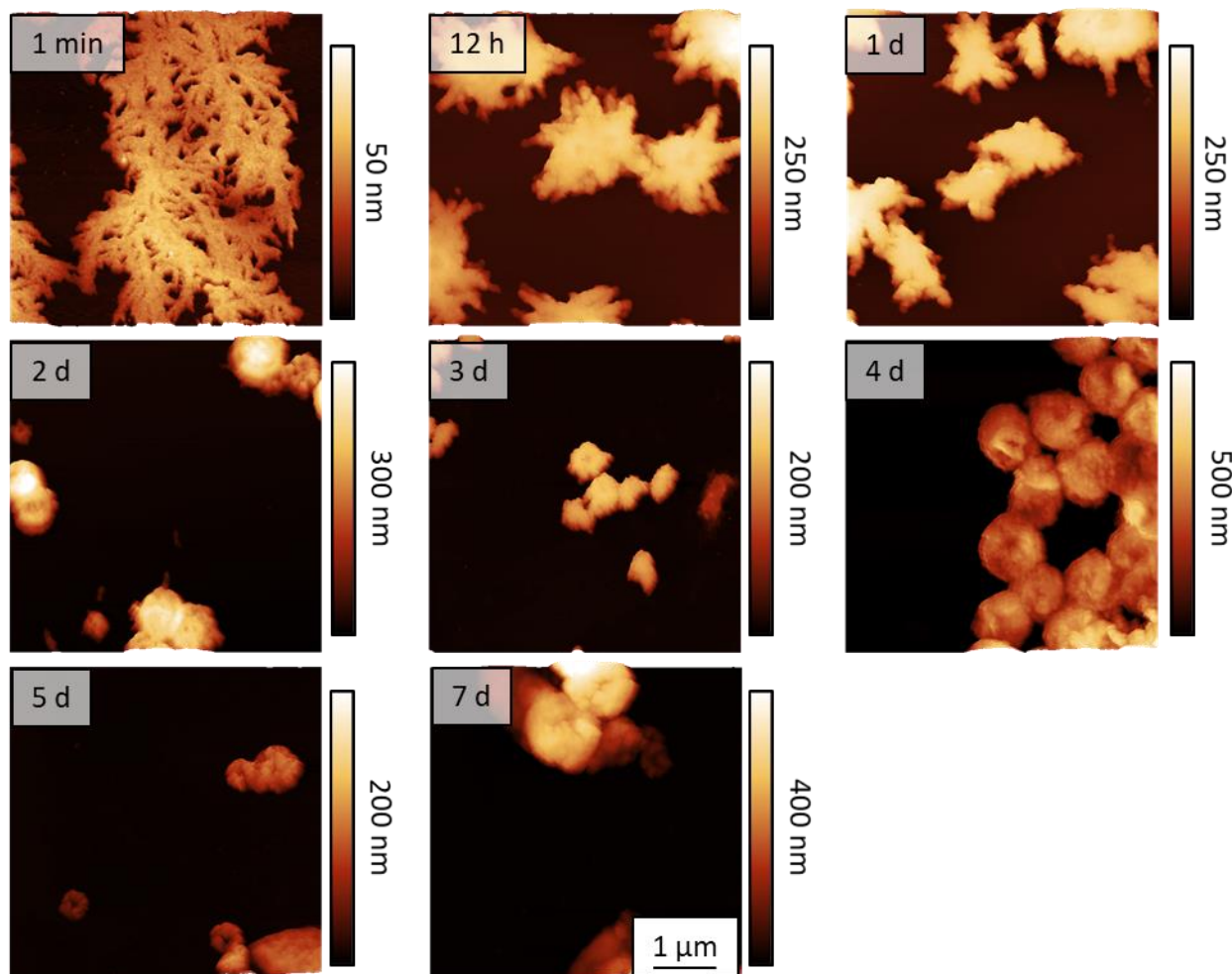
3

4



1
 2 **Figure S10.** Time dependent stereocomplexation in THF, D_H of SCs forming in THF over 7 d with
 3 0, 5, 10 and 20 mol% EtGly (DLS data).

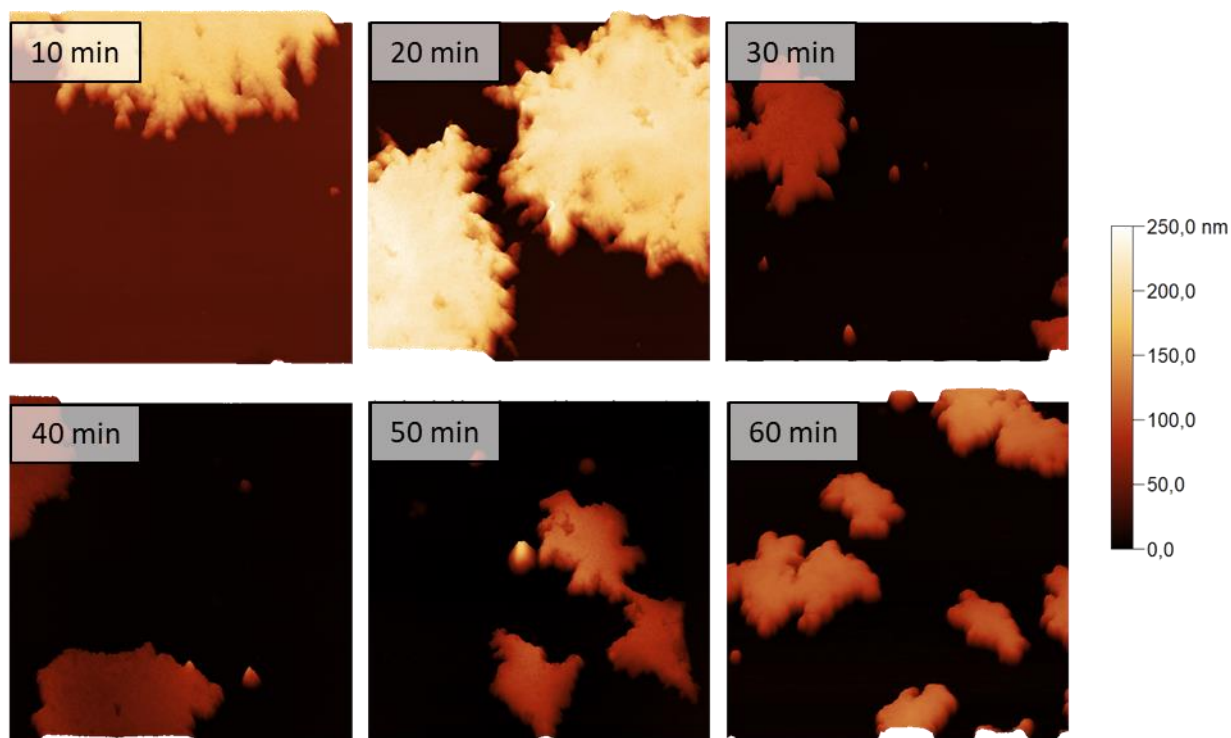
1



2

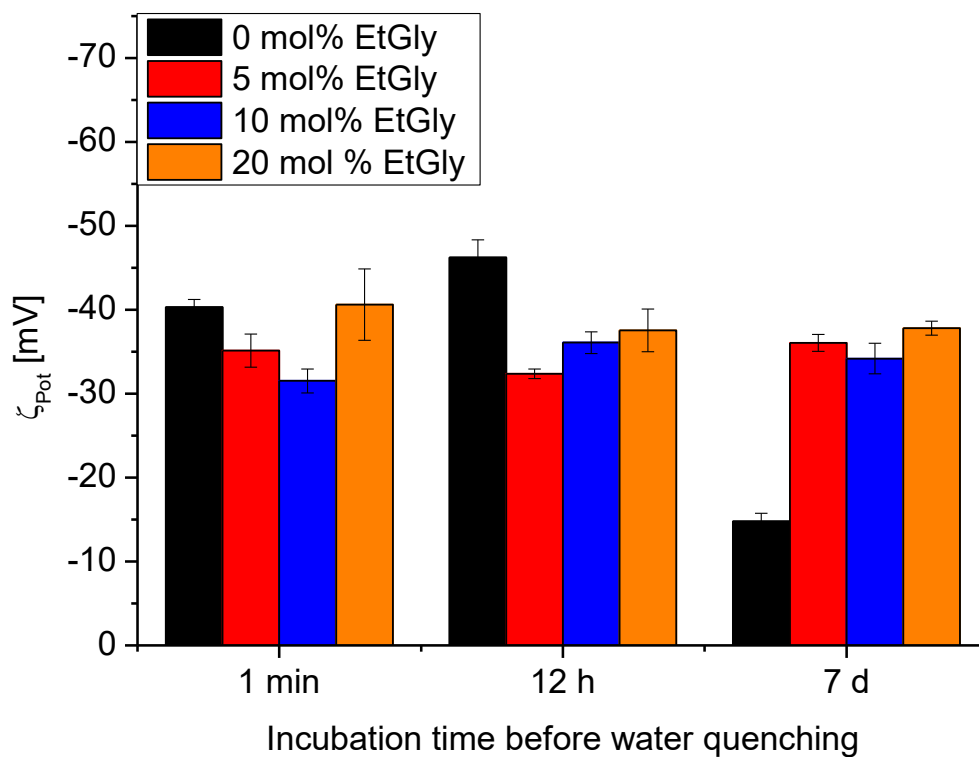
3 **Figure S11.** AFM height images of SCs containing 0 mol% EtGly from THF solution. The SCs
4 were incubated in THF for the time displayed on the images. Afterwards they were drop cast on
5 freshly cleaved mica and dried at room temperature prior to AFM investigation.

6

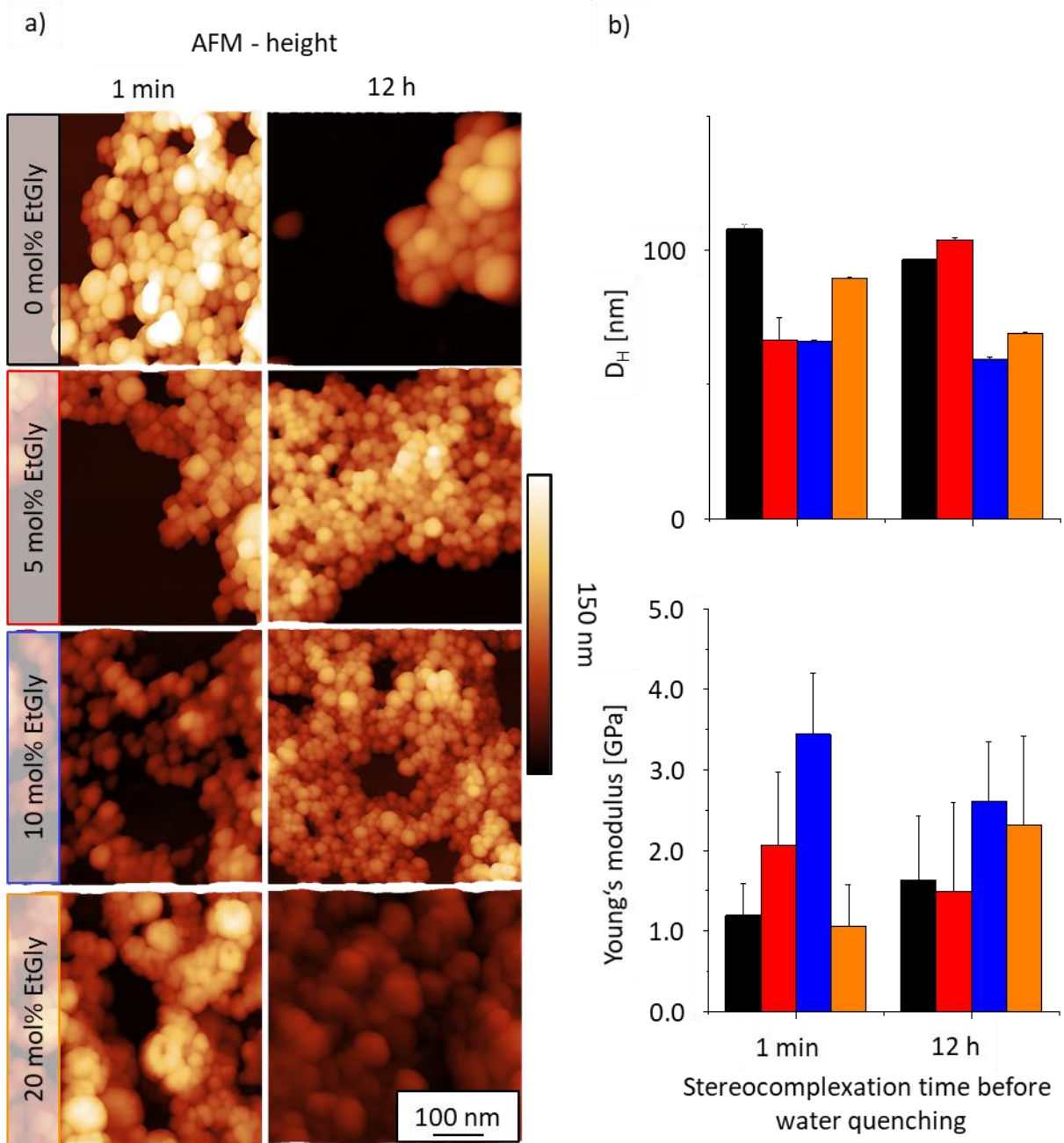


1
 2 **Figure S12.** AFM height images of SCs containing 0 mol% EtGly from THF solution. The SCs
 3 were incubated in THF for the time displayed on the images. Afterwards they were drop cast on
 4 freshly cleaved mica and dried at room temperature prior to AFM investigation. The triangular
 5 structures at 50 min are SC crystals.^{9 10}

6

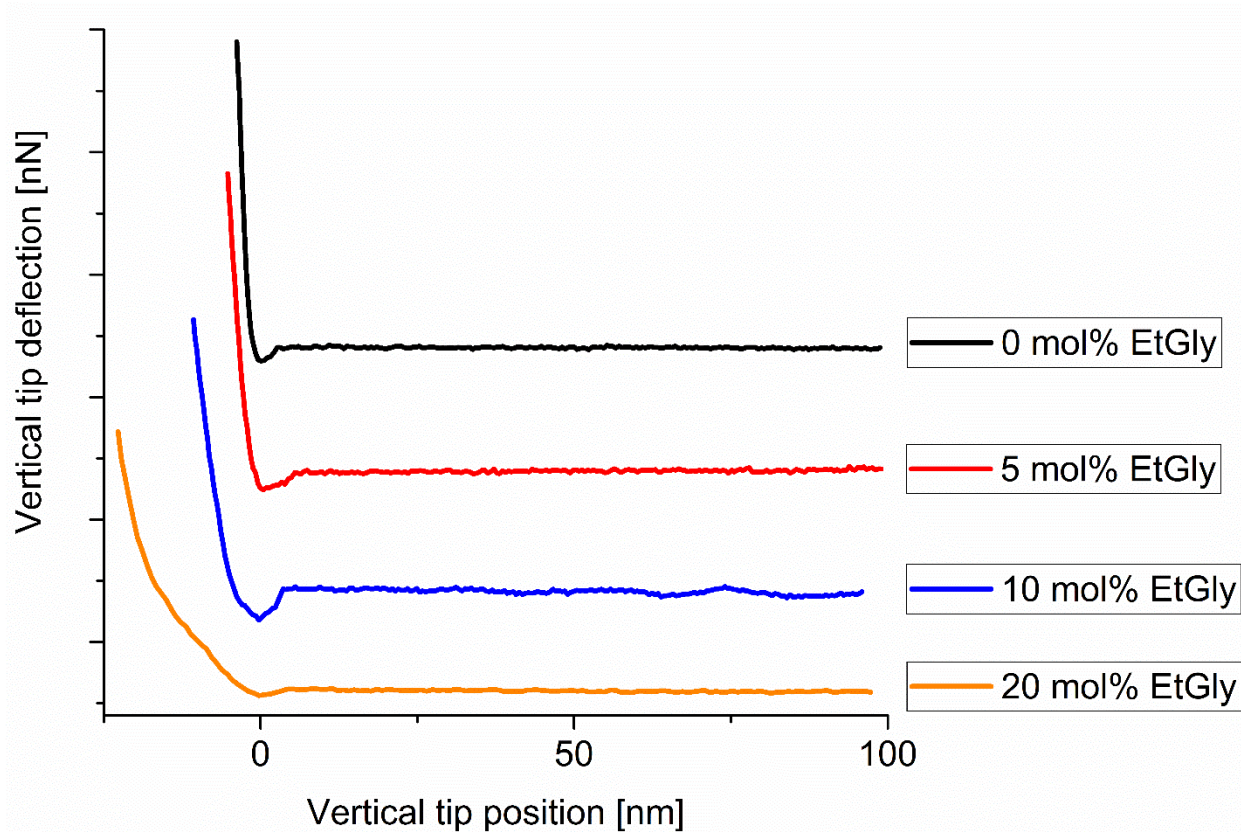


1
 2 **Figure S13.** ζ_{Pot} of water quenched nanoparticles containing 0, 5, 10 and 20 mol% EtGly. The SC
 3 solutions were quenched in MQW after 1 min, 12 h and 7 d of stereocomplexation in THF.

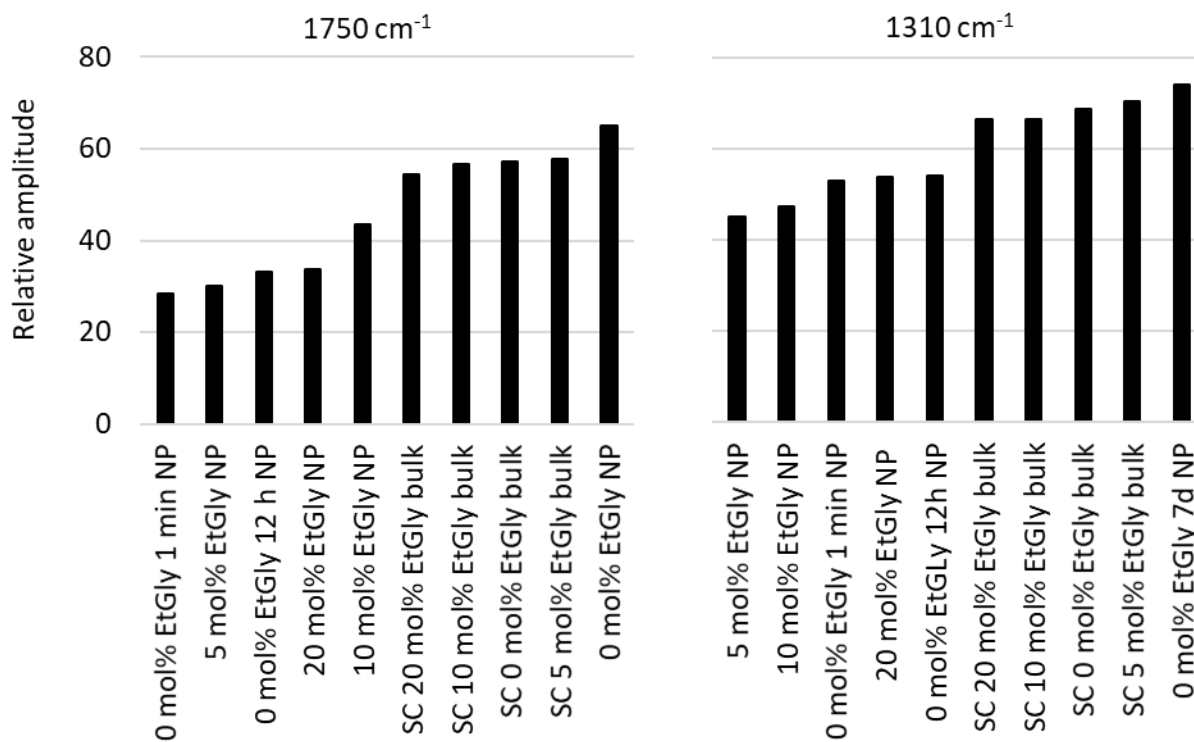


1
 2 **Figure S14.** Nanoparticles quenched from SC solution; a) representative AFM height images of
 3 the nanoparticles on mica; b) D_H and Young's modulus depending on the stereocomplexation time
 4 prior to nanoprecipitation and polymer composition.

5



1
2 **Figure S15.** Representative force distance curves of SC nanoparticles with 0, 5, 10 and
3 20 mol% EtGly, quenched after 7d of stereocomplexation in THF. Curves are shifted on the y-axis
4 for clarity.



1
 2 **Figure S16.** Using the relative amplitude of the “crystallinity Raman marker bands” around
 3 1310 cm⁻¹ and 1750 cm⁻¹, the nanoparticles and the bulk material can be ordered with increasing
 4 crystallinity.

5
 6
 7

1 **Table Ts3:** Degree of crystallinity, calculated from WAXS reflexes and T_m , determined *via* DSC
 2 of the bulk materials of P(DLA-*stat*-EtGly), P(LLA-*stat*-EtGly) with varying EtGly contents
 3 without stereocomplexation and from pure PEtGly.³

Base polymer	PDLA				PLLA				PEtGly
EtGly-content [mol%]	0	5	10	20	0	5	10	20	100
w_c^{WAXS} [%]	59	40	31	35	62	22	47	40	n.a.**
T_m [°C]*	163	151	143	121	163	151	140	121	n.a.***

4 * Values obtained from the third heating run (heating rate: 10 K min⁻¹).

5 ** No WAXS reflexes were observed.

6 *** No DSC peaks were observed.

7

8 References

- 9 (1.) Xu, P.; Huang, X.; Pan, X.; Li, N.; Zhu, J.; Zhu, X., Hyperbranched polycaprolactone
 10 through raft polymerization of 2-methylene-1,3-dioxepane. *Polymers* **2019**, *11*.
 11 (2.) Nojima, S.; Fujimoto, M.; Kakihira, H.; Sasaki, S., Effects of copolymer composition on
 12 the crystallization and morphology of poly(ϵ -caprolactone)-block-polystyrene. *Polymer Journal*
 13 **1998**, *30*, 968-975.
 14 (3.) Bandelli, D.; Alex, J.; Helbing, C.; Ueberschaar, N.; Görls, H.; Bellstedt, P.; Weber,
 15 C.; Jandt, K. D.; Schubert, U. S., Poly(3-ethylglycolide): A well-defined polyester matching the
 16 hydrophilic hydrophobic balance of pla. *Polym. Chem.* **2019**, *10*, 5440-5451.
 17 (4.) Kister, G.; Cassanas, G.; Vert, M., Effects of morphology, conformation and configuration
 18 on the ir and raman spectra of various poly(lactic acid)s. *Polymer* **1998**, *39*, 267-273.
 19 (5.) Furukawa, T.; Sato, H.; Murakami, R.; Zhang, J.; Noda, I.; Ochiai, S.; Ozaki, Y., Raman
 20 microspectroscopy study of structure, dispersibility, and crystallinity of
 21 poly(hydroxybutyrate)/poly(l-lactic acid) blends. *Polymer* **2006**, *47*, 3132-3140.
 22 (6.) Kawai, T.; Rahman, N.; Matsuba, G.; Nishida, K.; Kanaya, T.; Nakano, M.; Okamoto,
 23 H.; Kawada, J.; Usuki, A.; Honma, N.; Nakajima, K.; Matsuda, M., Crystallization and melting
 24 behavior of poly (l-lactic acid). *Macromolecules* **2007**, *40*, 9463-9469.

- 1 (7.) Suzuki, T.; Ei, A.; Takada, Y.; Uehara, H.; Yamanobe, T.; Takahashi, K., Modification
2 of physical properties of poly(l-lactic acid) by addition of methyl- β -cyclodextrin. *Beilstein J Org*
3 *Chem* **2014**, *10*, 2997-3006.
- 4 (8.) Yuniarto, K.; Purwanto, Y. A.; Purwanto, S.; Welt, B. A.; Purwadaria, H. K.; Sunarti,
5 T. C., Infrared and raman studies on polylactide acid and polyethylene glycol-400 blend. *AIP*
6 *Conference Proceedings* **2016**, *1725*, 020101.
- 7 (9.) Slager, J.; Domb, A. J., Biopolymer stereocomplexes. *Adv. Drug Deliv. Rev.* **2003**, *55*, 549-
8 83.
- 9 (10.) Slager, J.; Brizzolara, D.; Cantow, H. J.; Domb, A., Crystallization and
10 stereocomplexation governed self-assembling of poly(lactide)-b-poly(ethylene glycol) to
11 mesoscale structures. *Polym. Adv. Technol.* **2005**, *16*, 667-674.

12